

THE
INTERNATIONAL SERIES
OF
MONOGRAPHS ON PHYSICS

GENERAL EDITORS

J. BIRMAN S. F. EDWARDS
C. H. LLEWELLYN SMITH M. REES

The Physics of Liquid Crystals

SECOND EDITION

P. G. DE GENNES

and

J. PROST

*École Supérieure de Physique
et de Chimie Industrielles de la Ville
de Paris*

CLARENDON PRESS · OXFORD
1993

Oxford University Press, Walton Street, Oxford OX2 6DP

Oxford New York Toronto
Delhi Bombay Calcutta Madras Karachi
Kuala Lumpur Singapore Hong Kong Tokyo
Nairobi Dar es Salaam Cape Town
Melbourne Auckland Madrid
and associated companies in
Berlin Ibadan

Oxford is a trade mark of Oxford University Press

Published in the United States
by Oxford University Press, New York

© P. G. de Gennes and J. Prost, 1993

All rights reserved. No part of this publication may be reproduced, stored in a retrieval system, or transmitted, in any form or by any means, without the prior permission in writing of Oxford University Press. Within the UK, exceptions are allowed in respect of any fair dealing for the purpose of research or private study, or criticism or review, as permitted under the Copyright, Designs and Patents Act, 1988, or in the case of reprographic reproduction in accordance with the terms of licences issued by the Copyright Licensing Agency. Enquiries concerning reproduction outside those terms and in other countries should be sent to the Rights Department, Oxford University Press, at the address above.

This book is sold subject to the condition that it shall not, by way of trade or otherwise, be lent, re-sold, hired out, or otherwise circulated without the publisher's prior consent in any form of binding or cover other than that in which it is published and without a similar condition including this condition being imposed on the subsequent purchaser

A catalogue record for this book is available from the British Library

Library of Congress Cataloging in Publication Data

Gennes, Pierre Gilles de.

The physics of liquid crystals / P. G. de Gennes and J. Prost. —
2nd ed.

p. cm. — (The International series of monographs on physics; 83)
Includes bibliographical references.

1. Liquid crystals. I. Prost, Jacques. II. Title. III. Series:
International series of monographs on physics (Oxford, England); 83.
QD923.G46 1993 530.4'29—dc20 93-9154

ISBN 0 19 852024 7

Typeset by Integral Typesetting, Great Yarmouth, Norfolk
Printed in Great Britain by
Biddle's Ltd, Guildford and King's Lynn

PREFACE TO THE SECOND EDITION

The first version of this book came out about twenty years ago. Since then, our knowledge of liquid crystals has expanded considerably: the ‘blue phases’ of cholesterics have been essentially understood; columnar systems have been constructed; nematic polymers of various types have come up; microphases obtained with block copolymers have been clarified.

The first book was a hasty introduction to a rapidly growing field. Some friends convinced us that it was worthwhile to transform it into a more detailed review of a mature field. The process of going from a sketch to a full painting is long and hard: it was energetically undertaken by one of us—Jacques Prost—with very little help from the original designer.

The final painting is much larger in size: but it remains focused on a few central characters—with special emphasis on smectics and columnar phases. On the one hand, what was formally a single chapter on smectics has been split into four—retaining a spirit similar to what we originally had for nematics. On the other hand, there are many little corners in the painting where we do not shed much new light: surface phenomena, instabilities, electric field effects in nematics, chemical inventions, applications. . . . One beautiful figure is not really shown: this is the modern classification of defects, with its remarkable predictions for systems such as biaxial nematics.

The basic reasons for these omissions are (a) the need to keep to a ‘human’ size, (b) the recent appearance of many books where these features are duly emphasized.

As in most large classical paintings, this book is really a collective work, where the influence of famous ‘schools’ can be clearly recognized—and where some pieces may turn out to be done by some future Veronese. We acknowledge with particular warmth the participation of the Bordeaux group on liquid crystals (Centre de Recherches Paul Pascal); of the theory group at the Ecole de Physique et Chimie (Paris); of T. Lubensky whose teaching and advice have been essential to both of us; of J. Toner, who convinced one of us (J. P.) to start the project (the central argument being: ‘you will be so happy when it is finished’); of a number of visitors and friends—V. Amarias, J. P. Carton, E. Dubois Violette, C. Garland, S. Lagerwall, L. Limat, S. Ramaswamy—who participated both in stimulating discussions and painful proofreadings.

Last, but not least: our thanks to the late G. Berner; to M. Bertrand and G. Friedelance, who prepared the manuscript. And our nostalgic thanks to our companions, children and friends, who endured this long gestation.

PREFACE TO THE FIRST EDITION

Liquid crystals are beautiful and mysterious; I am fond of them for both reasons. My hope is that some readers of this book will feel the same attraction, help to solve the mysteries, and raise new questions.

We have known of the existence of liquid crystals for a comparatively long time—eighty years—yet many experiments which could have been done thirty years ago are only now being performed. The importance of potential applications to thermography and electro-optic display was realized only ten years ago (mainly through the work of Fergason and Hellmeier), but the apparent lack of applications in earlier times cannot, by itself, explain certain delays. More fundamentally, the study of liquid crystals is complicated because it involves several different scientific disciplines: chemistry, optics, and mechanics, more specialized tools such as nuclear magnetic resonance, and also a certain sense of vision in three-dimensional space in order to visualize complex molecular arrangements. A semi-theorist like myself is not very well trained in any of these techniques. For this reason, this book is very incomplete; certain aspects (and particularly the chemical aspects) are reduced to a bare minimum. On the other hand, what a theorist can and should systematically introduce is comparisons with other fields. In the present context, comparisons with magnetic systems are often useful and will be mentioned. Comparisons between the so-called smectic phases and the superfluid helium II and superconductors are also highly instructive. However, they imply a certain familiarity with low-temperature physics, which I did not want to impose as a prerequisite; for this reason, the references to superfluids are kept short.

As do all theorists, I relish exact calculations, but in the present case I have tried to insert qualitative discussions rather than equations whenever possible. Two parts remain particularly heavy and unpleasant, however: these are the sections of Chapters 3 and 5 concerned with the hydrostatics and hydrodynamics of nematics. This subject has been the source of some controversy between the classical mechanics group at Johns Hopkins and the theoretical physics group at Harvard. The two groups use very different languages; however (fortunately), their essential results are the same. I have tried to show this at the expense of a rather long and dull analysis, but, apart from this particular topic, the theoretical speculations have usually been condensed and replaced by one or two useful references.

I must emphasize that the references quoted (both for experimental data and for theoretical work) do not claim to be a complete list and do not refer to historical priority. For instance, I do *not* mention the books of Lehmann and of Schenk because an average reader will get a much more clear

presentation of their main observations through the later reviews by Friedel or Saupe[†]. Similarly, in the discussion of nematic order at the molecular level, I have omitted many theoretical papers which are interesting but still very tentative.

Even as regards the choice of topics, the present work is incomplete; in particular, the lyotropic materials are not discussed. I believe that we still need a few years to understand them better. The same remark holds for the ‘exotic’ smectic phases D, E, F, G . . . and for the ‘blue phase’ of certain cholesterol esters. These phases are extremely interesting, but (in my opinion at least) we grasp them too poorly to discuss them in this book; my purpose is clarification more than compilation. Having taught the corresponding material during the past three years, I know that the present version is still very far from achieving this purpose, but I hope that, in spite of its obvious defects, it will help ‘liquid crystallers’ to reach a universally common language.

My debt to a number of colleagues and friends is enormous. I would like to mention first G. Durand and M. Veyssié, who bravely started experiments on liquid crystals at Orsay during the autumn of 1968. Now, owing to their efforts and to the participation of other teams we have established a very active group; to a large extent, the present book represents its common views, based on constant discussions. The mistakes are my mistakes but the spirit is their spirit. I would also like to mention friends from outside the Orsay unit: J. Billard, who showed me the first liquid crystals that I ever saw and who, more recently, taught me a number of fundamental features of mesomorphic phases; R. B. Meyer, with whom I have been in constant correspondence and whom I hoped (in vain) to convince to write some chapters; our visitors from last year D. Litster, P. Pershan, and especially P. Martin, whose advice and positive criticism has been of constant help; F. C. Frank who, together with J. Friedel and M. Kleman, patiently instructed me on the structure of some difficult defects; G. Sarma and N. Boccardo, with whom I have been exchanging ideas for a long time; S. Alexander, D. Martire, and J. Vieillard Baron, who coached me on the hard-rod problem. A special mention is due to J. L. Ericksen, H. Gruler, W. Marshall, A. Rapini, and Y. R. Shen for their close scrutiny of the initial manuscript, to C. Williams, who prepared the list of elastic constants, and to L. Léger, who did the same for the friction constants. Most of the typing work—particularly painful in view of the unpredictable changes of mood of the author—was done, with charming patience, by Marie France Jestin. M. Crasson and R. Seveste have succeeded in producing figures and photographs from my vague indications and scribblings.

Last, but not least, I want to thank my wife Anne Marie for her

[†] The history of liquid crystals has been analysed recently by H. Kelker (*Molecular crystals and liquid crystals*, 21, 1 (1973)).

cooperation: so many sunny weekends have been sacrificed to this book. Now, looking at the result, I am not entirely convinced that it was worthwhile, and I certainly do not dare to dedicate the book to her.

'Well, now that we have seen each other,' said the unicorn 'If you believe in me, I'll believe in you. Is that a bargain?'

'Yes, if you like,' said Alice.

Orsay
December 1972

P. G. de G.

CONTENTS

1 LIQUID CRYSTALS: MAIN TYPES AND PROPERTIES	1
1.1 Introduction: what is a liquid crystal?	1
1.2 The building blocks	3
1.2.1 Small elongated organic molecules	3
1.2.2 Small discoid organic molecules	6
1.2.3 Long helical rods	6
1.2.4 Polymers	8
1.2.5 Associated structures	9
1.2.6 Summary	10
1.3 Nematics and cholesterics	10
1.3.1 Uniaxial nematics	10
1.3.2 Nematics of different symmetry	12
1.3.3 Cholesterics	13
1.3.4 Summary	17
1.4 Smectics	18
1.4.1 Smectics A	19
1.4.2 Smectics C	20
1.4.3 ‘Hexatic’ smectics	22
1.4.4 ‘Crystalline’ smectics	24
1.4.5 The D phase	26
1.5 Columnar phases	26
1.5.1 Hexagonal phases	26
1.5.2 Rectangular and oblique phases	27
1.5.3 ‘Antiphases’	27
1.6 More on long-, quasilong-, and short-range order	28
1.6.1 ‘Poor man’s’ elasticity of liquid crystals	29
1.6.2 Fluctuations	31
1.6.3 Long-range, quasilong-range, short-range order	32
1.7 Remarkable features of liquid crystals	34
2 LONG- AND SHORT-RANGE ORDER IN NEMATICS	41
2.1 Definition of an order parameter	41
2.1.1 Microscopic approach	41
2.1.2 Macroscopic approach	56
2.1.3 Relation between microscopic and macroscopic approaches	57
2.2 Statistical theories of the nematic order	59
2.2.1 Mean-field calculations for hard rods and platelets	59
2.2.2 Mean-field theory with S^2 interaction	66
2.2.3 Computer calculations	73

2.3	Phenomenological description of the nematic-isotropic transition	76
2.3.1	Landau free energy above T_c	76
2.3.2	Static pretransitional effects	78
2.3.3	Biaxial phase	82
2.3.4	Failures of the mean-field approach	85
2.4	Mixtures	91
2.4.1	Importance of mixed systems	91
2.4.2	General trends	92
3	STATIC DISTORTIONS IN A NEMATIC SINGLE CRYSTAL	98
3.1	Principles of the continuum theory	98
3.1.1	Long-range distortions	98
3.1.2	The distortion free energy	100
3.1.3	Discussion of the distortion-energy formula	102
3.1.4	Boundary effects	108
3.1.5	Nematics transmit torques	116
3.2	Magnetic field effects	117
3.2.1	Molecular diamagnetism	117
3.2.2	Definition of a magnetic coherence length	120
3.2.3	The Frederiks transition	123
3.3	Electric field effects in an insulating nematic	133
3.3.1	Dielectric anisotropy	133
3.3.2	Polarization induced by distortion (flexoelectric effect)	135
3.4	Fluctuations in the alignment	139
3.4.1	Light-scattering experiments	139
3.4.2	Orientation fluctuations and correlations in a nematic single crystal	141
3.4.3	Scattering of light by orientation fluctuations	144
3.5	Hydrostatics of nematics	150
3.5.1	Free energy and molecular field	150
3.5.2	Stresses and forces	151
3.5.3	The balance of torques	155
4	DEFECTS AND TEXTURES IN NEMATICS	163
4.1	Observations	163
4.1.1	Black filaments (' <i>structures à fils</i> ')	163
4.1.2	' <i>Structures à noyaux</i> ' ('Schlieren structures')	163
4.1.3	Types of defects	166
4.2	Disclination lines	168
4.2.1	Definition of the 'strength'	168
4.2.2	Distortion field around one line	170
4.2.3	The concept of line tension	178
4.3	Point disclinations	180
4.3.1	Instability theorem for lines of integral strength	180

4.3.2 Interpretation of the <i>noyaux</i>	183
4.3.3 Other observations on point defects	184
4.4 Walls under magnetic fields	185
4.4.1 180° walls	187
4.4.2 Walls associated with a Frederiks transition	189
4.4.3 Transformation from walls to lines (' <i>pincement</i> ')	190
4.5 Umbilics	194
4.6 Surface disclinations	194
 5 DYNAMICAL PROPERTIES OF NEMATICS	198
5.1 The equations of 'nematodynamics'	198
5.1.1 Coupling between orientation and flow	198
5.1.2 Choice of dynamical variables	199
5.1.3 The entropy source for a flowing nematic	200
5.1.4 The laws of friction	204
5.2 Experiments measuring the Leslie coefficients	209
5.2.1 Laminar flow under a strong orienting field	209
5.2.2 Attenuation of ultrasonic shear waves	213
5.2.3 Laminar flow in the absence of external fields	218
5.2.4 Variable external fields	220
5.2.5 Inelastic scattering of light	227
5.3 Convective instabilities under electric fields	230
5.3.1 Basic electrical parameters	230
5.3.2 Experimental observations at low frequencies	233
5.3.3 The Helfrich interpretation	236
5.3.4 Extension to higher frequencies	239
5.4 Molecular motions	245
5.4.1 Dielectric relaxation	245
5.4.2 Nuclear spin-lattice relaxation	246
5.4.3 Acoustic relaxation	248
5.4.4 Translational motions	250
5.4.5 Temperature variation of the friction coefficients	254
5.4.6 Semi-slow motions above T_c	255
 6 CHOLESTERICS	263
6.1 Optical properties of an ideal helix	263
6.1.1 The planar texture	263
6.1.2 Bragg reflections	264
6.1.3 Transmission properties at arbitrary wavelengths (normal incidence)	268
6.1.4 Interpretation	271
6.1.5 Conclusions and generalizations	279
6.2 Agents influencing the pitch	280
6.2.1 Physicochemical factors	281
6.2.2 External fields	286

6.3	Dynamical properties	294
6.3.1	Studies on small motions in a planar texture	295
6.3.2	Macroscopic flow	296
6.3.3	Convective instabilities	300
6.3.4	Torques induced by a heat flux	304
6.4	Textures and defects in cholesterics	308
6.4.1	Textures	308
6.4.2	Singular lines	313
6.5	Blue phases	320
6.5.1	Experimental observations	320
6.5.2	Double twist theories	323
6.5.3	Landau theory	329
7	MACROSCOPIC BEHAVIOUR OF SMECTICS AND COLUMNAR PHASES	337
7.1	Continuum description of smectics and columnar phases: statics	337
7.1.1	Choice of variables	337
7.1.2	Distortion free energy of (non-chiral) smectics	341
7.1.3	Distortion free energy of columnar phases	349
7.1.4	Boundary conditions	353
7.1.5	Particular geometries	357
7.1.6	Transitions induced by external forces: Helfrich–Hurault effect	361
7.1.7	Transitions induced by external forces: undulation by mechanical tension	364
7.1.8	Transitions induced by external forces: thermo-optic effect in smectics A	369
7.1.9	Fluctuations	370
7.2	Continuum description of chiral smectics and columnar phases	376
7.2.1	Chiral S_A^* and S_C^*	376
7.2.2	Chiral S_C^* (S_I^* , S_F^* , and S_K^*)	377
7.2.3	Electric terms	379
7.2.4	Unwinding of the helix by an electric field	385
7.2.5	Fluctuations	389
7.2.6	Surface anchoring	390
7.2.7	Particular geometries	393
8	DYNAMICAL PROPERTIES OF SMECTICS AND COLUMNAR PHASES	408
8.1	Unified description	408
8.1.1	Preliminary remarks	408
8.1.2	Basic equations	410
8.1.3	Smectics A and columnar hexagonal phases	415

8.1.4	The undulation mode	418
8.1.5	Permeation mode	420
8.1.6	Acoustic waves	421
8.1.7	Transverse modes	423
8.1.8	$S_{B\text{hex}}$ and S_C hydrodynamics	424
8.1.9	Remarks on the mode structure	429
8.2	Flow properties	430
8.2.1	Typical geometries	430
8.2.2	Flow past obstacles	435
8.2.3	Flow alignment	445
8.3	Breakdown of elasticity	452
8.3.1	Poor man's derivation	452
8.3.2	Splay modulus	454
8.3.3	Macroscopic non-linear stress-strain relation	455
8.3.4	Renormalization group results	455
8.4	Breakdown of hydrodynamics	457
8.4.1	Poor man's derivation	457
8.4.2	More general results	460
8.4.3	Columnar phases	461
8.4.4	Experimental situation	462
9	DEFECTS IN SMECTICS AND COLUMNAR PHASES	466
9.1	Observations	466
9.1.1	Large deformations in smectics	466
9.1.2	Large deformations in columnar phases	473
9.1.3	Dislocations	476
9.1.4	Disclinations	478
9.1.5	Walls	483
9.2	Dislocation and associated stress/strain	487
9.2.1	Distortions in smectics	487
9.2.2	Strain fields in columnar phases	500
10	PHASE TRANSITIONS IN SMECTICS	507
10.1	The $A \rightleftharpoons N$ transition	507
10.1.1	Mean-field description	507
10.1.2	The analogy with superconductors	509
10.1.3	Critical phenomena	514
10.1.4	Anisotropic scaling	517
10.1.5	Experimental situation	518
10.1.6	The search for an anisotropic fixed point	521
10.1.7	Nature of the $N-S_A$ transition	522
10.1.8	'Poor man's' dislocation unbinding transition	524
10.1.9	Twisted grain boundary phase	525
10.1.10	Current situation	527

10.2	Smectic A-smectic C transition	527
10.2.1	Superfluid analogy	527
10.2.2	Ginzburg criterion	529
10.2.3	Experimental findings	532
10.2.4	First-order $S_A \rightleftharpoons S_C$	532
10.2.5	N–A–C point	534
10.2.6	The S_A – S_C transition in two dimensions	540
10.3	Transitions involving hexatic phases	547
10.3.1	$S_A \rightleftharpoons S_{B\text{Hex}}$ transition	547
10.3.2	Harmonics of hexatic ordering and scaling properties	549
10.4	Frustrated smectics	551
10.4.1	Experimental facts	551
10.4.2	Frustrated smectics model	557
10.4.3	Bilayer, partial bilayer smectics, incommensurate phases, and antiphases	560
10.4.4	Re-entrant behaviour	568
10.4.5	S_A – S_A isolated critical point and nematic bubble	570
10.4.6	Molecular aspects	575
	Author index	587
	Subject index	595

LIQUID CRYSTALS: MAIN TYPES AND PROPERTIES

'Que m'a donné le monde que ce mouvement d'herbes'

Saint John Perse

1.1 INTRODUCTION: WHAT IS A LIQUID CRYSTAL?

During our years in high school, we have all been taught that matter only exists in three states: solid, liquid, and gas. However, this is not quite correct. In particular, certain organic materials do not show a single transition from solid to liquid, but rather a cascade of transitions involving new phases. The mechanical properties and the symmetry properties of these phases are intermediate between those of a liquid and those of a crystal. For this reason, they have often been called *liquid crystals*. A more proper name is ‘mesomorphic phases’ (*mesomorphic*: of intermediate form).

To understand the significance of these new states of matter, it may be useful to recall first the distinction between a *crystal* and a *liquid*.

In a crystal the components (molecules, or groups of molecules) are regularly stacked. The centres of gravity of the various groups are located on a three-dimensional periodic lattice. In the liquid the centres of gravity are not ordered in this sense. These two states of matter differ most obviously by their mechanical properties; a liquid flows easily. More fundamentally, a crystal is defined by the fact that, if a primitive pattern (or basis) is located at a point \mathbf{x}_0 , the probability of finding an equivalent pattern at the point $\mathbf{x} = \mathbf{x}_0 + n_1\mathbf{a}_1 + n_2\mathbf{a}_2 + n_3\mathbf{a}_3$ (n_i = integer; $i \in \{1, 2, 3\}$ and $\{\mathbf{a}_i\}$ basis vectors) stays finite when $|\mathbf{x} - \mathbf{x}_0| \rightarrow \infty$. As a result, its X-ray diffraction pattern shows sharp Bragg reflections characteristic of the lattice. In other words

$$\lim_{|\mathbf{x} - \mathbf{x}'| \rightarrow \infty} \langle \rho(\mathbf{x})\rho(\mathbf{x}') \rangle = F(\mathbf{x} - \mathbf{x}') \quad (1.1)$$

where $\langle \rho(\mathbf{x})\rho(\mathbf{x}') \rangle$ is the density–density correlation function and $F(\mathbf{x} - \mathbf{x}')$ a periodic function of basis vector \mathbf{a}_i .

An isotropic liquid may be defined in a similar way. One can say that, if one has been able to locate a molecule or some pattern at a given point \mathbf{x}_0 , there is just no way to express the probability of finding a similar one at the point \mathbf{x} far from \mathbf{x}_0 , except through the average particle density $\bar{\rho}$. In other

words,

$$\lim_{|\mathbf{x} - \mathbf{x}'| \rightarrow \infty} \langle \rho(\mathbf{x})\rho(\mathbf{x}') \rangle \simeq \bar{\rho}^2. \quad (1.2)$$

The important feature is the existence of an (isotropic) length scale ξ over which correlations are lost. The X-ray diffraction pattern of a liquid exhibits diffuse peaks of typical width ξ^{-1} .

We are now in a position to define liquid crystals. These are systems in which a liquid-like order exists at least in one direction of space and in which some degree of anisotropy is present (a better definition of ‘some degree of anisotropy’ is: the density–density correlation function does not depend solely on the modulus $|\mathbf{x} - \mathbf{x}'|$ but also on the orientation of $\mathbf{x} - \mathbf{x}'$ with respect to macroscopically defined axes).

With this definition in mind we see that mesophases can be obtained in two different ways

1. Imposing no positional order, or imposing positional order in one or two rather than in three dimensions. All this can happen in nature.
 - The first case obviously corresponds to a liquid but, if the correlation function is anisotropic, this is not an isotropic liquid; it is a *nematic* (there are at least two length scales ξ_{\parallel} and ξ_{\perp} over which correlations decay; \parallel (respectively \perp) indicate parallel (respectively perpendicular) to a macroscopically defined direction).
 - The second case describes one-dimensional order in three dimensions: the system can be viewed as a set of two-dimensional liquid layers stacked on each other with a well defined spacing; the corresponding phases are called *smectics*.
 - The third case corresponds to two-dimensionally ordered systems in three dimensions. They can be described as a two-dimensional array of liquid tubes and are called *columnar phases*.
2. Introducing degrees of freedom that are distinct from the localization of the centres of gravity. For non-spherical molecules, their orientation is the most natural candidate. Orientational transitions may take place in crystals, in liquid crystals, or in isotropic liquids. In the first two cases the freezing of orientational degrees of freedom does not generate very novel phases. On the other hand, freezing out orientational degrees of freedom in an isotropic liquid does yield anisotropy: certain organic liquids show a low-temperature phase in which the molecules are aligned preferentially along one direction. The correlations along the preferred direction are not equivalent to those in the perpendicular plane. The phase obeys our definition of a nematic: orientational freezing is the most transparent way of obtaining nematics.

Nematics, smectics, and columnar phases are the only known forms of liquid crystals. We also have ‘colloidal crystals’, which can sometimes flow almost like water. But they are not liquid crystals: they are genuine crystals, exhibiting long-range three-dimensional order, with an unusually small yield stress.

The type of liquid crystals that may be observed depends heavily on the structure of the constituent molecules or groups of molecules (the ‘building blocks’ as we shall call them). Nematics and smectics are often made of *elongated* objects, whereas some other nematics and most columnar phases are often made of *disk-like* molecules.

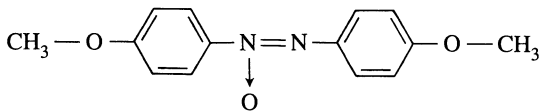
Depending upon the nature of the building blocks and upon the external parameters (temperature, solvents, etc.), we can observe a wide variety of phenomena and transitions amongst liquid crystals. This chapter therefore starts off by discussing the building blocks that give rise to the known types of liquid crystals and then goes on to give a broad classification of nematics, smectics, and columnar phases.

1.2 THE BUILDING BLOCKS

As explained above, to generate a liquid crystal one must use anisotropic objects, either elongated or disk-like. At the present time we know several ways to achieve this: with small molecules; with long helical rods that either occur in nature or can be made up artificially; with polymers; or with more complex units that are associated structures of molecules and ions.

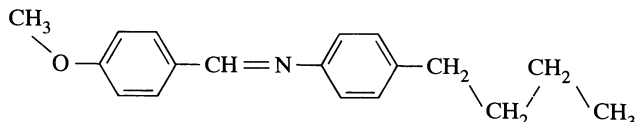
1.2.1 Small elongated organic molecules

The classical example is *p*-azoxyanisole (PAA) with the formula



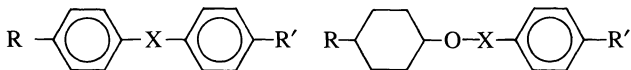
From a (rough) steric point of view, this is a rigid rod of length ~ 20 Å and width ~ 5 Å. (The two benzene rings are nearly coplanar.)

Another historical example is *N*-(*p*-methoxybenzylidene)-*p*-butylaniline (MMBA) with the formula



Both PAA and MBBA are ‘nematogens’. This word means that they give rise to the nematic type of mesophase that will be discussed in Section 1.3.1. However, for PAA the nematic state is found only at high temperatures (between 116°C and 135°C at atmospheric pressure), while MBBA is nematic from ~20°C to 47°C, thus allowing much easier experimentation. MBBA, however, lacks chemical stability. For many purposes cyanobiphenyls and cyanobicyclohexyl derivatives (and many others!) are preferred nowadays.

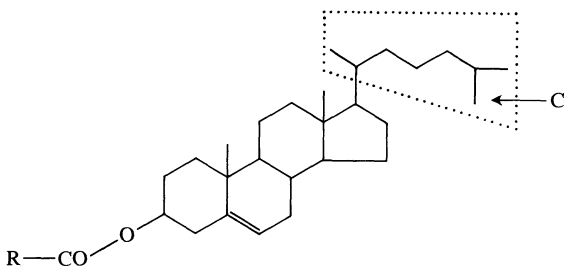
A broad class of organic molecules with the following general pattern are either nematogens or smectogens



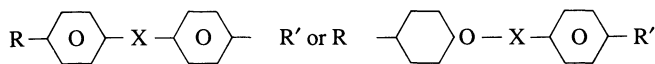
(i.e. two para-substituted aromatic rings linked by a large variety of functions preserving the long axis of the molecules, or one para-substituted aromatic ring and one para-substituted cyclohexane linked by the same type of functions; R and R' can be polar or non-polar). The major types inside this scheme are listed in Table 1.1.

Empirical rules describing the influence of the molecular nature on phase diagrams and related problems are reviewed in references 1–3. Smectics are favoured by long aliphatic chains, and amphiphilic interactions (i.e. a tendency for the aliphatic and polarizable part to segregate).

Another favourable class is obtained with *cholesterol esters*, of general formula



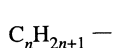
(We use a simplified convention in which the hydrogens are not explicitly shown.) Note that the rings are not aromatic and the structure is not planar. However, the ring system is rigid, while the saturated chain C and the radical R (when it is not too short) behave like two somewhat more flexible tails



R

X

R'



R

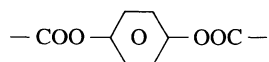
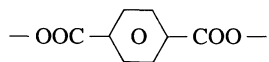
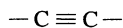
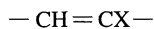
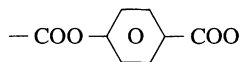
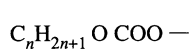
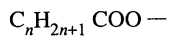
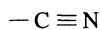
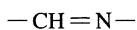
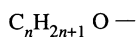


TABLE 1.1

attached to the rigid part; thus there is some steric similarity to the preceding group.[†]

We observe finally that, in all the pure systems that have been discussed here (PAA, cholesterol, esters, etc.), the simplest way to induce a transition is to vary the temperature. For this reason, such systems are commonly called *thermotropic*.

1.2.2 Small discoid organic molecules

The simplest examples are the hexasubstituted phenylesters (Table 1.2). This type of molecule yielded the first thermotropic columnar phase [4] made up of small entities. More general building blocks involve planar rigid cores‡ of different symmetries (note that both D_{2h} and D_{4h} cores do give columnar phases) a number (typically six) of aliphatic chains attached to the core with a suitable linkage. We give examples of such molecules in Table 1.2. The triphenylene has provided the first example of a thermotropic disk-like nematogen [6].

The importance of the length of the aliphatic chain suggests that the stability of columnar phases requires some kind of amphiphilic interaction: cores and chains tend to segregate, and the chains provide lubrication between the columns.

1.2.3 Long helical rods

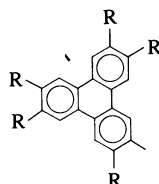
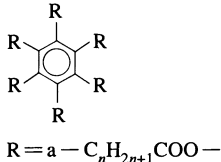
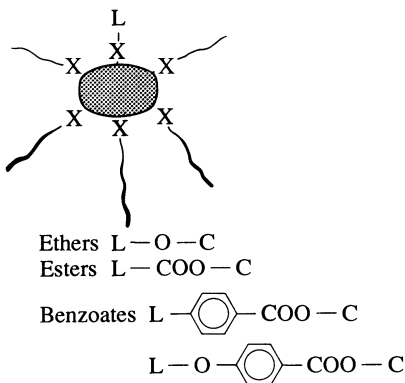
A number of *synthetic polypeptides* and other rigid polymers in suitable solvents, have a rod-like conformation with typical rod lengths of order 300 Å, and widths 20 Å [7]. In concentrated solutions these systems give mesophases [8]. Similar phases are found also with deoxyribonucleic acids (DNA) and with certain viruses [8]; the standard example is *tobacco mosaic virus* (TMV), with length 3000 Å, and width ~200 Å. One definite advantage of such viruses, from the point of view of physical experiments, is that all rods from one virus species are exactly the same size.

Finally, on a still larger scale, model systems made with glass or plastic fibres (diameters ~10 µm, lengths ~100 µm or more) floating in water can be of great interest. However, (1) these colloids must be stabilized against flocculation; (2) with these sizes thermal agitation becomes negligible and equilibrium must be enforced by other forms of noise (e.g. sonication).

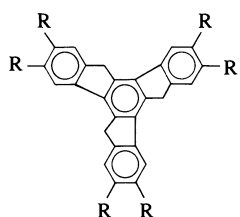
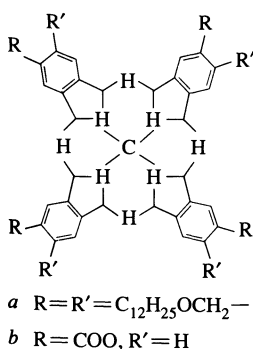
Note that, for all the systems listed in this section, the transitions are induced most easily by changing the concentration of rods rather than the temperature; for this reason they are commonly called *lyotropic*.

[†] Cholesterol itself has H instead of R-CO-, and does not give mesophases, probably because the OH groups creates strong hydrogen bonds between different molecules.

[‡] In fact, the core need not really be planar [5].



- a $R=n-C_nH_{2n+1}O-$
- b $R=a-C_nH_{2n+1}COO-$
- c $R=a-C_nH_{2n+1}-\text{C}_6\text{H}_4\text{COO}-$
- d $R=a-C_nH_{2n+1}O-\text{C}_6\text{H}_4\text{CO}-O-$



- a $R=n-C_nH_{2n+1}O-$
- b $R=n-C_nH_{2n+1}COO-$
- c $R=n-C_nH_{2n+1}-\text{C}_6\text{H}_4\text{COO}-$

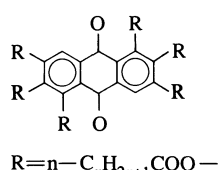
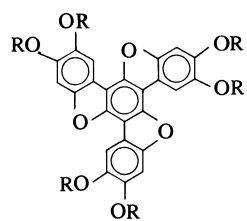


TABLE 1.2

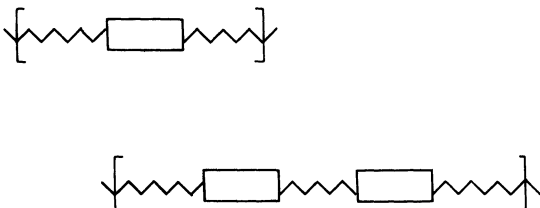


Fig. 1.1.

1.2.4 Polymers

In the preceding section we mentioned that rigid polymers in suitable solvents can give rise to mesophases (because they behave as rigid rods). A richer situation is obtained if one inserts flexible parts in the macromolecules. Two main classes are of interest.

1. *Main-chain polymers* are composed of rigid mesogenic parts attached to each other with flexible links (Fig. 1.1).

There is a large variety of possibilities since one can vary the nature of the mesogenic group, that of the flexible spacer, their length; one can also use copolymers with different mesogenic groups and spacers, either placed regularly or at random, change the degree of polymerization, etc.

2. *Side-chain polymers*. On rather classical polymers such as polysiloxanes, mesogenic groups are linked via flexible spacers (typically alkyl chains; Fig. 1.2).

Here again, a great variety of systems can be synthesized: one can change the main chain, the spacers, the mesogens, the degree of polymerization, use several mesogens (regularly spaced or not), etc.

For both classes 1 and 2, thermotropic mesomorphism is obtained. These systems are very stable, exhibit very large mesomorphic ranges (sometimes several hundred degrees), and give easily glassy states (most molecules may be trapped in an anisotropic matrix, easy to handle). A good survey of polymer properties may be found in reference 9.

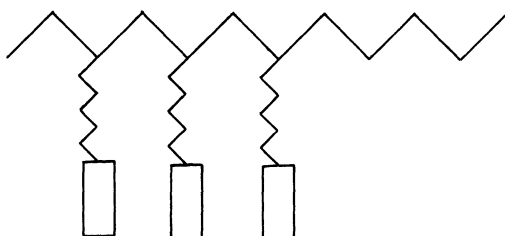


Fig. 1.2.

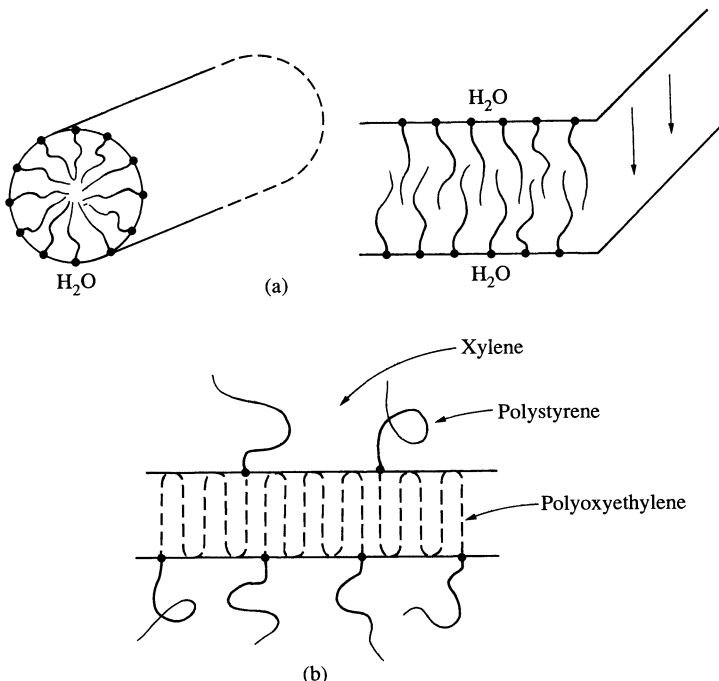


Fig. 1.3. A few typical building blocks for amphiphilic materials. (a) Rods and sheets for the system fatty acids–water (the polar head of the fatty acid is represented by the arrow). (b) Sheet structure for a copolymer: each chain has one soluble part (here polystyrene, the solvent being xylene) and one unsoluble part (here polyoxyethylene).

1.2.5 Associated structures

Typical examples of such structures are found in the soap–water systems.

Here we have an aliphatic anion $\text{CH}_3-(\text{CH}_2)_{n-2}-\text{CO}_2^-$ (with n in the range 12–20) plus a positive ion (Na^+ , K^+ , NH_4^+ , or others). The polar head of the acid (i.e. the $-\text{CO}_2^-$ group) tends to be in close contact with water molecules, while the apolar aliphatic chain avoids the water. These two opposite requirements define an amphiphile. A single molecule in solution cannot satisfy both of them, but a cluster of molecules can, as is shown in Fig. 1.3(a). Other examples of amphiphilic chains leading to similar geometries are the ‘block copolymers’ shown on Fig. 1.3(b) [11]. The resulting objects (e.g. rods or leaflets) may become the building units of larger mesomorphic structures [10]. Four-component mixtures (for instance, sodium dodecyl sulphate (SDS), decanol, hexane, water mixtures), important for oil recovery purposes, also give associated structures that yield liquid crystals. The same building block can give nematics, smectics, and columnar phases as well [12]. This is an important advantage over simpler molecules that usually

give smectics (and nematics) on one hand, columnar phases (and nematics) on the other, but not both with the exception of thermotropic soaps [13].

1.2.6 Summary

To summarize—we have found four types of building blocks:

- (1) small organic molecules, either rod-like or disk-like, for which an amphiphilic character may or may not be crucial (at least for getting the nematic phase). They are commonly designated as thermotropic.
- (2) rods in a liquid substrate. Here the temperature (T) effects are difficult to control (very often an increase in T will rapidly destroy the individual rods), and the natural parameter which we can adjust to induce phase transitions is the *concentration* of the rods. Such systems are called *lyotropic*.
- (3) main-chain or side-chain polymers that are thermotropic mesogens. Aside from temperature the molecular weight may also be considered as a variable.
- (4) amphiphilic compounds. These may give rise to associations and to mesomorphic behaviour, either in the presence of a selective solvent (e.g. water in soaps) or as a pure phase (for certain block copolymers and thermotropic soaps). Thus, depending upon which of the above conditions holds, amphiphilic compounds may be lyotropic or thermotropic.

In the present book, we shall be concerned only with thermotropic materials (except for a short discussion on biaxial nematics). Having in mind the various chemical species, we can now start to describe the unusual thermodynamic phases to which they give rise. The classification of mesophases (first clearly set out by G. Friedel in 1922 [14]) is essentially based on their symmetry. As we have seen there are three major classes: nematics; smectics; and columnar phases.

1.3 NEMATICS AND CHOLESTERICS

1.3.1 Uniaxial nematics

A schematic representation of the order of a ‘nematic’† phase is shown in Fig. 1.4(a), (b). The main features are as follows.

† The word ‘nematic’ was invented by G. Friedel. It comes from the Greek $\nu\eta\mu\alpha$ = thread, and refers to certain thread-like defects that are commonly observed in these materials. The physical nature of these defects (‘disclination lines’) will be discussed in Chapter 4.

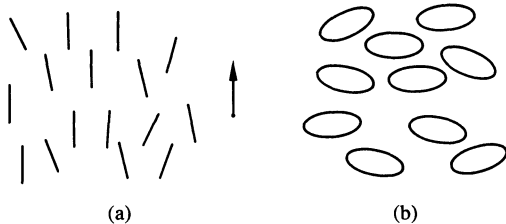
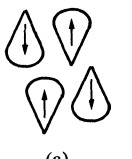


Fig. 1.4. The arrangement of molecules in the *nematic* mesophase: (a) made up of rod-like molecules; (b) made up of disk-like molecules.

1. The centres of gravity of the molecules have *no long-range order* and, consequently, as already stated, there is only diffuse scattering in the X-ray diffraction pattern. The correlations in position between the centres of gravity of neighbouring molecules are similar to those existing in a conventional liquid, aside from the anisotropy $\xi_{\parallel} \neq \xi_{\perp}$ in the length scale. In fact, nematics do flow like liquids. For a typical nematic such as PAA the viscosities are of order 0.1 poise.†
2. There is some order, however, in the *direction* of the molecules; they tend to be parallel to some common axis, labelled by a unit vector (or ‘director’) \mathbf{n} . This is reflected in all macroscopic tensor properties: for instance, optically, a nematic is a uniaxial medium with the optical axis along \mathbf{n} . (The difference between refractive indices measured with polarizations parallel or normal to \mathbf{n} is quite large: typically 0.2 for PAA.) In all known cases, there appears to be complete rotational symmetry around the axis \mathbf{n} .
3. The direction of \mathbf{n} is arbitrary in space; in practice it is imposed by minor forces (such as the guiding effect of the walls of the container). This is a situation of broken rotational symmetry, reminiscent of a Heisenberg ferromagnet, where all spins tend to be parallel but where the energy is independent of the direction of the total moment \mathbf{M} .
4. The states of director \mathbf{n} and $-\mathbf{n}$ are indistinguishable. For instance, if the individual molecules carry a permanent electric dipole, as in Fig. 1.5(a), there are just as many dipoles ‘up’ as there are dipoles ‘down’ and the system is not ferroelectric.
5. Nematic phases occur only with materials that do not distinguish between right and left; either each constituent molecule must be identical to its mirror image (achiral) or, if it is not, the system must be a ‘racemic’ (1:1) mixture of the right- or left-handed species (we shall come back to this point in Section 1.3.3). From a crystallographic point of view, properties 2, 4, and 5

† For comparison, the viscosity of water at room temperature is $\sim 10^{-2}$ poise.



(a)



(b)

Fig. 1.5. (a) In a nematic single crystal, if the molecules carry a dipole (represented by an arrow), there are as many dipoles ‘up’ as there are dipoles ‘down’. (b) If dipoles are forced to be ‘up’ the shape asymmetry of the molecules leads to a natural splay of the structure.

may be summarized by the symbol $D_{\infty h}$ in Schoenflies notation ($\infty/m\bar{m}$ in international notations).

The dual aspects of a nematic phase (liquid-like but uniaxial) are exhibited most spectacularly in the *nuclear magnetic resonance (NMR) spectrum*; the uniaxial symmetry causes certain line splittings (which are absent in the conventional isotropic liquid phase). On the other hand, the lines are relatively narrow; this implies rapid molecular motions and is a natural consequence of the fluidity. Some applications of these NMR measurements will be discussed in Chapters 2 and 5.

1.3.2 Nematics of different symmetry

1. Could we have a uniaxial liquid made with polar molecules, all the dipoles being aligned (Fig. 1.5(b))? This would be a liquid ferroelectric. Unfortunately, a phase like this is *unstable*: because the head and the tail of each molecule are generally different in size, the whole structure must deform [15]. (We analyse these deformations in Chapter 3.)
2. Could we have a uniaxial liquid made with molecules that carry magnetic moments along their long axis, and generate a liquid ferromagnet? From a formal point of view, this is possible [15]: the ‘head’ and ‘tail’ of the molecule may now be chemically identical and no mechanical instability appears. The difficulty here is in the physics, not with the symmetry. The exchange couplings between neighbouring magnetic moments are weaker than the conventional interactions between molecules (steric, Van der Waals, etc.); thus liquid ferromagnets should be very rare.
3. *Biaxial nematics* can be expected with building blocks shaped in the form of long rectangles (Fig. 1.6). The long expected *biaxial phase* $(D_{2h}; \frac{2}{m} m)$ has first been observed in lyotropic systems: when certain delicate conditions are met, one can have micelles of the required shape, and they do build up a remarkable anisotropic liquid [16]. Note that it is, however,

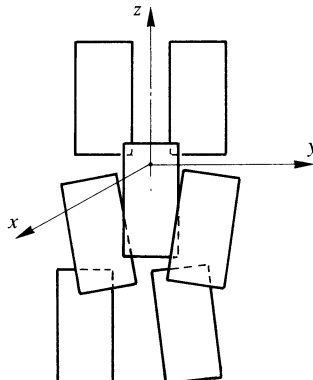


Fig. 1.6. Naïve representation of a biaxial nematic: the long sides and short sides of the rectangles are on the average parallel to, respectively, the z and y directions.

important to bear in mind that one can have an uniaxial phase with biaxial building blocks, and a biaxial phase with uniaxial building blocks! Biaxial nematics have also been observed in polymeric and low-molecular-weight thermotropic systems, as referred to in Chapter 2.

4. *Exotic nematics.* Nematics of higher symmetry, such as $D_{6h}\left(\frac{6}{m}, m\right)$

(hexagonal), $O_h(m\bar{3}m)$ (cubic) and $m\bar{5}m$ (icosahedral symmetry) may seem somewhat exotic. The existence of a hexagonal nematic has been conjectured (between a usual $D_{\infty h}$ nematic and a hexagonal columnar phase) [17]. Optically, a hexagonal phase is uniaxial just as that of a conventional nematic. Icosahedral nematics have been invoked in super-cooled liquids prior to the glass transition [18]. Another good candidate for generating an icosahedral nematic could be a melt of quasi-crystals: this new state of matter, obtained for instance by rapidly quenching samples of aluminium alloyed with manganese, iron, or chromium [19], is characterized by the existence of incommensurate lengths along icosahedral symmetry axes. The X-ray diffraction pattern reveals a dense distribution of Bragg spots that show the appropriate symmetry. Melting can well yield first a broadening of the peaks before losing the angular bond orientational order, which would be exactly that of the icosahedral nematic.

1.3.3 Cholesterics

If we dissolve in a nematic liquid a molecule that is *chiral* (i.e. different from its mirror image), we find that the structure undergoes a helical distortion.

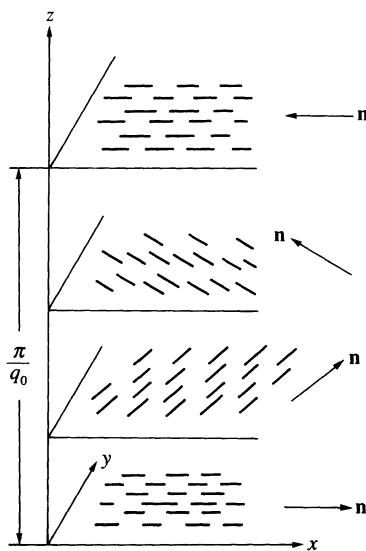


Fig. 1.7. The arrangement of molecules in the *cholesteric* mesophase. (The successive planes have been drawn for convenience, but do not have any specific physical meaning).

The same distortion is also found with pure cholesterol esters (which are also chiral). For this reason, the helical phase is called *cholesteric*.

1.3.3.1. The helical structure

Locally, a cholesteric is very similar to a nematic material. Again the centres of gravity have no long-range order and the molecular orientation shows a preferred axis labelled by a director \mathbf{n} . However, \mathbf{n} is not constant in space. The preferred conformation, shown in Fig. 1.7, is helical. If we call the z -axis the helical axis, we have the following structure for \mathbf{n}

$$\begin{aligned} n_x &= \cos(q_0 z + \phi) \\ n_y &= \sin(q_0 z + \phi) . \\ n_z &= 0 . \end{aligned} \quad (1.3)$$

Both the helical axis (z) and the value of ϕ are arbitrary; we see here another type of broken symmetry. The structure is periodic along z and (since the states \mathbf{n} and $-\mathbf{n}$ are again equivalent) the spatial period L is equal to one-half of the pitch:

$$L = \frac{\pi}{|q_0|} .$$

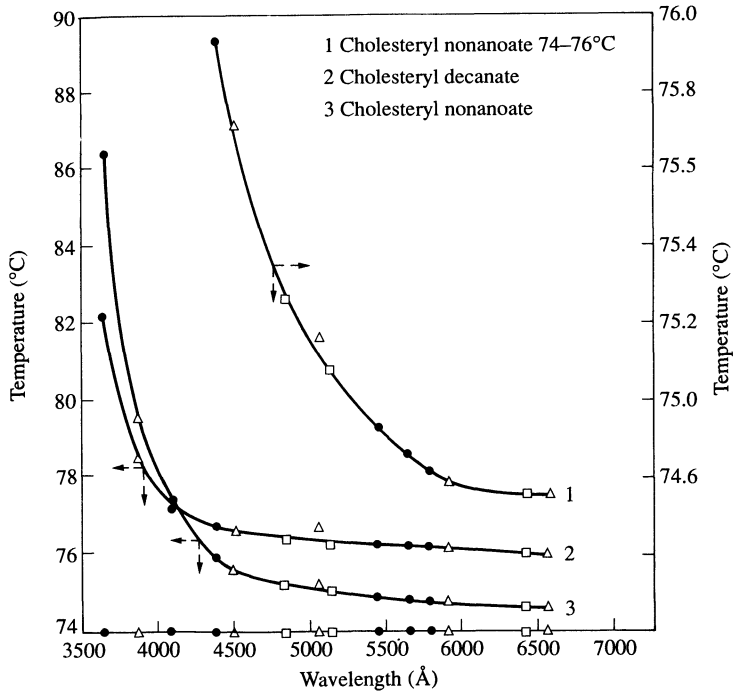


Fig. 1.8. Relation between pitch and temperature in typical cholesterics. What is plotted horizontally is the optical wavelength for Bragg reflection on the helical structure, which is equal to the pitch multiplied by the refractive index $\bar{n} \sim 1.5$ [20].

Typical values of L are in the 3000 Å range, i.e. much larger than the molecular dimensions. Since L is comparable to an optical wavelength, the periodicity results in Bragg scattering of light beams. We shall discuss these optical effects in Chapter 6.

Both the magnitude and sign of q_0 are meaningful. The sign distinguishes between right- and left-handed helices; a given sample at a given temperature always produces helices of the same sign. If we change the temperature T , q_0 changes (Fig. 1.8). In some particular cases $q_0(T)$ may even change sign at a particular temperature T^* . This case is interesting.

1. For $T = T^*$, the material is found to behave like a conventional nematic.
2. When we cross the temperature T^* , we find that the physical properties such as specific heats, etc. remain quite smooth.

Properties 1 and 2 show that the local molecular arrangements are indeed very similar in the nematic and in the cholesteric state, as was first noted by G. Friedel [14].

In the published literature, the cholesteric helix is sometimes visualized as

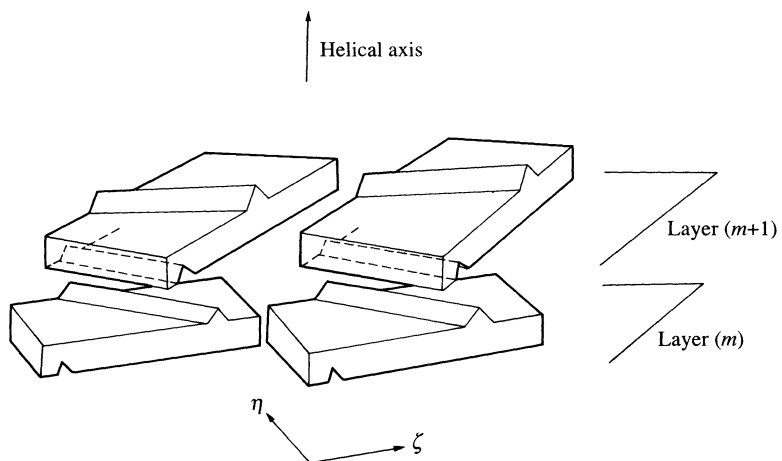


Fig. 1.9. An incorrect model for the cholesteric mesophase. The model assumes nearly flat molecules that pile up on each other and build up a helical structure. Central to the model is the assumption that the molecules form well defined layers normal to the helical axis; in reality, the planes of the molecules are completely free to rotate around the local optical axis (the ζ axis of the figure).

in Fig. 1.9, i.e. as a stacking of flat strips in the xy -planes. In this model the local optical symmetry is not uniaxial but biaxial (with axes ξ , η , and z). However, this would imply very strong differences on the molecular scale between the nematic and the cholesteric states and is in contradiction with the preceding paragraph; thus Fig. 1.9 is, in general, wrong.[†]

1.3.3.2. Cholesterics occur only with non-racemic systems

Let us consider a general twisted structure $n_x = \cos \theta(z)$, $n_y = \sin \theta(z)$ and find the form of the free energy F (per unit volume) as a function of the twist

$$q = \frac{\partial \theta}{\partial z}.$$

1. In materials that do not distinguish between the right and the left the plot of $F(q)$ must be symmetrical $F(-q) = F(q)$. Then there are two possibilities (Fig. 1.10(a)).
 - a. The minimum value of F occurs at $q = 0$; this corresponds to nematics.
 - b. Alternatively, F has two symmetrical minima at $q = \pm q_1$. This would be the analogue of the helimagnetic structures observed in certain rare-earth metals [21]. Steric interaction of dumb-bell-like molecules would tend to give rise to such lateral minima (Fig. 1.10(a)). At the

[†] More precisely, the difference in refractive index between the ξ and η directions is at most of order $(q_0 a)^2$, where a is a molecular dimension, i.e. of order 10^{-4} .

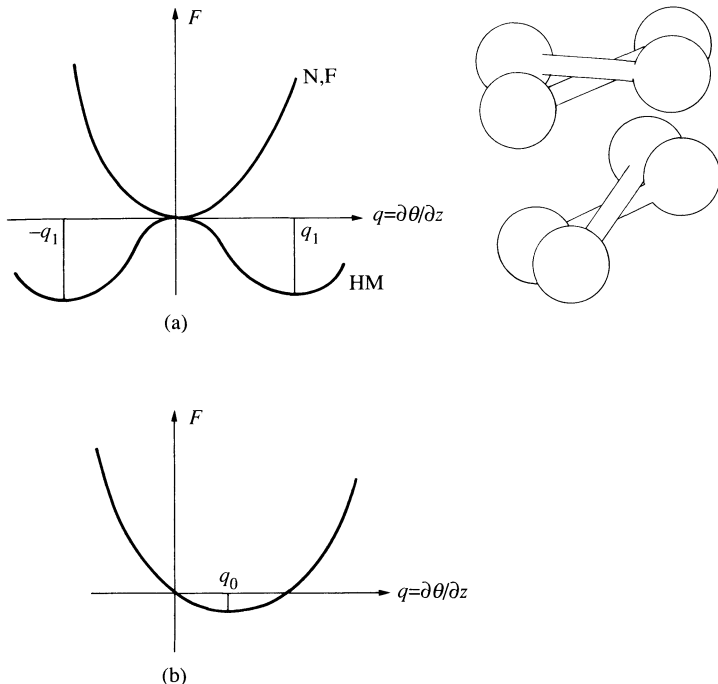


Fig. 1.10. Variation of the free energy with twist for various physical systems. (a) Systems that do not distinguish right and left. The curve labelled N, F applies to a nematic or a ferromagnet (minimum of energy at zero twist). The curve labelled HM applies to a helimagnet, or to the dumb-bells of the inset. (b) Systems distinguishing right from left such as actual cholesterics.

present stage no helices of this kind have been found in liquid crystals, but a similar short-range order has been observed in some columnar phases.

2. If the constituent molecules differ from their mirror image, the plot of $F(q)$ is not symmetrical (Fig. 1.10(b)). The minimum cannot fall at $q = 0$ and the optimum twist q_0 is non-zero.† This corresponds to the actual situation in cholesterics.‡

1.3.4 Summary

Thus nematics and cholesterics appear to some extent as two subclasses of the same family, with the correspondence rules

† Except at ‘accidental points’ such as $T = T^*$ in our earlier discussion.

‡ In fact, the problem is somewhat more complicated: cholesterics correspond to a one-dimensional development of the natural ‘twisting’ tendency of chiral mesogens. We will discuss other possibilities in Chapter 6.

Racemic or achiral system → nematic N,
System different from its mirror image → cholesteric N*.

A perhaps more rigorous way to think of the difference between cholesterics and nematics is to use a comparison with phase transitions: when subjected to a small external magnetic field a paramagnetic phase acquires a small but non-zero macroscopic magnetization. It has the same symmetry as a ferromagnetic phase although it is locally still very close to the initial paramagnetic state we started with. If one increases the field enough, and in well chosen conditions, we know that we can drive the system continuously to a state that is truly ferromagnetic. Whether the paramagnetic phase subjected to a magnetic field should be considered as ferromagnetic or not is purely a matter of order of magnitude. Similarly, chirality acts as a field on the natural twisting tendency. The natural twist being almost always small on a molecular scale ($q_0a \sim 10^{-2}, 10^{-3}$), we are in the small-field limit (i.e. the idea of cholesterics as twisted nematics is basically correct). On the other hand, the cholesteric state is really an original state of matter, and short-pitch cholesterics have probably little to do with nematics (i.e. the equivalent of the ferromagnetic phase). In fact, as we shall see, cholesterics could well be classified with smectics.

1.4 SMECTICS

Smectic (from the Greek $\sigma\mu\eta\gamma\mu\alpha$ = soap) is the name coined by G. Friedel for certain mesophases with mechanical properties reminiscent of soaps. From a structural point of view, all smectics are *layered structures* with a well-defined interlayer spacing that can be measured by X-ray diffraction.[†] Smectics are thus more ordered than nematics. For a given material, the smectic phases usually occur at temperatures below the nematic domain.

G. Friedel recognized only one type of smectic—the type now called smectic A. However, starting with some very early work by Vorlander, it became progressively clear that there are several different types of smectic, giving rise to different macroscopic textures, readily recognized by optical observation. Over the last decade the situation has been considerably clarified: many of the phases that were identified as smectics on the basis of microscopic observations turned out to be crystals characterized by a very low-yield stress [23]. For historical reasons they are often (improperly) referred to as ‘crystalline smectics’; we will briefly discuss them in Section 1.4.5. The natural classification of smectic phases should use the set G_1^3 of groups describing three-dimensional objects that are periodic in one direction (they are often called cylindrical helical or even rod groups because they

[†] The first X-ray evidence for the layers was obtained by E. Friedel (the son of G. Friedel) [22].

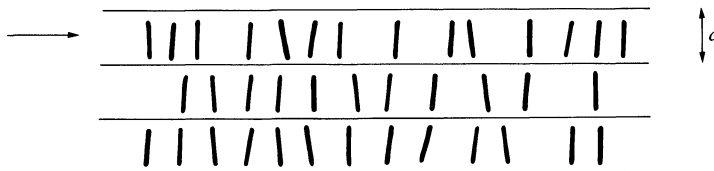


Fig. 1.11. The arrangement of molecules in a smectic A.

allow us to classify objects like rods, chain ribbons, or screws as well as smectics). There is an infinite number of such groups. However, we know a finite number of smectics only, and we will describe each case separately keeping the usual notation. The three main types of smectics are smectics A, smectics C, and hexatic smectics.

1.4.1 Smectics A

A picture of the molecular arrangement for smectic A is shown in Fig. 1.11. The major characteristics are as follows.

1. A layer structure. (The layer thickness in thermotropic materials can vary from values close to the full length of the constituent molecule to twice this value. Lyotropic smectics A can have periodicities as large as several thousand Ångströms!)
2. Inside each layer, the centres of gravity show no long-range order; each layer is a two-dimensional liquid.

Properties 1 and 2 together define a remarkable type of one-dimensional ordering, which is, in fact, quite singular and will be discussed in Section 1.6.3.

3. The system is optically uniaxial, the optical axis being the normal Oz to the plane of the layers. This is not enough by itself to identify a smectic A: large angle X-ray scattering shows complete rotational symmetry around Oz.
4. The directions z and $-z$ are equivalent: the same argument that we developed for nematics in Section 1.3.2 prevents, in principle, the existence of longitudinal ferroelectricity. On a more pragmatic basis, one can also say that in all clear-cut cases no spontaneous polarization has ever been measured.

Properties 3 and 4 lead to a symmetry D_∞ in the Schoenflies notation ($\infty.2$ in crystallographic notation). Note that it is different from the nematic $D_{\infty h}$ in that it accepts chirality. We have seen that, if we try to set up a nematic phase with a material that differs from its mirror image, it will in fact distort into a cholesteric. No similar distortion is found in smectics A. As we shall see in Chapter 7, the requirement of constant layer spacing imposes the

condition $\mathbf{n} \cdot \text{curl } \mathbf{n} = 0$ for all macroscopic deformations of smectics. The helical arrangement of eqn (1.3) has $\mathbf{n} \cdot \text{curl } \mathbf{n} = -q_0 \neq 0$ and is thus forbidden. Many cholesterol esters are in fact smectic A below their cholesteric domain.

Strictly speaking, smectic A made of chiral molecules should be labelled S_A^* , and considered as a phase different from the standard smectic A, with $D_{\infty h}$ symmetry. Indeed, the macroscopic properties of S_A and S_A^* are not equivalent: in S_A^* rotatory power and electroclinic effects[†] exist but not in S_A .

At last it is useful to remark that cholesterics, as described by eqn (1.3), obey the general definition of a smectic: they exhibit a periodic structure in the z direction, are liquid-like perpendicularly to it, macroscopically uniaxial, and respect the $z, -z$ symmetry.

These features are those of an S_A^* . However, the existence of a constant twist shows that the important symmetry element is a screw axis: cholesterics and smectics A^* differ by their space group ($S_M2/2$ for the former $t\infty/2$ for the latter in international notation). In any case the long-wavelength properties of the two phases are very similar.

1.4.2 Smectics C

The structure of a smectic C is defined as follows.

1. Each layer is still a two-dimensional liquid.
2. The X-ray pattern on aligned samples shows an anisotropic diffuse ring tilted with respect to the $00l$ reflection row. Or, if the molecular direction is specified by a magnetic field, the $00l$ row makes an angle with this direction. This proves in turn that the molecules are tilted with respect to the normal z of the layers (Fig. 1.12).

As a consequence of point 2 the material is optically (electrically, magnetically, etc.) biaxial. If the molecules are tilted in the x, z -plane, the principal axes of the dielectric or magnetic tensors are: two orthogonal directions in the x, z plane (which need not be identical in the electric and magnetic cases), plus the y direction.

This corresponds to the monoclinic symmetry C_{2h} . Note that the existence of biaxial smectics with symmetry D_{2h} is quite possible (i.e. orientational order of the type depicted in Fig. 1.6): we believe that with the synthesis of molecules bearing properties intermediate between rods and disks biaxial smectics will soon be discovered.[‡]

[†] Electroclinic effects demonstrated by Meyer and Garov [24] will be discussed in Chapter 7.

[‡] The racemic version of the antiferroelectric phase discovered by Galerne and Liebert [25] probably exhibits this point-group symmetry, although with a more complex local arrangement.

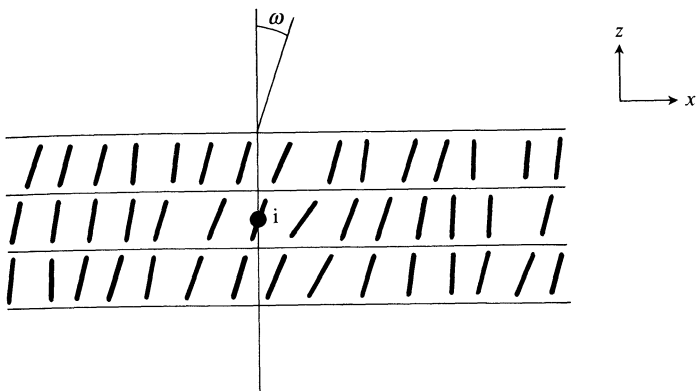


Fig. 1.12. The tilted arrangement of molecules in a smectic C (tilt angle ω ; i, inversion point).

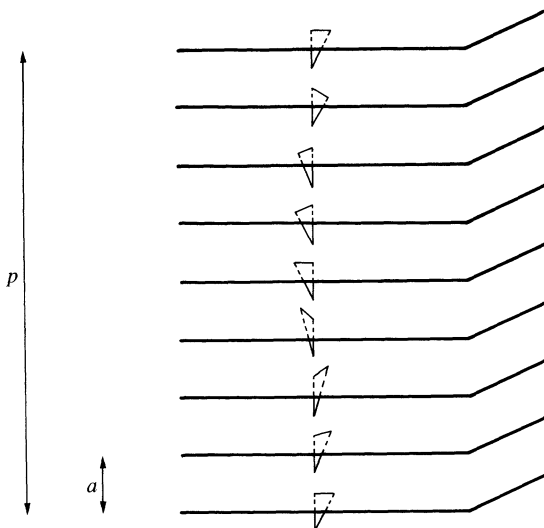


Fig. 1.13. Twist induced in a smectic C by the presence of a chiral agent. The pitch p is much larger than the interlayer distance a (typically $p/a \sim 10^3$). Note that p need not be an exact multiple of a .

3. The simple smectic C structure described in points 1 and 2 is obtained only when the constituent molecules are optically inactive (or with a racemic mixture). If we add optically active molecules to a smectic C, the structure distorts; the direction of tilt precesses around the z-axis and a helical configuration C* is obtained (Fig. 1.13; [26]).

At this point, it is worth re-examining the elements of the monoclinic symmetry:

- the plane of symmetry (z, x) of Fig. 1.12;
- a twofold axis C_2 perpendicular to it;
- an inversion point i .

Introducing chirality suppresses the plane and the inversion centre. Thus, if a polarization appears along the C_2 axis, no symmetry operation can cancel it. Hence it will exist in general. Thus, according to the beautiful remark made first by R. B. Meyer [27], chiral smectic C*'s are ferroelectric.[†]

We have illustrated in Fig. 1.14 how chirality can generate polarization [28].

1.4.3 ‘Hexatic’ smectics

1. Each layer is again a two-dimensional liquid, but of a very special sort. Locally, the molecules are distributed on a triangular lattice; however, the number of defects is such that the positional order does not propagate over distances larger than a few 100 Å, but the bond order extends over macroscopic distances. The azimuthally symmetrical diffuse X-ray ring of smectics A is replaced by a sixfold modulated diffuse pattern (Fig. 1.15(b)) [29]. The smectic A diffuse ring is shown in Fig. 1.15(a) for comparison. The phase is thus characterized by a D_{6h} point group symmetry.
2. The material is optically (electrically, etc.) uniaxial like a smectic A. One might think that such a phase should be obtained with molecules having themselves the D_{6h} point-group symmetry. This is not necessary. It results from the loss of the in-plane positional order, keeping that of the bond ordering. This phase, called ‘hexatic smectic B’ for historical reasons, was predicted [30, 31] before being observed [29].

It seems natural that, if one can identify phases with in-plane short-range positional but long-range bond order when molecules are perpendicular to the layers, that should also be true when molecules are tilted. This is indeed the case. The smectic F phase is such an example [see Part 1, Sections 4.1 and 4.2, and Part 2, Chapter 7 in reference 23] (Fig. 1.16(a)): in a given layer the molecules are distributed on a nearly triangular lattice; this order extends over a few hundred Å as in the uniaxial hexatic case, but the bond ordering exhibits long-range order. X-ray patterns of monodomain samples obtained by melting single crystals show sixfold (or nearly sixfold) symmetry in the diffuse outer ring (incoming X-ray beam parallel to the molecular direction).

[†] Because of the helical precession of the tilt angle, thus of the polarization, a more rigorous denomination is helielectric.

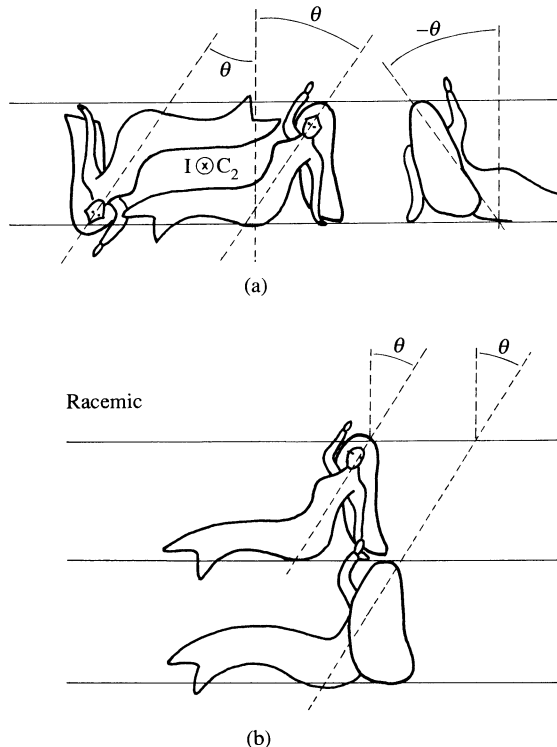


Fig. 1.14. Illustration of the polar symmetry of a smectic C*. (a) Consider a set of sirens gaining chirality by waving their right hand and leaning on their left hand. The C_2 symmetry allows an equal number of sirens upward and downward, but they all look at the reader (e.g. polarity); (note that the siren who shows her back does not belong to the same monodomain since her tilt angle is $-\theta$). (b) The racemic mixture has no polarity (equal number of sirens facing us or showing their backs).

A more refined analysis shows that the tilt points toward the side of the hexagons, which as a result are slightly distorted: this leads to a local rectangular lattice. The point group symmetry is thus $2/m$ (C_{2h}), and the space group $t\ 2/m$ is identical to that of smectic C: hence, although their local order is quite different, there is no reason to consider S_C and S_F as different phases. One can well imagine going continuously from one to the other without phase transition at all. Usually, however, S_C - S_F transitions are first order (a similarity with the liquid-vapour system).

When, instead of pointing toward the side of the hexagons, the tilt points toward the vertices (Fig. 1.16(b)), a new phase is obtained, the S_I .† The nearly sixfold outer ring is in some cases quite comparable to that of the hexatic,

† Intermediate tilt directions are known in the lecithin-water system [32].

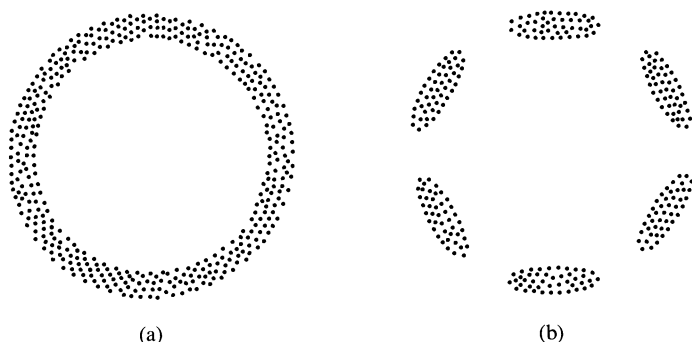


Fig. 1.15. Typical X-ray pattern (incident beam perpendicular to the smectic layers) probing in plane order: (a) diffuse ring revealing the two-dimensional isotropic liquid-like character of a smectic A; (b) six-fold modulation of the diffuse ring characteristic of the hexagonal long-range bond order of a hexatic smectic B.

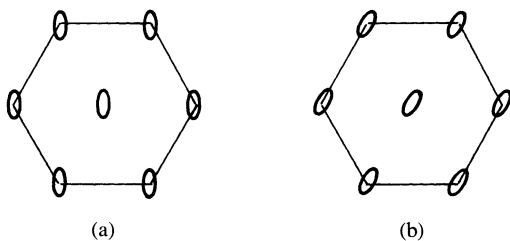


Fig. 1.16. Short-range in-plane structure (the ellipsoids represent the tilt direction): (a) smectic F; (b) smectic I.

in some others sharper. In this latter case the picture of a stack of uncorrelated two-dimensional crystals seems to fit the experimental data better [33]. If such phases exist, they are not included in our classification scheme. The natural framework would be the set of space groups of three-dimensional objects ordered in two directions.

A final remark: smectics with D_{4h} could, in principle, also exist but have not been found yet.

1.4.4 ‘Crystalline’ smectics

The liquid crystal community has considered for years phases called S_B , S_E , S_G , S_H , S_J , S_K . They all are genuine crystals that exhibit long-range positional order [see Part 1, Sections 4.3 and 4.4 and Part 2, Chapter 6 in reference 23]; the confusion came from the fact that they are three-dimensional stacks of layers weakly attached to each other. Very weak forces are able to impose

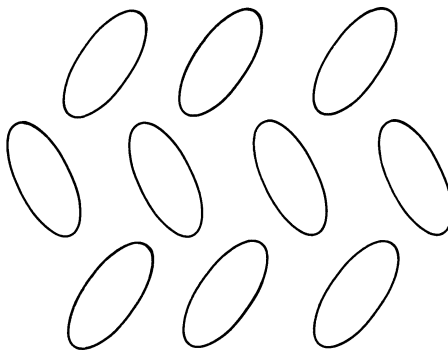


Fig. 1.17. ‘Chevron’ order (ellipsoids again represent the tilt direction).

plastic deformations that give them some resemblance to true smectics under usual experimental conditions. In fact S_B are much closer to graphite than to any of the liquid crystalline phases: they are characterized by an interplane shear elastic constant C_{44} that is unusually small. The difference between S_E and S_B results from the existence of a long-range chevron order in the former (Fig. 1.17). A clear description of these systems is given in references 2 and 23. Before being identified by careful crystallographic work, the originality of these phases had been spotted using the miscibility criterion [34]. Miscibility is a very convenient technique for guiding research into new phases. It is thus interesting to recall the type of information that one can expect from it.

When two materials X and Y give the same texture and are miscible in all proportions maintaining this texture, they are classified in the same group. When they do not mix continuously, no conclusion can be drawn, in principle. However, if a subgroup Y_1, Y_2, \dots, Y_p of materials is found, all of them showing the B texture, all of them intermiscible, but none of them miscible with standard B compounds, it is tempting to give them a new label Z. But the distinction that is defined in this way may reflect a difference in molecular size (or shape) between the Z group and the B group that is enough to prohibit miscibility rather than a fundamental difference in symmetry between the B and Z phases with the same texture. In fact, these size or shape effects are expected to be particularly important in the strongly ordered phases, just as they are in ordinary solids (this point has been stressed in particular by Schott†). Thus, this criterion allows us to reduce the number of investigations to only cases when miscibility is not observed (which is a great help).

† Verbal remark at the meeting on the physics of liquid crystals, Pont-à-Mousson (1971).

1.4.5 The D phase

The D phase is not smectic: it has an overall cubic symmetry. Some X-ray data have been obtained for polydomain samples [35]. One possible model for the D phase is the following. Start by bending the layers of a planar smectic obtaining, for example, concentric cylinders or concentric spheres. Using the resulting rods or balls as building blocks, set up a cubic packing. Arrangements of this sort have indeed been observed in the cubic phases of soap–water systems [10]. The D phase might be their counterpart in thermotropic systems [36].

1.5 COLUMNAR PHASES

It is surprising how theory has been ahead of experiment in the case of two-dimensionally ordered systems. Their stability was stressed in the 1930s [37] and a complete classification scheme developed according to group theory in 1929 [38]. Indeed, the correct framework for a classification of columnar phases is provided by the set G_2^3 of the symmetry group of three-dimensional doubly periodic objects. It contains 80 elements†; a little more than 10 of them have been identified up to now. The term ‘columnar phases’ seems most used now, although other appellations, such as ‘canonic’ (from the Greek *Kavov* = rod) and ‘calamitic’ (from the Latin *calamus* = reed), have also been proposed. The often used term ‘discotic’ is not quite proper, since it refers to building blocks (more properly labelled discoid) that are not a necessary prerequisite for obtaining this two-dimensional order.

1.5.1 Hexagonal phases

In solutions of large rod-like polymers [8], for certain soap phases [10], as well as with discoid molecules, we find a set of X-ray reflections that can be indexed in terms of a hexagonal packing of columns (or more exactly triangular). No long-range order can be observed along the columns (Fig. 1.18).

The relevant space group is P_{6mm} (equivalently $P_{\bar{m}\bar{m}m}^{622}$) (point group D_{6h}). Such phases are optically, electrically, and magnetically uniaxial. They cannot sustain a spontaneous electric polarization. The liquid crystal community prefers the level D_h (the D refers to the (often) discoid shape of the building blocks, and h stands for hexagonal). In the nomenclature

† An easy way to obtain these elements is to single out the three-dimensional space groups compatible with the absence of periodicity in one direction (A. L. Levelut, personal communication).

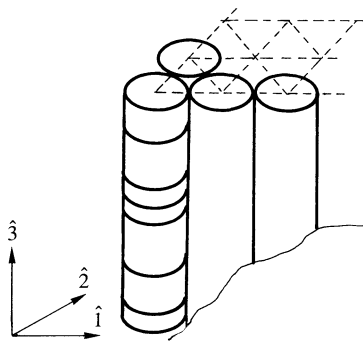


Fig. 1.18. Typical example of a columnar phase. Note the randomness of the intermolecular distance along the columnar axis.

commonly used a second subscript appears: one can see D_{ho} or D_{hd} . This second index refers to the range of position correlations along the columnar axis; o stands for ordered; d for disordered. In the second case, each column is a one-dimensional liquid with positional correlations limited to a short correlation length (\sim a few molecules). The difference between D_{ho} and D_{hd} is not sharp: all one-dimensional systems have a finite correlation length (see the problem at the end of the chapter).

1.5.2 Rectangular and oblique phases

The potentially rich polymorphism of columnar phases has led to the discovery of about half a dozen new phases made up of discoid molecules [39]. A feature common to all of them is a genuine liquid-like order along the columns: the extent of the positional correlations is over a few molecules only. Thus they are labelled D_{rd} and $D_{ob,d}$ (r, ob, d stand respectively for rectangular, oblique, and disordered). Rectangular means that the two-dimensional unit cell is a rectangle; oblique reflects the existence of an average tilt of the molecules with respect to a plane perpendicular to the column axis. Often a tilt of the molecules within a given column exists even in the rectangular phases. Other phases have a low enough symmetry to be polar but no polarization measurements have yet been reported.

1.5.3 ‘Antiphases’

Among two-dimensionally ordered systems the antiphases[†] play a special role. They are made of elongated molecules that possess a strong polar head

[†] The name ‘antiphase’ has been coined by A. M. Levelut in analogy with binary alloys, in which the position of atoms A and B plays a role similar to that of the polar heads in liquid crystals.

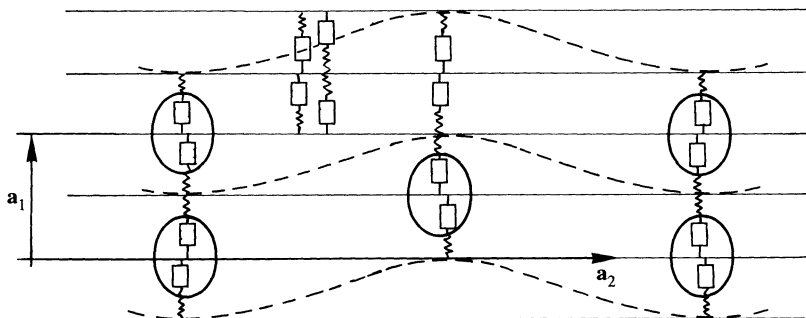


Fig. 1.19. Structure of an $S_{\bar{A}}$ antiphase (the polar head of the molecules is represented by a segment, the aliphatic chain by a wavy line, and the rigid core by a rectangle). Note that the location of the polar heads defines a two-dimensional lattice, even though the short-range order is smectic-like.

on one end, and a wavy aliphatic chain on the other. The local structure is that of a bilayer smectic but, as is shown in Fig. 1.19, the polar heads of the molecules jump periodically from one layer to the next perpendicularly to the \hat{z} direction [40] (i.e. \hat{x}) (for $S_{\bar{A}}$). There is thus a two-dimensional array, whereas the \hat{y} -direction stays liquid-like: this is the very definition of a columnar mesophase. We may wonder if there is any interest in classifying systems that are locally very similar to smectics (and made of rod-like polar molecules) together with others made of disk-like molecules. We believe that there is indeed some interest. We will show in the following chapters that the long-wavelength, low-frequency behaviour is the same for all these systems. Even the defect structure will be shown to depend on the symmetry of the phases.

The $S_{\bar{C}}$ antiphase differs from the $S_{\bar{A}}$ in that the lattice built by the polar head is tilted with respect to that of the smectic layers. As a result the optical axis is tilted with respect to both: $S_{\bar{C}}$ are biaxial phases of point-group symmetry C_{2h} . Thus, according to the argument developed in Section 1.4.2, $S_{\bar{C}}$, made of chiral molecules, ought to be polar. Furthermore, since the polarization is parallel to the liquid-like direction \hat{y} , the twisting tendency of the system cannot develop. Although such systems are known, no polarization has yet been measured.

1.6 MORE ON LONG-, QUASILONG-, AND SHORT-RANGE ORDER

In the preceding sections we have taken the existence of one-, two-, and three-dimensional orders for granted. Of course we all know of the existence of crystals in three dimensions; well known also is the absence of any

crystalline order in one dimension because of the importance of thermal fluctuations. What about liquid crystals? In the following subsections we give the simplest considerations that yield the essential results [37].

1.6.1 ‘Poor man’s’ elasticity of liquid crystals

Small deformations of crystals and liquid crystals (with the exception of nematics which will be considered separately) can be described by the displacement field \mathbf{u} of the lattice that represents their ground state. The vector \mathbf{u} is (Fig. 1.20):

- three-dimensional for crystals in three dimensions (respectively two- and one-dimensional in two and one dimensions);
- two-dimensional for columnar phases (in three dimensions);
- one-dimensional for smectics (in three and two dimensions).†

In what follows, the number of components does not matter and will not be specified. Thus we will just keep a scalar variable u . A more accurate discussion of the elastic theories is postponed to Chapter 7. We need first to remark that a uniform translation will produce a uniform u . Of course, this does not change the energy of the system: only the gradients of u can enter the free energy. Furthermore, stability requires that the lowest terms in the expression be quadratic: this is nothing but Hooke’s law.

The next point is that first-order derivatives involving the ‘liquid’ direction (parallel to the smectic planes or to the direction of the columns; Fig. 1.21) correspond to a mere rotation of the system. Hence, only second-order derivatives, corresponding to a curvature of the planes of the columns, can enter the free energy. Thus the poor man’s elastic energy of crystals (cr), columnar (co), and smectic (s) phases reads

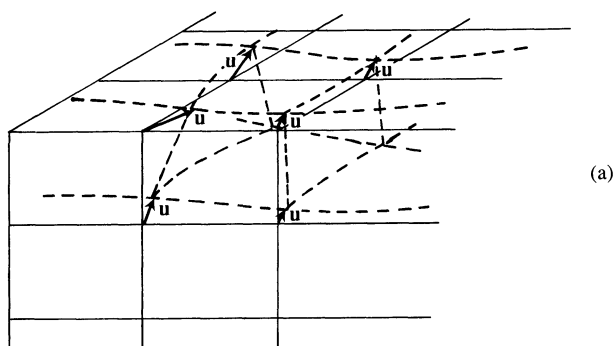
$$F_{\text{cr}} = \frac{C}{2} \int d^3x (\nabla \mathbf{u})^2, \quad (1.4a)$$

$$F_{\text{co}} = \frac{C}{2} \int d^3x [(\nabla_{\perp} \mathbf{u})^2 + \lambda^2 (\nabla_z^2 u)^2], \quad (1.4b)$$

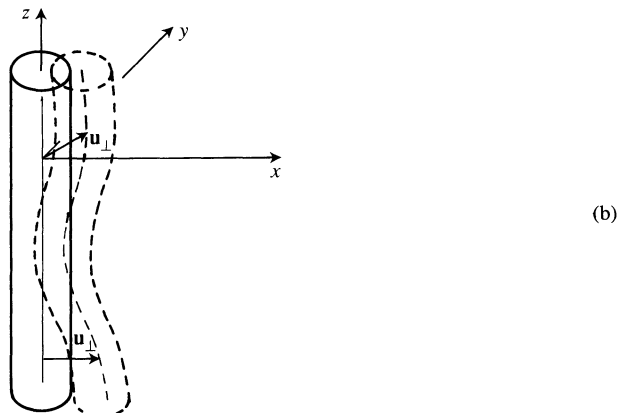
$$F_s = \frac{C}{2} \int d^2x [(\nabla_z u)^2 + \lambda^2 (\nabla_{\perp}^2 u)^2], \quad (1.4c)$$

where C is an elastic modulus characterizing the material. In Fourier space

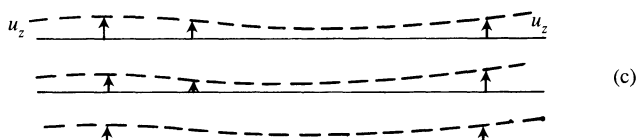
† Note that the convention of referring to smectic for one-dimensional order in two dimensions is not consistent with the convention for crystals: columnar phase in two dimensions would be more coherent, but the convention does not change the physics and corresponds to the accepted terminology.



(a)



(b)



(c)

Fig. 1.20. Displacement variables: (a) three-dimensional vector for a crystal (in a three dimensional space); (b) two-dimensional vector for a columnar phase; (c) one-dimensional vector for a smectic.

(for a unit volume),

$$F_{\text{cr}} = \frac{C}{2} \int \frac{d^3q}{(2\pi)^3} q^2 |u(q)|^2, \quad (1.5a)$$

$$F_{\text{co}} = \frac{C}{2} \int \frac{d^3q}{(2\pi)^3} (q_{\perp}^2 + \lambda^2 q_z^4) |u(q)|^2, \quad (1.5b)$$

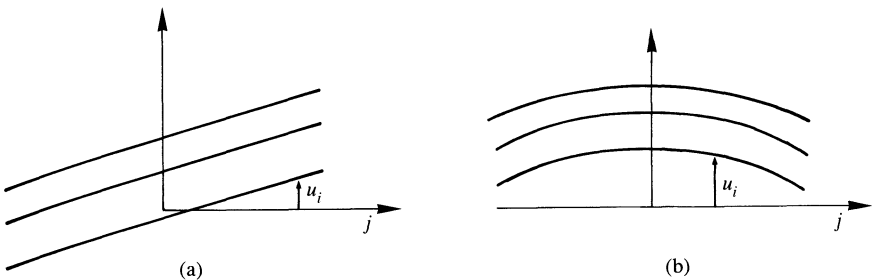


Fig. 1.21. (a) A rotation $\partial u_i / \partial x_j$ does not cost energy. (b) A curvature $\partial^2 u_i / \partial x_j^2$ costs energy. ($i = x$ or y , $j = z$ for columnar phases; $i = z$, $j = x$ or y for smectics.)

$$F_s = \frac{C}{2} \int \frac{d^3 q}{(2\pi)^3} (q_z^2 + \lambda^2 q_{\perp}^4) |u(q)|^2. \quad (1.5.c)$$

λ is the ‘penetration’ length and provides the scale over which curvature can compare to compression. C is an elastic modulus characterizing the material.

1.6.2 Fluctuations

The theorem of equipartition of energy yields

$$\begin{aligned} \langle |u(q)|^2 \rangle &= k_B T / C q^2 && \text{crystals,} \\ \langle |u(q)|^2 \rangle &= k_B T / C (q_{\perp}^2 + \lambda^2 q_z^4) && \text{columnar phases,} \\ \langle |u(q)|^2 \rangle &= k_B T / C (q_z^2 + \lambda^2 q_{\perp}^4) && \text{smectics} \end{aligned} \quad (1.6)$$

where k_B is Boltzmann’s constant. Thus

$$\begin{aligned} \langle u^2(r) \rangle &= \frac{k_B T}{(2\pi)^3 C} \int_{L^{-1}}^{q_c} \frac{d^3 q}{q^2} \simeq k_B T q_c / 2\pi^2 C && \text{crystals} \\ \langle u^2(r) \rangle &= \frac{k_B T}{(2\pi)^3 C} \int_{L^{-1}}^{q_c} \frac{d^3 q}{q_{\perp}^2 + \lambda^2 q_z^4} \simeq k_B T (q_c \lambda^{-1})^{1/2} / 2\pi^2 C && \text{columnar phases} \\ \langle u^2(r) \rangle &= \frac{k_B T}{(2\pi)^3 C} \int_{L^{-1}}^{q_c} \frac{d^3 q}{q_z^2 + \lambda^2 q_{\perp}^4} \simeq k_B T \log(q_c L) / 4\pi \lambda C && \text{smectics} \end{aligned} \quad (1.7)$$

where q_c is a cut-off wavevector beyond which the elastic theory breaks down and L is the linear size of the sample. In the first two cases the mean square displacement stays finite when L goes to infinity: it is controlled by short-range forces. In the third case, the mean square fluctuations diverge logarithmically with L : this conceptually important result is known as the Landau–Peierls instability [37]. Orders of magnitude are interesting to estimate.

With $k_B T = 4 \cdot 10^{-14}$ erg, $\lambda \simeq 30 \text{ \AA}$, $C \simeq 10^{10}$ for crystals (10^8 for columnar and smectic phases) erg cm $^{-3}$, $q_c \simeq 10^8$ for crystals ($2 \cdot 10^7$ for columnar and smectic phases) cm $^{-1}$ and $L = 1$ cm, we obtain

Crystals	$\sqrt{\langle u^2 \rangle} \simeq 0.4 \text{ \AA}$,
Columnar phases	$\sqrt{\langle u^2 \rangle} \simeq 1.5 \text{ \AA}$,
Smectics	$\sqrt{\langle u^2 \rangle} \simeq 4 \text{ \AA}$.

In all three cases the root mean square of the displacement variable is of the order of a tenth of the basic periodicity (a few tenths in the case of smectics). It is indeed larger in this case but, for $\sqrt{\langle u^2 \rangle}$ to be of the order of the lattice spacing, samples of linear size $L \simeq$ a few hundred metres would have to be prepared! This logarithmic divergence, known also for two-dimensional crystals, is said to correspond to quasilong-range order.

The case of nematics is similar to that of crystals if one replaces the layer displacement by the rotation angle θ, ψ of the director \mathbf{n} with respect to its ground-state direction. Indeed gradients of θ in any direction change the free energy (Fig. 1.10) and, forgetting about anisotropy in the elastic constants, we can write the elastic energy of nematics as

$$F_N = K \int d^3x (\nabla \theta)^2 \quad (1.8)$$

and

$$\langle \theta^2 \rangle = k_B T q_c / 2\pi^2 K. \quad (1.9)$$

where K is a Frank modulus to be defined in more detail in Chapter 3. Anticipating $K \simeq 10^{-6}$ dyn, and with $q_c \simeq 2 \cdot 10^7$ cm $^{-1}$, we get $\sqrt{\langle \theta^2 \rangle} \simeq 0.2$ rad, which is quite sizeable, but finite and independent of the sample size. Nematics exhibit genuine long-range orientational order.

Before closing this chapter, it is worth giving the implications of the foregoing concerning the density-density correlation function, and to return to the definition of liquid crystals.

1.6.3 Long-range, quasilong-range, short-range order

Saying that a system is periodic in a direction \mathbf{q}_0 , implies that a development of the density ρ in a Fourier series is possible

$$\rho = \bar{\rho}_0 + \rho_1 \cos(\mathbf{q}_0 \cdot \mathbf{r}_0) + \dots \quad (1.10)$$

If one includes the layer displacement \mathbf{u} , (1.10) becomes

$$\rho(\mathbf{r}) = \bar{\rho}_0 + \rho_1 \cos(\mathbf{q}_0 \cdot (\mathbf{r} + \mathbf{u})) + \dots \quad (1.11)$$

If \mathbf{u} is allowed to fluctuate, \mathbf{u} has to be considered as a function of \mathbf{r} . Then

$$\langle \rho(\mathbf{r})\rho(\mathbf{r}') \rangle - \langle \rho^2 \rangle \propto \cos(\mathbf{q} \cdot (\mathbf{r} - \mathbf{r}')) \langle \exp(i\mathbf{q}_0 \cdot (\mathbf{u}(\mathbf{r}) - \mathbf{u}(\mathbf{r}'))) \rangle \quad (1.12)$$

$$\langle \rho(\mathbf{r})\rho(\mathbf{r}') \rangle - \langle \rho^2 \rangle \propto \cos(\mathbf{q} \cdot (\mathbf{r} - \mathbf{r}')) \exp(-\frac{1}{2}q_0^2 \langle (\mathbf{u}(\mathbf{r}) - \mathbf{u}(\mathbf{r}'))^2 \rangle) \quad (1.13)$$

with

$$\langle (\mathbf{u}(\mathbf{r}) - \mathbf{u}(\mathbf{r}'))^2 \rangle = 2 \int \frac{d^3 q}{(2\pi)^3} (1 - \cos \mathbf{q} \cdot (\mathbf{r} - \mathbf{r}')) \langle |\mathbf{u}(\mathbf{q})|^2 \rangle. \quad (1.14)$$

$\langle |\mathbf{u}(\mathbf{q})|^2 \rangle$ is given by (1.6). As a result:

- In a crystal, eqn (1.14) is governed by the large wavevector cut-off (i.e. short length scale). X-rays exhibit Bragg peaks attenuated by a Debye–Waller factor.
- In a columnar phase eqn (1.14) is also governed by large wavevector cut-offs, and X-rays are also characterized by Bragg peaks attenuated by a slightly different Debye–Waller factor. The wings differ from those of a crystal: the $1/q^2$ dependence is replaced by $1/(q_{\perp}^2 + \lambda^2 q_z^4)$.
- Smectics are fundamentally different because of the logarithmic divergence in eqn (1.7)

$$\begin{aligned} \langle (\mathbf{u}(\mathbf{r}) - \mathbf{u}(\mathbf{r}'))^2 \rangle &= \frac{k_B T}{2\pi\lambda C} \log(q_c \sqrt{(\lambda|z - z'|)}), & \mathbf{x} - \mathbf{x}' = 0, \\ \langle (\mathbf{u}(\mathbf{r}) - \mathbf{u}(\mathbf{r}'))^2 \rangle &= \frac{k_B T}{2\pi\lambda C} \log(q'_c |X_{\perp} - X'_{\perp}|), & z - z' = 0, \end{aligned} \quad (1.15)$$

Hence,

$$\begin{aligned} \langle \rho(\mathbf{r})\rho(\mathbf{r}') \rangle - \langle \rho^2 \rangle &= \cos(q_0(z - z'))/q_c^{2\eta}\lambda^{\eta}|z - z'|^{\eta}, & \mathbf{x}_{\perp} - \mathbf{x}'_{\perp} = 0, \\ \langle \rho(\mathbf{r})\rho(\mathbf{r}') \rangle - \langle \rho^2 \rangle &= \cos(q_0(z - z'))/q_c^{2\eta}|X_{\perp} - X'_{\perp}|^{2\eta}, & z - z' = 0 \end{aligned} \quad (1.16)$$

where

$$\eta = \frac{q_0^2 k_B T}{8\pi\lambda C} \quad (1.17)$$

For large enough separation the correlation function tends toward the square of the average density: fluctuations wash out the density modulation on a large scale. This result is similar to that obtained in two-dimensional crystals. One might be tempted to say that, after all, smectics are liquids, but the fact that the modulation decreases with a power law denotes a profound difference. In a liquid any density modulation is washed out over a well defined length scale; in a smectic (in three dimensions) there is no such length scale. No strict Bragg reflection can be seen with X-rays: the observed peaks are power law divergences ($q_z^{-2+\eta}$ and $q_{\perp}^{-4+2\eta}$) [41]. These features have been carefully checked at MIT [42]. Including non-linear terms in the elastic free energy does not fundamentally alter these results [43].

We are now in a position to sharpen the definition we have given of crystals, columnar phases, smectics, and nematics (in three dimensions):

- Crystals exhibit genuine three-dimensional long-range order, as defined in eqn (1.1).
- Columnar phases exhibit genuine two-dimensional long-range order as defined in eqn (1.1).
- Smectics exhibit one-dimensional quasilong-range order as defined in eqn (1.16).
- Nematics are characterized by anisotropic positional short-range order (as defined in eqn (1.2)) and orientational, genuine, long-range order.

The simplicity of these definitions hides a rich variety of systems. Phases belonging to the same group may correspond to very different microscopic physics; although useful in many cases, symmetry considerations do not answer all questions.

1.7 REMARKABLE FEATURES OF LIQUID CRYSTALS

Liquid crystals have unusual optical properties. Nematics and smectics A are uniaxial. Cholesterics (because of their periodic structure) give rise to Bragg reflections at optical wavelengths. In nematics and cholesterics, these properties are carried by a fluid, flexible substrate; thus they are extremely sensitive to *weak external perturbations*.

The pitch of a cholesteric and hence the wavelength of the Bragg-reflected light depends on the temperature T . Thus the colour of the material can change drastically over a temperature interval of a few degrees. This leads to a number of applications: detection of hot points in microcircuits; localization of fractures and tumours in humans; conversion of infrared images; etc.

The pitch is also sensitive to other agents such as pressure, chemical contaminants, etc. For instance, a method of display for ultraviolet images based on a photochemical reaction and the resulting change in pitch has been worked out.

Both nematics and cholesterics are *very sensitive to external fields*; the first magnetic-field effects were shown long ago by the Russian groups of Frederiks and Tsvetkov [44]. But a variety of new magnetic phenomena have been discovered since. Electric-field effects are more complex (because their action is influenced by impurity carriers and electrochemical phenomena), but very spectacular and important for applications in particular for *display systems*. Liquid-crystal films are inexpensive and work under low voltage and low power; they can also often operate in the presence of sunlight (because they modulate the *reflected* light including the sunlight itself and

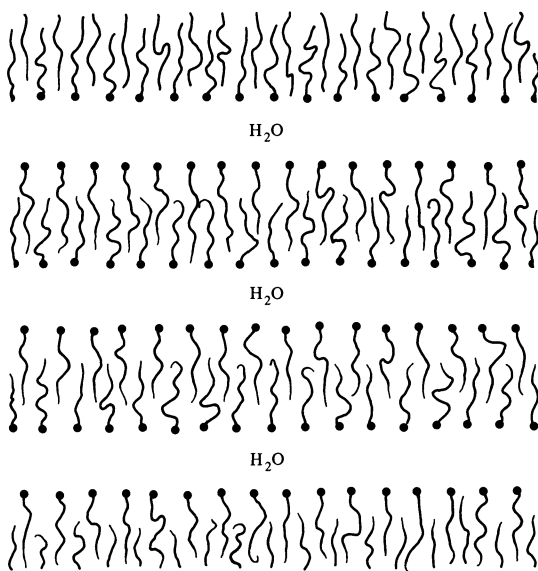


Fig. 1.22

thus maintain a good contrast). A few references on liquid-crystal display devices are listed [45, 46]. Every one knows the success of the *twisted-nematic* display in the watch and pocket calculator industry, and, more generally, in optoelectronics.

For all these reasons, interest in nematics and cholesterics was quite active in the 1970s. The action has progressively shifted to *smectics*. The motivations are both academic and applied. Among them let us mention the following.

1. *Physics of detergents.* As already mentioned, soaps and non-ionic detergents show a number of remarkable mesophases. The so-called ‘neat’ soaps, for example, correspond to a lamellar phase with successive sheets of water and lipid (Fig. 1.22).
2. *Membrane biophysics.* Biological membranes are thin (80 \AA) sheets made of lipids and proteins. They play a crucial role in many living processes, but little is known about their structure. Most physical techniques (e.g. NMR) cannot be used on a single membrane, because the amount of matter available is too small. But it is possible to set up model systems with lipids and water (or even with lipid + protein + water [47] that have a lamellar structure: it is hoped that each individual sheet will have some analogy with a membrane. With a bulk phase of this sort, one can use sample volumes large enough to allow for accurate physical studies.[†]

[†] In a similar way, the hexagonal phases of certain rod-like molecules (e.g. nucleic acids) may be useful for carrying out experiments on oriented molecules, while still retaining enough water to preserve biological functions.

3. *Unusual elastic and hydrodynamic properties of smectics.* These systems, being more rigid than nematics, are less easy to perturb. However, their time constants are much shorter than those of nematics: thermal excitation of S_{As} and primary electric excitation in S_{SC}^* provide very promising types of displays, which possess intrinsic memory and speed. A selective control of smectic textures (for instance S_{SC}^* domains), provides new types of memories addressable and readable optically and also displays compatible with video rates [46]. Furthermore, from a fundamental viewpoint the hydrodynamics of smectics is extremely original and illustrates the role of fluctuations in one-dimensionally ordered systems.

The research effort on *columnar phases* is still somewhat limited, but increasing steadily. Many structures are now well understood. Considering the rich variety of possible phases, interesting applications will probably exist. For instance, some of the phases are ferroelectric; hexastable devices could also be imagined. The hydrodynamics is strongly anisotropic and is basically as original as that of smectics.

In spite of their high viscosity, *mesogenic polymers* draw considerable attention nowadays. They provide examples of liquid crystal glasses that can be used as anisotropic hosts in many fields of applications, among them, non-linear optics. S_C^* polymers give flexible sheets, which have basically the same electro-optical properties as monomeric S_C^* . Copolymerization allows the inclusion in the matrix of molecules that would be insoluble otherwise. Another strong incentive for this research is the fact that certain high-modulus polymer fibres are aligned through a nematic phase during extrusion. The synergy between polymer and liquid crystals properties is also present in the new system formed by nematic droplets hosted in a polymer matrix [46].

In the following chapters, we will focus on fundamental questions in statistical mechanics and hydrodynamics, raised by the very existence of mesophases.

Problem. Show the absence of conventional long-range order along the z -axis of columnar phases (direction of the columns).

Solution. Assume first that such an order is possible. For simplicity we consider a uniaxial columnar phase. The location of a given molecule may be determined as in a solid by the vector displacement of components u_x, u_y, u_z . The free energy of a crystal of uniaxial symmetry reads

$$\begin{aligned} F_C = \frac{1}{2} \int d^3x &\{ C_1 (\nabla_z u_z)^2 + C_2 (\nabla_x u_x + \nabla_y u_y)^2 \\ &+ C_3 [(\nabla_x u_x - \nabla_y u_y)^2 + (\nabla_x u_y + \nabla_y u_x)^2] + C_4 \nabla_z u_z (\nabla_x u_x + \nabla_y u_y) \\ &+ \frac{C_5}{4} [(\nabla_x u_z + \nabla_z u_x)^2 + (\nabla_y u_z + \nabla_z u_y)^2] \}. \end{aligned}$$

The fact that the columns can glide freely over each other implies the absence of resistance to shears in the x , z - and y , z -planes. Thus $C_5 = 0$ for a columnar phase. According to our remark in Section 1.6.1, the bending of the columns costs energy

$$F_{\text{bending}} = \frac{K}{2} \int d^3x [(\nabla_z^2 u_x)^2 + (\nabla_z^2 u_y)^2]$$

or, in Fourier space for the total elastic free energy,

$$\begin{aligned} F = \frac{1}{2} \int \frac{d^3q}{(2\pi)^3} & \{ C_1 q_z^2 |u_z(q)|^2 + C_2 |\mathbf{q}_\perp \cdot \mathbf{u}_\perp(q)|^2 + C_3 q_\perp^2 |\mathbf{u}(q)|^2 \\ & + C_4 |q_z u_z(\mathbf{q}_\perp \cdot \mathbf{u}_\perp)| + K q_z^4 |\mathbf{u}_\perp(q)|^2 \} \end{aligned}$$

where

$$\mathbf{u}_\perp = \{u_x, u_y\}; \quad \mathbf{q}_\perp = \{q_x, q_y\}.$$

With U_q , U_θ taken as the polar coordinates of \mathbf{U}_\perp with respect to the radius vector \mathbf{q}_\perp ,

$$\begin{aligned} F = \frac{1}{2} \int \frac{d^3q}{(2\pi)^3} & \{ C_1 q_z^2 |u_z(q)|^2 + (C_3 q_\perp^2 + K q_z^4) |u_\theta(q)|^2 \\ & + ((C_2 + C_3) q_\perp^2 + K q_z^4) |U_q(q)|^2 + C_4 q_z q_\perp |u_z(q) u_q(q)| \}. \end{aligned}$$

With the further variable change

$$u_q(q) = u'(q) - \frac{C_4 q_z q_\perp u_z(q)}{2((C_2 + C_3) q_\perp^2 + K q_z^4)}$$

we get

$$\begin{aligned} F = \frac{1}{2} \int \frac{d^3q}{(2\pi)^3} & \{ C_1^{\text{eff}} q_z^2 |u_z(q)|^2 + (C_3 q_\perp^2 + K q_z^4) |u_\theta(q)|^2 \\ & + ((C_2 + C_3) q_\perp^2 + K q_z^4) |u'(q)|^2 \} \end{aligned}$$

where

$$C_1^{\text{eff}} = C_1 - \frac{C_4^2 q_z^2 q_\perp^2}{4((C_2 + C_3) q_\perp^2 + K q_z^4)^2}.$$

The expression is diagonal in u_z , u_θ , and u' , which means that the fluctuations of these quantities are independent. Note that the structure of the $|u_\theta|^2$ and $|u'|^2$ coefficients respects the general form of eqn (1.4b). All we said about these types of variables in Sections 1.6.2 and 1.6.3 holds here. Let us now consider u_z .

$$\langle |u_z^2(q)| \rangle = \frac{k_B T}{C_1^{\text{eff}} q_z^2}$$

so that

$$\langle u_z^2(r) \rangle = \frac{k_B T}{(2\pi)^3} \int_{L^{-1}}^{q_c} \frac{d^3q}{C_1^{\text{eff}} q_z^2}.$$

Remarking that the contribution from q_\perp comes from the upper cut-off while that

from q_z comes from the lower one, we can take C_1^{eff} as a constant $C_1^{\text{eff}} \simeq C_1$. Hence

$$\langle u_z^2(r) \rangle \simeq \frac{k_B T}{8\pi^2 C_1} q_c^2 L.$$

The mean square of the molecule position along the column diverges linearly with the size of the sample. This is a very strong divergence. The consequence of this result on the density correlation function is even more spectacular. We can use formula (1.13) to investigate the nature of the order within a given column (taken at the origin), such that

$$\begin{aligned} \langle \rho(z, 0)\rho(z', 0) \rangle &= \bar{\rho}_0^2 + \frac{\rho_1^2}{2} \cos q_0(z - z') \exp(-\frac{1}{2}q_0^2 \langle (u_z(z, 0) - u_z(z', 0))^2 \rangle), \\ \langle (u_z(z, 0) - u_z(z', 0))^2 \rangle &= 2 \int \frac{d^3 q}{(2\pi)^3} (1 - \cos q_0(z - z')) |U_z(q)|^2. \end{aligned}$$

The integration gives

$$\langle (u_z(z, 0) - u_z(z', 0))^2 \rangle = \frac{q_c^2 k_B T}{8\pi^2 C_1} |z - z'|.$$

Thus,

$$\langle \rho(z, 0)\rho(z', 0) \rangle = \bar{\rho}_0^2 + \frac{\rho_1^2}{2} \cos q(z - z') \exp(-|z - z'|/\xi)$$

where

$$\xi = \frac{8\pi^2 C_1}{q_0^2 q_c^2 k_B T}.$$

Thus, even though we started with the hypothesis of a crystalline type of order in the columnar direction, we find an exponential decay of the positional correlation. Fluctuations kill long-range order in this direction as in one-dimensional systems. Thus, as stated in Section 1.5.1 the so-called ‘ordered’ columnar phase does not, strictly speaking, exist.

With an elastic modulus $C_1 \simeq 2 \cdot 10^8 \text{ erg cm}^{-3}$, $q_0 = \pi/(4 \cdot 10^{-8}) \text{ cm}^{-1}$, and $q \simeq (\pi/3 \cdot 10^{-7}) \text{ cm}^{-1}$, we get $\xi \sim 100 \text{ \AA}$; this is indeed a typical number.

REFERENCES

1. Gray, G. W. *Molecular structure and the properties of liquid crystals*. Academic Press, London (1962); see also *Mol. Cryst. liquid Cryst.* **7**, 127 (1969), **21**, 161 (1973); the review by Brown, G. H. and Shaw, G. H., *Chem. Rev.* **57**, 1049 (1957); and the list of mesomorphs established by Kast, W. In *Landolt-Bornstein* (6th edn), Vol. II, Part 2a, p. 266. Springer, Berlin (1960).
2. Gray, G. W. and Goodby, J. W., *Smectic liquid crystals: textures and structures*. Heiden and Sons (1984).
3. Demus, D. and Zaschke, H. *Flüssige Kristalle in Tabellen*. VEB Deutscher Verlag für Grundstoffindustrie, Leipzig (1st edn, 1974; 2nd edn, 1984).

4. Chandrasekhar, S., Sadashiva, D. K., and Suresh, K. A. *Pramana* **9**, 471 (1977). Thermotropic soaps yield in fact similar structures, see ref. 13.
5. Lin, L. *Mol. Cryst. liquid Cryst.* **91**, 77 (1983); Zimmerman, H., et al. *Z. Naturforsch.* **40a**, 149 (1985); Malthète, J. and Collet, A. *Nouv. J. Chimie* **9**, 151 (1985).
6. Nguyen, H. T., Destrade, C., and Gasparoux, H. *Phys. Lett.* **72A**, 3 (1979).
7. For a review on physical determinations of the size of polypeptide molecules see Benoit, H., Freund, L., and Spach, G. *Poly- α -amino acids*, Vol. 1 (ed. G. Fasman), p. 105. Dekker, New York (1967).
8. Robinson, C. *Discuss. Faraday Soc.* **25**, 29 (1958); Robinson, C. In *Proceedings of the Kent conference on liquid crystals* (1965) (ed. G. Brown, G. Dienes, and M. Labes), p. 147. Gordon and Breach, New York (1966); Saludjan, P. and Luzzati, V. In *Poly- α -amino acids*, Vol. 1 (ed. Fasman, G.), p. 157. Dekker, New York (1967).
9. *Advances in Polymer Sciences*. Liquid crystal polymers, Parts II and III. Springer-Verlag, Berlin (1984); Ciferri, A., Krigbaum, W. R., and Meyer, R. B. (ed.) *Polymer liquid crystals*. Academic Press, New York (1982).
10. Luzzati, V. in *Biological membranes* (ed. Chapman). Academic Press, New York (1968); Skoulios, A. *Adv. colloid Interface Sci.* **1**, 79 (1967).
11. Szwarc, M., Levy, M., and Milkovich, R., *J. Am. chem. Soc.* **78**, 2656 (1956).
12. Meunier, J., Langevin, D., and Boccardo, N. (ed.) *The physics of amphiphilic layers*. Springer-Verlag, Berlin (1987).
13. Spegt, P. A. and Skoulios, A. E. *Acta Crystallog.* **16**, 301 (1962).
14. Friedel, G. *Ann. Phys.* **18**, 273 (1922). See also Chistiakov, I. G. *Sov. Phys. Usp.* **9**, 551 (1967); Brown, G. H., Doane, J. W., and Neff, V. D. *CRC Crit. Rev. Solid State Sci.* **1**, 303 (1970).
15. Boccardo, N. *Ann. Phys.* **76**, 72 (1973). More detailed considerations allowing for uniform ferroelectric fluid states may be found in Alexander, S., Hornreich, R. M., and Shtrikman, S. In *Symmetries and broken symmetries in condensed matter physics* (ed. N. Boccardo), p. 379. IDSET, Paris (1981).
16. Yu, L. J. and Saupe, A. *Phys. Rev. Lett.* **45**, 1000 (1980).
17. Giannessi, C. *Phys. Rev.* **A34**, 705 (1986).
18. Toner, J. and Nelson, D. R. *Phys. Rev.* **B23**, 363 (1981).
19. Shechtman, D., Blech, I., Gratias, D., and Chan, J. W. *Phys. Rev. Lett.* **53**, 1851 (1984).
20. Fergason, J., Goldberg, N., and Nadalin, R. *Mol. Cryst.* **1**, 315 (1966).
21. For a discussion of Heisenberg ferromagnetism see, for example, Mattis, D. C. *The theory of magnetism*. Harper, New York (1966).
22. Friedel, E. *C.R. Acad. Sci., Paris* **180**, 269 (1925).
23. See, for example, Pershan, P. S. Structure of liquid crystal phases. In *World scientific lecture notes in physics*, Vol. 23, Part 2, Chapter 6 World Scientific, Singapore (1988).
24. Meyer, R. B. and Garov, S. *Phys. Rev. Lett.* **38**, 848 (1971).
25. Galerne, Y. and Liebert, L. *Phys. Rev. Lett.* **64**, 906 (1990).
26. Helfrich, W. and Oh, C. S. *Mol. Cryst. liquid Cryst.* **14**, 289 (1971); Urbach, W. and Billard, J. *C.R. Acad. Sci., Paris* **274** 1287 (1972).
27. Meyer, R. B., Liebert, L., Strzelecki, L., and Keller, P. *J. Phys. (Paris) Lett.* **36**, L69 (1975).

28. This example is adapted from the 'whales' model of Guyon, E. and Pieransky, P. Orsay liquid crystals group, *La Recherche* **88**, 368 (1978).
29. Pindak, R., Moncton, D. E., Davey, S. C., and Goodby, J. W. *Phys. Rev. Lett.* **46**, 1135 (1981).
30. Halperin, B. I. and Nelson, D. R. *Phys. Rev. Lett.* **41**, 121 (1978); **E41**, 2514 (1980); Nelson, D. R. and Halperin, B. I., *Phys. Rev. B* **19**, 2457 (1979).
31. Birgeneau, R. J. and Litster, J. D. *J. Phys. (Paris) Lett.* **39**, L399 (1978).
32. Smith, G. S., Sirota, E. B., Safinya, C. R., and Clark, N. A. *Phys. Rev. Lett.* **60**, 813 (1988).
33. Benattar, J. J., Moussa, F., and Lambert, M. *J. Chim. Phys.* **80**, 99 (1983).
34. Demus, D., Diele, S., Klapperstruck, M., Link, V., and Zaschke, H. *Mol. Cryst. liquid Cryst.* **15**, 161 (1971).
35. Diele, S., Brand, P., and Sackmann, S. *Mol. Cryst. liquid Cryst.* **17**, 163 (1972).
36. Tardieu, A. and Billard, J. *J. Phys. (Paris) Colloq.* **37** (Suppl C3), (1976); Etherington, G., Leadbetter, A. J., Wang, X. J., Gray, G. W., and Tajbakhsh, A. *Liquid Crystals* **1**, 209 (1986).
37. Peierls, R. E. *Annales de l'Institut Henri Poincaré* **5**, 177 (1935); Landau, L. D. *Phys. Z. Sowjet Union* **2**, 26 (1937).
38. Alexander, E. and Herrmann, K. *Z. Kristallographie* **69**, 285 (1928); **70**, 328 (1929).
39. Levelut, A. M. *J. chem. Phys.* **80**, 149 (1983).
40. Sigaud, G., Hardouin, F., Achard, M. F., and Levelut, A. M. *J. Phys. (Paris)* **42**, 107 (1981).
41. Caillé, A. *C.R. Acad. Sci., Paris* **B274**, 891 (1972).
42. Als-Nielsen, J., Birgenau, R. J., Kaplan, M., Litster, J. D., and Safinya, C. R. *Phys. Rev. Lett.* **39**, 352 (1977); **E41**, 1626 (1978); **39**, 1668 (1977).
43. Grinstein, G. and Pelcovits, R. *Phys. Rev. Lett.* **47**, 856 (1981).
44. Frederiks, V. K., Zolina, V. *J.R.F. (Kharkov) (Phys.)* **62**, 457 (1969); Tsvetkov, V. N. and Sosnovskii, A. *Acta Phys. Chim. USSR* **18**, 358 (1943).
45. Williams, R. J. *Chem. Phys.* **39**, 384 (1963); Heilmeyer, G. H., Zanoni, J., and Barton, J., *Proc. IEEE* **56**, 1162 (1968); *Trans. IEEE* **17**, 22 (1970); Van Raulte, J. *Proc. IEEE* **56**, 2146 (1968); Orsay Group on liquid crystals, *La Recherche* **12**, 433 (1971).
46. A more recent and useful book on displays: Kaneko, E. (ed.) *Liquid crystals T.V. displays: principles and applications of liquid crystal displays* (ed. E. Kaneko). Published for Hitachi Co by K.T.K. Scientific Publisher, Tokyo (1987). A comprehensive overview of the state of the art for all current applications of liquid crystals may be found in Bahadur, B. (ed.) *Liquid crystals: applications and uses*, Vols I, II, and III. World Scientific, Singapore (1991). For ferroelectric liquid crystals see: Lagerwall, S. T., Clark, N. A., Dijon, J., and Clerc, J. F. *Ferroelectrics* **94**, 3 (1989).
47. Gulik-Krzywicki, T., Schechter, E., Luzzati, V., and Fauré, M. In *Biochemistry and biophysics of mitochondrial membranes* (ed. G. F. Arzone *et al.*), p. 241. Academic Press, New York (1972).

LONG- AND SHORT-RANGE ORDER IN NEMATICS

*'Quand tu penses, ne sens-tu pas que
tu déranges secrètement quelque chose?'*
Paul Valéry

2.1 DEFINITION OF AN ORDER PARAMETER

The nematic phase has a lower symmetry than the high-temperature isotropic liquid. We express this qualitatively by saying that the nematic phase is ‘more ordered’. To put this on a quantitative basis, we need to define an order parameter that is non-zero in the nematic phase but that vanishes, for symmetry reasons, in the isotropic phase. In some physical systems an adequate choice of the order parameter is obvious. For instance, in a ferromagnet, the order parameter is the magnetization \mathbf{M} ; this is a vector with three independent components M_x . In a nematic phase the choice is less trivial and we shall have to proceed in successive steps.

2.1.1 Microscopic approach

2.1.1.1 Simple rods

Rigid rods are the simplest type of objects that allow nematic behaviour. The axis of one rod will be labelled by a unit vector \mathbf{a} . The rod is assumed to have complete cylindrical symmetry about \mathbf{a} . The direction of the nematic axis \mathbf{n} (i.e. the average direction of alignment of the molecules) will be taken as the z -axis of the (x, y, z) laboratory frame. We shall define \mathbf{a} by its polar angles θ and ϕ where

$$a_x = \sin \theta \cos \phi,$$

$$a_y = \sin \theta \sin \phi,$$

and

$$a_z = \cos \theta.$$

The state of alignment of the rods can be described by a distribution function $f(\theta, \phi) d\Omega$ (giving the probability of finding rods in a small solid angle $d\Omega = \sin \theta d\theta d\phi$ around the direction (θ, ϕ)).

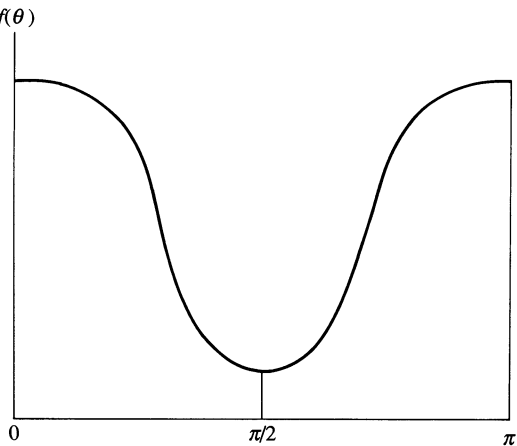


Fig. 2.1. The distribution function $f(\theta)$ for a system of rods in a nematic phase. $f(\theta)$ is large around $\theta = 0$ or π (i.e. for molecules parallel to the optical axis) and is small for $\theta \simeq \pi/2$.

From the discussion in Chapter 1 we know that, in conventional nematics:

1. $f(\theta, \phi)$ is independent of ϕ (the phase has complete cylindrical symmetry about \mathbf{n});
 2. $f(\theta) = f(\pi - \theta)$ (the directions \mathbf{n} and $-\mathbf{n}$ are equivalent). (2.1)
- The general appearance of $f(\theta)$ is shown in Fig. 2.1.

Now we wish to characterize the alignment not through the full function $f(\theta)$, but preferably by one related numerical parameter. The first idea would be to use the average

$$\langle \cos \theta \rangle = \langle \mathbf{a} \cdot \mathbf{n} \rangle = \int f(\theta) \cos \theta d\Omega,$$

but this vanishes identically as a result of property 2: there is no average dipole. Thus we must resort to higher multipoles. The first multipole giving a non-trivial answer is the quadrupole; this is defined as

$$S = \frac{1}{2} \langle (3 \cos^2 \theta - 1) \rangle = \int f(\theta) \frac{1}{2} (3 \cos^2 \theta - 1) d\Omega. \quad (2.2)$$

For instance, if $f(\theta)$ is strongly peaked around $\theta = 0$ and $\theta = \pi$ (parallel alignment), $\cos \theta = \pm 1$ and $S = 1$. If, on the other hand, $f(\theta)$ were peaked around $\theta = \pi/2$ (perpendicular alignment), we would have $S = -\frac{1}{2}$.[†] Finally,

[†] However, on physical grounds, it is hard to invent a system of rods that would prefer to have the perpendicular alignment.

if the orientation were entirely random ($f(\theta)$ independent of θ) we would have $\langle \cos^2 \theta \rangle = \frac{1}{3}$ and $S = 0$. Thus S is a measure of the alignment.

2.1.1.2 Relation to NMR spectra

The quantity S can be extracted from NMR data. To understand this, consider the following (simplified) example. The rod contains two (and only two) protons of spins \mathbf{I}_1 and \mathbf{I}_2 ($I_1 = I_2 = \frac{1}{2}$). An external field \mathbf{H} is applied. As we shall see later, nematics usually tend to line up in the direction of \mathbf{H} . Thus, in our notation, \mathbf{H} is parallel to the z -axis. Each spin is coupled to the external field \mathbf{H} and the dipolar field created by its partner. The spin Hamiltonian describing this situation has the structure [1]

$$\mathcal{H} = -\hbar\gamma\mathbf{H}(I_{1z} + I_{2z}) - \frac{(\hbar\gamma)^2}{d^3} \{3(\mathbf{I}_1 \cdot \mathbf{a})(\mathbf{I}_2 \cdot \mathbf{a}) - I_1 \cdot I_2\} \quad (2.3)$$

$$= \mathcal{H}_{\text{Zeemann}} + \mathcal{H}_{\text{dipolar}} = \mathcal{H}_Z + \mathcal{H}_D$$

where $\hbar\gamma\mathbf{I}_1$, $\hbar\gamma\mathbf{I}_2$ are the magnetic moments associated with the spins \mathbf{I}_1 , \mathbf{I}_2 , \mathbf{a} is the unit vector along the rod, and d is the distance between the protons.

The dipolar fields are conveniently measured in terms of

$$H_L = \hbar\gamma/d^3.$$

H_L is of order 1 G and the corresponding precession frequency $\gamma\mathcal{H}_L$ is of order 10^4 s $^{-1}$. In our liquids, the direction of the long molecular axis (the vector \mathbf{a}) changes with time on a much faster scale (typically 10^{-9} s). In this limit of rapid motion, $\mathcal{H}_{\text{dipolar}}$ may be replaced by its average over the orientations of \mathbf{a} , which we shall call \mathcal{H}_D . To derive \mathcal{H}_D we use the averages

$$\langle a_z^2 \rangle = \frac{1}{3} + \frac{2}{3}S,$$

$$\langle a_x^2 \rangle = \langle a_y^2 \rangle = \frac{1}{3} - \frac{1}{3}S,$$

and

$$\langle a_x a_z \rangle = \langle a_y a_z \rangle = \langle a_x a_y \rangle = 0.$$

This leads to the following average Hamiltonian

$$\mathcal{H}_D = \Delta(-2I_{1z}I_{2z} + I_{1x}I_{2x} + I_{1y}I_{2y}) \quad (2.4)$$

where, for brevity, we have put

$$\Delta = \hbar\gamma S H_L.$$

Since protons are of spin $\frac{1}{2}$ we have

$$I_{1z}^2 = I_{1x}^2 = I_{1y}^2 = \frac{1}{4}, \text{ etc.}$$

This allows us to write the Hamiltonian (2.4) very simply in terms of the

total spin $\mathbf{I} = \mathbf{I}_1 + \mathbf{I}_2$. Using the equality

$$I_z^2 = (I_{1z} + I_{2z})^2 = I_{1z}^2 + I_{2z}^2 + 2I_{1z}I_{2z} = \frac{1}{4} + \frac{1}{4} + 2I_{1z}I_{2z}$$

and other similar ones, we obtain

$$\mathcal{H}_D = \frac{1}{2}\Delta(-2I_z^2 + I_x^2 + I_y^2) + \text{constant}.$$

The constant terms do not contribute to the energy intervals with which we are concerned, and may be omitted. The spin Hamiltonian (2.3) is thus reduced to

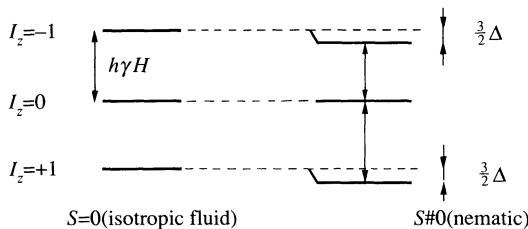
$$\bar{\mathcal{H}} = -\hbar\gamma HI_z + \frac{1}{2}\Delta(-3I_z^2 + \mathbf{I}^2). \quad (2.5)$$

$\bar{\mathcal{H}}$ may be shown to commute with the operators $\mathbf{I}^2 = I_x^2 + I_y^2 + I_z^2$ and I_z . Thus the levels of $\bar{\mathcal{H}}$ may be indexed by two quantum numbers: a number I such that $\mathbf{I}^2 = I(I+1)$ and a number I_z running from $-I$ to $+I$ by unit steps.

For two spins $\frac{1}{2}$, the total spin I may take only two values: $I = 0$ (singlet) or $I = 1$ (triplet). The singlet state may be shown to be unobservable in the resonance experiment. Thus we are left with the triplet state, with three levels corresponding to $I_z = -1, 0, 1$. The term involving \mathbf{I}^2 in eqn (2.5) is the same for these three levels and may again be omitted in discussion of the intervals. Thus we have the further reduction

$$\bar{\mathcal{H}} \rightarrow -\hbar\gamma HI_z - \frac{3}{2}\Delta I_z^2.$$

The corresponding levels are represented below:



Also shown on this plot are the two allowed transitions. (A third transition, from $I_z = +1$ to $I_z = -1$, is forbidden by a general spectroscopic rule.) They correspond to the frequencies

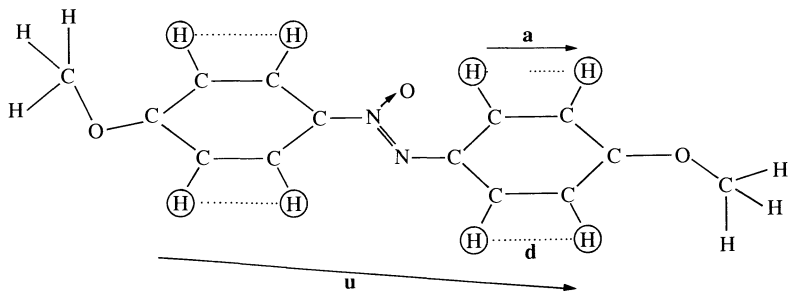
$$\omega = \gamma(H \pm \frac{3}{2}H_L S). \quad (2.6)$$

Thus, when going from the isotropic ($S = 0$) to the nematic phase ($S \neq 0$), the resonance line splits by an amount $3\gamma H_L S$.

If the distance d between the protons is fixed (rigid molecule) and is known, H_L is known and S can be extracted from the experimental splitting. Experiments of this type were performed very early; the first data on

p-azoxyanisole were obtained in about 1953 [2]. Here we have two types of protons.

1. The six methyl-group protons at both ends of the molecule have rapid rotations and do not give rise to any interesting splitting.
2. The eight protons linked to the aromatic ring fall into four pairs; each pair is nearly uncoupled to the others. The following diagram of PAA shows the pairs.



In a first approximation we may neglect the angle between **a** and the long axis **u**; then we recover the simple model described above. The distance *d* is 2.45 Å and $H_L = 2.9$ G. Typical values of *S* are in the range 0.4 (at the highest temperatures) to 0.6 (at the lowest temperatures). Detailed measurements of this sort have been performed by Saupe and his co-workers [3]. The data are accurate because each line is narrow: the ‘motional narrowing’ familiar in liquid phases [1] is also found in nematics. For general reviews on this subject see references 4–6.

2.1.1.3 Rigid molecules of arbitrary shape [7, 8]

Let **a**, **b**, **c** be three orthogonal unit vectors linked to the molecule; the degree of alignment may be defined by a natural generalization of eqn (2.2) through the quantities (often called ‘ordering matrix’)

$$S_{ij}^{\alpha\beta} = \frac{1}{2} \langle 3i_\alpha j_\beta - \delta_{\alpha\beta} \delta_{ij} \rangle \quad (2.7)$$

where $\alpha, \beta = x, y, z$ are indices referring to the laboratory frame, while $i, j = a, b, c$, and $\delta_{\alpha\beta}$ and δ_{ij} are Kronecker symbols. The brackets $\langle \rangle$ represent a thermal average. $S_{ij}^{\alpha\beta}$ is symmetric in ij and in $\alpha\beta$; it is also a traceless tensor in respect of either pair

$$S_{ij}^{xx} = 0 \quad \text{and} \quad S_{ii}^{z\beta} = 0. \quad (2.8)$$

(We use the usual notation where summations are implied by repeated indices $S^{\alpha\alpha} = S^{11} + S^{22} + S^{33}$.) We have seen in Chapter 1 that the usual nematic structure has complete rotational symmetry about the optical axis;

let us again take this as the z -axis. This property implies the equalities

$$S_{ij}^{xx} = S_{ij}^{yy} \quad \text{and} \quad S_{ij}^{xy} = 0. \quad (2.9)$$

Furthermore, the x, y -plane is a plane of reflection for the structure; from this we derive

$$S_{ji}^{zx} = S_{ij}^{zy} = 0. \quad (2.10)$$

Thus, in the usual uniaxial nematic structure, the only non-zero components of $S_{ij}^{\alpha\beta}$ are

$$S_{ij}^{zz} = -2S_{ij}^{xx} = -2S_{ij}^{yy} = S_{ij} \quad (2.11)$$

and the state of alignment of a rigid molecule is described by a (3×3) matrix S_{ij} , which is symmetric and of zero trace.

Note that $S_{ij}^{\alpha\beta}$ may describe less symmetric states. From the very construction of $S_{ij}^{\alpha\beta}$, the ‘ordering matrix’ S is symmetrical, real, and traceless. Thus it can be diagonalized in a well-chosen orthogonal frame of reference (x, y, z). Again we can write

$$S_{ij}^{xy} = S_{ij}^{xz} = S_{ij}^{yz} = 0$$

and

$$S_{ij}^{xx} + S_{ij}^{yy} + S_{ij}^{zz} = 0,$$

but, in general, $S_{ij}^{xx} \neq S_{ij}^{yy} \neq S_{ij}^{zz}$. A phase characterized by such an ordering matrix is less symmetric than the usual nematic we have just described. It possesses three planes of symmetry (xy , xz , and yz), three twofold axes (x, y, z) and an inversion point: this is the biaxial phase (Fig. 1.6). As pointed out in Chapter 1, these phases have been observed in lyotropic, polymeric, and low-molecular-weight thermotropic systems [9].

The average dipolar interaction $\bar{\mathcal{H}}_{12}$ between two arbitrary spins \mathbf{I}_1 and \mathbf{I}_2 carried by the molecule can be written entirely in terms of the S_{ij} . Equation (2.3) is generalized to

$$\bar{\mathcal{H}}_{12} = -\frac{\hbar^2 \gamma_1 \gamma_2}{d^3} \{3(\mathbf{I}_1 \cdot \mathbf{u})(\mathbf{I}_2 \cdot \mathbf{u}) - \mathbf{I}_1 \cdot \mathbf{I}_2\} \quad (2.12)$$

where $\hbar \gamma_1 \mathbf{I}_1$ and $\hbar \gamma_2 \mathbf{I}_2$ are the magnetic moments associated with the spins \mathbf{I}_1 and \mathbf{I}_2 , \mathbf{u} is the unit vector pointing in the $(\mathbf{r}_1 - \mathbf{r}_2)$ direction, and $d = |\mathbf{r}_1 - \mathbf{r}_2|$.

Equation (2.12) can easily be converted, in order to exhibit the ordering matrix (again with the summation convention), to

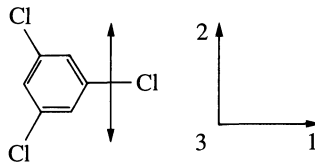
$$\bar{\mathcal{H}}_{12} = -\frac{2\hbar^2 \gamma_1 \gamma_2}{d^3} \left(\frac{3}{2} u_\alpha u_\beta - \frac{\delta_{\alpha\beta}}{2} \right) I_{1\alpha} I_{2\beta}. \quad (2.13)$$

And, after averaging,

$$\bar{\mathcal{H}}_{12} = -\frac{2\hbar^2\gamma_1\gamma_2}{d^3} S_{uu}^{\alpha\beta} I_{1\alpha} I_{2\beta}. \quad (2.14)$$

Thus, from the detailed high-resolution NMR spectrum of a rigid molecule in the nematic phase we can, in principle, reconstruct the matrix S_{ij} . In practice, however, this is often somewhat complicated, because the nematic molecules carry a number of nuclear spins and the spectra are complex. NMR quadrupolar splitting, which we will briefly describe in the next section, provides in fact more transparent data.

To avoid the complexities inherent in a heavy molecule, it is sometimes more convenient to study a well chosen solute in a nematic phase. If the solute is non-spherical in shape, it will be aligned by the neighbouring nematic molecules, and this alignment may also be characterized by a matrix \tilde{S}_{ij} . There is no direct way to relate \tilde{S}_{ij} (for the solute) to S_{ij} (for the nematic solvent); nevertheless, \tilde{S}_{ij} gives some indication of the amount or order. A good example of such a solute is 1,3,5-trichlorobenzene [10]



This is particularly simple: there are only three (equivalent) protons in the molecule. If we define the molecular axes as in the above diagram, the \tilde{S} matrix is diagonal. Furthermore, $\tilde{S}_{11} = \tilde{S}_{22}$ ($= -\frac{1}{2}\tilde{S}_{33}$) because of the trigonal symmetry around the axis 3. If \mathbf{u} is any one of the three proton-proton vectors, we also have $S_{uu} = \tilde{S}_{11} = \tilde{S}_{22}$. Let us call this single parameter \tilde{S} . In terms of \tilde{S} , the average Hamiltonian of the three protons, including dipolar coupling, is

$$\begin{aligned} \bar{H} &= -\gamma H(I_{1z} + I_{2z} + I_{3z}) \\ &+ \Delta \{ \mathbf{I}_1 \cdot \mathbf{I}_2 + \mathbf{I}_2 \cdot \mathbf{I}_3 + \mathbf{I}_3 \cdot \mathbf{I}_1 - 3(I_{1z}I_{2z} + I_{2z}I_{3z} + I_{3z}I_{1z}) \}, \\ \Delta &= \gamma H_L \tilde{S}. \end{aligned}$$

Introducing the total spin $\mathbf{I} = \mathbf{I}_1 + \mathbf{I}_2 + \mathbf{I}_3$, we have the very simple form

$$\bar{\mathcal{H}} = -\gamma H I_z + \frac{1}{2}\Delta(I^2 - 3I_z^2) + \text{constant}.$$

A complete analysis of the levels and of the allowed transitions shows that there are three resonance frequencies in the nematic phase, and the splitting directly measures \tilde{S} . Experimentally, in a variety of nematic solvents \tilde{S} ranges from +0.08 to +0.10 (depending on the temperature). Reviews of NMR

studies of solutes have been written by Diehl and Khetrapal and, more recently, by Emsley and Lindon [6].

2.1.1.4 Other determinations of the order by magnetic resonance and flexible molecules

Apart from these dipolar effects in NMR, there are also other resonance methods that permit a determination of S_{ij} : studies of NMR quadrupole splittings using nuclei with spin $I > 1$ such as ^{14}N [11] or deuterium [12]; and studies of the anisotropy of the Zeeman and hyperfine couplings in the electron spin resonance (ESR) of dissolved free radicals [13]. The latter method has one advantage: the high signal intensities make it possible to apply the method to very small samples. However, it also has some drawbacks. First, it is always concerned with the alignment of a solute and not of the nematic matrix itself. Second, the rapid-motion limit that applies for NMR (reducing \mathcal{H} to $\bar{\mathcal{H}}$) is not always obtained here; the characteristic electron frequencies can be comparable to $1/\tau_{\text{rotation}}$, for which we obtain a broad spectrum, and the determination of S_{ij} becomes inaccurate.

In view of its accuracy and ability to probe well defined parts of a molecule, we find it useful to recall the main features of the NMR quadrupole-splitting technique. The Hamiltonian of a nucleus possessing an electric quadrupole contains, aside from the Zeeman part, a contribution that corresponds to its interaction with the field gradients due to the neighbouring electron cloud [1]

$$Q = V_{\alpha\beta} Q_{\alpha\beta}. \quad (2.15)$$

(The summation convention is again used.) $V_{\alpha\beta} = \partial^2 V / (\partial x_\alpha \partial x_\beta)$ is the field gradient tensor. Very often, it can be considered to have uniaxial symmetry with a good accuracy (e.g. D–O and C–D bonds). $Q_{\alpha\beta}$ is the nuclear electric quadrupole moment, which can be expressed as a traceless dyadic of the nuclear spin,

$$Q_{\alpha\beta} = \frac{eQ}{6I(2I-1)} \left(\frac{3}{2}(I_\alpha I_\beta + I_\beta I_\alpha) - I(I+1)\delta_{\alpha\beta} \right). \quad (2.16)$$

(eQ is the electric quadrupole of the nucleus in the state $I_z = I$. It is different from zero for $I \geq 1$; hence the use of deuterium or ^{14}N .) If we consider uniaxial bonds and call \mathbf{u} the unit vector in the bond direction,

$$V_{\alpha\beta} = V_{uu} \left(\frac{3}{2} u_\alpha u_\beta - \frac{\delta_{\alpha\beta}}{2} \right) \quad (2.17)$$

which gives

$$Q = \frac{3}{2} V_{uu} Q_{uu}. \quad (2.18)$$

In these experiments the quadrupolar energy is a weak perturbation of the Zeeman term so that the difference in the energy levels can be simply

evaluated by perturbation theory. If m is the I_z quantum number, $|m\rangle$ the corresponding eigenvector, and if z is defined by the magnetic field direction (the principal axes of the nematic are not specified at this stage),

$$E_m = -\gamma\hbar H m + E'_m \quad (2.19)$$

where

$$E'_m = \langle m | \mathcal{H}_Q | m \rangle \quad (2.20)$$

To evaluate (2.20) it is convenient to express Q_{uu} first in the laboratory frame (Greek indices). From

$$Q_{uu} = \frac{eQ}{6I(2I-1)} (3I_u^2 - I(I+1)) \quad \text{and} \quad I_u = u_\alpha I_\alpha,$$

we obtain

$$Q_{uu} = \frac{eQ}{6I(2I-1)} (3u_\alpha u_\beta I_\alpha I_\beta - I(I+1))$$

or

$$Q_{uu} = \frac{1}{3} \frac{eQ}{I(2I-1)} \left(\frac{3}{2} u_\alpha u_\beta - \frac{\delta_{\alpha\beta}}{2} \right) I_\alpha I_\beta.$$

The angular average yields

$$\langle Q_{11} \rangle = \frac{1}{3} \frac{eQ}{I(2I-1)} \langle S_{uu}^{\alpha\beta} \rangle I_\alpha I_\beta. \quad (2.21)$$

The order parameter $\langle S_{uu}^{\alpha\beta} \rangle$ thus enters naturally the expression of the energy levels in the presence of quadrupolar interaction, in a way similar to (2.14). The advantage is that dipolar interactions are often negligible in deuterated samples; this allows us to resolve the spectra of complicated molecules.

With $\langle m | I_z^2 | m \rangle = m^2$; $\langle m | I_x^2 | m \rangle = \langle m | I_y^2 | m \rangle = \frac{1}{2}(I(I+1) - m^2)$ and all other elements being zero, the energy levels become

$$E_m = -\hbar\gamma H m + E'_m,$$

$$E'_m = \frac{V_{uu} eQ}{2I(2I-1)} (\frac{3}{2}m^2 - I(I+1)/2) \langle S_{uu}^{zz} \rangle. \quad (2.22)$$

The structure is similar to the one described in (2.5); again the transitions correspond to $|\Delta m| = 1$. Hence, for the deuteron ($I = 1$), the resonance line of the isotropic phase is split in a doublet for just the same reason as explained in the previous section

$$\delta\nu = \frac{3V_{uu} eQ}{2} \langle S_{uu}^{zz} \rangle. \quad (2.23)$$

Since $V_{11} eQ$ is a known quantity (the quadrupole splitting constant D), the measure of $\delta\nu$ is a direct measure of $\langle S_{uu}^{zz} \rangle$. If we call x, y, z the principal

axes of the ordering matrix we get

$$\delta v = \frac{3V_{11}eQ}{2} (\langle S_{uu}^{zz} \rangle a_z^2 + \langle S_{uu}^{yy} \rangle a_y^2 + \langle S_{uu}^{xx} \rangle a_x^2) \quad (2.24)$$

where a_i are the direction cosines between the magnetic field and the principal axes. Rotating the sample allows independent measurements of each component. In fact, diamagnetic interactions tend to align the direction of largest magnetic susceptibility in the field. Using a ‘dynamical trick’, Yu and Saupe were able to show the existence of a phase for which $\langle S_{uu}^{zz} \rangle \neq \langle S_{uu}^{yy} \rangle \neq \langle S_{uu}^{xx} \rangle$ in the ternary system potassium laurate-1-decanol-D₂O. Together with the sharpness of the lines, this proved the existence of a biaxial nematic phase [9].

Another interesting feature of this technique is that the ordering matrix is microscopically well defined: one measures the order of a given bond. For example if we deuterate alkyl chains at a particular location in a molecule, we can probe the degree of order of the C–D bond under consideration. Varying its position, we can get a map of S in the molecule. In fact, deuteration cannot be so selective. Yet, in their experiment on terephthalidene-di(*p*-₉-butyl-2-6-*d*₂ aniline) TBd-BA and *p*-butyloxybenzilidene-*p*-*d*₁₇-octyl-2-6-*d*₂ aniline BOBd-OA, Deloche *et al.* [14] were able to identify all C–D bonds contained in the molecules (the exceptional resolution is due to negligible dipolar interaction between deuterons as already mentioned).

$$-\underset{(n-1)}{C} \underset{(n)}{D_2} - CD_2 - \underset{(n+1)}{C} \underset{(n)}{D_2}.$$

The splitting, which is proportional to S_{uu}^{zz} (the z -direction being that of the largest diamagnetic susceptibility), varies considerably along the alkyl chain (Fig. 2.2). In both cases the outer methyl group exhibits little ordering in the nematic phase, and the degree of order decreases monotonically from the rigid core proximity to the chain ending. It is interesting to note that the chain seems hardly more distorted in the nematic than in lower temperature smectics. Furthermore, the temperature dependence of the order parameters depends on their location in the molecule. S decreases faster near the chain ends with increasing temperature than on the phenyl rings or close. This gives a measure of the rigid-rod picture and illustrates the difficulty of comparing statistical theories, in which the detailed nature of the molecules is ignored, with experiments that often measure ill defined weighted averages of the S corresponding to all bonds of the molecule. The case of lyophilic liquid crystals, such as hydrated soaps in which there is essentially no rigid part in the constituent molecule (at least for the high-temperature phases), is an extreme example.

However, for defining an order parameter, a collection of many quantities such as the S of all C–D bonds in a molecule is an *embarras de richesse*. This suggests that we should return to a more macroscopic definition of the order

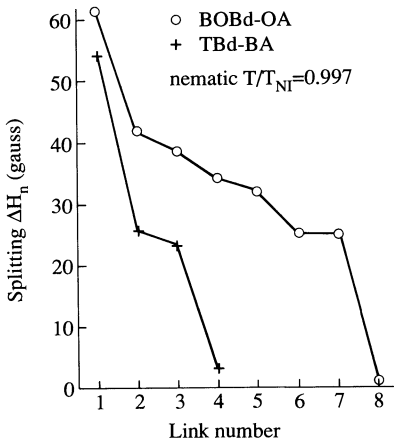


Fig. 2.2. Plot of orientational C–D bond order versus position along the alkyl chain of the mesogenic molecules (BOBd-OA; TBd-A) in their nematic phase. Note the abrupt decrease of the order at the extremity of the chain (increasing number = going away from the core). (After Deloche *et al.* [15].)

that will be applicable independently of any assumption on molecular rigidity. This is the object of Section 2.2.

2.1.1.5 Determination of higher moments of the distribution function

Let us come back for a moment to the rigid-rod picture we used in Section 2.1.1.1 to introduce the notion of order in uniaxial nematics. Because of the symmetry $\theta \rightarrow \pi - \theta$, it is clear that all odd moments of the one-particle distribution function $f(\theta)$ vanish. On the other hand, all even moments are non-zero and knowledge of them would allow us to calculate $f(\theta)$. One step toward the achievement of such a task is to measure the fourth moment, P_4 where

$$\langle P_4(\cos \theta) \rangle = \langle 35 \cos^4 \theta - 30 \cos^2 \theta + 3 \rangle / 8. \quad (2.25)$$

(P_4 can easily be constructed with the three requirements that it contain a $\cos^4 \theta$ term, that $\langle P_4(\cos \theta) \rangle_{\text{isotropic}} \equiv 0$, and that $P_4(1) = 1$.)

Several techniques allow such a measurement. Raman scattering, elastic neutron scattering, and electron paramagnetic resonance (EPR) line-shape analysis have been used [16–19]. Unfortunately, the results are in relative disagreement with each other.

Raman scattering of well chosen vibration bands (corresponding to C≡N or C–C bonds) allows us to probe the orientational order of selective parts of nematogenic molecules. The scattered light originates from a modulation of the electric polarizability due to the thermally excited vibration of the

considered bond. The radiating polarization at the Raman frequency, $\omega + \delta\omega$, reads

$$P_i(\omega + \delta\omega, \mathbf{r}) = \alpha_{ij}(\delta\omega, \mathbf{r}) E_j^{\text{loc}}(\omega, \mathbf{r}) \quad (2.26)$$

where α_{ij} is the polarizability of the bond located in \mathbf{r} . $E_j^{\text{loc}}(\omega, \mathbf{r})$ is the local field acting in \mathbf{r} , which is linearly related to the macroscopic field \mathbf{E} . On general grounds this relation reads

$$E_j^{\text{loc}}(\omega, \mathbf{r}) = \int l_{jk}(\omega, \mathbf{r} - \mathbf{r}') E_k(\mathbf{r}') d^3\mathbf{r}'.$$

Local field models suggest that the integral is heavily weighted by short-range correlation, i.e. $|\mathbf{r} - \mathbf{r}'|$ of the order of molecular sizes. Since the external field variation occurs on a much larger length scale, one usually writes

$$E_j^{\text{loc}}(\omega, \mathbf{r}) = L_{jk}(\omega, \mathbf{r}) E_k(\mathbf{r}). \quad (2.27)$$

Note that not only angular, but also short-range position correlations are hidden in the Lorentz tensor L_{ij} . Note also that L_{ij} need not exhibit the same principal axes as α_{ij} . On the grounds that short-range order does not vary critically and that refractive index measurements which suffer from the same type of remark do yield S values (Fig. 2.3) that are basically compatible with others, we can proceed further, considering $\alpha_{ij} L_{jk} = \alpha_{ik}^{\text{eff}}$ as an effective polarizability over which averaging processes can be conducted.

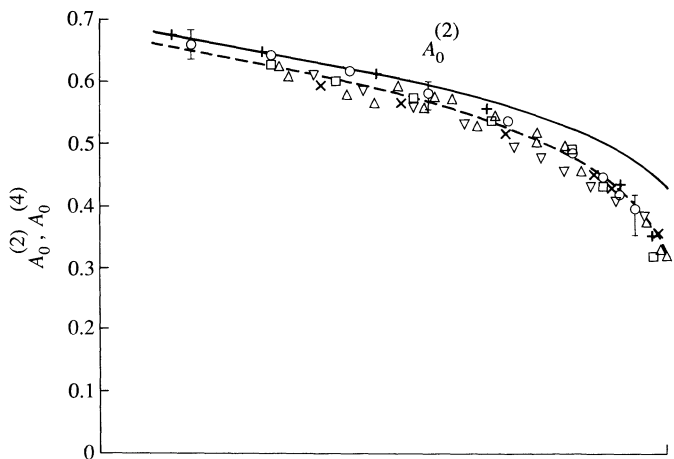


Fig. 2.3. Compatibility of different S measurements in MBBA using different techniques: circle, Raman; square, NMR; cross, birefringence; triangles, diamagnetic anisotropy (see reference 15 and references therein). The solid line corresponds to the Maier-Saupe theory described in Section 2.2.2.1. The dashed line corresponds to an improvement of this theory by Humphries, James, and Luckhurst [20].

From (2.26) and (2.27) it is clear that the scattered amplitude is proportional to

$$a = \alpha + \beta_{ij} S_{ij}$$

in which α, β_{ij} are functions of the experimental geometry (in particular the polarizations of the incident and scattered radiations) and S_{ij} is defined with respect to ‘molecular axes’ which are, in fact, the principal axes of α_{ik}^{eff} (before averaging).

The Raman intensity is then proportional to the average

$$\langle a^2 \rangle = \alpha^2 + 2\alpha\beta\langle S \rangle + \beta^2\langle S^2 \rangle$$

(where we omit all indices).

Suppose we know the α^{eff} principal axes. In this frame of reference

$$\alpha^{\text{eff}} = \alpha_0 \begin{pmatrix} a & 0 & 0 \\ 0 & b & 0 \\ 0 & 0 & 1 \end{pmatrix}.$$

Call β the angle of the third axis of α^{eff} with the nematic optical axis. Obviously, the average involves $\alpha_0, a, b\langle \cos^2 \beta \rangle$, and $\langle \cos^4 \beta \rangle$. Intensity ratios get rid of α_0 . In the nematic phase, in the back-scattering geometry, we can build three such ratios

$$\frac{I_{yz}}{I_{zz}}, \quad \frac{I_{zy}}{I_{yy}}, \quad \frac{I_{yx}}{I_{xx}}.$$

In $I_{\alpha\beta}$ the first index refers to the polarization of the incident radiation, the second to the scattered one ($z = \text{optical axis}$). If we add depolarization measurements in the isotropic phase we get a fourth equation and, with the assumption that neither the principal axes nor the principal values are sensitive functions of temperature, we can extract the four unknowns $a, b, \langle \cos^2 \beta \rangle, \langle \cos^4 \beta \rangle$. A consistency check is provided by the fact that a and b should be found independent of temperature. This procedure has been set by S. Jen *et al.* [16]. S measurements are consistent with the values obtained by other techniques. More striking are the results concerning P_4 . They are found to be quite small and often negative, close to T_{NI} the isotropic nematic transition temperature!

Other techniques have been used: quasi-elastic scattering of X-rays or neutrons gives access to the one-particle distribution function in the limit of large-angle scattering [18, 21]. Indeed, in that limit interferences can be neglected and the scattering cross-section is governed by the single-molecule term

$$\frac{d\sigma}{d\Omega} \simeq \sum_{MN} a_M a_N \langle e^{i\mathbf{q} \cdot \mathbf{r}_M} e^{-i\mathbf{q} \cdot \mathbf{r}_M} \rangle \quad (2.28)$$

where a_M is the (coherent) scattering length, \mathbf{r}_M the position in the laboratory frame of the M th nucleus and the molecule considered in the case of neutrons, of the M th electron cloud in the case of X-rays. The summation extends over all parts of the molecule. Expressing \mathbf{r}_M in the molecular frame (using the notation of Section 2.1.1.3 (note that overall translations of the molecule may be ignored since intermolecular interference terms are negligible in this limit),

$$\begin{aligned} \frac{d\sigma}{d\Omega} &\simeq \sum_{MN} a_M a_N^* \langle e^{iq_\alpha i_\alpha (\mathbf{r}_{Mi} - \mathbf{r}_{Ni})} \rangle, \\ \frac{d\sigma}{d\Omega} &\simeq \sum_M |a_M^2| - \frac{1}{2!} q_\alpha q_\beta \langle i_\alpha j_\beta \rangle \\ &\quad \times \sum_{MN} a_M a_N^* (\mathbf{r}_{Mi} - \mathbf{r}_{Ni})(\mathbf{r}_{Mj} - \mathbf{r}_{Nj}) + \frac{1}{4!} q_\alpha q_\beta q_\gamma q_\delta \langle i_\alpha j_\beta k_\gamma l_\delta \rangle \\ &\quad \times \sum a_M a_N^* (\mathbf{r}_{Mi} - \mathbf{r}_{Ni})(\mathbf{r}_{Mj} - \mathbf{r}_{Nj})(\mathbf{r}_{Mk} - \mathbf{r}_{Nk})(\mathbf{r}_{Ml} - \mathbf{r}_{Nl}). \end{aligned}$$

Thus the analysis of the angular dependence of the scattering cross-section provides a means of measuring the ordering matrix $S_{ij}^{\alpha\beta}$ and its higher moments, provided one knows the molecular form factors (such as $\sum_{MN} a_M a_N (\mathbf{r}_{Mi} - \mathbf{r}_{Ni})(\mathbf{r}_{Mj} - \mathbf{r}_{Nj})$). They could, in principle, be calculated using molecular models under the assumption of molecular rigidity. This would yield temperature-independent form factors and allow the estimate of the ordering matrix. The best procedure would probably be to take advantage of the experimental results obtained with NMR quadrupole splitting to estimate a temperature-dependent form factor. P_2 and P_4 have been estimated for PAA in the rigid-rod approximation. Although 'small' (in a way to be discussed shortly), the P_4 values are larger than those found with Raman scattering on pure 5CB(*p*-*n*-pentyl-*p'*cyanobiphenyl) and a mixture of 20 per cent BBCA in MBBA (BBCA: *N*-*p*'-butoxybenzylidene)-*p*-cyanoaniline) but fairly comparable to those obtained with neat MBBA (except close to T_{NI} , unfortunately, where the neutron data are not quite reliable because of degradation problems) and with 4.O.8 (*N*-(*p*'-butoxybenzylidene)-*p*-*n*-octyl-aniline).

EPR line shapes of nitroxide spin probes also allow P_4 measurements; indeed, the dominant relaxation processes depend on molecular angular fluctuations through the Landé and hyperfine tensors. Thus the line width will be controlled by 'friction' coefficients, which can be expressed by Kubo-type formulae [19]

$$D \propto \int \langle S_{ij}^{\alpha\beta}(0) S_{ij}^{\gamma\delta}(t) \rangle dt. \quad (2.29)$$

Again the analysis requires the 'rigid-rod' assumption and the information corresponds to a molecule that is a non-mesogenic 'guest'. Experiments

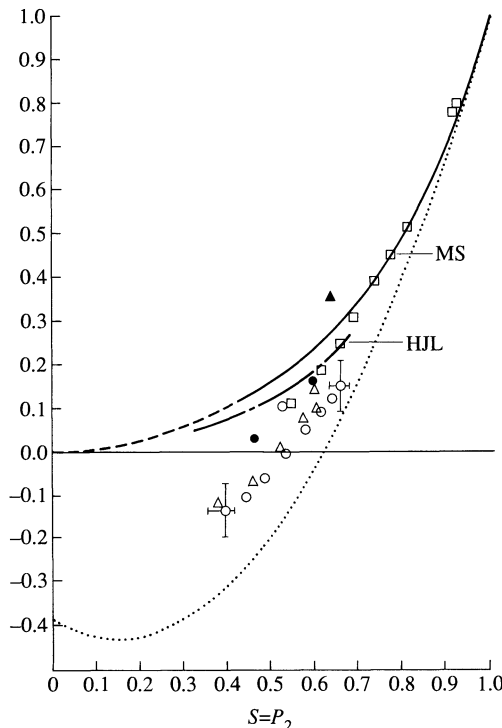


Fig. 2.4. Plot of the $P_4 = f(S)$ dependence. The dotted line corresponds to the limit discussed in the text. The upper solid line corresponds to the Maier-Saupe (MS) theory described in Section 2.2.21; the lower solid line to the Humphry-James-Luckhurst (HJL) theory. Solid triangle, EPR on a guest in 5CB as described in the text; square, Raman in pure MBBA; open triangle, Raman on 5CB; open circle, Raman on a mixture of 20 per cent BBCA in MBBA; solid circle, neutron scattering on PAA. Note the similarity of results between PAA and pure MBBA on one hand, and 5CB and the 20 per cent BBCA in MBBA mixture on the other.

performed with 3-spiro(2'-*N*-oxyl-3', 3'-dimethyloxazolidine)-5α-cholestane in MBBA and 5CB yield P_4 values that are significantly higher than those obtained in Raman scattering experiments [19]. Unfortunately, only a few temperatures far from T_{NI} were investigated.

We have plotted on Fig. 2.4 the curves $P_4 = f(P_2)$ obtained using different techniques and different compounds. The scatter may not be as large as it seems at first sight. The agreement between neutron and Raman scattering, although perhaps fortuitous, is encouraging; it further suggests that the differences may not be so much between techniques, but rather between cyano compounds and the other compounds. Pair correlations are quite important in these systems, and they can have a profound influence on the

interpretation of any of the data (all based on a one-particle approximation) on one hand, on the physics of the transition of the other. Solute molecules need not be sensitive to those pair correlations.

In Fig. 2.4, two other curves are also plotted: the $P_4 = f(P_2)$ dependence according to the Maier and Saupe (MS) theory of nematic order and the limit beyond which the (P_4, P_2) couple would not be coherent with their definition. This limit results from the Schwartz inequality

$$\langle \cos^4 \theta \rangle \geq \langle \cos^2 \theta \rangle^2$$

which implies

$$P_4 \geq (35P_2^2 - 10P_2 - 7)/18.$$

The limit itself corresponds to the absence of fluctuations in θ (the nematic order is obtained by the ϕ degeneracy only). The fact that P_4 is found to be smaller than predicted by the MS theory suggests that the θ fluctuations are not as large as expected from this theory. Note that the same type of arguments as those that show the existence of five independent components in the ordering matrix $S_{ij}^{\alpha\beta}$ predict nine components for the corresponding fourth moment $S_{ijkl}^{\alpha\beta\gamma\delta}$. Although it seems reasonable that P_4 provides the leading term, the importance of the others seems hard to assess. We are back to our *embarras de richesse* and to the need of a more macroscopic definition of the order.

2.1.2 Macroscopic approach

2.1.2.1 Tensor order parameter

A typical difference between the high-temperature isotropic liquid and the nematic mesophase is found in the measurement of all macroscopic tensor properties. For instance, the relation between the magnetic moment \mathbf{M} (due to the molecular diamagnetism) and the field \mathbf{H} has the form

$$M_\alpha = \chi_{\alpha\beta} H_\beta \quad (2.30)$$

where $\alpha, \beta = x, y, z$. When the field \mathbf{H} is static, the tensor $\chi_{\alpha\beta}$ is symmetric ($\chi_{\beta\alpha} = \chi_{\alpha\beta}$). In the isotropic liquid, we have

$$\chi_{\alpha\beta} = \chi \delta_{\alpha\beta},$$

while in the uniaxial nematic phase (always choosing the z -axis parallel to the nematic axis)

$$\chi_{\alpha\beta} = \begin{vmatrix} \chi_\perp & 0 & 0 \\ 0 & \chi_\perp & 0 \\ 0 & 0 & \chi_\parallel \end{vmatrix}. \quad (2.31)$$

To define an order parameter that vanishes in the isotropic phase, we

extract the anisotropic part $Q_{\alpha\beta}$ of the magnetic susceptibility

$$Q_{\alpha\beta} = G \left(\chi_{\alpha\beta} - \frac{1}{3} \delta_{\alpha\beta} \sum_{\gamma} \chi_{\gamma\gamma} \right). \quad (2.32)$$

We call $Q_{\alpha\beta}$ the tensor order parameter. It is real, symmetric, and of zero trace. The normalization constant G may be chosen at will; it is often convenient to define G by setting $Q_{zz} = 1$ in a fully oriented system. At this stage we can make the following remarks.

1. The choice of the magnetic response as a starting point is a pure matter of convention; we might as well have used another static response function such as the electric polarizability or the dielectric constant $\epsilon_{\alpha\beta}$.

Another possibility would be to define an order parameter through the dynamic dielectric tensor $\epsilon_{\alpha\beta}(\omega)$ at some standard frequency ω such as the yellow D-line of sodium. This has the advantage of being directly related to the refractive indices, which are easily and accurately obtained.

However, we prefer to define Q through the magnetic susceptibility χ , because the relation between χ and molecular properties is well understood whereas the relation between $\epsilon_{\alpha\beta}$ and molecular properties is much more obscure: we will come back to this point later.

2. Our definition of an order parameter $Q_{\alpha\beta}$ covers a wider class of liquid crystals than simple nematics. When the axes α, β are chosen properly to diagonalize the symmetric matrix Q , the most general structure is

$$Q_{\alpha\beta} = \begin{vmatrix} Q_1 & 0 & 0 \\ 0 & Q_2 & 0 \\ 0 & 0 & -(Q_1 + Q_2) \end{vmatrix}. \quad (2.33)$$

This corresponds to a ‘biaxial nematic’ already described in terms of the S matrix. In usual (uniaxial) nematics the diagonal form simplifies to

$$Q_{\alpha\beta} = G \begin{vmatrix} \frac{1}{3}(\chi_{\perp} - \chi_{\parallel}) & 0 & 0 \\ 0 & \frac{1}{3}(\chi_{\perp} - \chi_{\parallel}) & 0 \\ 0 & 0 & \frac{2}{3}(\chi_{\parallel} - \chi_{\perp}) \end{vmatrix} \quad (2.34)$$

as is easily seen from eqn (2.31). It is the structure of the thermodynamic free energy as a function of $Q_{\alpha\beta}$ that decides whether the optimum $Q_{\alpha\beta}$ is of the form (2.33) or (2.34), i.e. whether we have a uniaxial or a biaxial nematic.

2.1.3 Relation between microscopic and macroscopic approaches

When the molecules may be approximately taken as rigid, we might hope to find a simple connection between the macroscopic tensors $\chi_{\alpha\beta}$ or $\epsilon_{\alpha\beta}$ and

the microscopic quantities $S_{ij}^{\alpha\beta}$ introduced in eqn (2.7). In fact, our level of knowledge is not at all the same for χ as for ϵ .

2.1.3.1 Magnetic susceptibilities

Since the magnetic couplings between neighbouring molecules is very small, $\chi_{\alpha\beta}$ is, to a reasonable approximation, simply a sum of individual molecular responses. Let us call A_{ij} the magnetic polarizability tensor of one molecule, referred to the molecular frame ($i, j = \mathbf{a}, \mathbf{b}, \mathbf{c}$). Then, from the transformation rule of tensors,

$$\chi_{\alpha\beta} = c \sum_{ij} A_{ij} \langle i_\alpha j_\beta \rangle$$

where c = number of molecules cm⁻³. Using the definition (2.7) the anisotropic part of χ is seen to be

$$\chi_{\alpha\beta} - \frac{1}{3}\delta_{\alpha\beta}\chi_{\gamma\gamma} = cA_{ij}S_{ij}^{\alpha\beta}. \quad (2.35a)$$

The temperature dependence of the coefficient A_{ij} is expected to be weak. Thus, in principle, the A_{ij} may be derived from a study of the diamagnetism in the crystalline phase (assuming that the molecular orientations in this phase are known). The $S_{ij}^{\alpha\beta}$ can be simplified according to the rules of eqns (2.9) and (2.10). It is interesting to compare the experimental data on $\chi_{\alpha\beta}$ with the predicted values (2.35a) using the order parameters S_{ij} derived from NMR measurements. This has been carried out for PAA by Saupe and Maier [10]. They use a simplified model with uniaxial rods, in which case eqn (2.35a) reduces to

$$\chi_{\parallel} - \chi_{\perp} = c(A_{\parallel} - A_{\perp})S(T). \quad (2.35b)$$

The resulting values for $S(T)$ do show a temperature dependence very similar to those that are derived from NMR data.

2.1.3.2 Dielectric constants, refraction indices, etc.

The theory linking this type of quantity to the order parameters S_{ij} or S is in a much less satisfactory state, since the effective electric field seen by one molecule is a superposition of the field due to external sources, plus the field due to all other dipoles. The latter contribution is large; in the standard theory of dielectric response in isotropic dense media, it is included approximately in the form of a Lorentz field.

However, in liquid crystals there is no clear-cut way of extrapolating this procedure. As already stated, even in the simplest cases the dielectric response does not depend only on the angular distribution function f_a , but involves a correlation function $g(\mathbf{0}, \mathbf{a}|\mathbf{r}, \mathbf{a}')$ for two molecules, as a function of their relative distance \mathbf{r} and orientation (\mathbf{a} and \mathbf{a}'). All the approximations that have been proposed in the literature to relate S and $\epsilon_{\parallel} - \epsilon_{\perp}$ involve arbitrary

assumptions about the correlation function g . Thus, the values of $S(T)$ derived from refractive index data may be slightly incorrect.

Once calibrated at a given temperature, the different techniques for measuring S give fairly comparable results (Fig. 2.3). The absolute differences have been discussed in terms of the ordering matrix of a locally biaxial molecule [22]. They rarely exceed 10 per cent.

2.2 STATISTICAL THEORIES OF THE NEMATIC ORDER

The statistical mechanics of liquids is difficult; the statistical mechanics of nematics is still worse! Even for the simplest physical models, no exact solution has been worked out. We shall review but briefly here the approximate descriptions that are commonly employed.

2.2.1 Mean-field calculations for hard rods and platelets

2.2.1.1 *The Onsager approach*

As discussed in Chapter 1, we can prepare solutions of hard-rod macromolecules with well defined length L and diameter D (e.g. tobacco mosaic virus). Onsager in 1949 [23] discussed the statistics of such systems, with the following assumptions.

1. The only forces of importance correspond to steric repulsion; the rods cannot interpenetrate each other.[†]
2. The volume fraction $\Phi = c \cdot \frac{1}{4}\pi LD^2$ (c = concentration of rods) is much smaller than unity.
3. The rods are very long ($L \gg D$). It will turn out in practice that the values of Φ of interest near the isotropic nematic transition are such that $\Phi L/D \sim 4$. Thus requirements 2 and 3 are, in fact, linked.

To sketch Onsager's derivation, let us first start from the more familiar case of a dilute gas of hard spheres (concentration c , radius r , $cr^3 \ll 1$). Here the free energy (per sphere) has the form [24]

$$F = F_0 + k_B T \left\{ \log c + \frac{1}{2} c \beta_1 + O(c^2) \right\} \quad (2.36)$$

where F_0 is an additive constant, β_1 is the excluded volume (i.e. the volume that is not allowed for the centre of sphere '1' when sphere '2' is fixed at the origin), and $O(c^2)$ means terms of order of c^2 . Since the centres cannot come

[†] The effect of Coulomb repulsion between charged rods could also be included if desired; as shown by Onsager, it essentially amounts to an increase in the effective diameter of the rods.

closer than a distance $2r$,

$$\beta_1 = \frac{4}{3}\pi(2r)^3.$$

Let us now go to our system of hard rods. Here, we must specify not only the overall concentration c , but also the angular distribution of the rods; let us call $(\mathbf{c} f_{\mathbf{a}} d\Omega)$ the number of rods per unit volume pointing in a small solid angle $d\Omega$ around a direction labelled by the unit vector \mathbf{a} . Note incidentally that the sum of these solid angles overall must give the total concentration c , i.e.

$$\int f_{\mathbf{a}} d\Omega = 1. \quad (2.37)$$

The free energy is now given by a natural extension of eqn (2.36), namely

$$F = F_0 + k_B T \left(\int f_{\mathbf{a}} \log(4\pi f_{\mathbf{a}} c) d\Omega + \frac{1}{2} c \int \int f_{\mathbf{a}} f_{\mathbf{a}'} \beta_1(\mathbf{aa}') d\Omega d\Omega' \right) + O(c^2). \quad (2.38)$$

The second term in eqn (2.38) describes the drop in entropy associated with molecular alignment (i.e. a non-constant f). The third term describes the excluded volume effects; $\beta_1(\mathbf{aa}')$ is the volume excluded by one rod in direction \mathbf{a} as seen by one rod in direction \mathbf{a}' . The calculation of β_1 is simple for the long rods where end effects are ignored and is explained in Fig. 2.5. The result is

$$\beta_1 = 2L^2 D |\sin \gamma| \quad (L \gg D) \quad (2.39)$$

where γ is the angle between \mathbf{a} and \mathbf{a}' .

It must be emphasized that eqn (2.38), limited to order c , represents an approximation of the ‘mean-field’ type: correlations between different rods are not taken into account.

We can obtain a self-consistent equation for the distribution function $f_{\mathbf{a}}$ by specifying that the free energy (2.38) is a minimum for all variations of $f_{\mathbf{a}}$ that satisfy the constraint (2.37). This amounts to writing

$$\delta F = k_B T \lambda \int \delta f_{\mathbf{a}} d\Omega \quad (2.40)$$

where λ is an unknown Lagrange multiplier and gives the self-consistent equation

$$\log(4\pi f_{\mathbf{a}}) = \lambda - 1 - c \int \beta_1(\mathbf{aa}') f_{\mathbf{a}'} d\Omega'. \quad (2.41)$$

λ is then determined by the normalization condition (2.37).

Equations (2.39) and (2.41) show that the concentration c enters the problem only through the combination $cL^2 D = \text{const} \times \Phi L/D$.

Equation (2.41) always has an ‘isotropic’ solution ($f_{\mathbf{a}} = 1/4\pi$, independent of \mathbf{a}) but, if $\Phi L/D$ is large enough, it may also have anisotropic solutions,

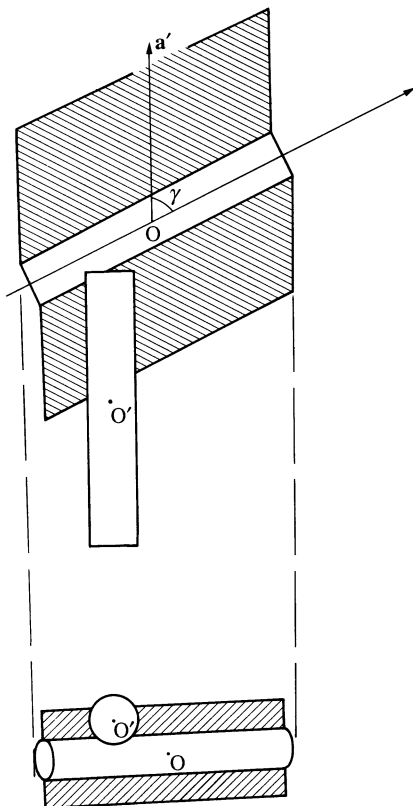


Fig. 2.5

describing a nematic phase. It is difficult to solve the non-linear integral equation (2.41) exactly. Onsager used a variational method, based on a trial function of the form

$$f_{\mathbf{a}} = (\text{const}) \cosh(\alpha \cos \theta) \quad (2.42)$$

where α is a variational parameter, and θ is the angle between \mathbf{a} and the nematic axis. (The constant factor is chosen to normalize f according to eqn (2.37).) In the region of interest, α turns out to be large (~ 20) and the function f is strongly peaked around $\theta = 0$ and $\theta = \pi$. The order parameter is

$$\begin{aligned} S &= \frac{1}{2} \int f_{\mathbf{a}} (3 \cos^2 \theta - 1) \sin \theta \, d\theta \\ &\simeq 1 - 3/\alpha \quad (\alpha \gg 1). \end{aligned} \quad (2.43)$$

Minimizing the energy F (eqn (2.38)) with respect to α , one obtains a function $F(c)$ showing a first-order phase-transition from isotropic ($\alpha = 0$) to nematic

($\alpha \geq 18.6$). (We shall come back to the fundamental symmetry reasons that make the transition first-order later in this chapter.) The volume fraction Φ occupied by the rods, in the nematic phase, just at the transition point, is

$$\Phi_{\text{nema}}^c = 4.5D/L. \quad (2.44)$$

At the same point, the value of Φ for the isotropic phase (in equilibrium with the nematic phase) is significantly smaller

$$\Phi_i^c = 3.3D/L.$$

Note that Φ_{nema}^c and Φ_i^c are independent of T in this model: hard rods are an ‘athermal’ system.

Of particular interest is the value of the order parameter S_c in the nematic phase just at the transition. This turns out to be quite high ($S_c \simeq 0.84$). Thus the Onsager solution leads to a rather abrupt transition between a strongly ordered nematic and a completely disordered, isotropic phase.

Problem. Discuss the existence of a nematic phase for a system of thin hard disks (radius of the disk b much larger than its thickness e) in the Onsager approximation.

Solution. Derive first the excluded volume $\beta_1(\gamma)$ for two disks with their plane making an angle γ . Define axes xyz such that the first disk is centred at the origin and is in the x, y -plane (Fig. 2.6).

The direction of intersection of the planes of the two disks parallel to Oy . The centre O' of the second disk is at an elevation z above the x, y -plane. The vector linking the point of contact c to O' has the components

$$\begin{aligned} \xi &= z/\tan \gamma, \\ \eta &= \sqrt{(b^2 - z^2/\sin^2 \gamma)}, \\ z. \end{aligned}$$

The intersection of the excluded volume for O' by a plane $z = \text{constant}$ is then made of two half-circles (derived by the translations (ξ, η) and $(\xi, -\eta)$ from the disk O) plus a rectangular region of dimensions $2b$ and 2η (see Fig. 2.6). The area inside this curve is $\pi b^2 + 4\eta b$ and the excluded volume is

$$\begin{aligned} -\beta_1(\gamma) &= 2 \int_0^{b \sin \gamma} \{\pi b^2 + 4\eta b\} dz \\ &= 4\pi b^3 \sin \gamma. \end{aligned}$$

Thus, the dependence of β_1 on γ is identical in form to eqn (2.23) and the Onsager results can be transposed immediately, by performing the substitution

$$L^2 D \rightarrow 2\pi b^3.$$

Thus, we expect to have a transition from isotropic to nematic, with the concentrations

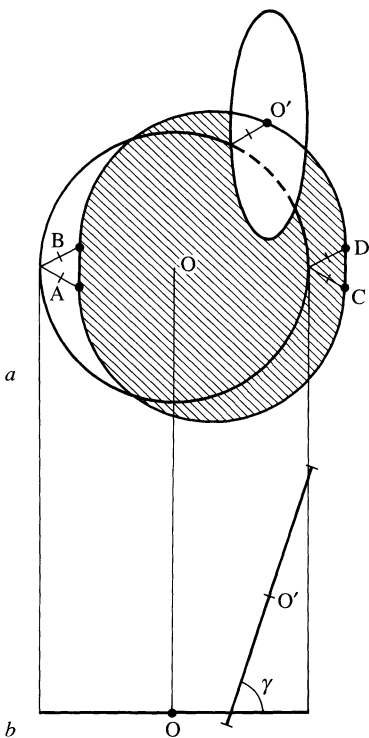


Fig. 2.6

of the two phases at equilibrium given by

$$b^3 c_{\text{nema}} = (2/\pi^2) \times 4.5 = 0.9,$$

$$b^3 c_i = (2/\pi^2) \times 3.3 = 0.67.$$

There are in fact a few observations suggesting the existence of ‘stacked phases’ for certain flat dye molecules [25]. As already quoted in Chapter 1, nematics made of disk-like molecules have been synthesized [26]; they are thermal systems, the properties of which cannot be directly compared to the Onsager model. Extended calculations for ellipsoids can be found in reference 27.

2.2.1.2 The Flory calculation

A slightly different mean-field calculation for the hard-rod problem has been used by Flory [28]. He describes a rod as a set of points inscribed on a lattice (see Fig. 2.7(a)). The number x of points on each rod plays the role of the parameter L/D in the preceding discussion. To describe a ‘tilted’ rod, Flory uses the picture of Fig. 2.7(b) where the rod is replaced by a family of smaller units, each unit still being aligned along the same lattice direction. One attractive feature of the model is that, when all rods are parallel ($S = 1$),

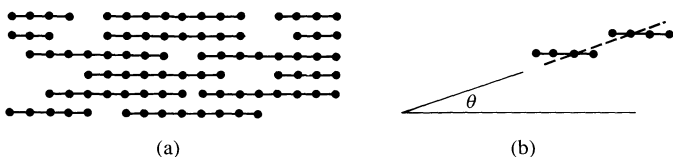


Fig. 2.7. Flory's lattice model for long rods: (a) conformation where all rods are parallel (the partition function for this case can be calculated exactly); (b) approximate method to describe tilted molecules.

the partition function can be calculated exactly. The approximate form of the free energy derived for $S < 1$ becomes the exact result for $S = 1$. Thus the Flory approach is useful for a dense, highly ordered phase. On the other hand, his treatment of the angular function f_a is rather crude, and this limits accuracy in the isotropic phase. Thus the Onsager and Flory calculations supplement each other but neither of them can be entirely reliable over the whole range of concentration c .

Numerically, Flory obtains higher values for the volume fractions at the transition

$$\Phi_{\text{nema}}^c \sim 12.5D/L, \quad \Phi_i^c \sim 8D/L \quad (L/D \gtrsim 10).$$

The critical value of the order parameter S^* is not quite meaningful, in view of the approximations in $f(\theta)$, but it turns out to be even larger than in the Onsager solution.

In Fig. 2.8 we show some experimental data on $\Phi^c(L/D)$ for polybenzyl-L-glutamate, in typical solvents. There is a decrease of Φ^c with L/D corresponding roughly to an inverse law. The coefficient is not too meaningful, because various complications are involved with the physical system.

1. van der Waals attractions between rods, and other possible effects on contact [30].
2. Polydispersity. If the rods are not uniform in length, the shorter ones are much more disordered than the long ones. This might have some effect on the equilibrium curves.

2.2.1.3 Strict lattice models

In the models of Onsager and Flory, the molecules have a continuous distribution of orientations. This corresponds to the actual physical situation. However, for purposes of calculation, it is tempting to work with a system where the number of allowed orientations is finite.

This is again obtained with a lattice where each molecule occupies a row of p consecutive points. The difference from the Flory model is that the molecules can point only in the directions defined by the nearest-neighbour vector (three directions for a simple cubic lattice, five directions for a

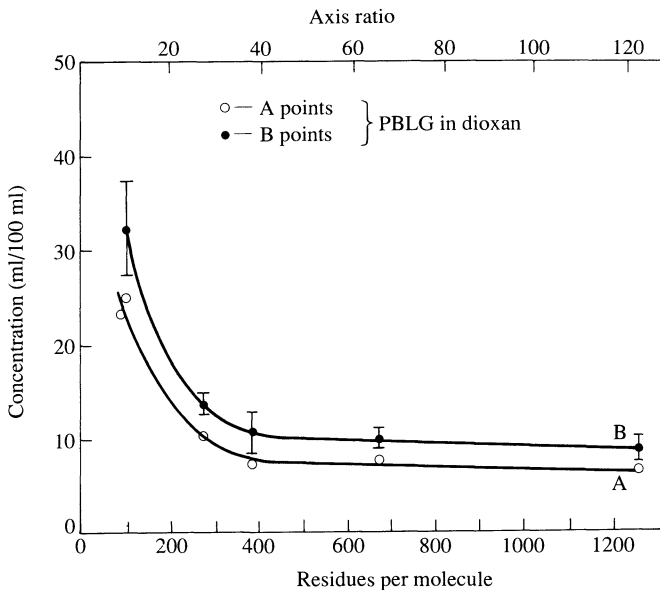


Fig. 2.8. Critical volume fraction Φ^0 for a suspension of long rods: poly(benzyl-L-glutamate) in dioxan. N is the number of peptide units per rod. The length L is estimated to be $N \times 1.5 \text{ \AA}$. The filled circles give Φ_{nema}^c and open circles give Φ_i^c . (After reference 29.)

face-centred cubic lattice). Figure 2.7(a) is allowed, but Fig. 2.7(b) is now eliminated.

In the mean-field approximation the statistics of such systems are not too hard to work out. At low densities the system is isotropic. At higher densities one direction is preferred (nematic order). A review of the results, and of some extensions of the method, has been given by M. Cotter and co-workers [31]. The qualitative features of the transition do not differ very much from what we have described above. But the strict lattice models suffer from at least two conceptual shortcomings.

1. The reduction of the continuous rotation group to a discrete point group destroys some important features of the fluctuations; this point will become clearer later, when we discuss light scattering by nematics (Chapter 3).
2. It is not quite certain that such a lattice model, even for a large p (long molecule), will actually lead to a transition from isotropic to nematic at high enough densities. The two-dimensional problem with dimers ($p = 2$) is known to show no ordering, even at the maximum (close packed) density [32]. The trouble may, in fact, be more general: for any p , at the close-packed density, the nematic conformation of Fig. 2.7(a) is not the

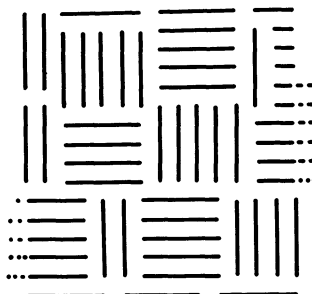


Fig. 2.9. One possible arrangement for close-packed molecules with purely repulsive forces on a lattice; in this arrangement there is no long-range nematic order. The molecules are grouped in small ‘disordered domains’.

only one allowed in a strict lattice model. This is explained in Fig. 2.9, which shows a typical ‘disordered domain’ configuration.†

A detailed examination of these disordered domains is also useful on more general grounds. With purely repulsive, hard-core interactions the domains have a good chance of being present, independently of the details of the model. This ‘hesitation’ between nematic and disordered configurations may, in fact, explain why higher virial expansions converge poorly for hard-rod systems.

Lattice models of systems made up of plates that are neither very square nor very rod-like [33], or of mixtures of plate-like and rod-like molecules [34], show the existence of a first-order isotropic–uniaxial nematic and a subsequent (i.e. at higher densities) uniaxial nematic–biaxial nematic transition. The existence of an isolated point at which a direct continuous isotropic–biaxial nematic phase change occurs is also found. These features will be described in Section 2.3.3.

2.2.2 Mean-field theory with S^2 interaction

2.2.2.1 Uniaxial nematics (Maier–Saupe)

With long, hard rods in three dimensions, we have a model that appears to lead to a nematic–isotropic transition. But this transition differs from the observations on actual thermotropic systems in many respects: the transition density is too low, and the jump in density at the transition is too high; the order parameter S_c at threshold is too high. Like all models involving only infinite repulsive forces, the system is ‘athermal’, so that the transition density, for example, is independent of temperature.

Clearly in the present situation we are still in need of a very simple

† I am indebted to J. Vieillard-Baron for pointing out this effect.

phenomenological theory, applicable independently on the detailed form of the interactions. This is the analogue, for nematics, of the ‘molecular field approximation’ introduced by P. Weiss for ferromagnets. Such a theory was worked out in detail by Maier and Saupe [35].

In general, to specify the orientation of the molecules, we would require a distribution function involving three Euler angles. However, we decide to ignore the details of the molecular structure. We assume that each molecule has a well defined long axis \mathbf{a} (with polar angles θ and ϕ) and we discuss only the distribution function $f(\theta, \phi)$ for the long axis.

The next step is to introduce a convenient thermodynamic potential, which will be a minimum in the equilibrium state. Here, since we work in practice at fixed pressure p rather than at fixed volume (and since our liquids do show some change in volume with temperature), we find it convenient to use the free enthalpy per molecule (or chemical potential) G . G depends on the angular distribution function $f_{\mathbf{a}}$

$$G(p, T) = G_i(p, T) + k_B T \int f_{\mathbf{a}} \log(4\pi f_{\mathbf{a}}) d\Omega + G_1(p, T, S) \quad (2.45)$$

where G_i is the free enthalpy of the isotropic phase. The second term, as in eqn (2.38), reflects the decrease in entropy due to an anisotropic angular distribution. The last term G_1 describes the effects of intermolecular interactions. We assume that G_1 is quadratic in S

$$G_1 = -\frac{1}{2}U(p, T)S^2. \quad (2.46)$$

The value of G_1 is decreased when S increases; thus U is positive. In the original presentation of Maier and Saupe [35] it was assumed that U is due entirely to van der Waals forces and is temperature-independent. In actual fact contributions from the steric repulsions (as in the Onsager calculation)[†] may be non-negligible and they do depend on T ; the overall temperature dependence may be rather complex.

We can minimize G with respect to all variations of f that satisfy the constraint (2.37). The variation equation is

$$\delta G = \lambda \int \delta f(\theta, \phi) d\Omega. \quad (2.47)$$

From eqn (2.46) the variation of the term G_1 has the form

$$\delta G_1 = -US \delta S = -US \int \frac{1}{2}(3 \cos^2 \theta - 1) \delta f(\theta, \phi) d\Omega.$$

[†] An example of a derivation involving forces other than of the van der Waals type may be found in reference 36.

Thus

$$\delta G = \int \delta f [k_B T \{ \log(4\pi f) + 1 \} - US(3 \cos^2 \theta - 1)/2] d\Omega$$

and eqn (2.47) gives

$$\log(4\pi f) = \lambda - 1 + (US/k_B T)(3 \cos^2 \theta - 1)/2. \quad (2.48)$$

The (correctly normalized) resulting form of the distribution function is

$$f(\theta) = \exp(m \cos^2 \theta)/4\pi Z \quad (2.49)$$

with

$$m = \frac{3}{2}(US/k_B T). \quad (2.50)$$

The normalization constant Z is defined by

$$Z = \int_0^1 e^{mx^2} dx \quad (2.51)$$

(and may be expressed in terms of error functions).

We must now write a self-consistency condition for S using eqn (2.2)

$$\begin{aligned} S &= -\frac{1}{2} + \frac{3}{2} \langle \cos^2 \theta \rangle \\ &= -\frac{1}{2} + \frac{3}{2Z} \int_0^1 x^2 e^{mx^2} dx, \\ S &= -\frac{1}{2} + \frac{3}{2} \frac{\partial Z}{Z \partial m}. \end{aligned} \quad (2.52)$$

Equations (2.50) and (2.52) may be solved graphically, as shown in Fig. 2.10, to obtain the values $S(T)$ and $m(T)$ relative to a certain temperature T . When $k_B T/U$ is small, there are two solutions for (2.50) and (2.52) which correspond to local minima in $G(S)$. One is associated with $S = 0$ and would correspond to an isotropic fluid. The other one corresponds to point M on Fig. 2.10, and described a nematic phase.[†] To decide which solution is realized physically, we must compare the values of G associated with both minima. When T is below a temperature T_c defined by

$$\frac{k_B T_c}{U(T_c)} = 4.55, \quad (2.53)$$

the nematic phase is the stable one. For higher temperatures, the isotropic fluid is stable; there is a first-order transition at $T = T_c$. The order parameter

[†] There may exist, in certain temperature ranges, other solutions to eqns (2.50) and (2.52) than those associated with the points O and M on Fig. 2.10 (e.g. point N). But they correspond to a maximum of G , not to a minimum.

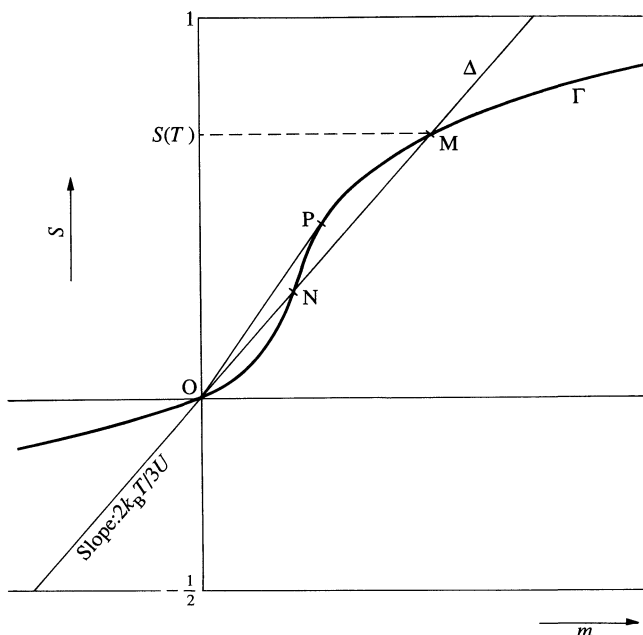


Fig. 2.10. Graphical solution for the self-consistency equation giving the order parameter $S(T)$ in the Maier-Saupe approximation. The curve Γ is defined by eqns (2.52) and (2.51). The straight line Δ is derived from eqn (2.50). When $T < T_c$, Δ intersects Γ at the origin, at the point M (and also eventually at a third point N , of lower S value than M). The point M gives the physical state of minimum free energy G . The point N would correspond to an unstable state (local maximum in G).

for T just below T_c is

$$S_c \equiv S(T_c) = 0.44.$$

Thus, with the expression (2.45) for the chemical potential, the value of S_c must be the same for all nematic-isotropic transitions. In particular, for a given compound, if we shift the transition point T_c by applying pressure, we should retain the same value of S_c ; this appears to be verified by NMR experiments under pressure [15, 37]. It must also be emphasized that the amount of order at T_c is much smaller in the Maier-Saupe theory than in the Onsager model ($S_c \sim 0.44$ instead of 0.84).

To reach a definite prediction on the temperature variation of S below T_c we must make an assumption concerning the temperature dependence of $U(T)$. As explained in eqn (2.46), this dependence is non-trivial. If we assume with Maier and Saupe that U is essentially independent of T , the order

parameter becomes a universal function of T/T_c . This function is plotted in Fig. 2.3 together with some experimental points.[†] There is good qualitative agreement but, as pointed out in Section 2.1.1.5, quantitative agreement is less satisfactory particularly for higher moments such as P_4 .

Difficulties are clearly illustrated if we use an independent experiment to determine the temperature variation of U . Consider for instance the heat of transition ΔH . This can be computed from the equation linking the entropy Σ to the chemical potential G given in eqn (2.45), $\Sigma = -(\partial G / \partial T)_p$.

Writing that the G values for both phases are equal at the transition point, one arrives at

$$\Delta H = T_c \Delta \Sigma = \frac{1}{2} S_c^2 \left\{ U - T_c \left(\frac{\partial U}{\partial T} \right)_p \right\}. \quad (2.54)$$

At $T = T_c$, U is given by eqn (2.53) and we have

$$T_c \left(\frac{\partial U}{\partial T} \right)_p \Big|_{U=1} = 1 - \frac{2\Delta H}{4.55 S_c^2 k_B T_c}.$$

This is approximately $\frac{2}{3}$ for PAA at atmospheric pressure; thus the temperature dependence of U near T_c is strong, and the agreement obtained when neglecting it may be, in fact, somewhat accidental.[‡]

The discrepancy may come from an intrinsic dependence of U on T , as well as a failure of the mean-field approximation near T_c . This last possibility is discussed in detail in Section 2.3.4.

2.2.2.2 Biaxial nematics

The natural generalization of (2.49) when non-cylindrically symmetric molecules are considered is [39]

$$f = \exp(+nS^{\alpha\beta}\bar{S}^{\alpha\beta}) = \exp(-W/kT), \quad (2.55)$$

in which $n = U(p, T)/kT$ is a measure of the interaction of the test molecule with its neighbours, mimicked by the mean field $\bar{S}^{\alpha\beta}$. In the frame of reference (x, y, z) for which $\bar{S}^{\alpha\beta}$ is diagonal,

$$\bar{S}^{\alpha\beta} = \begin{pmatrix} -\frac{1}{2}(S + \eta) & 0 & 0 \\ 0 & -\frac{1}{2}(S - \eta) & 0 \\ 0 & 0 & S \end{pmatrix}. \quad (2.56)$$

[†] Many other studies derived $S(T)$ from refractive index measurements. As pointed out earlier in this chapter, the relationship between birefringence and S involves delicate questions on dipole-dipole interactions in a dense medium; thus the ‘experimental’ $S(T)$ curves already involve some approximations.

[‡] A detailed discussion of thermodynamic derivatives near T_c has been given by R. Alben [38].

In the molecular frame of reference (i, j, k) in which $S^{\alpha\beta}$ is diagonal,

$$S^{ij} = \begin{pmatrix} -\frac{1}{2}(1+a) & 0 & 0 \\ 0 & -\frac{1}{2}(1-a) & 0 \\ 0 & 0 & 1 \end{pmatrix}. \quad (2.57)$$

Note that in (2.56) $S^{\alpha\beta}$ is a function of the direction cosines which transform i, j, k in x, y, z . Rectangular platelets would typically give interactions of that type.

Such a distribution function results from the existence of an angular interaction energy between molecules I and J of the type

$$W_{IJ} = -U' S_I^{\alpha\beta} S_J^{\alpha\beta}. \quad (2.58)$$

This expression is, of course, oversimplified, but its merit is to show unambiguously the trend towards biaxiality. Indeed, at low enough temperature, the equilibrium state is obtained by a simple minimization of W_{IJ} (i.e. maximization of $S_I^{\alpha\beta} S_J^{\alpha\beta}$). From the Schwartz inequality we know that

$$\frac{W^2}{U'^2} \leq (S_I^{\alpha\beta})^2 (S_J^{\alpha\beta})^2. \quad (2.59)$$

Equality holds when the eigendirections of $S_I^{\alpha\beta}$ and $S_J^{\alpha\beta}$ coincide. Thus the ground state of a system described by W_{IJ} is biaxial and, as remarked by Freiser, any reasonable statistical treatment should find a stable phase at low enough temperature. Of course the actual observation of biaxiality may be pre-empted by the occurrence of other transitions.

Developing this example a little further allows us to introduce the expansion to be used in the next section, and to reveal its characteristics.

The self-consistency condition now reads

$$\bar{S}^{\alpha\beta} = \frac{1}{Z} \int S^{\alpha\beta}(\Omega) \exp(nS^{\alpha\beta}(\Omega)\bar{S}^{\alpha\beta}) d\Omega \quad (2.60)$$

where Ω stands for the Euler angles that define the direction cosines, and

$$Z = \int \exp(nS^{\alpha\beta}(\Omega)\bar{S}^{\alpha\beta}) d\Omega. \quad (2.61)$$

The self-consistency condition (2.60) is obtained by minimization of the chemical potential

$$G(p, T) = G_1(p, T) + \frac{U'}{2} \bar{S}^{\alpha\beta} \bar{S}^{\alpha\beta} - kT \ln Z. \quad (2.62)$$

At this point, it is convenient to expand $\ln Z$ in a Taylor series with respect

to n

$$\begin{aligned} \ln Z(n) = \ln Z(0) + n \frac{\partial \ln Z}{\partial n}(n=0) + \frac{n^2}{2!} \frac{\partial^2 \ln Z}{\partial n^2}(n=0) \\ + \frac{n^3}{3!} \frac{\partial^3 \ln Z}{\partial n^3}(n=0) + \dots \end{aligned} \quad (2.63)$$

This leads to an expansion for G , the minimization of which gives the equilibrium state

$$G = G_0 + \frac{1}{2}A(T)\bar{S}^{\alpha\beta}\bar{S}^{\alpha\beta} + \frac{1}{3}B(T)\bar{S}^{\alpha\beta}\bar{S}^{\beta\delta}\bar{S}^{\delta\alpha} + \frac{1}{4}C(T)(\bar{S}^{\alpha\beta}\bar{S}^{\alpha\beta})^2 + \dots \quad (2.64)$$

It is important to remark that the coefficients $\partial^k \ln Z / \partial n^k$ are just numbers that cannot depend on any frame of reference

$$\frac{\partial^k \ln Z}{\partial n^k} \sim \underbrace{\bar{S}^{\alpha\beta} \dots \bar{S}^{\gamma\delta}}_{k \text{ times}} \int \underbrace{S^{\alpha\beta}(\Omega) \dots S^{\gamma\delta}(\Omega)}_{k \text{ times}} d\Omega. \quad (2.65)$$

Note further that there is no angle-dependent weighting term in (2.65): a fully isotropic integration is performed. This means that only tensorial invariants of $S^{\alpha\beta}$ can enter the coefficient. As a result, combinations in the $\bar{S}^{\alpha\beta}$ that are not fully invariant are multiplied by zero, and can also be omitted. Thus the expansion involves products of separate invariants of $S^{\alpha\beta}$ and $\bar{S}^{\alpha\beta}$ of the same order.

For example, the second-order and third-order ones necessarily involve the products (respectively)

$$\left(\frac{3+a^2}{2} \right) \left(\frac{3S^2 + \eta^2}{2} \right), \quad \text{i.e.} \quad (S^{\alpha\beta}S^{\alpha\beta})(\bar{S}^{\gamma\delta}\bar{S}^{\gamma\delta}) = \frac{3+a^2}{2} \bar{S}^{\gamma\delta}\bar{S}^{\gamma\delta}$$

and

$$\frac{3}{4}(1-a^2) \cdot \frac{3}{4}S(S^2 - \eta^2), \quad \text{i.e.} \quad (S^{\alpha\beta}S^{\beta\gamma}S^{\gamma\alpha})(\bar{S}^{\delta\mu}\bar{S}^{\mu\nu}\bar{S}^{\nu\delta}) = \frac{3}{4}(1-a^2)\bar{S}^{\delta\mu}\bar{S}^{\mu\nu}\bar{S}^{\nu\delta}.$$

It turns out that, because we are dealing with symmetric traceless tensors, all higher-order invariants may be expressed as a product of the two shown in the above formulae. For example, there is only one fourth-order invariant

$$\left(\sim \left(\frac{3+a^2}{2} \right)^2 (\bar{S}^{\gamma\delta}\bar{S}^{\gamma\delta})^2 \right),$$

one fifth-order

$$\left(\sim \left(\frac{3+a^2}{2} \right) \frac{3}{4} (1-a^2) \bar{S}^{\alpha\beta}\bar{S}^{\alpha\beta}\bar{S}^{\delta\mu}\bar{S}^{\mu\nu}\bar{S}^{\nu\delta} \right),$$

but two sixth-order

$$\left(\sim \left[\alpha \left(\frac{3+a^2}{2} \right)^3 + \beta \left(\frac{3}{4} (1-a^2) \right)^2 \right] [\alpha (\bar{S}^{\alpha\beta} \bar{S}^{\alpha\beta})^3 + \beta (\bar{S}^{\delta\mu} \bar{S}^{\mu\nu} \bar{S}^{\nu\delta})^2] \right).$$

The actual value of the coefficients is not very important. The main points are as follows.

- The coefficient A of the second-order term of G is positive at ‘high’ temperature and negative at ‘low’ temperature. It changes sign at

$$T_0 = \frac{3+a^2}{10} U/k_B.$$

(Note the similarity with (2.53), but pay attention to the fact that T_0 is not T_c).

- The coefficient of the third-order term is negative for $a^2 < 1$ and positive for $a^2 > 1$; it vanishes for $a^2 = 1$ (so does the coefficient of the fifth-order term. This is a particularity of the model linked to the simplicity of expression (2.55).)

- Other coefficients, C, E (of fourth, sixth order, etc.) are regular.

We postpone the discussion of the equilibrium states to the next chapter.

Let us just remark that for $a^2 = 1$, eqn (2.64) reads [with $\delta = \frac{3S^2 + \eta^2}{2}$, $\Delta = \frac{3}{4}S(S^2 - \eta^2)$]

$$G = G_0 + \frac{A}{2} \delta + \frac{C}{4} \delta^2 + \frac{E}{6} \Delta^2 + \dots \quad (2.66)$$

Minimizing with respect to the independent variables δ and Δ , we obtain immediately

For $T > T_0$ $\delta = \Delta = 0$, i.e. $S = \eta = 0$ isotropic phase,

For $T < T_0$ $\delta = -\frac{A}{c}$, $\Delta = 0$ i.e. $S^2 = \eta^2 = -\frac{A}{2c}$ biaxial phase.

Thus, when $a^2 = 1$ (i.e. when molecules have the appropriate biaxiality), this model predicts a direct continuous transition from the isotropic to a biaxial state.

Mixtures of rod-like and plate-like molecules are also expected to exhibit biaxial phases with similar treatments including excluded volume effects [40].

2.2.3 Computer calculations

All the calculations that have been presented up to now are of the ‘mean-field’ type; they neglect angular correlations between neighbouring

rods, which are certainly important at the actual physical densities and in particular near the transition point.

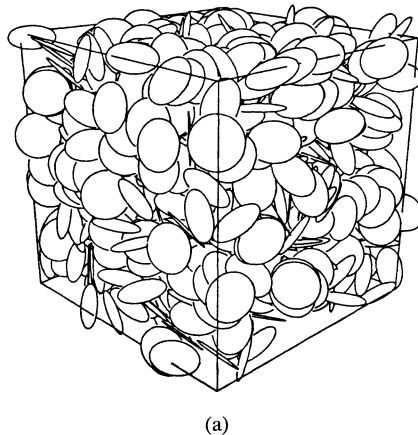
Direct computer calculations allow us to sample statistically allowed configurations, provided that the number of investigated particles is kept small enough and that simplifying assumptions are made concerning their shape and interactions laws. In Monte Carlo studies configurations are sampled with a weight proportional to their thermodynamical probability. In molecular dynamics, after an initial state is given, the system is allowed to evolve according to dynamical rules that have to be both simple and realistic. With this last technique dynamical properties can be obtained: for instance the role of molecular dipoles in self-diffusion has been studied in the vicinity of the isotropic–nematic transition [41]. However, the number of particles was too small to allow an accurate study of the transition itself. On the other hand the Monte Carlo technique allows us nowadays to consider systems of almost 10^3 particles [42b].[†] This is enough to obtain a reasonable description of the transition. The price is that we must work with simple objects and simple interaction laws. Fairly convincing results have been obtained with infinitely thin disks, interacting only via excluded volume effects (Fig. 2.11(a)).

In the limit of infinitely thin rods the Onsager theory becomes exact, since all virial coefficients higher than two vanish. This is not the case for infinitely thin disks and, thus, the influence of higher virial coefficients may be directly evidenced by the comparison of the Monte Carlo results and the Onsager theory. The transition discontinuities are found to be significantly smaller than with the mean-field approaches of Sections 2.2.1 and 2.2.2. For example, the density jump is found to be of the order of 2 per cent (26 per cent in the Onsager model), which is fairly close to the experimental results obtained with thermotropic systems; at the transition the order parameter is clearly smaller than in the Onsager, Flory, and Maier–Saupe models, but finite-size effects render an accurate determination difficult. Scaled particle theories [43], or virial expansions up to fifth order, are an improvement over simple mean-field calculations, but are inadequate close to the transition.

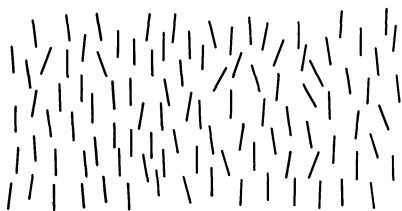
The distribution function may be evaluated. It has been shown that it can be expressed by the form (2.49), although only hard-core repulsions are considered. The $P_4(\cos \theta) = f(P_2(\cos \theta))$ dependence is the same as in the Maier–Saupe model. As a result, the discrepancy with experiment quoted in Section 2.1.1.5 cannot be blamed on fluctuations only, since they are treated correctly by the Monte Carlo technique.

At last, the phenomenological theory, which will be described in the next section, can also be tested. Being phenomenological, this theory should hold

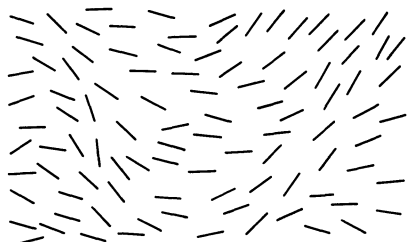
[†] In the early studies [42a] 170 ‘hard’ ellipses were already shown to undergo an isotropic–nematic transition in two dimensions. Problems linked to the absence of long-range order were, of course, out of reach.



(a)



(b)



(c)

Fig. 2.11. (a) Snapshot of a set of 800 hard disks just below the isotropic–nematic transition according to Eppenga and Frenkel [42b]. (b) Nematic phase. (c) Isotropic phase just above the clearing point I_c . In case (c) short-range order persists over distances $\zeta(T)$ much larger than the molecular size.

for thermotropic systems as well as for systems made of thin hard disks, provided that the variable T is replaced by the density ρ . Let us just anticipate that a free energy such as (2.64) will be introduced. In its mean-field version the coefficients B and C are assumed to be temperature-independent (as found in Section 2.2.2.2), and $A \propto (T - T^*)$. The Monte Carlo results indicate that $A \propto (\rho_c - \rho)$ (the accuracy of A does not seem to be sufficient to detect subtle deviations from this linear dependence, perhaps because of finite-size effects) and that B and C are strongly temperature-dependent. We will show in Section 2.3.4.2 how fluctuations can explain this result. Eventually the order parameter S is found to vary according to a law, $S \propto (\rho - \rho_c)^\beta$, with $\beta = 0.23 \pm 0.03$ in marked disagreement with mean-field calculations; again we postpone the discussion of this result to Section 2.3.4.2.

2.3 PHENOMENOLOGICAL DESCRIPTION OF THE NEMATIC-ISOTROPIC TRANSITION

2.3.1 Landau free energy above T_c

The statistical theories that we have described in the former section, suffer from different types of shortcomings, such as oversimplification of the intermolecular interactions, of the molecular structure, neglect of fluctuations (except for the Monte Carlo studies), etc. Yet, there is a need for correlating different experiments, sensitive to macroscopic properties. For that purpose, phenomenological theories, which can be constructed independently of the detailed nature of the interactions and of the molecular structure, are of much interest. Two different domains can be distinguished.

1. Below T_c the fluctuations of the magnitude S are weak, and the most spectacular effects are related to fluctuations in the *orientation* of the optical axis (Fig. 2.11(b)). This will be discussed in Chapter 3, after the introduction of continuum elasticity.
2. Just above T_c we have sizeable fluctuations both in magnitude and in orientation; they are described rather well by a simple (Landau-type) theory, which will be described qualitatively below.

If the discontinuities at T_c are small enough, the Landau theory may be expected to hold in a limited range below T_c . We will start with a mean-field analysis of the nematic-isotropic (N-I) free energy functional.

In the isotropic phase, there is no long-range order in the direction of alignment of the molecules; the tensor order parameter $Q_{\alpha\beta}$ vanishes on average. However, if we were to look closely enough at the molecules (Fig. 2.11(c)), we would see that, *locally*, they are still parallel to each other. This order persists over a certain characteristic distance $\xi(T)$, called the *coherence length*.

In a rough qualitative sense, in the isotropic phase (and in this phase only) one may speak of nematic ‘swarms’, i.e. small nematic droplets of size $\xi(T)$, the orientations of successive droplets being uncorrelated. This picture is qualitatively suggestive, but often leads to exponents in various physical laws (because it implies abrupt changes in orientation at the border between two swarms). To reach a more accurate description, it is useful to start from a continuum theory, where the free energy is expanded as a power series of the order parameter $Q_{\alpha\beta}$ and of its spatial derivatives. This approach ensures that the variations of Q are smooth. It is analysed in reference 44; a critical examination of experimental data on short-range order effects, comparing them to the continuum theory, is given in reference 45.

The main features that emerge are listed below. We shall discuss first the order of the transition.

For purely geometrical reasons, the nematic \rightleftharpoons isotropic transition must be of first order†; this was already recognized by Landau [46]. The argument may be summarized as follows: the free energy F may be expanded in powers of the order parameter, and the following terms occur (in the absence of external aligning fields \mathbf{H})

$$F = F_0 + \frac{1}{2}A(T)Q_{\alpha\beta}Q_{\beta\alpha} + \frac{1}{3}B(T)Q_{\alpha\beta}Q_{\beta\gamma}Q_{\gamma\alpha} + \frac{c(T)}{4}(Q_{\alpha\beta}Q_{\alpha\beta})^2 + O(Q^5). \quad (2.67)$$

(Summation over repeated indices is implied.) All these terms are invariant in respect to any rotation of the axes (x, y, z) as they should be.

\mathbf{Q} , which is symmetric and real, can always be diagonalized. It can thus be written in the proper frame of reference as

$$\mathbf{Q} = \begin{pmatrix} -\frac{q+\eta}{2} & 0 & 0 \\ 0 & -\frac{q-\eta}{2} & 0 \\ 0 & 0 & q \end{pmatrix} \quad (2.68)$$

where

$$\left. \begin{aligned} \delta &= Q_{\alpha\beta}Q_{\alpha\beta} = \frac{3q^2 + \eta^2}{2} \text{ is the second-order invariant} \\ \Delta &= Q_{\alpha\beta}Q_{\beta\gamma}Q_{\gamma\alpha} = \frac{3}{4}q(q^2 - \eta^2) \text{ is the third-order invariant.} \end{aligned} \right\} \quad (2.69)$$

and

The definitions are similar to those already used in Section 2.2.2.2 [34, 47]; note that they imply

$$\delta^3 \geq 6\Delta^2. \quad (2.70)$$

There is no linear invariant since $Q_{\alpha\alpha} = 0$. This ensures that the state of minimum F is a state of zero Q , that is to say, isotropic. It is very important to realize that there is a non-vanishing cubic term Δ . In the uniaxial case ($\eta = 0$), $\Delta > 0$ describes the alignment of molecules with their long axes on average parallel to the nematic c_∞ axis (optical axis); $\Delta < 0$ describes a physically distinct state in which the long axes are on average perpendicular to it. There is no reason for these two states to have the same free energy.

Note the similarity between (2.67) and (2.64), which we obtained in Section 2.2.2.2. Now, however, we have no *a priori* knowledge of the coefficients $A(T)$, $B(T)$, etc. but, in agreement with molecular theories, we postulate

† If we vary the pressure p , we have a certain transition line in the (p, T) diagram. All along this line the transition will be of first order, except possibly at one point. Fluctuation effects will be discussed in Section 2.3.4.2.

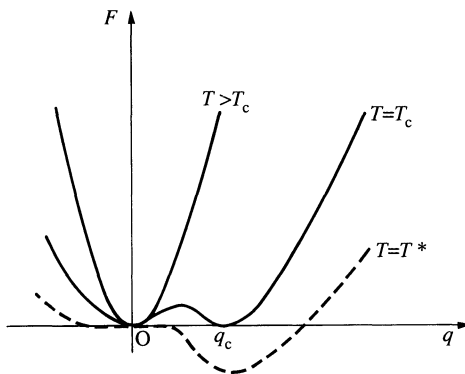


Fig. 2.12. Free energy as a function of order parameter for various temperatures. For $T > T_c$ the absolute minimum of GF corresponds to $q = 0$ (isotropic phase). For $T < T_c$ the minimum corresponds to $q \neq 0$ (nematic phase). For $T = T_c$ we can have coexistence of an isotropic phase and a nematic phase with a finite amount of order ($q = q_c$): the transition at T_c is of first order. The (lower) temperature T^* corresponds to the vanishing of the q^2 term in F . Below T^* the isotropic phase is completely unstable with respect to nematic ordering.

$A(T) \simeq a(T - T^*)$ with $B(T)$ and higher-order coefficients essentially independent of temperature. In the uniaxial case,

$$F = F_0 + \frac{3}{4} A q^2 + \frac{B}{4} q^3 + \frac{9c}{16} q^4 + O(q^5). \quad (2.71)$$

This q -dependence exhibits the characteristics outlined in Fig. 2.12.

As soon as there is a non-vanishing term of order q^3 in the expansion, the phase transition must be of first order; a qualitative explanation of this point is given in Fig. 2.12. Indeed, in all cases that have been studied up to now, the N-I transition has been found to be of first order; discontinuities have been observed in the density, in the heat content, etc. However, it must be emphasized that these discontinuities are small: the transition is ‘weakly first order’. This point will be re-examined in Section 2.3.4.

2.3.2 Static pretransitional effects

Since the transition is only weakly of first order, we expect that short-range order effects will be important at the temperatures just above the transition point T_c —in particular, that the coherence length $\xi(T)$ will be rather large—typically a few hundred Å (10 times the molecular length). This reacts on many physical properties. Here we shall outline them only very qualitatively; for a quantitative analysis, see reference 44.

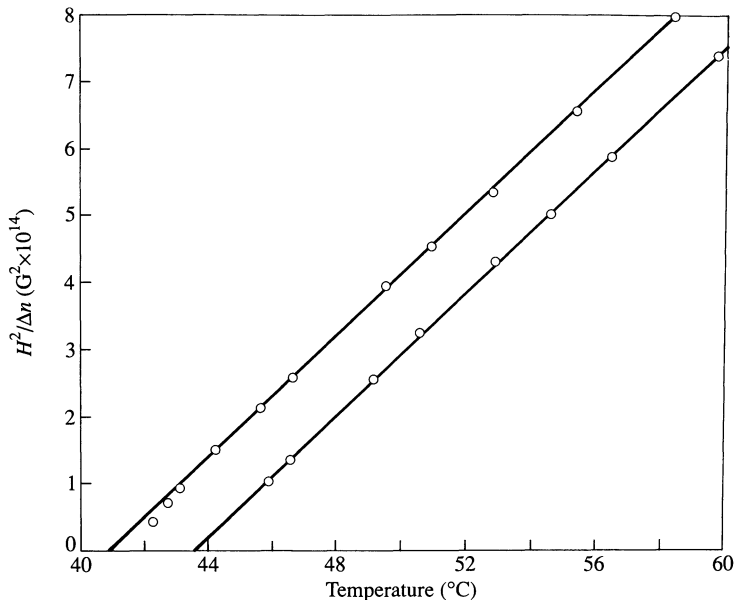


Fig. 2.13. Magnetic birefringence (Cotton–Mouton effect) in MBBA. The points give the inverse of the magnetic birefringence coefficient, as a function of temperature, for two different samples (with slightly different transition temperatures). In both samples the plots are nearly linear, in agreement with the Landau approximation. [After reference 45. Used with permission from McGraw-Hill.]

2.3.2.1 Magnetic birefringence

The swarms are rather easily aligned by a magnetic field if they are large enough. There is a magnetic birefringence

$$\Delta n = n_{\parallel} - n_{\perp} = CH^2 \quad (2.72)$$

where n_{\parallel} and n_{\perp} are the indices measured, respectively, along H and normal to H (see Fig. 2.13). The coefficient C is large just above T_c (typically a hundred times larger than in simple organic liquids such as nitrobenzene).

A strict swarm picture would predict that C could be proportional to the volume (ξ^3) of the swarms. But the continuum theory shows that, in fact,

$$C \sim \xi^2 \sim A^{-1}(T). \quad (2.73)$$

This law is simply obtained by minimizing the lowest-order terms in the free energy in the presence of a magnetic field (omitting all indices again), such that

$$F = \frac{A}{2} Q^2 - \Delta \chi Q H^2 \quad (2.74)$$

The requirement $\partial F / \partial Q = 0$, gives eqn (2.73).

2.3.2.2 Electric birefringence (Kerr effect)

Here there is also an alignment effect but it is more complicated. The temperature dependence of the Kerr constant $C' = (n_{||} - n_{\perp})/E^2$ is described by eqn (2.73) only for ultrahigh-purity samples [48]. In impure samples Helfrich has noticed that the anisotropic conduction currents induced by E inside a swarm, will lead to charge accumulation at the surface of the swarms [49]. This is related to the Carr–Helfrich effect described in Chapter 5 and gives rise to local forces, flows, and flow birefringence. At ultrahigh (optical) frequencies, when absorption effects are negligible, eqn (2.73) holds [50, 51]. In general, the situation is more complex [51]. The problem of electric fields may be summarized as follows. By symmetry, the anisotropy induced by the application of an external electric field reads

$$\langle Q^{\alpha\beta} \rangle_E = C'' \left(E_\alpha E_\beta - \frac{E^2}{3} \delta_{\alpha\beta} \right)$$

where $C'' \sim \xi^2$ only to the extent that the coupling between $Q^{\alpha\beta}$ and E_α is $Q^{\alpha\beta} \left(E_\alpha E_\beta - \frac{E^2}{3} \delta_{\alpha\beta} \right)$. In fact, one can write more generally

$$C'' \sim (A^{-1} + C_1 \langle Q^2 \rangle + \dots).$$

Since $\langle Q^2 \rangle \sim -(\text{constant})(T - T^*)^{1-\alpha}$ (with $\alpha = 1/2$ in the Gaussian approximation), the actual temperature dependence is never exactly A^{-1} . The same remark holds in principle for magnetic fields, but the absence of magnetic charges and the weakness of magnetic interactions justify the neglect of C_1 .

2.3.2.3 Light scattering

The scattering of light by the isotropic phase is much smaller than in the nematic phase (for this reason T_c is often called the clearing point). However, just above T_c , there will remain a sizeable scattering intensity I , due to the birefringent swarms (Fig. 2.14). The polarization dependence of I is indeed in agreement with what is expected for the scattering by a random distribution of anisotropic domains [45, 46].

Since the swarms are much smaller than the optical wavelength, the intensity I is essentially independent of scattering angle. It has been verified by the MIT group [45] that I and the magnetic birefringence coefficient C have the same temperature dependence near T_c . To a first approximation this is simply

$$C \sim I \sim 1/(T - T^*) \quad (2.75)$$

where T^* is a temperature slightly smaller than T_c . (Typically, $T_c - T^* \sim 1$ K). Physically, T^* is the temperature at which the size of the swarms would

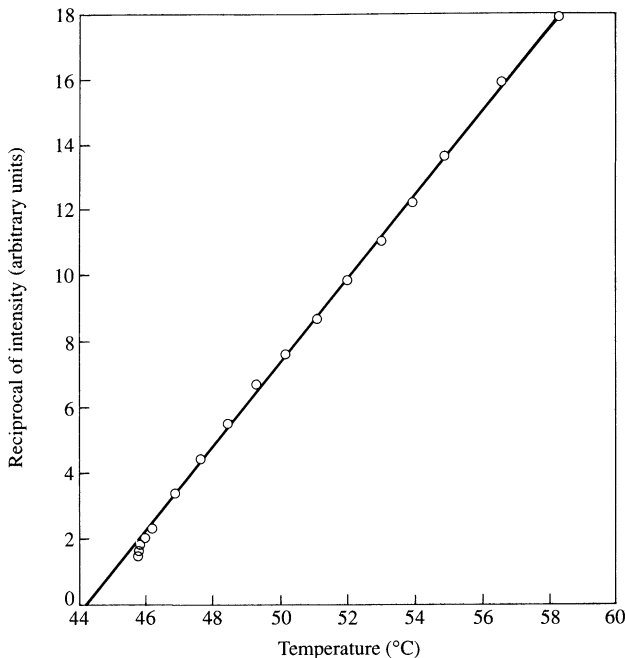


Fig. 2.14. Reciprocal of the light-scattering intensity in the isotropic phase of MBBA. (After reference 41. Used with permission from McGraw-Hill.) Note the systematic deviation from linearity close to T_c .

become infinite $\{\xi(T^*) = \infty\}$; it represents the lowest temperature down to which one could supercool the isotropic phase. It must be emphasized that, in a strict swarm model, one would expect $I \sim \xi^3$, while the more correct ‘Landau-type’ theory gives $I \sim \xi^2$. We may understand the latter result by the following qualitative argument.

The light-scattering amplitude at one point is proportional to the fluctuations of the dielectric tensor, i.e. to Q (we purposely omit all component indices).

The intensity is proportional to

$$I = \int \langle Q(\mathbf{R}_1)Q(\mathbf{R}_2) \rangle \exp(i\mathbf{k} \cdot \mathbf{R}_{1,2}) d\mathbf{R}_{1,2} \quad (2.76)$$

where \mathbf{k} is the scattering-wave vector. In the Landau approximation the $\langle QQ \rangle$ correlations have the Ornstein–Zernike form

$$\langle Q(0)Q(\mathbf{R}) \rangle \approx (e^{-R/\xi})/R.$$

As pointed out above, the swarms are small when compared to the optical

wavelength ($k\xi \sim 0$). Then

$$I \approx \int (e^{-R/\xi}/R) 4\pi R^2 dR = 4\pi \xi^2. \quad (2.77)$$

In the Landau approximation, the temperature dependence of ξ is of the form

$$\xi = \xi_0 \left(\frac{T^*}{T - T^*} \right)^v, \quad v = 1/2 \quad (2.78)$$

where ξ_0 is a molecular length.[†] This is compatible with the experimental law for I .

Alternatively, one can work in Fourier space

$$I \propto \langle Q(\mathbf{k})Q(-\mathbf{k}) \rangle. \quad (2.79)$$

Extending F to spatially varying Q , we may write to lowest order (ignoring all indices)

$$F = \int \left(\frac{A + Lk^2}{2} \right) Q(\mathbf{k})Q(-\mathbf{k}) \frac{d^3\mathbf{k}}{(2\pi)^3}.$$

In view of the Gaussian character of this expression we may use the equipartition theorem

$$\langle Q(\mathbf{k}) - Q(-\mathbf{k}) \rangle = \frac{kT}{A + Lk^2} = \frac{kT}{A(1 + k^2\xi^2)} \quad (2.80)$$

with

$$\xi = \frac{L}{A} \quad \left(\text{i.e. } \xi_0 = \frac{L}{aT^*} \right). \quad (2.81)$$

It is clear in this form that the \mathbf{k} dependence of the scattered intensity allows the measurement of ξ . However, since ξ is of the order of 100 Å, $k^2\xi^2 \ll 1$ in light scattering experiments and measurements are difficult. A small \mathbf{k} dependence has been detected on I , and the temperature variation of ξ has been studied [52]. It agrees basically with eqns (2.74) and (2.77).

2.3.3 Biaxial phase

It is easy to investigate the topology of a phase diagram in which we allow the A, B Landau coefficients to vary as in the molecular model of Section 2.2.2.2. Using the invariants $\delta = Q_{\alpha\beta}Q_{\alpha\beta}$, and $\Delta = Q_{\alpha\beta}Q_{\beta\gamma}Q_{\gamma\alpha}$ already intro-

[†] Until the end of this chapter, v will keep the same meaning but its value will be allowed to differ from 1/2.

duced in Section 2.3.1 (eqn (2.69)) [34, 47], the free energy reads

$$F = \frac{A}{2} \delta + \frac{B}{3} \Delta + \frac{C}{4} \delta^2 + \frac{D}{5} \delta \Delta + \frac{E}{6} \Delta^2 + \frac{E'}{6} \delta^3. \quad (2.82)$$

The discussion is greatly simplified if one sets $E' = 0$ (keeping $E' \neq 0$, would give quantitatively different but qualitatively similar results). Under these conditions the minimization of (2.82) is straightforward. If $CE > 6D^2/25$ the minimum of F is simply given by the zeros of $\partial F/\partial\delta$ and $\partial F/\partial\Delta$. One obtains:

$$\delta = \frac{2BD/5 - AE}{CE - 6D^2/25}, \quad \Delta = \frac{3AD/5 - CB}{CE - 6D^2/25}, \quad (2.83)$$

which corresponds to a biaxial phase. This solution is physically acceptable as long as $\delta^3 > 6\Delta^2$ (cf. condition (2.70)).

$$\Delta = \pm \delta^{3/2}/\sqrt{6} \quad (2.84)$$

defines the boundary between the biaxial and the uniaxial phase. When the inequality (2.70) cannot be satisfied, the equality necessarily holds and δ and Δ are no longer independent variables. One is back with the standard isotropic–uniaxial nematic problem as discussed in Section 2.3.1: the boundary is obtained by equating the free energies of the nematic and isotropic phases. For small B , the N–I line is defined by

$$A = \frac{B^2}{27C} \left(1 + \frac{4BD}{45C^2} \right). \quad (2.85)$$

The fact that the equality (2.84) can be approached continuously from the biaxial side shows that, according to mean-field calculations the uniaxial–biaxial transition is also continuous. Another way to understand this feature is to remark that the free energy (2.82) contains only even powers of η (cf. eqn (2.69)), which is the natural order parameter of this transition.

We thus get the phase diagram of Fig. 2.15(a) in the A, B -plane. It contains one remarkable point O (mentioned in Subsection 2.2.2.2) at which the isotropic phase condenses directly into the biaxial nematic. Its existence was first spotted by Alben [34].

The topology of the phase diagram of the potassium laureate/1 decanol/ D_2O system (in a T–KCl concentration plane at 6.24 weight per cent of 1 decanol) is in qualitative agreement with Fig. 2.15(a) in that the biaxial phase is sandwiched between a uniaxial positive and a uniaxial negative nematic.

Optical measurements of the invariants δ and Δ [53] reveal a good

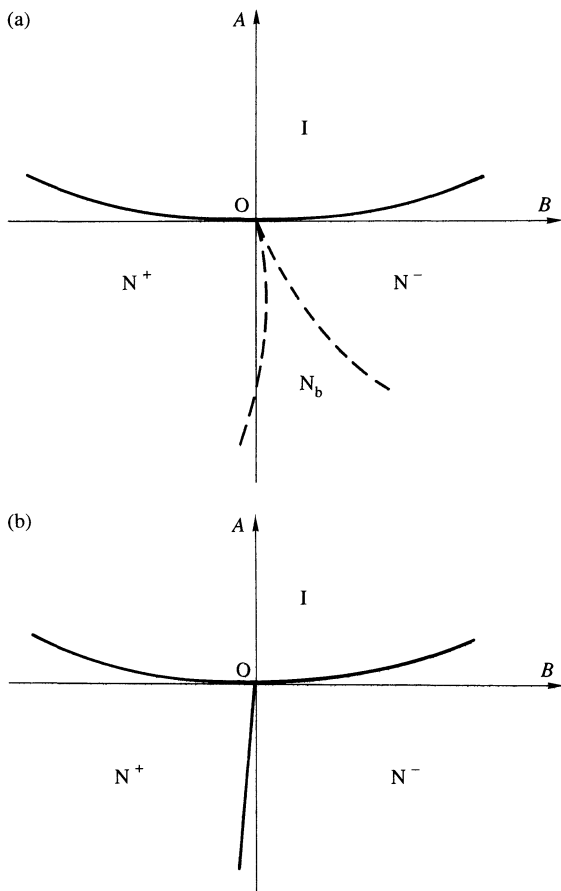


Fig. 2.15. Phase diagram in the A, B plane resulting from the minimization of (2.82). N^+ and N^- are uniaxial nematics with $S > 0$ and $S < 0$, respectively. N_b is a biaxial nematic. I is the isotropic phase. Solid lines are first-order and dashed lines are second-order lines. (a) $CE > 6D^2/25$. (The N^+N_b and N^-N_b lines have the same slope in O , the tilt of which depends on D ; $D < 0$ in the case of the figure.) (b) $CE < 6D^2/25$. (The tilt of the first order N^+N^- depends again on D ; $D > 0$ in the case of the figure.)

agreement with formula (2.82), which suggests that, in that case, local field corrections are either independent of temperature, or negligible.

If $CE < 6D^2/25$, the quadratic form is always minimized by choosing $|\delta|$ as large as possible; hence the equality $|\delta|^3 = 6\Delta^2$ holds everywhere: only uniaxial phases are stable. The I-N boundary is still given by (2.85), and a first-order line separates out the uniaxial positive and negative phases (Fig. 2.15(b)).

2.3.4 Failures of the mean-field approach

2.3.4.1 Experimental findings

Much attention has been paid to the N–I transition over the last 15 years. Although a qualitative agreement with the mean field is basically always reached, a number of points reveal that a finer analysis is required.

1. Light scattering experiments [54, 55] (Fig. 2.14) show that the $I \propto A^{-1}$ law (with $A = a(T - T^*)$) often breaks down near T_{NI} .[†] The same observation can be made with other techniques which measure A , such as Cotton–Mouton or Kerr effects [56].
2. A strict Landau analysis predicts for the specific heat: $C_p = C_{p0} = \text{cte}$ in the isotropic phase and

$$C_p = \frac{a^2}{2C} \left(1 + \frac{B}{(24aC)^{1/2}} \left(\frac{T^{**} - T}{T_c} \right)^{-1/2} \right) \quad (2.86)$$

in the nematic phase where T^{**} is the absolute limit of superheating of the nematic phase (see Fig. 2.12) which implies $\Delta C_p = 2a^2/C$ at the N–I transition.

Experiments show a more complex behaviour [58, 59] in which Gaussian and non-Gaussian fluctuations cannot be neglected. In particular ΔC_p and $(T^{**} - T_{NI})$ are found to be significantly smaller than predicted by the Landau theory.

3. The temperature dependence of the order parameter can be fitted with the form

$$Q = \text{const} + K(T^{**} - T)^\beta. \quad (2.87)$$

Minimization of (2.67) and keeping terms up to fourth order predict $\beta = 0.5$. Although some experiments have been fitted with this value [60], $\beta \approx 0.25$ seems to be a better candidate [61], in good agreement with the Monte Carlo simulation on hard disks. Moreover, the ratio $(Q(T = T^*)/(Q(T = T_c))$ is predicted to be exactly 3/2, independently of the system if the truncation to fourth order is valid. Experimentally $Q(T = T^*) - Q(T = T_c)$ is of the order of a few per cent instead of 50 per cent.

Point 3 and, to some extent, point 2 suggest that the most important interaction term in (2.67) is the sixth-order one. A small third-order coefficient could tentatively be justified on a molecular basis (cf. Section 2.3.3.1), but a small fourth-order one is much less intuitive.[‡] The Monte

[†] Some compounds like 20.4 follow the $(T - T^*)^{-1}$ law even close to T_{NI} [57].

[‡] It is an experimental fact that, in molar units (e.g. $A_m = A/RT$ per mole, $B_m = B/RT$ per mole, etc.), Landau coefficients are of the order unity in practically all known systems (superfluid helium, magnetic systems, etc.); nematogenic systems investigated yield B_m and C_m 10 times smaller if the mean-field approximation is assumed to hold [62].

Carlo results suggest that B and C decrease significantly upon approaching T_c .

Furthermore, $(T_{\text{NI}} - T^*)/T_{\text{NI}} \sim 10^{-3}\text{--}10^{-2}$; in all known systems, in which only short-range interactions are present, the Landau approximation is known to fail for such small values. We are thus naturally led to consider the role of fluctuations.

2.3.4.2 Importance of fluctuations

Looking for the minimum of F with respect to Q , as we have done in Section 2.3.1 (or with respect to δ and Δ as in Section 2.3.3.2), with the assumption $A = a(T - T^*)$ and B, C , ‘const’ independent of temperature is not the correct procedure. In principle, one should start from a microscopic Hamiltonian of the type (2.58) (but certainly considerably more complicated in order to be realistic), and calculate whatever thermodynamic quantity is needed, from the partition function Z), such that

$$Z = \int e^{-\beta \mathcal{H}(x_i)} \pi_i \delta x_i. \quad (2.88)$$

The symbol $\pi_i \delta x_i$ means that the integration is performed over all independent degrees of freedom in the system. This includes, intra- as well as intermolecular variables. It is possible to construct a free energy $F(\langle Q \rangle)$ such as (2.67), the minima of which do rigorously define equilibrium states ($\langle \rangle$ means the statistical average with the Boltzmann factor 2.88).

$$F(\langle Q \rangle) = -kT \log Z(\langle Q \rangle) \quad (2.89)$$

where $Z(\langle Q \rangle)$ obeys the definition (2.88) with the constraint that all the integrations are performed with a constant average order parameter $\langle Q \rangle$. Unfortunately, this procedure is too complicated to be tractable.

It is the current prejudice that, on scales l such that $a \ll l \lesssim \xi$ (a = typical molecular length), expansions such as (2.67) with coefficients depending analytically on temperature are valid. In other words, on that scale the Landau approximation holds and one can consider this ‘local’ free energy as a Hamiltonian.

If $F(\langle Q \rangle)$ is analytic in $\langle Q \rangle$, an expansion similar to (2.67) will, of course, exist

$$\begin{aligned} F(\langle Q \rangle) - F_0 = F_c(T) + \int & \left[\frac{\tilde{A}}{2} \langle Q_{ij} \rangle \langle Q_{ij} \rangle + \frac{\tilde{B}}{3} \langle Q_{ij} \rangle \langle Q_{jk} \rangle \langle Q_{ki} \rangle \right. \\ & \left. + \frac{\tilde{C}}{4} \langle Q_{ij} \rangle^2 \langle Q_{kl} \rangle^2 \right] dx^3. \end{aligned} \quad (2.90)$$

The problem is now how to relate $F_c(T)$, \tilde{A} , \tilde{B} , \tilde{C} , to the ‘bare’ coefficients A , B , C for which we have information from molecular theories.[†]

There are several techniques for estimating $F_c(T)$, \tilde{A} , \tilde{B} , \tilde{C} ; all of them are approximate. Let us summarize very roughly the situation.

1. The simplest approximation (which we have already used) is to identify \tilde{A} , \tilde{B} , \tilde{C} with A , B , C and set $F_c = 0$. The mere fact that C_p exhibits pretransitional behaviour on the isotropic side shows that $F_c(T)$ is non-zero; hence this approximation has a qualitative value only.
2. The next possibility is to expand the exponential in powers of B and C and integrate over Gaussian fluctuations of the type considered in Section 2.3.3.2. A detailed description of this procedure may be found in Gramsbergen *et al.* [55] and references therein. We obtain [63]

$$\tilde{A} \simeq A \left(1 + \frac{7Ck_B T \xi}{2\pi^2 L^2} - \frac{7B^2 k_B T \xi^3}{4\pi^2 L^3} \right). \quad (2.91)$$

Formula (2.91) is valid only to the extent that the corrections are small compared to one. This requirement defines the Ginzburg criteria for the N-I transition. Assuming the simplest analysis to be valid, it is possible to estimate ξ , C , B , and L from experimental data [62, 64]. Typically,

$$\xi \simeq 10^{-6} \text{ cm}, \quad C \simeq B \simeq 10^7 \text{ erg cm}^{-3}, \quad L \simeq 10^{-6} \text{ dyn}$$

with $k_B T_{NI} \simeq 4 \cdot 10^{-14}$ erg. One obtains

$$\frac{7Ck_B T_{NI} \xi}{2\pi^2 L^2} \simeq 0.1; \quad \frac{7B^2 k_B T_{NI} \xi^3}{4\pi^2 L^3} \simeq 4.$$

These figures show clearly that the corrections are not small in general near T_{NI} (the numbers depend, of course, on the systems under consideration). Another way to estimate ‘the critical domain’ (i.e. the domain beyond which the perturbation theory we briefly described breaks down) is to look for the temperature at which, say, the B^2 correction is of the order of one,

$$T - T^* = \frac{L}{a} \left(\frac{7B^2 k_B T}{4\pi^2 L^3} \right)^{2/3}.$$

With the same numbers as above and $a \simeq 10^5, 10^6$, one obtains $T - T^*$ of the order of 1–10 K.

[†] \tilde{A} , \tilde{B} , \tilde{C} (with a slightly different normalization) are called 2, 3, 4 point vertex functions in the ‘technical’ literature. $F_c(T)$ is the ‘critical’ part of the free energy on the isotropic side.

This is sufficient to show that, depending on the molecular properties of the system, fluctuations will or will not be important in the description of the transition. (Note that the sign and amplitude of the correction contained in (2.91) agree with light scattering experiments.) Other types of improvement over the mean-field approximation lead to similar results [65], but it is important to remark that, when the first-order correction is large, it is obvious that one has to consider the whole series: unfortunately, it does not converge! Similar calculations can be performed for \tilde{B} and \tilde{C} . It is remarkable that, because of biaxial fluctuations, the first corrections to B are negative [66]. As a result, we underestimate the critical region when using the experimental B (i.e. $\tilde{B}(T_{NI})$ instead of B). In this domain other types of approximations have to be made since the straightforward expansion diverges.

3. Close to T_{NI} the correlation length is found to be a few hundred Å. This is much larger than the molecular length and one may hope that techniques that are asymptotically correct at second-order critical points may have some relevance. This is the case for renormalization group calculations, which allow us to relate the effective coefficients $\tilde{A}, \tilde{B}, \tilde{C}$ to the bare ones A, B, C through a series of length-scale transformations [67].

One finds

$$\begin{aligned}\tilde{A}(A, B, C) &= (\xi/\xi_0)^{-2+\eta} L \xi_0^{-2}, \\ \tilde{B}(A, B, C) &= (\xi/\xi_0)^{-\frac{3}{2}} (\tilde{\Gamma}^\eta) b(B, C, \xi/\xi_0), \\ \tilde{C}(A, B, C) &= (\xi/\xi_0)^{-(1-2\eta)} c(B, C, \xi/\xi_0)\end{aligned}\quad (2.92)$$

where ξ_0 is the bare correlation length ($\xi_0 \simeq L/aT_c$) and the functions b and c are given by renormalization group equations, with the conditions: $b(B, C, 1) = B$; $c(B, C, 1) = C$. Since the B - and C -dependences come only through these initial conditions, we use from now on the simplified notation b_ξ, c_ξ . η is also a function of B, C , and ξ/ξ_0 .

With the variable change, $s = (\xi/\xi_0)^{(1+\eta)/2} \langle Q \rangle$, the free energy density transforms into

$$f(s) - f_0 = f_c(T) + \left(\frac{\xi_0}{\xi}\right)^3 \frac{3s^2}{4} \left(L \xi_0^{-2} + \frac{b_\xi}{3} s + \frac{3}{4} c_\xi s^2 \right). \quad (2.93)$$

The stability criterion is similar to the one used with mean-field theory. If $b_{\xi_c}^2 < 27c_\xi L \xi_0^{-2}$ (respectively $>$), the isotropic (respectively nematic) phase is stable. T_c is defined by

$$b_{\xi_c}^2 = 27c_\xi L \xi_0^{-2}.$$

Several approximation schemes allow us to estimate the leading behaviour

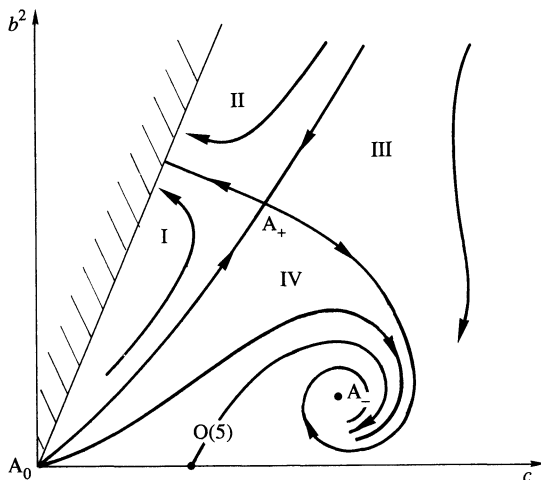


Fig. 2.16. Flow lines in the $b_\xi c_\xi$ plane, according to reference 71. The separatrix between the hatched area and the right-hand side, corresponds to the N-I transition. If, for $\xi = \xi_0$, the system starts out from regions I and II the transition is first order and (more or less) controlled by the unstable fixed point A_+ . If the system starts from III or IV the transition is continuous! This possibility is conjectural, however.

of b_ξ and c_ξ [68–71]. The results are best visualized in a parametric representation of the curves b_ξ^2 versus c_ξ ; one possible picture is represented in Fig. 2.16. The physical parameters B and C give the starting point and, as ξ/ξ_0 increases, the flow lines drawn on the figure show the evolution of b_ξ^2 and c_ξ .

If B and C are such that the initial point lies in regions III or IV, the flow lines go to the fixed point A_- without crossing the instability limit (see Fig. 2.16). This means that no first-order transition pre-empts ξ from going to infinity:[†] the transition is continuous despite the existence of the third-order invariant.[‡] In the vicinity of this point one would expect [71] $\gamma \simeq 1.6$, $v \simeq 0.85$, $\beta \simeq 0.48$, and $\eta \simeq 0.11$.

If B and C are such that the initial point lies in regions I or II, the flow lines go toward A_+ before hitting the instability limit. In the vicinity of A_+ [71], $\gamma \simeq 0.58$, $v = 0.35$, $\eta = 0.3$, and $\beta = 0.23$.

[†] Such a possibility has been spotted without the use of renormalization group by S. Alexander [72].

[‡] A word of caution. The fifth-order term is relevant in the renormalization group sense in three dimensions. Its influence on the fixed-point structure has not been studied yet. A_- is unstable and A_+ stable with respect to this perturbation. Whether the possibility for second-order transition would survive the inclusion of this term or not is an open question. Furthermore, A_- is not found in well controlled expansion schemes [68].

The fixed point O(5) is obtained with $\tilde{B} \equiv 0$ only (i.e. point O of Fig. 2.15). It corresponds to the $n = 5$ case of Wilson's n -vector model [67].

Experimentally, no clear-cut case of continuous N-I transition has been reported yet [73].† If A_- does exist, in the vicinity of the point O of Fig. 2.15, the transition should be continuous and controlled by A_- . As B grows, at some point the separatrix $A^0 A_+$ is crossed and the transition switches to first order. In the neighbourhood of this separatrix the behaviour is controlled by A_+ .

The value of the ratio $(T_{NI} - T^*)/T^*$ is determined by the proximity of the initial point to the separatrix: it can be made arbitrarily small if chosen close enough to that line. This may explain why all mean-field theories of reasonably uniaxial systems predict $(T_{NI} - T^*)/T^*$ to be much larger than found experimentally. Another attractive feature is the β value which agrees well with Monte Carlo simulations and experiment. Furthermore, the small \tilde{B} and \tilde{C} found experimentally may be connected to the small values of b and c that characterize A_+ ,

$$b_+ \simeq L^{3/2} q_c^{3/2} / 2\sqrt{2\pi(k_B T)^{1/2}}, \quad c_+ \simeq (0.15)L^2 q_c / \pi 4! k_B T,$$

or, with $q_c \simeq v_0^{-1/3} \simeq 10^7 \text{ cm}^{-1}$, $L \simeq 10^{-6} \text{ dyn}$, $k_B T \simeq 4 \cdot 10^{-14} \text{ erg}$, and $\xi/\xi_0 \simeq 10$ to T_c ,

$$\begin{aligned} \tilde{B}_{T_c} &\simeq \left(\frac{\xi}{\xi_0}\right)^{-\frac{3}{2}(1-\eta)} \times 3 \cdot 10^7 \simeq 3 \cdot 10^6 \text{ erg cm}^{-3}, \\ \tilde{C}_{T_c} &\simeq \left(\frac{\xi}{\xi_0}\right)^{-(1-2\eta)} \times 10^6 \simeq 0.5 \cdot 10^6 \text{ erg cm}^{-3}. \end{aligned}$$

These numbers compare rather well with experiment and illustrate the role of fluctuations in reducing both \tilde{B} and \tilde{C} . Note that Monte Carlo simulations also find \tilde{B} and \tilde{C} strongly temperature-dependent near T_c .

To sum up, depending on the details of the system, fluctuations may or may not play a role in the transition. When they do play a role, the temperature dependences of \tilde{A} , \tilde{B} , and \tilde{C} are given by (2.93), and this could account for the observed temperature dependence of the order parameter. Furthermore, a possibility for second-order transition exists despite the presence of a cubic invariant: this would be a violation of Landau's rule. This point, conceptually important although somewhat conjectural, could be checked with experiments in the vicinity of the biaxial phase [73].

† The observation of an anomalously small birefringence has been reported in thermotropic compounds intermediate between the rod-like and disk-like molecules (G. Sigaud, personal communication).

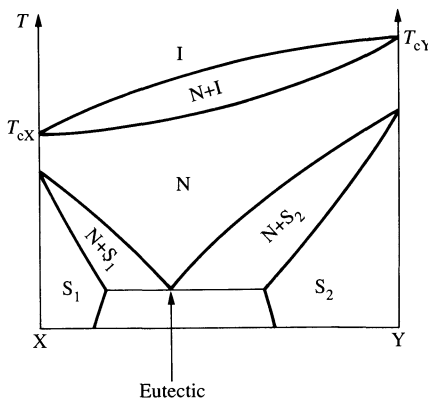


Fig. 2.17. Typical phase diagram for a mixture of two nematogens X, Y that are well miscible in the nematic phase N, but not entirely miscible in the solid phase S. (This is often obtained when the terminal chains of X and Y differ widely in this length.) I represents the isotropic phase.

2.4 MIXTURES

2.4.1 Importance of mixed systems

By mixing two nematogens X and Y one can often obtain a material with a lower melting point, while the ‘clearing point’ T_c is not much depressed. Many of the commercial room-temperature nematics are mixtures of this type, with the composition of the solid–liquid eutectic of minimal melting point (Fig. 2.17).

Miscibility studies are also important from a more fundamental point of view—to identify new phases. The rule that is used is the following:[†] if two phases (I) and (II) are continuously miscible without crossing any (first- or second-order) transition line, they have the same symmetry (cf. Section 1.4.4). Of course, a nematic phase can often be assigned simply from its optical appearance, especially from the defects which are present (see Chapter 4). However, these texture studies are not sufficient: for instance, a smectic C may have a nematic-like texture.[‡] To distinguish between the two we can take an X-ray picture. This method is fundamental but slow. A simpler method (among others) is to perform miscibility studies. This can often be carried out under the microscope (in a concentration gradient) and is faster.

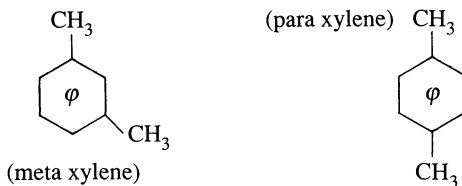
Mixtures of nematogens X with molecules Y of different shapes are also useful. For instance, the internuclear distances of molecules Y can be measured accurately by NMR if the solvent X is nematic (see reference 6).

[†] The rule is discussed in more detail in Chapter 10.

[‡] They have subtle differences (absence of 1/2 disclination lines in S_C ; see Chapter 8), which may not easily be seen in all cases.

Also, if Y is a chiral molecule, it twists the nematic into a cholesteric: this leads to a new form of polarimetry, where the chiral solute Y is not probed by the optical properties of its own molecule, but rather the long-range distortions which it creates in X [74]. In many cases it is of great interest to enhance a certain property (such as the magnetic anisotropy, conductance, nematic range) in a nematic phase X by adding a suitable solute Y. Mixtures are widely used in the display industry.

The selective solution of certain isomers by a nematic solvent is also of interest for gas chromatography. For instance, if we compare the following species



we find that the para-derivative accommodates better in nematic solvents (because of its elongated shape). The applications to chromatography have been discussed by H. Kelker.

For all of these reasons data on the phase diagrams of mixtures are very important. Some useful examples are given by Gray (reference 1 of Chapter 1) and a general discussion has been given by Billard [75]. We shall present here only a few major facts.

2.4.2 General trends

Two nematogens X and Y usually show a continuous miscibility in the nematic phase, and, if X and Y are not too different chemically, this solution is even nearly ideal. This property is convenient; it allows us to predict the nematic-isotropic (N-I) transition curves of the mixtures in terms of data taken on the pure compounds (X and Y) only, namely, the clearing points T_{cX} , T_{cY} , and the transition enthalpies ΔH_X , ΔH_Y .† The relevant formulae were established long ago by Schroder and Van Laar [76]. Note that this situation of good miscibility holds not only between some (biaromatic) nematogens, but also between them and the cholesterol esters.

Nearly ideal mixtures can also be obtained with a nematogen X and non-nematogen Y, when Y is not too different from X. The concentration of the N phases widens. In this case using the Schroder–Van Laar formulae backwards, and knowing T_{cX} , ΔH_X , one can assign a set of values T_{cY} , ΔH_Y .

[†]In principle, certain specific heat data are also required, but in practice they give only weak corrections.

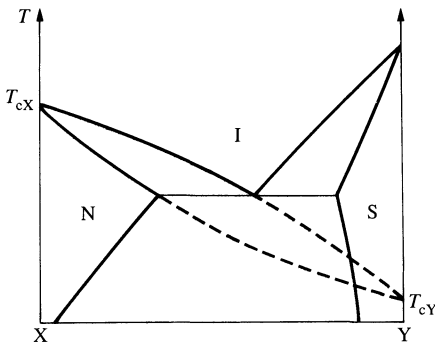


Fig. 2.18. Phase diagram for a mixture XY where X is a nematogen (i.e. has a nematic phase) while Y is not, but Y is still close to having a nematic phase. By extrapolation of the equilibrium curves for the nematic mixtures, one can ascertain the hidden transition point T_{cY} of Y. The phase S that masks the transition may be solid or smectic.

that would represent the transition N-I for the pure Y compound [77]. This transition is hidden in reality by another phase of Y (see Fig. 2.18). But knowledge of the fictitious T_{cY} can be of great interest in discussions of nematic order inside a chemical series Y_1, Y_2, \dots where certain members have a nematic phase and others do not.

In a few favourable cases, one can, in principle, start with two compounds X and Y that are not nematogens, and find a mixture X + Y that is nematic in a certain domain of concentrations and temperatures. In this case, both T_{cX} and T_{cY} are hidden by other low-temperature phases.

In general, the situation is more complex: even if X and Y are comparable chemically (i.e. $U_X \simeq U_Y = U$ as defined by (2.46) in a Maier-Saupe treatment), the angular interaction between species X and Y (i.e. U_{XY}) may be quite different from U_X , U_Y and a large variety of phase diagrams can be predicted [78].† If $U_{XY} < U$, the mixture does not favour the appearance of a nematic phase. If $U_{XY} > U$, the nematic order is increased by mixing.

The most striking result is perhaps the possibility under plausible conditions of a consolute point in the nematic phase. Such mixtures are far from ideal.

The calculations can be applied to polymer-polymer and to monomer-polymer mixtures by treating the isotropic part of the free enthalpy in a Flory-Huggins approximation [78]. In the monomer-polymer case the

† The angular interaction energy reads (where Φ is the volume fraction of Y and $S_X(S_Y)$ the order parameter of X(Y))

$$G_1 = -\frac{1}{2}U_X S_X^2(1-\Phi)^2 - \frac{1}{2}U_Y S_Y^2\Phi^2 - U_{XY} S_X S_Y \Phi(1-\Phi).$$

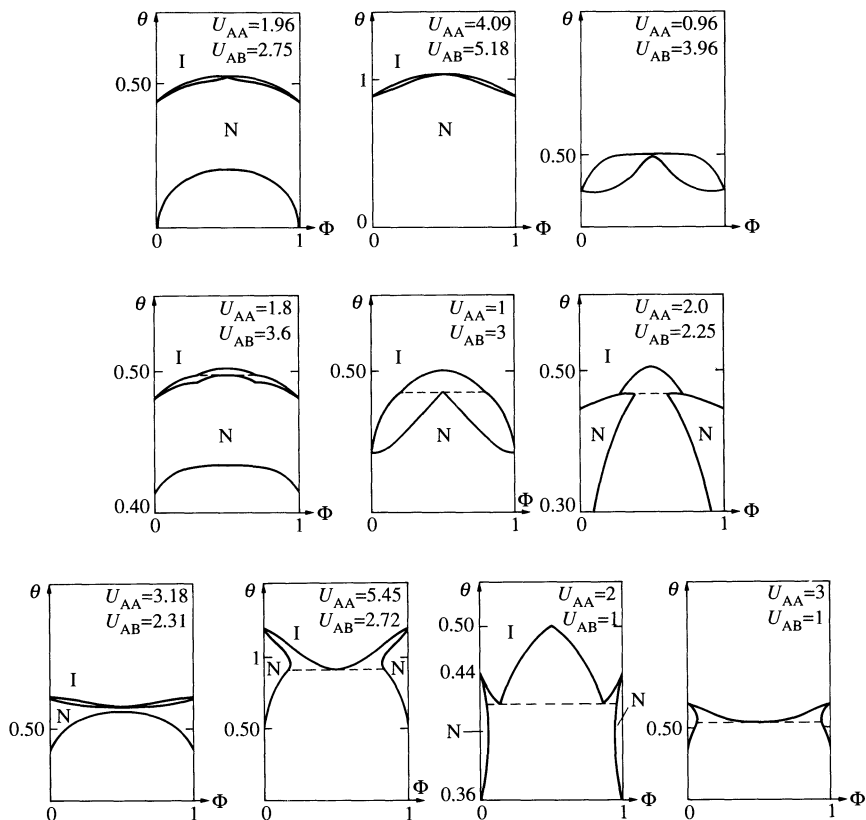


Fig. 2.19. Different topologies of the XY binary mixtures described in the text. The perfect symmetry of the diagrams is not to be expected in experiments. (After Brochard *et al.* [78].)

diagrams are very asymmetrical. The miscibility of the polymer is very small as soon as $U_{XY} < U$; on the contrary, if $U_{XY} > U$, the solubility is significantly increased. In the polymer-polymer mixtures, the effect is even more dramatic: if $U_{XY} > U$, there is complete miscibility but, if $U_{XY} < U$, complete immiscibility! Note that a consolute point has been experimentally observed in polymeric mixtures [79].

REFERENCES

1. See, for instance, Abragam, A. *The principles of nuclear magnetism*, Chapter 8. Oxford University Press (1961).
2. Spence, R. D., Gutowsky, H. S., and Nolm, C. H. *J. Chem. Phys.* **21**, 1891 (1953).
3. Saupe, A. and Englert, G. *Phys. Rev. Lett.* **11**, 462 (1963).

4. Saupe, A. *Angew. Chem. (int. edn)* **7**, 97 (1968); *Mol. Cryst.* **16**, 87 (1972).
5. Pincus, P. *J. Phys. (Paris) Colloq.* **30** (Suppl. C4), 8 (1969).
6. Diehl, P. and Khetrapal, C. L. In *N.M.R. basic principles and progress*, Vol. 1, Springer, Berlin (1969). For a more recent review see Emsley, J. W. and Lindon, J. C. *NMR spectroscopy using liquid crystal solvents*, Pergamon, New York (1975).
7. Saupe, A. *Z. Naturforsch.* **A19**, 161 (1964).
8. Snyder, L. C. *J. chem. Phys.* **43**, 4041 (1965).
9. For lyotropic systems see Yu, L. J. and Saupe, A. *Phys. Rev. Lett.* **45**, 1000 (1980). For polymeric ones see Windle, A. H., Vincy, C., Golombok, R., Donald, A. M., and Mitchell, G. R. *Faraday Disc. Chem. Soc.* **79**, 55 (1985) and Hessel, F. and Finkelmann, H., *Polym. Bull.* **15**, 349 (1986). For low-molecular-weight thermotropic systems see Malthète, J., Liebert, L., and Levelut, A. M. *C.R. Acad. Sci., Paris* **303**, 1073 (1986); Chandrasekhar, S., Sadashiva, B. K., Rameska, S., and Srikanta, B. C. *Pramaña (India)* **27**, L713 (1986); and Chandrasekhar, S., Sadashiva, B. K., Ratna, B. R., and Raja, V. N. *J. Phys. (Paris)* **30**, L491 (1988).
10. Saupe, A. and Englert, G. *Mol. Cryst.* **1**, 503 (1966); Nehring, J. and Saupe, A. *Mol. Cryst. liquid Cryst.* **8**, 403 (1969).
11. Cabane, B. and Clarke, W. G. *Phys. Rev. Lett.* **25**, 91 (1970).
12. Rowell, J. C. et al. *J. chem. Phys.* **43**, 3442 (1965).
13. Luckhurst, G. R. *Mol. Cryst. liquid Cryst.* **21**, 125 (1973).
14. Deloche, B., Charvolin, J., Liebert, L., and Strzelecki, L. *J. Phys. (Paris) Colloq.* **36** (Suppl. C1), 21 (1975).
15. Deloche, B., Cabane, B., and Jérôme, D. *Mol. Cryst. liquid Cryst.* **15**, 197 (1971).
16. Jen, S., Clark, N. A., Pershan, P. S., and Priestley, E. B. *J. chem. Phys.* **66**, 4635 (1977).
17. Miyano, K. *J. chem. Phys.* **69**, 4807 (1978).
18. Kohli, M., Otnes, K., Pynn, R., and Riste, T. *Z. Phys.* **B24**, 147 (1976).
19. Luckhurst, G. R. and Yeates, R. N. *J. chem. Soc., Faraday Trans.* **72**, 996 (1976).
20. Humphries, R. L., James, P. G., and Luckhurst, G. R. *Chem. Soc. Faraday Trans. II* **68**, 1031 (1972).
21. de Gennes, P. G. *C.R. Acad. Sci. Paris* **B247**, 62 (1972).
22. Alben, R., McColl, J., and Shih, C. S. *Solid State Commun.* **11**, 1081 (1972).
23. Onsager, L. *Ann. NY Acad. Sci.* **51**, 627 (1949); see also Wadati, M. and Isihara, A. *Mol. Cryst. liquid Cryst.* **17**, 95 (1972).
24. See Landau, L. D. and Lifshitz, E. M. *Statistical physics*, Section 71. Pergamon, London (1958).
25. Dreyer, J. F. *J. Phys. (Paris) Colloq.* **30** (Suppl. C4), 114 (1969).
26. Nguyen, H. T., Destrade, C., and Gasparoux, H. *Phys. Lett.* **72A**, 251 (1979).
27. Isihara, A. *J. chem. Phys.* **19**, 1142 (1951).
28. Flory, P. J. *Proc. R. Soc. A234*, 73 (1956).
29. Robinson, C., Ward, and Bevers. *Discuss. Faraday Soc.* **25**, 29 (1958).
30. Some of these effects, related to the existence of flexible side-chains in materials such as PBLG, have been analysed in detailed by Flory, P. J. and Leonard, M. *J. Am. chem. Soc.* **87**, 2102 (1965).
31. Cotter, M. and Martire, D. *Mol. Cryst.* **7**, 295 (1964); Martire, D. E. et al. *J. chem. Phys.* **64**, 1456 (1976).
32. Kastelein, P. W. *Physica* **27**, 1209 (1962); Lieb, E. H. *J. Math. Phys.* **8**, 2339 (1967).
33. Chuen-Shyr, Shih and Alben R. *J. chem. Phys.* **57**, 3055 (1972).

34. Alben, R. *J. chem. Phys.* **59**, 4299 (1973).
35. Maier, W. and Saupe, A. *Z. Naturforsch.* **A13**, 564 (1958); **A14**, 882 (1959); **A15**, 287 (1960).
36. Sluckin, T. J. and Shukla, P. *J. Phys.* **A16**, 1539 (1983).
37. McColl, J. and Shih, C. *Phys. Rev. Lett.* **29**, 85 (1972); McColl, J. *Phys. Lett.* **A38**, 55 (1972).
38. Alben, R. *Mol. Cryst. liquid Cryst.* **10**, 21 (1970).
39. Freiser, M. *J. Phys. Rev. Lett.* **24**, 1041 (1970).
40. Robin, Y., McMullen, W. E., and Gelbart, W. M. *Mol. Cryst. liquid Cryst.* **89**, 67 (1982).
41. Decoster, D., Constant, E., and Constant, M. *Mol. Cryst. liquid Cryst.* **97**, 263 (1983).
42. (a) Vieillard-Baron, J. *J. Phys. (Paris) Colloq.* **30** (Suppl. C4), 22 (1969). (b) Eppenga, R. and Frenkel, D. *Mol. Phys.* **52**, 1303 (1984); *Phys. Rev. Lett.* **49**, 1089 (1982).
43. Savithramma, K. L. and Madhusudana, N. V. *Mol. Cryst. liquid Cryst.* **74**, 243 (1981).
44. de Gennes, P. G. *Phys. Lett.* **A30**, 454 (1969); *Mol. Cryst. liquid Cryst.* **12**, 193 (1971). See also references 55, 56, and 63.
45. Litster, J. D. In *Critical phenomena* (ed. R. E. Mills), p. 393. McGraw-Hill, New York (1971).
46. Landau, L. D. In *Collected papers* (ed. D. Ter Haar), p. 193. Gordon and Breach, New York (1965).
47. Vigman, P. B., Larkin, A. I., and Filev, V. M. *Sov. Phys. JETP* **41**, 944 (1976).
48. Dunmur, D. A. In *Molecular electro-optics* (ed. S. Kranse), p. 435. Plenum, New York (1981).
49. Helfrich, W. and Schadt, M. *Mol. Cryst. liquid Cryst.* **17**, 355 (1972); *Phys. Rev. Lett.* **27**, 561 (1971).
50. Wong, George K. L. and Shen, Y. R. *Phys. Rev. Lett.* **30**, 895 (1973).
51. Pouliquen, B. Thesis, Bordeaux, No. 764 (1983); Pouliquen, B., Marcerou, J. P., Lalanne, J. R., and Coles, H. J. *Mol. Phys.* **49**, 583 (1983).
52. Litster, J. D. and Stinson, T. *Phys. Rev. Lett.* **28**, 688 (1972); Gulari, E. and Chu, B. *J. chem. Phys.* **62**, 798 (1975).
53. Galerne, Y. and Marcerou, J. P. *Phys. Rev. Lett.* **51**, 2109 (1983); *J. Phys. (Paris)* **46**, 589 (1985).
54. Stinson, T. W., Litster, J. D., and Clark, N. A. *J. Phys. (Paris)* **33**, 69 (1972).
55. Gramsbergen, E. F., Longa, L., and De Jeu, W. H. *Phys. Rep.* **135**, 195 (1986).
56. Anisimov, M. A. *Mol. Cryst. liquid Cryst.* **162A**, 1 (1988).
57. Gohin, A., Destrade, C., Gasparoux, H., and Prost, J. *J. Phys. (Paris)* **44**, 427 (1983).
58. Anisimov, M. A., Mamnitskii, V. M., and Sorkin, E. L. *J. engng Phys. (USSR)* **39**, 1385 (1981).
59. Thoen, J., Marynissen, H., and Van Dael, W. *Phys. Rev.* **A26**, 2886 (1982).
60. Poggi, Y., Atten, P., and Filippini, J. C. *Mol. Cryst. liquid Cryst.* **37**, 1 (1976).
61. Keyes, P. H. *Phys. Lett.* **67A**, 132 (1978).
62. Anisimov, M. A., Zaprudskii, V. M., Mamnitskii, V. M., and Sorkin, E. L. *JETP Lett.* (1079).
63. Fan, C. P. and Stephen, M. J. *Phys. Rev. Lett.* **25**, 500 (1970).

64. Wong, G. and Shen, Y. R. *Phys. Rev.* **A10**, 1277 (1974).
65. Lin, L. *Phys. Rev. Lett.* **43**, 1604 (1979).
66. Priest, R. G. In *Liquid crystals*, Proceedings of the International Conference, Bangalore 1979, p. 361. Heyden, Philadelphia (1980).
67. Wilson, K. and Kogut, J. *Phys. Rep.* **12C**, 77 (1974).
68. Priest, R. G. and Lubensky, T. C. *Phys. Rev.* **B13**, 4159 (1976).
69. Korzhenevskii, A. L. *Sov. Phys. JETP* **48**, 744 (1978).
70. Nelson, D. and Toner, J. *Phys. Rev.* **B24**, 363 (1981).
71. Korzhenevskii, A. L. and Shalaev, B. N. *Sov. Phys. JETP* **49**, 1094 (1979).
72. Alexander, S. *Solid State Commun.* **14**, 1069 (1974).
73. Rosenblatt, C. *J. Phys. (Paris) Lett.* **46**, L1191 (1985). In this article a nearly second-order transition is reported.
74. See Billard, J. *C.R. Acad. Sci. Paris* **B274**, 333 (1972).
75. Billard, J. *Bull. Soc. Fr. Mineral Cristallogr.* **95**, 206 (1972).
76. Schroder, I. *Z. Phys. Chem.* **II**, 449 (1983); Van Laar, J. *J. Z. Phys. Chem.* **63**, 216 (1903); **64**, 257 (1908).
77. Domon, M. and Billard, J. *Pramana (India)* Suppl. N.1, 131 (1975).
78. Brochard, F., Jouffroy, J., and Levinson, P. *J. Phys. (Paris)* **45**, 1125 (1984) and references therein.
79. Casagrande, C., Veyssie, M., and Finkelmann, H. *J. Phys. (Paris) Lett.* **43**, L671 (1982); Casagrande, C., Veyssie, M., and Knobler, C. *Phys. Rev. Lett.* **58**, 2079 (1987).

STATIC DISTORTIONS IN A NEMATIC SINGLE CRYSTAL

Avec des courbes pareilles à celle des osiers quand on prépare la corbeille

J. Giono

3.1 PRINCIPLES OF THE CONTINUUM THEORY

3.1.1 Long-range distortions

In an ideal, nematic, single crystal, the molecules are (on average) aligned along one common direction $\pm \mathbf{n}$. The system is uniaxial, and the tensor order parameter has the form

$$Q_{\alpha\beta} = Q(T)(n_\alpha n_\beta - \frac{1}{3}\delta_{\alpha\beta}). \quad (3.1)$$

However, in most practical circumstances, this ideal conformation will not be compatible with the constraints that are imposed by the limiting surfaces of the sample (e.g. the walls of a container) and by external fields (magnetic, electric, etc.) acting on the molecules. There will be some deformation of the alignment; the order parameter $Q_{\alpha\beta}$ will vary from point to point. Three typical examples are shown in Fig. 3.1.

For most situations of interest, the distances l over which significant variations of $Q_{\alpha\beta}$ occur are much larger than the molecular dimensions a (typically $l \gtrsim 1 \mu\text{m}$, while $a \sim 20 \text{ \AA}$).

Thus the deformations may be described by a *continuum theory* disregarding the details of the structure on the molecular scale. To construct such a theory, one possible starting point would be the free energy density F , expressed as a function of $Q_{\alpha\beta}$ as in eqn (2.67). When $Q_{\alpha\beta}$ becomes a function of \mathbf{r} , we must add in F new terms involving the gradients of $Q_{\alpha\beta}$. This approach is indeed useful to study space-dependent properties above the nematic \rightarrow isotropic transition, because in this region $Q_{\alpha\beta}$ is small, and the structure of the gradient terms is simple. Below T_c this approach would become rather clumsy, because, for large $Q_{\alpha\beta}$, there are many phenomenological coefficients involved. It is better then to start from the following observation. In a weakly distorted system ($a/l \ll 1$), at any point, the local optical properties are still those of a uniaxial crystal; the magnitude of the anisotropy is unchanged; it is only the orientation of the optical axis (\mathbf{n}) that has been rotated. In

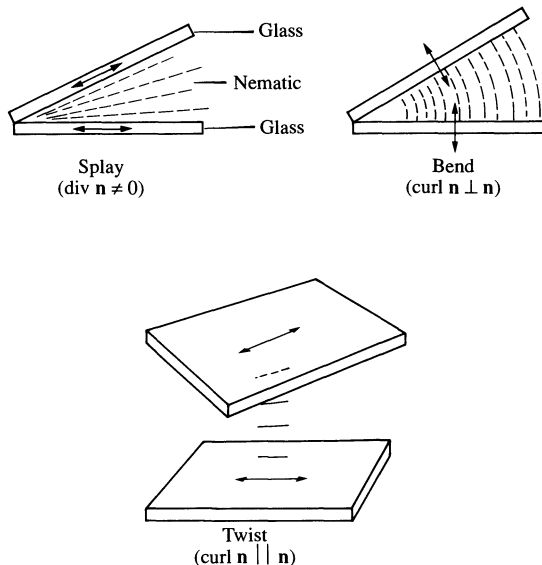


Fig. 3.1. The three types of deformation occurring in nematics. The figure shows how each type may be obtained separately by suitable glass walls. The twisted geometry between parallel walls, commonly called *plage tordue*, was used as early as 1911 by C. Mauguin.

terms of an order parameter $Q_{\alpha\beta}$ this means that

$$Q_{\alpha\beta}(\mathbf{r}) = Q(T)\{n_\alpha(\mathbf{r})n_\beta(\mathbf{r}) - \frac{1}{3}\delta_{\alpha\beta}\} + \text{terms of higher order in } (a/l). \quad (3.2)$$

(For similar reasons, the changes in density of the liquid, induced by a long-range distortion, are very small.)

The distorted state may then be described entirely in terms of a vector field $(\mathbf{r}).\dagger$ The ‘director’ \mathbf{n} is of unit length but of variable orientation. It is assumed that \mathbf{n} varies slowly and smoothly with \mathbf{r} (except possibly on a few singular points or singular lines).

This type of description was initiated by Oseen [1] and Zocher [2]. More recently, it has been examined critically by Frank [3], and its relations to the hydrostatic properties of nematic liquids have been considered by Ericksen [4]. In the present chapter, we shall insist mainly on the physical properties of the distorted conformations.

[†] This is similar to the conventional description of Bloch walls in ferromagnets where the changes of the *length* of the magnetization in the wall are neglected: the description is correct provided that the wall thickness is much larger than the interatomic distance.

3.1.2 The distortion free energy

Let us impose on our nematic a certain state of distortion, described by a variable director $\mathbf{n}(\mathbf{r})$. We make the following assumptions about this distorted system.

The variations of \mathbf{n} are slow on the molecular scale

$$a \nabla \mathbf{n} \ll 1.$$

(This does *not* imply, however, that \mathbf{n} remains nearly parallel to one fixed direction; a simple counterexample is the helical deformation shown in Fig. 3.7.)

The only forces of importance between molecules are *short range*: this omits some possible long-range electric effects that will be discussed separately.

Let us then call F_d the free energy (per cm^3 of nematic material) due to the distortion of \mathbf{n} . F_d will vanish if $\nabla \mathbf{n} = 0$, and, with our assumptions, it may be expanded in powers of $\nabla \mathbf{n}$. The following conditions must be imposed on F_d .

1. F_d must be even in \mathbf{n} ; as explained in Chapter 1, the states (\mathbf{n}) and $(-\mathbf{n})$ are indistinguishable.
2. There are no terms linear in $\nabla \mathbf{n}$. The only terms of this form that are invariant by rotations are

$$\begin{cases} \text{div } \mathbf{n}; \text{ this is ruled out by requirement 1;} \\ \mathbf{n} \cdot \text{curl } \mathbf{n}; \text{ this changes sign by the transformation, } x \rightarrow -x, y \rightarrow -y, \\ z \rightarrow -z, \end{cases}$$

and is thus forbidden in a centrosymmetric material. (In cholesterics, which are not centrosymmetric, this term will be present.)

3. Terms in F_d which are of the form $\text{div } \mathbf{u}$, where $\mathbf{u}(\mathbf{r})$ is an arbitrary vector field, may be discarded. This is a consequence of the identity:

$$\int \text{div } \mathbf{u} \, d\mathbf{r} \equiv \int d\sigma \cdot \mathbf{u},$$

where $\int d\sigma$ represents a surface integral and $d\sigma$ is normal to the surface at each point. The integral is taken on the limiting surface of the nematic. The identity shows that such terms describe only certain contributions to the surface energies, and not to the volume energies: for the present discussion of bulk properties we may omit them.[†]

We shall now list all possible terms in F_d of order $(\nabla \mathbf{n})^2$. This represents a rather tedious operation; readers who are mainly interested in the physical results should skip this part and proceed directly to eqn (3.15).

[†] The question of surface energies will be discussed later in this section.

To construct F_d , let us now consider explicitly the spatial derivatives of \mathbf{n} : they form a tensor of rank two $\partial_\alpha n_\beta$ (where we put $\partial_\alpha \equiv \partial/\partial x_\alpha$). As usual it is convenient to separate this tensor into a symmetric part

$$e_{\alpha\beta} = \frac{1}{2}(\partial_\alpha n_\beta + \partial_\beta n_\alpha) \quad (3.3)$$

and an antisymmetric part, related to the curl of \mathbf{n}

$$(\text{curl } \mathbf{n})_z = \frac{\partial}{\partial x} n_y - \frac{\partial}{\partial y} n_x \quad \text{etc.} \quad (3.4)$$

In general a symmetric tensor $e_{\alpha\beta}$ has six independent components, but here these components are further restricted by the fact that \mathbf{n} is a unit vector. This is most conveniently expressed by going to a local (orthogonal) frame of reference with the z -axis parallel to local direction of \mathbf{n} . Then all gradients of n_z vanish, because of the identity

$$0 = \nabla(n_z^2 + n_x^2 + n_y^2) = 2n_z \nabla n_z + 0 = 2\nabla n_z. \quad (3.5)$$

Thus

$$\begin{aligned} e_{zz} &= 0, \\ e_{zx} &= \frac{1}{2}(\text{curl } \mathbf{n})_y, \\ e_{zy} &= -\frac{1}{2}(\text{curl } \mathbf{n})_x \end{aligned} \quad (3.6)$$

It will also be useful to recall that

$$e_{xx} + e_{yy} + e_{zz} = e_{xx} + e_{yy} = \text{div } \mathbf{n}. \quad (3.7)$$

From requirement 1, F_d will be a quadratic function of the components $e_{\alpha\beta}$ and of curl \mathbf{n} . It is convenient to separate the contributions as follows

$$F_d = F_e + F_c + F_{ec}$$

where F_e comes from terms quadratic in $e_{\alpha\beta}$, F_c from terms quadratic in curl \mathbf{n} , and F_{ec} represents cross-terms. Let us start with F_e ; finding the number of independent terms in F_e is formally equivalent to finding the number of elastic constants in a medium of symmetry C_∞ around z . The most general form for F_e can thus be found in textbooks on elasticity [5] and involves five arbitrary constants

$$F_e = \lambda_1 e_{zz}^2 + \lambda_2(e_{xx} + e_{yy})^2 + \lambda_3 e_{\alpha\beta} e_{\beta\alpha} + \lambda_4 e_{zz}(e_{xx} + e_{yy}) + \lambda_5(e_{xz}^2 + e_{yz}^2). \quad (3.8)$$

(In the λ_3 term we have used the convention of summing over repeated indices.) Taking into account the properties of eqn (3.6), this reduces to three terms

$$F_e = \lambda_2(\text{div } \mathbf{n})^2 + \lambda_3 e_{\alpha\beta} e_{\beta\alpha} + \frac{1}{4}\lambda_5(\mathbf{n} \times \text{curl } \mathbf{n})^2. \quad (3.9)$$

We now use the identity†

$$e_{\alpha\beta} e_{\beta\alpha} = (\operatorname{div} \mathbf{n})^2 + \partial_\alpha(n_\beta \partial_\beta n_\alpha) - \partial_\beta(n_\beta \partial_\alpha n_\alpha) + \frac{1}{2}(\operatorname{curl} \mathbf{n})^2. \quad (3.10)$$

The second and third terms in eqn (3.10) must be dropped in agreement with requirement 3. Recalling that

$$(\operatorname{curl} \mathbf{n})^2 \equiv (\mathbf{n} \cdot \operatorname{curl} \mathbf{n})^2 + (\mathbf{n} \times \operatorname{curl} \mathbf{n})^2,$$

we see that F_e is finally a sum of three contributions of the form

$$(\operatorname{div} \mathbf{n})^2, \quad (\mathbf{n} \cdot \operatorname{curl} \mathbf{n})^2, \quad \text{and} \quad (\mathbf{n} \times \operatorname{curl} \mathbf{n})^2. \quad (3.11)$$

Turning now to the terms F_c , which are quadratic in the curl, in a medium of C_∞ symmetry they must have the structure

$$\begin{aligned} F_c &= \mu_1(\operatorname{curl} \mathbf{n})_z^2 + \mu^2\{(\operatorname{curl} \mathbf{n})_x^2 + (\operatorname{curl} \mathbf{n})_y^2\} \\ &= \mu_1(\mathbf{n} \cdot \operatorname{curl} \mathbf{n})^2 + \mu_2(\mathbf{n} \times \operatorname{curl} \mathbf{n})^2. \end{aligned} \quad (3.12)$$

Finally we discuss the cross-terms F_{ec} . The only term linear in $(\operatorname{curl} \mathbf{n})_z$ compatible with C_∞ symmetry is

$$(\operatorname{curl} \mathbf{n})_z(e_{xx} + e_{yy}) = (\mathbf{n} \cdot \operatorname{curl} \mathbf{n}) \operatorname{div} \mathbf{n}. \quad (3.13)$$

This is odd in \mathbf{n} and thus ruled out by requirement 2. The only terms linear in $(\operatorname{curl} \mathbf{n})_x$ and $(\operatorname{curl} \mathbf{n})_y$ compatible with C_∞ symmetry are

$$\begin{aligned} (\operatorname{curl} \mathbf{n})_x e_{xz} + (\operatorname{curl} \mathbf{n})_y e_{yz} &\equiv 0 \quad (\text{see eqn (3.6)}), \\ (\operatorname{curl} \mathbf{n})_y e_{zx} - (\operatorname{curl} \mathbf{n})_x e_{zy} &= \frac{1}{2}(\mathbf{n} \times \operatorname{curl} \mathbf{n})^2, \end{aligned}$$

Thus the most general form for F_{ec} is

$$F_{ec} = v(\mathbf{n} \times \operatorname{curl} \mathbf{n})^2. \quad (3.14)$$

Regrouping eqns (3.11), (3.12), and (3.14), we may write the distortion energy in the form

$$F_d = \frac{1}{2}K_1(\operatorname{div} \mathbf{n})^2 + \frac{1}{2}K_2(\mathbf{n} \cdot \operatorname{curl} \mathbf{n})^2 + \frac{1}{2}K_3(\mathbf{n} \times \operatorname{curl} \mathbf{n})^2. \quad (3.15)$$

Equation (3.15) is the fundamental formula of the continuum theory for nematics.

3.1.3 Discussion of the distortion-energy formula

3.1.3.1 Three elastic constants

The constants K_i ($i = 1, 2, 3$) introduced in eqn (3.15) are respectively associated with the three basic types of deformation displayed in Fig. 3.1:

† I am indebted to Dr L Brun for correcting a mistake in eqn (3.10).

- K_1 : conformations with $\operatorname{div} \mathbf{n} \neq 0$ (splay);
 K_2 : conformations with $\mathbf{n} \cdot \operatorname{curl} \mathbf{n} \neq 0$ (twist);
 K_3 : conformations with $\mathbf{n} \times \operatorname{curl} \mathbf{n} \neq 0$ (bend).

It is possible to generate deformations that are pure splay, pure twist, or pure bend. Thus each constant K_i must be *positive*; if not, the undistorted nematic conformation would not correspond to a minimum of the free energy F_d .

A remark on dimensions and order of magnitude: F_d is an energy per cm^3 , \mathbf{n} is dimensionless; thus from eqn (3.15) the elastic constants K_i have the dimension of energy/cm (or dynes). By a purely dimensional argument, we expect the K s to be of order U/a where U is a typical interaction energy between molecules, while a is a molecular dimension. Taking $U \sim 2 \text{ kcal/mol}$ (0.1 eV or 10^3 K) and $a \simeq 14 \text{ \AA}$ we expect $K_i \sim 1.4 \cdot 10^{-13} \text{ erg}/1.4 \cdot 10^{-7} \text{ cm} = 10^{-6} \text{ dyn}$. This is indeed the correct order of magnitude; for PAA at 120°C the measured elastic constants [6] are

$$K_1 = 0.7 \times 10^{-6} \text{ dyn},$$

$$K_2 = 0.43 \times 10^{-6} \text{ dyn},$$

$$K_3 = 1.7 \times 10^{-6} \text{ dyn}.$$

Note that the bending constant is much larger than the others, while the twist constant is small (this difference can be understood qualitatively by looking at models with hard rods). It must also be emphasized that the K_i values decrease rather strongly when T increases (they behave roughly like the square of the order parameter†) but their ratio is nearly independent of T (except for some special cases to be discussed in Chapter 7).

It is also useful to estimate the magnitude of the distortion energy, per molecule, for a typical distortion taking place in a distance l : this will be roughly $F_d a^3 \sim (K/l^2)a^3 \sim U(a/l)^2$. Thus, in the continuum limit ($a \ll l$) it represents only a very small fraction of the total energy.

The number of independent elastic constants has been a matter of wide discussion in the past; from a microscopic analysis. Oseen [1] produced eqn (3.15) plus a term of the form (3.13), because, at that early time (1933), the equivalence of \mathbf{n} and $-\mathbf{n}$ was not fully recognized. Frank [3] showed that the term (3.13) should be discarded, but then added to eqn (3.15) an extra term, closely related to the coefficient λ_3 of eqn (3.9). Ericksen [8] first recognized that this extra term could be integrated by parts and lumped into the other ones, as shown here through eqn (3.10). Thus it took about 30 years to define the distortion free energy unambiguously! A compilation of values of the elastic constants in PAA and MBBA, as obtained by different methods, is listed in Tables 3.1 and 3.2.

† The detailed behaviour of the elastic constants versus temperature is reviewed (and compared with certain theoretical proposals) in reference 7a. See also reference 7b.

Table 3.1. Elastic constants of PAA.

$T(^{\circ}\text{C})$	Elastic constants (10^{-7} dyn)			References ^a
	K_1	K_2	K_3	
120	5.0	3.8	10.1	1
125	4.5	2.9	9.5	1
129	3.85	2.4	7.7	1
120	7.01	4.26	—	2
124.9	6.06	3.7	—	2
130	4.84	2.89	—	2
129	—	3.1 ± 0.6	—	3

^a References:

1. Zvetkov, V. *Acta Phys. Chem. USSR* **6**, 866 (1937). (Method: Frederiks; see Section 3.2.3.) The χ values used here are those of Zvetkov, V. and Sosnovskii, A. *Acta Phys. Chem. USSR* **18**, 358 (1943).
2. Saupe, A. Z. *Naturforsch.* **15a**, 815 (1960). (Method: Frederiks; see Section 3.2.3.)
3. Durand, G., Léger, L., Rondelez, F., and Veysie, M. *Phys. Rev. Lett.* **22**, 227 (1969) and Orsay Liquid Crystal Group. In *Liquid crystals and ordered fluids* (ed. J. Johnson and R. S. Porter), p. 447. Plenum Press, New York (1970). (Method: transition, cholesteric \rightleftharpoons nematic induced by a magnetic field.)

3.1.3.2 The one-constant approximation

Experimental applications of eqn (3.15) and the possible methods of determination for the three elastic constants K_i will be reviewed in the following sections. However, as we shall see, in many cases the full form of eqn (3.15) is still too complex to be of practical use—either because the relative values of the three elastic constants K_i are unknown, or because the equilibrium equations derived from (3.15) are prohibitively difficult to solve. In such cases, a further approximation is often useful; this amounts to assuming all three elastic constants equal

$$K_1 = K_2 = K_3 = K. \quad (3.16)$$

The free energy then takes the form

$$\begin{aligned} F_d &= \frac{1}{2}K\{(\text{div } \mathbf{n})^2 + (\text{curl } \mathbf{n})^2\} \\ &= \frac{1}{2}K \partial_\alpha n_\beta \partial_\alpha n_\beta \end{aligned} \quad (3.17)$$

(the latter form of F_d differing from the preceding one only by surface terms).

The numerical values quoted above for PAA show that eqn (3.17) cannot be quantitatively correct. Nevertheless, the simpler form of eqn (3.17) makes it a valuable tool to reach a qualitative insight into distortions in nematics.

Table 3.2. Elastic constants of MBBA^a.

T (°C)	Elastic constants (10^{-7} dyn)			Ratios	Refs ^b
	K_1	K_2	K_3		
22	5.8		7	$K_3/K_1 \cong 1.25 \pm 0.05$	1
~24		$K_{2,\max} = 3.8$			1
22	6.2 ± 0.6		8.6 ± 0.4		2
22			7.3 ± 1.5		3
22		3.4 ± 0.3	8 ± 0.8		4
22		3.34 ± 0.04			5
22	5.3 ± 0.5	2.2 ± 0.7	7.45 ± 1.1	$K_3/K_1 = 1.4 \pm 0.2$	6
25	3.5				7
22		3.35			8
23			8.1	$K_3/K_1 = 1.38$	9
23				$K_3/K_2 = 2.89$	9
24			7.2 ± 1		10
26	3.2 ± 1		6.1 ± 1	$0.85 < K_3/K_1 < 1.4$	11
22				$K_3/K_1 = 1.16 \pm 0.05$	12
23.5 ± 0.5	3.88		4.66		13

^a In many of the methods used what is measured is the ratio K/χ_a of an elastic constant K to a diamagnetic anisotropy χ_a . To make meaningful comparisons we have systematically used the χ_a values of Gasparoux, H. et al. *C.R. Acad. Sci. (Paris)* **272B**, 1168 (1971).

^b References:

1. Haller, I. *J. chem. Phys.* **57**, 1400 (1972).
2. Robert, J., Labrunie, G., and Borel, J. *Mol. Cryst.* **23**, 197 (1973).
3. Galerne, Y., Durand, G., Veyssie, M., and Pontikis, V. *Phys. Lett.* **38A**, 449 (1972).
4. Williams, C. and Cladis, P. E. *Solid State Commun.* **10**, 357 (1972).
5. Cladis, P. E. *Phys. Rev. Lett.* **28**, 1629 (1972).
6. Rondelez, F. and Hulin, J. P. *Solid State Commun.* **10**, 1009 (1972).
7. Regaya, B., Gasparoux, H., and Prost, J. *Revue Phys. appl. (Paris)* **7**, 83 (1972).
8. Léger, L. *Solid State Commun.* **10**, 697 (1972).
9. Léger, L. *Mol. Cryst.* **24**, 33 (1973).
10. Martinand, J. L. and Durand, G. *Solid State Commun.* **10**, 815 (1972).
11. Pieranski, P., Brochard, J., and Guyon, E. *J. Phys. (Paris)* **33**, 681 (1972).
12. Wahl, J. and Fischer, F. *Mol. Cryst.* **22**, 359 (1973).
13. Gruler, H., unpublished results.

3.1.3.3 A comparison with magnetism

Equation (3.17) is identical in form to the Landau–Lifshitz free energy [9] for distortions in the direction of magnetization $\mathbf{M}(\mathbf{r})$ in a cubic ferromagnet

$$F_m = \frac{1}{2} A \partial_\alpha M_\beta \partial_\alpha M_\beta. \quad (3.18)$$

But it must be realized that F_m is rigorous for a Heisenberg ferromagnet, while eqn (3.17) represents only an arbitrary simplification of the correct eqn

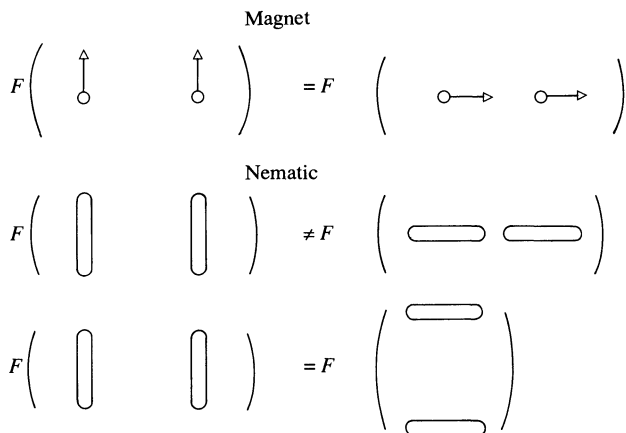


Fig. 3.2. Rotational properties of the free energy. In a Heisenberg ferromagnet F is invariant by a rotation of the spins. In a nematic F is *not* invariant by a rotation of the molecular axes. But, of course, it remains invariant by a rotation of both axes and centres of gravity.

(3.15) for a nematic. The source of this difference is as follows. In a Heisenberg ferromagnet, rotation of the spins (keeping the atoms fixed) does not change the energy; as shown in reference 9 this immediately leads to eqn (3.18). On the other hand, in a nematic phase, a rotation of the molecules (keeping their centres of gravity fixed) changes the energy (see Fig. 3.2). Thus the free energy (3.15) is invariant only by a *simultaneous* rotation of both molecular axes and centres of gravity.

3.1.3.4 Equilibrium conditions (in the absence of external fields)

To obtain the conditions for equilibrium in the bulk we write that the total distortion energy $\mathcal{F}_d = \int F_d dr$ is a minimum with respect to all variations of the director $\mathbf{n}(\mathbf{r})$ which keep $\mathbf{n}^2 = 1$. According to the rule of Lagrange, the latter condition may be taken into account by writing

$$\delta\mathcal{F}_d = \int dr \frac{1}{2} \lambda(\mathbf{r}) \delta(\mathbf{n}^2) = \int dr \lambda(\mathbf{r}) \mathbf{n} \cdot \delta\mathbf{n}(\mathbf{r}), \quad (3.19)$$

where $\lambda(\mathbf{r})$ is an arbitrary function of \mathbf{r} and $\delta\mathbf{n}$ is an arbitrary variation of the vector \mathbf{n} .

In our case F_d , as given by eqn (3.15), is a quadratic function of the gradients $g_{\alpha\beta} = \partial_\alpha n_\beta$, and is also a function of \mathbf{n} itself. Imposing a small variation $\delta\mathbf{n}(\mathbf{r})$ at all points we have

$$\delta\mathcal{F}_d = \int \left\{ \frac{\partial F_d}{\partial n_\beta} \delta n_\beta + \frac{\partial F_d}{\partial g_{\alpha\beta}} \partial_\alpha (\delta n_\beta) \right\} dr \quad (3.20)$$

We integrate the second term by parts and neglect the surface term†

$$\delta \mathcal{F}_d = \int \left\{ \frac{\partial F_d}{\partial n_\beta} - \partial_\alpha \left(\frac{\partial F_d}{\partial g_{\alpha\beta}} \right) \right\} \delta n_\beta \, d\mathbf{r}.$$

Inserting this in eqn (3.19) and writing that the Lagrange condition must be satisfied for any function $\delta \mathbf{n}(\mathbf{r})$ we reach the equilibrium equation

$$h_\beta \equiv -\frac{\partial F_d}{\partial n_\beta} + \partial_\alpha \left(\frac{\partial F_d}{\partial g_{\alpha\beta}} \right) = -\lambda(\mathbf{r}) n_\beta. \quad (3.21)$$

We call the vector \mathbf{h} the *molecular field* (a notation derived from magnetism). Equation (3.21) then states that, in equilibrium, *the director must be at each point parallel to the molecular field*. (In this form, we dispose of the arbitrary function $\lambda(\mathbf{r})$.)

Inserting eqn (3.15) for F_d into eqn (3.21), one arrives at a rather complicated form for the molecular field

$$\mathbf{h} = \mathbf{h}_S + \mathbf{h}_T + \mathbf{h}_B$$

where the three parts refer to splay, twist, and bending, respectively, and are given by

$$\begin{aligned} \mathbf{h}_S &= K_1 \nabla (\operatorname{div} \mathbf{n}) \\ \mathbf{h}_T &= -K_2 \{ A \operatorname{curl} \mathbf{n} + \operatorname{curl}(A\mathbf{n}) \} \\ \mathbf{h}_B &= K_3 \{ \mathbf{B} \times \operatorname{curl} \mathbf{n} + \operatorname{curl}(\mathbf{n} \times \mathbf{B}) \} \end{aligned} \quad (3.22)$$

where $A = \mathbf{n} \cdot \operatorname{curl} \mathbf{n}$ and $\mathbf{B} = \mathbf{n} \times \operatorname{curl} \mathbf{n}$.

In the one-constant approximation \mathbf{h} becomes simpler:‡ from eqns (3.17) and (3.21)

$$\mathbf{h} = K \nabla^2 \mathbf{n}. \quad (3.23)$$

A general discussion of eqn (3.21) has been given by Ericksen [10]. However, in practice, the equilibrium equations are rarely used in this general form; it is often more convenient to express the unit vector \mathbf{n} in terms of suitably chosen polar angles, and to write that \mathcal{F}_d is a minimum with respect to all variations in these angles.

Let us show this by an example: the pure twist deformation shown in Fig. 3.1 and in more detail in Fig. 3.7. The director \mathbf{n} is a function of y only, with the following components

$$n_z = \cos \theta(y), \quad n_x = \sin \theta(y). \quad (3.24)$$

† The surface term is discussed in Section 3.5.

‡ There is an apparent discrepancy between (3.23) and the form obtained from (3.22) by putting the three elastic constants equal. In fact the two expressions are equivalent, for the following reason: one can always add to F a term of the form $\frac{1}{2}\mu(\mathbf{r})\mathbf{n}^2 = \frac{1}{2}\mu$ without changing the distortion energy. This changes \mathbf{h} into $\mathbf{h} + \mu\mathbf{n}$: two fields differing only by $\mu(\mathbf{r})\mathbf{n}$ are equivalent.

Inserting this form into eqn (3.15) shows that

$$F_d = \frac{1}{2}K_2 \left(\frac{\partial \theta}{\partial y} \right)^2. \quad (3.25)$$

The energy \mathcal{F}_d (calculated per unit area at the $y0z$ plane) is

$$\mathcal{F}_d = \frac{1}{2}K_2 \int \left(\frac{\partial \theta}{\partial y} \right)^2 dy.$$

We write that $\delta\mathcal{F}_d = 0$ for an arbitrary variation in form of the twist $\delta\theta(y)$. This gives

$$\begin{aligned} 0 = \delta\mathcal{F}_d &= K_2 \int \frac{\partial \theta}{\partial y} \frac{\partial}{\partial y} \delta\theta dy \\ &= -K_2 \int \frac{\partial^2 \theta}{\partial y^2} \delta\theta dy + \text{surface terms}. \end{aligned}$$

Thus the condition for local equilibrium is

$$K_2 \frac{\partial^2 \theta}{\partial y^2} = 0, \quad (3.26)$$

and this may readily be integrated to give

$$\frac{\partial \theta}{\partial y} = \text{constant}. \quad (3.27)$$

Distortions of this type have been produced and were studied very early on by Mauguin [11]—they are called ‘*plages tortues*’ (twisted areas) in the French literature. To understand in detail how these distortions are produced, however, we must discuss how one can impose the orientation of \mathbf{n} at the boundaries of the sample; this will be done in Section 3.1.2.4.

A final word of caution: when we start with a postulated form of the distortion, such as eqn (3.24), we must always check at the end of the calculation that the molecular field \mathbf{h} is collinear with \mathbf{n} , in agreement with (3.21). For the present case this is true; $\text{div } \mathbf{n}$ and \mathbf{B} are equal to zero, \mathbf{h} reduces to \mathbf{h}_T , $A = \partial\theta/\partial y = \text{constant}$, and $h_T = -2K_2A^2\mathbf{n}$.

3.1.4 Boundary effects

Equation (3.15) defining the distortion energies in the bulk of the nematic phase must be, in principle, supplemented by a description of the energies associated with the *surface* of the sample. We shall now show, however, that in most practical conditions the surface forces are strong enough to impose a well-defined direction to the director \mathbf{n} at the surface; this is what we call ‘strong anchoring’. Then, instead of minimizing the sum of bulk + surface

energies, it is sufficient to minimize only the bulk terms, with fixed boundary conditions for \mathbf{n} .

3.1.4.1 Easy directions at the surface

Let us restrict our attention to a plane surface, separating the nematic from an external medium (solid, liquid, or gas). We assume first that the bulk of the nematic is undistorted with a certain (constant) director \mathbf{n} ; thus there is no bulk contribution from eqn (3.15). What are the ‘easy’ directions, i.e. the directions of \mathbf{n} which minimize the energy of the surface region? The answer depends on the nature of the external medium.

1. If the external medium is a *single crystal*, and the interface corresponds to a well-defined crystallographic plane, the easy directions form a discrete manifold; this has been shown experimentally in a certain number of cases by Grandjean [12]. For instance, with *p*-azoxyanisole on a (001) face of sodium chloride, there are two preferred directions lying in the plane of the surface, namely (110) and (1 $\bar{1}$ 0) (see Fig. 3.3). It often happens, as in this example, that the easy directions are parallel to some simple crystallographic axes; but from a purely geometrical point of view there is no rule which imposes this; a counterexample is shown in Fig. 3.4. When there is more than one easy direction we say that the problem is *degenerate*.

2. Chatelain has shown that, when a glass surface is carefully *rubbed in one direction*, the nematic molecules of materials such as PAA tend to line up along this direction [13a]. A clear-cut microscopic explanation of this

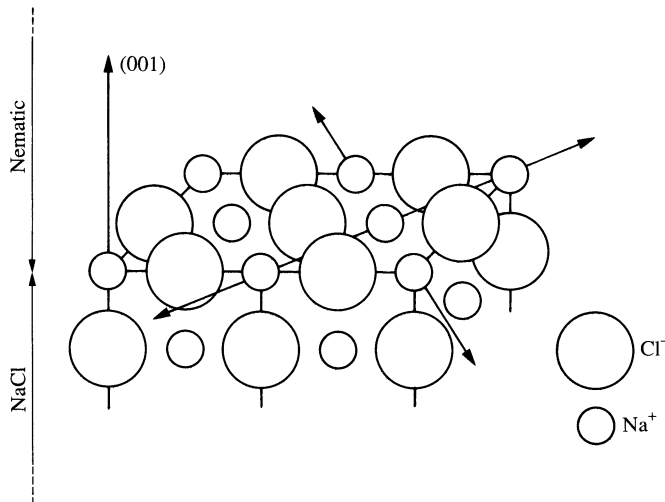


Fig. 3.3. Two easy directions for PAA molecules at the surface of a sodium chloride crystal (surface plane 001).

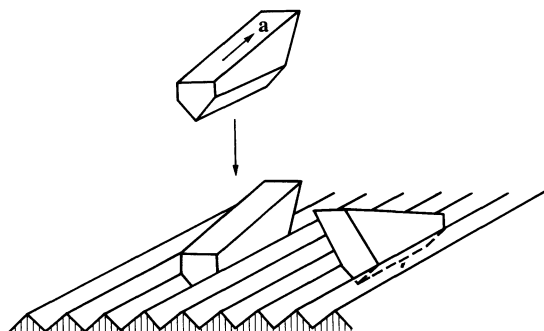


Fig. 3.4. A mechanical model showing how certain molecules may have an easy axis at a finite angle from the crystallographic axes of the surface plane

effect is still lacking,[†] but in any case the rubbing has created one easy direction in the plane of the glass.[‡] Another very powerful technique giving this type of anchoring has been invented [13b]: certain thin films (nominal thickness 3–30 nm) evaporated on glass at an *oblique* incidence give an excellent anchoring, with the easy axis in the plane of incidence. Depending on the angle of incidence, the size of the constituent grains, etc. the easy axis may be either in the plane of the glass, or tilted with respect to this plane [15].

3. If the external medium is *isotropic* (a fluid, a clear glass surface, etc.) we can have the following three situations:

- a. The normal to the surface is the easy direction. In the early days, this condition was difficult to achieve; it could sometimes be obtained on glass surfaces etched with chromic acid. More recently it has been found that suitable detergents, when incorporated by small amounts in the nematic, tend to attach their polar head on a glass surface, as shown in Fig. 3.5. This imposes a normal orientation. With such a treatment, between two parallel glass plates, it is thus easy to prepare a ‘homotropic texture,’ i.e. a single domain with optical axis normal to the walls. Similar results are obtained by treating the surfaces with polyamides or with certain lipids, such as lecithin [14].
- b. All directions in the plane of the surface are easy directions, this is probably found for the free surface of PAA.
- c. The easy directions make an angle ψ with the surface, and are thus distributed on a cone (Fig. 3.6). It has been shown (by a study of optical reflectance) that this is the situation for the free surface of MBBA [16].

[†] Fatty acids brought on to the surface by the rubbing process may play an important role. Another explanation is discussed in the problem on p. 115, see reference 14b.

[‡] It has not always been proved, however, that the easy direction is exactly in the plane of the glass.

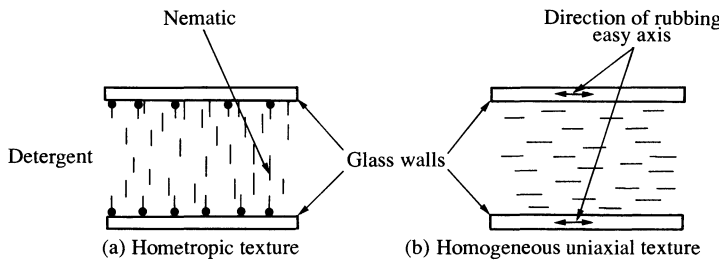


Fig. 3.5. Two types of nematic single crystals obtained between parallel glass walls

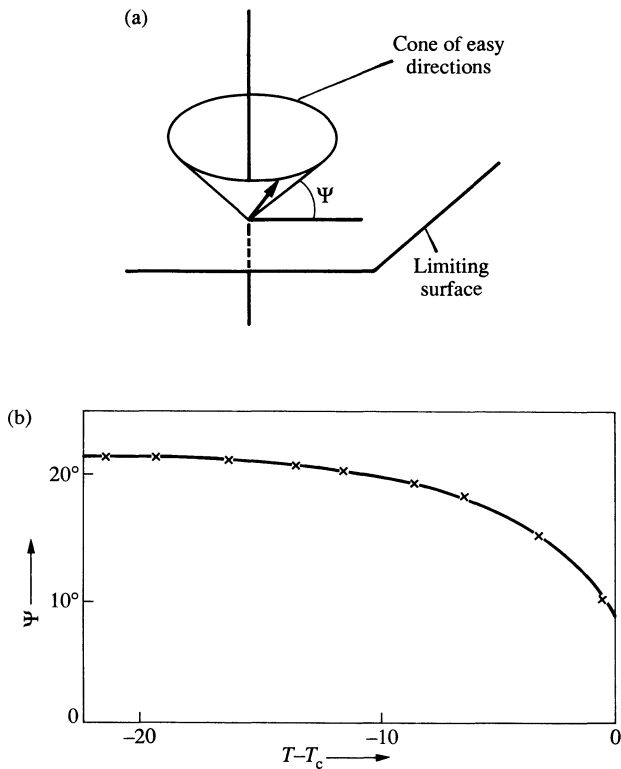


Fig. 3.6. (a) ‘Conical’ boundary conditions at the interface between a nematic and an isotropic medium. (b) Variation of the angle ψ with temperature for the MBBA–air interface. (After reference 16.)

The angle ψ is somewhat dependent on temperature, and probably also very sensitive to surface contaminants.

In cases (b) and (c) there is a continuous manifold of easy directions; we call these cases *continuously degenerate*.

3.1.4.2 Reaction of bulk distortions on the surface state

We now turn our attention to cases where the nematic arrangement is distorted in the bulk, and investigate the effects of the distortion on the surface properties. Let us start with our simple situation, corresponding to pure twist (Fig. 3.7). We assume that the surface (the $x0z$ plane) has one easy direction ($0z$). At a distance y from the surface the angle between \mathbf{n} and $0z$ is $\theta(y)$. The bulk distortion energy (per unit area in the $y0z$ plane) is, as we have seen,

$$\mathcal{F}_{\text{bulk}} = \int_0^L \frac{1}{2} K_2 \left(\frac{\partial \theta}{\partial y} \right)^2 dy$$

and writing that \mathcal{F} is a minimum leads to the condition $\partial \theta / \partial y = \text{constant}$ (eqn 3.27).

To impose a non-zero value of the bulk twist $\partial \theta / \partial y$ we fix the value of θ at a large distance L from the surface which we call $\theta(L)$. On the other hand, the value of θ near the surface will turn out to be small (since $\theta = 0$ is the easy direction). Thus the bulk twist will be nearly equal to $\theta(L)/L$.

Near the surface, eqn (3.27) no longer holds: a possible curve for $\theta(y)$ in this region is shown in Fig. 3.8. One important property of this profile is the following: provided that in all the surface region θ is small, the equations ruling θ will be linear; if we change the bulk torsion $\theta(L)$, the profile $\theta(y)$ will simply scale up or down. The ‘extrapolation length’ b defined in Fig. 3.8 is independent of the magnitude of the torsion. All the information of interest for the continuum theory is contained in b .

To derive the profile $\theta(y)$ near the surface, and the length b , from microscopic calculations is far beyond our present means. However, we can

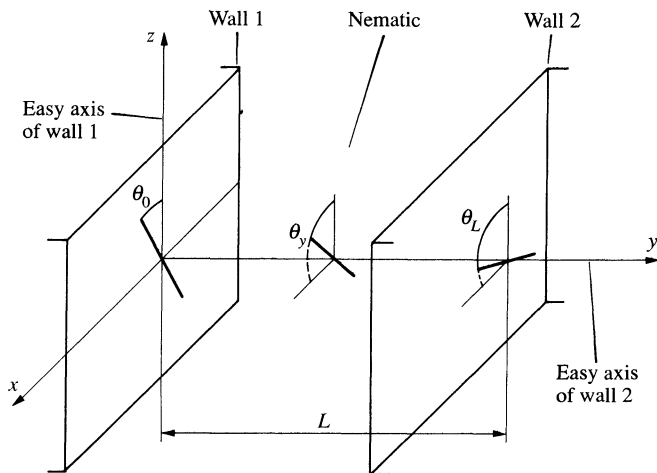


Fig. 3.7. Plage tordue between two polished glass plates.

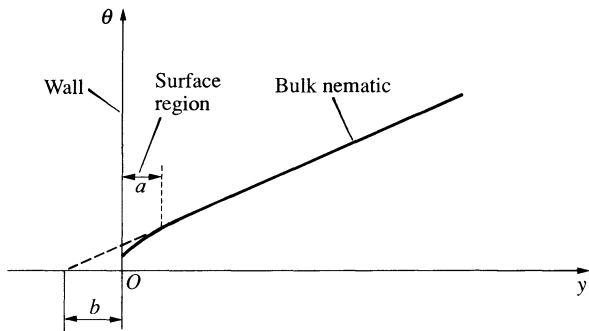


Fig. 3.8. Shape of the twisted conformation near the first wall of Fig. 3.7. In a region of molecular thickness a near the surface, the twist $\partial\theta/\partial y$ is dependent on detailed molecular properties. Out of this region the twist is essentially constant. b is the ‘extrapolation’ length. Depending on the strength of the alignment along the easy axis at the wall, b may be $\sim a$ or $\gg a$.

obtain a qualitative estimate of b through a simple argument; let us assume that eqn (3.27) holds down to the surface, i.e.

$$\frac{\partial\theta}{\partial y} = \frac{\theta(L) - \theta(0)}{L} \quad (3.28)$$

but that there is a surface term in the energy, favouring $\theta(0) = 0$.

$$\mathcal{F}_{\text{surf}} = \frac{1}{2}A\theta^2(0) \quad (\theta(0) \ll 1) \quad (3.29)$$

where A is a positive constant with the dimensions of surface tension. Then the total energy (bulk + surface) per cm^2 of wall is

$$\mathcal{F} = \frac{1}{2}A\theta^2(0) + \frac{1}{2}K_2 L \left\{ \frac{\theta(L) - \theta(0)}{L} \right\}^2. \quad (3.30)$$

Minimizing this with respect to $\theta(0)$ we find

$$\theta(0) = \frac{K_2}{A} \frac{\partial\theta}{\partial y}, \quad (3.31)$$

$$\mathcal{F} = \mathcal{F}_{\text{bulk}} + \frac{1}{2} \frac{K_2^2}{A} \left(\frac{\partial\theta}{\partial y} \right)^2. \quad (3.32)$$

Comparing eqn (3.31) with the definition of the extrapolation length b in

Fig. 3.8 we see that, in our approximation,

$$b = K_2/A. \quad (3.33)$$

The constant A is of order U_{WN}/a^2 where U_{WN} is the anisotropic part of the interaction between the wall and one nematic molecule lying against the wall, and a represents an average molecular dimension. We have already seen that $K_{22} \sim U/a$, where U is the nematic–nematic interaction. This leads to

$$b \sim a \frac{U}{U_{WN}}. \quad (3.34)$$

Equation (3.34) is the fundamental formula for boundary effects. In practice there are two possibilities:

1. *Strong anchoring.* If U_{WN} is comparable to (or larger than) U , the extrapolation length b is comparable to the molecular dimensions. Also from eqn (3.32) we see that the ratio

$$\frac{\mathcal{F}_{\text{surf}}}{\mathcal{F}_{\text{bulk}}} = \frac{K_2}{AL} = \frac{b}{L} \sim \frac{a}{L}. \quad (3.35)$$

Thus, in the continuum limit ($a/L \ll 1$) we may neglect the surface energy, put $b = 0$, and use the effective boundary condition $\theta(0) = 0$. We call this situation ‘strong anchoring.’ We expect it to hold usually for a crystalline wall.

2. *Weak anchoring.* If $U_{WN} \ll U$, the extrapolation length b may become much larger than the molecular dimensions a . The angle of rotation of the molecules at the surface is $\theta(0) \sim b\theta(L)/L$. If the torsion is strong enough ($\theta(L) \sim 1/b$), the angle $\theta(0)$ becomes large;† an external constraint can disrupt the surface alignment. We call this ‘weak anchoring’: it might be found with certain glass surfaces polished by the method of Chatelain [13]. (See also reference 17.)

The above results have been obtained for a particularly simple geometry (twist deformation, plane surface, etc.) and for a non-degenerate problem (one single easy direction on the surface). A complete formal discussion, covering all cases (and in particular the continuously degenerate cases), has not yet been carried out. However, it appears plausible that the results will remain meaningful; we are thus led to the following formulation.

In all cases where $U_{WN} \sim U$ (strong anchoring) the \mathbf{n} -dependent terms in the surface energies may be omitted. The effect of the surface is simply to impose certain easy directions on \mathbf{n} .

† Of course if $\theta(0) \sim 1$ the surface energy term (3.29) must be amended.

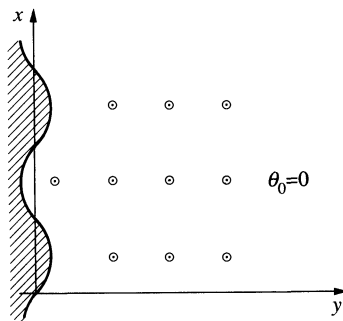
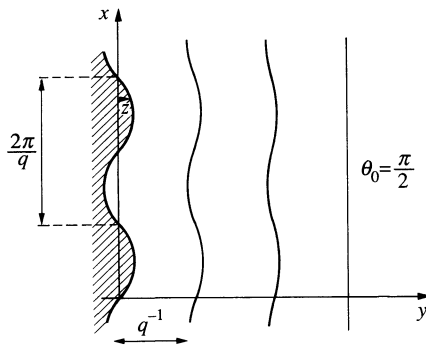


Fig. 3.9. Contact between a nematic and an undulating wall; the molecules are supposed to be tangential to the local wall surface. For $\theta_0 = 0$ this can be obtained without distortion. For $\theta_0 = \pi/2$ there must be some distortions extending up to a thickness q^{-1} in the nematic

Problem. Study the contact of a nematic with a rubbed solid surface, assuming that rubbing has created an undulating surface, departing from the plane $x0y$ by a small amount (see Fig. 3.9)

$$\zeta(x, z) = u \cos(qx) \quad (qu \ll 1).$$

Assume that at all points of the surface, the director must be *tangential*. Derive the energy of the conformation where the director \mathbf{n} , at large distances from the surface, takes a fixed orientation ($n_y = 0$, $n_x = \sin \theta_0$, $n_z = \cos \theta_0$).

Solution. For $\theta_0 = 0$ there is no distortion energy. For $\theta_0 = \pi/2$ the arrangement is distorted; at the surface we must have (to first order in $\nabla \zeta \sim qu$)

$$n_y = -\frac{\partial \zeta}{\partial x} = uq \sin(qx).$$

Inside the nematic n_y is small (of first order in qu), $n_x = 1$ (to order $q^2 u^2$), and $n_z = 0$.

Making, for simplicity, the one-constant approximation (eqn 3.17), we obtain for the free energy

$$\mathcal{F} = \int \frac{1}{2}K(\nabla n_y)^2 d\mathbf{r}, \quad (3.36)$$

and the condition \mathcal{F} = minimum leads to $\nabla^2 n_y = 0$. The solution compatible with the value of n_y at the boundary is

$$n_y = uq \sin qx e^{-qy}.$$

The energy per unit area of wall is

$$\mathcal{F}_{\text{surf}} = \frac{1}{2}K \int u^2 q^4 e^{-2qy} \{\sin^2 qx + \cos^2 qx\} dy = \frac{1}{4}Ku^2 q^3. \quad (3.37)$$

A similar calculation for arbitrary values of the angle θ_0 gives

$$\mathcal{F}_{\text{surf}} = \frac{1}{4}Ku^2 q^3 \sin^2 \theta_0. \quad (3.38)$$

In particular, comparing this with eqn (3.29), we find

$$A = \frac{1}{2}Ku^2 q^3. \quad (3.39)$$

The corresponding extrapolation length b would be of order

$$\frac{K}{A} = \frac{2}{u^2 q^3} = \frac{1}{4\pi^3} \cdot \frac{\lambda^3}{u^2} \quad \left(\lambda = \frac{2\pi}{q} \right). \quad (3.40)$$

Taking $\lambda = 10^{-4}$ cm and $u = 3 \times 10^{-5}$ cm would give $b = 10^{-4}$ cm = 1 μm . This effect has been noticed independently, and is discussed in much more detail in reference 18. Relevant experiments are described in reference 19

3.1.5 Nematics transmit torques

Conventional liquids cannot transmit static torques, but nematics can. To understand this property, we shall start once more from the problem of pure one-dimensional twist between two parallel plates (Fig. 3.7). The first plate ($y = 0$) imposes one preferred direction (θ_0) and the other one ($y = L$) imposes another preferred direction (θ_L). Strong anchoring is assumed on both plates. In this situation, as already shown, the optimum state for the nematic is a uniform twist

$$\frac{\partial \theta}{\partial y} = \frac{\theta_L - \theta_0}{L} = \text{constant}.$$

The distortion energy \mathcal{F}_d (per unit area of the plates) is

$$\mathcal{F}_d = \frac{K_2}{2L} (\theta_L - \theta_0)^2.$$

\mathcal{F}_d depends on the relative orientation of the two plates. Thus the second plate (at $y = L$) is submitted to a torque, due to the nematic near it, of magnitude

(per cm² of wall)

$$-\frac{\partial \mathcal{F}_d}{\partial \theta_L} = \frac{K_2}{L} (\theta_0 - \theta_L) = C. \quad (3.41)$$

Similarly, the first plate is submitted to a torque from the nematic

$$-\frac{\partial \mathcal{F}_d}{\partial \theta_0} = \frac{K_2}{L} (\theta_L - \theta_0) = -C. \quad (3.42)$$

Equation (3.42) may also be interpreted by saying that the first plate exerts the torque C on the nematic, and eqn (3.41) means that the same torque C is transmitted from the nematic to the second plate; thus nematics transmit torques. Note that $C = -K_2(\partial\theta/\partial y)$. Now consider the inside of the nematic and imagine it cut along a plane parallel to the plates ($y = y_0$); the left half exerts in the right half a torque $-K_2(\partial\theta/\partial y)_{y_1}$. Finally let us consider a slab ($y_0 < y < y_1$) is an arbitrary state of twist $\theta(y)$; the slab suffers from the left side a torque $-K_2(\partial\theta/\partial y)_{y_0}$ and from the right side a torque $+K_2(\partial\theta/\partial y)_{y_1}$. If we want the slab to be in equilibrium (and there are no other forces acting on it) these two torques must balance each other

$$K_2 \left\{ \left(\frac{\partial \theta}{\partial y} \right)_{y_1} - \left(\frac{\partial \theta}{\partial y} \right)_{y_0} \right\} = 0, \quad \text{hence} \quad \frac{\partial \theta}{\partial y} = \text{constant}. \quad (3.43)$$

Thus the equilibrium equation (3.27) may be interpreted as expressing the balance of torques.

We shall present later (in Section 3.5) a more general discussion of stresses and torques in nematics, after the introduction of magnetic and electric field effects.

3.2 MAGNETIC FIELD EFFECTS

3.2.1 Molecular diamagnetism

Most organic molecules are diamagnetic, the diamagnetism being particularly strong when the molecule is aromatic. A benzene ring, for instance, when it experiences a magnetic field \mathbf{H} *normal* to its plane, builds up a current inside the ring, which tends to reduce the flux going through it; thus the lines of force tend to be expelled, as shown in Fig. 3.10(a), and this raises the energy. On the other hand, if the field \mathbf{H} is applied *parallel* to the ring, no current is induced, the lines of force are nearly undistorted and the energy is not raised (Fig. 3.10(b)). Thus a benzene molecule tends to choose an orientation such that \mathbf{H} is in the plane of the ring.

Typical nematogenic molecules such as MBBA or PAA have two aromatic rings (see the formulae in Chapter 1). If we have a nematic monodomain with a magnetic field \mathbf{H} parallel to its optical axis \mathbf{n} , \mathbf{H} will be in the plane

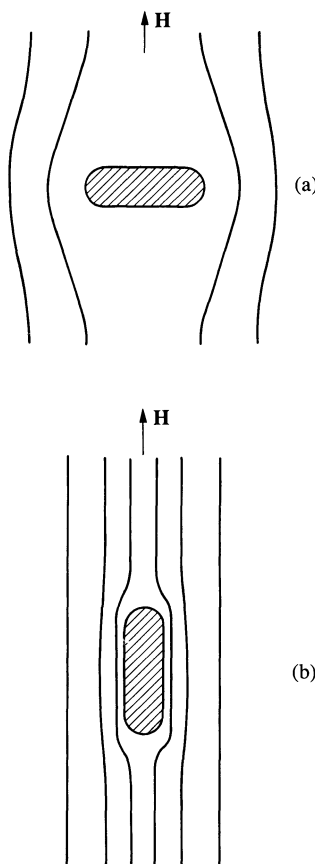


Fig. 3.10. Anisotropic diamagnetism of an aromatic ring. (The ring is normal to the sheet.) In case (a) the lines of force are more distorted and the energy is higher.

of the rings. But, if \mathbf{H} is normal to \mathbf{n} , for most molecules in the sample \mathbf{H} will be at a finite angle with the rings; thus the lowest energy is obtained when the optical axis is *parallel to the field*. This is indeed what is observed for both PAA and MBBA.

Of course, the coupling we have just discussed is very small. In fact, quantum mechanical calculations show that the coupling energy per molecule is of order $(\mu H)^2/E$ where μ is a Bohr magneton and E an electronic excitation energy.

Typically for $H \sim 10^4$ oersteds, $\mu H \sim 1$ K, $E \sim 10$ eV $\sim 10^5$ K and $(\mu H)^2/E \sim 10^{-5}$ K is very small when compared to $k_B T$. Thus a single molecule (e.g. in the vapour phase) would not be aligned in practice by any achievable field \mathbf{H} , because of thermal agitation. However, if, instead of considering an isolated molecule, we go to a large nematic sample, we have

now ($N \sim 10^{22}$) molecules which can only rotate in unison. Then the coupling energy is of order $N(\mu H)^2/E_{el} \gg k_B T$ and the sample will indeed put its optical axis parallel to \mathbf{H} . We shall see in this section that a sample of linear dimensions $\gtrsim 0.1$ mm can be aligned in fields $H \sim 10^3$ oersteds. This provides a method of preparing nematic single crystals that supplements very usefully the technique of Chatelain (using rubbed glass walls).

In smaller samples there is often a competition between the alignment favoured by the wall and that favoured by the field, giving rise to *curved conformations*. We shall see that from an experimental study of these conformations one may extract useful information on the Frank elastic constants.

To investigate these effects we need first to write down quantitatively the effect of the field \mathbf{H} on a nematic of director \mathbf{n} ; the magnetization \mathbf{M} induced by \mathbf{H} is of the form:

$$\begin{aligned}\mathbf{M} &= \chi_{\parallel} \mathbf{H} && \text{if } \mathbf{H} \text{ is parallel to } \mathbf{n} \\ \mathbf{M} &= \chi_{\perp} \mathbf{H} && \text{if } \mathbf{H} \text{ is perpendicular to } \mathbf{n}.\end{aligned}\quad (3.44)$$

Here both χ_{\parallel} and χ_{\perp} are negative (diamagnetism) and small ($\sim 10^{-7}$ to 10^{-6} in cgs electromagnetic units). If \mathbf{H} makes an arbitrary angle with \mathbf{n} , the formula for \mathbf{M} becomes

$$\mathbf{M} = \chi_{\perp} \mathbf{H} + (\chi_{\parallel} - \chi_{\perp})(\mathbf{H} \cdot \mathbf{n})\mathbf{n}. \quad (3.45)$$

In usual nematics the difference

$$\chi_a = \chi_{\parallel} - \chi_{\perp} \quad (3.46)$$

is positive.[†] From eqn (3.45) giving the magnetization we can derive the free energy (per cm³)

$$F = F_d - \int_0^H \mathbf{M} \cdot d\mathbf{H} = F_d - \frac{1}{2}\chi_{\perp}H^2 - \frac{1}{2}\chi_a(\mathbf{n} \cdot \mathbf{H})^2. \quad (3.47)$$

The term $\frac{1}{2}\chi_{\perp}H^2$ is independent of the molecular orientation (i.e. independent of \mathbf{n}) and may be omitted in all the cases to be discussed below. The last term is the interesting one; note that for $\chi_a > 0$ this term is minimized when \mathbf{n} is collinear with \mathbf{H} , as stated before.

As already seen in Section 3.1.5, it is sometimes convenient to discuss a distorted state in terms of torques, rather than in terms of energies. According to a classic formula of high school physics, the magnetic torque Γ_M (per cm³) acting on the magnetization \mathbf{M} is

$$\Gamma_M = \mathbf{M} \times \mathbf{H} = \chi_a(\mathbf{n} \cdot \mathbf{H})\mathbf{n} \times \mathbf{H}. \quad (3.48)$$

[†] $\chi_a = 1.21 \cdot 10^{-7}$ for PAA at 122°C. $1.23 \cdot 10^{-7}$ for MBBA at 19°C
More detailed references on χ_a are listed in reference 20).

To write the equilibrium conditions under a field \mathbf{H} we may operate in two (equivalent) ways:

1. We minimize $\int F \, d\mathbf{r}$, where F is given by eqn (3.47). The result is still that \mathbf{n} must, at each point, be parallel to a certain molecular field \mathbf{h} , defined by an equation similar to (3.21), but F substituted for F_d . This amounts to inserting in \mathbf{h} , in addition to the terms in eqn (3.22), a magnetic contribution

$$\mathbf{h}_M = \chi_a(\mathbf{n} \cdot \mathbf{H})\mathbf{H}. \quad (3.49)$$

2. We may also write that for any volume element in the nematic the bulk torque (3.48) is balanced at equilibrium by the surface torques (3.41, 3.42) due to neighbouring regions.

We shall see examples of both approaches in the following discussions. Historically, equations equivalent to (3.47) and (3.48) seem to have been recorded first by Zocher [2].

3.2.2 Definition of a magnetic coherence length

3.2.2.1 Simple twist

Let us consider the competing effects of a wall and of a magnetic field on the alignment of a nematic sample. Let us take the plane of the wall as the ($x0z$) plane, the nematic lying in the region $y > 0$. We assume that, at the wall, there is one easy direction for the molecules ($\pm 0z$) and that ‘strong anchoring’ (in the sense of Section 3.1.5) prevails.

We shall consider first the case where the magnetic field is along the x direction, i.e. normal to the wall’s easy axis, but in the plane of the wall (Fig. 3.11). Certainly, if we go far enough from the wall (y large and positive) we will find the nematic aligned along \mathbf{H} , as explained in Section 3.2.1. Closer to the wall, there will be a transition layer, where the nematic molecules stay parallel to the $x0z$ plane, but make a variable angle $\theta(y)$ with the z direction. This is a situation of pure twist, which is particularly simple to analyse.

The magnetic torque Γ_M (eqn (3.48)) is parallel to the y -axis, and of magnitude

$$\Gamma_M = \chi_a H^2 \sin \theta \cos \theta. \quad (3.50)$$

Consider a slab (of area 1 cm^2 in the $x0z$ plane) extending from y to $y + dy$ in the nematic. As seen in Section 3.1.5 this slab experiences a surface torque $-K_2(d\theta/dy)|_y$ at (y) and a torque $+K_2(d\theta/dy)|_{y+dy}$ at $(y + dy)$. Furthermore, it is subjected to the bulk torque $\Gamma_M dy$. Writing that the sum of these three contributions vanishes, we arrive at the equilibrium equation

$$K_2 \frac{d^2\theta}{dy^2} + \chi_a H^2 \sin \theta \cos \theta = 0. \quad (3.51)$$

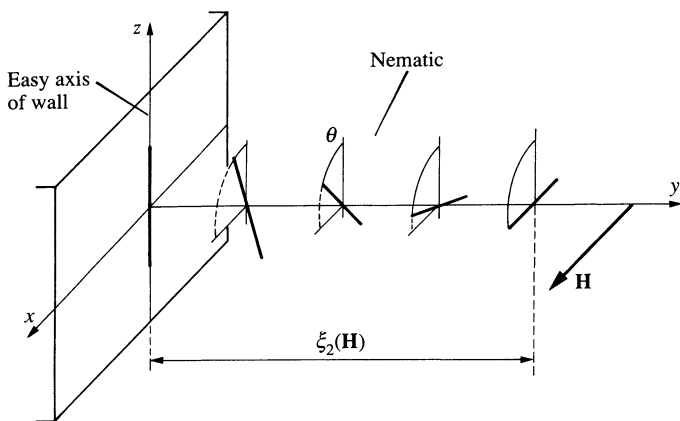


Fig. 3.11. Competition between wall alignment and field alignment. Case of pure twist.

Let us define a length $\xi_2(H)$ through the equation

$$\xi_2(H) = (K_2/\chi_a)^{1/2}/H \quad (3.52)$$

In terms of ξ_2 , eqn (3.51) takes the form

$$\xi_2^2 \frac{d^2\theta}{dy^2} + \sin \theta \cos \theta = 0.$$

It can be solved by the following trick; multiplying by $d\theta/dy$ we get

$$\xi_2^2 \frac{d}{dy} \left\{ \frac{1}{2} \left(\frac{d\theta}{dy} \right)^2 \right\} + \frac{d}{dy} \left(-\frac{1}{2} \cos^2 \theta \right) = 0.$$

This may be integrated to give

$$\xi_2^2 \left(\frac{d\theta}{dy} \right)^2 = \cos^2 \theta + \text{const.} \quad (3.53)$$

Far from the wall ($y \rightarrow +\infty$) we expect $\theta = \pi/2$ and $d\theta/dy = 0$. Thus the integration constant in eqn (3.53) must vanish

$$\xi_2 \frac{d\theta}{dy} = \pm \cos \theta. \quad (3.54)$$

Both choices of sign are permissible, corresponding to a ‘right-handed’ or a ‘left-handed’ transition region. (These conformations are related to each other by a mirror reflection in the $y0z$ plane.) Choosing for instance the

positive determination in eqn (3.54) we have

$$\frac{dy}{\xi_2} = \frac{d\theta}{\cos \theta} = -\frac{du}{\sin u} \quad (3.55)$$

where we have found convenient to introduce $u = (\pi/2) - \theta$. Equation (3.55) may be integrated in terms of

$$t = \tan(u/2),$$

$$\sin u = \frac{2t}{1+t^2}, \quad du = \frac{2 dt}{1+t^2},$$

giving

$$\begin{aligned} \frac{dy}{\xi_2} &= -\frac{dt}{t} \\ t &= \exp(-y/\xi_2). \end{aligned} \quad (3.56)$$

The integration constant in eqn (3.56) has been chosen to ensure that for $y = 0$ (at the wall) $u/2 = \pi/4$, $u = \pi/2$, and $\theta = 0$ as required.

Equation (3.56) shows that the thickness of the transition layer is essentially $\xi_2(H)$, as defined in eqn (3.52). Taking $K_2 = 10^{-6}$, $\chi_a = 10^{-7}$, and $H = 10^4$ oerstedts, we get from (3.52) $\xi_2(H) \sim 3 \mu\text{m}$. We meet here for the first time one of the fascinating properties of liquid crystals: with a rather weak external perturbation we can induce distortions on a scale comparable to an optical wavelength.

3.2.2.2 Generalization

The competition between the effects of a wall and the effects of a field may occur in a number of different geometries. One example is shown in Fig. 3.12 where the wall again imposes one easy direction Oz, but the field \mathbf{H} is now normal to the wall (along y). In this case the distortion is a combination of bend and splay.

An interesting experiment, probing optically the transition layer, has been carried out on MBBA [21].

The algebra is slightly more involved, and will not be discussed here in detail. But the same general features are found; the effects of the wall decrease exponentially at large distances, and the thickness of the transition layer is a certain weighted mean of the lengths

$$\xi_1 = \left(\frac{K_1}{\chi_a} \right)^{\frac{1}{2}} \frac{1}{H}, \quad \xi_3 = \left(\frac{K_3}{\chi_a} \right)^{\frac{1}{2}} \frac{1}{H}, \quad (3.57)$$

related to the elastic constants K_1 and K_3 for splay and bend. The three lengths ξ_i ($i = 1, 2, 3$) are usually of comparable magnitude. In the one-

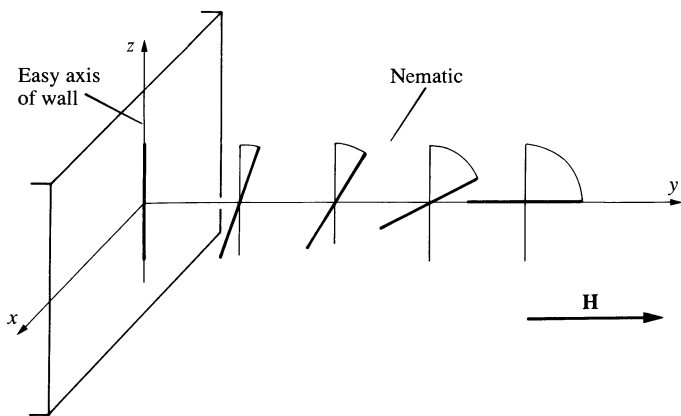


Fig. 3.12. Competition between wall alignment and field alignment. The case shown involves a mixture of bending and splay.

constant approximation ($K_i = K$) they become equal

$$\xi(H) = \left(\frac{K}{\chi_a}\right)^{\frac{1}{2}} \frac{1}{H}. \quad (3.58)$$

We call $\xi(H)$ the *magnetic coherence length* of the nematic. The general significance of ξ may be explained with the following '*gedanke experiment*'.† A large nematic sample is first aligned under a magnetic field \mathbf{H} . Then, in a small region around one point 0 in the nematic, we act on the molecules with some other perturbing force of arbitrary strength. This creates a long-range distortion in the surrounding nematic. It may be shown [22] that the angle between \mathbf{n} and \mathbf{H} decreases at large distances r from 0, according to

$$\frac{1}{r} \exp - \{r/\xi(\mathbf{H})\}.$$

Thus the nematic alignment is perturbed only in a region of linear dimensions ξ .

3.2.3 The Frederiks transition

3.2.3.1 Experimental set-up

Let us now consider a nematic single crystal, of thickness d ($\sim 20 \mu\text{m}$), oriented between two solid plates. Various geometrical possibilities are shown in Fig. 3.13. At the surface of the plates we assume strong anchoring. The easy direction imposed by both surfaces may be in the plane of the

† *Gedanke experiment* = thought experiment, i.e. one carried out in the imagination, not in reality.

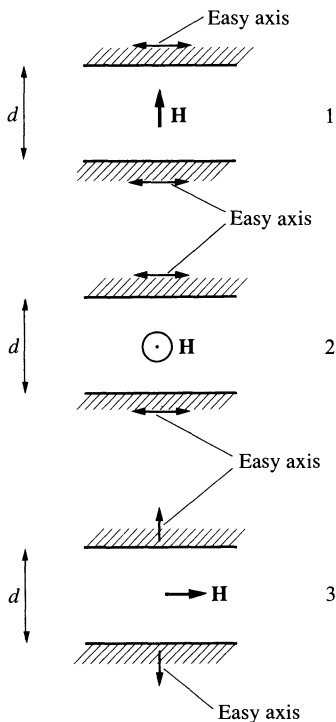


Fig. 3.13. The Frederiks transition for a nematic slab under a magnetic field \mathbf{H} . At low H the molecules are parallel to the easy axis of the wall. For $H > H_c$ the molecules near the centre of the slab rotate towards \mathbf{H} .

surfaces (cases 1 and 2) or normal to it (case 3). A magnetic field \mathbf{H} is applied *normal to the easy axis*. This choice implies that the magnetic torque

$$\Gamma_M = \chi_a(\mathbf{n} \cdot \mathbf{H})\mathbf{n} \times \mathbf{H} \quad (\text{see eqn (3.28)})$$

vanishes in the unperturbed configuration ($\mathbf{n} \cdot \mathbf{H} = 0$). Thus the unperturbed configuration does satisfy the conditions for local equilibrium, even in the presence of \mathbf{H} . However, it is clear that for large \mathbf{H} (i.e. when $\xi(\mathbf{H}) \ll d$) the optimum state will correspond to a different conformation, with molecules aligned along H in most of the slab, except for two thin transition regions (of thickness ξ) near each wall. There will be a phase transition, at a certain critical value H_c of the field, between the unperturbed conformation and the distorted conformation (see Fig. 3.14).

A transition of this type was detected optically and studied by Frederiks in 1927 [6]. He was mainly concerned with case 3; he showed that the critical field H_c was inversely proportional to the sample thickness d

$$H_c d = \text{const.} \quad (3.59)$$

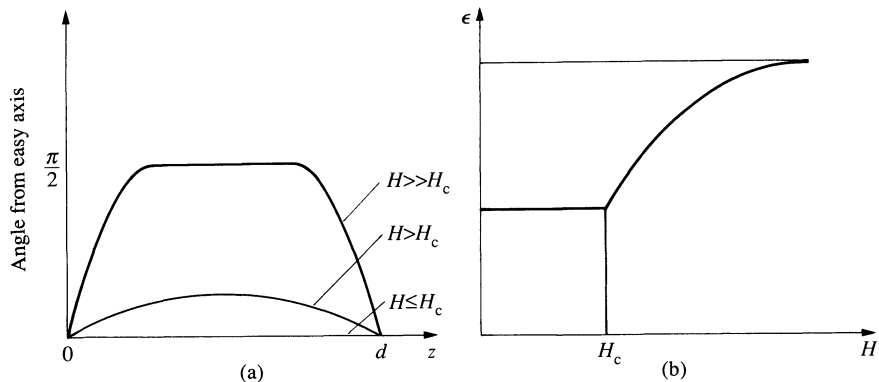


Fig. 3.14. (a) Progressive stages of the Frederiks transition as observed at different points in the slab. (b) Typical plot of apparent dielectric constant $\bar{\epsilon}$ versus field in a Frederiks transition of type 1 or 3.

(typical values being in the range of 10^4 oersteds for $d = 10 \mu\text{m}$). Soon afterwards H. Zocher [2] set up a first version of the continuum theory and showed that Frederiks' law (3.59) is a natural consequence of it.

Let us first review briefly the methods which can be used to monitor the transition. They fall essentially into two classes: macroscopic measurements and optical measurements.

1. *Macroscopic measurements.* Any anisotropic property, such as the dielectric constant [23] (or the thermal conductivity [24]), may be used as a probe of the average state of alignment. Usually the probing field (electric field, or thermal gradient) is applied *normal* to the slab. This turns out to be convenient in cases 1 and 3. The average dielectric constant $\bar{\epsilon}(H) = \bar{\epsilon}(0)$. For $H = H_c$ there is a discontinuity in the slope $d\bar{\epsilon}/dH$, which allows for a rather precise determination of H_c . (This, as we shall see later, gives one elastic constant.) For $H \gg H_c$, $\bar{\epsilon}(H)$ saturates, since nearly all the sample is aligned along H . From a study of the saturation law one can derive further information about the elastic constants.

The method does not work for case 2 where the molecules stay constantly normal to the probing field. In fact, it could still be used, if the probing field was now made *parallel* to the slab; this is feasible if one measures certain transport properties such as electric conductance or diffusion of a dye.

2. *Optical observations.* The distortion induced by H are usually very weak on the scale of an optical wavelength; this makes them rather hard to detect. To understand this more precisely considering, for instance, the following experiment, corresponding to case 2: a light beam is admitted normal to the slab (along Z), and is linearly polarized parallel to the rubbing

direction of the plates (we call this direction X). We explore the state of polarization of the transmitted beam, under a field H applied along Y .

The answer is a consequence of a certain ‘adiabatic theorem’ which was already recognized by Mauguin [11]: even when $H > H_c$, and when a good fraction of the sample has become aligned along Y , the outgoing beam is still linearly polarized along X (inside the sample, the direction of polarization remains everywhere parallel to the local optical axis. Since this axis is fixed along X at both plates, the light beam must thus come out polarized along X). Thus, in this experiment, it is *not* possible to detect the transition. In fact, changes in the outgoing polarization start to occur only at much higher fields, namely when $\xi(H)$ becomes comparable to the optical wavelength λ ; then the adiabatic theorem breaks down and, for instance, if we operated between crossed polarizers the dark field observed at low H would become progressively brighter. Thus, to follow the transition optically, more advanced techniques are required, such as *conoscopy* (Fig. 3.15). Convergent light illuminates the slab. The interference between the two allowed polarizations for one beam, depends on the beam direction, and gives rise to a characteristic interference pattern. The method is particularly suited to case 3, here, for $H < H_c$, the configuration is homeotropic, the interference pattern has full rotational symmetry around the normal to the slab, and is made of

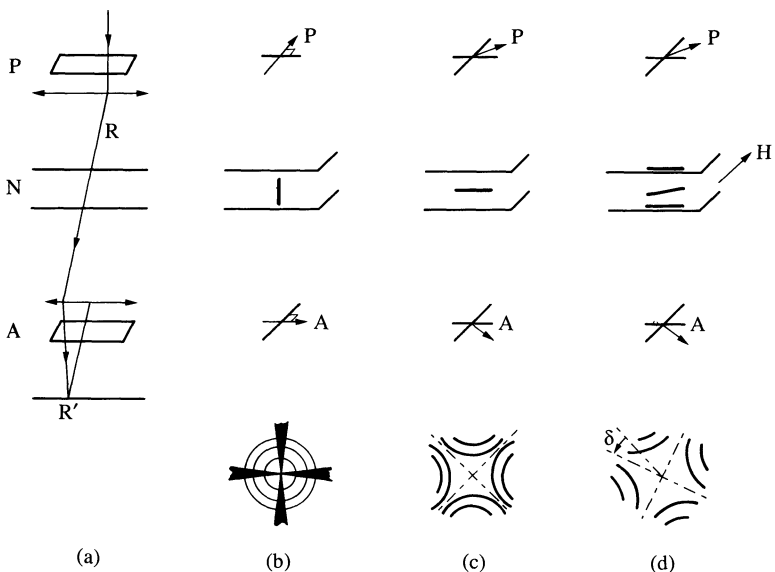


Fig. 3.15. Principle of conoscopy measurements. (a) Set up with polarizer P , analyser A , and light converging on nematic sample N . To each direction for the incident light ray R there corresponds one image point R' in the observation plane. (b) Homeotropic texture \rightarrow circles. (c) Planar texture \rightarrow hyperbolas. (d) Planar texture deformed by a field H \rightarrow hyperbolas expanded and rotated by an angle δ .

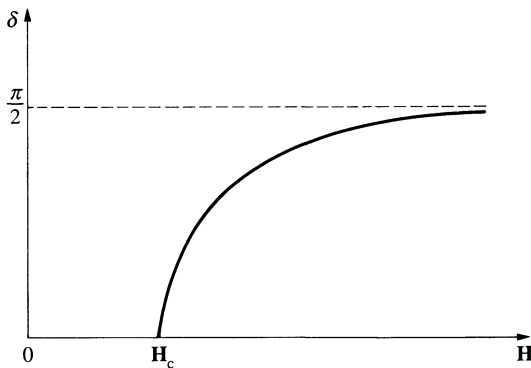


Fig. 3.16. Rotation angle δ versus field in the experiment of Fig. 3.14(d) (qualitative plot).

dark and bright circles. For $H > H_c$ the symmetry is reduced and the circles become distorted. Finally, for $H \gg H_c$ one obtained the characteristic pattern of a birefringent slab, which corresponds to hyperbolas with one axis parallel to \mathbf{H} .

The conoscopic method was applied to nematics long ago by Mauguin [25], and revived more recently at Harvard (by Meyer, private communication) and at Orsay, [21]. It is of use not only in case 3, but also in some other geometries; in case 2 for instance, we start at $H = 0$ with a set of hyperbolas with one axis parallel to the rubbing direction. For $H > H_c$ the main effect is a rotation of the pattern, by an angle

$$\delta = \frac{1}{2} \tan^{-1} \left(\frac{\overline{\sin 2\phi}}{\overline{\cos 2\phi}} \right)$$

where ϕ is the local tilt of the optical axis induced by \mathbf{H} , and the bars represent an average over the thickness of the slab [26]. The aspect of $\delta(H)$ is shown in Fig. 3.16.

3.2.3.2 Calculation of the critical fields

It may be shown rigorously that the Frederiks transition is of second order, i.e. that the distortions found just above the threshold field are small. Accepting this result, for the three situations of Fig. 3.13 the critical field H_c may be derived by a simple argument. Starting from the unperturbed state ($\mathbf{n} = \mathbf{n}_0$) we consider a slight deflection

$$\mathbf{n} = \mathbf{n}_0 + \delta\mathbf{n}(\mathbf{r})$$

where $\delta\mathbf{n}$ is normal to \mathbf{n}_0 (since $\mathbf{n}^2 = 1$) and is parallel to \mathbf{H} (since this is the direction in which the molecules are solicited). It is natural to assume that the distortion depends only on z (where z is the normal to the slab). The

distortion energy (3.15) reduces to

$$F_d = \frac{1}{2} K_i \left(\frac{\partial \delta \mathbf{n}}{\partial z} \right)^2 \quad (\text{case } i), \quad (3.60)$$

where $K_i = K_1$ (for case 1), K_2 (for case 2), K_3 (for case 3). The magnetic energy (3.47) gives a contribution

$$F_M = -\frac{1}{2} \chi_a H^2 \delta \mathbf{n}^2. \quad (3.61)$$

Since we have assumed strong anchoring, at both boundaries ($z = 0$ and $z = d$) $\delta \mathbf{n}$ must vanish. It is then convenient to analyse $\delta \mathbf{n}$ in a Fourier series

$$\begin{aligned} \delta \mathbf{n} &= \sum_q \delta n_q \sin qz \\ q &= v \frac{\pi}{d} \quad (v = \text{positive integer}). \end{aligned} \quad (3.62)$$

Inserting this form of $\delta \mathbf{n}$ in the free energy and integrating over the thickness one obtains (per cm^2 of slab)

$$\mathcal{F} = d(\bar{F}_d + \bar{F}_M) = \frac{d}{4} \sum_q \delta n_q^2 (K_i q^2 - \chi_a H^2). \quad (3.63)$$

If we want the unperturbed state to be stable, the increase in free energy \mathcal{F} must be positive for all values of the parameters δn_q

$$\chi_a H^2 < K_i q^2.$$

The smallest value of q is $q = \pi/d$ ($v = 1$) corresponding to a distortion of half-wavelength d . Thus the threshold field $H_{c,i}$ corresponds to

$$\begin{aligned} \chi_a H_{c,i}^2 &= K_i (\pi/d)^2 \\ H_{c,i} &= (\pi/d)(K_i/\chi_a)^{\frac{1}{2}}. \end{aligned} \quad (3.64)$$

Equation (3.64) may also be stated in the following terms: at the critical field the coherence length $\xi_i(H_{ci})$ is equal to d/π . The result (3.64) does show the $1/d$ dependence found experimentally by Frederiks. It also gives the principle of a simple *determination of the three classic constants*; for applications of the method see the references listed in reference 6.

However, it must be emphasized that such determinations are meaningful only under the following conditions.

1. Strong anchoring prevails [14]
2. The easy direction is normal or parallel to the slab. If, instead, we had conical boundary conditions, there would be a non-zero magnetic torque on the molecules (and distortions would occur) for arbitrarily weak fields.

Problem. Starting from case (1) of Fig. 3.13, in low fields H , one twists the nematic by rotating the upper plate. What is the change in the critical field H_c as a function of the rotation angle ψ_0 ? [27]

Solution. Let us call z the normal to the plates (\mathbf{H} is parallel to z) and look for a configuration of the form.

$$n_x = \cos \theta(z) \cos \phi(z),$$

$$n_y = \cos \theta(z) \sin \phi(z),$$

$$n_z = \sin \theta(z).$$

The free-energy density derived from eqns (3.15) and (3.47) is

$$\begin{aligned} F = & \frac{1}{2}(K_1 \cos^2 \theta + K_3 \sin^2 \theta)(d\theta/dz)^2 \\ & + \frac{1}{2} \cos^2 \theta(K_2 \cos^2 \theta + K_3 \sin^2 \theta)(d\phi/dz)^2 - \frac{1}{2}\chi_a H^2 \sin^2 \theta. \end{aligned}$$

The unperturbed solution corresponds to $\theta = 0$ and $\phi = \phi_0(z) = \psi_0 z/L$ (L = plate thickness). Let us look for a small deviation from this state $\theta \rightarrow \theta_1(z)$, $\phi = \phi_0 + \phi_1(z)$. To second order in θ_1 and ϕ_1 we have

$$F = F_0 + \frac{1}{2}K_1(d\theta_1/dz)^2 + \frac{1}{2}(K_3 - 2K_2)(\psi_0/L)^2\theta_1^2 + \frac{1}{2}K_2(d\phi_1/dz)^2 - \frac{1}{2}\chi_a H^2\theta_1^2.$$

The term involving ϕ_1 is not coupled to θ_1 , and is positive; it leads to no instability. But the terms involving θ_1 do lead to an instability provided that H is larger than a certain threshold $H_c(\psi_0)$. Operating as in eqns (3.62) and (3.63) one obtains

$$H_c^2(\psi_0) = H_c^2(0)[1 + \{(K_3 - 2K_2)/K_1\}(\psi_0/\pi)^2].$$

In practice, one cannot achieve values of the twist angle ψ_0 which are larger than $\pi/2$, because larger twists are always relaxed by the nucleation of a ‘disclination loop’ on some defect in the structure (for a definition of the disclination loop, see Chapter 4). This implies that

$$\frac{H_c^2(\psi_0) - H_c^2(0)}{H_c^2(0)} \leq \frac{K_3 - 2K_2}{4K_1}.$$

Taking the accepted values of the constants K for PAA one finds that the right-hand side is of order $\frac{1}{3}$. The experiment has been performed by Gerritsma, de Jeu, and van Zanten [28]; it agrees very well with the formulae above,† except for very thin slabs ($\sim 7 \mu\text{m}$) where surface irregularities, etc. probably become important.

At fields $H > H_c$, the set-up can be used as a magneto-optic device; take for instance the incident light polarized parallel to the easy axis of the first plate X . Depending on the size of H , we have two regimes.

1. When H is not too high, the light wave sees a slowly twisted nematic, and the polarization follows the angle $\phi(z)$.
2. When H is large the slab behaves essentially as a homeotropic monodomain, and the emerging polarization is not rotated. A detailed calculation of the optical transmission as a function of field has been carried out by Van Doorn [31].

† The behaviour above the threshold was analysed by Shtrikman *et al.* [29].

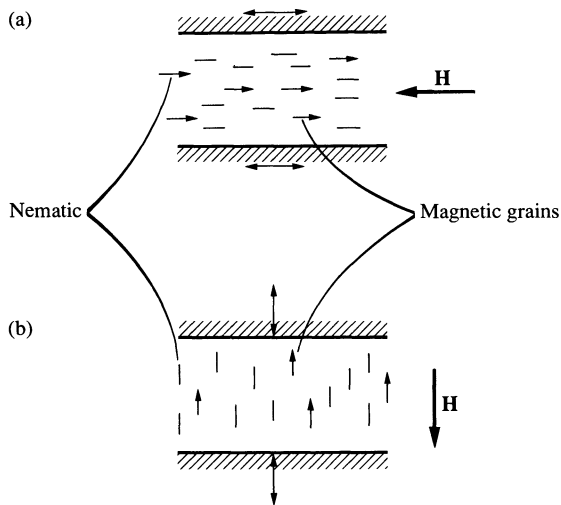


Fig. 3.17. Two possible geometries for the study of hysteresis cycles in feronematics.

The transition between the two regimes is progressive, but reasonably sharp. This application (using electric rather than magnetic fields as the orienting agent) was invented independently by Helfrich and by Fergason.

Problem. A nematic slab (of thickness d) contains a homogeneous suspension of elongated magnetic grains. Assume that the grains always have their moment parallel to the director \mathbf{n} ('feronematic'). In the absence of external fields there is one easy direction (\mathbf{n}_0) either parallel or normal to the slab. A field \mathbf{H} is now applied antiparallel to the magnetization. Compute the critical field H_c at which the conformation begins to be distorted (F. Brochard, 1970).

Solution. The two possible geometrical situations (a) and (b) are shown on Fig. 3.17. Again we look at small distortions

$$\mathbf{n} = \mathbf{n}_0 + \delta\mathbf{n}(z)$$

The magnetization \mathbf{M} is the form $\mathbf{M} = M\mathbf{n}$ where the magnitude M is fixed by the grain moments μ and concentration c_g ($M = \mu c_g$). We assume that the fields due to \mathbf{M} itself are small in comparison with \mathbf{H} , and neglect them in what follows. The distortion free-energy is

$$F_d = \begin{cases} \frac{1}{2}K_1\left(\frac{\partial \delta n_z}{\partial z}\right)^2 + \frac{1}{2}K_2\left(\frac{\partial \delta n_y}{\partial z}\right)^2 & (\text{Case a}) \\ \frac{1}{2}K_3\left(\frac{\partial}{\partial z} \delta \mathbf{n}\right)^2 & (\text{Case b}) \end{cases}$$

The magnetic energy density (neglecting now all diamagnetic effects) is

$$-\mathbf{M} \cdot \mathbf{H} \approx MH(1 - \frac{1}{2}(\delta \mathbf{n})^2).$$

As in the Frederiks transition, the instability occurs first for the Fourier component $\delta \mathbf{n}_q$ of wavevector $q = \pi/d$.

For this component the integrated free energy is given by

$$\frac{4\mathcal{F}}{d^2} = \begin{cases} (K_1 \delta n_z^2 + K_2 \delta n_y^2) \frac{\pi^2}{d^2} - MH(\delta n_z^2 + \delta n_y^2), \\ \left(K_3 \frac{\pi^2}{d^2} - MH \right) \delta \mathbf{n}^2. \end{cases} \quad \begin{array}{l} (\text{a}) \\ (\text{b}) \end{array}$$

Case a. If $K_1 < K_2$ we have an instability with respect to splay and a critical field

$$H_{cs} = \frac{\pi^2 K_1}{Md^2}.$$

If $K_1 > K_2$ we have an instability with respect to twist, and a critical field

$$H_{ct} = \frac{\pi^2 K_2}{Md^2}.$$

Case b. Here the instability is associated with a bending distortion, and the critical field is

$$H_{cb} = \frac{\pi^2 K_3}{Md^2}.$$

Note the $1/d^2$ dependence of these critical fields. Typically for $M = 1$ gauss, $K = 10^{-6}$ dyn, and $d = 3 \mu\text{m}$, $H_c = 100$ gauss. The main experimental problem is to achieve a stable colloid with the required properties.

Problem. A horizontal field \mathbf{H} is applied to the free surface of a nematic. Discuss the effect of \mathbf{H} on the energy per unit area, for a small tilt of the free surface around a horizontal axis normal to \mathbf{H} (Fig. 3.18).

Solution. We take the (xy) plane as representing the unperturbed surface (\mathbf{H} being parallel to the x -axis). The perturbed surface has an altitude $\zeta = \epsilon x$ where $\epsilon (\ll 1)$ is the tilt angle. The director \mathbf{n} is in the (x, y) plane, and makes a variable angle $\theta(z - \zeta)$ with the x -axis. Deep in the nematic $(-z + \zeta > \xi(\mathbf{H}))\mathbf{n}$ is parallel to $\mathbf{H}(\theta = 0)$. At the free surface, we assume strong anchoring $= \mathbf{n}$ must make a fixed angle ψ with the surface plane ($\psi = 0$ is the tangential case, $0 < \psi < \pi/2$ is a conical case, $\psi = \pi/2$ is the normal case). This means

$$\theta(z = \zeta) = \pm \psi + \epsilon.$$

The two signs correspond to two types of distortion (see Fig. 3.18). Let us consider for instance the case $\epsilon > 0$. Then the state of lowest distortion energy will correspond to $\theta(\zeta) = -\psi + \epsilon$. The distortion energy is easily derived in the one-constant

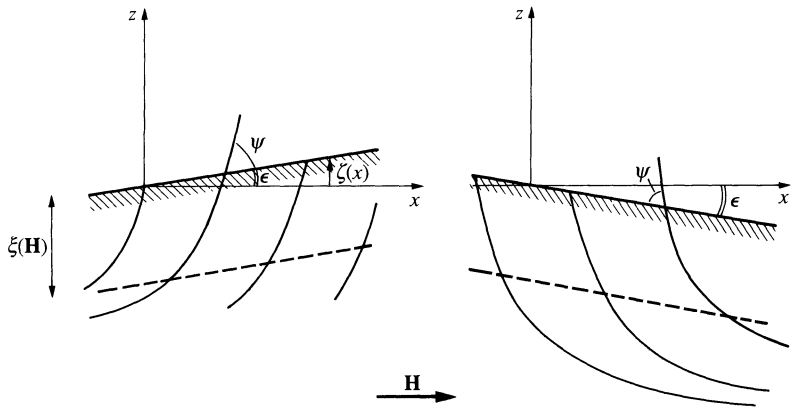


Fig. 3.18. Distortion of the free surface of a nematic under a magnetic field.

approximation. The equations are similar in form to those of Section 3.2.2, namely

$$\xi^2 \frac{d^2\theta}{dz^2} = \sin \theta \cos \theta,$$

$$\xi^2 \left(\frac{d\theta}{dz} \right)^2 = \sin^2 \theta,$$

$$\xi \frac{d\theta}{dz} = -\sin \theta$$

(— determination, corresponding to the more favourable distortion).

The distortion energy per cm² is

$$\begin{aligned} \mathcal{F}_d &= \frac{1}{2} K \int_{-\infty}^{\zeta} \left\{ \frac{\sin^2 \theta}{\xi^2} + \left(\frac{d\theta}{dz} \right)^2 \right\} dz = \frac{K}{\xi^2} \int_{-\infty}^{\zeta} \sin^2 \theta dz \\ &= \frac{K}{\xi} \int_0^{-\psi + \epsilon} \sin \theta d\theta = \frac{K}{\xi} \{1 - \cos(\psi - \zeta)\}. \end{aligned}$$

Expanding to first order in ϵ we have

$$\mathcal{F}_d - \mathcal{F}_d^0 - \frac{K \sin \psi}{\xi} \epsilon$$

Note that the other type of distortion, with θ going from 0 to $\psi + \epsilon$, would lead to a symmetrical formula

$$\mathcal{F}_d = \mathcal{F}_d^0 + \frac{K \sin \psi}{\xi} \epsilon.$$

To this energy must be added the conventional terms due to the surface tension A and to gravity g ;† calling ρ the density difference between the nematic and the over medium, this gives in general.

$$\mathcal{F}_{\text{surface}} = \int \int \left\{ \frac{1}{2} A \left(\frac{d\zeta}{dx} \right)^2 + \frac{1}{2} \rho g \zeta^2(x) \pm \frac{K \sin \psi}{\xi} \frac{d\zeta}{dx} \right\} dx dy$$

where we have generalized the result to arbitrary (slow) distortions $\zeta(x)$. For $\rho = 0$ the optimum slope would be

$$|\epsilon| = \left| \frac{d\zeta}{dx} \right| = \frac{K \sin \psi}{A \xi} \sim \frac{a}{\xi} \sin \psi \sim 10^{-3}$$

where we always call U a typical interaction energy, and put $A \sim U/2$. This tilt could be observed only if the densities are very nearly equal. If not, choosing a *definite sign* in $\mathcal{F}_{\text{surface}}$ and minimizing gives the standard equation [31]

$$\frac{d^2\zeta}{dx^2} = \zeta/\lambda^2, \quad \lambda = \sqrt{\left(\frac{A}{\rho g} \right)} \sim 1 \text{ mm.}$$

The new term comes only in the boundary conditions at the walls of the container. Thus a surface of dimensions $\gg \lambda$ will remain horizontal, if the distortion is everywhere of the same type. But if we allow for alternative regions, using *both* types of distortion, then we have a rugged surface; this will be discussed in Chapter 4.

3.3 ELECTRIC FIELD EFFECTS IN AN INSULATING NEMATIC

A static electric field \mathbf{E} imposed on a nematic have many physical effects, some of which are quite complex [32]. In the present section we restrict our attention to the case of a *perfect nematic insulator*.†

Even in this ideal situation, the coupling of an external electric field to a nematic medium involves at least two different processes. One is the anisotropy of the dielectric constant, and is similar in its consequences to the diamagnetic anisotropy described in Section 3.2. The second effect (invented by R. B. Meyer [33]) is far less trivial; in a deformed nematic, there should appear in many cases a spontaneous dielectric polarization. Conversely, an electric field may in some cases induce distortions in the bulk.

3.3.1 Dielectric anisotropy

The static dielectric constants, measured along ($\epsilon_{||}$) or normal (ϵ_{\perp}) to the nematic axis, are different. For a more general direction of the electric field

† Also, to avoid all possible injections of current carriers, the sample must be separated from all electrodes by suitable insulating layers.

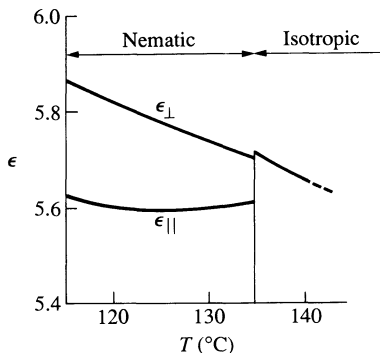


Fig. 3.19. Low-frequency dielectric constants for PAA. (After reference 20.)

E. the relation between electric displacement \mathbf{D} and field has the form

$$\mathbf{D} = \epsilon_{\perp} \mathbf{E} + (\epsilon_{\parallel} + \epsilon_{\perp}) (\mathbf{n} \cdot \mathbf{E}) \mathbf{n}. \quad (3.65)$$

The difference

$$\epsilon_a = \epsilon_{\parallel} - \epsilon_{\perp}, \quad (3.66)$$

may be positive or negative, depending on the detailed chemical structure of the constituent molecules.

1. If each molecule carries a permanent dipole moment parallel (or nearly parallel) to its long axis, the dipole can be oriented efficiently by a field \mathbf{E} along the nematic axis (if the field is, say, along $+\mathbf{n}$, there will be more dipoles along $+\mathbf{n}$ than along $-\mathbf{n}$). But a field \mathbf{E} normal to \mathbf{n} has only weak effects. Thus in this case we have $\epsilon_{\parallel} > \epsilon_{\perp}$. In practice, to realize large values of ϵ_a , it is efficient to attach at one end of the molecule a rather strongly polar group (assuming that it does not destroy the nematic order), pointing along the long axis, such as a $-\text{C}\equiv\text{N}$ group.
2. If there is a permanent dipole moment which is more or less normal to the long axis, the situation is reversed and $\epsilon_{\parallel} < \epsilon_{\perp}$. This is the case in particular with PAA, where the moment associated with the $\text{N}-\text{O}$ groups is dominant. A plot of dielectric constants versus temperature for PAA is shown in Fig. 3.19.

The dielectric anisotropy leads, in principle, to a method of alignment by electric fields. The electric contribution to the thermodynamic potential is (per cm^3)†

$$-\frac{1}{4\pi} \int \mathbf{D} \cdot d\mathbf{E} = -\frac{\epsilon_{\perp}}{8\pi} E^2 - \frac{\epsilon_a}{8\pi} (\mathbf{n} \cdot \mathbf{E})^2. \quad (3.67)$$

† The potential used here is that one must be minimized for fixed voltages applied on external conductors.

The first term is independent of orientation. The second term is the interesting one; it favours parallel alignment (\mathbf{n} collinear with \mathbf{E}) if $\epsilon_a > 0$, and perpendicular alignment if $\epsilon_a < 0$. For instance, pure PAA aligns perpendicular to E .†

The electric analogue of the Frederiks transition has been known since the days of Frederiks and Zvetkov; recent experiments and detailed theoretical calculations have been worked out by Gruler and Meier [23a]. The formula for the threshold field is identical to eqn (3.64), if one makes the substitution

$$\frac{1}{2}\chi_a H^2 \rightarrow \frac{\epsilon_a E^2}{8\pi}.$$

It is of interest to compare the relative efficiencies of an \mathbf{H} -field and of an \mathbf{E} -field. With the above correspondence we get $\mathbf{E} = (4\pi\chi_a/\epsilon_a)^{\frac{1}{2}}\mathbf{H}$. Taking $\chi_a = 10^{-7}$, $\epsilon_a = 0.1$, and $H = 1$ gauss, this gives $E \cong 3 \times 10^{-3}$ ues ≈ 1 V cm⁻¹. Thus roughly, one V cm⁻¹ is equivalent to one gauss. But in certain favourable cases ϵ_a can be made much larger. Above threshold ($E > E_c$) the detailed analysis differs for the electric case, because the distortions of the director field react on the field distribution inside the slab. Studies of the alignment for large specimens (no wall effects) in competing \mathbf{H} and \mathbf{E} fields have been carried out by Carr [23b].

3.3.2 Polarization induced by distortion (flexoelectric effect)

In certain solids, a strain will induce a polarization \mathbf{P} . The source of the strain may be an external pressure; for this reason the effect is called *piezoelectric*. In liquid crystals, a splay or a bending distortion can create a polarization: the physical origin of the effect is exemplified in Fig. 3.20 which is extracted from the work of R. B. Meyer [33]. He has also used the word ‘piezoelectric’ to describe this effect. This terminology might create some misunderstandings, since pressure does not influence the director \mathbf{n} in a nematic, and is thus unable to induce distortions and the associated polarizations: for this reason, we prefer the word ‘flexoelectric.’

To make the description of Fig. 3.20 quantitative, let us construct the most general form of the polarization \mathbf{P}_d which is induced by weak distortions. This means that we want \mathbf{P}_d to be proportional to the first-order space derivatives of the director \mathbf{n} (higher derivatives being smaller by successive powers of a/l and negligible in the continuum limit). Also \mathbf{P}_d must be an *even* function of \mathbf{n} , since, as repeatedly stated, the states \mathbf{n} and $-\mathbf{n}$ are equivalent. Finally \mathbf{P}_d must transform like a vector. The most general form of \mathbf{P}_d

† In impure PAA conductivity effects come into play and the trend may be reversed: see Chapter 5.

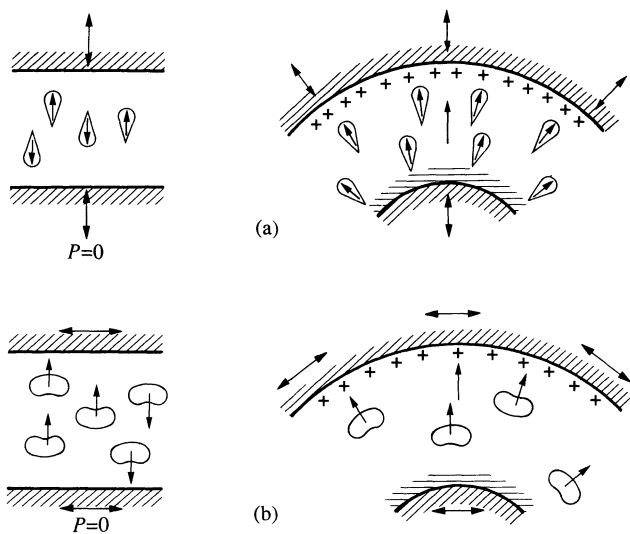


Fig. 3.20. Origin of the two flexoelectric constants in nematics (after R. B. Meyer). Case (a): Wedge-shaped molecules carrying permanent moments give $P \neq 0$ when a splay is imposed (for instance by suitable walls). Case (b): Banana-shaped molecules with a moment normal to their long axis give $P \neq 0$ under bending

satisfying these requirements is

$$\mathbf{P}_d = e_1 \mathbf{n}(\operatorname{div} \mathbf{n}) + e_3 (\operatorname{curl} \mathbf{n}) \times \mathbf{n}. \quad (3.68)$$

It involves two coefficients e_1 and e_3 , with the dimensions of an electric potential, and of arbitrary sign; we call them flexoelectric coefficients. With molecules which are very asymmetric in shape and carry a strong electric dipole moment μ_e the flexoelectric coefficients might reach values of order μ_e/a^2 where a is a typical molecular dimension. In all other cases (and in particular if the molecules do not have a permanent moment) they will be smaller [34].

In principle, e_1 and e_3 could be obtained from two types of experiment:

1. Measuring the polarizations (or the surface charges) induced by an imposed distortion. This could be done with bent condensers, as shown on Fig. 3.20(b). However, in practice, the charges on the condenser plates are easily screened out by impurity conduction; the experiments would require ultrapure materials.

2. Using the inverse effect: when a field \mathbf{E} is applied on a nematic single crystal, the alignment may become distorted, since a suitable distortion will imply a polarization \mathbf{P}_d parallel to \mathbf{E} . This inverse effect has apparently been observed by Schmidt, Schadt, and Helfrich on MBBA [35]. The principle is shown in Fig. 3.21. The sample is limited by two parallel glass surfaces,

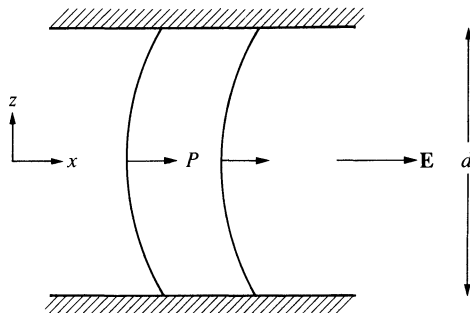


Fig. 3.21. Measurement of the flexoelectric coefficient e_3 . The molecules are assumed to be weakly anchored on both plates. Under the field E the molecular pattern distorts like a bow. The figure is drawn for e_3 positive.

treated with lecithin to achieve a homeotropic texture. However, it is necessary for the proposed interpretation of the experiment that the boundary conditions do *not* correspond to strong normal anchoring; the angle of the molecules at the surface must not be fixed. A field E is applied in the plane of the slab (along X); since $\epsilon_{\parallel} < \epsilon_{\perp}$ in MBBA, if dielectric effects were present alone, they would stabilize the alignment along the normal (z) to the plates. But in practice a distortion is observed, as described in Fig. 3.21. Such a distortion is a natural consequence of the flexoelectric effect, if weak anchoring is assured at both boundaries. To see this, let us write down the polarization $P_{d(x)}$ corresponding to a distortion of the form

$$n_z = \cos \phi(z) \approx 1 \quad (\phi \ll 1)$$

$$n = \sin \phi(z) \approx \phi(z).$$

From eqn (3.68) we get

$$P_{d(x)} = e_3 \frac{\partial \phi}{\partial z}. \quad (3.69)$$

For simplicity let us restrict ourselves to a case where the dielectric anisotropy ϵ_a is negligible. Then the free energy reduces to two contributions: the coupling of P_d with E , and the Frank elastic energy, which for the present case (with ϕ small) corresponds to a pure-bending type of deformation. The free energy per unit volume is thus

$$F = -P_{d(x)}E + \frac{1}{2}K_3 \left(\frac{\partial \phi}{\partial z} \right)^2.$$

Inserting the form found for $P_{d(x)}$ and minimizing F with respect to $\partial \phi / \partial z$

we find

$$\begin{aligned}\frac{\partial\phi}{\partial z} &= \frac{e_3}{K_3} E, \\ \phi &= \frac{e_3}{K_3} Ez.\end{aligned}\quad (3.70)$$

(In this last equation we took the origin in the midplane of the slab.) Clearly this form, leading to non-zero ϕ values on both plates, is valid only for weak anchoring. Typically, for fields E of order 300 V cm^{-1} the curvature $\partial\psi/\partial z$ is in the range of 10 cm^{-1} .

In the experiment of reference 35 the distortion was monitored by an interference method, measuring the different Δl in optical path lengths for rays propagating (along z) through the slab, with respective polarizations among x and y . The difference is easily shown to be

$$\Delta l = d(n_e - n_0)\bar{\psi}^2 \quad (\psi \ll 1)$$

where $n_e - n_0$ is the difference between extraordinary and ordinary indices, and $\bar{\psi}^2$ represents an average over the slab thickness d . Here we have

$$\bar{\psi}^2 = \frac{d^2}{12} \left(\frac{\partial\phi}{\partial z} \right)^2.$$

Thus, collecting our results, we find that

$$\Delta l = \frac{1}{12} \left(\frac{e_3}{K_3} \right)^2 (n_e - n_0) E^2 d^3. \quad (3.71)$$

The proportionality to $E^2 d^2$ is well confirmed by the experimental data. From the measured Δl , one can thus extract $|e_3| = 4.5 \cdot 10^{-5}$ cgs units.

The sign of e_3 must be obtained by a separate experiment; in reference 35 the space-charge $\rho = -\text{div } \mathbf{P}$ was probed through the resulting bulk force $\rho \mathbf{E}$; in suitable conditions (a sample with open ends) this force induces a hydrodynamic flow, the sign of which is easy to detect. From this it was concluded that $e_3 > 0$.

Some information on the flexoelectric coefficients can also be obtained from careful studies on simple Frederiks transitions under electric fields [36].

Another interesting consequence of the flexoelectric effect is that two distorted regions, remote from one another, in a nematic material may interact significantly through the Coulomb forces associated with their polarization charge. These charges are small, but the Coulomb force is of such long range that the effect may be sizeable. In fact, if the flexoelectric coefficients were large, the resulting contribution to the free energy would become comparable to F_d : the description based on the Frank elasticity only (i.e. on F_d) would then be quite incorrect [37]. In practice, however, the Frank elasticity is found to provide an acceptable description for PAA; this

may be due to the fact that the flexoelectric coefficients are not very large. Also, even if they are large, since PAA is usually not a very good insulator, the flexoelectric charges are screened out by impurity conduction.

3.4 FLUCTUATIONS IN THE ALIGNMENT

3.4.1 Light-scattering experiments

Nematics are turbid in appearance. The scattering of visible light by nematics is higher, by a factor of the order of 10^6 , than the scattering by conventional isotropic fluids. This was in fact one of the things which cast doubt on the very existence of liquid crystals in the early years; it was tempting to assume; that they were made of a suspension of small crystallites in a fluid phase, with crystallite dimensions comparable to an optical wavelength. However it became progressively clear that the high scattering power was in fact an intrinsic property of well-defined nematic phases. The first detailed experimental studies in this field are due to P. Chatelain [38]. As we shall see, they give us a very direct probe of the *spontaneous fluctuations of the alignment* in a nematic medium.

Typical scattering geometries are shown in Fig. 3.22. In all cases the crucial parameters are the wave vector \mathbf{k}_i , \mathbf{k}_f of the ingoing and outgoing beam inside the sample, and also the corresponding polarizations, defined by the unit vector \mathbf{i} and \mathbf{f} . The difference

$$\mathbf{g} = \mathbf{k}_i - \mathbf{k}_f$$

is the ‘scattering vector’. The plane (\mathbf{k}_i , \mathbf{k}_f) is the ‘scattering plane,’ and the angle between \mathbf{k}_i and \mathbf{k}_f is the ‘internal scattering angle’.

In the most simple case (case 1 of Fig. 3.22) both beams (\mathbf{k}_i and \mathbf{k}_f) are normal to the nematic axis. Depending on whether the polarizations \mathbf{i} and \mathbf{f} are normal or parallel to the optical axis, the beams propagate with the ‘ordinary’ refractive index n_{\perp} or with the ‘extraordinary’ index n_{\parallel} . (For PAA at 125°C with the sodium D-line, $n_{\perp} \approx 1.83$ and $n_{\parallel} \approx 1.57$). This allows us to compute the lengths of the wavevectors as a function of the optical frequency $\omega_0/2\pi$, using the relation†

$$k = n\omega_0/c \quad (c = \text{speed of light}).$$

Finally one can then construct the scattering wavevector \mathbf{q} for a given scattering angle, as shown in Fig. 3.22. Similar (but somewhat more complicated) rules hold for case 2.

Having specified these geometrical parameters, we can now list the main results obtained by Chatelain

† Note that, if the polarizations \mathbf{i} and \mathbf{f} are crossed, the lengths of \mathbf{k}_i and \mathbf{k}_f are different.

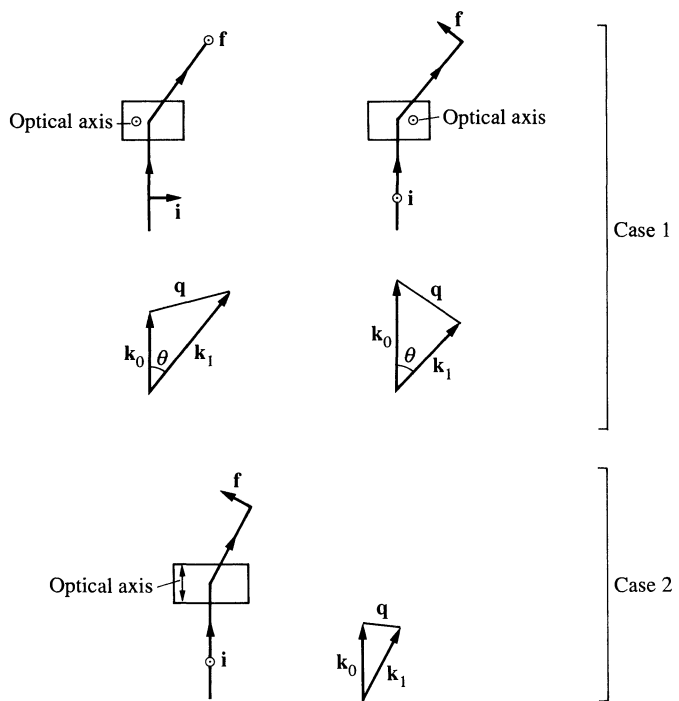


Fig. 3.22. A few typical geometries for the study of light scattering by a nematic single crystal. \mathbf{i} and \mathbf{f} are polarization vectors. (For the three examples shown the choices shown for \mathbf{i} and \mathbf{f} ensure a large scattering intensity.)

1. The scattering is intense only for cross polarizations (i.e. when \mathbf{i} and \mathbf{f} are not parallel). The weak residual intensity observed for \mathbf{i} parallel to \mathbf{f} is probably due mainly to multiple scattering.
2. The scattering is particularly strong at small \mathbf{q} . The precise law of intensity versus \mathbf{q} could not be derived, since, for technical reasons (collimation, multiple scattering, etc.), Chatelain could not work at very small \mathbf{q} s (which corresponds to small scattering angles: see Fig. 3.22, case 2).

As already mentioned, a tempting model for the interpretation of these scattering data is to invoke small objects (of diameter D in the micron range) each of these being optically anisotropic, and sending out depolarized light with no phase coherence between different objects. This is the essence of the so-called ‘swarm theory’ which has plagued the field of nematic liquid crystals for 30 years. In actual fact there is no reason for the director \mathbf{n} to stay constant in a region of dimension D and then to shift abruptly to another orientation; the energies associated with the abrupt shift would be prohibitively

large. The actual situation is much more continuous, and can be described rigorously in terms of small fluctuations of $\mathbf{n}(\mathbf{r})$: we shall now discuss this in detail.

3.4.2 Orientation fluctuations and correlations in a nematic single crystal [39]

We consider a nematic sample with optical axis z . The average director \mathbf{n}_0 is parallel to z . The fluctuations of the optical axis at any point \mathbf{r} will be described by small, non-zero components $n_x(\mathbf{r}), n_y(\mathbf{r})$. To second order in n_x, n_y the distortion energy (3.15) reduces to

$$\mathcal{F}_d = \frac{1}{2} \int \left\{ K_1 \left(\frac{\partial n_x}{\partial x} + \frac{\partial n_y}{\partial y} \right)^2 + K_2 \left(\frac{\partial n_x}{\partial y} - \frac{\partial n_y}{\partial x} \right)^2 + K_3 \left[\left(\frac{\partial n_x}{\partial z} \right)^2 + \left(\frac{\partial n_y}{\partial z} \right)^2 \right] \right\} d\mathbf{r}. \quad (3.72)$$

We may also impose a magnetic field H along z : this will add a term (derived from eqn (3.47))

$$\mathcal{F}_{\text{mag}} = \frac{1}{2} \int \chi_a H^2 (n_x^2 + n_y^2) d\mathbf{r} + \text{const.} \quad (3.73)$$

It is convenient to analyse $n_x(\mathbf{r})$ and $n_y(\mathbf{r})$ in Fourier components, defined by

$$n_x(\mathbf{q}) = \int n_x(\mathbf{r}) e^{i\mathbf{q} \cdot \mathbf{r}} d\mathbf{r}, \quad \text{etc.}$$

In terms of these Fourier components the free energy becomes

$$\begin{aligned} \mathcal{F} = \mathcal{F}_0 + \frac{1}{2} \Omega^{-1} \sum_{\mathbf{q}} & \{ K_1 |n_x(\mathbf{q}) q_x + n_y(\mathbf{q}) q_y|^2 + K_2 |n_x(\mathbf{q}) q_y - n_y(\mathbf{q}) q_x|^2 \\ & + (K_3 q_z^2 + \chi_a H^2) \{ |n_x(\mathbf{q})|^2 + |n_y(\mathbf{q})|^2 \} \} \end{aligned} \quad (3.74)$$

where Ω is the sample volume. For a given \mathbf{q} , it is convenient to diagonalize the quadratic form in eqn (3.74) by a linear transformation $(n_x, n_y) \rightarrow (n_1, n_2)$. The meaning of the axes (1) and (2) is the following. We introduce for each \mathbf{q} two unit vectors \mathbf{e}_1 and \mathbf{e}_2 in the (xy) plane: \mathbf{e}_2 is normal to \mathbf{q} ; \mathbf{e}_1 is normal to \mathbf{e}_2 . The component of $\mathbf{n}(\mathbf{q})$ along \mathbf{e}_α is called $n_\alpha(\mathbf{q})$ ($\alpha = 1, 2$). $n_1(\mathbf{q})$ describes a periodic distortion which is a mixture of splay and bend. $n_2(\mathbf{q})$ describes a periodic distortion which is a mixture of twist and bend. In terms of n_1 and n_2 the free energy takes a very simple form

$$\mathcal{F} = \mathcal{F}_0 + \frac{1}{2} \Omega^{-1} \sum_{\mathbf{q}} \sum_{\alpha=1,2} |n_\alpha(\mathbf{q})|^2 (K_3 q_{||}^2 + K_\alpha q_\perp^2 + \chi_a H^2) \quad (3.75)$$

where $q_{||} = q_z$ is the component of the wavevector parallel to the optical axis, while $\mathbf{q}_\perp = \mathbf{q} \cdot \mathbf{e}_1$ is the normal component. In eqn (3.75) the various

degrees of freedom are decoupled. We are now in a position to derive the thermal average of $|n_\alpha(q)|^2$. For this, we apply the *equipartition theorem*: for a classical system,[†] with free energy quadratic in the amplitudes $n_\alpha(\mathbf{q})$, the average \mathcal{F} , per degree of freedom, at thermal equilibrium, is equal to $\frac{1}{2}(k_B T)$.

$$\begin{aligned}\langle \frac{1}{2}\Omega^{-1}|n_\alpha(\mathbf{q})|^2(K_3 q_{||}^2 + K_\alpha q_\perp^2 + \chi_a H^2) \rangle &= \frac{1}{2}k_B T \\ \langle |n_\alpha(q)|^2 \rangle &= (\Omega k_B T)/(K_3 q_{||}^2 + K_\alpha q_\perp^2 + \chi_a H^2)\end{aligned}\quad (3.76)$$

where the brackets $\langle \rangle$ denote a thermal average. Equation (3.76) is the central formula of fluctuation theory for nematics.

From eqn (3.76) we may derive the correlation between values of the director \mathbf{n} taken at two different points \mathbf{r}_1 and \mathbf{r}_2 in the nematic. From the general theorem on Fourier transforms we have, for instance

$$\langle n_x(\mathbf{r}_1) n_x(\mathbf{r}_2) \rangle = \Omega^{-2} \sum_{\mathbf{q}, \mathbf{q}'} \langle n_x(\mathbf{q}) n_x(-\mathbf{q}') \rangle \exp\{i(\mathbf{q}' \cdot \mathbf{r}_2 - \mathbf{q} \cdot \mathbf{r}_1)\}.$$

The Fourier components $\mathbf{n}(\mathbf{q}), \mathbf{n}(\mathbf{q}')$ for different values of the wavevector are uncorrelated. Thus

$$\langle n_x(\mathbf{r}_1) n_x(\mathbf{r}_2) \rangle = \Omega^{-2} \sum_{\mathbf{q}} \langle |n_x(\mathbf{q})|^2 \rangle \exp(-i\mathbf{q} \cdot \mathbf{R}),$$

$$\mathbf{R} = \mathbf{r}_2 - \mathbf{r}_1.$$

We can now transform from $n_x(\mathbf{q})$ to $n_\alpha(\mathbf{q})$ and use the equipartition formula (3.76). The algebra is rather tedious, except in one case; if we make the one-constant approximation, the denominator of (3.76) becomes simply $K(q^2 + \xi^{-2})$ where ξ is the magnetic coherence length. Then

$$\begin{aligned}\langle n_x(\mathbf{r}_1) n_x(\mathbf{r}_2) \rangle &= \langle n_y(\mathbf{r}_1) n_y(\mathbf{r}_2) \rangle = (2\Omega)^{-2} \sum_{\mathbf{q}} \langle |n_1(\mathbf{q})|^2 + |n_2(\mathbf{q})|^2 \rangle \exp(-i\mathbf{q} \cdot \mathbf{R}) \\ &= (2\pi)^{-3} \int k_B T / \{K(q^2 + \xi^{-2})\} \exp(-i\mathbf{q} \cdot \mathbf{R}) \\ &= (k_B T / 4\pi K R) \exp(-R/\xi).\end{aligned}\quad (3.77)$$

Equation (3.77) is valid only in the continuum limit, i.e., for $R \gg a$. Let us discuss it first in the case of zero field. Then ξ is infinite (see eqn (3.58)) and the correlations $\langle n_x n_x \rangle$ decrease slowly with distance; the $1/R$ dependence is the direct analogue of that found for the distortion around a floating object in the Problem in Section 3.2.5.

Note that, in zero field, it is not possible to define a characteristic length D above which the correlations die out rapidly. This is in sharp contradiction

[†] Quantum corrections to the equipartition theorem come in only when $\hbar\omega_\alpha(\mathbf{q}) > k_B T$, where $\omega_\alpha(\mathbf{q})$ is a characteristic oscillation or relaxation frequency for the mode (α, \mathbf{q}) [40]. These modes will be discussed in Chapter 5. For long wavelengths ($qs \ll 1$), their characteristic frequencies are indeed much lower than $k_B T$.

with the swarm model, which assumes strong correlation at distances R smaller than the swarm diameter, and zero correlation at larger R .

When the differences between the three elastic constants K_i are allowed for, one still finds a slow decrease essentially like $1/R$. The exact formula is

$$\begin{aligned} & \langle n_x(\mathbf{r}_1) n_x(\mathbf{r}_2) + n_y(\mathbf{r}_1) n_y(\mathbf{r}_2) \rangle \\ &= (k_B T / 4\pi) \{ (K_3 K_1)^{-\frac{1}{2}} R_1^{-1} \} + \{ (K_3 K_2)^{-\frac{1}{2}} R_2^{-1} \} \quad (H = 0) \end{aligned} \quad (3.78)$$

where

$$\begin{aligned} R_\alpha &= \sqrt{(x^2 + y^2 + z_\alpha^2)}, \\ z_\alpha &= z(K_\alpha/K_3)^{\frac{1}{2}}. \end{aligned}$$

This type of $1/R$ decrease is found for the transverse correlations of all physical systems where:

1. The ordered state is characterized by a privileged axis (\mathbf{n}_0), but the direction of \mathbf{n}_0 is arbitrary.
2. The interactions are short range. For instance, similar correlations are found in the ordered phase of a Heisenberg ferromagnet in zero field.

In a finite field \mathbf{H} , eqn (3.77) shows that the range of the correlations of \mathbf{n} is the magnetic coherence length ξ . We had defined ξ earlier by the range of the distortions induced in the nematic by a local perturbation (a wall, a floating object, etc.). The equivalence of these two definitions for ξ is a consequence of general relations existing between response functions and correlation functions [35].

Problem. Discuss the corrections to the fluctuation intensities $\langle |\delta n_\alpha(\mathbf{q})|^2 \rangle$ when flexoelectric effects are included for a pure (insulating) nematic in zero external electric fields [37].

Solution. Let us call $\delta\mathbf{n}$ the vector $(n_x, n_y, 0)$. The flexoelectric polarization (eqn (3.68)) has the components $P_{||} = e_1 \operatorname{div} \delta\mathbf{n}$ and $P_{\perp} = e_3 \frac{\partial}{\partial z} \delta\mathbf{n}$. Introducing the electric field $\mathbf{E} = -\nabla V$ and the displacement $D = \epsilon \cdot \mathbf{E} + 4\pi\mathbf{P}$, writing that $\operatorname{div} \mathbf{D} = 0$ one arrives at the following equation for the Fourier component V_q of the potential

$$\mathbf{q} \cdot \boldsymbol{\epsilon} \cdot \mathbf{q} V_q = 4\pi e q_{||} (\mathbf{q} \cdot \mathbf{n}_q) = 4\pi e q_{||} q_{\perp} n_1(\mathbf{q})$$

$$e = e_1 + e_3.$$

We can then compute the thermodynamic potential at constant \mathbf{E} , G_E (using eqn (3.75) or the thermodynamic potential at constant \mathbf{D} , $G_D = G_E + \mathbf{E} \cdot \mathbf{D} / 4\pi$; for the present problem they are in fact equal, because D_q is normal to \mathbf{q} , while E_q is parallel

to \mathbf{q} . The result is

$$\begin{aligned} G &= \mathcal{F}_d + \Omega^{-1} \sum_q \frac{\mathbf{q} \cdot \boldsymbol{\varepsilon} \cdot \mathbf{q}}{8\pi} |V_q|^2 \\ &= \frac{1}{2}\Omega^{-1} \sum_q [|n_1(q)|^2 \{K_1 q_\perp^2 + K_3 q_\parallel^2 + \chi_a H^2 + (4\pi e^2 q_\parallel^2 q_\perp^2 / q_\parallel^2 \varepsilon_\parallel + q_\perp^2 \varepsilon_\perp)\} \\ &\quad + |n_2(q)|^2 \{K_2 q_\perp^2 + K_3 q_\parallel^2 + \chi_a H^2\}]. \end{aligned}$$

Thus the contribution of the modes (1) to the thermodynamic potential is modified, and the correction brings in a novel angular dependent on \mathbf{q} . One can then derive the change in $\langle |n_1(\mathbf{q})|^2 \rangle$ by the equipartition theorem. The shift in $|n_1^2|$ and the resulting effect on light scattering may become an efficient way of displaying flexoelectric effects in pure nematics.

3.4.3 Scattering of light by orientation fluctuations

The propagation of light is sensitive to fluctuations in the dielectric tensor

$$\epsilon_{\alpha\beta} = \epsilon_\perp \delta_{\alpha\beta} + (\epsilon_\parallel - \epsilon_\perp) n_\alpha n_\beta.$$

(The reader may verify for himself that this form of $\boldsymbol{\varepsilon}$ gives $\epsilon = \epsilon_\parallel$ for an electric field parallel to \mathbf{n} , etc.)

The fluctuations of $\boldsymbol{\varepsilon}$ may come from two sources: (1) fluctuations in the magnitude of ϵ_\parallel and ϵ_\perp , due to small, local, changes in the density, the temperature, etc.; and (2) fluctuations in the orientation of \mathbf{n} ; this is the dominant effect, specific to the nematic phase, which we shall now discuss.

In general, the analysis of light scattering in an *anisotropic* medium including the correct variations of refraction indices with beam orientation, and the correct definition of photometric intensities is delicate. For this reason we will restrict our attention to the limiting case where $\epsilon_a = \epsilon_\parallel - \epsilon_\perp$ is small, so that both the ingoing and the outgoing beams may be described as propagating in an isotropic medium. This approximation is not too good for a material like PAA (where $\epsilon_\parallel = n_\parallel^2 \approx 3.3$ and $\epsilon_\perp = n_\perp^2 = 2.3$ at 125°C), but it allows for a much more explicit display of the important physical features.

Let us first derive a formula for the *scattering cross-section*. Our starting point is the formula giving the field radiated by a dipole \mathbf{P} , oscillating at the angular frequency ω , and located at point \mathbf{r}

$$\mathbf{E}(\mathbf{r}') = (\omega^2/c^2 R) \exp(ikR) \mathbf{P}_v(r) \quad (3.79)$$

where $k = \bar{n}\omega/c$, \bar{n} being the average refraction index, and \mathbf{P}_v is the component of \mathbf{P} normal to the observation direction $\mathbf{R} = \mathbf{r}' - \mathbf{r}$ (c is the velocity of light).

Let us write that the dipoles \mathbf{P} are induced by the ingoing radiation field $\mathbf{E}_{in}(\mathbf{r}) = E_i \exp(i\mathbf{k}_0 \cdot \mathbf{r})$ (E =amplitude, i =unit vector specifying the

polarization)

$$\mathbf{P}(\mathbf{r}) = (4\pi)^{-1}(\boldsymbol{\epsilon}(\mathbf{r}) - \mathbf{1})\mathbf{E}_{\text{in}}(\mathbf{r}),$$

where $\mathbf{1}$ represents a unit tensor.

The outgoing field $\mathbf{E}_{\text{out}}(\mathbf{r}')$ is obtained by summing all the contributions (3.79) over the volume of the sample. If \mathbf{r}' is far enough from the scattering region the factor $1/R$ may be taken out of the integral. We may also write $kR = \mathbf{k}_1 \cdot \mathbf{R} = \mathbf{k}_1(r' - r)$ where \mathbf{k}_1 is the wavevector in the direction of the outgoing beam. Projecting \mathbf{E}_{out} on the final polarization direction \mathbf{f} (\mathbf{f} normal to \mathbf{k}_1) we arrive at

$$\begin{aligned} \mathbf{f} \cdot \mathbf{E}_{\text{out}}(\mathbf{r}') &= (E/R) \exp(i\mathbf{k} \cdot \mathbf{r}') \alpha, \\ \alpha &= \omega^2/4\pi c^2 \int_{(\Omega)} \{\mathbf{f} \cdot (\boldsymbol{\epsilon}(\mathbf{r}) - \mathbf{1}) \cdot \mathbf{i}\} \exp(-i\mathbf{q} \cdot \mathbf{r}) d\mathbf{r}, \quad (3.80) \\ \mathbf{q} &= \mathbf{k}_0 - \mathbf{k}. \end{aligned}$$

The length α is called the *scattering amplitude*. Note that for $q \neq 0$ the term $(-\mathbf{1})$ in $(\boldsymbol{\epsilon}(\mathbf{r}) - \mathbf{1})$ does not contribute to the integral $\int d\mathbf{r}$. In terms of the Fourier transform

$$\boldsymbol{\epsilon}(\mathbf{q}) = \int_{(\Omega)} \boldsymbol{\epsilon}(\mathbf{r}) \exp(-i\mathbf{q} \cdot \mathbf{r}) d\mathbf{r},$$

we may write

$$\alpha = (\omega^2/4\pi c^2)\mathbf{i} \cdot \boldsymbol{\epsilon}(\mathbf{q}) \cdot \mathbf{f} \quad (3.81)$$

The differential cross-section (per unit solid angle of the outgoing beam around the direction \mathbf{k}_1) is

$$\sigma = \langle |\alpha|^2 \rangle \quad (3.82)$$

where the brackets $\langle \rangle$ as always denote a thermal average.

Let us now restrict our attention to the contribution in $\boldsymbol{\epsilon}(\mathbf{q})$ which are due to fluctuations in the optical axis \mathbf{n} , putting $\mathbf{n} = \mathbf{n}_0 + \delta\mathbf{n}$, with $\delta\mathbf{n} = (n_x n_y 0)$, and expanding $\boldsymbol{\epsilon}$ to first order in $\delta\mathbf{n}$, using (3.78) we get

$$\mathbf{f} \cdot \boldsymbol{\epsilon} \cdot \mathbf{i} = \mathbf{f} \cdot \langle \boldsymbol{\epsilon} \rangle \cdot \mathbf{i} + \epsilon_a(\mathbf{f} \cdot \delta\mathbf{n})(\mathbf{n}_0 \cdot \mathbf{i}) + \epsilon_a(\mathbf{f} \cdot \mathbf{n}_0)(\delta\mathbf{n} \cdot \mathbf{i}).$$

The first term, being independent of \mathbf{r} , does not contribute to the Fourier transform at finite \mathbf{q} . The second and third terms are linear in $\delta\mathbf{n}(\mathbf{q})$. It is convenient to analyse $\delta\mathbf{n}(\mathbf{q})$ into the eigenmodes n_1, n_2 , defined in the preceding paragraph

$$\delta\mathbf{n}(\mathbf{q}) = \mathbf{e}_1 n_1(\mathbf{q}) + \mathbf{e}_2 n_2(\mathbf{q}).$$

When we square the scattering amplitude (3.81) and take the average, the cross terms involving $n_1 n_2^*$ disappear, the two modes being uncorrelated.

Thus we are left with

$$\sigma = (\epsilon_a \omega^2 / 4\pi c^2)^2 \sum_{\alpha=1,2} \langle |n_\alpha(\mathbf{q})|^2 \rangle (i_\alpha f_z + i_z f_\alpha)^2 \quad (3.83)$$

where $\mathbf{i}_\alpha = \mathbf{e}_\alpha \cdot \mathbf{i}$, etc. The final formula for σ is obtained by inserting eqn (3.76) for the thermal averages.

$$\sigma = \Omega (\epsilon_a \omega / 4\pi c^2)^2 \sum_{\alpha=1,2} (k_B T / (K_3 q_{||}^2 + K_\alpha q_\perp^2 + \chi_a H^2)) (i_\alpha f_z + i_z f_\alpha)^2, \quad (3.84)$$

Let us discuss first the order of magnitude of σ ; it is proportional to the sample volume Ω , as it should be, and roughly given by

$$\sigma \sim \Omega (\epsilon_a \omega^2 / 4\pi c^2)^2 (k_B T / K q^2) \quad (\text{in zero magnetic field}). \quad (3.85)$$

To get a better feeling for this result let us compare it to the scattering by an isotropic liquid, of dielectric constant ϵ . Here the fluctuations of ϵ are mainly due to fluctuations in the density. Defining a local dilation $\theta(\mathbf{r})$ we may write $\epsilon = \bar{\epsilon} + \epsilon' \theta(\mathbf{r})$. The corresponding cross-section, as derived from eqns (3.81) and (3.82) is

$$\sigma|_{\text{isotropic}} = \Omega (\epsilon' \omega^2 / 4\pi c^2)^2 (\mathbf{f} \cdot \mathbf{i})^2 \langle |\theta(\mathbf{q})|^2 \rangle. \quad (3.86)$$

To find $\langle |\theta(\mathbf{q})|^2 \rangle$ we write down a compressional free energy

$$f_e = \frac{1}{2} \int W \theta^2(\mathbf{r}) d\mathbf{r} = W/2\Omega \sum_q |\theta_q|^2 \quad (3.87)$$

where W^{-1} is the isothermal compressibility. Applying the equipartition theorem we get $\langle |\theta_q|^2 \rangle = \Omega k_B T / W$. Inserting this into (3.86) and comparing with σ we get

$$\sigma/\sigma|_{\text{iso}} \sim (\epsilon_a / \epsilon)^2 (W / K q^2).$$

For an order of magnitude estimate we can put $\epsilon_a / \epsilon' \sim 1$, $K \sim U/a$, and $W \sim U/a^3$ where U is a typical binding energy. This gives

$$\sigma/\sigma|_{\text{iso}} \sim 1/(qa)^2.$$

$2\pi/q$ is comparable to an optical wavelength (or even larger for scattering at small angles). Thus $qa \sim 10^{-3}$ and the scattering in the nematic phase may be a million times larger than the scattering in the isotropic phase. Physically, we may say that in isotropic liquids, a long wavelength modulation of ϵ requires a uniform *dilation*, and this implies a finite elastic energy. On the other hand, in a nematic fluid, we may modify ϵ simply by a *rotation* of the optical axis. If the rotation is nearly uniform ($q \rightarrow 0$) this requires very little energy (see eqn (3.75), with $H = 0$). Thus eqn (3.84) does explain why the scattering is large, and particularly large at small q values. The polarization effects may also be accounted for; consider for instance the case 1 of

Fig. 3.22, with an ingoing polarization \mathbf{i} normal to the optical axis ($i_z = 0$), and 0 angle scattering (\mathbf{k}_1 nearly parallel to \mathbf{k}_0). Then, if \mathbf{f} is parallel to \mathbf{i} ($f_z = 0$), the polarization factor in (3.84) vanishes, while if \mathbf{f} is normal to \mathbf{i} ($f_z = 0$) we get a large cross-section. Similar agreement is found for the other cases.

The above calculations have been refined by Langevin and Bouchiat [41] to include the anisotropy in the initial and final states (ϵ_a being now not necessarily small). They have applied their results to a discussion of the total scattering cross-section, i.e. of the *turbidity* of a nematic. They measured this turbidity in MBBA, after careful elimination of multiple scattering effects. Using beams which are parallel or normal to the optical axis, and different polarizations, they are able to extract the *three* elastic constants from the data: the results are in rather good agreement with the direct measurements compiled in Table 3.2.

Let us end this paragraph with a discussion of the information that could be obtained from more detailed scattering measurements, particularly in the small- q region.[†] In most experiments, absolute values of cross-sections are not measured. But, by a suitable choice of geometry and using formulae such as (3.83), one could extract from the data the thermal averages $\langle |n_\alpha(\mathbf{q})|^2 \rangle$, except for a constant scale factor.

When $H = 0$, we expect from (3.76) that $\langle |n_\alpha(\mathbf{q})|^2 \rangle$ should be inversely proportional to $K_3 q_{\parallel}^2 + K_\alpha q_{\perp}^2$. Studying the dependence of the cross-section on the angle between \mathbf{q} and the optical axis, one should be able to extract the ratios K_α/K_3 .

With a strong field \mathbf{H} , the fluctuations $\langle |n_\alpha(\mathbf{q})|^2 \rangle$ are decreased; they become inversely proportional to $K_3 q_{\parallel}^2 + K_\alpha q_{\perp}^2 + \chi_a H^2$.[‡] If χ_a is known, it then becomes possible to measure the *magnitudes* of the three elastic constants from relative intensity measurements at various \mathbf{q} s. The experiment has been performed (with electric fields \mathbf{E} , instead of magnetic fields \mathbf{H} , as the orienting agent) [43].

In practice, there are some slight complications due to the anisotropy of the medium: for instance, as we have already mentioned, q does not tend to zero at zero scattering angle in case I with crossed polarizations, because the magnitudes of \mathbf{k}_0 and \mathbf{k}_1 are different. But, independently of these details, light scattering studies do allow for quantitative measurements of the elastic constants.

A final word of comment on the *temperature dependence* of the scattering. The main factors, displayed in eqn (3.85), are the dielectric anisotropy $\epsilon_a(T)$ and the elastic constant K . (The factor $k_B T$ gives but weak effects in the narrow range of existence of the nematic phase.) The intensity (at fixed \mathbf{q})

[†] This limit is interesting for two reasons: (1) because the scattering is very large; (2) because (in cases I and II) the outgoing beam propagates in a direction for which the refraction indices are well known and only weakly dependent on the scattering angle.

[‡] An increase in transmission under magnetic fields was observed long ago by Moll and Ornstein [42].

is essentially proportional to ϵ_a^2/K . Both ϵ_a and K tend to decrease rather strongly when $T \rightarrow T_c$ (the nematic-isotropic transition point). But the ratio ϵ_a^2/K is only weakly temperature dependent; in a mean field theory of the Maier/Saupe type, ϵ_a is linear in S while $K \sim S^2$; thus ϵ_a^2/K is independent of S . Indeed the temperature effects found by Chatelain [39] are small.

Problem. Discuss the effect of a large magnetic field \mathbf{H} on the birefringence of a nematic single crystal.

Approximate solution. The effect of \mathbf{H} is to decrease the magnitude of the fluctuations in the nematic. Putting always \mathbf{H} (and \mathbf{n}_0) parallel to the z -axis, we estimate the fluctuations of the director \mathbf{n} at one point \mathbf{r} by inverting the Fourier transform at (3.76)

$$\langle n_x^2(\mathbf{r}) \rangle = (2\pi)^{-3} \int k_B T / \{K(q^2 + \xi^{-2})\} d\mathbf{q}$$

where for simplicity we make the one-constant approximation. The integral over \mathbf{q} must be cut off at certain $q_{\max} \sim 1/a$ (limit of validity of the continuum theory). Performing the integration gives

$$\langle n_x^2 \rangle = k_B T / 2\pi^2 K (q_{\max} - \pi/2\xi) = \langle n_y^2 \rangle.$$

From this we get $\langle n_z^2 \rangle = 1 - \langle n_x^2 \rangle - \langle n_y^2 \rangle$ and the effective anisotropy of the dielectric constant

$$\langle \epsilon_{\parallel} - \epsilon_{\perp} \rangle = \epsilon_{a0} \langle n_z^2 \rangle$$

where ϵ_{a0} is the dielectric anisotropy for full alignment. This result contains a term independent of H , and a term linear in $|H|$, in which we are primarily interested

$$\langle \epsilon_{\parallel} - \epsilon_{\perp} \rangle = \epsilon_a(T) + \epsilon_{a0} k_B T / 2\pi K \xi = \epsilon_a(T) + \epsilon_{a0} k_B T \chi_a^{1/2} / 2\pi K^{3/2} |H|$$

Taking $\epsilon_{a0} \approx 1$, $T = 400$ K, $\chi_a = 10^{-7}$, $K = 10^{-6}$, and $H = 10^5$ oersteds, the correction term is of order 4×10^{-4} , corresponding to a change in refractive index anisotropy of order 10^{-4} . The anomalous exponent $|H|$ has been predicted independently by J. Alcantara† for a similar problem in magnetic systems. However, it must be emphasized that the solution is only approximate. But in any case it would be interesting to observe this effect, possibly with pulsed magnetic fields.

Problem. Discuss the correlations and the scattering of light in a nematic film floating at the surface of a fluid (two-dimensional nematic).

Solution. We assume that the film is of molecular thickness; such films might possibly be achieved with certain long molecules floating on a liquid surface. If the temperature is not too high, and if the surface density is suitable, we may postulate that, locally, at any point $\mathbf{p}(x, y)$ the nematic molecules are aligned along a certain direction $\mathbf{n}(x, y)$ in the film plane. However, as we shall see, there is no long-range order.

Let us start from the distortion free energy: there are two types of distortion (splay

† To be published.

and bend). For simplicity, we shall make the one-constant approximation, and write

$$F_d = \frac{1}{2}K(\nabla\theta)^2 = \frac{1}{2}K \left\{ \left(\frac{\partial\theta}{\partial x} \right)^2 + \left(\frac{\partial\theta}{\partial y} \right)^2 \right\}.$$

Here F_d is an energy per cm^2 and K has the dimensions of energy (ML^2T^{-2}). θ is the angle between \mathbf{n} and a fixed direction (x) in the plane of the film. Applying the equipartition theorem as in eqn (3.76) we get for a two-dimensional Fourier component of wavevector $\mathbf{q}(q_x q_y, 0)$,

$$\langle |\theta_{\mathbf{q}}|^2 \rangle = \frac{k_B T}{K q^2}$$

and, by inversion,

$$\begin{aligned} \sigma^2(\rho_{12}) &= \langle \{(\theta_{\mathbf{p}_1}) - \theta_{\mathbf{p}_2}\}^2 \rangle = \int \int (2\pi)^{-2} 2 \{1 - \exp(i\mathbf{q} \cdot \mathbf{p}_{12})\} \langle |\theta_0|^2 \rangle d\mathbf{q}_x d\mathbf{q}_y \\ &= (k_B T / \pi K) \ln(\rho_{12} a) \end{aligned}$$

where $\rho_{12} = |\mathbf{p}_2 - \mathbf{p}_1|$ and a is a cut-off distance, of the order of the molecular length. This formula shows that the mean-square deviation $\sigma^2(\rho_{12})$ diverges when the distance ρ_{12} between the two observation points becomes large; there is no long-range order. The distribution law for $\delta = \theta(\mathbf{p}_2) - \theta(\mathbf{p}_1)$ is a Gaussian

$$p(\delta) = \sigma^{-1} (2\pi)^{-\frac{1}{2}} \exp(-\delta^2/2\sigma^2).$$

As we shall see, the correlation function which is directly of interest for light scattering experiments is

$$\langle \cos\{2\theta(\mathbf{p}_1) - 2\theta(\mathbf{p}_2)\} \rangle = \int \cos(2\delta) p(\delta) = \exp(-2\sigma^2) = (a/\rho_{12})^x.$$

where $x(T) = 2k_B T / \pi K$ is a temperature-dependent quantity, and is probably of the order of unity in the temperature range where local nematic order exists.

Let us now apply this to the scattering of light by orientation fluctuations. We call \mathbf{q} the projection of the scattering wave vector on the plane of the film. A dimensionless scattering amplitude at point \mathbf{p} may be defined as

$$\alpha = \{2(\mathbf{i} \cdot \mathbf{n})(\mathbf{f} \cdot \mathbf{n}) - (\mathbf{i} \cdot \mathbf{f})\} e^{i\mathbf{q} \cdot \mathbf{p}}$$

where \mathbf{i} and \mathbf{f} are the incident and emergent polarizations; for simplicity we assume that both light beams are nearly vertical, so that \mathbf{i} and \mathbf{f} are in the plane of the film. If θ_i and θ_f are the angles of \mathbf{i} and \mathbf{f} with the x -axis we may write

$$\begin{aligned} \alpha &= \cos(2\theta - \theta_i - \theta_f) e^{i\mathbf{q} \cdot \mathbf{p}} = \cos 2(\theta - \bar{\theta}) e^{i\mathbf{q} \cdot \mathbf{p}}, \\ 2\bar{\theta} &= \theta_i + \theta_f. \end{aligned}$$

The scattered intensity is then proportional to

$$\begin{aligned} I(\mathbf{q}) &= \int \langle \cos 2(\theta_1 - \bar{\theta}) \cos 2(\theta_2 - \bar{\theta}) \rangle e^{i\mathbf{q} \cdot \mathbf{p}_{12}} d\mathbf{p}_{12} \\ &= \frac{1}{2} \int \langle \cos 2(\theta_1 - \theta_2) \rangle e^{i\mathbf{q} \cdot \mathbf{p}_{12}} d\mathbf{p}_{12} \\ &= \text{const}(a^x/q^{2-x}). \end{aligned}$$

Since $x > 0$, the divergence of $I(\mathbf{q})$ at small q is weaker than in a three-dimensional nematic.

This must be compared to the scattering caused by capillary waves at the liquid surface. The dimensionless scattering amplitude for the latter process is of the form

$$\alpha_c = \{\zeta(\mathbf{p})/b\}(\mathbf{i} \cdot \mathbf{f}) e^{i\mathbf{q} \cdot \mathbf{p}}$$

where ζ is the vertical displacement at the interface and b is a molecular length. The corresponding intensity is

$$I_c(\mathbf{q}) = \langle |\zeta(\mathbf{q})|^2 \rangle (\mathbf{i} \cdot \mathbf{f})^2 / b^2 = (k_B T / Ab^2 q^2) (\mathbf{i} \cdot \mathbf{f})^2$$

where A is the surface tension.

The ratio of the two intensities is thus

$$I/I_c = Ab^2/k_B T (qa)^x (\mathbf{i} \cdot \mathbf{f})^{-2}.$$

$Ab^2/k_B T$ will often be of order unity, but $qa \ll 1$. Thus the scattering due to orientation fluctuations can be dominant only if: (1) $x(T)$ is not too large; and (2) the polarization vectors \mathbf{i} and \mathbf{f} are orthogonal.

3.5 HYDROSTATICS OF NEMATICS

3.5.1 Free energy and molecular field

In Sections 3.1.5 and 3.2.2 we discussed the transmission of torques through nematics for situations of simple twist. It is sometimes useful to define stresses and torques for more general cases, as was first done by Ericksen [44]. We shall describe this here, restricting our attention (for simplicity) to incompressible nematics, under a homogeneous magnetic field \mathbf{H} (we postulate no electric field and no flexoelectric effect). The free-energy density then includes three contributions

$$F = F_d + F_m + F_g. \quad (3.88)$$

F_d is the distortion energy (eqn 3.15), F_m is the magnetic energy (defined in eqn (3.47)), and $F_g = \rho\phi$ where ϕ is the gravitational potential and ρ the density.

One basic concept, introduced by eqns (3.21) and (3.49) is that of the *molecular field* $\mathbf{h}(\mathbf{r})$

$$h_\alpha = \partial_\gamma \pi_{\gamma\alpha} - \frac{\partial F_d}{\partial n_\alpha} + \gamma_a (\mathbf{n} \cdot \mathbf{H}) H_\alpha \quad (3.89)$$

where we use the notation

$$\pi_{\gamma\alpha} = \frac{\delta F_d}{\delta(\partial_\gamma n_\alpha)} = \frac{\delta F_d}{\delta g_{\gamma\alpha}}. \quad (3.90)$$

As explained in Section 3.1, the equilibrium condition for the director is that

\mathbf{h} be parallel to \mathbf{n} at all points

$$h_\alpha = \lambda(\mathbf{r})n_\alpha. \quad (3.91)$$

3.5.2 Stresses and forces

Equation (3.91) was obtained by considering the change in total free energy δf_{tot} due to small rotations of \mathbf{n} . We shall now study δf_{tot} for another type of transformation, where the centres of gravity of the molecules are displaced in space, but *each molecule retains its orientation*. There will be a non-zero δf_{tot} for such a case; to see this we might start again from our usual simple case: a nematic slab of area S and thickness L , between two walls with tangential boundary condition. An angle α is imposed between the preferred axis of both walls, and the slab is under twist $\theta(0) - \theta(L) = \alpha$. The distortion energy is

$$f_d = \frac{1}{2}K_{22}(\alpha/L)^2LS = \frac{1}{2}K_{22}\alpha^2S/L \quad (3.92)$$

If we increase the thickness L by δL (keeping the same volume: $SL = \text{constant}$) we get a non-zero δf_d

$$\frac{\delta f_d}{f_d} = \delta S/S - \delta L/L = -2\delta L/L. \quad (3.93)$$

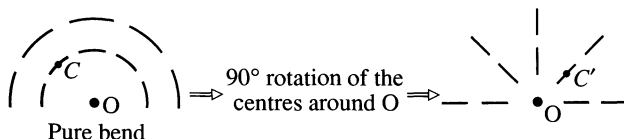
(The nematic wishes to decrease f_d by increasing its thickness.) The deformation just described may be obtained by displacing the molecules without changing their director: if $\mathbf{u}(\mathbf{r})$ is the displacement of a molecule initially located at \mathbf{r} , we might have chosen

$$u_y = y(\delta L/L) \quad (\text{along the normal to the slab})$$

$$\left. \begin{array}{l} u_x = -x(\delta L/L) \\ u_z = 0 \end{array} \right\} \quad (\text{in the plane of the slab})$$

and obtained a non-zero δf_d given by eqn (3.93).

Even a displacement $\mathbf{u}(\mathbf{r})$ corresponding to a pure rotation may change f_d if the molecules retain their initial orientation: this was already stressed in Fig. 3.2. Another example is the following.



We start from a state of pure bending, then displace the centres of all molecules by a 90° rotation, and reach a state of pure splay: thus if the splay and the bend elastic constants differ, f_d will be changed.

Let us now compute δf_d in detail; we start with a molecule at point \mathbf{r} , with director $\mathbf{n}(\mathbf{r})$. Then we displace it from \mathbf{r} to $\mathbf{r}' = \mathbf{r} + \mathbf{u}(\mathbf{r})$, keeping the director frozen: the final distribution of the director in space is given by a new function $\mathbf{n}'(\mathbf{r}')$, and

$$\mathbf{n}'(\mathbf{r}') = \mathbf{n}'(\mathbf{r} + \mathbf{u}) = \mathbf{n}(\mathbf{r}). \quad (3.94)$$

The new state of distortion involves the derivatives

$$\frac{\partial n'_\gamma}{\partial r'_\beta} = \frac{\partial n_\gamma}{\partial r_\alpha} \frac{\partial r_\alpha}{\partial r'_\beta}. \quad (3.95)$$

Since $\mathbf{r} = \mathbf{r}' - \mathbf{u}$ we have

$$\begin{aligned} \frac{\partial r_\alpha}{\partial r'_\beta} &= \delta_{\alpha\beta} - \frac{\partial u_\alpha}{\partial r'_\beta} \simeq \delta_{\alpha\beta} - \partial_\beta u_\alpha \\ \frac{\partial n'_\gamma}{\partial r'_\beta} - \frac{\partial n_\gamma}{\partial r_\beta} &= -(\partial_\alpha n_\gamma)(\partial_\beta u_\alpha) \end{aligned} \quad (3.96)$$

where we keep only the terms which are of first order in \mathbf{u} , and write as usual $\partial/\partial r_\beta \equiv \partial_\beta$.

Consider now a nematic element ($d^3\mathbf{r}$) around a point with position vector \mathbf{r} , which becomes \mathbf{r}' ($d^3\mathbf{r}' = d^3\mathbf{r}$ because of our assumption of incompressibility). The change in distortion energy of this element will be, from eqns (3.90) and (3.96)

$$d^3\mathbf{r} \pi_{\beta\gamma}(-\partial_\alpha n_\gamma)(\partial_\beta u_\alpha). \quad (3.97)$$

Thus we may write the total change δf_d as an integral over the initial sample volume

$$\delta F_d = \int \sigma_{\beta\alpha}^d \partial_\beta u_\alpha d^3\mathbf{r} \quad (3.98)$$

where we have introduced a second-rank tensor σ^d (the ‘distortion stress tensor’) by the equation

$$\sigma_{\beta\alpha}^d = -\pi_{\beta\gamma} \partial_\alpha n_\gamma. \quad (3.99)$$

Note that σ^d is *not symmetric* in general ($\sigma_{\beta\alpha}^d \neq \sigma_{\alpha\beta}^d$). In eqn (3.98) a displacement \mathbf{u} corresponding to a pure rotation for the centres of gravity (and fixed \mathbf{n}) will usually change the energy, as explained before eqn (3.94). The asymmetry in σ^d describes this effect. The only case where σ^d becomes symmetric is obtained when the three elastic constants are equal: then it can easily be verified that F^d becomes invariant separately by rotations in \mathbf{u} space, or in \mathbf{n} space.

Let us now return to eqn (3.98). To obtain a complete expression for the changes of the free energy, we must now make the following changes.

1. Since we restrict our attention to incompressible regimes

$$\operatorname{div} \mathbf{u} = 0,$$

we must not use the total free energy f_{tot} but a slightly different quantity

$$f = f_{\text{tot}} - \int p(\mathbf{r}) \operatorname{div} \mathbf{u} d^3\mathbf{r}$$

where $p(\mathbf{r})$ is an unknown function of \mathbf{r} , which we call the *pressure*. Here p plays the role of a Lagrange multiplier: the minimum of f for arbitrary displacements \mathbf{u} , will coincide with the minimum of f_{tot} for displacements \mathbf{u} which leave the density constant. The form of the function $p(\mathbf{r})$ will be found later from the conditions for equilibrium (see eqn (3.107)). The introduction of the pressure leads to a modified form of stress; we shall put

$$\delta f = \int \sigma_{\beta\alpha}^e \partial_\beta u_\alpha d^3\mathbf{r}$$

where

$$\sigma_{\beta\alpha}^e = \sigma_{\beta\alpha}^d - p \delta_{\alpha\beta}. \quad (3.100)$$

We call σ^e the '*Ericksen stress*.' Note that σ^e , just like σ^d , is not in general a symmetric tensor.

2. We must include the effect of F_m and F_g . For simplicity, we shall assume now that the magnetic field \mathbf{H} is constant in space. This is correct for essentially all experiments carried out up to now. Then the only external force acting on the molecules is gravitation: this adds to the integrand in eqn (3.98) a term $+u_\alpha \partial_\alpha F_g$.

3. We must allow now for small changes in \mathbf{n} at each point, $\mathbf{n} \rightarrow \mathbf{n} + \delta\mathbf{n}$, as in the equations defining the molecular field. This adds to the integrand the terms listed in eqn (3.20). We transform them by a partial integration, as was done after eqn (3.20), but now we are careful to keep the surface terms; they are explicitly

$$\int \pi_{\beta\gamma} \delta n_\gamma dS_\beta$$

where dS_β is the vectorial surface element on the boundary.

Grouping all the contributions, we arrive at the total variation of f

$$\delta f = \int \{\sigma_{\beta\alpha}^e \partial_\beta u_\alpha + u_\alpha \partial_\alpha F_g - h_\gamma \delta n_\gamma\} d^3\mathbf{r} + \int \pi_{\beta\gamma} \delta n_\gamma dS_\beta. \quad (3.101)$$

We now integrate by parts the first term, and obtain

$$\delta f = \int \{-u_\alpha \phi_\alpha - h_\gamma \delta n_\gamma\} d^3\mathbf{r} + \int \{\sigma_{\beta\alpha}^e u_\alpha + \pi_{\beta\gamma} \delta n_\gamma\} dS_\beta. \quad (3.102)$$

From eqn (3.102), the vector

$$\phi_\alpha = \partial_\beta \sigma_{\beta\alpha}^e - \partial_\alpha F_g \quad (3.103)$$

appears as the *force per unit volume* in the bulk of the sample.

The condition for hydrostatic equilibrium is $\phi = 0$. We shall now show that this condition is automatically satisfied when eqn (3.91) holds, provided that the pressure distribution is chosen properly. Inserting the definitions (3.100) and (3.99) for the Ericksen stress in (3.103), we arrive at:

$$\phi_\alpha = -\pi_{\beta\gamma} \partial_\alpha \partial_\beta n_\gamma - \partial_\alpha n_\gamma (\partial_\beta \pi_{\beta\gamma}) - \partial_\alpha (p + F_g). \quad (3.104)$$

The quantity $\partial_\beta \pi_{\beta\gamma}$ in the second term may be related to the molecular field h_γ by eqn (3.89). This gives

$$\phi_\alpha = -\pi_{\beta\gamma} \partial_\alpha \partial_\beta n_\gamma - \partial_\alpha n_\gamma \frac{\partial F_d}{\partial n_\gamma} - \partial_\alpha (p + F_g) + \partial_\alpha n_\gamma \chi_a H_\gamma n_\delta H_\delta - h_\gamma \partial_\alpha n_\gamma. \quad (3.105)$$

Recalling that $\pi_{\beta\gamma}$ is a partial derivative of F_d (eqn 3.90) we recognize that the first two terms of (3.105) add up to $-\partial_\alpha F_d$. The fourth term is $-\partial_\alpha F_m$. Finally, when eqn (3.91) holds, the last term reduces to

$$-\lambda n_\gamma \partial_\alpha n_\gamma = -\frac{1}{2}\lambda \partial_\alpha(\mathbf{n}^2) = 0.$$

Then ϕ_α reduces to

$$\phi_\alpha = -\partial_\alpha (F_d + F_m + F_g + p) \quad (3.106)$$

and the condition of hydrostatic equilibrium ($\phi_\alpha = 0$) imposes the following choice for p

$$p(\mathbf{r}) = -(F_d + F_m + F_g) + \text{const.} \quad (3.107)$$

Returning to eqn (3.102), let us look now at the two surface terms. The first term represents the work done on the sample by the limiting walls, if the walls are displaced by u_α , but with no change in the director at the walls ($\delta\mathbf{n} = 0$). The second term represents another type of work, done by the walls, when their motion implies a change of \mathbf{n} at the surface: we discussed an example of this effect in Section 3.1.5, where we had a nematic slab twisted between two polished glasses.

Other definitions of the stress The Ericksen definition of a stress tensor is based on the work done when the molecules are displaced, but each molecule retains its initial orientation. However, this set of defining operations for the stress is not unique; a different set will lead to a different stress tensor. To illustrate this point, we shall now describe another stress tensor σ_{ab}^M which is in fact related to the tensor used by the Harvard group [45]. The defining operations for σ^M are the following:

1. The molecular centres of gravity are displaced by $\mathbf{u}(\mathbf{r})$. At the same time, the director is rotated by an amount equal to the local rotation of the centres of gravity; the corresponding rotation vector is $\frac{1}{2} \operatorname{curl} \mathbf{u}$, and the change in \mathbf{n} involved, which we shall call $\delta^{(1)}\mathbf{n}$, is thus given by

$$\delta^{(1)}\mathbf{n} = \frac{1}{2}(\operatorname{curl} \mathbf{u}) \times \mathbf{n}$$

or, in terms of the components,

$$\delta^{(1)}n_\alpha = \frac{1}{2}(n_\beta \partial_\beta u_\alpha - n_\alpha \partial_\beta u_\beta).$$

The change in the total free energy f resulting from the first operation is defined to be

$$\delta f^{(1)} = \int \sigma_{\beta\alpha}^M \partial_\beta u_\alpha d\mathbf{r} + \int \pi_{\beta\gamma} \delta^{(1)}n_\gamma dS_\beta.$$

Comparing this with our earlier equations, the reader may check that

$$\sigma_{\alpha\beta}^M = \sigma_{\alpha\beta}^e + \frac{1}{2}(h_\beta n_\alpha - h_\alpha n_\beta).$$

2. The second operation amounts to an arbitrary rotation of the director at each point, giving rise to a change $\delta\mathbf{n}^{(2)}(\mathbf{r})$. The overall shift of \mathbf{n} is thus split into two parts

$$\delta\mathbf{n} = \delta^{(1)}\mathbf{n} + \delta^{(2)}\mathbf{n}.$$

The free-energy change associated with the second operation is

$$\delta f^{(2)} = \int (-\mathbf{h} \cdot \delta^2\mathbf{n}) d\mathbf{r} + \int \pi_{\beta\gamma} \delta^{(2)}n_\gamma dS_\beta.$$

This new set of definitions may appear more complicated at first sight. In fact the separation of $\delta\mathbf{n}$ into $\delta\mathbf{n}^{(1)} + \delta\mathbf{n}^{(2)}$ has a very physical meaning for dynamical studies; $\delta\mathbf{n}^{(1)}$ corresponds to a non-dissipative motion, while $\delta\mathbf{n}^{(2)}$ is always associated with some friction.

3.5.3 The balance of torques

The external agents acting on our sample are the magnetic field \mathbf{H} and the gravitational force $\rho\mathbf{g} = -\nabla F_g$. The resulting torques are

$$\int \{(\mathbf{M} \times \mathbf{H}) + \mathbf{r} \times \rho\mathbf{g}\} d_3r.$$

In equilibrium, these torques must be balanced by the action of the walls: the above volume integral must be convertible into a surface integral, which we shall now derive.

Our starting point is a *rotational identity* satisfied by the deformation energy F_d . As already pointed out in section I, F_d is invariant if (and only if) we rotate both the centres of gravity and the director by the same angle

ω . This means that if simultaneously

$$\begin{aligned}\mathbf{u}(\mathbf{r}) &= \boldsymbol{\omega} \times \mathbf{r} \\ \delta\mathbf{n}(\mathbf{r}) &= \boldsymbol{\omega} \times \mathbf{n}\end{aligned}\quad (3.108)$$

The deformation energy must be unaltered.

Let us write (3.108) in tensor notation

$$\begin{aligned}\partial_\beta u_\alpha &= \epsilon_{\alpha\mu\beta} \omega_\mu \\ \delta n_\gamma &= \epsilon_{\gamma\mu\rho} n_\rho \omega_\mu\end{aligned}\quad (3.108a)$$

where $\epsilon_{\alpha\mu\beta}$ is the alternate symbol ($\epsilon_{xyz} = -\epsilon_{yxz} = 1$, $\epsilon_{xx\beta} = 0$, etc.). We now insert (3.108a) into δf_d (see eqn 3.101) and obtain

$$\delta f_d = \omega_\mu \int \left\{ \sigma_{\beta\alpha}^d \epsilon_{\alpha\mu\beta} + \frac{\partial F_d}{\partial n_\gamma} \epsilon_{\gamma\mu\rho} n_\rho + \pi_{\beta\gamma} \epsilon_{\gamma\mu\rho} \partial_\beta n_\rho \right\} d^3 r = 0. \quad (3.109)$$

For each μ value (x , y , or z) the coefficient of ω_μ must vanish. This gives a rotational identity, which is satisfied by all scalar functions F_d (all functions of $\operatorname{div} \mathbf{n}$, $\mathbf{n} \cdot \operatorname{curl} \mathbf{n}$, and $(\mathbf{n} \times \operatorname{curl} \mathbf{n})^2$). Transforming the second term in eqn (3.109) by eqn (3.89), we obtain

$$\int \epsilon_{\alpha\mu\beta} \sigma_{\beta\alpha}^d d^3 r + \int \epsilon_{\gamma\mu\rho} \{ -h_\gamma n_\rho + n_\rho \partial_\beta \pi_{\beta\gamma} + \chi_a (\mathbf{n} \cdot \mathbf{H}) H_\gamma n_\rho + \pi_{\beta\gamma} \partial_\beta n_\rho \} d^3 r = 0. \quad (3.110)$$

The term $\epsilon_{\gamma\mu\rho} h_\gamma = (\mathbf{n} \times \mathbf{h})_\mu$ vanishes at equilibrium. The term involving χ_a is simply $(\mathbf{M} \times \mathbf{H})_\mu$ since $\mathbf{M} = \chi_\perp \mathbf{H} + \chi_a (\mathbf{n} \cdot \mathbf{H}) \mathbf{n}$. The other terms in the bracket add up to a total differential, giving

$$\int \{ \epsilon_{\alpha\mu\beta} \sigma_{\beta\alpha}^d + (\mathbf{M} \times \mathbf{H})_\mu \} d^3 r + \int \epsilon_{\gamma\mu\rho} \pi_{\beta\gamma} n_\rho dS_\beta = 0. \quad (3.111)$$

The first term on eqn (3.111) would vanish if the tensor σ^d were symmetric, but, as can be seen from eqns (3.99) and (3.15), σ^d is not symmetric in general.[†] We can transform the first term by writing that the bulk force ϕ_α vanishes at equilibrium

$$\begin{aligned}0 &= \int \epsilon_{\alpha\mu\rho} \phi_\alpha r_\rho d^3 r \\ &= \int \epsilon_{\alpha\mu\rho} (\partial_\beta \sigma_{\beta\alpha}^\epsilon) r_\rho + G_\mu d^3 r\end{aligned}\quad (3.112)$$

where

$$G_\mu = \int \epsilon_{\alpha\mu\rho} (-\partial_\alpha F_g) r_\rho d^3 r \quad (3.113)$$

[†] In the one-constant approximation σ^d becomes symmetric, because F_d is then invariant separately for rotations of \mathbf{n} and for rotations of \mathbf{r} .

is the torque of the gravitational forces.[†] Integrating by parts the first term in (3.112) we have in

$$\int \epsilon_{\alpha\mu\beta} \sigma_{\beta\alpha}^e d^3r = \int \epsilon_{\alpha\mu\rho} \sigma_{\beta\alpha}^e r_\rho dS_\beta + G_\mu. \quad (3.114)$$

On the left-hand side of (3.114) we can replace σ^e by σ^d , since both tensors differ only by a symmetric tensor ($p \delta_{\alpha\beta}$). Inserting (3.114) into (3.111) we finally obtain

$$\int \epsilon_{\alpha\mu\rho} \{r_\rho \sigma_{\beta\alpha}^e + n_\rho \pi_{\beta\alpha}^e\} dS_\beta + \int \{(M \times H)_\mu + G_\mu\} d^3r = 0. \quad (3.115)$$

Equation (3.115) shows that in a nematic sample, at equilibrium, the body torques ($\mathbf{M} \times \mathbf{H}$) and \mathbf{G} are balanced by surface torques. There are two contributions to these surface torques, one deriving from the Ericksen stress σ^e , and one deriving from the tensor π . We shall now try to make the discussion of these torques less abstract, by a consideration of specific examples.

Problem (1): a floating object. We consider a single small object, of arbitrary shape, suspended in a nematic matrix. In practice the object may be a large solute molecule, or a colloidal grain—the case of a magnetic grain being of particular interest [22]. We want to know what are the long-range distortions induced in the nematic by such an object.

Solution. Let us take a frame of reference with the origin at the centre of gravity of the grain, and the z -axis parallel to the unperturbed director \mathbf{n}_0 . At large distances from the grain ($r \rightarrow \infty$) the director will deviate only slightly from \mathbf{n}_0

$$\begin{aligned} \mathbf{n}(r) &= \mathbf{n}_0 + \delta\mathbf{n}, \\ \delta\mathbf{n} &= (n_x, n_y, 0). \end{aligned}$$

In the one-constant approximation the free energy density (3.17) becomes

$$F_d = \frac{1}{2}K\{(\nabla n_x)^2 + (\nabla n_y)^2\}$$

and the local equilibrium equations are

$$\nabla^2 n_x = \nabla^2 n_y = 0.$$

It is convenient to introduce a rotation vector $\boldsymbol{\omega}(\mathbf{r})$ such that $\delta\mathbf{n} = \boldsymbol{\omega} \times \mathbf{n}_0$. Then $\nabla^2 \omega_x = \nabla^2 \omega_y = 0$. Since ω_z is arbitrary we may also impose $\nabla^2 \omega_z = 0$. The most general form for $\boldsymbol{\omega}$ vanishing at large \mathbf{r} , is

$$\boldsymbol{\omega} = \alpha r^{-1} + \beta \cdot \nabla(r^{-1}) + \dots$$

where α is a vector and β a dyadic; α and β are independent of \mathbf{r} ; they depend, however, on the orientation of the grain. We shall now show that α is directly related to the torque Γ_t which the grain applied to the nematic. Since nematics transmit torques,

[†] We could dispose of G_μ by choosing the origin of coordinates at the centre of gravity of the sample.

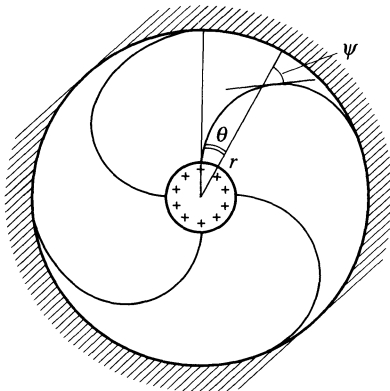


Fig. 3.23. The ‘magic spiral’: nematic contained between two cylinders with different boundary conditions

we may compute Γ_t by integration of eqn (3.115) over a large surface Σ surrounding the grain, and far enough from it to use the asymptotic for $\delta\mathbf{n}$, or ω . To first order in $\delta\mathbf{n}$, the contributions come only from the α term; only the π contribution remains, and gives

$$\Gamma_t = K\alpha \int_{(\Sigma)} d\Sigma \cdot \nabla(r^{-1}) = 4\pi K\alpha.$$

If the grain is subjected to other external forces (gravitational, magnetic, etc.) it will in general feel, from these forces, a torque Γ_{ext} . It feels from the nematic a torque $-\Gamma_t$. In equilibrium, the sum of these two torques must vanish

$$\alpha = \Gamma_{ext}/4\pi K.$$

Thus, when $\Gamma_{ext} \neq 0$, there is a long-range distortion in the nematic, decreasing only like $1/r$.

Problem (2): the ‘magical spiral’. A nematic liquid is enclosed between two concentric cylinders, with the following boundary conditions: on the inner cylinder the molecules are normal to the wall; on the outer cylinder they are tangential. One possible equilibrium conformation is then the spiral shown on Fig. 3.23. Clearly each of the cylinders must feel no overall torque when the nematic has settled to equilibrium (each cylinder can rotate without changing the energy stored in the nematic). On the other hand, the molecular conformation is bent and the molecules do experience some torques; for instance, if we relaxed slightly the boundary condition at the inner surface, the molecules would immediately rotate to decrease the bending. The question (raised by R. Meyer, and solved by O. Parodi) is to reconcile these two aspects, through the Ericksen equations.

[†] If a magnetic field H is applied to the grain, we assume H to be small, or $\xi(H)$ to be large in comparison to the distances r of interest: in this limit the distortions inside the nematic will not be affected by the direct action of H .

Solution. Let us introduce cylindrical coordinates, r and θ , and call ψ the angle between the local optical axis and the radial direction. For the spiral, ψ will be a function of r only. In the one-constant approximation, the free energy (per unit length along z) is found to be

$$\int_{r_0}^{r_1} 2\pi r \, dr \frac{1}{2} K \left(\frac{\partial \psi}{\partial r} \right)^2.$$

Writing that this is a minimum with respect to all variations of $\psi(r)$ leads to the equation

$$\frac{\partial}{\partial r} \left(r \frac{\partial \psi}{\partial r} \right) = 0$$

and the solution (correctly fitted to the boundary conditions) is

$$\psi = \frac{\pi}{2} \cdot \frac{\ln(r/r_0)}{\ln(r_1/r_0)}.$$

Let us consider first the π contributions to the torque on a surface element dS of the inner cylinder. From the definition (3.90) of $\pi_{\beta\gamma}$ we find

$$\pi_{\beta\gamma} dS_\beta = K dS \frac{\partial n_\gamma}{\partial r}.$$

The corresponding torque is thus, according to eqn (3.115),

$$\begin{aligned} dc_z(\pi) &= K dS \left(n_x \frac{\partial n_y}{\partial r} - n_y \frac{\partial n_x}{\partial r} \right) \\ &= K dS \frac{\partial \phi}{\partial r} \end{aligned}$$

where $\phi = \theta + \psi$ is the angle between the director and the x -axis. The torque $C(\pi)$ is perfectly finite; per unit length along z it is

$$C(\pi) = K 2\pi r_0 \left(\frac{\partial \phi}{\partial r} \right)_{r_0} = \pi^2 K / \ln(r_1/r_0).$$

However, we must also consider the contribution from σ^e in eqn (3.115). We note first that the scalar pressure p (eqn 3.107) has cylindrical symmetry and thus does not contribute to the torque: the only term of interest in the stress is σ^d . Using eqn (3.99) for σ^d , we find

$$\sigma_{ij}^d = -K \frac{\partial \phi}{\partial x_i} \frac{\partial \phi}{\partial x_j}$$

$(i, j) = (x, y)$

The corresponding force df on the element dS is given by

$$df_i = \sigma_{ij}^d dS_j$$

or, explicitly,

$$df = -K dS \frac{\partial \phi}{\partial r} \nabla \phi.$$

The vector $\nabla\phi = \nabla\psi + \nabla\theta$ has one radial component ($\nabla\psi$) which does not contribute to the torque; the tangential component ($\nabla\theta$) does contribute, however, and gives

$$dC_z(\sigma) = -K dS \frac{\partial\phi}{\partial r} \cdot \frac{1}{r} \cdot r = -K dS \frac{d\phi}{\partial r}.$$

Thus the sum of the two torques cancels exactly

$$dC_z(\sigma) + dC_z(\pi) = 0$$

This is gratifying because, if the sum did not cancel, we would have discovered perpetual motion!

Problem (3). What are the conditions to be imposed on the Frank equations for the director, at the interface between a nematic and an isotropic phase, when the manifold of easy directions at the interface is continuously degenerate (i.e. = 'conical,' or 'tangential' situations)?

Answer. The bulk free-energy f must be stationary for any small rotation of the director \mathbf{n} (at the surface) around the normal (z) to the interface, because the surface energy does not change in such a rotation. This leads to the condition, derived from eqn (3.115)

$$\epsilon_{az\rho} n_\rho \pi_{za} = 0$$

or, more explicitly,

$$n_x \pi_{zy} - n_y \pi_{zx} = 0.$$

REFERENCES

1. Oseen, C. W. *Trans. Faraday Soc.* **29**, 883 (1933).
2. Zocher, H. *Trans. Faraday Soc.* **29**, 945 (1933).
3. Frank, F. C. *Discuss. Faraday Soc.* **25**, 19 (1958).
4. Ericksen, J. L. *Arch. ration. Mech. Analysis* **23**, 266 (1966).
5. See, for example, Landau, L. D. and Lifshitz, E. M. *Theory of elasticity*, Section 10. Pergamon, London (1959). This is the section of hexagonal crystals (for the elastic coefficients, the symmetries C_6 and C_∞ are equal).
6. (a) Frederiks, V. and Zolina, V. *Trans. Faraday Soc.* **29**, 919 (1933); (b) Frederiks, V. and Zvetkoff, V. *Sov. Phys.* **6**, 490 (1934); (c) Zwetkoff, V. *Acta Phys. Chem. USSR* **6**, 865 (1937); (d) Saupe, A. Z. *Naturforsch. A* **15**, 815 (1960); (e) Gruler, H., Scheffer, T., and Meier, G. Z. *Naturforsch. A* **27**, 966 (1972).
7. (a) Gruler, H. Z. *Naturforsch. A* **28** 494 (1973). (b) Gruler, H. and Meier, G. *Mol. Cryst.* **23**, 261 (1973).
8. Ericksen, J. L. *Arch. ration. Mech. Analysis* **10**, 189 (1962); see also Oseen, C. W. *Ark. Math. Abo. Phys. K. Svenska Vetenskapsakademien* **A19**, 1–19 (1925).
9. See Landau, L. D. and Lifshitz, E. M. *Electrodynamics of continuous media*, Section 39. Pergamon, London (1960).
10. Ericksen, J. L. *Trans. Soc. Rheol.* **11**, 5 (1967).
11. Mauguin, C. *Phys. Z.* **12**, 1011 (1911); *C.R. Acad. Sci., Paris* **156**, 1246 (1913).
12. Grandjean, F. *Bull. Soc. fr. Minér.* **29**, 164 (1916).

13. (a) This was noticed already by Lehmann, O. *Verh. Naturwiss. Vereins. Karlsruhe* **19**, Sonderdruck 275 (1906), but the precise recipe giving reproducible planar textures was established and utilized only much later by Chatelain, P. *Bull. Soc. fr. Minér.* **66**, 105 (1943). (b) Lanning, J. L. *Appl. Phys. Lett.* **21** (4), 15 August (1972).
14. (a) Haller, I. and Huggins, H. A. US Patent 3 656 834 (Cl. 350/150; G02f) (1972); Haas, W., Adams, J., and Flannery, J. *Phys. Rev. Lett.* **25**, 1326 (1970). (b) Creagh, L. T. and Kmetz, A. R. *Mol. Cryst.* **24** (4), 15 August (1972). (c) Proust, J. E., Ter-Minassian, L., and Guyon, E. *Solid State Commun.* **11**, 1227 (1972).
15. Guyon, E., Pieranski, P., and Boix, M. *Lett. appl. Engng Sci.* **1**, 19 (1973); Urbach, W., Boix, M., and Guyon, E. *Appl. Phys. Lett.* **25**, 479 (1974).
16. Bouchiat, M. and Langevin, D. *Phys. Lett.* **A34**, 331 (1971).
17. For a discussion of weak anchoring and magnetic field effects see Rapini, A. and Papoulier, M. *J. Phys. (Paris) Colloq.* **30** (Suppl. C4), 54 (1969).
18. Berreman, D. *Phys. Rev. Lett.* **28**, 1683 (1972).
19. Berreman, D. *Mol. Cryst.* **23**, 215 (1973); Wolff, U., Grubel, W., and Kruger, A. *Mol. Cryst.* **23**, 187 (1973).
20. Maier, W. and Meier, G. *Z. Naturforsch.* **A16**, 470, 1200 (1961); Gasparoux, H., Regaya, B., and Prost, J. *C.R. Acad. Sci., Paris* **B272**, 1168 (1971); *J. Phys. (Paris)* **32**, 953 (1971); Rose, P. I. *Mol. Cryst.* **26**, 75 (1974).
21. Prost, J. and Gasparoux, H. *C.R. Acad. Sci., Paris* **C273**, 355 (1972).
22. Brochard, F. and DeGennes, P. G. *J. Phys. (Paris)* **31**, 691 (1970).
23. (a) Gruler, H. and Meier, G. *Mol. Cryst. liquid Cryst.* **16**, 299 (1972). (b) Carr, E. F. *Mol. Cryst. liquid Cryst.* **7**, 279 (1969). (c) Carr, E. F. In *Ordered fluids and liquid crystals*, p. 76. American Chemical Society (1967).
24. Guyon, E., Pieranski, P., and Brochard, F. *C.R. Acad. Sci., Paris* **B273**, 487 (1971); *J. Phys. (Paris)* **33**, 681 (1972).
25. Mauguin, C. *Bull. Soc. fr. Minér.* **34**, 71 (1911).
26. Cladis, P. *Phys. Rev. Lett.* **28**, 1629 (1972).
27. Leslie, F. M. *Mol. Cryst.* **12**, 57 (1970).
28. Gerritsma, G., de Jeu, W., and van Zanten, P. *Phys. Lett.* **36A**, 389 (1971).
29. Shtrikman, S. et al. *Phys. Lett.* **37A**, 369 (1971).
30. Van Doorn, D. *Phys. Lett.* **42A**, 537 (1973).
31. See Landau, L. D. and Lifshitz, E. M. *Fluid mechanics* Chapter 7. Pergamon, London (1959).
32. For a review, see Helfrich, W. *Mol. Cryst.* **21**, 187 (1973).
33. Meyer, R. B. *Phys. Rev. Lett.* **22**, 918 (1969).
34. Helfrich, W. *Mol. Cryst.* **26**, 1 (1974).
35. Schmidt, D., Schadt, M., and Helfrich, W. *Z. Naturforsch.* **A27**, 277 (1972).
36. Deuling, H. *Mol. Cryst.* **26**, 281 (1974).
37. Orsay Liquid Crystal Group. In *Liquid crystals and ordered fluids* (ed. J. Johnson and R. S. Porter), p. 195. Plenum Press, New York (1970).
38. Chatelain, P. *Acta Cristallogr.* **1**, 315 (1948).
39. De Gennes, P. G. *C.R. Acad. Sci., Paris* **266**, 15 (1968).
40. See, for example, Martin, P. In *The many-body problem* (ed. C. de Witt and R. Balian). Gordon and Breach, New York (1968).

41. Langevin, D. and Bouchiat, M. *J. Phys. (Paris) Colloq.* **36** (Suppl. C1), 197 (1975)
42. Moll and Ornstein *Proc. Acad. Sci., Amsterdam* **21**, 259 (1918).
43. Martinand, J. L. and Durand, G. *Solid State Commun.* **10**, 815 (1972).
44. Ericksen, J. L. *Arch. ration. Mech. Analysis* **9**, 371 (1972).
45. Forster, D., Lubensky, T., Martin, P., Swift, J., and Pershan, P. *Phys. Rev. Lett.* **26**, 1016 (1971).

DEFECTS AND TEXTURES IN NEMATICS

'Il y a de certains défauts qui, bien mis en œuvre, brillent plus que la vertu même'

La Rochefoucauld

4.1 OBSERVATIONS

In Chapter 3 we restricted our attention to distortions of the nematic arrangement that involved continuous variations of the director $\mathbf{n}(\mathbf{r})$. But there are other, important, physical situations where $\mathbf{n}(\mathbf{r})$ is not a smooth function of \mathbf{r} at all points. Two current examples are described below.

4.1.1 Black filaments ('*structures à fils*')

In rather thick nematic samples, both with and without crossed polarizers, it is common to observe a system of dark, flexible filaments: as explained in Chapter 1, this thread-like structure is responsible for the name '*nematic*' (see Fig. 4.4). Some of the filaments appear to float freely in the fluid. Others are attached by both ends to the walls. Some are less mobile and seem to stick entirely to the walls.

A first analysis of the optical properties of these filaments was carried out very early by Grandjean and refined by G. Friedel [1]. Both had already recognized that the filaments were not due to impurities or the like, but corresponded to lines of singularity in the molecular alignment: the word 'disclinations' was introduced later for these lines by Frank [2].

4.1.2 '*Structures à noyaux*' ('*Schlieren structures*')

When the boundary conditions imposed by the glass walls to the nematic are *continuously degenerate* (tangential or conical, without any preferred axis in the plane of the walls), one often sees a system of singular points on the surface (Fig. 4.1). Between crossed Nicol prisms, the singular points are connected by black stripes, showing the regions where the optical axis (projected on the plane of the preparation) is parallel to one of the Nicols. The points have been called *noyaux* by G. Friedel. The general texture

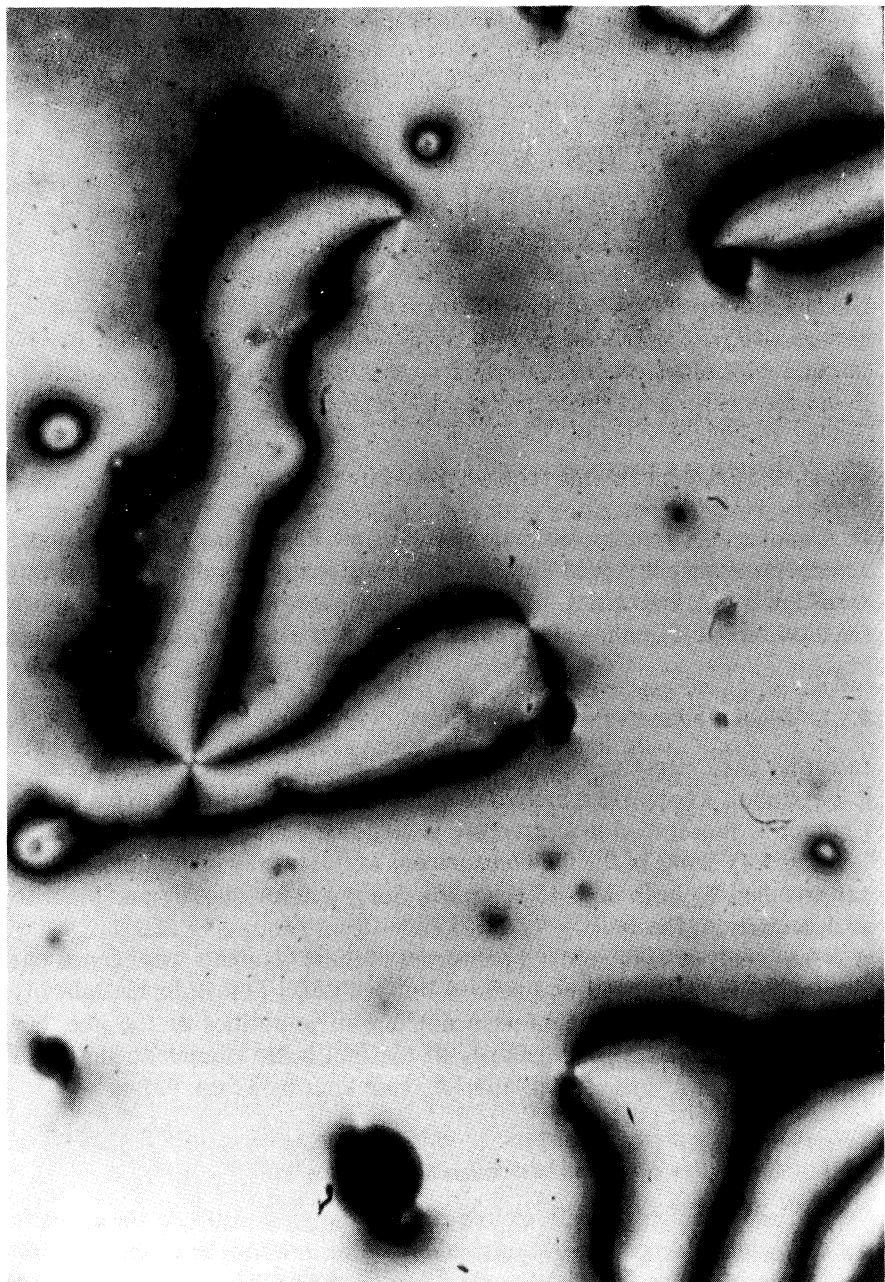


Fig. 4.1. Schlieren texture observed between crossed Nicols with a nematic giving tangential boundary conditions on the glass slide (courtesy J. Dreyer). This particular photograph is remarkable because it also shows the disclination lines in the bulk

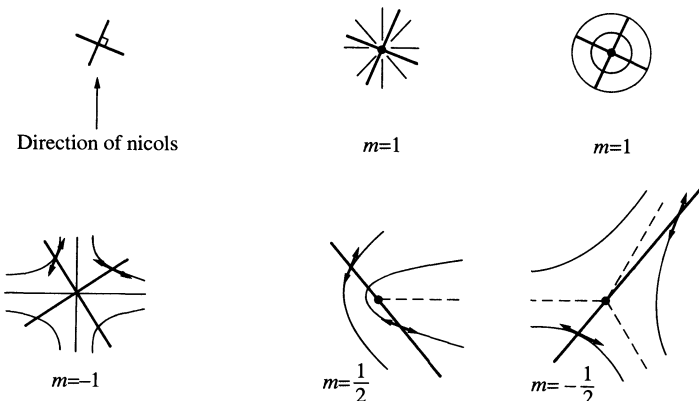


Fig. 4.2. Geometrical arrangement of the molecules at the sample surface around a *noyau*. The thick black lines give the regions of extinction between crossed Nicols.

resulting from those points is often called ‘*Schlieren texture*’ in the German literature.

The arrangement of the molecules in the vicinity of the limiting surface may be detected by various means. One is the polarizing microscope: the principle of the experiment is shown in Fig. 4.2. Alternatively, physico-chemical changes, such as precipitation [3] or bubble formation [4], can be induced at the limiting surface: the microcrystallites (or the bubbles) that appear show an oriented texture, revealing the local optical axis (Figs 4.3 and 4.4). With all these methods of observation, one detects four essential types of *noyaux* with molecular arrangements as shown in Fig. 4.2. We shall classify these four types with an index m taking the values

$$-1, \quad -\frac{1}{2}, \quad \frac{1}{2}, \quad 1.$$

The two-dimensional structure of the various types (in the plane of the wall that is observed) may be summarized in the following way. Assume that the director \mathbf{n} is in the plane of the wall (tangential boundary condition) and define two orthogonal axes (x, y) in this plane. Call \mathbf{r} the distance between the singularity and the observation point, and $\phi(\mathbf{r})$ the angle between \mathbf{r} and x ($\tan \phi = y/x$). The angle between \mathbf{n} and x will be named $\theta(\mathbf{r})$. An approximate relation for θ , which is correct from the point of view of symmetries, is

$$\theta(\mathbf{r}) = m\phi(\mathbf{r}) + \text{const.} \quad (4.1)$$

(white lines) that connect to the *noyaux*. Note that all *noyaux* with two black lines have one disclination line, while those with four black lines have none.



Fig. 4.3. Microprecipitate decoration technique displaying the arrangement of the molecules at a surface (courtesy J. Rault). This particular example is a (-1) defect.

Thus, if we follow a closed circuit around the singular point, and make one full turn ($\Delta\phi = 2\pi$), we find that the director has rotated by $\Delta\theta = 2\pi m$. This is acceptable only if m is an integer, or a half-integer (since the states (\mathbf{n}) and $(-\mathbf{n})$ are indistinguishable).

4.1.3 Types of defects

4.1.3.1 Disclination

The word disclination was invented by F. C. Frank [2] and comes from the Greek *kline* = slope. A disclination is a discontinuity in orientation, i.e. a discontinuity in the director field $\mathbf{n}(\mathbf{r})$. The discontinuity may be located at one point, on a line, or on a surface, and is referred to as a point, line, or sheet disclination. However, it is easy to see that sheet disclinations are completely unstable and can thus be omitted from the list. This instability



Fig. 4.4. Bubble decoration technique displaying the arrangement of the molecules at a free surface (courtesy P. Pieranski) [4]. In the present example we see two singular points of strength (+1) and (-1) between crossed polarizers.

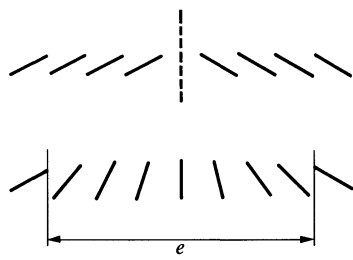


Fig. 4.5. Spontaneous smearing out of a sheet discontinuity.

can be understood from Fig. 4.5: in an abrupt sheet singularity the energy stored per unit area on the surface Σ of the sheet is of the order of U/a^2 (where U is a molecular binding energy and a an average molecular dimension). If we substitute for the discontinuous change of \mathbf{n} at Σ , a gradual

variation taking place in a finite thickness $e \gg a$, the distortion energy (per unit area) is of the order of $(K/e^2)e = K/e \cong U/ea \ll U/a^2$. Thus smearing out is favourable. The smearing operation is allowed, except possibly at some points or lines on Σ^\dagger and the sheet discontinuity will fade out, leaving at most a few disclination lines.

Thus we have only two types of disclinations in nematics: lines and points. It is well established that the black filaments, described at the beginning of this section, correspond to the lines. They will be discussed in Section 4.2. The meaning of the *noyaux* is less obvious. They can be either point disclinations located at the boundary surface, or lines normal to the plane of the surface: both cases occur in practice. A simple experiment, quoted by G. Friedel, sometimes allows one to decide: if the *noyaux* are observed at the boundary between the nematic and a cover glass, the cover glass is displaced in its own plane. If the *noyau* corresponds to a line that was initially vertical, the line becomes tilted and is then observable as a black thread in the preparation. It is found that the *noyaux* of half-integral index ($m = \pm \frac{1}{2}$) are always associated with a line, while the *noyaux* of integral index may be either lines, or point disclinations, and are nearly always of the latter type in usual materials. We shall discuss this in Section 4.2.

4.1.3.2 Walls

We have seen that a sheet singularity always tends to smear out into a continuously distorted region of finite thicknesses. With our simple argument (which ignored all effects due to boundaries or magnetic fields) the energy was minimized when the thickness e became very large. In practice, e is limited by size effects, or by the magnetic coherence length $\xi(\mathbf{H})$. It is thus possible to find, in nematics under fields, a *wall* separating two regions that are optically aligned in the field \mathbf{H} . These walls will be analysed in Section 4.4.

4.2 DISCLINATION LINES

4.2.1 Definition of the ‘strength’

A simple geometrical process, generating a closed disclination line L (or ‘loop’), in a nematic single crystal, is the following (Fig. 4.6): choose a surface (Σ) limited by the loop L . Call the two sides of (Σ) Σ^+ and Σ^- . Take the molecules that are in contact with Σ^+ ; by some ‘external force,’ rotate their director around an axis (Ω) normal to the optical axis \mathbf{n}_0 of the unperturbed crystal. Ω defines both the axis and the magnitude of the rotation. On the other side (Σ^-), maintain the unperturbed direction \mathbf{n}_0 .

At finite distances from (Σ) the director $\mathbf{n}(\mathbf{r})$ will then adjust itself and vary

[†] E.g. at the intersection of Σ and of the wall of the container, if the latter imposes a well defined easy direction. After smearing out, this intersection may remain as a disclination line.

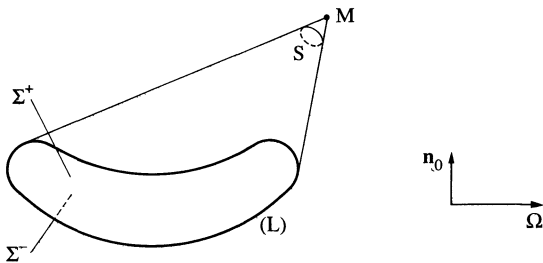


Fig. 4.6. Generation of a disclination loop L by the 'Volterra process'. M , Observation point at radius vector.

continuously with r . The resulting configuration is continuous except on (Σ) ; in general we have on (Σ) a sheet of discontinuity, which can be maintained only in the presence of the external forces. However, if the rotation angle Ω is such that the optical axes above and below the cut coincide, we may switch off the external forces and retain a non-trivial conformation. The condition for this is that Ω be a multiple of π

$$\Omega = 2\pi m \quad (m \text{ integer or half integer}). \quad (4.2)$$

The resulting conformation is everywhere continuous, except on the line L . We say that L is a disclination of 'strength' m (following a notation proposed by Friedel and Kleman [5]).

In Figs 4.7 and 4.8 we show the molecular arrangement around a straight portion of a disclination line, for two particular cases of importance: Ω

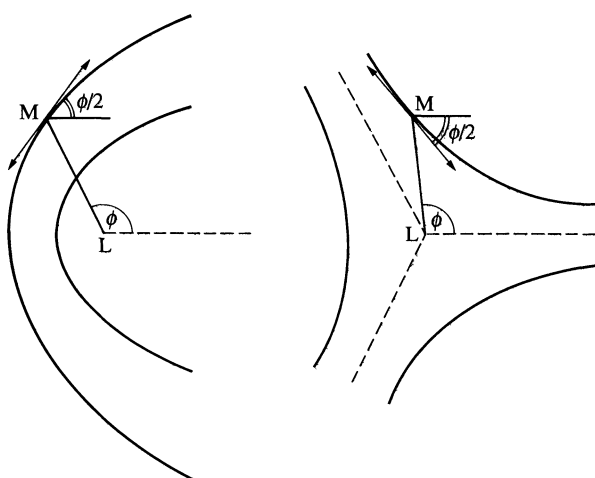


Fig. 4.7. Shape of a wedge disclination of strength $m = \pm 1/2$. (The line L is normal to the sheet.)

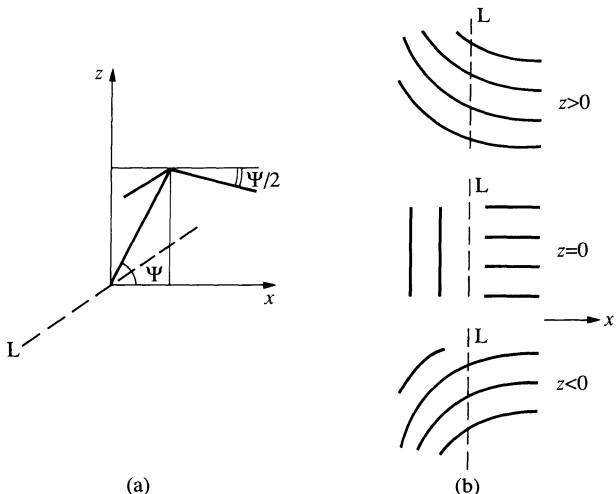


Fig. 4.8. Shape of a twist disclination of strength 1/2. (a) Geometrical construction; (b) molecular pattern: the molecules are always horizontal. The arrangement in three successive horizontal planes is shown. The pattern shown is only one particular example. To obtain other allowed patterns one may rotate the molecules inside each horizontal plane by a constant angle.

parallel to the line ('wedge disclination': Fig. 4.7); and Ω normal to the line ('twist disclination': Fig. 4.8).

Note that different parts of one, curved, disclination line L , may be successively wedge-like and twist-like as in Fig. 4.6; the quantity which is really characteristic of each line, and conserved all along its length, is the strength m .

4.2.2 Distortion field around one line

4.2.2.1 Straight lines

Just as for dislocations in solids, the calculation of the distortions around one line is often difficult. Here, as a first step towards simplification, we shall always use the one-constant approximation for the distortion energy. We start with simple wedge disclinations (Fig. 4.7). The z -axis is set along the line. The director \mathbf{n} is in the x, y -plane and makes an angle $\theta(x, y)$ with the x -axis. The distortion energy (eqn (3.17)) reduces to

$$F_d = \frac{1}{2}K(\nabla\theta)^2. \quad (4.3)$$

The minimization of $\mathcal{F}_d = \int F_d d\mathbf{r}$ leads to the equilibrium condition (first formulated by F. C. Frank [2])

$$\nabla^2\theta = 0. \quad (4.4)$$

The solutions of eqn (4.4) that are discontinuous on the z -axis are precisely of the form found empirically by G. Friedel (4.1). At the *noyaux*, θ is a linear function of the angle $\phi = \tan^{-1} y/x$. Rotation by 2π around the line restores the initial direction of the optical axis: θ can change at most by π , or $2\pi, \dots$. Thus the coefficient $m = d\theta/d\phi$ must be an integer or a half integer.

To check that eqn (4.1) is indeed compatible with eqn (4.4) it may be convenient to investigate the vector $\nabla\theta$. According to eqn (4.1), this vector is everywhere tangential and of magnitude

$$|\nabla\theta| = m/\rho \quad (4.5)$$

where $\rho = \sqrt{x^2 + y^2}$ is the distance to the line. It is easy to verify that such a vector field has no divergence $\text{div}(\nabla\theta) \equiv \nabla^2\theta = 0$.

Let us now discuss the energy \mathcal{T} (per unit length of line) associated with these distortions. According to eqns (4.3) and (4.5) this is given by

$$\mathcal{T} = \int_a^{\rho_{\max}} 2\pi\rho \, d\rho \frac{1}{2} Km^2/\rho^2. \quad (4.6)$$

We have set a lower limit a (of the order of molecular dimensions) to the integral, and also an upper limit ρ_{\max} may be given either by the distance between the line and the walls of the container, or by the distance to other disclinations screening out the distortion (4.5)—whichever is the smallest [6]. The precise value of ρ_{\max} is not very important, because it enters only in a logarithm

$$\mathcal{T} = \pi Km^2 \ln(\rho_{\max}/a). \quad (4.7)$$

Thus \mathcal{T} is proportional to the average elastic constant K . The (\ln) factor in eqn (4.7) is typically of order 10, and $\mathcal{T} \sim 30K$.

Equation (4.7) does not include the contributions of the inner region or ‘core’ ($\rho < a$). These contributions are hard to calculate with any accuracy (except near the nematic-isotropic transition point) but we may guess that they will be of the order of $U/a \sim K$: thus they may be lumped together in eqn (4.7) by a slight change in the argument of the logarithm.

Problem. Compute the energy of two parallel wedge disclinations (L_1 and L_2) of opposite strengths, separated by a distance d .

Solution. If the strengths are m and $-m$ respectively, the angle θ defining the direction still obeys eqn (4.4) and may be taken to be of the form

$$\theta = m(\phi_1 - \phi_2) + \text{const.}$$

where ϕ_1 and ϕ_2 are the azimuthal angles relative to both lines (see Fig. 4.9). To integrate the distortion energy (4.3) it will be convenient to arrange that θ , or $\phi_1 - \phi_2$, be a single-valued function. To ensure this, we must introduce a cut from L_1 to L_2 ; crossing the cut from below decreases $\phi_1 - \phi_2$ by 2π (on the other hand, if we follow

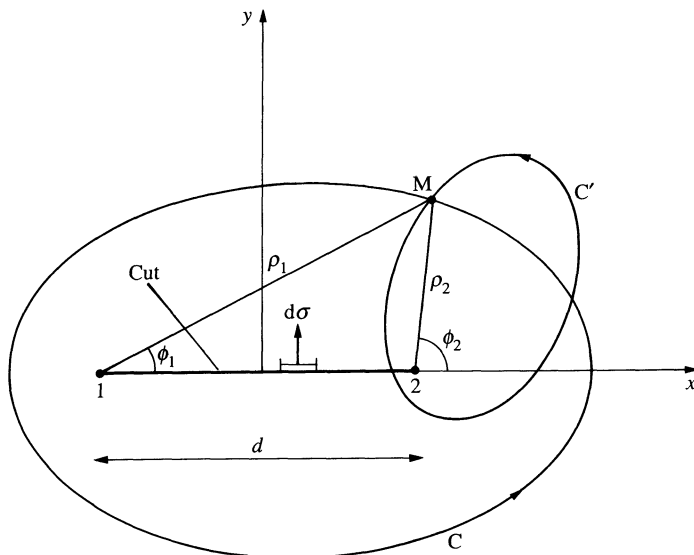


Fig. 4.9. Configurations with two parallel wedge disclinations of opposite strengths $\pm 1/2$. If the observation point M makes a closed circuit C without crossing the cut, the angle θ defining the director is unchanged. If the circuit C' crosses the cut, θ changes by π on every turn. In the one-constant approximation $\theta = (\phi_1 - \phi_2)/2$.

a large circle surrounding both lines, which does not cross the cut, we recover the same value of $\phi_1 - \phi_2$ after one turn). The energy (4.3) may then be integrated by parts

$$\frac{1}{2}K \int (\nabla\theta)^2 \, d\mathbf{r} = -\frac{1}{2}K \int \theta \nabla^2 \theta \, d\mathbf{r} + \frac{1}{2}K \int \theta \nabla \theta \, d\sigma.$$

The first integral vanishes since $\nabla^2\theta = 0$. The second integral is taken: (1) on a very remote surface (distance R from the lines); this part is easily seen to be of order $R(1/R)^2 \rightarrow 0$; (2) on the surface of the cut, where θ has a discontinuity

$$\{\theta\} = 2\pi m.$$

On the cut both the vector $d\sigma$ and $\nabla\theta$ are parallel to the y -axis, and

$$|\nabla\theta| = \frac{m}{\rho_1} + \frac{m}{\rho_2} = m \left\{ \frac{1}{\rho_1} + \frac{1}{d - \rho_1} \right\}.$$

Thus the distortion energy (per unit length of the lines) reduces to

$$\mathcal{F}_{12} = \frac{K}{2} \int_a^{d-a} \{\theta\} m \left\{ \frac{1}{\rho_1} + \frac{1}{d - \rho_1} \right\} d\rho_1$$

(where we have introduced suitable cut-offs corresponding to the core radius). This

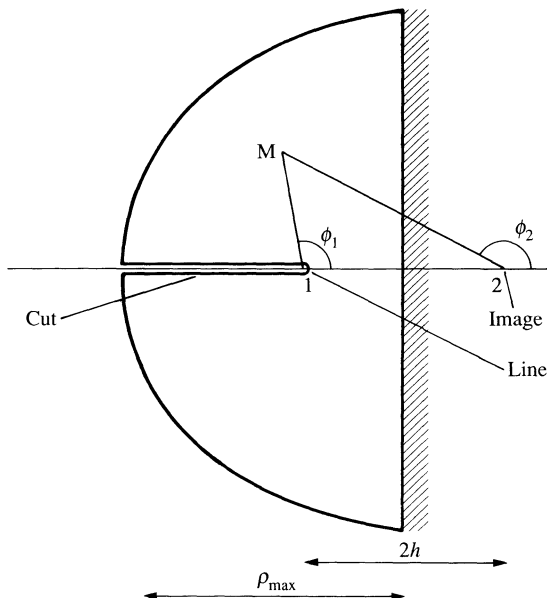


Fig. 4.10. A wedge disclination (a) parallel to a wall in a nematic. The line is repelled by its image (2). Also shown is the contour used to calculate the elastic energy of the system.

leads to

$$\mathcal{F}_{12} = 2\pi Km^2 \ln\left(\frac{d}{a}\right).$$

\mathcal{F}_{12} increases with d ; the interaction between two lines of opposite strength is *attractive*, and the attraction force per unit length is $2\pi Km^2/d$.

Problem. A wedge disclination of strength m is parallel to a wall, at a distance h from it. The wall imposes tangential (or normal) boundary conditions. What is the force acting on the line?

Solution. Introduce an image (L_2) of the line, at a distance $d = 2h$ from it (Fig. 4.10). The form of θ , satisfying eqn (4.4) and the boundary conditions, is

$$\theta = m(\phi_1 + \phi_2) + \theta_0.$$

On the wall $\phi_1 + \phi_2 = \pi$ and θ has a prescribed value $\theta_{\text{wall}} = m\pi + \theta_0$. This defines θ_0 . To compute the energy we again use the equation

$$\mathcal{F} = \frac{1}{2}K \int \theta \nabla \theta \cdot d\sigma.$$

The contour is represented in Fig. 4.10. The part of the integral taken along the wall vanishes, because $\theta = \theta_{\text{wall}}$ is constant while $\nabla \theta$ is an odd function of y . The

integration along the large semicircle does not contribute, because $\nabla\theta$ is tangential in this region. Finally we are left with the contribution from the cut

$$\mathcal{F} = \frac{1}{2}K\{\theta\} \int_a^{\rho_{\max}} m \left[\frac{1}{\rho} + \frac{1}{\rho + 2h} \right] = \pi m^2 K \left[\ln \frac{\rho_{\max}}{a} + \ln \frac{\rho_{\max}}{2h} \right],$$

$$\mathcal{F} = \mathcal{T} - \pi m^2 K \ln \frac{2h}{a}.$$

Thus the line is *repelled* from the wall, with a force per unit length

$$-\frac{\delta\mathcal{F}}{\delta h} = \frac{\pi Km^2}{h} = \frac{2\pi Km^2}{d}.$$

This is called the image force.

Problem. A field \mathbf{H} is applied horizontally to the free surface of a nematic: discuss the shape of this free surface, including possible disclination lines at the boundary [7].

Solution. As shown in the problem on pp. 131–3, the free energy per unit area of surface is

$$F_{\text{surf}} = \frac{1}{2}A \left\{ \left(\frac{d\zeta}{dx} \right)^2 + \left(\frac{\zeta}{\lambda} \right)^2 \right\} \pm \frac{K}{\xi} \sin \psi \frac{d\zeta}{dx}$$

where $\zeta(x)$ gives the vertical displacement of the surface (and is assumed to vary in one direction x only), A is the surface tension, $\lambda = \sqrt{(A/\rho g)}$, ρ is the density difference between the two phases in contact, and ψ is the angle of the director with the plane of the surface. The (\pm) sign refers to two possible types of distortion below the surface.

One lowers the energy F by choosing a suitable, non-zero value for $d\zeta/dx$, provided that this does not imply too large values for the gravitational term (ζ^2/λ^2) . As seen in the former problem, this term forces the surface to remain flat if the type of distortion is the same everywhere and the dimensions of the surface are $\gg \lambda$. On the other hand, if we use alternatively the two types of solutions, as shown in Fig. 4.11(a)), we may benefit from the last term in P_{surf} , while retaining small ζ values; the regions with different types of distortions will be separated by disclination lines, lying in the surface, parallel to the y -axis.

Locally, at all regular points, the minimum of F_{surf} still gives the usual equation $\lambda^2(d^2\zeta/dx^2) = \zeta$. The solution for a regular array of lines, separated by the distance L , is

$$\zeta(x) = \epsilon \frac{\sinh(x/\lambda)}{\cosh(L/2\lambda)} \quad -\frac{L}{2} < x < \frac{L}{2},$$

$$\zeta(x + L) = -\zeta(x)$$

where 2ϵ is the angle of the cusp on a disclination line.

One may derive ϵ either by minimizing the free energy or, more physically, by an argument based on capillary forces (Fig. 4.11(b)); integrating the last term in F_{surf} on one side of a cusp gives an energy contribution $-(K/\zeta) \sin \psi$. The other side

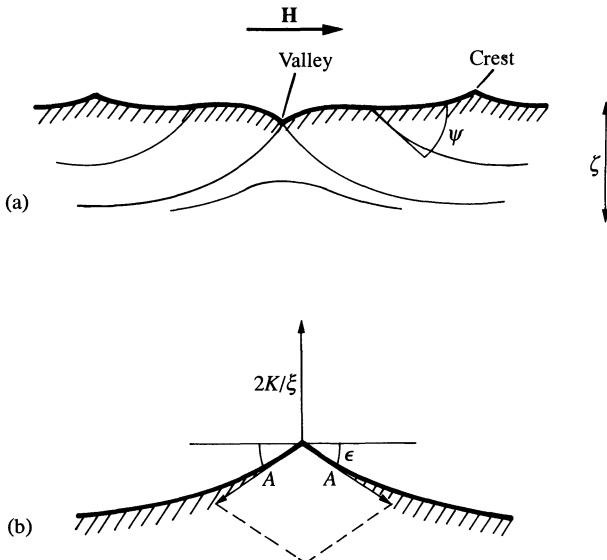


Fig. 4.11. (a) Valleys and crests induced by a horizontal magnetic field on the free surface of a nematic with conical or normal boundary conditions. (b) Determination of the slope ϵ near a crest (typically $\epsilon \sim 10^{-3}$).

doubles this force. Balancing these forces against the surface tensions gives

$$\epsilon = \frac{K}{\xi A} \sin \psi.$$

The free energy obtained for this solution is, per cm²,

$$\bar{F} = -\frac{\lambda A \epsilon^2}{L} \tanh u + \frac{\mathcal{T}}{L},$$

$$u = \frac{L}{2\lambda}$$

where \mathcal{T} is the line energy of the disclination at the cusp. We may roughly estimate \mathcal{T} for this problem as for a wedge disclination of strength 1, with distortions limited to a half space and a cut-off at thickness ξ

$$\mathcal{T} \simeq \frac{1}{2} K \int_a^\xi \pi \rho d\rho \frac{1}{\rho^2} = \frac{\pi}{2} \ln \frac{\xi}{a} K = c_1 K$$

where $c_1 \sim 10$ and is nearly independent of the magnitude of H . One must finally write that \bar{F} is a minimum with respect to variations of L . This gives the condition

$$\left(\frac{H_1}{H} \right)^2 = \tanh u - \frac{u}{\cosh^2 u}, \quad H_1 = \left(\frac{c_1}{\chi_a} \right)^{\frac{1}{4}} (\rho g A)^{\frac{1}{4}},$$

which defines implicitly u and L as a function of H . The right-hand side is always smaller than unity. Thus the field H_1 is the threshold field, above which the solution with crests and valleys is thermodynamically more stable than a flat free surface. Typically $H_1 \sim 10^4$ gauss. When H increases above H_1 , L decreases from ∞ to 0 but is typically of order λ . Domain structures under horizontal magnetic fields have indeed been observed by Williams on PAA [8a], with interline distances of a few millimetres. They might correspond to the situation described in the problem, if the contact angle ψ were different from zero. (It is commonly accepted that $\psi = 0$ for the PAA-air interface, but it is also known in similar cases that ψ may be quite sensitive to chemical contaminants.)

More recent work on MBBA by the same group [8b] tends to confirm the effect and the present interpretation.

It might also be possible to detect the slight deformation of the surface (vertical displacements of order 1 μm) which is predicted by the model, using an interferometric technique (Newton's rings). However, to reach a significant result, it is important to use light polarized perpendicular to the field direction (i.e. normal to the plane of Fig. 4.11); for this particular polarization, the refracting index inside the liquid is constantly equal to the 'ordinary' index b_0 , and the optical paths for vertical beams are not complicated by the deformations of the director field that take place under the interface.

4.2.2.2 'Planar' distortions for arbitrary line shapes [9]

We shall now discuss the shape of the distortion for somewhat more general line structures (always keeping, however, the one-constant approximation). Let us assume that at all points the director \mathbf{n} is parallel to a constant plane (which we take as the x , y -plane). We retain the same notation and call $\theta(\mathbf{r})$ the angle between $\mathbf{n}(\mathbf{r})$ and the x -axis. Equations (4.3) and (4.4) remain valid. It is possible to check first that the solutions of eqn (4.4) do give admissible configurations; the molecular field

$$\mathbf{h} = K\nabla^2\mathbf{n}$$

is given explicitly by

$$\begin{aligned} h_x &= -K\nabla^2\theta \sin\theta - K(\nabla\theta)^2 \cos\theta = -K(\nabla\theta)^2 \cos\theta \\ h_y &= +K\nabla^2\theta \cos\theta - K(\nabla\theta)^2 \sin\theta = -K(\nabla\theta)^2 \sin\theta. \\ h_z &= 0. \end{aligned} \quad (4.9)$$

Thus $\mathbf{h} = -K(\nabla\theta)^2 \mathbf{n}$ is correctly collinear with \mathbf{n} . We call these configurations with $n_z \equiv 0$, 'planar' configurations.

Let us now restrict our attention to planar configurations, and construct a loop (L) of arbitrary shape, and strength m (see Fig. 4.6). We wish to describe a planar distortion around such a loop; this means that we must find a function $\theta(\mathbf{r})$ with the following properties.

1. $\theta(\mathbf{r})$ satisfies the eqn $\nabla^2\theta = 0$ and is regular except on the contour L .
2. $\theta(\mathbf{r})$ does not diverge far from the loop.

3. $\theta(\mathbf{r})$ increases by $2\pi m$ if, starting from point \mathbf{r} , we make one turn around the line L and come back to \mathbf{r} .

This problem has a direct magnetic analogue: we may interpret $\nabla\theta$ as the magnetic field \mathbf{b} due to a current loop L with current $I = m/2$.[†] The solution for θ (i.e. for the magnetic potential) is

$$\theta(\mathbf{r}) = \frac{1}{2}mS(\mathbf{r}) \quad (4.10)$$

where $S(\mathbf{r})$ is the solid angle subtended by the loop at the observation point M of radius vector \mathbf{r} (see Fig. 4.6). If we make one turn around the line, S increases by 4π and condition 3 is correctly obeyed. Equation (4.10) is often helpful in visualizing the molecular arrangement around a loop.

The main interest of this magnetic analogy is to relate the distortion energy to a self-induction coefficient L_s for the magnetic loop; formulae and tables of L_s values are available for all sorts of loop shapes. The connection is given by the equation

$$\frac{1}{2}L_s I^2 = \int \frac{b^2}{8\pi} d\mathbf{r}. \quad (4.11)$$

Thus, putting $\mathbf{b} = \nabla\theta$ and $I = m/2$, we get

$$\frac{1}{2}K \int (\nabla\theta)^2 d\mathbf{r} = \frac{\pi}{2} K L_s m^2. \quad (4.12)$$

For instance, a circular loop of radius R (with a core of radius a) has a self-induction coefficient

$$L_s = 4\pi R \log(R/a). \quad (4.13)$$

It is worthwhile to note that (apart from weak differences due to the logarithmic factors) the energy derived from eqns (4.12) and (4.13) is the product of the line tension \mathcal{T} (eqn (4.7)) and the length of the loop $2\pi R$.

Problem. Discuss the energy of a loop in a uniformly twisted nematic [9].

Solution. Let us take the helical axis of the twist along z , and consider planar solutions with $n_z \equiv 0$. Keeping the same notations, a suitable solution $\theta(\mathbf{r})$, satisfying the equation $\nabla^2\theta = 0$, is

$$\theta(\mathbf{r}) = qz + \frac{1}{2}mS(\mathbf{r}) = \theta_0 + \theta_1$$

where q is the rate of twist. The energy is

$$\mathcal{F} = \mathcal{F}_0 + K \int \nabla\theta_0 \cdot \nabla\theta_1 d\mathbf{r} + \frac{1}{2}K \int (\nabla\theta_1)^2 d\mathbf{r}.$$

The first term is the energy in the absence of disclinations. The last term is given by

[†] We use electromagnetic cgs units.

eqn (4.12). The cross-term may be integrated by parts

$$\int \nabla \theta_0 \cdot \nabla \theta_1 \, d\mathbf{r} = \int \{\theta_1\} \nabla \theta_0 \, d\sigma - \int \theta_1 \nabla^2 \theta_0 \, dr.$$

The volume integral on the right-hand side vanishes: the surface integral is taken on a cut surface (Σ) limited by the loop L. The discontinuities $\{\theta_1\}$ across Σ is equal to $m\pi$. This gives

$$\mathcal{F} - \mathcal{F}_0 = \pi K m \left\{ \frac{1}{2} D_S m - q \Sigma \right\}$$

where Σ is the projected area of the loop on the x, y -plane.[†] For instance, with a circular loop parallel to the x, y -plane, of radius R , of strength $m = \frac{1}{2}$,

$$\mathcal{F} - \mathcal{F}_0 = \frac{1}{2} \pi^2 K \{R \log(R/a) - qR^2\}.$$

\mathcal{F} first increases with R , reaches a maximum for $R = R^* \sim (1/4q) \log(1/qa)$, and then decreases; large loops are favourable, but there is a very high energy barrier (of order K/q) for loop nucleation. In practice nucleation never takes place in the bulk, but on defects at the wall surfaces, etc.

4.2.3 The concept of line tension

For a line of arbitrary shape, creating distortions that may be planar or non-planar, the calculation of the energy becomes more delicate. However, in the one-constant approximation, the result is a simple generalization of eqn (4.7). The energy E of the line is related to the length L by

$$E/L = \mathcal{F} = \pi K m^2 l \tag{4.14}$$

where l is a logarithmic factor, which is nearly independent of line size or line shape. Thus we may also write, with logarithmic accuracy that

$$\delta E/\delta L = \mathcal{F}.$$

This later definition of \mathcal{F} coincides with the usual definition of a *line tension*, as it used, for instance, in connection with vibrating strings. Many concepts which we have been taught concerning vibrating strings in secondary school may thus be transposed to disclination lines; for instance the forces at both ends of a bent disclination are obtained by the construction shown on Fig. 4.12.

Line tensions can be measured; we shall describe here one typical set up used by R. B. Meyer in this connection [10]. A nematic slab, of thickness D is contained between two polished glasses. The easy axes of the two plates are at right angles. (We shall call x the easy direction of the lower plate, and

[†] This equation is the analogue of a classic theorem for dislocations under stress in solids.

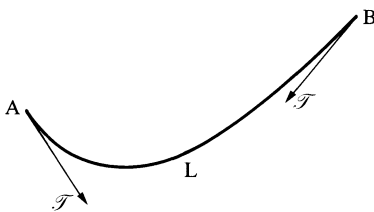


Fig. 4.12. Typical application of the line tension concept. A line L is anchored at points A and B on the sample boundary and urged towards the bottom part of the figure by some external agent (e.g. a flow). The forces on points A and B due to the deformed line are shown on the figure. They are equal in magnitude to the line tension \mathcal{T}

y the easy direction of the upper plate.) This leads to the ‘*plages tordues*’, first observed long ago by Mauguin, and mentioned in Chapter 3. In one *plage* we have a uniform twist, described by an angle

$$\theta(z) = \pm \pi z / 2D, \quad (4.15)$$

whose z measures the level counted from the lower plate. The two possible signs for the twist give equal energies; some *plages* are (+) and some are (−). Two (+) and (−) regions are separated by a line (lying more or less at $z = D/2$), of strength $\frac{1}{2}$. Most of these lines are closed into loops.

When no special precaution is taken a loop tends to shrink (to decrease its line-like energy $2\pi R\mathcal{T}$) and disappear rapidly. However, when a given loop is observed under the microscope, it can be stabilized by the following trick: let us assume for instance that the inside of the loop is (+). To avoid shrinkage, we apply a weak magnetic field \mathbf{H} at an angle θ_H from the x -axis such that $0 < \theta_H < \pi/2$. Then the (+) region is slightly favoured; by a suitable choice of θ_H (in practice by rotating the sample in a fixed field) one can achieve an exact balance between the magnetic effect and the line effect; the loop is then immobile, and its radius R may be measured accurately.

Let us write down the corresponding equations, assuming that the field is weak ($\xi(H) \gg D$) so that the local twist in each (+) or (−) is not altered and that the radius R of the loop is large compared with D . Then, each (+) or (−) region is macroscopic and has a magnetic energy (per unit area in the x, y -plane)

$$\begin{aligned} F_{\text{mag}} &= -\frac{1}{2}\chi_a H^2 \int_0^D dz \cos^2(\theta(z) - \theta_H) \\ &= -\frac{1}{2}\chi_a H^2 D \left\{ \overline{\cos^2 \theta(z)} \cos^2 \theta_H + \overline{\sin^2 \theta(z)} \sin^2 \theta_H \right. \\ &\quad \left. + \frac{1}{2} \sin 2\theta_H \overline{\sin 2\theta(z)} \right\}. \end{aligned} \quad (4.16)$$

The bars represent averages over the slab thickness. The averages of $\cos^2 \theta$ (or $\sin^2 \theta$) are the same for $a(+)$ or $a(-)$. The average

$$\overline{\sin 2\theta(z)} = 1/D \int_0^D dz (\pm \sin \pi z/D) = \pm 2/\pi \quad (4.17)$$

differs for the two signs of the twist. The difference in magnetic energies between the two regions is thus

$$\Delta F_{\text{mag}} = F_{\text{mag}}^{(-)} - F_{\text{mag}}^{(+)} = -(\chi_a H^2 D/\pi) \sin 2\theta_H. \quad (4.18)$$

Consider now the loop of radius R , surrounding an area πR^2 of the $(+)$ region. The overall energy of the form

$$\mathcal{F} = -\pi R^2 \Delta F + 2\pi R \mathcal{T} + \text{const.} \quad (4.19)$$

and the loop will be in equilibrium when $\partial \mathcal{F}/\partial R = 0$, or

$$\mathcal{T}/R = \Delta F_{\text{mag}}. \quad (4.20)$$

Equation (4.20) could have been derived in terms of known rules for vibrating strings; $/R$ is the inward restoring force (per unit length) for a bent line: this is balanced by the magnetic force ΔF_{mag} . Thus, if R is measured and if the magnetic parameters (H , θ_H , χ_a) are known, one can derive \mathcal{T} from eqn (4.20). For a more detailed discussion of these measurements, see reference 10.

Remark: anisotropy of the line tension \mathcal{T} When the differences between K_1 , K_2 , and K_3 are taken into account, twist and wedge disclinations will have different line tensions. If this anisotropy of \mathcal{T} is very strong, it can lead to angular cusps in the shape of the line.[†] In practice, however, these cusps do not seem to have been observed in nematics; the angular dependence of \mathcal{T} is probably too weak.

4.3 POINT DISCLINATIONS

4.3.1 Instability theorem for lines of integral strength

The distortions around a line of integral strength ($m = \pm 1, \pm 2, \dots$) may always be continuously transformed into a smooth structure with no singular line. A typical example of this smoothing process is shown in Fig. 4.13(a), (b); the sample is cylindrical, with a large radius R , and normal boundary conditions. Figure 4.13(a) shows the simplest arrangement, where the director is everywhere radial. The deformation is pure splay; on the axis of the cylinder we have a disclination line of strength $m = \pm 1$. The energy per unit length of line is easily calculated to be

$$\mathcal{T} = \pi K_1 \ln(R/a). \quad (4.21)$$

[†] This was pointed out to the author by J. Friedel.

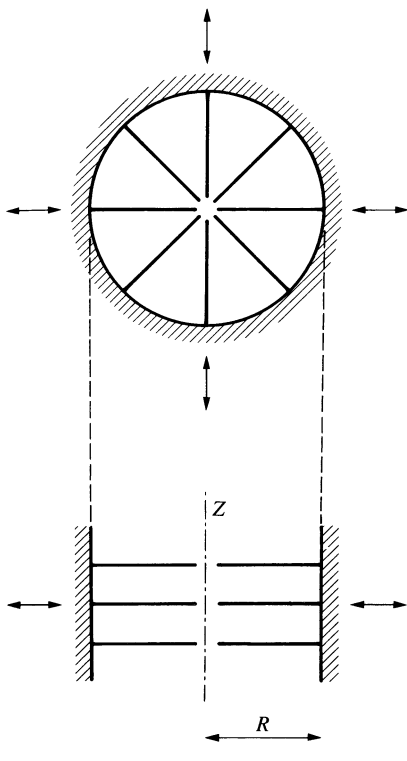


Fig. 4.13. (a) Wedge disclination of strength +1 in a cylinder: the arrangement near the centre has a discontinuity and must involve a core. (b) 'Escape' of the disclination in the third dimension: the arrangement is now continuous (no core). (c) Visualization of the 'escaped' arrangement in a capillary (courtesy C. Williams).

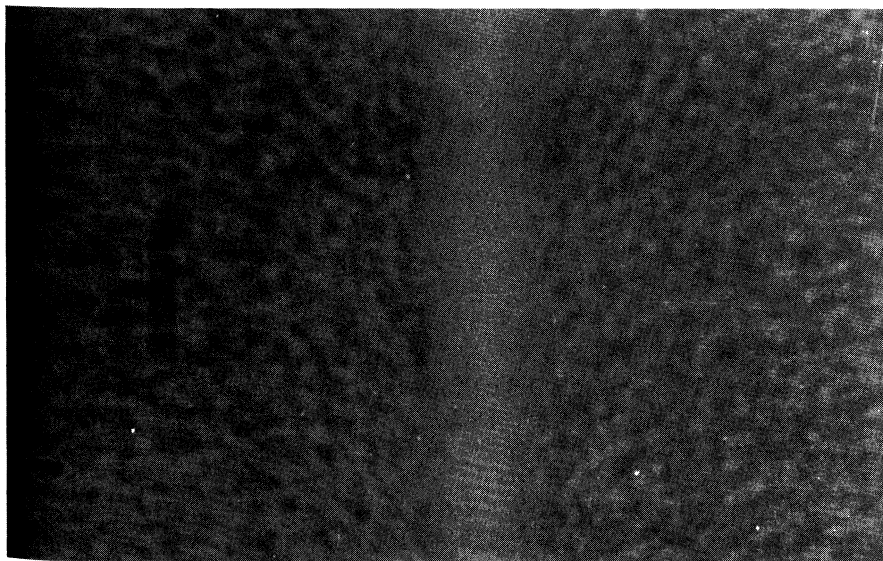
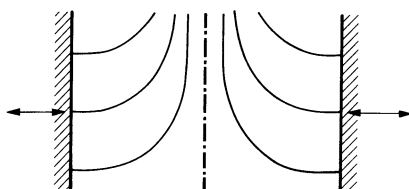


Figure 4.13(b) shows another possible conformation, involving both splay and bend. With cylindrical coordinates (ρ, ϕ, z) this is described by a director field of the form

$$\begin{aligned} n_z &= \cos u(\rho), \\ n_\rho &= \sin u(\rho), \\ n_\phi &= 0 \end{aligned} \quad (4.22)$$

where $u(R) = \pi/2$ and $u(0) = 0$. In the one-constant approximation the form of $u(\rho)$ turns out to be very simple [11, 12]

$$\tan \frac{1}{2}u = \rho/R. \quad (4.23)$$

We can see in eqn (4.23) that u vanishes linearly when $\rho \rightarrow 0$ and that the gradients of \mathbf{n} are not singular on the axis; thus, in this splay–bend solution, the disclination line has vanished.

The calculation can also be performed for the more realistic case where $K_1 \neq K_3$. The functional form of $u(\rho)$ is then modified, but the qualitative features shown by eqn (4.23) remain unchanged. The energy can be derived exactly for instance, when $K_3 > K_1$, we have an energy per unit length [12]

$$\mathcal{T}' = \pi(2K_1 + K_3(k/\tan k)), \quad (4.24)$$

where

$$\tan^2 k = K_3/K_1 - 1. \quad (4.25)$$

In most practical cases K_3/K_1 is close to unity and

$$\mathcal{T}' \cong 3\pi K \quad (4.26)$$

Then the splay–bend conformation is more favourable than the line, provided that $\ln R/a > 3$ or $R > 20a \sim 40$ nm. Thus for all physical sizes R , the line is not stable. This has been noticed independently by R. B. Meyer [11] and by Cladis and Kleman [12]. Meyer describes the effect as an ‘escape in the third dimension.’ On the experimental side, the ‘rule of escape’ has also been established very early in cholesterics by Rault [13].

The line could become stable only if K_1 were much smaller than K_3 (and K_2). Consider for instance the limit $K_3 \gg K_1$ in eqn (4.24). Then $k \rightarrow \pi/2$ and the energy of the ‘escaped’ configuration becomes

$$\mathcal{T}' \rightarrow \frac{1}{2}\pi^2(K_3 K_1)^{\frac{1}{2}} \quad (K_3 \gg K_1). \quad (4.27)$$

Comparing this with eqn (4.21), we see that the disclination line may become

stable if

$$\ln(R/a) < \frac{1}{2}\pi(K_3/K_1)^{\frac{1}{2}}. \quad (4.28)$$

As we shall see later, in Chapter 10, there is one case where the ratio K_3/K_1 may be very large—namely in the vicinity of a transition from nematic to smectic A. For instance if $K_3/K_1 = 16$ the condition (4.28) corresponds to $R \gtrsim 400a \simeq 1 \mu\text{m}$. Thus, in such a case and using fine capillaries, one might possibly stabilize a line with integral m . But, excluding such extreme cases, we see that the line will escape in practice.

The argument may be extended to cover other types of ‘escape’ (involving twist) and other types of lines; in all cases, when the elastic constants are comparable, the lines of integral m are found to be unstable. This theorem will be very important for our discussion of the *noyaux*.

On the other hand, the lines of half-integral strength ($m = \pm \frac{1}{2}$) are stable, simply because there is no way for them to ‘escape’ into a smooth structure, while retaining the same m ; if we follow a closed contour C surrounding the distorted region, starting from one point A with direct $\mathbf{n}(A)$, we reach point A again after one turn, but with a director $-\mathbf{n}(A)$. Now if we decrease the contour C we must at some moment hit a point I where \mathbf{n} is discontinuous. The locus of these points I defines a disclination line, which is thus present whatever efforts we make.

In lateral views, there is a rather striking difference between the optical aspect of the $|S| = \frac{1}{2}$ and $|S| = 1$ lines. The $|S| = \frac{1}{2}$ lines appear as thin threads, while the (escaped) $|S| = 1$ lines appear as *thick threads*. This distinction is emphasized by Williams and Bouligand [14].

4.3.2 Interpretation of the *noyaux*

The *structure à noyaux* or ‘Schlieren texture’ was presented in Section 4.1. We have seen that each *noyer* (node) has a characteristic strength m that can be integral ($m = \pm 1$) or half-integral ($m = \pm \frac{1}{2}$). We also noted that the nodes could be interpreted in terms of two different models; either as point disclinations, or as line disclinations normal to the plane of the slab. We are now in a position to discuss this more fully.

Since all lines with integral m are unstable, the nodes with $m = \pm 1$ must be disclination points; a typical geometry for such points is shown in Fig. 4.14. Any node with $m = \pm \frac{1}{2}$ must be the end point of a disclination line of the same strength, since (as explained at the end of the last paragraph) it is not possible to eliminate such a line by continuous deformations.

This very fundamental distinction between two types of nodes was not appreciated by G. Friedel. It has been established mainly through the work of R. B. Meyer [11]. All the existing observations appear to agree with it. A typical photograph showing both types of node, and the lines emerging only from the $\pm \frac{1}{2}$ species, is shown in Fig. 4.1.

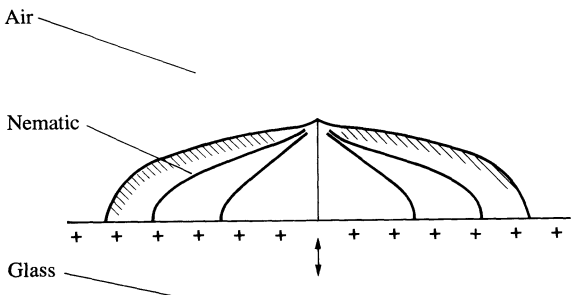


Fig. 4.14. One singular point at the free surface of a flat nematic droplet. Boundary conditions: homeotropic at the glass–nematic interface; tangential or conical at the nematic–air interface.

4.3.3 Other observations on point defects

4.3.3.1 Points on an interface

A number of point defects, geometrically similar to *noyaux* of integral strength ($m = \pm 1$) can be observed at the *free surface* of a nematic, or at the *interface* between a nematic and an isotropic phase, provided that the boundary conditions at the interface are tangential or conical. Typical geometries are shown in Figs 4.14 and 4.15. A detailed study of these points has been carried out by R. B. Meyer [7a].

In most cases, the distortions taking place below the surface will react on the shape of the surface itself [7b]. The singular points are associated with cusps (or dips) on the surface. These cusps are expected to be very weak (typical height of order $1\text{ }\mu\text{m}$), but the energy of the singular point does contain significant contributions from surface tensions and gravitational potentials, associated with the cusp.

4.3.3.2 Points in the bulk

When a line, such as the wedge disclination of Fig. 4.13(a), with $m = 1$, ‘escapes’ in the third dimension, it may do it in two ways (‘upwards’ or ‘downwards’). An upwards portion and a downwards portion will be linked by a singular point, as shown in Fig. 4.16. A systematic classification of the singular points has been constructed by Nabarro [15].

At first sight, the simplest geometry allowing for one singular point in the bulk corresponds to a spherical nematic droplet, floating in an isotropic liquid, with normal boundary conditions at the interface. In the most naïve solution for this problem, the director is everywhere radial, the singular point being at the centre of the droplet and the deformation being pure splay [16a]. However, this conformation is not usually observed. A much more complex arrangement, involving a strong twist in the central region, is preferred [16b].

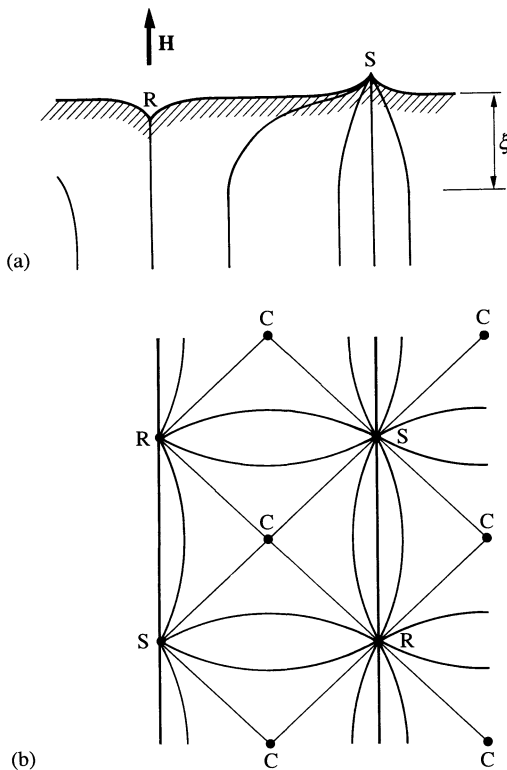


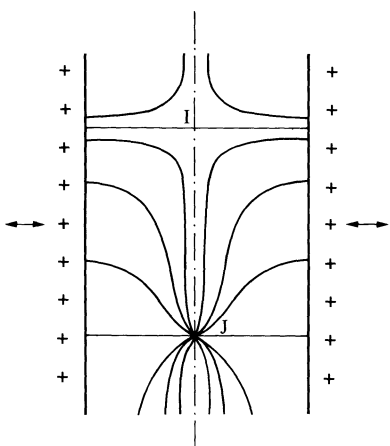
Fig. 4.15. Ideal array of point disclinations at the free surface of a nematic liquid: (a) view in a vertical plane; (b) horizontal pattern—sketch of one possible lattice (square lattice). S, peak; R, hole; C, saddle point. In practice, only disordered points have been observed up to now.

This is probably due to the fact that the twist constant K_2 is significantly smaller than K_1 in typical nematics.[†]

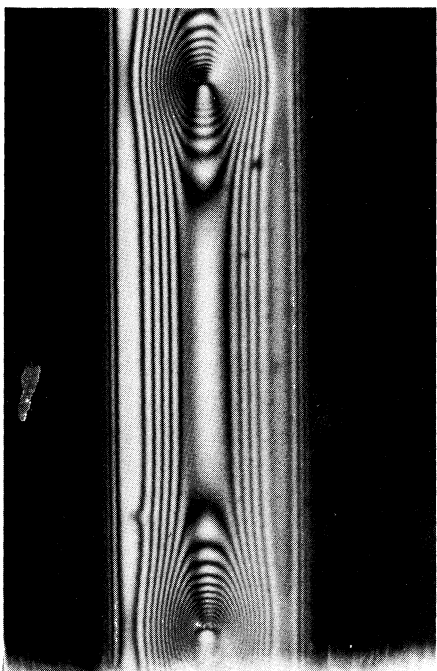
4.4 WALLS UNDER MAGNETIC FIELDS

In Section 4.1 we saw that sheet singularities are not stable in nematics, but that diffuse walls are allowed under a magnetic field. We now discuss these walls in more detail, starting from a simple example—which unfortunately is hard to realize experimentally—and then progressing towards more realistic situations.

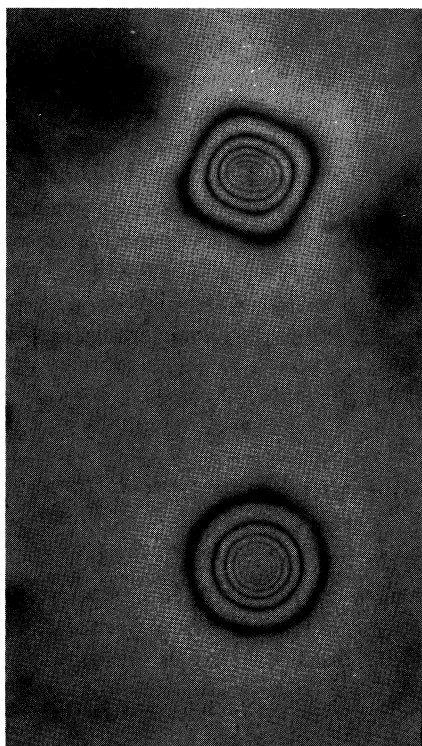
[†] Near a nematic-smectic transition A the ratio K_2/K_1 is expected to increase, and the ‘naïve’ solution might prevail.



(a)



(b)



(c)

Fig. 4.16. (a) Singular points in a capillary with normal boundary conditions. The diagram is schematic. In the vicinity of the points I or J a more complicated distortion may occur as shown in Fig. 4.17. (b) Optical observation of a pair of defects in a capillary (cross Nicols at 45° from the capillary axis). The director field corresponds to (a). (Courtesy H. Gruler and T. Scheffer.) (c) Singular points in a slab of MBBA with normal boundary conditions (courtesy R. B. Meyer). The drawing in (a) applies: point J gives circular rings. (Observation with crossed circular polarizers.)

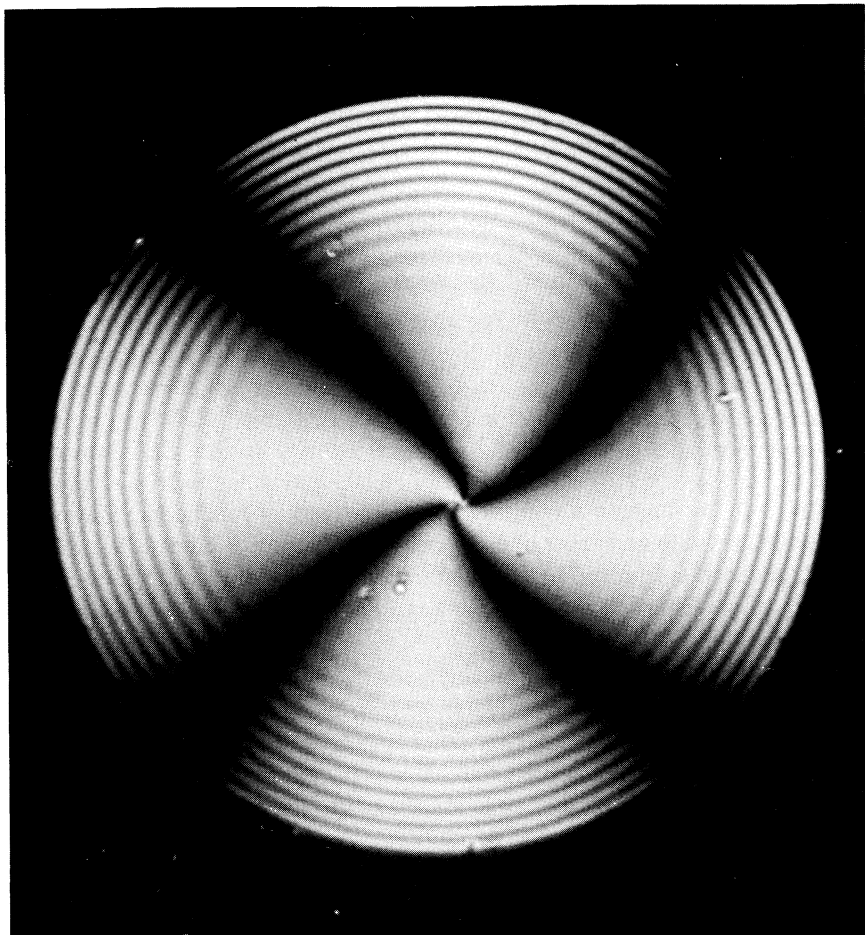


Fig. 4.17. Point defect at the centre of a nematic droplet (courtesy S. Candau). The boundary conditions at the surface of the droplet are normal (or nearly so). Instead of a simple radial arrangement (of the type shown at point J in Fig. 4.16(a)), there is a twisted arrangement, clearly shown here by the black cross observed under cross Nicols.

4.4.1 180° walls

4.4.1.1 *Structure of the wall*

Under a field \mathbf{H} a bulk nematic will align with the director \mathbf{n} parallel or antiparallel to \mathbf{H} ; both situations are physically equivalent, and lead to equal energies. It may happen that in one domain \mathbf{n} and \mathbf{H} are parallel, while in another domain they are antiparallel; the border region between the two domains is then called a 180° wall. It is similar to a Block wall in a

ferromagnetic with uniaxial anisotropy; the analogue of the easy axis in the ferromagnetic is the field axis in the nematic.

For the nematic problem, these walls were first considered by Helfrich [17]. The wall surface may be normal or parallel to \mathbf{H} . In the latter case, the only deformation involved is twist, and, since in usual materials K_2 is the smallest elastic constant, the twist wall is the least expensive from an energy point of view. It is also the simplest one to compute, and we shall restrict our attention to this type.

Let us put the field \mathbf{H} along the x -axis, and assume that the director \mathbf{n} depends only on y , with the form

$$\begin{aligned} n_x &= \cos u(y), \\ n_z &= \sin u(y), \\ n_y &= 0. \end{aligned} \quad (4.29)$$

At $y = +\infty$ we impose $u = 0$, and at $y = -\infty$, $u = \pi$. The calculation of $u(y)$ coincides with an earlier one, described in Chapter 3 (eqns (3.50)–(3.56)) to introduce the concept of a coherent length; the only change is in the domain of variation of y . The implicit equation for $u(y)$ is

$$\tan \frac{1}{2}u = \exp(-y/\xi_2(H)) \quad (4.30)$$

where ξ_2 is defined as usual as $(K_2/\chi_a)^{\frac{1}{2}}H^{-1}$. We can check that eqn (4.30) is compatible with the boundary conditions. Most of the variation of u takes place in a thickness $2\xi_2$, centred at $y = 0$. Typically for $H = 5000$ G, $2\xi_2 \sim 10$ μm . The energy per unit area, or ‘surface tension’ σ , of the wall may be derived from eqns (3.47) and (3.54). The result is

$$\sigma = 2K_2/\xi_2. \quad (4.31)$$

With the above values for H , $\sigma \sim 4 \times 10^{-3}$ erg cm^{-2} . The wall is a very smooth structure, and requires only low energies.

4.4.1.2 Boundary effects

In practice, it is often important to understand the interactions of the wall with the boundaries of the sample. If the wall intersects the boundary surface the situation is usually rather complex (in particular disclination lines may nucleate at the intersection). If the wall is parallel to the surface, the situation is somewhat simpler. Let us further assume that the boundary conditions at the surface are tangential, and that the distance d between the wall and the surface is much larger than ξ_2 . Then a generalization of the above calculations leads to the following predictions [18].

1. If the surface is rubbed, with an easy axis parallel to \mathbf{H} , the wall is repelled from it. The repulsive force per unit area, or pressure, is given by

$$p = 8\chi_a H^2 \exp(-2d/\xi_2). \quad (4.32)$$

2. If the boundary condition is degenerate (e.g. at a free surface, the molecules being tangential) the wall is *attracted* towards the surface; the pressure is equal in magnitude, but opposite in sign, to eqn (4.32). In both cases these pressures may be understood as resulting from the interaction between the wall and its image, separated from it by a distance $2d$.

In principle, relying on statement 1, it appears possible to stabilize one wall between two anchored plates, which would both repel it. One might think of the following sequence to generate the wall: (a) in zero field, starting from a planar texture, rotate one of the glass plates by 180° , thus creating a *plage tordue*. Apply \mathbf{H} along the easy axis of the plates; the *plage tordue* should shrink in a wall at the midlane of the slab. However, in practice, as soon as we twist the sample by more than 90° , disclination loops nucleate at the edges of the slab, and relax the torsion. Thus operation (a) can be performed only during a short transient period. (We shall come back to a discussion of these transient effects in Chapter 5.)

4.4.2 Walls associated with a Frederiks transition

The Frederiks transitions were discussed in Section 3.2. In all these transitions we start with a nematic monodomain, apply to it a field normal to the optical axis, and observe a distortion above a certain threshold field H_c . For a given $H > H_c$, the system may choose between two different (but equivalent) distortion patterns: one example is shown in Fig. 4.18, corresponding to case 1 in our classification of the various Frederiks transition (see Fig. 3.13)—i.e., a transition from planar towards homeotropic texture.

For $H > H_c$ the nematic slab will thus break into domains, corresponding to either of the two distortion patterns. The border between two domains of opposite distortions involves a wall.[†] The theoretical structure of these walls has been analysed by F. Brochard [19]. It is significantly different from the structure of the Helfrich walls described above.

[†] At least for H not too large. At high fields the situation is more complex, and will be discussed later in this section.

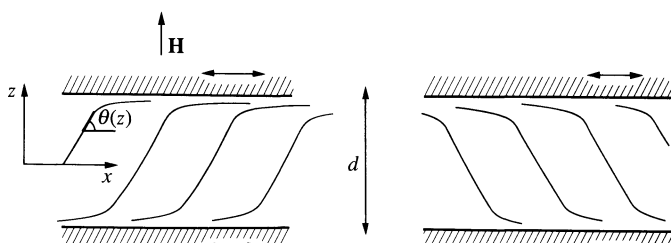


Fig. 4.18. Two types of domains above the Frederiks critical field

Again the walls may be either parallel or normal to the easy axis; we choose to discuss the parallel case (twist wall). The thickness of the wall is *very large* when H is close to H_c . It is of order $2\kappa_2^{-1}$ where the inverse length κ_2 is defined by

$$\xi_2^2 \kappa_2^2 = 1 - (H_c/H)^2 \quad (H \rightarrow H_c).$$

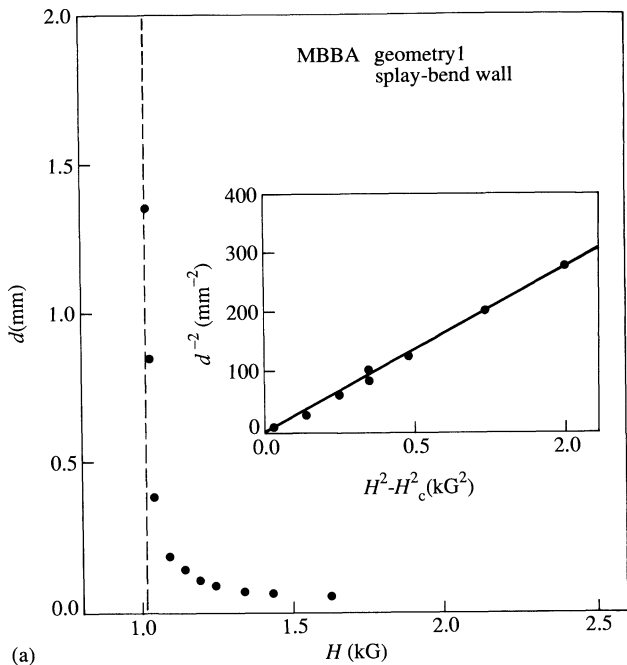
From the point of view of the general theory of phase transitions, the divergence of κ^{-1} when $H \rightarrow H_c$ is natural. The Frederiks transition is of second order, and near a usual second-order transition point the correlation lengths diverge [20]. Figure 4.19 shows the increase in size of a wall when $H \rightarrow H_c$.

When the field $H > H_c$ is suddenly applied, a number of domains appear. After some time, many small domains shrink to zero, and we are left with a few large loops. By slightly tilting the field, it is possible to favour the inside of a loop, and to make it stationary (just as in the Meyer technique for disclinations). The loop is not circular; the portions of the wall which are parallel to the easy axis (twist wall) are less expensive in energy than the normal positions (bend wall for case 1). Thus, from a study of the ellipticity of the loops, it is possible to infer the ratio of two elastic constants. Experiments of this type (but using case 2 in the classification of Fig. 3.13, Section 3.2) have been performed by L. Léger [21].

On the whole, the most interesting feature of the walls (as opposed to the disclination lines) is that all their properties can be nearly analysed in terms of the continuum theory—while for the lines, the core effect is often non-negligible. For instance, the nucleation of a wall at a surface involves large regions (of the order of the wall thickness) and is thus rather insensitive to atomic defects on the surface. On the other hand, the nucleation of a line takes place on the molecular scale and is not easily controlled.

4.4.3 Transformation from walls to lines ('*pincement*')

Consider for instance the wall of Fig. 4.20 and increase the field H ; the distortion in the wall region becomes progressively larger (κ^{-1} decreases) and finally, at a certain field H' , a set of two disclinations (of strengths $m = -\frac{1}{2}$ and $m = +\frac{1}{2}$) appears. This process has been called '*pincement*' by Y. Bouligand. The field H depends on the choice of the system, but is typically of the order of $2H_c$. This transition from walls to lines was observed first by R. B. Meyer (private communication). A similar transition in cholesterics (with a more complex wall structure) was found by Rault [22]. *Pincements* induced by electric fields have been studied at Freiburg [23].



(a)

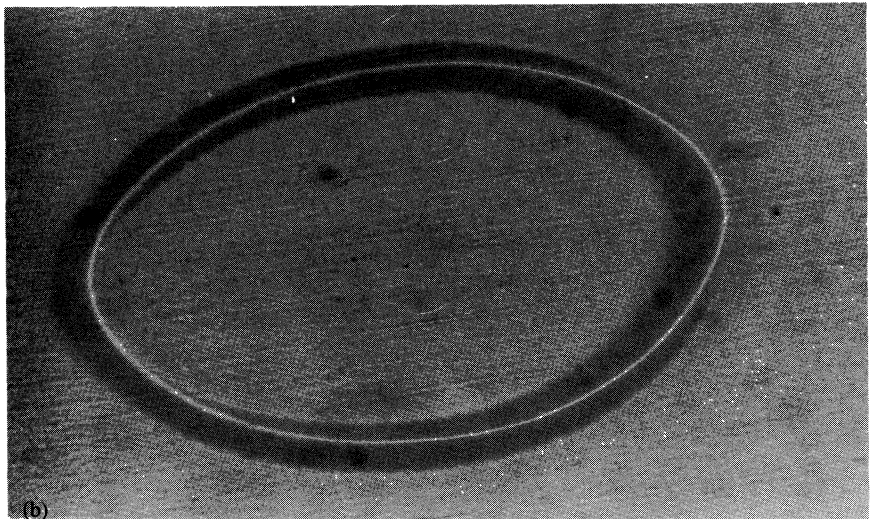
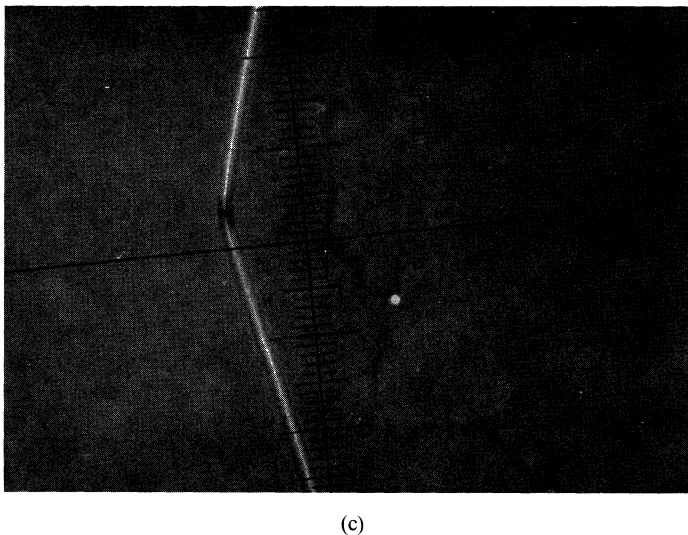
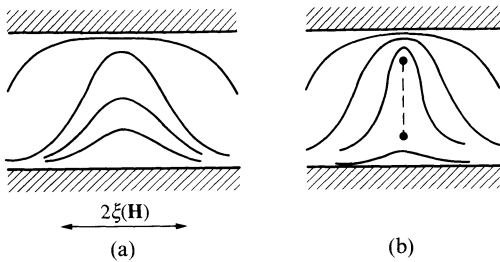
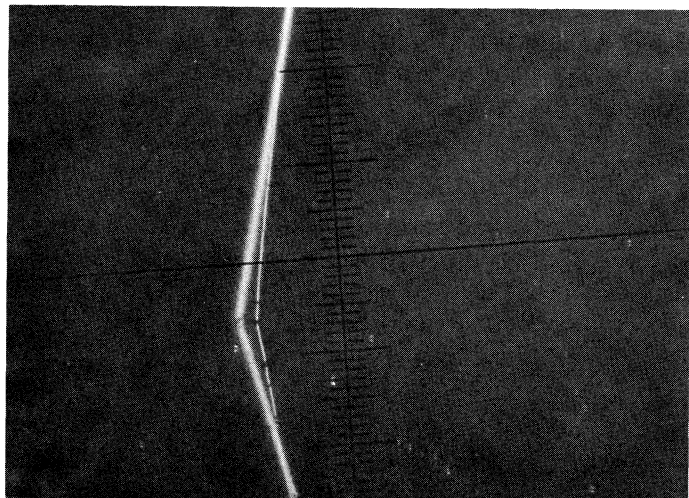
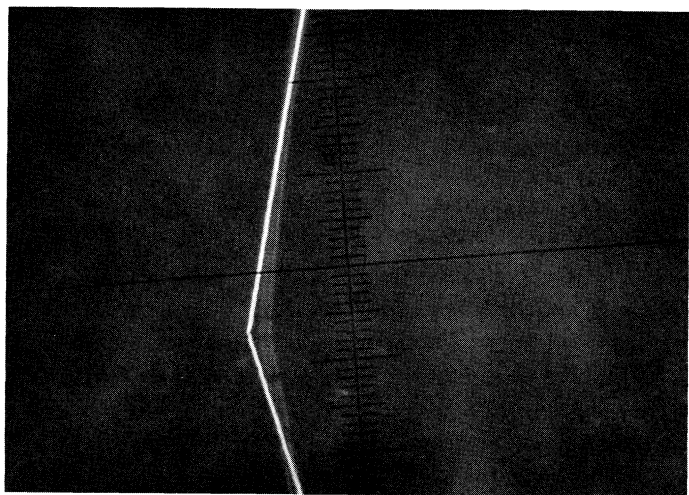


Fig. 4.19. (a) Thickness d of a wall as a function of the field \mathbf{H} (d is derived from a study of interference fringes for normally incident monochromatic light). Note the divergence of d at the Frederiks threshold ($H/H_c \rightarrow 1$). (Courtesy L. Léger.) (b) A closed wall in a homeotropic \rightarrow planar transition. The long angle of the ellipse is along the field \mathbf{H} .



(c)

Fig. 4.20. *Pincement*: transformation of a wall (a) into a system of lines (b). The wall as seen under polychromatic light is shown in (c). In (d) the same region is observed at higher H . The image is focused on the upper line, and the lower line is blurred. In (e) the image is focused on the lower line. The use of a bent wall is convenient to avoid exact superposition of the two lines (courtesy L. Léger).



(e)

4.5 UMBILICS

Another type of Frederiks transition is of interest in generating smooth defects. It is obtained with materials of negative dielectric anisotropy, prepared in a homeotropic texture, and subjected to a field \mathbf{E} normal to the plates (direction z) (Fig. 4.21). Above a certain Frederiks threshold E_c the molecules in the midplane of the slab tend to tilt, but they can tilt towards any direction in the x, y -plane. One can define the chosen tilt direction by a unit vector \mathbf{c} . When observed with vertical light beams, a region tilted along \mathbf{c} behaves as a birefringent slab with one neutral line parallel to \mathbf{c} . It must be noticed, however, that \mathbf{c} and $-\mathbf{c}$ are not equivalent.

In an ideal sample \mathbf{c} would be independent of x and y . But in practice the lateral boundary conditions impose some distortions upon the \mathbf{c} field. One can in fact construct a two-dimensional Frank elasticity for this problem, involving two elastic constants (' c splay' and ' c bend'). Also one can find *singular points* in the \mathbf{c} field (Fig. 4.22). These singular points have been called umbilics by the Orsay group [24]. They can have only integral strength (± 1). An interesting feature of the umbilics is that (at least for fields E that are not too high) their core is continuous; the size of the core is essentially

$$\kappa^{-1} = \frac{DE_c}{\pi(E_c^2 - E^2)^{\frac{1}{2}}}$$

(D being always the sample thickness), and the director \mathbf{n} varies smoothly inside the core [24]: thus the static and dynamic properties of the umbilics can be calculated accurately. The umbilics show remarkable distortions and motions under shear flows (the upper limiting plate moving parallel to the lower plate). (See reference 25.)

4.6 SURFACE DISCLINATIONS

The special features of disclination lines sticking at a solid-nematic interface have been observed in particular by M. Kleman and C. Williams [26] and more recently by M. Kleman and G. Ruschenkov [27]. These lines are not mobile, and their path is often sensitive to microscopic regularities on the solid. They are easily distinguished from the lines in the bulk.

The structure of these lines has been analysed in detail by Vitek and Kleman [28]; some earlier work by Meyer [11] is also relevant to this problem. The structure depends mainly on the magnitude of the anchoring energy, favouring one particular orientation at the surface. When this energy is weak or, equivalently, when the extrapolation length b defined in Fig. 3.8 is large, a surface line becomes *spread out over a distance of order b* . This

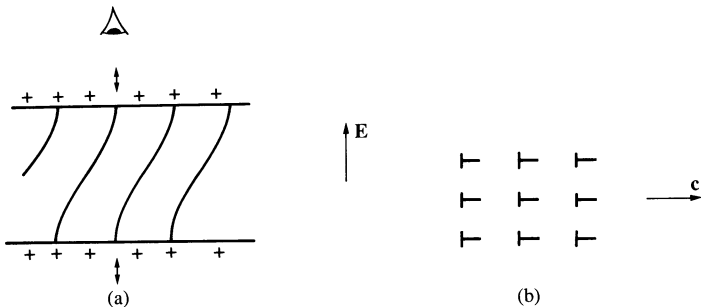


Fig. 4.21. ‘Degenerate’ Frederiks transition under a field E with homeotropic boundary conditions and negative dielectric anisotropy $\epsilon_a < 0$ (all electrohydrodynamic effects are assumed to be absent). Above the threshold field E_c the molecules tilt towards an arbitrary direction c of the slab plane. (a) Side view; (b) the alignment as seen by an observer looking through the plates

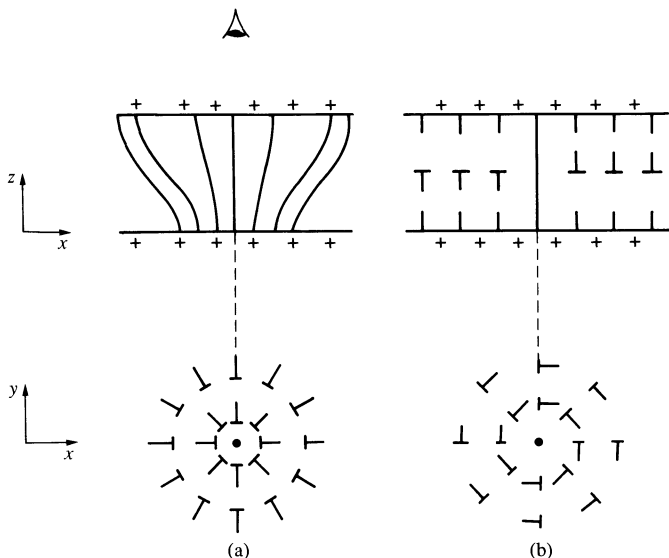


Fig. 4.22. ‘Umbilics’ obtained in the degenerate case of Fig. 4.21. (a) Splay dominant in the core. (b) Twist dominant in the core.

can be understood as follows. Consider, for instance, an interface in the x, y -plane with tangential boundary conditions and an anchoring energy (per cm^2)

$$f_{\text{surf}} = \frac{1}{2}A \sin^2 \theta \quad (4.33)$$

for a director making an angle θ with the easy axis. With the one-constant approximation a planar distortion of the type in Section 4.2.2.2) is again

governed by $\nabla^2\theta = 0$ in the whole nematic region ($z > 0$). The boundary condition at the wall expresses the balance of torques and is

$$\frac{\partial f_{\text{surf}}}{\partial \theta} = K \left. \frac{\partial \theta}{\partial z} \right|_{z=0}$$

or, in terms of the extrapolation length b (eqn (3.33)),

$$\frac{1}{b} \sin \theta \cos \theta - \left. \frac{\partial \theta}{\partial z} \right|_{z=0} = 0. \quad (4.34)$$

The solution $\theta(xyz)$ can be obtained from the discussion following eqn (4.4). For a line parallel to the y -axis, it is given by [11, 28]

$$\tan \theta = \frac{z + b}{x}. \quad (4.35)$$

It is easily checked that the boundary condition (4.34) is correctly satisfied. Equation (4.35) taken exactly at the interface ($z = 0$) shows that θ varies from 0 to π when x goes from $-\infty$ to $+\infty$, the main variation taking place in an interval $2b$.

This is interesting, since in many practical conditions b lies in the micrometre range: by careful optical measurements of $\theta(z = 0)$ one can then determine b , or, more generally, measure anchoring energies.

REFERENCES

1. Friedel, G. *Ann. Phys., Paris* **19**, 273 (1922).
2. Frank, F. C. *Discuss. Faraday Soc.* **25**, 19 (1958).
3. Rault, J. *C.R. Acad. Sci., Paris* **272**, 1275 (1971).
4. Cladis, P., Kleman, M., and Pieranski, P. *C.R. Acad. Sci., Paris* **B273**, 275 (1971).
5. Friedel, J. and Kleman, M. In *Fundamental aspects of the theory of dislocations*, National Bureau of Standards Special Publication no 317, Vol. I, p. 607. National Bureau of Standards, Washington DC (1970); Kleman, M. and Friedel, J. *J. Phys. (Paris) Colloq.* **30** (Suppl. C4), 43 (1969). For a more recent analysis see: Kleman, M. *Points, lignes, parois*, Vols I and II. Les Editions de Physique (1977).
6. Detailed studies on groups of disclinations have been carried out by Ericksen, J. L. In *Liquid crystals and ordered fluids* (ed. J. Johnson and R. S. Porter), p. 181. Plenum Press, New York (1970); Dafermos, C. *Quart. J. Mech. appl. Math.* **33**, 49 (1970).
7. (a) Meyer, R. B. *Mol. Cryst. liquid Cryst.* **16**, 355 (1972); (b) de Gennes, P. G. *Solid State Commun.* **8**, 213 (1970).
8. (a) Williams, R. J. *chem. Phys.* **50**, 1324 (1969). The optical rotations observed by Williams are due to his use of a binocular microscope with beams tilted from the vertical. When such a beam propagates, for example, in the y, z -plane, it

- enters into the thickness ξ below the surface through regions where the optical axis is progressively rotating. (b) Williams, R. et al. *J. Appl. Phys.* **43**, 3685 (1972).
9. Friedel, J. and de Gennes, P. G. *C.R. Acad. Sci., Paris* **258**, 257 (1969).
10. Meyer, R. B. *Phys. Rev. Lett.* **22**, 918 (1969); unpublished D.Phil. thesis, Harvard University (1969).
11. Meyer, R. B. *Phil. Mag.* **27**, 405 (1973).
12. Cladis, P. and Kleman, M. *J. Phys. (Paris)* **33**, 591 (1972).
13. Rault, J. Unpublished D.Phil. thesis, Orsay (1971).
14. Williams, R. and Bouligand, Y. *J. Phys. (Paris)* **35**, 589 (1974).
15. Nabarro, F. R. N. *J. Phys. (Paris)* **33**, 1089 (1972).
16. (a) Dubois Violette, E. and Parodi, O. *J. Phys. (Paris)* **30** (Suppl. C4), 57 (1969); (b) Candau, S., LeRoy, P., and Debeauvais, F. *Mol. Cryst.* **23**, 283 (1973); Press, M. and Arrot, A. *J. Phys. (Paris) Colloq.* **36** (Suppl. C1), 177 (1975); (c) Saupe, A. *Mol. Cryst.* **21**, 211 (1973); (d) Williams, C., Cladis, P., and Kleman, M. *Mol. Cryst.* **21**, 355 (1973).
17. Helfrich, W. *Phys. Rev. Lett.* **21**, 1518 (1968).
18. de Gennes, P. G. *J. Phys. (Paris)* **32**, 789 (1971).
19. Brochard, F. *J. Phys. (Paris)* **33**, 607 (1972).
20. See, for example, Stanley, H. E. *Introduction to phase transitions*. Oxford University Press, Oxford (1971).
21. Léger, L. *Mol. Cryst.* **24**, 33 (1973).
22. Rault, J. *Mol. Cryst. liquid Cryst.* **16**, 143 (1972).
23. Stieb, A., Baur, G., and Meier, G. *J. Phys. (Paris) Colloq.* **36** (Suppl. C1), 185 (1975).
24. Rapini, A. *J. Phys. (Paris)* **34**, 629 (1973).
25. Rapini, A., Léger, L., and Martinet, A. *J. Phys. (Paris) Colloq.* **36** (Suppl. C1), 194 (1975).
26. Kleman, M. and Williams, C. *Phil. Mag.* **28**, 725 (1973); see also Williams, C. Thèse 3e cycle, Orsay (1973).
27. Ruschenkov, G. Thèse 3e cycle, Orsay (1975). Ruschenkov, G. and Kleman, M. *J. Chem. Phys.* **64**, 23 (1976).
28. Vitek, B. and Kleman, M. *J. Phys. (Paris)* **36**, 59 (1975).

DYNAMICAL PROPERTIES OF NEMATICS

'Before us the thick dark current runs. It talks to us in a murmur become ceaseless and myriad.'

W. Faulkner

5.1 THE EQUATIONS OF 'NEMATODYNAMICS'

5.1.1 Coupling between orientation and flow

A nematic flows very much like a conventional organic liquid with molecules of similar size. However, the flow regimes are more complex and more difficult to study experimentally than in isotropic liquids for the following reasons.

The translational motions are coupled to inner, orientational motions of the molecules; in most cases, the flow disturbs the alignment. Conversely, a change in the alignment (e.g. by application of an external field) will, in many instances, induce a flow in the nematic.

To measure these effects quantitatively, optical observations of the local state of affairs under flow would be extremely helpful. Unfortunately, nematics are turbid (for reasons that are not accidental; see Section 3.4). In practice, optical studies are restricted to thin samples (below 300 µm). Conventional viscometric equipment (based on capillaries, falling spheres, rotating cylinders, etc.) is thus not adequate for optical observations. Also, the boundaries (e.g. at the inner surface of the capillary) are not controlled, and the state of nematic alignment is unknown. For these reasons, many of the existing data in the literature cannot be used for quantitative purposes.

It is possible, however, to improve on this situation, either by imposing an alignment by an external field or by selecting some more refined probes: attenuation of acoustic shear waves, inelastic scattering of light, etc. (We shall discuss these experiments on 'nematodynamics' in Section 5.2.)

From a theoretical point of view, the coupling between orientation and flow is a very delicate matter. It has been analysed essentially by two groups who represent very different schools of thought.

1. A macroscopic approach, based on classical mechanics, has been used by Ericksen [1], Leslie [2], and Parodi [3] (hereafter referred to as ELP). Most of the existing data have been analysed in this language.
2. A microscopic approach, based on a study of correlation functions, has been set up more recently by the Harvard group [4a]. The results have been later rewritten directly in macroscopic terms, and extended to other mesomorphic phases [4b].

The two approaches are essentially identical in content. We shall present here a (slightly amended) version of the ELP theory and then show how, by a slight change in the choice of variables, one can obtain the Harvard formulation.

5.1.2 Choice of dynamical variables

The first assumption of the ELP approach is that in a nematic liquid crystal a dynamical situation must be specified by:

1. a velocity field $\mathbf{v}(\mathbf{r})$ giving the flow of matter;
2. a unit vector $\mathbf{n}(\mathbf{r})$ (the director) describing the local state of alignment.

This formulation was questioned in an early contribution by the Harvard group [5]. They proposed a completely different theory, where it was assumed that the velocity field $\mathbf{v}(\mathbf{r})$ is enough to specify the state of affairs; in this theory the director is not an independent variable, but its orientation is deduced from the gradients of \mathbf{v} . Thus, in this picture, a rotation of the optical axis can occur only if there is a macroscopic (non-uniform) flow.

Experimentally, it is in fact possible, in suitable geometries, to rotate the director \mathbf{n} by an external field, without any macroscopic displacement of the molecules ($\mathbf{v} \equiv 0$). A good example of this property is found with planar distortions of pure twist (Fig. 5.1). Starting with a nematic single crystal between two polished plates, one applies a magnetic field \mathbf{H} in the plane of the plates at a finite angle ψ ($< \pi/2$) to the unperturbed optical axis. If H is large enough ($\xi(H)$ much smaller than the sample thickness d) the molecules in the central part of the slab rotate by an angle ψ . To see if this is accompanied by backflow, one watches a dust particle floating in the nematic (Y. Galerne, unpublished). The result is negative; in this geometry a rotation of the optical axis is achieved without any macroscopic displacements. More refined versions of this experiment have also been carried out by inelastic scattering of light [6], and they lead to the same conclusion: the choice of state variables proposed in reference 5 is not sufficient to describe a nematic, while the ELP choice is adequate.

We should also add one word of comment on the use of a director $\mathbf{n}(\mathbf{r})$ of *constant length* ($\mathbf{n}^2 \equiv 1$). Of course, as already mentioned in connection with the static continuum theory (Section 3.1), in a distorted state the

magnitude of the birefringence is slightly modified. However, this effect is very small at all temperatures below the nematic isotropic transition T_c . Also, in ordered phases the characteristic frequencies associated with a change of magnitude of the order parameter are high, and thus not amenable to a hydrodynamic description. Thus we must omit these changes.[†]

5.1.3 The entropy source for a flowing nematic

5.1.3.1 Nature of the losses

We wish to write down equations of motion for the variables \mathbf{v} and \mathbf{n} in the limit of slow space-variations and low frequencies ('hydrodynamic limit'). The first step is to construct a formula giving the dissipation or, as it is called, the entropy source due to all friction processes in the fluid. For simplicity we shall restrict our attention to *isothermal* processes (no thermal gradients); then we shall find two types of dissipative losses—conventional viscosity effects and losses associated with a rotation of the optical axis \mathbf{y} with respect to the background fluid.

Our derivation of the entropy source follows rather closely the approach of de Groot and Mazur [7] for isotropic fluids. The free energy stored in our nematic has the form

$$\int \left\{ \frac{1}{2} \rho v^2 + F_0 + F_d + F_m \right\} d^3r.$$

The first term represents kinetic energy (ρ is the density). F_0 is an internal free energy, depending on the density. F_d is the Frank free energy for distortions. F_m represents the coupling between the director and an external magnetic field \mathbf{H} . Note that we did not include any surface terms in the free energy; this means that we restrict ourselves to situations with strong anchoring.

In all that follows we shall assume (as in Chapter 3) that \mathbf{H} is uniform in space. Also, for simplicity, we have not included in our discussion the coupling with an electric field, or the effect of bulk forces such as gravitation.

For an isothermal process, the dissipation $T\dot{S}$ is equal to the decrease in stored free energy

$$T\dot{S} = -\frac{d}{dt} \int \left\{ \frac{1}{2} \rho v^2 + F_0 + F_d + F_m \right\} d^3r. \quad (5.1)$$

We shall now write down explicitly the various contributions to eqn (4.1). The kinetic term will be derived from an equation for the local acceleration; the internal free-energy terms will be taken directly from our discussion of hydrostatics in Chapter 3.

[†] Above T_c the situation is quite different, and it will be discussed separately in Section 5.4.

5.1.3.2 Definition of the total stress and of the viscous stress

We shall write the acceleration equation for the fluid in the form

$$\rho \frac{d}{dt} v_\beta = \partial_\alpha \sigma_{\alpha\beta} \quad (5.2)$$

where $\sigma_{\alpha\beta}$ is called the *stress tensor*. It must be emphasized that $\sigma_{\alpha\beta}$ is not uniquely defined by eqn (5.2). Changes of the form $\sigma_{\alpha\beta} \rightarrow \sigma_{\alpha\beta} + g_{\alpha\beta}$ leave the acceleration unchanged, provided that $\partial_\alpha g_{\alpha\beta} \equiv 0$.

Inserting eqn (5.2) into eqn (5.1) and integrating by parts we obtain

$$-\frac{d}{dt} \int (\frac{1}{2} \rho v^2) d^3 r = \int \sigma_{\alpha\beta} \partial_\alpha v_\beta d^3 r + \text{surface terms.} \quad (5.3)$$

Let us now turn to the contribution of $F_0 + F_d + F_m$ to the entropy source. It can be obtained from eqn (3.101) putting $F_g = 0$ and is

$$-\frac{d}{dt} \int \{F_0 + F_d + F_m\} d^3 r = \int (-\sigma_{\alpha\beta}^e \partial_\alpha v_\beta + \mathbf{h} \cdot \dot{\mathbf{n}}) d^3 r + \text{surface terms} \quad (5.4)$$

where σ^e is the *Ericksen stress* (3.100), \mathbf{h} is the molecular field (3.89), and

$$\dot{\mathbf{n}} = \frac{d\mathbf{n}}{dt} = \frac{\partial \mathbf{n}}{\partial t} + (\mathbf{v} \cdot \nabla) \mathbf{n} \quad (5.5)$$

is the *material derivative* of \mathbf{n} (change of \mathbf{n} per unit time as experienced by a moving molecule).

Adding the contributions from eqns (5.3) and (5.4) we arrive at

$$T \dot{S} = \int \{(\sigma_{\alpha\beta} - \sigma_{\alpha\beta}^e) \partial_\alpha v_\beta + \mathbf{h} \cdot \dot{\mathbf{n}}\} d^3 r + \text{surface terms.} \quad (5.6)$$

The difference σ' between the actual stress σ and the equilibrium stress σ^e will be called the *viscous stress*

$$\sigma'_{\alpha\beta} = \sigma_{\alpha\beta} - \sigma_{\alpha\beta}^e. \quad (5.7)$$

5.1.3.3 The antisymmetric part of the viscous stress

The tensor $\sigma'_{\alpha\beta}$ is not symmetric in general. To characterize the antisymmetric part, we shall introduce a vector Γ

$$\Gamma_z = -\sigma'_{xy} + \sigma'_{yx}, \quad \text{etc.} \quad (5.8)$$

Our first task now is to derive an explicit expression for Γ . Consider the integral

$$\dot{L} = \frac{d}{dt} \int d^3 r \mathbf{r} \times \rho \mathbf{v}. \quad (5.9)$$

This represents the rate of change of the angular momentum of the sample, i.e. the *total torque* applied to our liquid. In our case, \dot{L} contains the following contributions: (1) magnetic torques

$$\int d^3\mathbf{r} \mathbf{M} \times \mathbf{H} \quad (5.10)$$

where $\mathbf{M}(\mathbf{r})$ is the local magnetization in the nematic (see eqns (3.45) and (3.48)); (2) torques due to external stresses (σ) acting on the sample boundary

$$\int \mathbf{r} \times (d\mathbf{S} : \sigma) \quad (5.11)$$

where $d\mathbf{S}$ is the surface element vector (pointing outwards from the fluid) on the boundary, and $(d\mathbf{S} : \sigma)_x = dS_\beta \sigma_{\beta x}$; 3) torques on the director at the boundary. For equilibrium situations, these have been discussed in Chapter 3 (3.115), and are given by

$$\int \mathbf{n} \times (d\mathbf{S} : \pi) \quad (5.12)$$

where $\pi_{\alpha\beta}$ is defined in eqn (3.90). Here we have chosen to discuss ‘strong anchoring’ situations for which there are no specific losses at the surface. Then eqn (5.12) for the surface torques remains true even out of equilibrium.

Collecting the contributions from eqns (5.10)–(5.12) we arrive at

$$\frac{d}{dt} \int (\mathbf{r} \times \rho \mathbf{v}) d^3\mathbf{r} = \int (\mathbf{M} \times \mathbf{H}) d^3\mathbf{r} + \int \{\mathbf{r} \times (d\mathbf{S} : \sigma) + \mathbf{n} \times (d\mathbf{S} : \pi)\}. \quad (5.13)$$

We now make use of eqn (5.2) to transform the left-hand side of eqn (5.13), and integrate the result by parts, to obtain

$$\int (\sigma_{yx} - \sigma_{xy}) d^3\mathbf{r} = \int (\mathbf{M} \times \mathbf{H})_z d^3\mathbf{r} + \int \{\mathbf{n} \times (d\mathbf{S} : \pi)\}_z. \quad (5.14)$$

On the left-hand side of (5.14) we write $\sigma = \sigma^e + \sigma'$. The contribution from σ' is simply Γ_z . The contribution from σ^e has already been calculated in eqn (3.11)†

$$\int (\sigma_{yx}^e - \sigma_{xy}^e) d^3\mathbf{r} = \int \{\mathbf{M} \times \mathbf{H} - \mathbf{n} \times \mathbf{h}\}_z d^3\mathbf{r} + \int \{\mathbf{n} \times (d\mathbf{S} : \pi)\}_z. \quad (5.15)$$

Inserting these results into eqn (5.14) we see that the magnetic term and the π term drop out, leaving us with

$$\int \{\Gamma - \mathbf{n} \times \mathbf{h}\} d^3\mathbf{r} = 0. \quad (5.16)$$

† Equation (3.110) is written in terms of another tensor σ^d , but σ^d and σ^e have the same antisymmetric part (see eqn (100)).

Thus we conclude that

$$\Gamma = \mathbf{n} \times \mathbf{h}. \quad (5.17)$$

Physically we may say that Γ is the torque (per unit volume) exerted by the internal degree of freedom (\mathbf{n}) on the flow. This torque is non-zero only out of equilibrium, since we know from Chapter 3 that \mathbf{n} is collinear to \mathbf{h} at equilibrium. The lack of symmetry of the tensor σ' (5.8) simply reflects the presence of these bulk torques.

5.1.3.4 Final formula for the entropy source

Let us now return to eqn (5.6) giving the dissipation; it is convenient at this stage to separate the velocity gradient tensor $\partial_\alpha v_\beta$ into a symmetric part

$$A_{\alpha\beta} = \frac{1}{2}(\partial_\alpha v_\beta + \partial_\beta v_\alpha) \quad (5.18)$$

and an antisymmetric part, associated with the vector

$$\boldsymbol{\omega} = \frac{1}{2} \operatorname{curl} \mathbf{v}. \quad (5.19)$$

Similarly we shall call σ^s the symmetric part of σ' . Making use of these definitions, and of eqn (5.8) for \mathbf{F} , we can transform eqn (5.6) and obtain

$$T\dot{S} = \int \{\mathbf{A} : \sigma^s - \Gamma \cdot \boldsymbol{\omega} + \mathbf{h} \cdot \dot{\mathbf{n}}\} d^3r \quad (5.20)$$

We now substitute $\Gamma = \mathbf{n} \times \mathbf{h}$ (eqn (5.17)) into this result, and arrive at

$$T\dot{S} = \int \{\mathbf{A} : \sigma^s + \mathbf{h} \cdot \mathbf{N}\} d^3r \quad (5.21)$$

where

$$\mathbf{N} = \dot{\mathbf{n}} - \boldsymbol{\omega} \times \mathbf{n}. \quad (5.22)$$

The vector \mathbf{N} represents the rate of change of the director with respect to the background fluid. Equation (5.21) is the fundamental equation of 'nematodynamics'. It displays the two types of dissipation that we announced at the beginning of this section: dissipation by shear flow and dissipation by rotation of the optical axis.

It is also interesting to note that the entropy source vanishes for rigid rotations, i.e. if both the molecules and the director rotate around a certain axis, at the same angular velocity, we have $A_{\alpha\beta} = 0$, and $N_\alpha = 0$, and thus, by eqn (5.21), $T\dot{S} = 0$. This property is sometimes considered as obvious, and then used as a starting point to derive (5.21). The more detailed (and painful) derivation that was used here is essentially based on eqn (5.15). As explained in Chapter 3 this equation simply expresses that the distortion free energy F_d is a scalar (a function of $\operatorname{div} \mathbf{n}$, of $\mathbf{n} \cdot \operatorname{curl} \mathbf{n}$, and of $(\mathbf{n} \times \operatorname{curl} \mathbf{n})^2$): thus the physical content is the same in both directions.

5.1.4 The laws of friction

5.1.4.1 Definitions of fluxes and forces

It is customary, when dealing with irreversible processes, to write each contribution to the entropy source as the product of a ‘flux’ by the conjugate ‘force’. (For a general introduction to these notions, we again refer the reader to the book by de Groot and Mazur [7].) Here the entropy source is given by eqn (5.21). We choose to take as fluxes the components of the symmetric tensor $A_{\alpha\beta}$ and the components of the vector N_μ .[†] The tensor \mathbf{A} has six independent components, and the vector \mathbf{N} has three components.[‡] According to eqn (5.21) we may then say that:

$$\begin{aligned}\sigma_{xx}^s &\text{ is the force conjugate to } A_{xx} \\ 2\sigma_{xy}^s &\text{ is the force conjugate to } A_{xy} \text{ etc.} \\ h_\alpha &\text{ is the force conjugate to } N_\alpha\end{aligned}\quad (5.23)$$

The factor of 2 occurring in the non-diagonal elements expresses the fact that the term such as $\sigma_{xy}^s A_{xy}$ appears twice in the entropy source (5.21).

5.1.4.2 The friction coefficients

We may now proceed to write down a set of phenomenological equations expressing the forces in terms of the flux (or vice versa). At this stage we assume that the fluxes are *weak on the molecular scale*—for instance that the rotation velocities described by \mathbf{N} are very small in comparison with the rotation frequencies characteristic of one molecule. This limit of slow motions is required for all hydrodynamic theories.

In the limit of weak fluxes, the forces will be linear functions of the fluxes; we write this in the form

$$\sigma_{\alpha\beta}^s = L_{\alpha\beta\gamma\delta} A_{\gamma\delta} + M_{\alpha\beta\gamma} N_\gamma, \quad (5.24)$$

$$h_\gamma = M'_{\alpha\beta\gamma} A_{\alpha\beta} + P_{\gamma\delta} N_\delta. \quad (5.25)$$

All the coefficients L, M, M', P have the dimension of a viscosity, namely mass \times length $^{-1}$ \times time $^{-1}$; to see this, it is enough to note that σ and \mathbf{h} have the dimensions energy per unit volume, while \mathbf{A} and \mathbf{N} have the dimensions of frequency.

For the diamagnetic materials of interest, the influence of the magnetic field \mathbf{H} on the friction constants is completely negligible; this observation simplifies the situation considerably.

Another simplification is provided by the Onsager theorem [7], which

[†] With this choice, all the fluxes are odd under time reversal, while all forces are even.

[‡] The components of \mathbf{N} are linked by one relation ($N_\mu n_\mu = 0$). However, a linear dependence between fluxes does not invalidate the Onsager relations. See de Groot and Mazur (reference 7, Section 6.3.)

asserts that the matrices M and M' are identical

$$M_{\alpha\beta\gamma} = M'_{\alpha\beta\gamma}. \quad (5.26)$$

To check that the factors of two occurring in the definition (5.23) of the forces are correctly included in eqn (5.26), the reader may consider, for instance, the coefficient of N_γ in the expression (derived from eqn (5.24)) for the force $2\sigma_{xy}^s$; this is equal to $2M_{xy\gamma}$. Now the coefficient of A_{xy} , in eqn (5.25) for h_y , is $2M'_{xy\gamma}$. These two coefficients must be equal by Onsager's theorem; the result is in agreement with (5.26).

Finally, the structure of the matrices, L, M, P must be compatible with the local symmetry ($D_{\infty h}$) of the nematic. Thus the only vector that may appear in the definition of L, M, P is the local director \mathbf{n} . Also, as we have repeatedly pointed out, all measurable properties must be invariant when we change \mathbf{n} into $-\mathbf{n}$. In such a change \mathbf{A} and $\boldsymbol{\sigma}^s$ are invariant, while \mathbf{N} and \mathbf{h} are odd. The most general structure for eqns (5.25) and (5.26) compatible with these requirements is

$$\begin{aligned} \sigma_{\alpha\beta}^s &= \rho_1 \delta_{\alpha\beta} A_{\mu\mu} + \rho_2 n_\alpha n_\beta A_{\mu\mu} + \rho_3 \gamma_{\alpha\beta} n_\gamma n_\mu A_{\gamma\mu} + \alpha_1 n_\alpha n_\beta n_\mu n_\rho A_{\mu\rho} \\ &\quad + \alpha_4 A_{\alpha\beta} + \frac{1}{2}(\alpha_5 + \alpha_6)(n_\alpha A_{\mu\beta} + n_\beta A_{\mu\alpha})n_\mu + \frac{1}{2}\gamma_2(n_\alpha N_\beta + n_\beta N_\alpha), \end{aligned} \quad (5.27)$$

$$h_\mu = \gamma'_2 n_\alpha A_{\alpha\mu} + \gamma_1 N_\mu. \quad (5.28)$$

Again all the coefficients ($\rho'_s, \alpha'_s, \gamma'_s$) have the dimension of a viscosity. The Onsager relation (5.26) imposes that

$$\gamma'_2 = \gamma_2. \quad (5.29)$$

Thus, in the general case, the equations of nematodynamics (eqns (5.27) and (5.28)) involve eight independent coefficients. However, for the majority of the experiments, one is concerned only with motions that are very slow in comparison with sound waves. It is then permissible to treat the fluid as *incompressible*: we shall now focus our attention on this case.

5.1.4.3 Incompressible nematics: the Leslie presentation

If the density of the fluid is constant, the trace of the A tensor vanishes

$$A_{\mu\mu} = \operatorname{div} \mathbf{v} = 0. \quad (5.30)$$

Thus the (ρ_1) and (ρ_2) terms in eqn (5.27) drop out. The term (ρ_3) does not contribute to the entropy source (5.21) because it reduces to three equal diagonal components; it can be lumped into the scalar pressure p and omitted from the equations (recall that, for an incompressible fluid, p is not given by an equation of state, but is an unknown, to be fixed at the end of the calculation by the condition of constant density).

For the current applications, where the starting point is the acceleration equation (eqn 5.2), it is convenient to transform eqn (5.27) into an equation for the complete viscous stress $\boldsymbol{\sigma}'$. The antisymmetric part of $\boldsymbol{\sigma}'$ is given

explicitly in terms of the molecular field \mathbf{h} by eqns (5.8) and (5.17). The field \mathbf{h} , in turn, is written in eqn (5.28). Collecting these results, one arrives at the equations

$$\begin{aligned}\sigma'_{\alpha\beta} &= \alpha_1 n_\alpha n_\beta n_\mu n_\rho A_{\mu\rho} + \alpha_4 A_{\alpha\beta} + \alpha_5 n_\alpha n_\mu A_{\mu\beta} \\ &\quad + \alpha_6 n_\beta n_\mu A_{\mu\alpha} + \alpha_2 n_\alpha N_\beta + \alpha_3 n_\beta N_\alpha,\end{aligned}\quad (5.31)$$

$$h_\mu = \gamma_1 N_\mu + \gamma_2 n_\alpha A_{\alpha\mu} \quad (5.32)$$

together with the relations

$$\gamma_1 = \alpha_3 - \alpha_2, \quad (5.33)$$

$$\gamma_2 = \alpha_2 + \alpha_3 = \alpha_6 - \alpha_5. \quad (5.34)$$

The coefficients α_i are usually called the *Leslie coefficients*: there are six α_i s, linked by one relation (5.34) (first derived by Parodi [3]). Thus the dynamics of an incompressible nematic involves *five independent coefficients*, all with the dimension of a viscosity. For the few examples where data are available at the present time—the five coefficients appear to be of comparable magnitude—typically in the range 10^{-2} to 10^{-1} poise. Values for MBBA are given in Table 5.1.

5.1.4.4 Another choice of fluxes and forces

In the preceding paragraphs, starting from the entropy source (5.21) we defined as fluxes the quantities $A_{\alpha\beta}$ and N_α (all of which are odd under time reversal), and as forces the quantities $\sigma_{\alpha\beta}^s$ and h_α (all of which are even under time reversal).

However, it is sometimes convenient to make a different choice, and to take $\sigma_{\alpha\beta}^s$ and N_α as fluxes, while $A_{\alpha\beta}$ and h_α are now the forces. This choice does lead to very compact formulae for the study of *small motions* in a nematic single crystal, which were introduced first by the Harvard group [4], and which we shall now write down.

Let us immediately restrict our attention to the problem of small amplitude motion. The unperturbed director \mathbf{n}_0 is taken along the z -axis. The perturbed director has small components $n_x(\mathbf{r})$, $n_y(\mathbf{r})$. We shall discuss the stresses only to first order in n_x and n_y . As already explained, the component of \mathbf{h} along \mathbf{n} may be chosen arbitrarily. For the present problem, we may then assume that h_z vanishes identically and write the entropy source as

$$T\dot{S} = \sigma_{\alpha\beta}^s A_{\alpha\beta} + h_x N_x + h_y N_y, \quad (5.35)$$

thus displaying explicitly the only independent components of \mathbf{h} and \mathbf{n} (h_x , h_y and N_x , N_y). Let us now write a set of linear relations given σ^s and N in terms of A and h : for an incompressible fluid, the most general form is

$$\begin{aligned}\sigma_{\alpha\beta}^s &= 2v_2 A_{\alpha\beta} + 2(v_3 - v_2)(A_{\alpha\mu} n_\mu^0 n_\beta^0 + A_{\beta\mu} n_\mu^0 n_\alpha^0) \\ &\quad + 2(v_1 + v_2 - 2v_3)n_\alpha^0 n_\beta^0 n_\mu A_{\mu\rho} n_\rho - \frac{1}{2}\lambda(n_\alpha^0 h_\beta + n_\beta^0 h_\alpha);\end{aligned}\quad (5.36)$$

$$N_i = h_i/\gamma_1 + \lambda A_{iz} \quad (i = x, y). \quad (5.37)$$

A number of comments are required to help the reader at this point.

The parameters v_1, v_2, v_3 have the dimensions of viscosity. Why they are chosen as the fundamental parameters in this version of the theory will become more apparent if we write down explicitly the components of σ^s

$$\begin{aligned}\sigma_{xx}^s &= 2v_2 A_{xx} \\ \sigma_{xy}^s &= 2v_2 A_{xy} \\ \sigma_{xz}^s &= 2v_3 A_{xz} - \frac{1}{2}\lambda h_x \\ \sigma_{zz}^s &= 2v_1 A_{zz} \\ \sigma_{yz}^s &= 2v_3 A_{yz} - \frac{1}{2}\lambda h_y.\end{aligned}\quad (5.38)$$

The parameter λ is a dimensionless number. For a system of fluxes, one group of which is odd under time reversal (namely \mathbf{A}) while the other (\mathbf{h}) is even, the Onsager relations demand that the crossed coefficients be *opposite* (see de Groot and Mazur [7]). This is why we have $(-\lambda)$ in eqn (5.36) while we have $(+\lambda)$ in eqn (5.37).

Equations (5.36) and (5.37) must be identical in content with equations (5.31) and (5.32) of the Leslie formulation. Comparing the two sets (and also making use of the identities (5.33) and (5.34)) we arrive at the relations

$$\begin{aligned}2v_2 &= \alpha_4 \\ 2v_3 &= \alpha_4 + \beta\end{aligned}\quad (5.39)$$

(where $\beta = \alpha_6 + \alpha_3\lambda = \alpha_5 + \alpha_2\lambda$).

$$2v_1 = \alpha_1 + \alpha_4 + \alpha_5 + \alpha_6,$$

and also

$$\lambda = -\gamma_2/\gamma_1. \quad (5.40)$$

The entropy source may be expressed in terms of the fluxes A and h in the form

$$T\dot{S} = 2v_1 A_{zz}^2 + 4v_2(A_{zx}^2 + A_{zy}^2) + 2v_3(A_{xx}^2 + A_{yy}^2) + (h_x^2 + h_y^2)/\gamma_1. \quad (5.41)$$

The dissipation does not involve λ : for this reason the parameter λ is classified as a 'reactive parameter' by the Harvard group [4]. The condition of increasing entropy ($T\dot{S} > 0$), (evaluated with the constraint $A_{xx} \equiv \operatorname{div} \mathbf{v} = 0$ for an incompressible fluid) imposes that v_1, v_2, v_3 , and γ_1 be positive.

Let us now discuss the equation giving the *bulk force* (per unit volume) in a nematic with distortions and flow. This is defined by eqn (5.2), namely

$$\rho \frac{dv_\beta}{dt} = \partial_\alpha \{\sigma_{\alpha\beta}^e + \sigma_{\alpha\beta}^s + \frac{1}{2}(n_\beta h_\alpha - n_\alpha h_\beta)\}. \quad (5.42)$$

Here σ^e is the Ericksen stress, and (as can be seen from eqn (3.100)) it is of second order in the deviations n_x, n_y : thus, in the small-motion approximation,

it drops out completely. σ^s is defined by eqn (5.36) or eqn (5.38). The last term in eqn (5.42) represents the antisymmetric part of σ' , as derived from eqns (5.8) and (5.17). In this term, to first order in n_x, n_y , we replace $n_\beta h_\alpha$ by $n_\beta^0 h_\alpha$, etc. Finally, we obtain for the bulk force

$$\rho \frac{dv_\beta}{dt} \cong \partial_\alpha \sigma_{\alpha\beta}^s + \frac{1}{2}(n_\beta^0 \partial_\alpha h_\alpha - n_\alpha^0 \partial_\alpha h_\beta). \quad (5.43)$$

As already pointed out at the beginning of this chapter, the stress tensor leading to this bulk force is not unique. The Harvard group has made use of this observation, and has constructed a *symmetric* stress tensor $\sigma_{\alpha\beta}^H$ which gives rise to the same set of bulk forces, provided that $H = 0$ (no external torques in the bulk). The Harvard stress σ^H is defined by

$$\sigma_{\alpha\beta}^H = \sigma_{\alpha\beta}^s + \frac{1}{2}\{-n_\mu^0 \partial_\mu \pi_{\alpha\beta} - n_\mu^0 \partial_\mu \pi_{\beta\alpha} + n_\alpha^0 \partial_\mu \pi_{\beta\mu} + n_\beta^0 \partial_\mu \pi_{\alpha\mu}\}. \quad (5.44)$$

The corresponding force is

$$\partial_\alpha \sigma_{\alpha\beta}^H = \partial_\alpha \sigma_{\alpha\beta}^s + \frac{1}{2}\{-n_\mu^0 \partial_\mu h_\beta - n_\mu^0 \partial_\mu \partial_\alpha \pi_{\beta\alpha} + n_\alpha^0 \partial_\alpha \partial_\mu \pi_{\beta\mu} + n_\beta^0 \partial_\mu h_\mu\} \quad (5.45)$$

where we have made use of the equation for the molecular field \mathbf{h} , which reduces here (for $H = 0$) to $h_\alpha = \partial_\mu \pi_{\mu\alpha}$.[†] The second and third terms in the bracket of eqn (5.45) cancel out, and (5.45) is seen to be identical to (5.43).

For many applications connected with small distortions of a nematic single crystal, the calculations are somewhat simpler when performed with the Harvard stress tensor—especially because the structure of σ^s is very simple. On the other hand the ELP approach gives a more detailed insight for the internal torques, etc.

5.1.4.5 Summary of equations and unknowns

Let us now summarize what are the unknowns, and what are the equations, for a study of motions in an incompressible nematic.

- *The unknowns:*

- (1) the velocity field $\mathbf{v}(\mathbf{r}, t)$;
- (2) the director $\mathbf{n}(\mathbf{r}, t)$;
- (3) the pressure $p(\mathbf{r}, t)$.

Since \mathbf{n} is a unit vector, it involves only two independent parameters. Thus the total number of unknown quantities is $3 + 2 + 1 = 6$.

- *The equations* (for definiteness we shall refer to the ELP presentation):

- (1) the acceleration equation (5.2) where the stresses are defined by eqn (3.100) for the reversible part σ^e , and by eqn (5.31) for the viscous part;

[†] h_α is defined by eqn (3.89). In this equation the term $\partial F_d / \partial n_\alpha$ is of second order n_x, n_y , and may thus be omitted here.

(2) the equations (5.32) giving the rate of change of the director in terms of the velocity gradients plus the molecular field \mathbf{h} . The latter is given explicitly in terms of the director by eqn (3.89). At first sight we have three equations (5.32), since they involve the components of a vector. However it must be recalled that the molecular field $\mathbf{h}(\mathbf{r}, t)$ is defined only within the transformation

$$\mathbf{h}(\mathbf{r}, t) \rightarrow \mathbf{h}(\mathbf{r}, t) + \lambda(\mathbf{r}, t)\mathbf{n}(\mathbf{r}, t)$$

since this transformation leaves the torque Γ (eqn (5.17)) unchanged and it is only Γ which is observable. Because of this freedom we obtain only two conditions from (5.32);

(3) the incompressibility condition (5.30).

We see that the number of equations is then $3 + 2 + 1 = 6$, just equal to the number of unknowns.

In principle we have an adequate tool for the study of macroscopic motions. In practice there are many difficulties.

1. The equations are quite complicated—their consequences have been explored only for very simple types of macroscopic flows, or for small deviations from a fully aligned state.
2. The description does not include disclination lines (or points). In practice the lines may play a significant role in certain dissipative flow properties. This implies that all hydrodynamic experiments devised to check the ELP equations are meaningful only if all disclinations are carefully eliminated from the sample, and from all upstream regions.

5.2 EXPERIMENTS MEASURING THE LESLIE COEFFICIENTS

A number of quantitative studies on the flow properties of nematics (with controlled boundary conditions and conditions for aligning fields) are now available. We list only those methods for which the interpretation is reasonably simple.

5.2.1 Laminar flow under a strong orienting field

In this type of experiment, the molecules are firmly aligned in one direction by a constant magnetic field \mathbf{H} .† The word ‘firmly’ corresponds to the following conditions.

† Alignment by an electric field \mathbf{E} may also be used (if the material has a positive dielectric anisotropy); however this method requires special care to avoid all possible electrohydrodynamic instabilities (see Section 5.3).

1. The lateral walls limiting the flow may tend to impose some preferred direction of alignment, different from the direction of \mathbf{H} . To avoid this, the diameter D of the flow must be much larger than the coherence length ξ defined in Chapter 3. Then the misalignments due to wall effects are confined to a small sheet of thickness ξ near the walls, and are thus negligible

$$\xi \ll D \quad \text{or} \quad H \gg \sqrt{\left(\frac{K}{\chi_a}\right) \frac{1}{D}}. \quad (5.46)$$

2. The flow itself tends to disrupt the alignment; in a velocity gradient A there will be, in general, a hydrodynamic torque acting on the molecules. It is given by eqns (5.17) and (5.32), and is of order γA (per cm³) where γ is some average of γ_1 and γ_2 . It must be balanced by the restoring torque due to the magnetic field, which is $\chi_a H^2 \sin \theta$, θ being the angle between \mathbf{n} and \mathbf{H} . (For a discussion of this torque, see Chapter 3, eqn (3.48)). Thus $\sin \theta \sim \gamma A / \chi_a H^2$. The alignment will be essentially unperturbed if $\theta \ll 1$, or

$$A \ll \chi_a H^2 / \gamma. \quad (5.47)$$

Let us now assume that the two conditions (5.46) and (5.47) are satisfied, and discuss the possible types of laminar flow. Depending on the relative orientation of the field \mathbf{H} , the velocity \mathbf{v} , and the velocity gradient, we find three typical geometries for *simple shear*. These possibilities are shown and listed under (a), (b), (c) in Fig. 5.1. The corresponding viscosities have been measured by Miesowicz, using a slowly moving plate to create the shear (Fig. 5.2) [8]. He studied *p*-azoxyanisole and found the following values at 122°C†

$$\begin{aligned} \eta_a &= 3.4 \times 10^{-2} \text{ poise}, \\ \eta_b &= 2.4 \times 10^{-2} \text{ poise}, \\ \eta_c &= 9.2 \times 10^{-2} \text{ poise}. \end{aligned}$$

How are the measured values of η_a , η_b , η_c related to the Leslie coefficients? To find this we return to eqn (5.31) giving the viscous stress in terms of the shear rate tensor $A_{\alpha\beta}$ and of the effective director velocity $\mathbf{N} = d\mathbf{n}/dt - (\boldsymbol{\omega} \times \mathbf{n})$. In the present cases $d\mathbf{n}/dt = 0$ along each flow line and $\boldsymbol{\omega} = \frac{1}{2} \operatorname{curl} \mathbf{v}$ is simply expressed in terms of the velocity gradient.

If β is the direction of \mathbf{v} , and α the direction of the velocity gradient, we must derive the viscous force along β per unit area in a plane normal to α . With our convention for ordering of indices (see eqn (5.2)), this force is given by the component $\sigma'_{\alpha\beta}$ of the stress tensor. When $\sigma'_{\alpha\beta}$ is known, we can derive

† The value of η_a is an extrapolation from data at different temperatures.

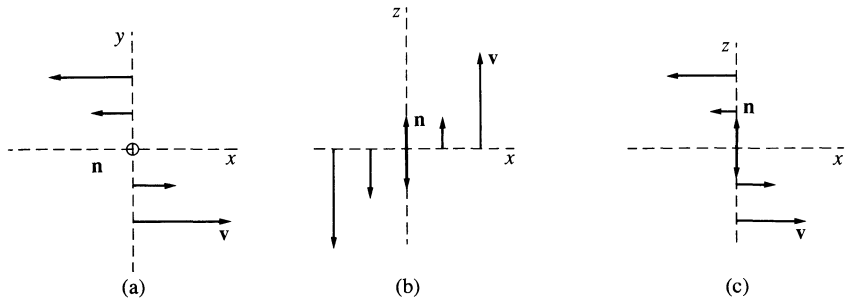


Fig. 5.1. The three fundamental geometries for viscosity measurements in a well aligned nematic (director \mathbf{n}).

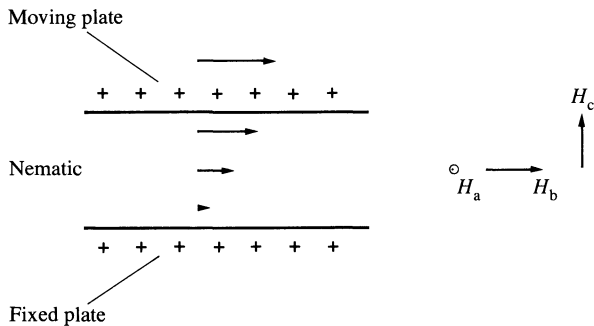


Fig. 5.2. Principle of the Miesowicz experiment. The field \mathbf{H} aligning the molecule is applied in one of the three fundamental directions a , b , and c . The moving plate oscillates at a very low frequency and viscosity is derived from the damping of the oscillations.

an effective viscosity η by using equation

$$\eta = \frac{\sigma'_{\alpha\beta}}{2A_{\alpha\beta}}. \quad (5.48)$$

Let us now consider explicitly the three cases in Fig. 5.1 and label the axes as shown. (The molecules and the field \mathbf{H} are always along the z -axis.) We get for these situations

$$(a) \quad A_{yx} = \frac{1}{2} \frac{\partial v}{\partial y} \quad \sigma'_{yx} = \alpha_4 A_{yx} \quad (5.49)$$

$$\eta_a = \frac{\sigma'_{yx}}{2A_{yx}} = \frac{1}{2}\alpha_4$$

$$(b) \quad A_{zx} = \frac{1}{2} \frac{\partial v}{\partial x}$$

$$N_x = -\omega_y = A_{xz} \quad (5.50)$$

$$\sigma'_{xz} = \alpha_3 N_x + (\alpha_4 + \alpha_6) A_{xz}$$

$$\eta_b = \frac{1}{2}(\alpha_2 + \alpha_4 + \alpha_6)$$

$$(c) \quad A_{zx} = \frac{1}{2} \frac{\partial v}{\partial z}$$

$$N_x = -\omega_y = -A_{zx} \quad (5.51)$$

$$\sigma_{zx} = \alpha_2 N_x + (\alpha_4 + \alpha_5) A_{zx}$$

$$\eta_c = \frac{1}{2}(-\alpha_2 + \alpha_4 + \alpha_5) = \eta_b - \gamma_2.$$

These may also be expressed in terms of the Harvard coefficients $(v_1, v_2, v_3, \gamma_1, \lambda)$ by a suitable application of eqns (5.39) and (5.40)

$$\begin{aligned} \eta_a &= v_2, \\ \eta_b &= v_3 + \frac{1}{4}\gamma_1(1 - \lambda)^2, \\ \eta_c &= \eta_b + \lambda\gamma_1. \end{aligned} \quad (5.52)$$

Thus, from measurements on simple shear flow we can extract three relations between the five friction coefficients.

Up to now, our discussion has been restricted to simple shear flows. The case of *Poiseuille flows* taking place between two horizontal planes under a horizontal pressure gradient is also of interest. The situation is represented in Fig. 5.3. The direction of flow is along y , the normal to the plates is z .

If the strong field \mathbf{H} is applied parallel to one of the three principal directions (x , y , or z) we again measure the set of Miesowicz viscosities. But a more remarkable effect occurs if the field is *oblique* [9]. Let us assume that \mathbf{H} (and the director \mathbf{n} which is aligned along \mathbf{H}) lies in the x , y -plane, at an angle ϕ from the flow lines. We apply a driving gradient $\partial p/\partial y$ along the flow lines but, if we probe the pressure (by a simple manometric technique) along the axis y , we find that to maintain the flow a *transverse pressure gradient* $\partial p/\partial x$ must be maintained. The ratio $\partial p/\partial x : \partial p/\partial y$ depends only on ϕ and is an odd function of ϕ , vanishing both for $\phi = 0$ and $\phi = \frac{1}{2}\pi$. As pointed out by Pieranski and Guyon [9], this effect is a simple consequence of the Leslie stress tensor. If, using eqn (5.31), we compute the viscous force in the flow field $v_y(z)$, we find

$$F_y = (\eta_a \sin^2 \phi + \eta_b \cos^2 \phi) \frac{ds}{dz} = \eta(\phi) \frac{ds}{dz},$$

$$F_x = (\eta_b - \eta_a) \sin \phi \cos \phi \frac{ds}{dz}$$

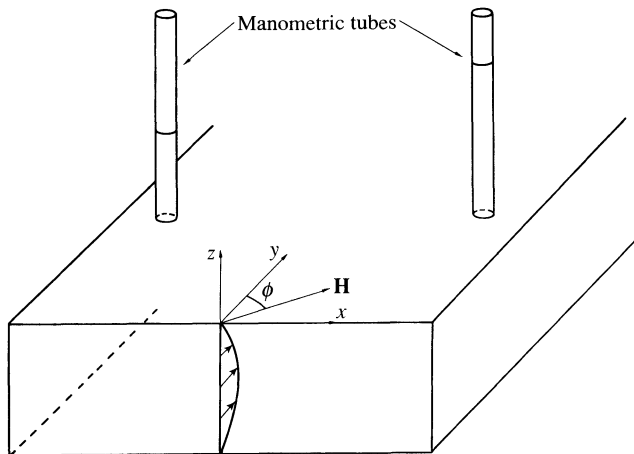


Fig. 5.3. Poiseuille flow under a strong oblique field (Pieranski Guyon). In this example the molecules tend to deflect the flow to the right. This effect is balanced by a *transverse pressure gradient*, the pressure being higher on the right-hand side ($x > 0$).

where $s = dv_y/dz$ is the local shear rate. The transverse force F_x has no counterpart in isotropic fluids. In steady state the forces F_x, F_y must be balanced by pressure gradients. Thus we must have

$$\frac{\partial p}{\partial x} : \frac{\partial p}{\partial y} = \frac{\eta_b - \eta_a}{\eta(\phi)} \sin \phi \cos \phi.$$

The experimental data on this ratio for MBBA fit very well with the values of η_a and η_b deduced from the measurements by Gahwiller (Table 5.1).

5.2.2 Attenuation of ultrasonic shear waves

This type of experiment has been set up recently for nematics by Candau and Martinoty [10a]. The principle is shown in Fig. 5.4. An ultrasonic shear wave (of frequency ω) propagates in a solid crystal, penetrates slightly into the nematic, and is reflected back; what is measured is a reflection coefficient. In reference 10a the incidence is oblique (for practical reasons). In the present analysis, to avoid some minor complications, we shall restrict our attention to normal incidence (Fig. 5.4(b)).

There is an apparent similarity between the set-up of Fig. 5.4(b) and the Miesowicz experiment (Fig. 5.2) where an oscillating plate was moved in the fluid. However, there are some crucial differences.

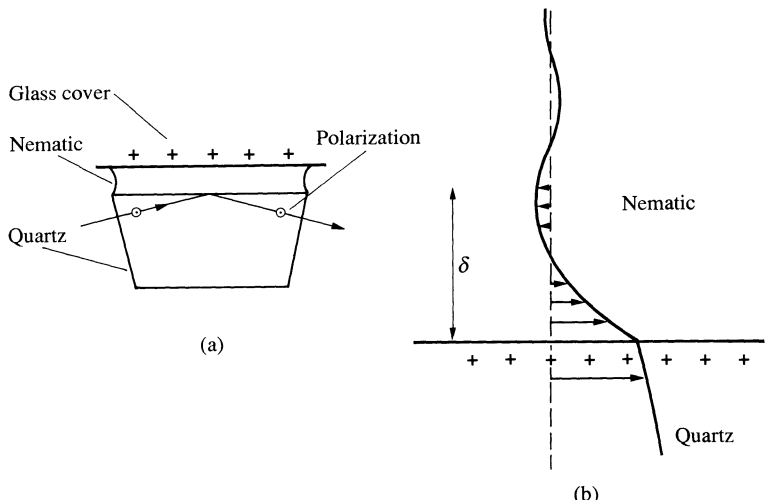


Fig. 5.4. The Candau–Martinoty experiments on shear wave attenuation in nematics: (a) set-up; (b) aspect of the wave penetration in the nematic. The penetration thickness δ is in the micron range.

1. *The frequency range.* In the high-frequency ultrasonic experiment shear is induced only in a very small thickness of the nematic, near the vibrating solid. For a conventional fluid of viscosity η and density ρ , this penetration thickness δ is known to be [11]

$$\delta = \left\{ \frac{\eta}{\rho \omega} \right\}^{\frac{1}{2}}. \quad (5.53)$$

As we shall see, this result remains correct for a nematic fluid, η being a certain combination of the Leslie coefficients. Typically, with $\rho = 1$, $\omega/2\pi = 10$, and $\eta = 0.1$ poise, we have $\delta = 4 \mu\text{m}$. On the other hand, in the Miesowicz experiment, the plate oscillates very slowly ($\omega \rightarrow 0$) the thickness δ is larger than the sample dimensions, and the velocity gradient is the same at all points in the nematic.

2. *The orienting agent.* In the Miesowicz experiment the molecules are aligned by a strong magnetic field \mathbf{H} . In the ultrasonic experiment, a preferred direction is defined by the boundary conditions at the crystal–nematic interface. (Three typical situations are displayed in Fig. 5.5.)

However, as we shall see, in spite of the directional effects of the wall, the ultrasonic shear does in general impose a non-negligible tilt angle to the optical axis. For this reason the effective viscosities derived from the ultrasonic experiment differ from the Miesowicz viscosities η_a , η_b , η_c .

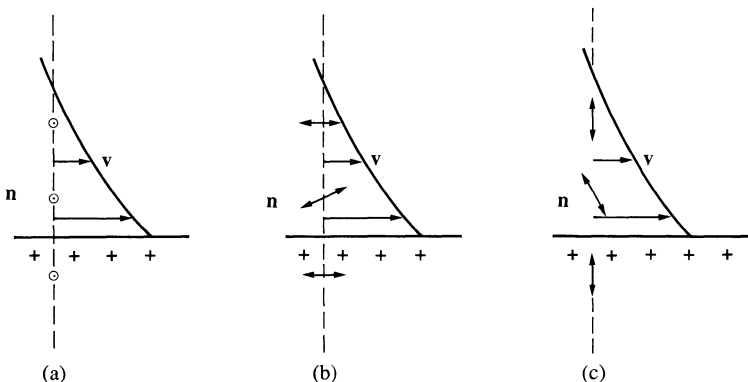


Fig. 5.5. The three fundamental geometries for acoustic measurements of shear viscosities. Note that in cases (b) and (c) the direction \mathbf{n} is significantly tilted by the flow.

Let us now show one example of how the effective ‘ultrasonic viscosities’ $\tilde{\eta}_a$, $\tilde{\eta}_b$, $\tilde{\eta}_c$ can be related to the friction coefficients. We shall not consider the case 1 (which is a very particular case with no tilt of the optical axis) but rather focus our attention on case 2, as being more illustrative. We call $0x$ the axis normal to the interface, and $0z$ the easy direction at the wall. The flow velocity $v(x)$ is also parallel to $0z$. The director \mathbf{n} is nearly parallel to $0z$, but is slightly tilted in the (x, z) plane ($n_z \sim 1$, $n_x \ll 1$, $n_y = 0$). The shear rate tensor $A_{\alpha\beta}$ has one non-vanishing component $A_{xz} = \frac{1}{2}\partial v/\partial x$ and the local rotation vector $\boldsymbol{\omega}$ reduces to $\omega_y = -\frac{1}{2}(\partial v/\partial x)$. We are interested in the component σ_{xz} of the strain, giving the force (along z) per unit area in the y, z -plane. This is given by Leslie’s equation (5.31) which may be written as

$$\sigma_{xz} = \eta_b \frac{\partial v}{\partial x} + \alpha_3 i \omega n_x. \quad (5.54)$$

The tilt of the director is derived from eqn (5.32), which reads

$$\gamma_1 i \omega n_x = h_x - \frac{1}{2}(\gamma_1 + \gamma_2) \frac{\partial v}{\partial x}. \quad (5.55)$$

By eqn (3.23) the molecular field h_x is of order $K \nabla^2 n_x \sim K n_x / \delta^2$ where δ is defined in eqn (5.53). Thus

$$\begin{aligned} h_x &\sim \frac{K \rho \omega}{\eta} n_x, \\ \frac{h_x}{\gamma_1 \omega n_x} &\sim \frac{K \rho}{\eta \gamma_1} \sim \frac{K \rho}{\eta^2} \end{aligned} \quad (5.56)$$

where we do not distinguish between γ_1 and the average viscosity η . The parameter

$$\mu = \frac{K\rho}{\eta^2} \quad (5.57)$$

is a dimensionless quantity that plays an important role in many dynamical problems connected with nematics.[†] In all known cases μ is small. Typically with $K = 10^{-6}$ dyn, $\rho = 1$ g cm⁻³, where $\eta = 10^{-2}$ poise, we have $\mu = 10^{-2}$. Higher values of η would make μ even smaller. The order-of-magnitude estimate (5.56) shows that h_s may be neglected in eqn (5.55). Inserting the resulting form for $i\omega n_x$ in eqn (5.54) we arrive at $\sigma_{xz} = \tilde{\eta}_b(\partial v/\partial x)$ where the effective viscosity $\tilde{\eta}_b$ is given by

$$\tilde{\eta}_b = \eta_b - \alpha_3 \frac{\gamma_1 + \gamma_2}{2\gamma_1}. \quad (5.58)$$

The main interest of this derivation based on the Leslie approach is to show explicitly that there is a tilt in the optical axis ($n_x \neq 0$). On the other hand, if one is interested only in the final result (5.58), one may reach it more concisely through the Harvard formulation; using eqn (5.38) we have

$$\sigma_{xz}^s = 2v_3 A_{xz} - \frac{\lambda}{2} h_x.$$

As shown above, h_x is negligible. The differences between the complete Harvard tensor σ^H (eqn 5.44)) and σ^s are also of order h , and may be omitted. Thus one arrives at

$$\tilde{\eta}_b = v_3, \quad (5.58')$$

which is in fact identical to (5.58), but much simpler in notation. Repeating this argument for the three cases (a), (b), (c) one obtains

$$\begin{aligned} \tilde{\eta}_a &= \eta_a = v_2, \\ \tilde{\eta}_b &= \tilde{\eta}_c = v_3. \end{aligned} \quad (5.59)$$

The equality between $\tilde{\eta}_b$ and $\tilde{\eta}_c$ was noticed first by A. Rapini by careful scrutiny of the equations (such as (5.58)) in the Leslie formulation that had been derived by Candau and Martinoty [10].[‡] In the Harvard formulation the equality is obvious (as first pointed out by P. Martin): clearly this formulation is more suitable for the ultrasonic problem, since the variables

[†] μ may be interpreted as the ratio of two diffusion constants: $\mu = D_n/D_v$, where D_v describes the diffusion of the vorticity, well known for isotropic fluids $D_v = \eta/\rho$. The other constant D_n describes the diffusion of orientation, and is given by $D_n = K/\eta$. This formula for D_n will be justified later (eqns (5.70)–(5.72))

[‡] The experts in classical mechanics (Ericksen, Truesdell, etc.) consider that the use of the Onsager relations in hydrodynamics requires special caution. The Rapini equality, which does depend on the validity of these relations, provides a direct experimental check on this point.

are **A** and **h**, and h may be neglected. On the other hand, in the Miesowicz problem, the Leslie choice of variables (**A** and **n**) is more suitable, because **n** is fixed by the magnetic field.

Finally, it may be shown that, for all relevant mechanical parameters (acoustic impedances, wave reflection coefficients, etc.) the nematic should behave exactly like an ordinary fluid of viscosity $\tilde{\eta}_a$ (or $\tilde{\eta}_b$ or $\tilde{\eta}_c$) depending on the geometrical conditions. A careful reader may find this simple result somewhat surprising—his point being that the tilt $n_x(x)$ derived from eqn (5.55), with $h_x \approx 0$, does not satisfy the correct boundary condition for strong anchoring ($n_x(0) = 0$). However, this defect is not serious when μ (as defined by eqn (5.57)) is small. One can show that there is a thin layer (thickness $\mu^{\frac{1}{2}}\delta$) near the crystal surface, where h_x cannot be neglected and where n_x adjusts to the boundary condition. But this layer is so thin that it plays a negligible role in the mechanical properties of the fluid.

Measurements of the reflected intensity at the interface between quartz and MBBA have been undertaken by Candau and Martinoty [10a] for the geometries (a) and (b). It is very much to be hoped that case (c) will also be feasible, and that the Rapini equality ($\tilde{\eta}_b = \tilde{\eta}_c$) will be compared to experimental data.

At first sight, one might also be tempted to repeat the ultrasonic experiments under a strong magnetic field **H**, parallel to the easy axis on the walls; then the tilt of the optical axis would be negligible and the effective viscosities would be given by the Miesowicz set η_a, η_b, η_c . However, this is not feasible in practice. To understand why, let us consider for instance case (b) and insert a magnetic contribution into eqn (5.55). In the limit of small μ we now have

$$\left(i\omega + \frac{\chi_a H^2}{\gamma_1}\right) n_x = -\frac{\gamma_1 + \gamma_2}{2\gamma_1} \frac{\partial v}{\partial x}.$$

To reduce n_x significantly we should achieve $\chi_a H^2 / \gamma_1 > \omega$ or $H > (\gamma_1 \omega / \chi_a)^{\frac{1}{2}}$. Taking $\gamma_1 = 0.1$ poise, $\frac{1}{2}\omega/\pi = 10^7$, and $\chi_a = 10^{-7}$ cgs units, this would correspond to fields of order 10^8 gauss!

Another method for generating shear waves in nematics is based on the capillary waves which propagate at a nematic-air interface. These waves could be generated by mechanical means. In practice, it is convenient to observe the spontaneous thermal fluctuations of the surface by inelastic light scattering [10b].

At first sight, one might expect two types of novel effects to be connected with these waves in nematics.

- When the surface undulates (with a certain wave vector **q**) the molecular arrangement below it is distorted (within a thickness $\sim q^{-1}$). Thus the effective surface tension \tilde{A} might be modified. In fact, we have qualitatively

$$\tilde{A} - A = Kq^2 \frac{1}{q} = Kq$$

where A is the natural surface tension and K is a Frank constant. The relative shift $(\bar{A} - A)/A$ is then very small (of order qa) for the long wavelengths ($\gtrsim 10 \mu\text{m}$) of interest, and the effect is negligible.

2. The damping of the capillary waves depends on the Leslie coefficients; in particular, for tangential (or conical) boundary conditions at the interface, the damping depends on the angle between the direction of wave propagation (\mathbf{q}) and the nematic axis (\mathbf{n}).

These friction effects have been studied with great care, on MBBA, by the Kastler group [10b]. They do give certain combinations of the Leslie coefficients (see Table 5.1).

5.2.3 Laminar flow in the absence of external fields

With conventional isotropic fluids, studies on laminar flow in a capillary, or between rotating cylinders ('Couette flow') represent the most direct means of measuring the viscosity. In nematics, measurements of this type have also been carried out, mainly by Porter, Johnson, and co-workers [12]. However, as already mentioned in the introduction to this chapter, the interpretation of these early experiments is delicate for the following reasons.

1. The boundary conditions at the walls were not controlled.
2. The possible role of disclination lines was not ascertained.

More precise experiments were carried out by Fisher and Wahl [13a, b] in a situation of simple shear flow between two parallel plates, with homeotropic boundary conditions on both plates. What is measured in these experiments is **not** a mechanical property. Rather, by optical methods, one probes the distortions of the molecular alignment due to the flow. The aspect of these distortions depends critically on the parameter $\lambda = -\gamma_2/\gamma_1$.

1. If $|\lambda| > 1$ there is a certain critical angle θ between \mathbf{n} and \mathbf{v} (defined by $\cos 2\theta = 1/\lambda$) for which the hydrodynamic torque Γ (given by eqns (5.17) and (5.32)) vanishes. Then, far from the walls, the molecules tend to lie precisely at this angle. In the vicinity of the walls, since the molecules must adjust to a prescribed boundary condition, their orientation changes progressively; this takes place in a certain 'transition layer' of thickness $e \sim \{K/\eta s\}^{\frac{1}{2}}$, K being an elastic constant, η an average viscosity, and s the shear rate. This behaviour is shown on Fig. 5.6(a) for simple shear flow. The slightly more complicated case of laminar flow between two fixed walls is displayed in Fig. 5.6(b).
2. If $|\lambda| < 1$ the hydrodynamic torque Γ is non-zero for all orientations of the molecules.[†] This implies that the nematic structure is very strongly

[†] This is true except for the configuration in Fig. 5.1(a), where the hydrodynamic torque vanishes for symmetric reasons.

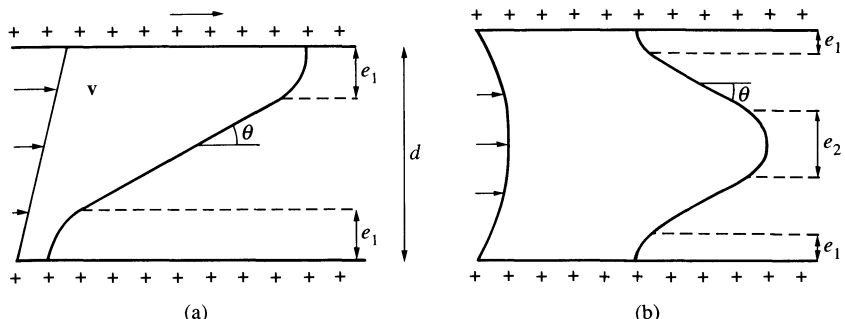


Fig. 5.6. Distortions induced in a nematic plate by laminar flows. Strong normal anchoring is assumed on both walls; $|\lambda| > 1$. (a) Simple shear flow: at high enough shear rates the nematic molecules tend to make a fixed angle θ with the flow lines except in the two boundary layers of thickness $e_1 \cong (K/\eta s)^{1/2}$. (b) Poiseuille flow: we now have two regions of alignment at the angle θ separated by an adjustment sheet of thickness $e_2 = d^{1/3}e_1^{2/3}$. The difference between e_2 and e_1 stems from the fact that the local shear $\partial v / \partial z$ is small in the central region.

deformed. For the simplest case of shear flow between two plates, the director, as seen by an observer moving from one plate to the other, rotated by many turns. However, this particular regime is often found to be unstable towards three-dimensional distortion.

In most nematics, $|\lambda|$ is slightly larger than unity; in a thick nematic sample, the molecules tend to become aligned along the direction of flow (θ close to 0). For instance, in MBBA at 22°C, Wahl and Fisher find [13]

$$\theta = 8^\circ, \quad |\lambda| = +1.04.$$

If $\theta \sim 0$, we are automatically in case (b) of Fig. 5.1. Provided that λ is close to 1, we expect that a bulk viscosity measurement in a thick capillary will give η_b as the effective viscosity: this has indeed been approximately verified in a few cases.

Detailed theoretical calculations on the distortions induced by flow are listed in reference 14a. As regards the mechanical properties, the most important consequence of these distortions is that the apparent viscosity η_{app} becomes a *function of the shear rate s*. Ericksen has shown, by a purely dimensional argument [14b] that

$$\frac{\eta_{app}(s)}{\eta_{app}(0)} = f\left(\frac{e_1}{d}\right) = f\left[\left(\frac{K}{\gamma_1 s}\right)^{1/2} \frac{1}{d}\right].$$

In this formula e_1 is the thickness of the boundary layer defined for instance in Fig. 5.6(a), and d is the flow diameter. The function f is dimensionless and depends only on:

- (1) the ratio between various Leslie coefficients, such as λ ;
- (2) the particular laminar flow under study.[†]

The Ericksen law holds for all (disclination free) laminar flows with strong anchoring boundary conditions and agrees very well with the existing data [14c]. To appreciate the importance of this law, it may be useful to compare it with the scaling law that holds for dilute polymer solutions

$$\frac{\eta(s)}{\eta(0)} = f(st)$$

where τ is the relaxation time of one macromolecule, and is independent of the flow size d .

Finally, it must be emphasized that all the preceding discussion was restricted to *stable flows*. In fact, inside the laminar domain (i.e. keeping the Reynolds number low) we do sometimes find remarkable instabilities due to coupling between orientation and flow. For instance, the simple shear flow of case (a) in Fig. 5.2 becomes unstable above a certain critical shear rate [15].

5.2.4 Variable external fields

It is possible to induce motions in a nematic fluid by suitable time-dependent external fields. The motions may concern the director (rotation of the optical axis) or the molecular centres of gravity (hydrodynamic flow) or both. The fields may be electric or magnetic. However, in most practical situations, the coupling between a nematic and an electric field involves very special charge transport processes. For this reason all electric effects will be discussed separately, later in this chapter (Section 5.3). For the moment we restrict our attention to the comparatively simpler case of a magnetic field $\mathbf{H}(t)$. We also assume that \mathbf{H} is spatially uniform. These restrictions still allow many possible set-ups, which can be interesting either for a determination of certain Leslie coefficients or to induce some remarkable magneto-optic effects. Here, we shall discuss briefly a few typical examples.

5.2.4.1 Oscillating fields

Consider for instance the nematic slab with one free surface shown in Fig. 5.7. At the bottom of the slab the molecules are strongly anchored (among the x direction) by a polished glass surface. Furthermore, a static field \mathbf{H}_0 may also be added in the same direction. At the free surface, the boundary condition is assumed to be tangential.

We apply to this system a small a.c. field \mathbf{H}_1 (of angular frequency ω) along the y -axis (i.e. in the plane of the slab, but normal to \mathbf{H}_0). The

[†] In Fig. 5.6(b) we find two characteristics lengths e_1 and e_2 . But their ratio is only a function of e_1/d and the scaling property is maintained.

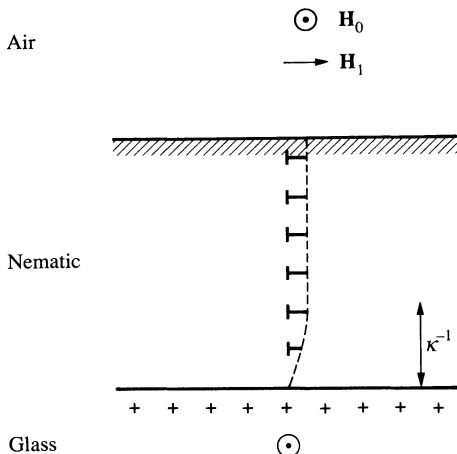


Fig. 5.7. A nematic droplet (with tangential boundary conditions) under a large static field \mathbf{H}_0 (normal to the sheet) plus a small oscillating field \mathbf{H} . We use here the Friedel-Kleman graphical notation to show tilted molecules: each ‘nail’ represents a molecule pointing partly out of the sheet, the tip of the nail being directed towards the observer.

molecules then assume a slightly twisted arrangement; at all points the director is still in the x, y -plane, but it makes a small angle $\phi(z, t)$ with the unperturbed direction (x). There are at least two methods for detecting the distortion ϕ .

1. *Magnetic detection.*† The magnetization density in the liquid crystal is given by eqn (3.45)

$$\mathbf{M} = \chi_{\perp} \mathbf{H} + \chi_a (\mathbf{H} \cdot \mathbf{n}) \mathbf{n},$$

where $\mathbf{H} = \mathbf{H}_0 + \mathbf{H}_1$. The transverse component of interest (modulated at the frequency ω) is

$$M_y = \chi_{\perp} \mathbf{H}_1 + \chi_a \mathbf{H}_0 \phi. \quad (4.50)$$

The two terms may be separated through their frequency dependence, since, as we shall see, the ϕ terms drops out at high frequencies. What is measured finally is the average of ϕ over the sample volume. Since M_y is a small (diamagnetic) response, it can be measured only on rather large samples.

2. *Optical detection.* A plane wave, moving vertically upwards, enters the nematic slab from below. The initial polarization is along $0x$. On distances

† This method was first described to the author in a private communication by Dr D. Johnson (Kent State University).

of order λ (the optical wavelength) the changes in twist angles ϕ are small; thus, inside the nematic slab, the polarization of the light wave follows adiabatically the direction of the optical axis. When the wave emerges at the free surface, its plane of polarization has been rotated by an angle $\phi(z_s)$ (z_s being the surface level). Thus in this method one probes the molecular rotation at the free surface.

From a theoretical point of view, this situation of oscillating twist is particularly simple; it can be shown from the Leslie equations (5.31) and (5.32) that there is no hydrodynamic flow ($v \equiv 0$). Then the torque equation—deduced from eqns (5.17) and (5.32)—reduces to

$$\Gamma_z = \gamma_1 \frac{\partial \phi}{\partial t} = K_2 \frac{\partial^2 \phi}{\partial z^2} + \chi_a H_0 (H_1 - H_0 \phi). \quad (5.61)$$

In eqn (5.61) we have retained only terms of first order in H_1 or ϕ . The boundary conditions to be imposed on ϕ are

$$\phi = 0 \text{ at the glass-nematic interface,} \quad (5.62)$$

$$\frac{\partial \phi}{\partial z} = 0 \text{ at the free surface.}$$

(The latter condition is a condition of zero surface torque.) Replacing $\partial/\partial t$ by $i\omega$ in eqn (5.61) and solving, one finds

$$\phi = \frac{H_1}{H_0} \frac{1}{1 + i\omega\theta} \left\{ 1 - \frac{\cosh(\kappa z)}{\cosh(\kappa d)} \right\}. \quad (5.63)$$

In eqn (5.63), θ is a characteristic time, defined by

$$\theta = \frac{\gamma_1}{\chi_a H_0^2}. \quad (5.64)$$

Typically with $\gamma_1 = 10^{-1}$ poise, $\chi_a = 10^{-7}$, and $H = 10^3$ gauss, $\theta \sim 10^{-2}$ s. The origin of ordinates (z) in eqn (5.63) has been taken at the free surface; d is the thickness of the nematic slab, and κ^{-1} is a (complex) length, defined by

$$\kappa^2 = \frac{\chi_a H_0^2 + i\omega\gamma_1}{K_2} = \frac{1}{\xi_2^2} (1 + i\omega\theta), \quad (5.65)$$

ξ_2 being the magnetic coherence length.

In practice the frequencies of interest are $\omega \sim 1/\theta$ and thus κ^{-1} is comparable to ξ .

For $\kappa d > 1$, eqn (5.63) shows that the response ϕ is essentially equal to

$$\phi_{\text{bulk}} = \frac{H_1}{H_0} \frac{1}{1 + i\omega\theta} \quad (5.66)$$

except for a thin layer of thickness κ^{-1} near the anchored wall. Using eqn (5.66) and measuring the amplitude and phase angle of the response ϕ at various frequencies ω , one can determine θ . Finally, if the anisotropy of the susceptibility χ_a is known, one can derive the friction constant γ_1 through eqn (5.64).

Similar considerations should apply to more complicated geometries; if we have a large sample, subjected to a static field H_0 plus a crossed oscillating field H_1 , we expect to measure in the bulk a tilt of the optical axis which is still given by eqn (5.66). Again, we should find no hydrodynamic flow (except possibly in a thin sheet near the outer surface of the sample) for the following general reason: in a region where the field \mathbf{H} and the magnetization \mathbf{M} are both spatially uniform, there is no bulk magnetic force tending to induce a flow. Thus we can have driving forces only near the sample surface. But, at finite frequencies ω , such forces will induce flow only in a thin shell below the surface (see eqn (5.53)).

5.2.4.2 Rotating fields

Early experiments on the torque received by a nematic sample subjected to a large, rotating, magnetic field were carried out by Tsvetkov [16]. But it has progressively become clear that the effects of the walls of the container may be quite complex in a situation of this kind. Let us illustrate this by returning to the nematic slab of Fig. 5.6 with one anchored surface and one free surface. Instead of the fields $H_0 + H_1$, we now apply a rotating field in the plane of the slab†

$$H_x = H \cos \omega t,$$

$$H_y = H \sin \omega t.$$

If ω is low ($\omega\theta \ll 1$, where θ is always defined by eqn (5.64)) and if the slab thickness d is much larger than the magnetic coherence length ξ , the molecules in the bulk of the sample would like to rotate essentially in phase with H . However, this cannot give a steady-state regime; because the molecules at the glass surface are anchored, it would in fact correspond to a twist between both surfaces which would increase linearly with time.

The nematic must invent a process to relax the twist. There are many ways for it to do this; we shall quote two of them.

1. Relaxation of twist by *disclination loops*. This is probably the most common procedure. The loop separates a region of low twist from a region of higher twist, and expands.

How is the loop created? As explained in Chapter 4, nucleation of a loop in the bulk is difficult. In practice, it is observed to take place on a

† Experimentally, it may sometimes be more convenient to rotate the sample in a fixed field. Both situations are equivalent.

'source' (a speck of dust, or some irregularity on the glass surface). The loop then grows and detaches from the source.

2. Relaxation of twist by *emission of 180° walls*. The walls are emitted by the glass surface, and move towards the free surface.† This process has been observed in flat samples, where disclination loops cannot nucleate easily [17].

These two examples lead us to think that the dissipation measured in the Tsvetkov experiment [16] may be influenced by the nucleation, migration, and annihilation of orientational defects in the nematic structure—lines or walls. The experiment is thus meaningful only if the anchoring conditions at the interfaces and the type of defect involved, are well under control.

However, in a *bulk* sample at low ω the boundary effects are found experimentally to be rather unimportant: this probably means that process 1 is dominant and that the fraction of the sample volume where the orientation is perturbed by the lines is small.

In this regime, the optical axis rotates and follows the field \mathbf{H} with a certain phase lag ϕ . The value of ϕ is such that the friction torque and the magnetic torque $\frac{1}{2}\chi_a H^2 \sin 2\phi$ balance. It may be shown that there is no hydrodynamic flow ($v \equiv 0$) and thus the friction torque reduces to $\gamma_1 \omega$. The equation

$$\gamma_1 \omega = \frac{1}{2} \chi_a H^2 \sin 2\phi$$

has solutions ϕ provided that $\omega\theta < \frac{1}{2}$. Measuring the mechanical torque, on the sample, and knowing ω , one derives γ_1 : this Tsvetkov method has been revived recently [13d, 16b, 18]. Another approach has been used by Luckhurst and co-workers [16c]; they probe the angle ϕ by an ESR technique.

Finally we should discuss the case of higher frequencies ($\omega\theta > \frac{1}{2}$). If one again neglects all boundary effects, one finds theoretically that the director should still rotate (although not with constant speed). The average rotation velocity $\bar{\omega}$ is then smaller than ω . However, in this regime it is more difficult to obtain reproducible data; the role of the boundaries is probably more important.

An experiment under rotating fields, but with *controlled* boundary conditions has been performed recently by Brochard, Léger, and Meyer [19]. Here the sample is prepared in a homeotropic texture between two flat plates and the field rotates in the plane of the plates. With this particular set-up, a steady state can be achieved *without* nucleation of any defects. The molecular distortions are followed by optical means. Depending on the magnitude of the field \mathbf{H} , and on the rotation frequency ω , three distinct regions are found:

† If, instead of a sample of thickness d with one free surface, we had a sample of thickness $2d$ between two polished glass surfaces, the process would be very similar; walls (of opposite twist) would be emitted by both glass surfaces, then migrate towards the centre and annihilate by pairs.

- (1) homeotropic;
- (2) synchronous—here the molecular pattern is inclined towards the field directions (except for a certain phase lag); the pattern rotates at the same frequency ω ;
- (3) asynchronous—here the phase lag varies with time, and the pattern rotates with an average velocity smaller than ω .

This experiment gives much more information than the original Tsvetkov set-up. It requires only a small mass of the nematic. It is also interesting to observe the defects that can nucleate accidentally in the system, particularly near the border of the synchronous and asynchronous regimes. Finally, the fluctuations in the alignment for fields just below the limit of region (1) are remarkable: thus the method may be of wide interest in the future.

5.2.4.3 Pulsed fields

Measurements on a physical system using pulsed fields or oscillating fields are usually equivalent in content, provided that the physical system under study responds linearly to the applied field. On the other hand, the two approaches become non-equivalent, if the response is strongly non-linear. For liquid crystals, this will occur in the vicinity of a phase transition induced by the field, the typical case for nematics being the Frederiks transition between two orienting glass plates (see Chapter 3). For each of the three typical ‘Frederiks geometries’ (listed as 1, 2, 3 in Fig. 3.13) there is a well-defined critical field H_c . Two simple ways of conducting the experiment are then the following: to raise the field abruptly from 0 to a certain value H_0 (larger than H_c) and study the subsequent distortions in the nematic; or to decrease the field from H_0 to 0, starting from an equilibrium distorted state in the field H_0 , and following its relaxation towards the unperturbed state.

The instantaneous state of distortion may be monitored by optical methods, or by various types of transport studies. For instance, we mentioned thermal conductance measurements as a probe of static distortions. It turns out that they also provide an adequate means of following the dynamics of the Frederiks transition for the following reasons. Thermal lags in the thermocouples can be made very small by using evaporated metallic films, and the intrinsic time lags associated with heat transport in the nematic film are of order $d^2/\pi^2 D_t$, where d is the thickness and D_t is the thermal diffusivity (the ratio thermal conductance: specific heat). On the other hand, as we shall see, the time constants associated with the orientational effects of interest are of order $d^2\eta/\pi^2 K$ where η is an average viscosity and K a Frank elastic constant. The thermal diffusivity D_t turns out to be at least 10 times larger than the orientational diffusivity K/η : thus thermal lags are negligible. Dynamical experiments of this type have been carried out recently by Guyon and Pieranski, and interpreted theoretically by F. Brochard and co-workers [20].

To explain the main dynamical features, we shall restrict our attention here to the Frederiks transition of type 2, involving pure twist (see Fig. 3.13). This case is, in fact, not suitable for transport measurements across the slab, but it is pedagogically convenient because (as already mentioned) there is no hydrodynamic flow: the molecules rotate without any translational motion, and this simplifies considerably the analysis based on the Leslie equations. We shall also assume that the maximum field H_0 is only slightly larger than the critical field H_c . Then, as explained in Fig. 3.14, the tilt angle ϕ of the molecules is small, and its value at equilibrium $\phi_0(z)$ is, to a good approximation, given by a simple sine wave

$$\phi_0(z) = a_0 \sin\left(\frac{\pi z}{d}\right) \quad (5.67)$$

(where the glass surfaces are located at $z = 0$ and $z = d$). The amplitude a_0 may be derived from a variational calculation, and is given by

$$a_0 \cong 2 \left\{ \frac{H_0 - H_c}{H_c} \right\}^{\frac{1}{2}}. \quad (5.68)$$

The dynamical equation for $\phi(z, t)$ (deduced from eqns (5.17) and (5.32) with $v \equiv 0$) has the form

$$\Gamma_z = \gamma_1 \frac{\partial \phi}{\partial t} = K_2 \frac{\partial^2 \phi}{\partial z^2} + \chi_a H^2 \sin \phi \cos \phi \quad (5.69)$$

together with the boundary conditions $\phi(0) = \phi(d) = 0$.

Let us consider first the case where H is decreased abruptly from H_0 to 0 at time $t = 0$. Equation (5.69) then reduces to

$$\gamma_1 \frac{\partial \phi}{\partial t} = K_2 \frac{\partial^2 \phi}{\partial z^2}, \quad (5.70)$$

and the solution—coinciding with $\phi_0(z)$ at $t = 0$ —is

$$\phi(z, t) = \phi_0(z) e^{-t/\theta}, \quad (5.71)$$

with a relaxation time

$$\theta = \frac{\gamma_1 d^2}{\pi^2 K_2}. \quad (5.72)$$

With $d = 10 \mu\text{m}$, $\gamma_1 = 10^{-1}$ poise, $K_2 = 10^{-6}$ dyn, we have $\theta = 10^{-2}$ s. Equation (5.72) is quite typical of nematic relaxation processes in zero field, which are very important for many technical applications of nematics.

Let us now turn to the case where H is abruptly increased (from 0 to H_0) at time $t = 0$. Since, even in the final state described by eqn (5.67), ϕ will still be small, we may expand the dynamical eqn (5.69) in powers of ϕ .

However, to reach the correct equilibrium condition at large times, we must include non-linear terms up to order ϕ^3 . This leads to

$$\gamma_1 \frac{\partial \phi}{\partial t} = K_2 \frac{\partial^2 \phi}{\partial z^2} + \chi_a H_0^2 \phi (1 - \frac{2}{3} \phi^2) + \dots \quad (5.73)$$

To a first approximation $\phi(zt)$ is always a simple sine wave in z

$$\phi(z, t) = a_0 u(t) \sin\left(\frac{\pi z}{d}\right) \quad (5.74)$$

where $u(0)$ and $u(\infty) = 1$. Multiplying both sides in eqn (5.73) by $\sin(\pi z/d)$ and integrating over the thickness d , one arrives at

$$\theta' \frac{du}{dt} = u - u^3 \quad (5.75)$$

with

$$\theta' \cong \frac{H_c}{2(H_0 - H_c)} (\gg 0).$$

Equation (5.75) is readily integrated to give

$$\begin{aligned} u(t) &= m(t) \{1 + m^2(t)\}^{-\frac{1}{2}}, \\ m(t) &= \text{const.} \times \exp(t/\theta'). \end{aligned} \quad (5.76)$$

Equation (5.76) describes first the exponential growth of a small fluctuation (regime $m \ll 1$)—followed by saturation (regime $m \gg 1$, $u \rightarrow 1 - \frac{1}{2}m^{-2}$). The time constant for each of these steps is of order θ' . On the whole, we see that these studies on dynamical twist provide a means of measuring the friction constant γ_1 . For the other types of Frederiks transitions (cases 1 and 3 of Fig. 3.13) the situation is more complicated, but also more interesting; various combinations of the Leslie coefficients are involved and can be measured. For a more thorough experimental and theoretical discussion the reader is referred to reference 20.

5.2.5 Inelastic scattering of light

We have seen (Section 3.4) that, in a nematic single crystal, the long wavelength fluctuations of the optical axis give rise to a large scattering of light. It must be realized that these fluctuations are not static; in fact their dynamical character was already displayed in the early observations on ‘flicker effects’ by Friedel, Grandjean, and Mauguin [21]. If, in a region of space, the director \mathbf{n} differs from its average orientation \mathbf{n}_0 , the fluctuation $\delta\mathbf{n} = \mathbf{n} - \mathbf{n}_0$ will relax towards zero in a certain time. For long-wave length fluctuations, this relaxation process may be predicted by the macroscopic equations of nematodynamics. Experimentally, we can prove these time-

dependent fluctuations of \mathbf{n} because they result in a frequency modulation of the scattered light. The corresponding frequency broadenings are small (in the kilocycle range), but measurable with the present laser sources and photon beat techniques [22]. This type of study has been carried out in some detail on *p*-azoxyanisole by the Orsay Group [23]. As we shall see, these experiments give rather detailed information on the Leslie coefficients.

The scattered amplitude, for a given scattering wavevector \mathbf{q} , depends on the two independent Fourier components $n_1(\mathbf{q})$ and $n_2(\mathbf{q})$ of the fluctuation $\delta\mathbf{n}$. These components have been defined (and studied from a static point of view) in Chapter 3 (see in particular Fig. 3.20). For a general \mathbf{q} , the component n_1 describes a mixed deformation involving splay and bend, while n_2 involves twist and bend. Each of them may be analysed separately by a suitable choice of polarizations in the light scattering experiment. When this separation is performed, the main experimental results appear to be the following

1. For each mode the power spectrum (or frequency distribution) has the form of *one single Lorentzian*, centred on the incident beam frequency. This means that the behaviour of the fluctuations is purely viscous (no oscillations).
2. When q retains a fixed orientation, but varies in magnitude, the line widths $\Delta\omega_1(\mathbf{q})$, $\Delta\omega_2(\mathbf{q})$ are essentially *proportional to q^2* (in the absence of any external magnetic field)
3. The widths $\Delta\omega_\alpha(\mathbf{q})$ ($\alpha = 1, 2$) do depend somewhat on the orientation of \mathbf{q} .

An interpretation of these facts can be given in terms of the Leslie equations, suitably linearized for small deviations from equilibrium [24]. The conclusions may be summarized as follows.

1. A fluctuation $n_\alpha(\mathbf{q})$ sees a restoring ‘force’ in the Onsager sense, which is simply the corresponding component of the molecular field

$$h_\alpha = -(K_\alpha q_\perp^2 + K_3 q_z^2) n_\alpha = -K_\alpha(\mathbf{q}) n_\alpha \quad (\alpha = 1, 2). \quad (5.77)$$

Equation (5.77) is a direct consequence of eqn (3.74). (Here for simplicity we have also assumed that no magnetic field is applied.)

2. If the parameter μ (defined by eqn (5.57)) is much smaller than unity (as it always appears to be) the Leslie equations predict a purely viscous type of relaxation, i.e. they can be reduced to the form

$$\frac{\partial}{\partial t} n_\alpha(\mathbf{q}) = -\frac{1}{\tau_\alpha(\mathbf{q})} n_\alpha(\mathbf{q}) \quad (5.78)$$

(the time τ being real). In terms of a power spectrum, this gives a single Lorentzian of width $\Delta\omega_\alpha(\mathbf{q}) = 1/\tau_\alpha(\mathbf{q})$, and is in agreement with the experiments on PAA.

3. The relaxation rate (i.e. the right-hand side of eqn (5.78) is proportional to the restoring force (5.77), and inversely proportional to a certain effective viscosity $\eta_\alpha(\mathbf{q})$

$$\frac{1}{\tau_\alpha(\mathbf{q})} = \frac{K_\alpha(\mathbf{q})}{\eta_\alpha(\mathbf{q})} \quad (5.79)$$

(note the dimensions: $K_\alpha(\mathbf{q}) \sim Kq^2$ is an energy/cm³ and the viscosity η has the dimensions $ML^{-1}T^{-1}$). The viscosity $\eta_\alpha(\mathbf{q})$ depends only on the orientation of \mathbf{q} , and is given explicitly by [22b]

$$\begin{aligned}\eta_1(\mathbf{q}) &= \gamma_1 - \frac{(q_\perp^2\alpha_3 - q_z^2\alpha_2)^2}{q_\perp^4\eta_b + q_\perp^2q_z^2(\alpha_1 + \alpha_3 + \alpha_4 + \alpha_5) + q_z^4\eta_c}, \\ \eta_2(\mathbf{q}) &= \gamma_1 - \frac{\alpha_2^2q_z^2}{q_\perp^2\eta_a + q_z^2\eta_c}.\end{aligned}\quad (5.80)$$

In eqn (5.80) η_a, η_b, η_c are the Miesowicz viscosities defined by eqns (5.49)–(5.52). Some limiting cases of eqn (5.80) deserve special mention

1. Omitting first all the angular factors, we find $1/\tau = D_0q^2$ where $D_0 = K/\eta \sim 10^{-5}$ cm²/sec may be interpreted as the diffusion coefficient for orientation.
2. If \mathbf{q} is along the nematic axis (along 0z) the deformation for both modes reduces to a pure bend, and the effective viscosity is

$$\eta_{\text{bend}} = \gamma_1 - \frac{\alpha_2^2}{\eta_c}.$$

3. If \mathbf{q} is normal to the nematic axis, mode (2) becomes a pure twist deformation, of viscosity $\eta_{\text{twist}} = \gamma_1$. Mode (1) is then a case of pure splay, and $\eta_{\text{splay}} = \gamma_1 - \alpha_3^2/\eta_b$.

The data on mode (2) in PAA at 125°C can be fitted with $\gamma_1 = 5.9 \times 10^{-2}$, $\alpha_2^2/\eta_a = 0.1$, $\alpha_2^2/\eta_c = 0.05$ (all viscosities being measured in poise). For technical reasons, the data on mode (1) are more difficult to obtain. All that has been possible to extract from them at present is a rough estimate of the splay viscosity

$$4.8 \times 10^{-2} < \eta_{\text{splay}} < 6.5 \times 10^{-2}.$$

Thus, at the present stage, the light scattering experiments provide us with three relations between the five unknown Leslie coefficients, plus another approximate relation (for η_{splay}). An interesting comparison between these results and the Miesowicz data [8] on η_a, η_b, η_c has been carried out by the Harvard Group [4]. Using as a starting point η_a, η_b, η_c , plus the Orsay value for γ_1 , they derive

$$\lambda = -\frac{\gamma_2}{\gamma_1} = 1.15,$$

$$\nu_3 = 2.4 \times 10^{-2} \text{ poise}.$$

Then they show that the three other Orsay data (α_2^2/η_a , α_2^2/η_c , and η_{splay}) are reproduced with reasonable accuracy. This does confirm to some extent the validity of the general nematodynamic equations, involving five independent parameters. In the future, the light scattering experiments will undoubtedly prove more and more useful to check these equations. In particular, recent improvements in detection methods should soon allow for a complete study of mode (1).

In Table 5.1 we give a list of data for the friction coefficients of MBBA. The coefficient γ , which is particularly important, has been compiled for eight nematic liquids by C. K. Yun [25].

5.3 CONVECTIVE INSTABILITIES UNDER ELECTRIC FIELDS

The alignment in a nematic single crystal may often be destroyed by a rather small voltage (of the order of 10 V) applied between two points in the sample. This type of electro-optic effect was discovered independently by a number of experimentalists but its practical importance was first realized by the RCA group under G. Heilmeier [24]. The fundamental process underlying the effect was at first mysterious, but W. Helfrich [32] proposed an explanation—based on a combination of charge transport and convection effects—that seems to account for the most salient facts. Because convection is involved, the problem essentially belongs to nematodynamics, and we shall try to summarize here the main experimental results together with their interpretation. The effect is rather complex. For this reason, we shall present only a very special selection of experiments, with no reference to historical order, and often omitting contributions that were important in their time, but that did not point to (what we now believe to be) the crucial phenomena.

5.3.1 Basic electrical parameters

We shall be concerned here with experiments that involve only d.c. or low-frequency a.c. electric fields (typical frequency range 0– 10^3 Hz), for which the most important parameters are the static dielectric constant and the static conductivity.

5.3.1.1 Dielectric constants

In Chapter 3 we discussed briefly the static dielectric constants $\epsilon_{||}$ (measured along the optical axis) and ϵ_{\perp} (normal to the axis). By suitable insertion of permanent dipoles in the chemical formula of the material, one can often achieve either $\epsilon_{||} > \epsilon_{\perp}$ (if the dipole is parallel to the long axis of the molecule)

Table 5.1. Viscosities of MBBA (centipoise).

Leslie coefficients ((5.31) and (5.34))

Miesowicz ((5.49) and (5.51))

α_1	α_2	α_3	α_4	α_5	α_6	$\alpha_3 + \alpha_2 + \alpha_5$	$\alpha_3 - \alpha_2$	$\alpha_3 + \alpha_2$	$\alpha_4/2$	$\frac{-\alpha_2 + \alpha_4 + \alpha_5}{2}$	$\frac{\alpha_3 + \alpha_4 + \alpha_6}{2}$
6.5 ± 4	-77.5 ± 1.6	-1.2 ± 0.1	83.2 ± 1.4	46.3 ± 4.5	-34.4 ± 2.2	γ_1	76.3 ± 1.7	γ_2	23.8 ± 0.3	η_b	η_c
							78.7 ± 1.7			103.5 ± 1.5	41.6 ± 0.7
											$T (\text{ }^\circ\text{C})$
						155					
						110					
							42				
								25.2			
									$\gamma_1/\gamma_2 = 0.959 \pm 0.05$		
									125		
									80		
									130 ± 5		
									86 \pm 2		

Light scattering (5.80)

Ultrasound (5.58)

Capillary waves

Dynamical Frederiks transition

$\gamma_1(\alpha_3^2/\eta_b)$ (bend)	$\gamma_1 - (\alpha_2^2/\eta_c)$ (splay)	γ_1 (twist)	$\eta_1 - (\alpha_3^2/\gamma_1)$ $\tilde{\eta}_b = \tilde{\eta}_c$	$\alpha_4/2$ $\tilde{\eta}_a$	$\gamma_1 + (\gamma_2^2/\gamma_1)$	$\gamma_1 + (\alpha_2^2/\eta_c)$ γ^*	$T (\text{ }^\circ\text{C})$
19 \pm 3			27	42			25
21 \pm 2	126		16.3	25.2	16.1		$T - T_c = 3^\circ\text{C}$
							24
							25
							22
							23
						107	
						110 \pm 5	

Data from references 10a, b, 27–29 and 31a, References 10a, b and 31a also give data as a function of temperature.

or $\epsilon_{\parallel} < \epsilon_{\perp}$ (if the dipole is normal). Typical values for MBBA at room temperature are $\epsilon_{\parallel} = 4.7$, $\epsilon_{\perp} = 5.4$.

5.3.1.2 Conductivities

Another important electrical property is the static conductance; it is usually small (typically in the range 10^{-9} to 10^{-8} ohm $^{-1}$ cm $^{-1}$) and anisotropic: The anisotropy of σ was measured very early by Svedberg [33]. In most of the examples studied up to now the parallel conductance σ_{\parallel} is somewhat larger than the perpendicular conductance σ_{\perp} [34]. With usual samples of MBBA, $\sigma_{\parallel}/\sigma_{\perp} \sim 1.5$.

It must be emphasized, however, that all conductance results are strongly dependent on the amount, and on the chemical nature, of the impurities present in the sample; it is helpful to have charge carriers; they are required for the electro-optic effects to be described below. In MBBA the conduction process involves a weak dissociation of molecules into ions, which has been studied by careful electrodialysis experiments [35]. But one can act on the conductance of a nematic by various means. (a) Starting with a pure material, and doping it with ions which are (slightly) soluble in it—such as certain crown salts [36]—one can in principle vary at will the magnitude of σ_{\parallel} and σ_{\perp} , keeping a constant ratio $\sigma_{\parallel}/\sigma_{\perp}$. (b) By changing the stereochemical shape of the dissolved ions by suitable chemical substitutions, one should be able to change the ratio $\sigma_{\parallel}/\sigma_{\perp}$. (c) Values of $\sigma_{\parallel}/\sigma_{\perp}$ smaller than unity have been achieved in the vicinity of a smectic–nematic transition [37].

For notational purposes, it may sometimes be helpful to divide nematics into four classes (+ +) (+ -) (- +) (- -) where the first symbol gives the sign of $\epsilon_{\parallel} - \epsilon_{\perp}$, and the second symbol the sign of $\sigma_{\parallel} - \sigma_{\perp}$. Spectacular electro-optic effects have been found and studied principally in the (- +) class: we shall mainly focus our attention on this case.

5.3.1.3 Electrode effects

One important complication connected with electric currents in organic materials such as nematics, is brought in by electrode effects. All d.c. studies require metallic electrodes in direct contact with the fluid. Chemical reactions take place at these electrodes, with the following consequences.

1. *Injection* of supplementary carriers. These injection effects have been studied in isotropic fluids of high purity, and they can, by themselves, lead to certain convective instabilities [38]. Unfortunately, the injection process is often chemically complex. It can be controlled accurately only for very special electrodes (semipermeable membranes).
2. *Chemical degradation* of the nematic material (this may be a serious nuisance for technical applications).

5.3.1.4 Elimination of electrode effects

Clearly, from the point of view of fundamental studies at least, it is preferable to eliminate the complications due to specific electrode effects. At present, the best method that has been found to achieve this in nematics amounts to the use of *low-frequency a.c. fields* rather than d.c. fields.

Using a.c. fields, it is possible to insert thin insulating foils (e.g. Teflon) between the electrodes and the nematic slab. There does remain a field (or a voltage drop V) between the foils because, at finite frequencies, the electrical carriers in the nematic are not able to screen out entirely the charges Q on the electrodes; for a conventional lossy dielectric the relation between V and Q reads

$$V = \frac{Q}{C} \frac{i\omega\tau}{1 + i\omega\tau}$$

where C is the capacitance in the absence of losses, $\tau = 4\pi\sigma/\epsilon$ is the dielectric relaxation time, and ω the angular frequency.

Even using a.c. fields, the effects observed with or without the Teflon shields are often identical! This probably means that, in the latter case, the injected carriers are confined to a thin sheet near the electrode, and are not able to generate extra instabilities.

5.3.2 Experimental observations at low frequencies

A nematic material of the $(-+)$ class is placed between two semitransparent electrodes (typical slab thickness $30\text{ }\mu\text{m}$). A d.c. or (preferably) low-frequency a.c. voltage V is applied across the slab. For increasing values of the r.m.s. amplitude V we then observe the following sequence of regimes.

5.3.2.1 Single crystal regime

At low voltages V (typically in the range $V \sim 1\text{ V}$) the molecules are aligned normal to the electric field \mathbf{E} (along a certain axis x) as expected for a dielectric material with $\epsilon_{||}/\epsilon_{\perp}$. In this regime we have a nematic single crystal; in particular any light beam incident on the slab is reflected (or transmitted) specularly.

5.3.2.2 Williams domains

When V reaches a critical threshold V_c (of the order of 5 V) a periodic distortion of the nematic alignment is observed. In many cases, it is a simple one-dimensional type of distortion, which was first observed by Williams and studied in particular by the groups at IBM, Orsay, and Ford [40, 41]. The aspect of the distortion is shown in Fig. 5.8. It can be detected by various optical means.

Consider a light wave propagating along z and polarized along x . At a

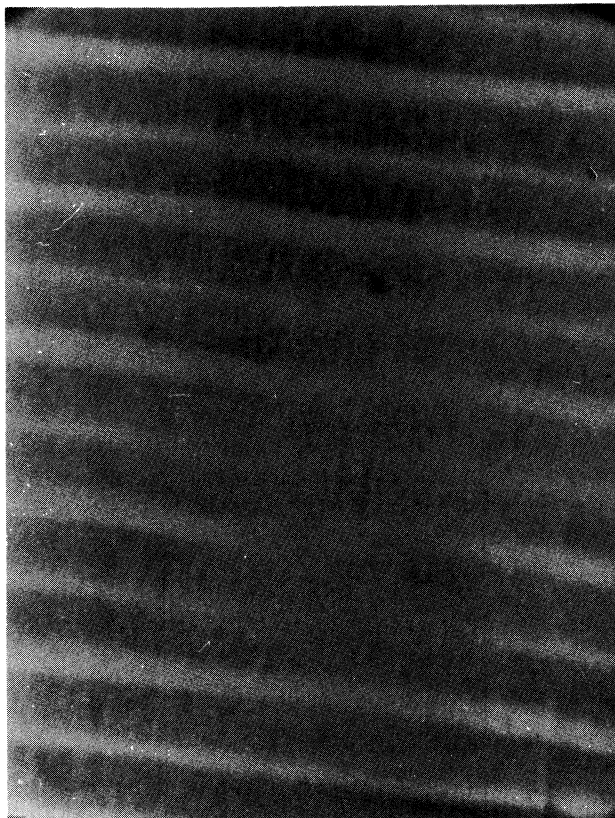
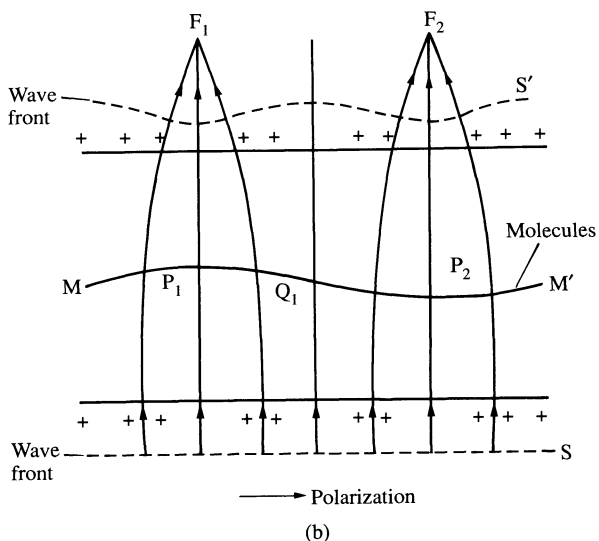
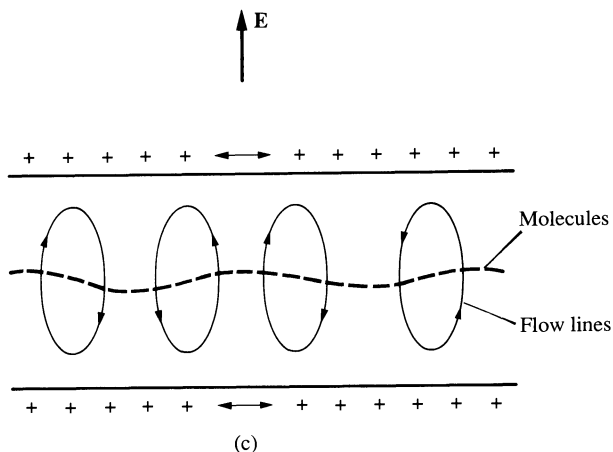


Fig. 5.8. (a) The 'Williams domains' in MBBA. Glass plates impose tangential boundary conditions. The strips are normal to the easy axis of the plates (courtesy G. Durand). (b) Light focusing by a distorted nematic arrangement. The molecular arrangement is represented by the line MM'. Plane parallel light is sent through the bottom plate. The initial wave front S is flat. Inside the sample the refractive index is larger at P₁ than at Q₁. Thus the light velocity is larger at Q₁ and the outgoing wave front S' is bent: this corresponds to a focusing of the rays (normal to S') at points F₁, F₂, etc. (c) Flow pattern associated with the distortion in the Williams domains.

point such as P₁ the polarization is parallel to the optical axis: the refraction index is then the 'extraordinary' index n_e . On the other hand, at point Q₁, the polarization makes a certain angle with the optical axis and the effective index n_{eff} is a certain combination of n_e and of the ordinary index n_0 ($< n_e$). Thus at point Q₁, $n_{\text{eff}} < n_e$. We conclude that, for a polarization along x, the slab behaves as a periodic array of cylindrical lenses P₁, P₂, ... An incident plane wave is then focused at a series of lines F₁, F₂, ... A



(b)



(c)

photograph showing these focusing effects is shown in Fig. 5.8(a). Note that the focusing effects disappear completely if the light is polarized along y ; this proves that the molecules do remain in the x, z -plane.

With the (x) polarization, the sample may be used as a periodic grating, and the periodicity may be derived from a study of the selective reflections on this grating; the repeat period along $x(\lambda_x)$ is observed to be a linear function of the sample thickness d .

At low frequencies ω , the distortions in the molecular alignment are found to be *static*; the pattern stays the same when the electric field reverses.

The distortions are also accompanied by a certain amount of *cellular flow* in the nematic liquid; this motion may be displayed by following the motion of a dust particle floating in the slab. The flow lines are observed to have the same periodicity as the distortions; the geometrical relations between the two effects are shown in Fig. 5.8(c). This flow pattern is somewhat reminiscent of what is observed when a slab of isotropic fluid is heated from below (the Benard phenomenon [42]). The analogy strongly suggests that a convective instability is involved.

The voltage threshold V_c is essentially *independent of the sample thickness*; at first sight one might be tempted to interpret this property in terms of an electrochemical process at a metal–nematic interface. However, this cannot be correct, since the same voltage V_c is maintained with Teflon shields in a.c. regimes. We shall see that a constant V_c is a natural consequence of the Helfrich model.

5.3.2.3 Dynamic scattering

If the voltage V is increased above V_c , the distortion amplitudes and the associated flow velocities increase. Finally, at some higher voltage V_t , a new regime is reached.

1. The Williams domains become disordered and mobile.
2. The flow is now turbulent.
3. The long-range nematic alignment is completely upset.

Optically the new, fluctuating, disordered state can be observed without any special specification on the light polarization; this shows that the molecules are not confined any more to orientations in the x, z -plane. Observation under the microscope also shows a number of disclination loops nucleating near the limiting surface.

On a macroscopic scale, the practical consequence of point 3 is a strong, diffuse, scattering of light. This ‘dynamic scattering’—as it has been called by the RCA group—is technologically interesting because it involves low voltages, low power dissipation, and small sample size, and also because it operates by reflection of any type of light (e.g. sunlight).

On the other hand, the processes involved in the transition towards turbulence (particularly the role of disclination lines) are very poorly understood at present: most fundamental studies have been directed towards the interpretation of the lower threshold V_c ; in the following discussion, we shall restrict our attention to V_c .

5.3.3 The Helfrich interpretation

The effects that we have listed above are observed mainly with materials of the $(-+)$ class prepared in the *planar* texture.

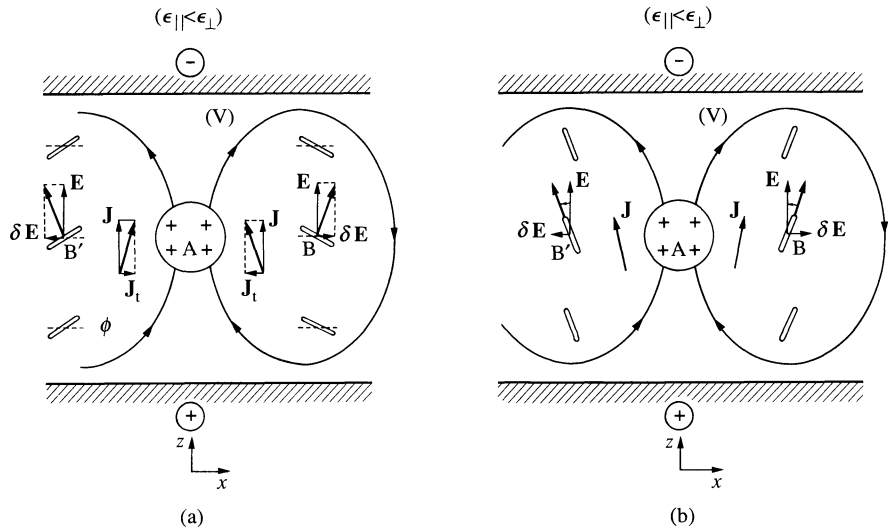


Fig. 5.9. (a) Carr–Helfrich effect for a material with negative dielectric anisotropy and positive conductance anisotropy $(-+)$ (boundary conditions: tangential). (b) Carr–Helfrich effect for a $(++)$ material (boundary conditions: normal). The molecules are represented by small rods.

They can be explained rather simply in terms of convective instabilities. The general idea was first invoked by Tsvetkov and Carr [43] but the detailed discussion of small motion instabilities is due to W. Helfrich [32].

To understand the basic concepts, let us consider a slab of a $(-+)$ material under electric fields \mathbf{E} as shown in Fig. 5.9(a). In the unperturbed situation the molecules are in the planar texture (say along x).

The perturbed state has a small periodic distortion of the bending type. Of course, the Frank elastic energy is increased by the distortion and gives rise to a restoring force. On the other hand, if $\sigma_{||} > \sigma_{\perp}$ there is a component J_t of the current, along x , which tends to pile up a positive charge density q in the region around point A. This charge accumulation has two main effects.

1. The field at point B is shifted from \mathbf{E} to $\mathbf{E} + \delta\mathbf{E}$. The molecules at B tend to remain orthogonal to the overall field; as seen in Fig. 5.9(a), this *electrostatic torque* tends to increase the initial distortion.
2. The fluid around A is subjected to a bulk force $q\mathbf{E}$: this gives rise to a certain flow pattern, shown qualitatively on the figure. The result at point B is a strong *hydrodynamic torque* which also tends to increase the distortion.

If ϕ is the angular amplitude of the distortion, and \mathbf{k} its wavevector along x , the restoring torque due to elastic distortions is $-K_3 k^2 \phi$. On the other hand, both the electrostatic and the hydrodynamic torques are proportional to $E^2 \phi$. We also know, from the experiments described above, that the wavelength of the distortion (along x) is comparable to the sample thickness d (i.e. $k \sim 1/d$).

Thus we conclude that there is a threshold in field E_c defined by

$$E_c^2 = \text{const. } K/d^2, \quad (5.81)$$

or that $V_c = E_c d$ is independent of sample thickness, as is indeed observed. The exact value of the constant in eqn (5.81) would have to be derived from a rather complex two-dimensional nematodynamic calculation. An approximate value has been derived by Helfrich using a one-dimensional approximation; all quantities such as the tilt angle ϕ are assumed to depend only on the transverse coordinate x , and not on z : the boundary conditions at both sides of the plate are omitted, except that the magnitude of the wavevector k is taken to be equal to C/d where C is a fixed numerical constant (or order unity). The result is then comparatively easy to reach, and reads

$$V_c^2 = \frac{V_0^2}{\zeta^2 - 1} \quad (5.82)$$

where

$$V_0^2 = 4\pi C^2 \frac{K_3 \epsilon_{||}}{\epsilon_{\perp}(\epsilon_{\perp} - \epsilon_{||})} \quad (5.83)$$

and ζ^2 is a dimensionless parameter, which must be larger than unity to obtain an instability

$$\zeta^2 = \left(1 - \frac{\sigma_{\perp} \epsilon_{||}}{\sigma_{||} \epsilon_{\perp}}\right) \left(1 + \frac{\alpha_2 \epsilon_{||}}{\eta_c \epsilon_a}\right). \quad (5.84)$$

For MBBA, (assuming that the ratio $\alpha_2 : \eta_c$ is close to those estimated for PAA) one finds $\zeta^2 \sim 3.2$.

Helfrich has shown that, with plausible values for K_3 and a constant C of order π (i.e. a half-wavelength equal to the sample thickness), the estimated values of V_c are of the order of a few volts—quite acceptable in view of the many unknowns involved. Experimental studies [44a] and improved calculations of the boundary effects [44b] essentially confirm these results.

Let us now discuss the instabilities that may occur with the other nematic classes. For simplicity, we shall assume that for all cases, in low fields \mathbf{E} , the easy direction imposed by the walls coincides with that imposed by \mathbf{E} ; this avoids further complications due to Frederiks transitions in the field \mathbf{E} .

Consider for instance a sample of the (+ +) class (Fig. 5.9(b)); here the unperturbed state has the molecules normal to the slab, and the fluctuation that may induce local charge accumulation is a splay. However it is seen that the electric torque at point B now tends to stabilize the structure. To study the hydrodynamic torque, we note that at point B the flow lines are nearly parallel to the molecules. As explained in Section 5.2, the hydrodynamic torque is then very weak (in other words, the parameter $\lambda = -\gamma_2/\gamma_1$ is close to unity, and the torque is proportional to $\lambda - 1$). For points above or below B, we do have some hydrodynamic torques but their sign depends on the precise location studied. Finally, in this case, we find only two strong torques (elastic and electric) and both tend to stabilize the structure: no instability is expected.

A similar conclusion can be derived for the (--) class. On the other hand, for the (+-) class an instability is predicted (created mainly by the electric torques).

The limiting case $\epsilon_a = 0$ is delicate. Consider for instance a (0+) sample in the homeotropic texture of Fig. 5.9(b). If $\lambda > 1$ and $\epsilon_a = 0$, the one-dimensional argument (based on the torque at point B) predicts instability. If we go to an improved, two-dimensional calculation, and choose $k \sim \pi/d$ ('cylindrical' rolls), we find that the system is stable: the torques near the top and bottom surfaces are opposed in sign to the torques at B. But if we choose $\gg \pi/d$ ('thin' rolls), the one-dimensional argument *must* become correct: an instability should occur for thin rolls.

5.3.4 Extension to higher frequencies

5.3.4.1 Williams domains and chevrons

The experimental variation of the threshold V_c with frequency ($\omega/2\pi$) is displayed in Fig. 5.10. Note that, to obtain this type of curve, the sample must not be too thin (typically, we require $d > 10 \mu\text{m}$). Then one observes two very different regimes, respectively below and above a certain threshold frequency ($\omega_c/2\pi$).

For $\omega < \omega_c$ the threshold V_c is rather low, and also independent of sample thickness. For $V \gtrsim V_c$ we have Williams domains, with a spatial periodicity comparable to the thickness d .

For $\omega > \omega_c$ the threshold is much higher, and V_c is proportional to d ; the real threshold parameter in this regime is the field $E_c = V_c/d$, where E_c varies like $\omega^{\frac{1}{2}}$. The onset of instability at V_c is manifested optically by parallel striations (shown in Fig. 5.11). The distance between striations is now much smaller than d , and depends on ω (or on E_c). It is proportional to $1/E_c \sim \omega^{-\frac{1}{2}}$.

This second type of instability has been detected first by Heilmeyer and Helfrich [45] and studied in some detail by the Orsay Group [46]—who coined the name '*chevrons*' for the pattern of Fig. 5.11. A very useful 16 mm

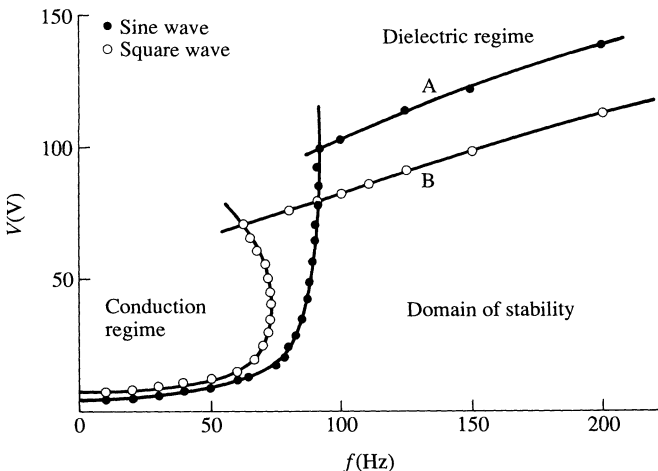


Fig. 5.10. Typical threshold voltage versus frequency for commercial MBBA (courtesy G. Durand).

film, showing the Williams domains, the chevrons, and also the turbulent structures observed as voltages $V \gg V_c$, has been taken by R. Kashnow [47].

The cut-off frequency $\omega_c/2\pi$ is typically of the order of 100 Hz and is found to increase linearly with the sample conductivity [46]. Thus with very pure materials of low conductance, the a.c. effects should always correspond to the chevron regime.

5.3.4.2 Interpretation

All the features displayed above may be interpreted in terms of the Carr–Helfrich model, suitably extended to cover time-dependent phenomena [48]. The geometrical conditions are still those of Fig. 5.7(b) or 5.9(a). In the distorted state the molecules are deflected by a small angle ϕ in the x, y -plane. The most important parameter from the point of view of charge accumulation is not exactly ϕ , however, but rather the curvature $\psi = \partial\phi/\partial x$ of the molecular pattern. We use ψ and the charge density q as our fundamental variables. Again, as in the original Helfrich calculation for static regimes [32], we consider only a one-dimensional problem (ϕ and q depend only on x).

Positive charges pile up in the regions of negative curvature (when E is along $+z$) as is shown on Fig. 5.9(a): the charge source is proportional to $-\psi E$. This leads to an equation for the charge of the form

$$\dot{q} + \frac{q}{\tau} + \sigma_H \psi E \rightarrow 0 \quad (5.85)$$

where τ describes dielectric relaxation, and σ_H is associated with the Carr

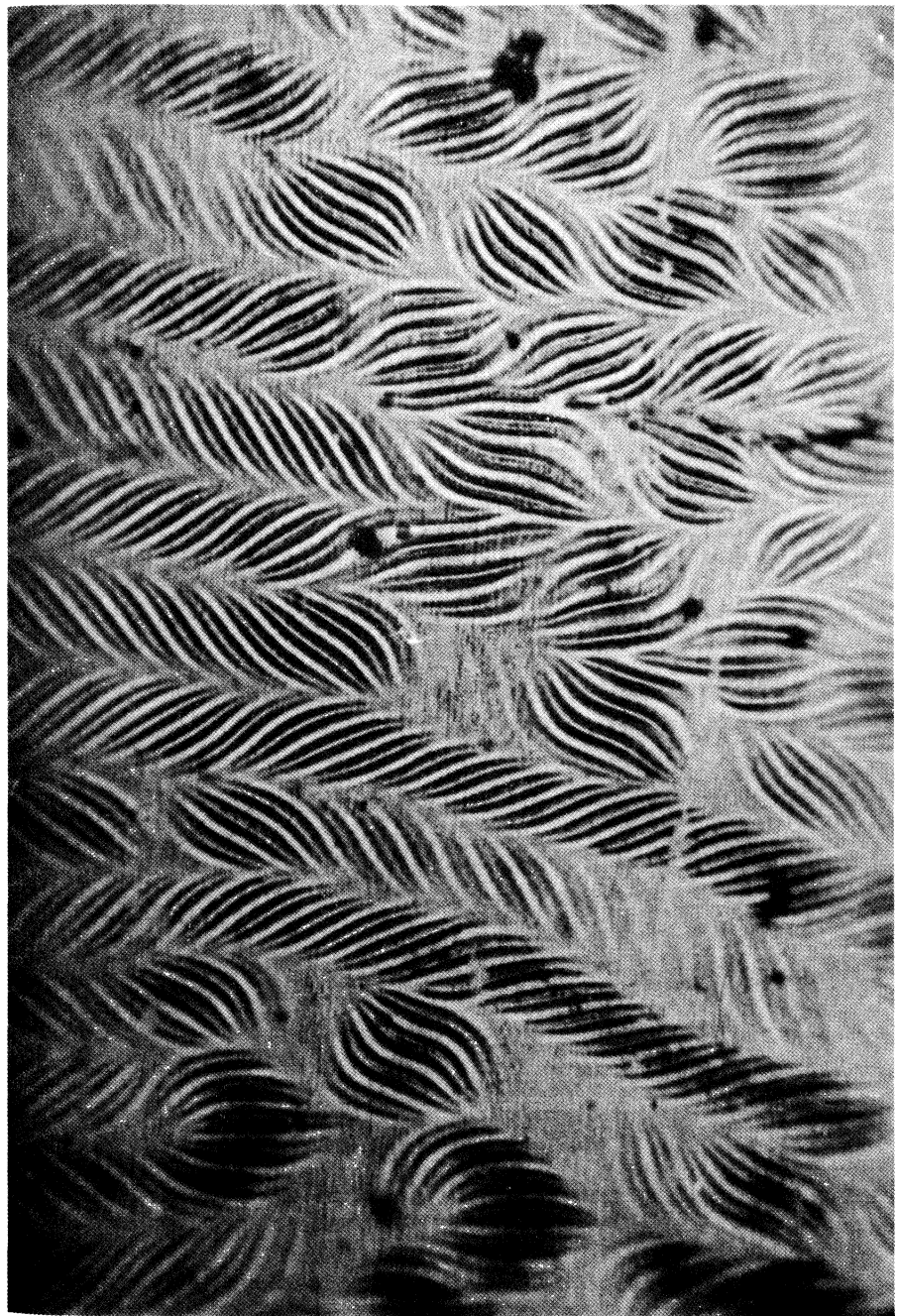


Fig. 5.11. The 'chevron' domains characteristic of the instabilities at high frequencies (courtesy G. Durand).

process. Using Ohm's law and Poisson's equation in an anisotropic medium, one obtains [48]

$$\frac{1}{\tau} = \frac{4\pi\sigma_{||}}{\epsilon_{||}}, \quad (5.86)$$

$$\sigma_H = \sigma_{||} \left(\frac{\epsilon_{\perp}}{\epsilon_{||}} - \frac{\sigma_{\perp}}{\sigma_{||}} \right) \quad (\sigma_H > 0) \quad (5.87)$$

(for MBBA $\sigma_H \sim \frac{1}{2}\sigma_{||}$).

We must also write down an equation for the curvature ψ . One origin for ψ is the bulk electrostatic force qE , giving rise to cellular flow and hydrodynamic torques. From Fig. 5.9(a) we see that a negative qE will tend to give a positive increase in ψ . This suggests an equation of the form

$$\dot{\psi} + \frac{\psi}{T} + \frac{qE}{\eta} = 0 \quad (5.88)$$

where $1/T$ is a relaxation rate for molecular orientation, and η has the dimensions of a viscosity. In fact, the complete calculation, including both hydrodynamic and electric torques, leads to eqn (5.88) with the coefficients

$$\begin{aligned} \frac{1}{T} &= \frac{\eta_c}{\gamma_1 \tilde{\eta}_c} \left[\frac{(\epsilon_{\perp} - \epsilon_{||})\epsilon_{\perp}}{4\pi\epsilon_{||}} E^2 + K_3 k^2 \right], \\ \frac{1}{\eta} &= \frac{\eta_c}{\gamma_1 \tilde{\eta}_c} \left[\frac{\epsilon_{\perp} - \epsilon_{||}}{\epsilon_{||}} - \frac{\alpha_2}{\eta_c} \right]. \end{aligned} \quad (5.89)$$

In these formulae, η_c and $\tilde{\eta}_c$ are the effective viscosities defined by eqns (5.51) and (5.58), while \mathbf{k} is the wavevector of the bend deformation.[†]

Equations (5.85) and (5.88) must then be solved, in the presence of a given a.c. field $E = E_m \cos \omega t$. The general solutions have the form

$$q(t) = q_p(t) e^{st},$$

$$\psi(t) = \psi_p(t) e^{st}$$

where q_p and ψ_p are periodic functions (of period $2\pi/\omega$), and s is a parameter depending on the field amplitude E_m . The threshold is obtained when the real part s vanishes.[‡]

The complete discussion is rather complex—especially since the relaxation rate for orientation $1/T$ (eqn (5.89)) does depend on the instantaneous value of the field $E(t)$. Here we shall give only a simplified discussion of the two regimes.

1. At low frequencies ω , the fields E near threshold are rather small, and

[†] I am very much indebted to A. Rapini, who noticed earlier that the simplified forms (5.89) could be used instead of the heavier expressions found in reference 48.

[‡] For the cases at hand s appears to be real at threshold.

T is rather large. Thus $\omega T > 1$, and the only important Fourier component of $\psi(t)$ is at zero frequency

$$\psi(t) \rightarrow \bar{\psi}.$$

Then the charge source, proportional to $-\psi E$ (eqn 5.85) is a simple sinusoidal wave $-\sigma_H \bar{\psi} E_m \cos \omega t$. The corresponding charge is given by

$$q(t) = q' \cos \omega t + q'' \sin \omega t, \quad (5.90)$$

$$q' = -\sigma_H \tau E_m \bar{\psi} \frac{1}{1 + \omega^2 \tau^2}.$$

Let us now turn to the equation for the average curvature $\bar{\psi}$, obtained by averaging eqn (5.88) over one period; it may be shown to reduce to

$$\frac{\bar{\psi}}{T} + \frac{1}{2} q' E_m = 0 \quad (5.91)$$

where $1/T$ is the time-average of the relaxation rate (5.89). This gives a threshold condition

$$1 = \frac{E_m^2}{2} \cdot \frac{\sigma_H \tau \bar{T}}{\eta} \cdot \frac{1}{1 + \omega^2 \tau^2},$$

which, after using (5.89), may be cast in the form

$$\bar{E}^2 = \frac{1}{2} E_m^2 = \frac{4\pi\epsilon_{||}}{(\epsilon_{\perp} - \epsilon_{||})\epsilon_{\perp}} K_3 k^2 \frac{1 + \omega^2 \tau^2}{\zeta^2 - (1 + \omega^2 \tau^2)} \quad (5.92)$$

where ζ^2 has been defined in eqn (5.84). The threshold field will correspond to the minimum allowable wavevector k : following the Helfrich assumption, we may assume that this is of the form C/d . This gives a voltage threshold (r.m.s.)

$$V_c(\omega) = V_c(0) \left(\frac{1 + \omega^2 \tau^2}{\zeta^2 - (1 + \omega^2 \tau^2)} \right)^{\frac{1}{2}}. \quad (5.93)$$

Equation (5.93) shows that $V_c(\omega)$ increases with ω and finally becomes very large when ω approaches a cut-off frequency

$$\omega_c = \frac{1}{\tau} \sqrt{(\zeta^2 - 1)}. \quad (5.94)$$

The theoretical curve (5.93) is in rather good agreement with the data on MBBA [46]. Also, according to eqn (5.86), $1/\tau$ (and thus ω_c) is a linear function of the conductivity σ —in agreement with experiment.

Thus, at the threshold, for all frequencies $\omega < \omega_c$, the instability pattern corresponds to a static distortion ($\psi \neq 0$) and to oscillating charges; for this reason it is often referred to as the *conducting regime*.

2. The above calculation breaks down when ω reaches ω_c , because in this region the fields become large, ωT reaches values of the order of unity, and the curvature ψ becomes time-dependent. The situation is comparatively simple if we consider only the domain $\omega \gg \omega_c$. This implies $\omega\tau > 1$. Then the charge q cannot follow the excitation

$$q \rightarrow \bar{q},$$

The bulk force $qE \rightarrow \bar{q}E_m \cos \omega t$ is sinusoidal, and the curvature response $\psi(t)$, given by eqn 5.88), is a more or less complicated periodic function of time. Qualitatively we may guess that, to get a sizeable response, the phase lag of ψ must not be too large; the threshold condition corresponds to

$$\omega \bar{T} = \text{constant}.$$

Thus, in this regime, \bar{T} must be short. The system achieves this by two means which can be understood from eqn (5.89). One is to have high field amplitudes. The other (first pointed out by O. Parodi and E. Dubois Violette) is to use a high value of the wavevector k . At threshold, both effects contribute roughly equally, and we have

$$\frac{\epsilon E_c^2}{4\pi} \sim K_3 k^2 \sim \eta \omega$$

where ϵ and η are suitable combinations of dielectric and viscosity coefficients. These rules do explain the experimental observations that we quoted before:

- threshold field $E_c \sim \omega^{\frac{1}{2}}$;
- E_c independent of sample thickness;
- spatial period of the striations $\pi/k \sim \omega^{-\frac{1}{2}}$.

In the high-frequency regime (for $\omega \gg \omega_c$) the molecular pattern oscillates while the charges are static; for this reason this is often called the *dielectric regime*. Another name is the *fast turn-off mode* [45]; if the a.c. voltage is turned off from a value slightly above V_c to 0, the striation pattern disappears rapidly. A plausible explanation for this feature is that the relaxation rate in zero field (deduced from eqn (5.89)) is

$$1/T \simeq K_3 k^2 / \eta$$

and is still high because the wavevector k of the striations is large.

On the whole, the Helfrich model [32] appears well substantiated by these a.c. studies near the threshold V_c , and some information on the Leslie coefficients will probably be extracted from the data.†

5.4 MOLECULAR MOTIONS

Very little is known—and even less is understood—concerning the dynamics of nematic fluids on the molecular scale. Here we shall present only a selected list of experiments that appear to be relevant.

5.4.1 Dielectric relaxation

For a few typical nematics, the dielectric constants $\epsilon_{\parallel}(\omega)$ and $\epsilon_{\perp}(\omega)$ have been measured on oriented samples and over a wide frequency range (radiofrequencies and microwaves). The main results appear to be the following.

1. Both ϵ_{\parallel} and ϵ_{\perp} usually show a normal (Debye) type of relaxation at microwave frequencies ($\omega/2\pi \sim 10^{10}$) [50]. Similar relaxation times are also found in the isotropic phase.
2. If the molecule under study has a non-zero component of electric dipole along its long axis, there is an additional relaxation process at much lower frequencies, which concerns only the parallel dielectric constant ϵ_{\parallel} . In materials where the nematic range falls around 100°C (such as PAA) this occurs in the radiofrequency range. The effect was discovered by Maier and Meier [51], and interpreted in some detail by Meier and Saupe [52] in terms of a 180° rotation of the molecule around one of the *short* axes of the molecule. For a long molecule, such a rotation is clearly difficult in the nematic phase, and the resulting relaxation rate is correspondingly slow—typically 10^3 times slower than for rotations around the long axis. It is tempting to relate this slowing down to the (small) probability for one molecule to be orthogonal to the nematic axis. However, these considerations cannot be made very precise; because of short-range order effects two neighbouring molecules, whose dipoles are accidentally parallel, may rotate synchronously and cross the perpendicular conformation more easily than a single one, etc.

† The instabilities under a field E stem from a coupling between charge transport and molecular orientation. Similar instabilities are generated by *thermal* transport—see P. Pieranski, E. Guyon, and E. Dubois-Violette [49].

5.4.2 Nuclear spin-lattice relaxation

The spin-lattice relaxation rate $1/T_1$ of a nucleus inside the nematic liquid gives some information on the motion of its immediate surroundings, on a time scale *ca.* 10^{-6} seconds. Some of the most salient results for the nematic phase are reviewed in references 53–55.

In practice, we have two slightly different types of nuclear probes, as exemplified by the following (current) cases: protons (spin $\frac{1}{2}$) where the main relaxing agent is the dipole-dipole interaction between nuclear spins; and deuterons (^2H) or nitrogen nuclei (^{14}N) [56] where the agent is a local electric field gradient.

In isotropic liquids, the molecular motions that dominate the relaxation process can usually be described in terms of one single correlation time τ_c ; as a result, the dependence of the relaxation rate on the nuclear frequency ω_n is simple [57]. In nematic liquids the situation is very different: the frequency dependence of $1/T_1$ is more complex and cannot be discussed in terms of one correlation time τ_c .

In fact, it is clear that many processes can contribute to $1/T_1$. Let us first restrict ourselves to an ideal situation, with rigid molecules and relaxation by intramolecular couplings only.† Then we can (at least) think of contributions due to:

- (1) rotations around the long molecular axis;
- (2) large-angle rotations around a short molecular axis (such as those involved in low-frequency relaxation of $\epsilon_{||}$);
- (3) small-amplitude oscillations of the long axis around its average orientation.

Process (1) has a short correlation time $\tau_1 \sim 10^{-10}$ s ($\omega_n \tau_1 \ll 1$). It should give a small frequency-independent contribution to the relaxation rate $1/T_1$.‡ Process (2) is rare, as we have seen, but it has a long correlation time, which enhances its efficiency for nuclear relaxation. It can contribute to the frequency dependent of $1/T_1$. Process (3) cannot be characterized by one correlation time: we know this, because the lower end of the frequency spectrum corresponds to the slow motions of long wavelength fluctuations, and such motions can be analysed by the Leslie equations. Using eqn (5.79) we see that a fluctuation of wavevector \mathbf{q} has a correlation time of order η/Kq^2 (where η is a viscosity and K a Frank constant): thus different Fourier components have different correlation times. In fact the most important fluctuations (for nuclear relaxation) are those for which the correlation time

† This means, for instance, that we neglect all dipole-dipole interactions between nuclei belonging to different molecules.

‡ Of course this type of rotation is efficient only if the vector linking the two nuclei involved in the dipole-dipole coupling is not parallel to the long axis.

is comparable to the nuclear period $\eta/Kq^2 \sim \omega_n^{-1}$. This corresponds to wavelengths

$$\lambda = \frac{2\pi}{q} = 2\pi \left(\frac{K}{\eta\omega_n} \right)^{\frac{1}{2}}.$$

Taking $\omega_n = 10^7$, $K = 10^{-6}$, and $\eta = 10^{-1}$ we find $\lambda = 600 \text{ \AA}$. λ is thus significantly larger than the molecular length a , and a discussion in terms of the continuum theory is not unreasonable. This has been carried out by Pincus [58] with subsequent improvements by Doane and Johnson [59] and by Lubensky [60]. Qualitatively, the resulting contribution to the nuclear spin-lattice relaxation may be written as

$$\frac{1}{T_1} \sim (\gamma H_L)^2 \frac{k_B TS^2}{K} \left(\frac{K}{\eta} + D \right)^{-\frac{1}{2}} \omega_n^{-\frac{1}{2}} \quad (5.95)$$

where H_L is the local field describing the relaxing agent, γ is the nuclear gyromagnetic factor, S is the nematic order parameter, and D is a translational self-diffusion coefficient. To understand why D plays a role, consider the limiting case where the fluctuations relax very slowly ($K/\eta \rightarrow 0$): the nematic is still distorted by thermal agitation, but the distortions are frozen. The molecule carrying the nuclear spin under study, moves in this structure by Brownian motion and has a variable position $\mathbf{r}(t)$. It is plausible to assume that the molecule constantly adjusts its long axis parallel to the local (distorted) director $\mathbf{n}\{\mathbf{r}(t)\}$; thus, when $\mathbf{r}(t)$ changes the local field seen by the nuclear spin is modulated.

Experimental relaxation rates in PAA can be fitted (between 5 and 10 megacycles) by the law of the form

$$\frac{1}{T_1} = A + B\omega_n^{-\frac{1}{2}}.$$

This would appear as the superposition of two relaxation processes: one of them (A) due to the local motions with a short correlation time, the other ($B\omega_n^{-\frac{1}{2}}$) being of the Pincus type. In early experiments, this agreement was not entirely significant, for various reasons.

1. As emphasized by Vilfan *et al.* [54a] it is known that, in certain isotropic liquids, the intermolecular spin interactions (modulated by the relative motion of the molecules) can lead to a relaxation rate of the form

$$\frac{1}{T_1} = C - D\omega_n^{+\frac{1}{2}}.$$

This is not easily distinguished from the ‘augmented Pincus form’ quoted above.

2. The slow motions listed under (2) above may play an important role.
3. In materials like PAA, the aromatic protons of interest are strongly perturbed by dipolar coupling with the methyl protons at both ends of the molecule: this has been proven by selective deuteration of the methyl protons [55].

However recent experiments have been performed at ultra low frequencies (kilocycles) by the so-called $T_1\rho$ technique [54b]. Here the Pincus process is dominant and is clearly proven.

5.4.3 Acoustic relaxation

Acoustic waves provide a tool to study relaxation processes in liquids, if these processes are comparatively slow ($\sim 10^{-7}$ s). The case of nematics is particularly complex, and the results are only partly understood. Nevertheless the technique is interesting and the existing data deserve a short description.

5.4.3.1 Low-frequency limit

At very low frequencies (say, well below 1 MHz), longitudinal waves propagate in a nematic with a velocity c_0 which is *independent of direction*. This is one characteristic feature of a liquid, where c_0 depends only on the bulk rigidity coefficient

$$E_0 = -V \left(\frac{\partial p}{\partial V} \right)_{\text{adiabatic}},$$

$$c_0 = [E/\rho]^{\frac{1}{2}} \quad (\rho = \text{density}).$$

Experimentally, c_0 is (as usual) mainly a decreasing function of temperature. But it shows a dip near the nematic-isotropic transition point T_c [61, 62]. This dip can be qualitatively understood by a thermodynamic argument based on the Maier-Saupe free energy [63].

5.4.3.2 Dispersion of the sound velocity: $c(\omega)$

At finite frequencies ω , the sound velocity $c(\omega)$ is slightly modified. This has been studied in MBBA by the groups at Rutgers [64] and MIT [65]. In particular, the dip that we mentioned above disappears above $\omega/2\pi \sim 10$ MHz. At these high frequencies, the order parameter S of the nematic phase is not able to follow the density fluctuations, and the sound velocity c measures a rigidity *at constant S*, which is not singular near T_c .

5.4.3.3 Anisotropy of the velocity: $c(\theta)$

At finite frequencies, the sound velocity c becomes slightly dependent on the angle between the optical axis and the direction of propagation. This effect has been shown by the Rutgers group, using a refined method of phase detection, in MBBA samples aligned by a magnetic field H . The result (at

one given frequency) is of the form

$$c(\theta) = c(0)[1 - \Delta \sin^2 \theta]$$

where Δ is typically of order 10^{-3} , and is positive (maximum velocity along the optical axis).

At temperatures well below T_c , Δ increases with frequency (more or less linearly). Near T_c , Δ becomes essentially independent of ω (in the range $2M_c < \omega/2 < 10M_c$)—presumably because the relaxation time of the order parameter becomes longer than the period in this temperature interval.

5.4.3.4 Attenuation as a function of frequency and temperature: $\alpha(\omega)$

A detailed study of the attenuation (for frequencies in the range 0.3 to 23 MHz_c) has been carried out recently by the MIT group on MBBA [65]. Unfortunately, the data were taken on unoriented samples where many disclinations are probably present and may influence the damping. However, the main results are probably unaffected by this complication. Far from T_c , the attenuation α is well described in terms of a single relaxation time τ . Closer to T_c , α increases considerably, as expected from the coupling to the order parameter S : this is a general feature of order-disorder transitions, emphasized in particular by Landau and Khalatnikov [66] in connection with superfluid helium, and refined in subsequent theories. The relaxation rates involved are found to be in the range 10^6 – 10^7 s⁻¹, as could be expected from the results on $c(\omega)$ near T_c . But a picture using a single exponential relaxation is not sufficient to explain the data.

5.4.3.5 Anisotropy of the attenuation

For usual frequencies (in the megacycle range) the attenuation α is much more angular dependent than the velocity c . This has been shown by various groups [67–69]. As a function of the angle θ between the optical axis and the direction of propagation, one can usually fit the attenuation by the form

$$\alpha(\theta) = \alpha(0)[1 - \delta \sin^2 \theta]$$

with $\delta > 0$ and $\delta \sim 0.1$.

It is of some interest to compare this form with predictions of a purely hydrodynamical theory, including the friction coefficients $\alpha_1 \dots \alpha_5$ for an incompressible fluid plus two ‘bulk viscosities’. The relevant formulae have been written down by the Harvard group [4]. They have the form

$$\alpha(\theta) = a + b \sin^2 \theta + c \sin^2 2\theta.$$

The coefficient b involves the bulk viscosities, while the coefficient c depends only on $\alpha_1 \dots \alpha_5$. The experimental results lead us to conclude that the bulk viscosities dominate the attenuation ($b \gg c$).

There is of course a correlation between the attenuation $\alpha(\omega)$ and the velocities $c(\omega)$, which are related respectively to the imaginary and to the real part of certain elastic constants. In an isotropic liquid this correlation is of limited use, because there are too many unknowns; for instance, two velocities at least must be known, $c(\omega = 0)$ and $c(\omega \rightarrow \infty)$. If one studies the anisotropies, however, the correlation is more useful, as first noted by Jähnig [70a], because $\Delta c(\omega = 0)$ vanishes identically in a liquid. From his analysis, it appears that at least two different relaxation processes control the frequency dependence of the bulk viscosities in MBBA: (a) a specific mode of the butyl terminal chain is probably important [70b]; (b) near the clearing point T_c , the order parameter S relaxes rather slowly (as expected for a nearly second-order transition) and is strongly coupled to the density fluctuations. But its effect cannot be described by a simple exponential relaxation.

5.4.4 Translational motions

5.4.4.1 Self-diffusion

A self-diffusion coefficient D has been qualitatively introduced in the last paragraph. More accurately, one must define two diffusion coefficients D_{\parallel} and D_{\perp} . In principle, they can be measured by various techniques, using:

1. Radioactive tracers [71]. For PAA the results at 125°C are $D_{\parallel} = 4 \times 10^{-6} \text{ cm}^2 \text{ s}^{-1}$, $D_{\perp} = 3.3 \times 10^{-6} \text{ cm}^2 \text{ s}^{-1}$.
2. Inelastic scattering of neutrons; this makes use of the large, incoherent scattering due to the protons of the molecule. With a monoenergetic ingoing beam, and a scattering wavevector \mathbf{q} , the energy width of the outgoing beam $\Delta\omega_{\mathbf{q}}$ is given by

$$\Delta\omega_{\mathbf{q}} = D_{\parallel} q_z^2 + D_{\perp} q_{\perp}^2 \quad (5.96)$$

However, eqn (5.96) applies only when $qa \ll 1$; this corresponds to small widths $\Delta\omega_{\mathbf{q}}$, which are rather hard to measure accurately.

Early experiments with low flux reactors were open to some doubt [72, 73]. More recent measurements with higher energy resolution and low q values have recently been performed at Julich, and seem to give diffusion coefficients that are in better agreement with values from other sources.

3. Studies on nuclear spin precession in a magnetic field gradient: the principles of this method can be found for instance in Abragam's treatise [57]. The application to nematic fluids is difficult, because the spin-spin relaxation time T_2 is rather short. However, an interesting progress has been achieved: a special sequence of spin echoes can remove most

of the dipolar interactions that are responsible for T_2 ; this elaborate technique has been set up recently by the Ljubljana group [74], and has allowed for a good measurement of D_{\parallel} in MBBA.

Theoretical estimates of the self-diffusion constants have been given by Franklin [75].

5.4.4.2 Diffusion of a solute

It is often easier to measure D_{\parallel} and D_{\perp} for a solute in the nematic phase than for the nematic molecules themselves. For instance, if the solute is a dye, injected at time $t = 0$ in one small region of the sample, a study of the spatial spread in coloration at later times t is enough to measure D . This technique was used as early as 1917 (to study the diffusion anisotropy of nitrophenol dissolved in azoxyphenetol) by Svedberg [76]: his sample was aligned by a field $H \sim 3000$ G, and he could measure diffusion with concentration gradients either parallel or normal to \mathbf{H} . For this particular example he found $D_{\parallel}/D_{\perp} = 1.41$.

These diffusion studies can give some useful information of solvent-solute interactions. They could also be used to detect a macroscopic conformational change in a nematic; one example is discussed in the following problem.

Problem. A nematic slab is twisted by a field \mathbf{H} larger than the Frederiks threshold H_c . How does the twist react on diffusion in the plane of the slab?

Solution. The geometrical conditions are shown in Fig. 5.12. The slab is in the x, y -plane, with the walls at $z = 0$ and $x = d$. The concentration gradient is taken along x . The easy axis of the walls (\mathbf{n}_0), is at a finite angle ψ from x in the x, y -plane. The field \mathbf{H} is applied to the plane of the slab, normal to \mathbf{n}_0 . Below the threshold field H_c we have a single crystal with optical axis along \mathbf{n}_0 . Above threshold, the molecules at point (x, y, z) make an angle $\psi + \theta(z)$ with the x -axis. For instance, if H is slightly larger than H_c , we have (see Section 3.2)

$$\theta \sim a_0 \sin\left(\frac{\pi z}{d}\right),$$

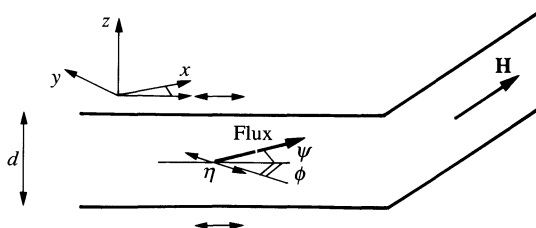


Fig. 5.12. Lateral diffusion in a nematic twisted by a magnetic field \mathbf{H} .

$$a_0 = 2 \left\{ \frac{H - H_c}{H_c} \right\}^{\frac{1}{2}}.$$

The diffusion coefficient, for a concentration gradient along x , is

$$D(z) = D_{\perp} + (D_{\parallel} - D_{\perp}) \cos^2 \{\psi + \theta(z)\}.$$

We shall restrict our attention to diffusion times $t \gg d^2/D$. In this limit the dye concentration becomes independent of z , and depends only on x . The effective diffusion coefficient is then the average of $D(z)$ over the sample thickness

$$\bar{D} = D_{\perp} + (D_{\parallel} - D_{\perp}) \overline{\cos^2(\psi + \theta)}.$$

In particular, for H slightly larger than H_c , this becomes

$$\bar{D} = D_{\psi} - (D_{\parallel} - D_{\perp}) \sin(2\psi)\bar{\theta}$$

$$D_{\psi} = D_{\perp} + (D_{\parallel} - D_{\perp}) \cos^2 \psi$$

$$\bar{\theta} = a_0 \frac{1}{d} \int_0^d \sin\left(\frac{\pi z}{d}\right) dz = \frac{2}{\pi} a_0.$$

Clearly, the optimum situation to detect a threshold amounts to take $\psi = \pi/4$.

5.4.4.3 Mobility of the charge carriers

In an organic semiconductor, the mobility μ of the charge carriers is never easy to measure. In an organic fluid, the situation is still worse; convective motions induced by the electric field give rise to an apparent mobility that is much larger than the intrinsic μ . However, some information on the carrier mobilities in materials such as MBBA can be obtained by (at least) two methods.

1. Studies on transient regime in ultrapure specimens with electrodes suppressing all injection [77].
2. Studies on a.c. instabilities in the limit of very small ‘chevrons’ [78]. The analysis of instabilities in Section 5.2 was based on Ohm’s law $\mathbf{J} = \sigma \mathbf{E}$.† However, when spatial variations become rapid, we must also include a diffusion term

$$\mathbf{J} = \sigma \mathbf{E} - D_c \nabla q \quad (5.97)$$

where the diffusion constant of the carriers D_c is related to σ by Einstein’s relation

$$D_c = \frac{k_B T \sigma}{ne^2} = \frac{k_B T}{e} \mu \quad (5.98)$$

(e = charge of the carriers, n = number of carriers per cm^3).

† For simplicity, we neglect here the anisotropy of σ , μ , etc.

If we take the divergence of \mathbf{J} and use Poisson's equation to eliminate \mathbf{E} we find

$$\operatorname{div} \mathbf{J} = \frac{4\pi\sigma}{\epsilon} \tau - D_c \nabla^2 \mathbf{q} = \left(\frac{4\pi\sigma}{\epsilon} + D_c k^2 \right) q \quad (5.99)$$

where \mathbf{k} is the wavevector of the perturbation. This may also be written as

$$\operatorname{div} \mathbf{J} = \frac{4\pi\sigma}{\epsilon} q(1 + k^2 r_D^2) \quad (5.100)$$

where the length r_D is defined by

$$r_D = \left\{ \frac{D_c \epsilon}{4\pi\sigma} \right\}^{\frac{1}{2}} = \left\{ \frac{\epsilon k_B T}{4\pi n e^2} \right\}^{\frac{1}{2}}.$$

r_D is nothing else but the Debye–Hückel screening radius, associated with the mobile carriers, and familiar from the theory of electrolytes [79]. Equation (5.100) shows that diffusion begins to play an important role in the charge balance when $kr_d \sim 1$; when the size of the parallel striations decreases down to r_d , the formulae of Section 5.3 break down. This observation, due to Dubois Violette and Parodi [48], allows for a measurement of r_d (which turns out to be typically of order 1 μm). Knowing r_d , one can derive the carrier density n from (5.101), and from n plus the measured conductivity σ , one finally reaches the mobility μ (eqn (5.98)).

Both methods for the measurement of μ have been put into practice only recently, and the results are not yet firmly established. But the existing data (for MBBA at room temperature) give rather low values of μ

$$\mu \sim 10^{-6}\text{--}10^{-5} \text{ cm}^2 \text{ s}^{-1} \text{ V}^{-1}.$$

These numbers are significantly smaller than might be expected from viscous friction on a Stokes' sphere of molecular size. Various interpretations of this effect may be suggested.

1. The mobile ions may be of unusually large size.
2. A charged ion deforms the nematic alignment (through its electric field) up to rather large distances. When the ion moves, the distortion must adjust accordingly; this provides an additional friction.
3. Apart from any distortion, when the ion moves, there is a certain lag in the electric polarization cloud surrounding it. As explained in Section 5.4.1, the component of the dielectric response due to longitudinal dipoles has a slow relaxation; this tends to increase the lag and the resulting friction [80]. In practice, as pointed out by R. B. Meyer, when the individual dipoles in the nematic flip very slowly, the main relaxation channel for the polarization cloud is by spatial diffusion of the dipoles around the ion. A rough calculation

based on this idea gives an enhancement of friction

$$\frac{\Delta f}{f} \sim 0.1 \frac{\epsilon_\infty(\epsilon_0 - \epsilon_\infty)}{\epsilon_\infty} \frac{c}{a}$$

where a is the ionic radius, ϵ_0 and ϵ_∞ are the low- and high-frequency dielectric constants, and c is a characteristic length defined by

$$c \sim \frac{e^2}{\epsilon_0 k_B T}.$$

Typically c is of order 100 Å and $\Delta f/f \sim 2$. Clearly, to see if these processes are indeed important, detailed studies with nematics of different dielectric properties will be required.

5.4.5 Temperature variation of the friction coefficients

The Leslie coefficients introduced in Section 5.1 (eqn (5.27)) are related to certain local correlations in the fluid. From their temperature dependence two simple features emerge.

1. The friction coefficients show an activation energy behaviour (as is found in most fluids far below their gas–liquid critical point).
2. However, in the vicinity of the clearing point ($T \lesssim T_c$) there is a difference in behaviour between the various coefficients: α_4 , which does not involve the alignment properties, is a rather smooth function of temperature; but all the other α s describe couplings between orientation and flow, and are thus affected by a decrease in the nematic order.

For instance, near T_c , the α_1 term of eqn (5.27)

$$\alpha_1 n_\alpha n_\beta n_\mu n_\rho A_{\mu\rho},$$

is more usefully written in the form

$$\tilde{\alpha}_1 Q_{\alpha\beta} Q_{\mu\rho} A_{\mu\rho}$$

where $Q_{\alpha\beta}$ is the tensor order parameter introduced in Chapter 2, and $\tilde{\alpha}_1$ is a new coefficient which (in mean-field theory) remains finite for $Q \rightarrow 0$. This means that α_1 should then be proportional to Q^2 (or S^2 in the Maier–Saupe notation). A similar argument suggests that α_2 , α_3 , α_5 , and α_6 , should be linear in S [81]. However, certain combinations of these coefficients are expected to vanish faster. For instance, $\gamma_1 = \alpha_3 - \alpha_2$ should be proportional to S^2 in the mean-field approximation [82]. This will be explained in the next section.

5.4.6 Semi-slow motions above T_c

In Chapter 2, we discussed some short-range order effects occurring above the nematic-isotropic transition temperature T_c . We concluded that, just above T_c , the fluid contained correlated regions of size $\xi(T_c) \sim 200 \text{ \AA}$. Let us consider the dynamical properties of such a structure in more detail.

One molecule in the fluid rotates with a very short time constant (10^{-11} s). But, for an object of size $\xi(T_c)$, any overall rotation or deformation is less rapid (time constant of the order of 10^{-7} s). We shall say that such a process is *semi-slow*. Our information on these motions comes from the following types of measurements (some of which have been announced in Chapter 2):

- flow birefringence [83];
- inelastic scattering of light [84];
- nuclear spin lattice relaxation [56];
- ultrasonic attenuation of shear waves [85], and also (less directly) of longitudinal waves;
- time constants of the electric birefringence (Kerr effect) [86], [87]

Since these phenomena involve rather large regions and semi-slow motions in the fluid, they may be described macroscopically in terms of rate equations for the order parameters $Q_{\alpha\beta}$ (defined as in Chapter 2) [88]. However, just as below T_c , we have a certain coupling between orientation and flow. To describe it, we must again introduce two sets of fluxes.

The first is the rate of change of the order parameter

$$\frac{\delta Q_{\alpha\beta}}{\delta t} = \dot{Q}_{\alpha\beta}. \quad (5.101)$$

Note that, in principle, the derivative $\delta/\delta t$ should represent the variation of Q , along one flow line, and with respect to the background fluid; $\delta Q/\delta t$ is the analogue, above T_c , of the vector $\mathbf{N} = \dot{\mathbf{n}} - \boldsymbol{\omega} \times \mathbf{n}$ of Section 5.1. However, for the motion of interest above T_c , we may usually treat $Q_{\alpha\beta}$ and the flow velocities v_α as infinitesimal quantities of first order; then, the difference between $\delta Q/\delta t$ and the partial derivative $\partial Q/\partial t$ is negligible.

The other set of fluxes remains, as in Section 5.1, the shear rate tensor $A_{\alpha\beta}$ defined by eqn (5.18). We also restrict our attention to incompressible flows ($A_{\alpha\alpha} \equiv 0$): this will be justified for the applications listed above, because the semi-slow motions of interest are at much lower frequencies than sound waves.

We now write the entropy source

$$T\dot{S} = \dot{Q}_{\alpha\beta}\Phi_{\alpha\beta} + \sigma'_{\alpha\beta}A_{\alpha\beta} \quad (5.102)$$

where $\sigma'_{\alpha\beta}$ is again the viscous stress. The force $\Phi_{\alpha\beta}$ is the restoring force

derived from the free energy F : (eqn (2.67)) of Chapter 2

$$\Phi_{\alpha\beta} = -\frac{\partial F}{\partial Q_{\alpha\beta}} = -A(T)Q_{\alpha\beta}. \quad (5.103)$$

In eqn (5.103) we have kept only the term that was linear in Q , and we have assumed $\mathbf{H} = 0$. We can now construct a set of phenomenological equations relating the forces to the fluxes—all of them being symmetric traceless tensors of rank 2. The most general form for these equations, compatible with rotational invariance and with the Onsager symmetry relation, is then [88]

$$\sigma'_{\alpha\beta} = 2\eta A_{\alpha\beta} + 2\mu \dot{Q}_{\alpha\beta}, \quad (5.104)$$

$$\Phi_{\alpha\beta} = 2\mu A_{\alpha\beta} + v \dot{Q}_{\alpha\beta}. \quad (5.105)$$

If Q is dimensionless (and normalized so that $Q_{zz} = 1$ in a completely ordered phase) the three coefficients η, μ, v have the dimension and the magnitude of a viscosity. Nematodynamics above T_c involves only three parameters, while below T_c , five parameters were required (in an incompressible fluid). This simplification comes from the fact that $Q_{\alpha\beta}$ is small above T_c . Writing that TS is positive definite for all motions, and inserting into eqn (5.102), one obtains the conditions

$$\eta > 0, \quad 2\mu^2 < v\eta, \quad v > 0. \quad (5.106)$$

Let us now show briefly how the three parameters η, μ, v can be related to experimental data.

5.4.6.1 Flow birefringence

Consider, for instance, a shear flow with v along x , and a velocity gradient along z ($A_{xz} \neq 0$). This is a steady state, with $\dot{Q}_{\alpha\beta} = 0$. Inserting this into eqn (5.105) we get, after making use of eqn (5.103)

$$Q_{xz} = -\frac{2\mu}{A(T)} A_{xz} = -\frac{\mu}{A(T)} \frac{\partial v}{\partial z}, \quad (5.107)$$

while all other components of $Q_{\alpha\beta}$ are equal to zero. The tensor $Q_{\alpha\beta}$ has then two principal axes (labelled 1 and 2) that are the bisectors of x and z .

$$Q_{11} = -Q_{22}, \quad Q_{33} = 0,$$

$$|Q_{11} - Q_{22}| = \frac{2\mu}{A(T)} \left| \frac{\partial v}{\partial z} \right|. \quad (5.108)$$

Thus the material is birefringent, and the magnitude of the birefringence is large, since $A(T)$ is small near T_c .

5.4.6.2 Inelastic scattering of light

At small scattering wavevectors \mathbf{q} the fluctuations of the hydrodynamic velocity are very slow (relaxation rates $\eta q^2/\rho$) while those of Q are only

semi-slow; then the coupling between orientation and flow becomes ineffective and, in eqn (5.105), the shear rate component $A_{\alpha\beta}$ is negligible. This gives a simple exponential relaxation for $Q_{\alpha\beta}$, with a rate (deduced from eqns 5.103 and 5.105)

$$\Gamma(T) = \frac{A(T)}{\nu} \quad (5.109)$$

Because of the small factor $A(T)$, $\Gamma(T)$ is reduced: this is the origin of the semi-slow motions. We may say that the restoring force (5.103) is small near T_c .

The width in frequency of the light scattered by orientation fluctuations is equal to $\Gamma(T)$: it has been measured on MBBA using refined Fabry–Perot techniques [84]. The values of Γ are in the range 10^7 s^{-1} and $\Gamma(T)$ increases rapidly when T increases above T_c . This increase is due mainly to the factor $A(T)$, which can be derived from the data on magnetic birefringence (see Chapter 2). By comparing $\Gamma(T)$ and $A(T)$, it appears that the friction coefficient varies with temperature very much like the average viscosity η (Fig. 5.13).

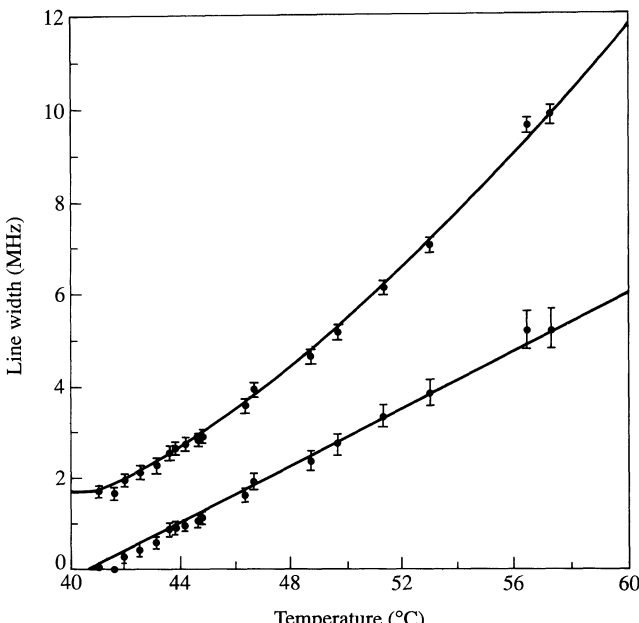


Fig. 5.13. Line width $\Gamma(T)$ of the inelastic scattering of light. Upper curve: raw data for MBBA; lower curve: $\Gamma\eta(T_c)/\eta(T)$. (The temperature dependence of the friction coefficients is removed.) (After reference 72.)

The above discussion was restricted to very small scattering wavevectors \mathbf{q} . At larger q values,[†] the admixture between orientational and hydrodynamic modes complicates the situation slightly (see reference 74) but the orders of magnitude remain the same.

5.4.6.3 Shear wave attenuation

From eqns (5.104) and (5.105) after elimination of the internal variables $Q_{\alpha\beta}$, it is easy to derive an effective, frequency-dependent, viscosity $\eta(\omega)$

$$\eta(\omega) = \eta - \frac{2\mu^2}{\nu} \frac{i\omega}{\Gamma + i\omega}. \quad (5.110)$$

Equation (5.110) shows a dispersion anomaly at $\omega \simeq \Gamma$: above this frequency, the molecular alignment is not able to adjust to the shear. In the transient Kerr effect [86, 87] it is also the constant Γ that gives the relaxation rate.

5.4.6.4 Nuclear spin-lattice relaxation

This is also a probe for the dynamical fluctuations of $Q_{\alpha\beta}$. In this case, the analysis requires more sophistication: the spatial derivatives of Q must be included in the free energy and in the friction equations.

Qualitatively, one may understand the relaxation line T_1 from the following argument. The relaxation rate contains a component, due to the fluctuations of Q , of the form

$$\frac{1}{T_1} \cong (\gamma H_L)^2 \langle Q^2 \rangle \tau_c \quad (5.111)$$

where $H_L Q$ measures the local field seen by one nucleus (we omit all component indices). γ is the nuclear gyromagnetic ratio, and τ_c a correlation time for the fluctuations of Q :[‡] here τ_c will be essentially equal to Γ^{-1} . The average $\langle Q^2 \rangle$ is not exactly to be taken at one point, but must be taken as a smeared out average $\langle Q(0)Q(R) \rangle$ with $R \sim \xi$.[§] To a good approximation, the correlation function $\langle Q(0)Q(R) \rangle$ has the Ornstein-Zernike form

$$\langle Q(0)Q(R) \rangle = \frac{a}{R} \exp(-R/\xi_c) \quad (5.112)$$

where a is a molecular length. Equations (5.111) and (5.112) lead to a

[†] I.e. when $\eta q^2/\rho \sim \Gamma$.

[‡] Equation (5.111) holds only for nuclear resonance frequencies ω_n which are not too high ($\omega_n \tau_c < 1$). For an introduction to the concepts leading to eqn (5.111), see for instance, reference 57.

[§] Among other reasons for this smearing is the fact that, during the time τ_c , the molecule diffuses through the swarm.

relaxation rate

$$\frac{1}{T_1} \cong (\gamma H_L)^2 \frac{a}{\xi} \tau. \quad (5.113)$$

We have seen that τ_c varies essentially as ξ^2 . Thus we expect $1/T_1$ to be proportional to ξ , i.e. to $(T - T^*)^{-\frac{1}{2}}$ in the Landau approximation. A power law of this type has indeed been observed with the relaxation of ^{14}N (controlled by modulations of a quadrupolar field) in PAA [56].

5.4.6.5 Connection between the dynamics above and below T_c

Whenever the nematic-isotropic transition is nearly of second order, there is a certain link between the five Leslie coefficients (defined below T_c) and the three friction coefficients defined above T_c by eqns (5.104) and (5.105). We shall show this here for the coefficient $\gamma_1 = \alpha_3 - \alpha_2$. Consider a situation without flow ($A_{\alpha\beta} \equiv 0$), the nematic molecules rotating at a constant speed ω , $n_x = \cos \omega t$, $n_y = \sin \omega t$, $n_z = 0$.

The corresponding dissipation is, from eqn (5.21),

$$T\dot{S} = \gamma_1 \omega^2 = \gamma_1 \left(\frac{d\mathbf{n}}{dt} \right)^2. \quad (5.114)$$

But if we are in the vicinity of T_c (Q small), we can also derive $T\dot{S}$ from eqns (5.102)–(5.105),

$$T\dot{S} = v \dot{Q}_{\alpha\beta} \dot{Q}_{\alpha\beta}. \quad (5.115)$$

Writing $Q_{\alpha\beta} = Q(3n_\alpha n_\beta - \delta_{\alpha\beta})$, performing the operations in eqn (5.115), and keeping in mind the fact that \mathbf{n} is a unit vector ($n_\alpha \dot{n}_\beta = 0$), one arrives at the form (5.114) with

$$\gamma_1 = 18vQ^2. \quad (5.116)$$

Thus, in the Landau approximation, γ_1 vanishes like Q^2 , as first noticed, on a specific model, by Farinha Martins.

REFERENCES

1. Ericksen, J. L. *Arch. ration. Mech. Analysis* **4**, 231 (1960); *Phys. Fluids* **9**, 1205 (1966).
2. Leslie, F. M. *Quart. J. Mech. appl. Math.* **19**, 357 (1966); *Arch. ration. Mech. Analysis* **28**, 265 (1968).
3. Parodi, O. *J. Phys. (Paris)* **31**, 581 (1970).
4. Forster, D., Lubensky, T., Martin, P., Swift, J., and Pershan, P. *Phys. Rev. Lett.* **26**, 1016 (1971); Martin, P. C., Parodi, O., and Pershan, P. *J. Phys. Rev. A* **6**, 2401 (1972). See also Stephen, M. J. *Phys. Rev. A* **2**, 1558 (1970); Jähnig, F. and Schmidt, M. *Ann. Phys.* **71**, 129 (1971).
5. Martin, P. C., Pershan, P. J., and Swift, J. *Phys. Rev. Lett.* **25**, 844 (1970).

6. Haller, I. and Litster, J. D. *Phys. Rev. Lett.* **25**, 1550 (1970).
7. de Groot, S. and Mazur, P. *Non-equilibrium thermodynamics*. North-Holland, Amsterdam (1962); Dover Publications, New York (1984).
8. Miesowicz, M. *Nature* **17**, 261 (1935); *Bull. Acad. Pol. Sci.* **A228** (1936); *Nature* **158**, 27 (1946).
9. Pieranski, P. and Guyon, E. *Phys. Lett.* **49A**, 237 (1974).
10. (a) Martinoty, P. and Candau, S. *Mol. Cryst. liquid Cryst.* **14**, 243 (1971); Martinoty, P. Unpublished D.Phil. thesis, Strasbourg University (1972); (b) Langevin, D. *J. Phys. (Paris)* **33**, 249 (1971).
11. See, for example, Landau, L. D. and Lifshitz, E. M. *Fluid mechanics*, Section 24. Pergamon, London (1959).
12. Porter, R. S. and Johnson, J. F. *J. phys. Chem.* **66**, 1826 (1962); *J. chem. Phys.* **45**, 1452 (1966). See also *J. appl. Phys.* **34**, 51, 55 (1963).
13. (a) Fisher, J. and Wahl, J. *Mol. Cryst.* **22**, 359 (1973). (b) Fisher, J. and Wahl, J. *Opt. Commun.* **5**, 341 (1972). (c) See also Gahwiller, J. *Phys. Rev. Lett.* **28**, 1554 (1972); (d) Meiboom, S. and Hewitt, R. C. *Phys. Rev. Lett.* **30**, 261 (1973).
14. (a) Leslie, F. M. *Arch. ration. Mech. Analysis* **28**, 265 (1968); Atkin, R. J. and Leslie, F. M. *Quart. J. Mech. appl. Math.* **23**, 3 (1970); Currie, P. K. *Arch. ration. Mech. Analysis* **37**, 222 (1970). (b) Erickson, J. L. *Trans. Soc. Rheol.* **13**, 9 (1969). (c) Fisher, J. and Frederikson, A. G. *Mol. Cryst. liquid Cryst.* **8**, 267 (1969).
15. Pieranski, P. and Guyon, E. *Solid State Commun.* **13**, 435 (1973); *Physica* **73**, 184 (1974); *J. Phys. (Paris) Colloq.* **36** (Suppl. C1), 209 (1975).
16. (a) Tsvetkov, V. *Zh. eksp. teor. Fiz.* **9**, 603 (1935); Tsvetkov, V. and Sosnovskii, A. *Acta physicochem. USSR* **18**, 358 (1943). (b) Gasparoux, H. and Prost, J. *Phys. Lett.* **A36**, 245 (1971). (c) Leslie, F. M., Luckhurst, G. R., and Smith, H. J. *Chem. Phys. Lett.* **13**, 368 (1972).
17. de Gennes, P. G. *J. Phys. (Paris)* **32**, 789 (1971); Léger, L. *Solid State Commun.* **10**, 697 (1972).
18. Gasparoux, H. and Prost, J. *J. Phys. (Paris)* **32**, 953 (1971); Flanders, P. J. *Mol. Cryst.* **29**, 19 (1974).
19. Brochard, F., Léger, L., and Meyer, R. B. *J. Phys. (Paris)* **36** (Suppl. C1), 209 (1975).
20. Brochard, F., Guyon, E., and Pieranski, P. *Phys. Rev. Lett.* **28**, 1681 (1972).
21. See, for example, Friedel, G. *Ann. Phys., Paris* **18**, 273 (1922) (in particular, p. 359).
22. (a) Orsay Group on Liquid Crystals. *J. chem. Phys.* **51**, 816 (1969). (b) See, for example, the review by Benedek, G. In *Polarisation, matière, rayonnement*. Presses Universitaires de France, Paris (1969).
23. Orsay Group on Liquid Crystals. *Mol. Cryst. liquid Cryst.* **13**, 187 (1971); Léger, L. Thèse 3e cycle, Orsay (1971).
24. Heilmeier, G., Zanoni, L. A., and Barton, L. *Proc. IEEE* **56**, 1162 (1968).
25. Yun, C. K. *Phys. Lett.* **43A**, 369 (1973).
26. Gahwiller, J. *Phys. Lett.* **36A**, 311 (1971); see also *Mol. Cryst.* **20**, 301 (1973).
27. Martinand, J. L. and Durand, G. *Phys. Rev. Lett.* **29**, 562 (1972).
28. Haller, I. *J. chem. Phys.* **57**, 1400 (1972); Haller, I. and Litster, J. D. *Mol. Cryst.* **12**, 277 (1971).
29. Brochard, F., Pieranski, P., and Guyon, E. *C.R.Acad. Sci., Paris* **273**, 486 (1971); *Phys. Rev. Lett.* **28**, 1681 (1972).
30. Cladis, P. E. *Phys. Rev. Lett.* **28**, 1629 (1972).

31. (a) Léger, L. *Solid State Commun.* **11**, 1499 (1972); (b) **10**, 697 (1972).
32. Helfrich, W. *J. chem. Phys.* **51**, 4092 (1969).
33. Svedberg, T. *Ann. Phys.* **44** (1914); **46** (1916).
34. See, for example, Klingbiel, R., Genova, D., and Bucher, H. *Mol. Cryst.* **27**, 1 (1974).
35. See Gaspard, F., Herino, R., and Mondon, F. *Mol. Cryst.* **24**, 145 (1973).
36. See Haller, I., Young, W., and Gladstone, G. *Mol. Cryst.* **24**, 249 (1973).
37. Rondelez, F. *Solid State Commun.* **12**, 1675 (1972).
38. See the review by Felici, N. *Revue gén. elect.* **78**, 77 (1969).
39. Williams, R. J. *chem. Phys.* **39**, 384 (1963).
40. Teaney, D. and Migliori, A. *J. appl. Phys.* **41**, 998 (1970); Orsay Group on Liquid Crystals. *C.R. Acad. Sci., Paris* **270**, 97 (1970); Penz, P. A. *Phys. Rev. Lett.* **24**, 1405 (1970).
41. For a review see Helfrich, W. *Mol. Cryst.* **21**, 187 (1972).
42. See, for example, Chandrasekhar, S. *Theory of hydrodynamic stability*. Oxford University Press, Oxford (1961).
43. Carr, E. F. In *Ordered fluids and liquid crystals*, Advanced Chemistry Series, p. 76. American Chemical Society, Washington DC (1967).
44. (a) Gruler, H. *Mol. Cryst.* **27**, 31 (1974). (b) Penz, P. A. and Ford, G. W. *Phys. Rev.* **6**, 414 (1972).
45. Heilmeier, G. and Helfrich, W. *Appl. Phys. Lett.* **16**, 1955 (1970).
46. Rondelez, F. Thèse 3e cycle, Orsay (1970); Orsay Group on Liquid Crystals. *Mol. Cryst. liquid Cryst.* **12**, 251 (1971).
47. Film available from the General Electric Company.
48. Dubois Violette, E., de Gennes, P. G., and Parodi, O. *J. Phys. (Paris)* **32**, 305 (1971).
49. Pieranski, P., Guyon, E. and Dubois Violette, E. *Phys. Rev. Lett.* **30**, 736 (1973); *Mol. Cryst.* **26**, 193 (1974).
50. See, in particular, Carr, E. F. *J. chem. Phys.* **38**, 1536 (1963); **39**, 1979 (1963); **42**, 738 (1965); **43**, 1536 (1965).
51. Maier, W. and Meier, G. *Z. Naturforsch.* **A16**, 262 (1961).
52. Meier, G. and Saupe, A. *Mol. Cryst.* **1**, 515 (1966); Martin, A. J., Meier, G., and Saupe, A. *Symp. Faraday Soc.* **5**, 119 (1971).
53. Visintainer, J., Doane, J. W., and Fishel, D. *Mol. Cryst.* **13**, 69 (1971).
54. (a) Vilfan, M., Blinc, R., and Doane, J. W. *Solid State Commun.* **11**, 1073 (1972); (b) Doane, W., Tarr, C., and Nickerson, M. *Phys. Rev. Lett.* **33**, 620 (1974).
55. Farinha Martins, A. *Phys. Rev. Lett.* **28**, 289 (1972).
56. Cabane, B. and Clarke, G. *Phys. Rev. Lett.* **25**, 91 (1970); Gosh, S., Tettamanti, E., and Indovina, E. *Phys. Rev. Lett.* **29**, 638 (1973).
57. See, for example, Abragam, A. *Principles of nuclear magnetism*, Chapter 8. Clarendon Press, Oxford (1961).
58. Pincus, P. *Solid State Commun.* **7**, 415 (1969). See also Blinc, R., Hogenboom, D., O'Reilly, D., and Peterson, E. *Phys. Rev. Lett.* **23**, 969 (1969).
59. Doane, J. W. and Johnson, D. L. *Chem. Phys. Lett.* **6**, 291 (1970).
60. Lubensky, T. *Phys. Rev. A2*, 2497 (1970).
61. Hoyer, W. and Nolle, A. W. *J. chem. Phys.* **24**, 803 (1956).
62. Kapustin, A. and Evereva, G. *Kristallographia* **10**, 723 (1965).

63. Kapustin, A. and Martianova, L. *Kristallographia* **16**, 649 (1970).
64. Mullen, M., Lüthi, B., and Stephen, M. J. *Phys. Rev. Lett.* **28**, 799 (1972).
65. Eden, D., Garland, C., and Williamson, R. *J. chem. Phys.* **58**, 1861 (1973).
66. Landau, L. and Khalatnikov, I. *Dokl. Akad. Nauk SSSR* **96**, 469 (1954).
67. Lord, A. E. and Labes, M. *Phys. Rev. Lett.* **25**, 570 (1970).
68. Kemp, K. and Letcher, S. *Phys. Rev. Lett.* **27**, 1634 (1971).
69. Lieberman, E., Lee, J., and Moon, F. *Appl. Phys. Lett.* **18**, 280 (1971).
70. (a) Jähnig, F. *Z. Phys.* **258**, 199 (1973). (b) Jähnig, F. *Chem. Phys. Lett.* **23**, 262 (1973).
71. Yin, G. and Frederikson, G. *Mol. Cryst. liquid Cryst.* **12**, 73 (1970).
72. Blinc, R., Dimic, V., Pirš, J., Vilfan, M., and Zupančič, I. *Mol. Cryst. liquid Cryst.* **14**, 97 (1971); Murphy, J. A. and Doane, J. W. *Mol. Cryst. liquid Cryst.* **13**, 93 (1971).
73. Janik, J. A., Janik, J. M., Otnes, K., and Riste, T. *Mol. Cryst. liquid Cryst.* **15**, 189 (1971).
74. Blinc, R., Pirš, J., and Zupančič, I. *Phys. Rev. Lett.* **30**, 546 (1973).
75. Franklin, W. *Mol. Cryst. liquid Cryst.* **14**, 227 (1971).
76. Svedberg, T. *Kolloidzeitschrift* **22**, 68 (1918).
77. (a) Heilmeier, G., Ranoni, L., and Barton, L. *IEEE Trans. electron Devices* **ED17**, 22 (1970); Koelmans, H. and van Boxtel, A. *Mol Cryst.* **7**, 395 (1969). (b) Brière, G., Gaspard, F., and Herino, R. *Chem. Phys. Lett.* **9**, 285 (1971); Brière, G., Herino, R., and Mondron, F. *Mol. Cryst.* **19**, 157 (1972).
78. See Galerne, Y., Durand, G., and Veyssie, M. *Phys. Rev. A* **6**, 484 (1972).
79. See, for example, Landau, L. D. and Lifshitz, E. M. *Statistical physics*, Section 91. Pergamon Press, London (1958).
80. de Gennes, P. G. *Comments Solid State Phys.* **3**, 148 (1971).
81. Imura, H. and Okano, K. *Jap. J. appl. Phys.* **11**, 440 (1972).
82. Farinha Martins, A. *Part. Phys.* **9** (1), 1 (1974).
83. Zvetkov, V. *Acta phys. chim. USSR* **19**, 86 (1944).
84. Litster, J. D. and Stinson, T. W. *J. appl. Phys.* **41**, 996 (1970); *Phys. Rev. Lett.* **25**, 503 (1970). Litster, J. D. In *Critical phenomena* (ed. R. E. Mills), p. 394. McGraw-Hill, New York (1971).
85. Martinoty, P., de Beauvais, F., and Candau, S. *Phys. Rev. Lett.* **27**, 1123 (1971).
86. Prost, J. and Lalanne, J. R. *Phys. Rev.* **8**, 2090 (1973).
87. Wong, W. and Shen, Y. *Phys. Rev. Lett.* **30**, 895 (1973); *J. chem. Phys.* **59**, 2068 (1973).
88. de Gennes, P. G. *Phys. Lett.* **A30**, 454 (1969); *Mol. Cryst. liquid Cryst.* **12**, 193 (1971).

CHOLESTERICS

‘Dove sono quei vortici di foco pien d’orrore?’

Don Giovanni

6.1 OPTICAL PROPERTIES OF AN IDEAL HELIX

6.1.1 The planar texture

The helical arrangement characteristic of the cholesteric phase has been presented in Chapter 1. In this ideal state the director $\mathbf{n}(\mathbf{r})$ varies in space according to the law

$$\begin{aligned} n_x &= \cos \theta \\ n_y &= \sin \theta \end{aligned} \tag{6.1}$$

$$\begin{aligned} n_z &= 0 \\ \theta &= q_0 z + \text{constant} \end{aligned} \tag{6.2}$$

where we have taken the helical axis along z . A cholesteric single crystal, described by eqns (6.1) and (6.2), can often be obtained in thin slabs (thickness d in the 100 μm range)—provided that the boundary conditions on both sides of the slab are *tangential*. The configuration is represented in Fig. 6.1; it is usually called the ‘planar texture’ or ‘Grandjean texture’. Typical examples include the following.

1. Between one polished glass surface and a free surface. At the glass surface ($z = 0$) the angle $\theta(0)$ is fixed by the polishing direction. At the free surface ($z = d$), the angle $\theta(d)$ is free to adjust.
2. Between two polished glass surfaces, or in a cleavage gap between two mica sheets. Here both angles $\theta(0)$ and $\theta(d)$ are fixed. The helix must in general adjust its pitch slightly in order to comply to these conditions: the wavevector q' in eqn (6.2) is now different from q_0

$$\begin{aligned} q'd &= \theta(d) - \theta(0) + n\pi \\ (n &= \text{integer}), \end{aligned}$$

the value of n being chosen to minimize the distortion energy—i.e. to minimize $|q' - q_0|$.

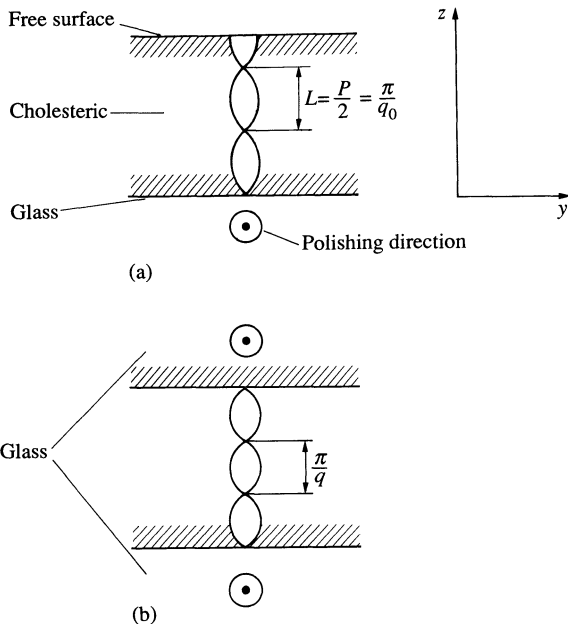


Fig. 6.1. The planar texture of cholesterics. The director is horizontal everywhere. In case (a) the helix has the optimum pitch. In case (b) the pitch is enforced by the boundary conditions.

Let us now recall briefly a point of notation: the nominal pitch P of the helical structure is equal to $2\pi/q_0$; however, since the states (\mathbf{n}) and $(-\mathbf{n})$ are indistinguishable, the periodicity interval along z is $L = P/2 = \pi/q_0$.

We must also remember the question of sign: if the (xyz) frame used in eqn (6.1) is a right-handed frame, and if the wave vector q_0 is positive, we have a right-handed helix; this is found for instance with cholesterol chloride. If q_0 is negative, we have a left-handed helix: most of the aliphatic esters of cholesterol belong to this class.

6.1.2 Bragg reflections

A light beam, of angular frequency ω , is sent parallel to the helical axis (z). In a zero-order approximation, we may think of the cholesteric as of a nearly isotropic medium, with a certain average index of refraction \bar{n} . The optical wavelength in the medium is then

$$\lambda = \frac{2\pi c}{\bar{n}\omega}. \quad (6.3)$$

We may also define the beam by the wave vector \mathbf{k}_0 , directed along z , and of magnitude $\omega n/c$: both notations will be useful.

In the next approximation, we note that the medium is not exactly isotropic; the optical properties are modulated with a spatial period q_0 . This may in principle give rise to Bragg reflections, provided

$$2L = m\lambda \quad (m = \text{integer}). \quad (6.4)$$

Experimentally, one does observe *one* Bragg reflection ($m = 1$). The higher order reflections ($m = 2, 3, \dots$) are forbidden for normal incidence. The polarization features of the waves are also remarkable [1].

1. The reflected light is circularly polarized: at any instant t the electric field pattern in the reflected wave is a helix, identical in shape to the cholesteric helix (see Fig. 6.2(a)), in sharp contrast with a reflection from a mirror (Fig. 6.3).
2. If we analyze the incident wave into two components of opposite circular polarizations, we find that only one component is strongly reflected—i.e. the component for which the instantaneous electric pattern is again identical in shape to the cholesteric helix. The other component is transmitted without any significant reflection through the slab. These features are also displayed in Fig. 6.2.

All these properties can be explained in terms of the scattering amplitude α introduced in Chapter 3 (eqn (3.81))

$$\alpha = \mathbf{f} \cdot \boldsymbol{\epsilon}(\mathbf{q}) \cdot \mathbf{i} \quad (6.5)$$

where \mathbf{f} and \mathbf{i} represent the polarizations of the reflected waves (of wave vector \mathbf{k}_1) and of the incident wave (wavevector \mathbf{k}_0). $\mathbf{q} = \mathbf{k}_0 - \mathbf{k}_1$ is the scattering wavevector, and $\boldsymbol{\epsilon}(\mathbf{q})$ the Fourier transform of the dielectric tensor. In the present case, the three vectors \mathbf{k}_0 , \mathbf{k}_1 , and \mathbf{q} will be parallel to (z) . As explained in Chapter 1, at any point \mathbf{r} a cholesteric behaves locally like a uniaxial material: the dielectric tensor may thus be written

$$\epsilon_{\alpha\beta}(\mathbf{r}) = \epsilon_{\perp} \delta_{\alpha\beta} + (\epsilon_{\parallel} - \epsilon_{\perp}) n_{\alpha}(\mathbf{r}) n_{\beta}(\mathbf{r}). \quad (6.6)$$

Using eqn (6.1) for $\mathbf{n}(\mathbf{r})$ we can compute $\boldsymbol{\epsilon}(\mathbf{r})$ and then $\boldsymbol{\epsilon}(\mathbf{q})$. For $q \neq 0$ a constant term like ϵ_{\perp} does not contribute. To illustrate the calculation let us discuss the (xx) component of the dielectric tensor

$$\epsilon_{xx}(\mathbf{q}) = \epsilon_a \int d\mathbf{r} \cos^2(q_0 z) e^{iqz} \quad (6.7)$$

$$(\epsilon_a = \epsilon_{\parallel} - \epsilon_{\perp}).$$

Writing

$$\cos^2(q_0 z) = \frac{1}{2} + \frac{1}{4}(e^{2iq_0 z} + e^{-2iq_0 z})$$

and eliminating again the constant term, we see that the integral (6.7)

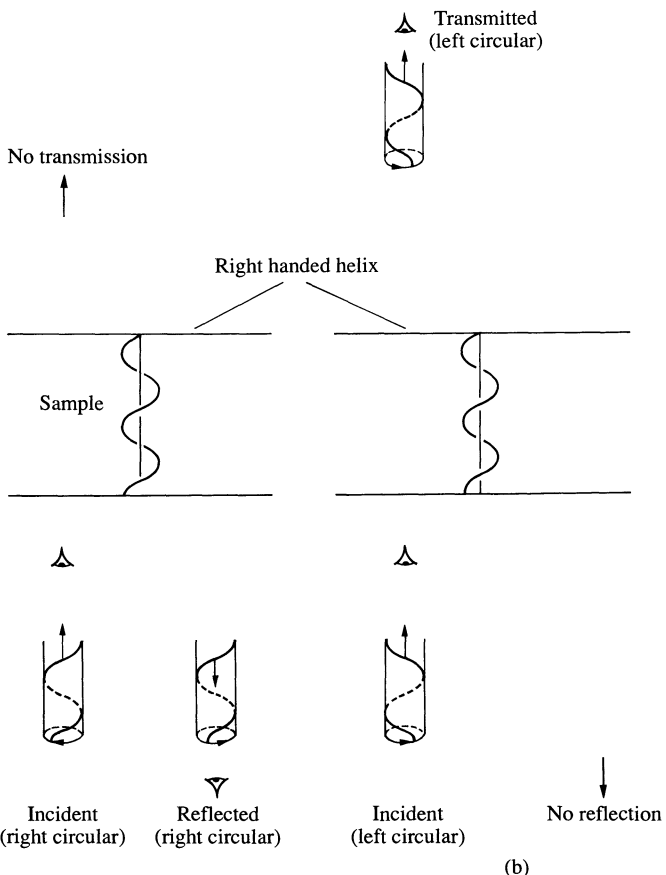


Fig. 6.2. Bragg reflection and transmission by a slab in the planar texture. The cylinders with helices S represent ‘snapshots’ of the electric field \mathbf{E} associated with one wave. The vertical arrows give the direction of propagation. The circles C show the rotation of \mathbf{E} as seen by an observer at one fixed point in space. The reflected wave emitted by the sample is an image of the cholesteric helix, translated downwards. Examination of the corresponding projected path C shows that it is *right circular*.

vanishes except when $q = \pm 2q_0$. Let us take $q_0 > 0$ (right-handed helix). Then the case $q = -2q_0$ corresponds to k_1 larger than k_0 , and is forbidden, since the frequency of the scattered wave must coincide with ω .

The case of interest is $q = 2q_0$, corresponding to $k_0 = -k_1 = q_0$. The reader will check that this condition is identical to eqn (6.4) with $m = 1$. Then

$$\epsilon_{xx}(2q_0) = \frac{1}{4}\epsilon_a V$$

where V is the sample volume.

Similar manipulations give the other components of $\epsilon(2q_0)$: the only

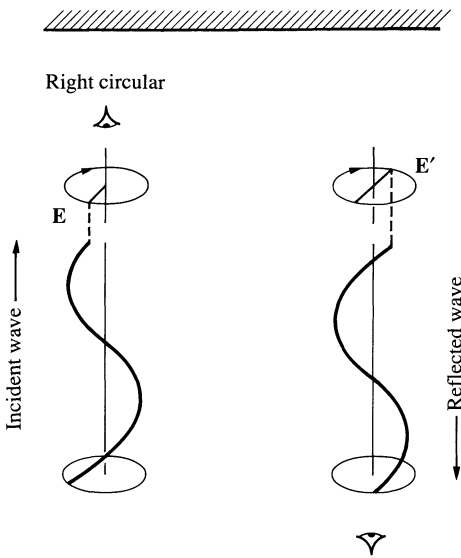


Fig. 6.3. Reflection of a circular wave on a conventional mirror. At the mirror surface the reflected field \mathbf{E}' is just opposite to the incident field \mathbf{E} . Compare the reflected wave with the reflected wave of Fig. 6.2. They are of opposite circular polarizations.

non-vanishing components correspond to polarizations in the x , y -plane, and the resultant 2×2 matrix is

$$\hat{\epsilon}(2q_0) = \frac{1}{4}\epsilon_a V \hat{M}, \quad (6.8)$$

$$\hat{M} = \begin{pmatrix} 1 & i \\ i & -1 \end{pmatrix}.$$

Omitting the constant factor, the polarization of the reflected wave \mathbf{f} is related to the incident polarization \mathbf{i} by

$$\begin{pmatrix} f_x \\ f_y \end{pmatrix} = \hat{M} \begin{pmatrix} i_x \\ i_y \end{pmatrix}$$

or, explicitly,

$$\begin{aligned} f_x &= i_x + ii_y, \\ f_y &= ii_x - i_y. \end{aligned} \quad (6.9)$$

We see that $f_y = +if_x$: the reflected light is circularly polarized. In one case we do *not* get a reflected wave: namely when $i_y = ii_x$; this defines the transmitted wave of Fig. 6.2.

We may also explain why the higher-order Bragg reflections are forbidden, in terms of the matrix amplitude \hat{M} .

Let us look for instance at the reflection $m = 2$, which would correspond to $q = 4q_0$. This can be obtained by scattering from the initial state k_0 to a virtual photon state $k_0 - 2q_0$, followed by a second scattering from $k_0 - 2q_0$ to $k_0 - 4q_0$. The matrix amplitude for this process is proportional to M^2 . But, from eqn (6.8), it is easily verified that $\hat{M}^2 = 0$. The proof can be extended to higher-order processes involving more than one virtual photon, and to larger values of m ; all higher Bragg reflections are forbidden for normal incidence.

Let us now discuss briefly the case of oblique incidences. Here, we observe reflections with the geometrical condition

$$2L \cos r = m\lambda \quad (6.10)$$

where r is the angle of the refracted beam in the slab (related to the angle of incidence i by $\sin i = \bar{n} \sin r$). The main differences from the case of normal incidence are that [2]:

1. All order ($m = 1, 2, 3, \dots$) are observed.
2. The polarizations are elliptical.

A detailed discussion of oblique propagation and reflections requires heavy numerical calculations [2–4]. We may summarize the explanation of point (i) as follows, taking as an example the second reflection $m = 2$. The intermediate photon (of wavevector $\mathbf{k}_0 - 2\mathbf{q}_0$) is oblique. The corresponding polarization vectors are not both in the x, y -plane: it is only their projection in this plane that contributes to the scattering amplitude; this complication is described mathematically by a certain projection operator \hat{P} . The second-order amplitude is then proportional to $\hat{M}\hat{P}\hat{M}$, and this does not vanish in general.

6.1.3 Transmission properties at arbitrary wavelengths (normal incidence)

6.1.3.1 The Mauguin limit

Cholesterics of large, adjustable pitch P are easily obtained by dilution of an optically active material in a nematic matrix: with such dilute solutions, P is typically in the range 10–50 μm and is much larger than the optical wavelength λ . In this limit the optical properties are comparatively simple: they were discussed first in 1911 by Mauguin [5] (in connection with mechanical twist of nematics).

A thin sheet (corresponding to an interval $z, z + dz$ in the slab), of thickness small compared with P , but large compared to λ , behaves as a uniaxial slab, of optical axis \mathbf{n} : in the sheet the eigenmodes of vibration are linearly polarized: one mode along \mathbf{n} , with the extraordinary index $n_e = (\epsilon_{||})^{\frac{1}{2}}$, and one mode normal to \mathbf{n} , with the index $n_0 = (\epsilon_{\perp})^{\frac{1}{2}}$. The structure of the

two modes may be written down explicitly in the form

$$\begin{aligned} \text{Mode 'e', } & \begin{cases} E_x = \cos \theta \cos[\omega\{(zn_e/c) - t\}], \\ E_y = \sin \theta \cos[\omega\{(zn_e/c) - t\}], \end{cases} \\ \text{Mode 'o', } & \begin{cases} E_x = \sin \theta \cos[\omega\{(zn_0/c) - t\}], \\ E_y = -\cos \theta \cos[\omega\{(zn_0/c) - t\}] \end{cases} \end{aligned} \quad (6.11)$$

where $\mathbf{n} = (\cos \theta, \sin \theta, 0)$.

Let us now consider the whole sample; the successive sheets (dz) do not have the same optical axes. However, in the limit $\lambda \ll P(n_e - n_0)$ it may be shown† that eqns (6.11) still correctly define the eigenmodes of vibration.

Knowing this mode structure, we may then deduce the transmission properties of the slab. Let us take our x -axis along the easy direction of the bottom plate [$\theta(0) = 0$]. Let us also define two auxiliary axes (ξ, η) in the slab plane, coinciding with the optical axes at the upper end of the slab. If we send a wave polarized along x , entering through the bottom plate, it will come out at $z = d$, as a linear wave, polarized along ξ , and with a phase lag $\phi_e = \omega n_e d/c$. Similarly, an incident wave polarized along y , comes out along η , with a phase lag $\phi_0 = \omega n_0 d/c$. On the other hand, an incident wave of arbitrary linear polarization:

$$E_x(z = 0) = \cos \alpha \cos(\omega t)$$

$$E_y(z = 0) = \sin \alpha \cos(\omega t),$$

will come out in the form

$$E_\xi(d) = \cos \alpha \cos\{\omega t - \phi_e\}$$

$$E_\eta(d) = \sin \alpha \cos\{\omega t - \phi_0\}$$

and, because of the phase difference $\phi_e - \phi_0$, it will be elliptical in general.

The simple ‘wave guide’ effect obtained with ingoing waves polarized along x or y provides a convenient optical method for measuring the total twist angle $\theta(d) - \theta(0)$; this is sometimes of interest with a planar texture between one polished glass plate and a free surface, and leads to a measurement of the pitch P .

A remark about signs; if the cholesteric helix is right-handed, and if $\theta(d) - \theta(0)$ is small, an observer, measuring the rotation of the plane of polarization for the extraordinary wave (the angle between x and ξ), will call the material laevogyric‡ (or more shortly *laevo*), according to the usual convention in optics. The geometry is shown in Fig. 6.4.

† The proof will be described in Section 6.1.4.

‡ Laevogyric means: turning to the left.

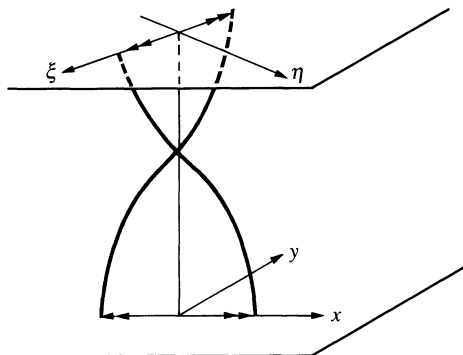


Fig. 6.4. Definition of local axes in a twisted nematic.

6.1.3.2 Rotatory power

Let us assume now that

$$\lambda > P(n_e - n_0) \quad (6.12)$$

(excluding however, for the moment, the case of exact Bragg reflection $\lambda = P$). Then the experimental observations show that, with normal incidence, the planar texture behaves like an ‘optically active’ medium; this means that, for a given frequency ω , the two eigenmodes of vibration propagating along $+z$ are circular waves, with different indices $n_1 n_2$.

If we illuminate the slab (at $z = 0$) with a wave of linear polarization

$$\begin{aligned} E_x &= \cos \alpha \cos \omega t, \\ E_y &= \sin \alpha \cos \omega t, \end{aligned} \quad (6.13)$$

and if we analyse it in terms of the eigenmodes, we find that the corresponding outgoing wave (at $z = d$) is also linear but rotated by an angle

$$\psi = \frac{d\omega}{2c} \{n_1 - n_2\}. \quad (6.14)$$

This is geometrically similar to what is observed in an isotropic, optically-active liquid (IOAL). But the orders of magnitude are strikingly different

$$\text{IOAL} \qquad \frac{\psi}{d} \sim 1 \text{ deg cm}^{-1},$$

$$\text{cholesteric} \qquad \frac{\psi}{d} \sim 10^4 \text{ deg cm}^{-1}.$$

The dependence of the optical rotation ψ/d on the wavelength λ of the light is shown in Fig. 6.8. Note in particular the singularity at the Bragg

wavelength. A review on optical rotation can be found in the Ph.D. work of Cano [6].

6.1.4 Interpretation

6.1.4.1 Assumptions on the local dielectric properties

The huge optical rotations observed in the cholesteric phase are clearly not due to an intrinsic spectroscopic property of the constituent molecules (since they do not persist in the isotropic phase). They must reflect the properties of light waves propagating in a twisted anisotropic medium. This has been studied by many authors, the most clear, rigorous, and accessible reference being that of de Vries [7].

The starting point is an assumption on the form of the local dielectric tensor $\epsilon(\mathbf{r})$ at any point \mathbf{r} in the cholesteric fluid: neglecting the weak intrinsic rotation that persists in the isotropic phase, we may write that the electric displacement $\mathbf{D}(\mathbf{r})$ is a linear functional of the electric field $\mathbf{E}(\mathbf{r})$, taken at the same point \mathbf{r} , and use eqn (6.6),

$$\begin{aligned}\mathbf{D} &= \epsilon \mathbf{E} = \epsilon_{\perp} \mathbf{E} + \epsilon_a \mathbf{n}(\mathbf{n} \cdot \mathbf{E}), \\ \epsilon_a &= \epsilon_{\parallel} - \epsilon_{\perp}.\end{aligned}\tag{6.15}$$

For a wave propagating along the helical axis z , \mathbf{D} and \mathbf{E} are restricted to the x, y -plane and eqn (6.15), involving two parameters (ϵ_{\parallel} and ϵ_{\perp}), is the most general local form. On the other hand, for oblique propagation, eqn (6.15) represents an approximation; at each point \mathbf{r} the medium is described as *uniaxial* (with axis \mathbf{n}), while by symmetry it might be biaxial (with dielectric constants $\epsilon_{\perp}, \epsilon_{\parallel}$ in the x, y -plane, and with another constant ϵ_{zz} along the helical axis). However, as already mentioned in Chapter 1, the deviations from uniaxiality ($\epsilon_{\perp} - \epsilon_{zz}$) are expected to be of order $(q_0 a)^2 \sim 10^{-4}$, and the approximation is probably excellent in all cases.

6.1.4.2 Equation of propagation

Let us now consider specifically the propagation, along z , of an electromagnetic wave of frequency ω . The non-zero field components are

$$\begin{aligned}E_x(zt) &= \text{Re}\{E_x(z) e^{-i\omega t}\}, \\ E_y(zt) &= \text{Re}\{E_y(z) e^{-i\omega t}\}\end{aligned}\tag{6.16}$$

(Re = real part of), and the Maxwell equations reduce to

$$-\frac{d^2}{dz^2} \left(\frac{E_x}{E_y} \right) = \left(\frac{\omega}{c} \right)^2 \hat{\epsilon}(z) \left(\frac{E_z}{E_y} \right).\tag{6.17}$$

The explicit form of the matrix $\hat{\epsilon}$ deduced from eqns (6.15) and (6.1) is

$$\hat{\epsilon}(z) = \frac{\epsilon_{\parallel} + \epsilon_{\perp}}{2} \begin{pmatrix} 1 & 0 \\ 0 & 1 \end{pmatrix} + \frac{\epsilon_a}{2} \begin{pmatrix} \cos 2q_0 z & \sin 2q_0 z \\ \sin 2q_0 z & -\cos 2q_0 z \end{pmatrix}. \quad (6.18)$$

Equation (6.17) does not have exactly the structure of an eigenvalue problem. However, there are some simple features. The operators on both sides are unchanged by a translation of length L along (z). This implies a Bloch–Floquet theorem [8]; a complete set of solutions can be found, such that, for each of them

$$\begin{pmatrix} E_x \\ E_y \end{pmatrix}_{z+L} = \text{const} \times \begin{pmatrix} E_x \\ E_y \end{pmatrix}_z. \quad (6.19)$$

Here we shall find it convenient to write the constant in the form $-e^{ilL}$ (the minus sign is chosen because the helical pitch is $P = 2L$). The wavevector l defines the mode under consideration; note that l may be real (propagating wave) or complex (evanescent wave).

6.1.4.3 Dispersion relation

To derive the solutions explicitly it is convenient to analyse all fields in terms of circular (rather than linear) waves. This amounts to choosing as new variables the quantities

$$E = E_x \pm iE_y.$$

Equation (6.17) then becomes

$$\begin{aligned} -\frac{d^2 E^+}{dz^2} &= k_0^2 E^+ + k_1^2 \exp(2iq_0 z) E^-, \\ -\frac{d^2 E^-}{dz^2} &= k_1^2 \exp(-2iq_0 z) E^+ + k_0^2 E^-. \end{aligned} \quad (6.20)$$

where we have put

$$\begin{aligned} k_0^2 &= \left(\frac{\omega}{c}\right)^2 \frac{\epsilon_{\parallel} + \epsilon_{\perp}}{2}, \\ k_1^2 &= \left(\frac{\omega}{c}\right)^2 \frac{\epsilon_a}{2}. \end{aligned} \quad (6.21)$$

From eqn (6.20) we can immediately find the form of the modes

$$\begin{aligned} E^+ &= a \exp\{i(l + q_0)z\}, \\ E^- &= b \exp\{i(l - q_0)z\} \end{aligned} \quad (6.22)$$

where a and b are two constants, linked by the relations

$$\begin{aligned} \{(l + q_0)^2 - k_0^2\}a - k_1^2 b &= 0, \\ -k_1^2 a + \{(l - q_0)^2 - k_0^2\}b &= 0. \end{aligned} \quad (6.23)$$

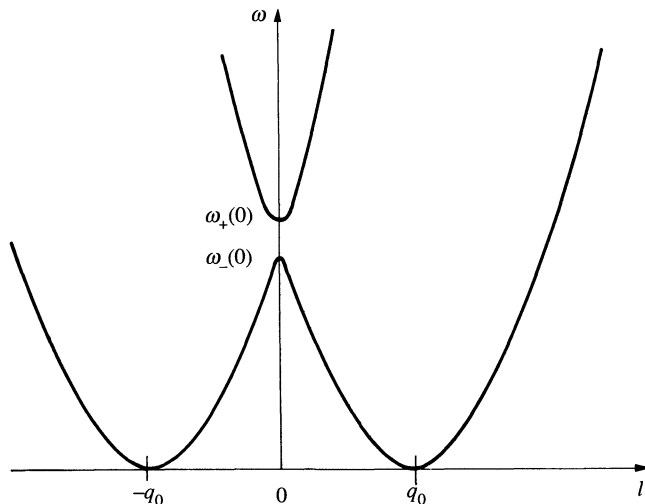


Fig. 6.5. Relation between frequency and wavevector l for propagation of electromagnetic modes in a cholesteric spiral. The mode l defined by eqn (6.22) is a coherent superposition of two plane waves with wavevectors $l \pm q_0$.

The reader may check that eqn (6.22) is compatible with the Bloch–Floquet theorem (eqn (6.19)).

The two eqns (6.23) have a non-trivial solution only if the corresponding determinant vanishes

$$(-k_0^2 + l^2 + q_0^2)^2 - 4q_0^2 l^2 - k_1^4 = 0. \quad (6.24)$$

For a given frequency, ω , k_0 , and k_1 are fixed and eqn (6.24) gives four possible values of l (real or complex). The relation between ω and l for real l is called the *dispersion relation*; it is shown in Fig 6.5.

There are two distinct branches, which we call (+) and (-). To locate them, it is useful to consider first the case $l = 0$. This gives

$$k_0^2 - q_0^2 = \pm k_1^2.$$

Returning to the definitions of k_0 and k_1 (eqn 6.21) one obtains the frequencies

$$\begin{aligned} \omega_+(0) &= \frac{cq_0}{n_0} & n_0 &= \epsilon_{\perp}^{\frac{1}{2}} = \text{ordinary index}, \\ \omega_-(0) &= \frac{cq_0}{n_e} = & n_e &= \epsilon_{\parallel}^{\frac{1}{2}} = \text{extraordinary index}. \end{aligned} \quad (6.25)$$

$\omega_+(0)$ corresponds to $a = -b$. From eqn (6.22) this describes a linear wave polarized along the direction $\theta(z) + \frac{1}{2}z$ (ordinary axis). Similarly, $\omega_-(0)$

corresponds to $a = b$, i.e. a linear wave polarized along the local extraordinary axis.

6.1.4.4 Eigenmodes for travelling waves

The interval $\omega_-(0) < \omega < \omega_+(0)$ will be called the frequency gap. Let us, for the moment, choose an ω value outside of this interval. Then, as can be seen from Fig. 6.5, we have four real values of l (grouped in two pairs, $l_1, -l_1, l_2, -l_2$). If we are interested in waves that travel along the $(+z)$ direction, we must retain only the roots which give a positive group velocity $v_g = \partial\omega/\partial l > 0$. There are *two* such roots (see Fig. 6.5) which we call l_1 and l_2 .[†]

Each of them defines an eigenmode of vibration. Attached to the eigenmode (l_i) is an eigenvector

$$\begin{pmatrix} a_i \\ b_i \end{pmatrix}$$

defined only within a multiplicative constant.

In the present regime (l real) eqn (6.23) shows that a and b may both be taken as real. Then, returning from eqn (6.22) to the real variables of eqn (6.16), one can see that the electric field associated with the eigenmode is elliptically polarized; furthermore at each point, the axes of the ellipse coincide with the local optical axes of the cholesteric. A useful parameter to describe the ellipse is the real number

$$\rho = \frac{-a + b}{a + b}.$$

The axial ratio of the ellipse is $|\rho|$, and the sign of ρ gives the sign of rotation of the vibration in the x, y -plane (at fixed z and increasing t). To calculate ρ in terms of l or ω , we start from the eqns (6.23) written in the form

$$\frac{a}{b} = \frac{k_1^2}{A} = \frac{B}{k_1^2} \quad (6.26)$$

where

$$A = (l + q_0)^2 - k_0^2,$$

$$B = (l - q_0)^2 - k_0^2.$$

Then we can write

$$\begin{aligned} \rho &= \frac{-k_1^2 + A}{k_1^2 + A} = \frac{-B + k_1^2}{B + k_1^2} \\ &= \frac{-B + A}{B + A + 2k_1^2} = \frac{-2lq_0}{k_0^2 - l^2 - q_0^2 - k_1^2}. \end{aligned} \quad (6.27)$$

Equation (6.27) may be transformed, using eqn (6.24). If we define a

[†] For definiteness we shall call l_1 the larger of the two roots.

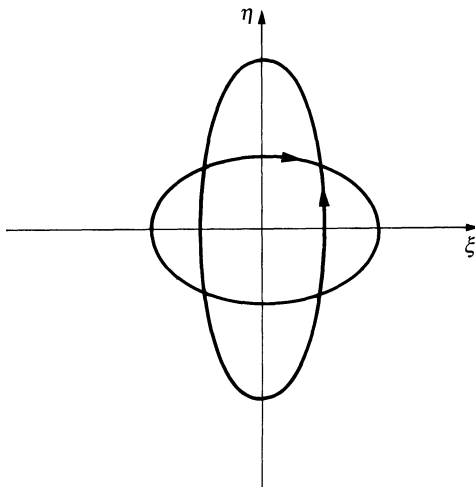


Fig. 6.6. Precession ellipses for the electric field $\mathbf{E}(t)$ at one fixed observation point. The two curves correspond to two eigenmodes with the same ω but different l . Note that the two ellipses do not have the same axial ratio.

positive quantity s^2 by

$$s^2 = +\sqrt{(k_1^4 + 4q_0^2 l^2)}, \quad (6.28)$$

we have

$$\rho = \frac{-2lq_0}{\pm s^2 - k_1^2}. \quad (6.29)$$

The sign (\pm) in eqn (6.29) depends on the branch used for $\omega(l)$ (Fig. 6.5). The general aspect of the two ellipses associated with one frequency ω is shown in Fig. 6.6. The signs and magnitude of ρ on the various branches associated with travelling waves (real l) are shown in Fig. 6.7.

Note that the ratio long axis:short axis is *not the same* for the ellipses associated with one ω value. This is obvious if we compare the point A_+ and B_+ (both corresponding to $\omega = \omega_+(0)$) on Fig. 6.7. At point A_+ we have a linear polarization as explained after eqn (6.25). At point B_+ , we can see from eqn (6.28) that $s^2 \sim 2lq_0$ and $\rho \sim +1$, i.e. the polarization is circular.

Mathematically, to have two ellipses of identical shape (differing only by a 90° rotation in the x, y plane) we would require $\rho_1 \rho_2 = -1$. This can also be written as

$$a_1 a_2 + b_1 b_2 = 0.$$

But this relation does *not* hold; the eigenvectors $\begin{pmatrix} a \\ b \end{pmatrix}$ of eqn 6.23 belonging to the same ω and different l are *not* orthogonal. This point has been emphasized in particular by Billard [3].

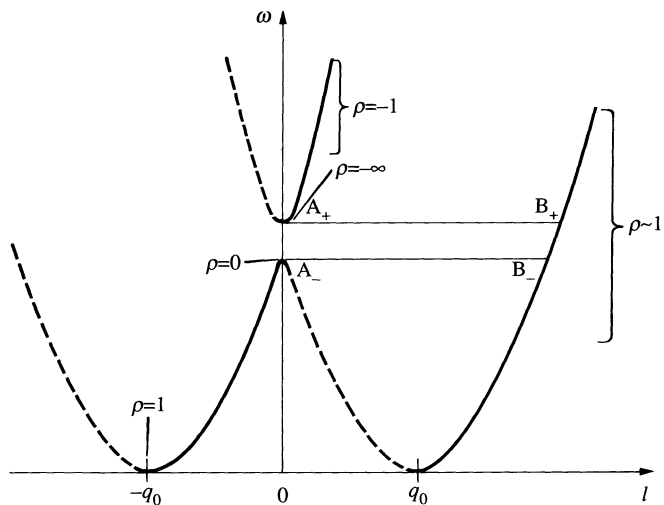


Fig. 6.7. Axial ratio of the ellipses associated with various modes.

6.1.4.5 ‘Waveguide’ regimes

Equations (6.28) and (6.29) show that the mode structure depends critically on the value of the parameter

$$x = \frac{2q_0 l}{k_1^2}. \quad (6.30)$$

Let us consider first the regimes where $x \ll 1$. This can be obtained in two ways:

- (1) by going to small l values, i.e. in the vicinity of the points A_+ and A_- of Fig. 6.5.
- (2) by going to very large l values. Then $l \sim k_0$ and

$$x \sim \frac{2q_0(n_e^2 + n_0^2)}{k_0(n_e^2 - n_0^2)} \sim \frac{2q_0\bar{n}}{k_0(n_e - n_0)}. \quad (6.31)$$

The criterion $x \ll 1$ is the criterion for the *Mauguin limit* $\lambda \ll (n_e - n_0)P$.

In both cases (1) and (2) we find one mode associated with the (+) branch which has $\rho \rightarrow \infty$, and represents a linear *ordinary* wave guided by the helix.† The (-) mode has $\rho \rightarrow 0$ and represents a linear *extraordinary* wave, guided in the same way; these conclusions are in agreement with our earlier remarks concerning the gap edges (case 1) and the Mauguin limit (case 2).

6.1.4.6 Circular regimes

In many practical cases the two indices n_e and n_0 are not very different. Then k_1^2 , as defined by eqn (6.21), tends to be small and the parameter x defined

† i.e. where the polarization remains everywhere parallel to the ordinary axis.

in eqn (6.30) is *large* for most frequencies of interest. Then $s^2 \rightarrow 2q_0|l|$ and by eqn (6.29) we see that $\rho \rightarrow \pm 1$. In this regime the eigenmodes are nearly circular—in agreement with the observations described in Section 6.1.4.3.

In fact, all essential properties can be derived directly from the initial eqns (6.22) and (6.23). If we neglect k_1^2 completely (zero-order approximation) we see in eqn (6.23) that the l values are

$$l_1 = k_0 + q_0 \text{ associated with } a_1 = 0 \quad b_1 = 1,$$

$$l_w = k_0 - q_0 \text{ associated with } a_2 = 1 \quad b_2 = 0.$$

In the next approximation, we find from eqn (6.24)

$$\begin{aligned} l_1 &= k_0 + q_0 + \frac{k_1^4}{8k_0 q_0(k_0 + q_0)} + O(k_1^8), \\ l_2 &= k_0 - q_0 + \frac{k_1^4}{8k_0 q_0(q_0 - k_0)} + O(k_1^8). \end{aligned} \quad (6.32)$$

Since $a_1 \cong 0$ the mode (1) is, according to eqn (6.22), a circular wave of wavevector $l_1 - q_0$. To make contact with the notation of section 6.1.2. we shall represent this wavevector in terms of a refractive index n_1

$$l_1 - q_0 = \frac{\omega}{c} n_1. \quad (6.33)$$

Similarly, for mode (2) we have a circular wave, of opposite sense, and of wavevector

$$l_2 + q_0 = \frac{\omega}{c} n_2. \quad (6.34)$$

The optical rotation per unit length ψ/d is then obtained simply by taking one half of the difference between these two wavevectors (see eqn (6.14))

$$\frac{\psi}{d} = \frac{\omega}{2c} (n_1 - n_2) = \frac{k_1^4}{8q_0(k_0^2 - q_0^2)}. \quad (6.35)$$

This formula is often expressed in terms of a reduced wavelength $\lambda' = \lambda/P = q_0/k_0$. Transforming k_1 by eqn (6.21), one obtains

$$\frac{\psi}{d} = \frac{q_0}{32} \left(\frac{n_e^2 - n_0^2}{n_e^2 + n_0^2} \right)^2 \frac{1}{\lambda'^2(1 - \lambda'^2)}. \quad (6.36)$$

Equation (6.36) is due to de Vries [7]. Note the following features.

1. Very large magnitude of the rotation: for $\lambda' = 0.7$ and $(n_e^2 - n_0^2)/(n_e^2 + n_0^2) = 0.1$ we get $\psi/d \sim 10^{-3}q_0$. With a pitch P of 1 μm , corresponding to $q_0 = 6 \times 10^4$, we expect $\psi/d \sim 60 \text{ rad cm}^{-1}$ or 3500 deg cm^{-1} ! An example is shown in Fig.6.8
2. ‘Dispersion’ anomaly (with a change in sign) at the Bragg reflection ($\lambda' = 1$). Of course, when discussing this point, we must remember that

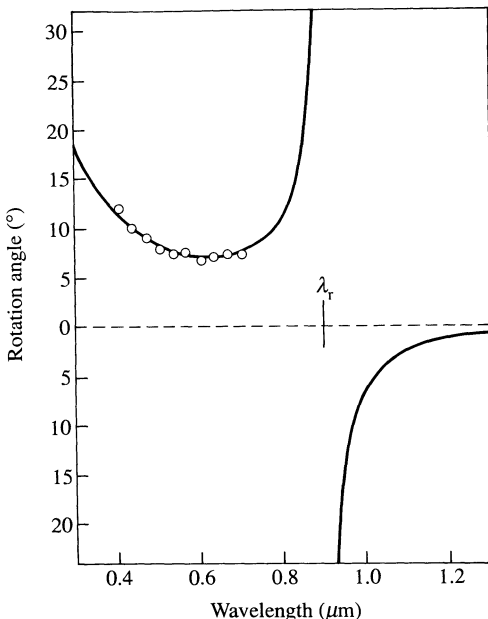


Fig. 6.8. Optical rotation as a function of wavelength for a cholesteric ester. Pitch $P = 600 \text{ nm}$. Average refractive index $\bar{n} = 1.50$. Sample thickness, $25.4 \mu\text{m}$. The theoretical curve was obtained from the de Vries formula (6.36) by assuming $(n_e - n_0)/\bar{n} = 3.07 \times 10^{-2}$ (after reference 10)

very near the Bragg reflection, eqn (6.36) breaks down and the ‘waveguide’ regime takes over. This compares rather well with the data of Mathieu [1].

3. Optical rotational proportional to P^3/λ^4 at long wavelengths.
4. At wavelengths $\lambda \ll P$ (but still too large to be in the Mauguin regime) the rotation becomes proportional to P/λ^2 : this regime has been probed in detail by Cano [6] in mixtures of adjustable pitch.

6.1.4.7 Bragg reflection

Let us now choose a frequency ω inside the gap

$$\frac{cq_0}{n_e} < \omega < \frac{cq_0}{n_0}.$$

For such a case, we see from Fig. 6.5 that eqn (6.24) has only two real roots ($l = \pm l_1$). The other two roots are pure imaginary $l = \pm ik$.

Consider now a thick slab ($d \rightarrow \infty$) attacked from below, at normal incidence, by a light beam of polarization $i(i_x i_y)$. This will in general induce in the slab two waves†

† The two other waves would correspond to light sources on the upper side of the slab.

1. One travelling wave [amplitude proportional to $\exp(il_1 z)$]. According to eqn (6.29) the parameter ρ associated with this wave is close to +1 (for a right-handed cholesteric helix): the wave is circularly polarized, and the sign of circulation is in agreement with Fig. 6.3.
2. One evanescent wave (amplitude $\sim e^{-\kappa z}$).

By a suitable choice of the polarization \mathbf{i} , ($\mathbf{i} = \mathbf{i}_R$) it is possible to extinguish the travelling wave component: this means that a beam of polarization \mathbf{i}_R will be totally reflected. We conclude that the gap $[\omega_-(0), \omega_+(0)]$ corresponds to the frequency range for possible Bragg reflections.

It is easy to check that this property agrees with the more elementary description of Section 6.1.2 in the appropriate limit—namely when $n_e \rightarrow n_0$. Then the gap shrinks down to one frequency $\omega = cq_0/\bar{n}$; the corresponding wavelength is $\lambda = 2\pi c/\omega\bar{n} = 2\pi/q_0 = P$, in agreement with the usual Bragg condition for first-order reflections.

6.1.5 Conclusions and generalizations

The optical properties observed on a planar cholesteric texture (Bragg reflection and optical rotation) are very spectacular: when P corresponds to an optical wavelength in the visible range, the sample shows some very bright colours in reflection. Also the optical rotations are huge. All these properties were quite mysterious in the early days of liquid crystal physics. However, they are explained very accurately by the dielectric model of Mauguin, Oseen, and de Vries—i.e. by eqn (6.15)—involving only two dielectric constants $\epsilon_{||}$ and ϵ_{\perp} .

We have deliberately skipped the discussion of oblique incidences in Section 6.1.4; this case is complicated and does not add much to our insight. It is important, however, from two points of view.

1. It is only with oblique waves that one can check the validity of eqn (6.15) for all electric field directions. A complete comparison between optical data and theoretical calculations, based on eqn (6.15), for oblique waves has been carried out on cholesteric mixtures by Berreman and Scheffer [2]. The agreement found is excellent, and proves unambiguously that a cholesteric fluid is *locally uniaxial*.

2. Oblique Bragg reflections are often important, in practice especially if we have a polydomain sample rather than a single-domain planar texture. This situation has been studied experimentally by Fergason [11]. A typical geometry is shown in Fig. 6.9. The beam enters the sample with a certain incidence θ_1 , is refracted to ϕ'_1 , then propagates in the sample up to a certain domain, with helical axis \mathbf{q}_0 , where it suffers a Bragg reflection. We restrict our attention to the case where \mathbf{q}_0 is in the plane of incidence. Then the outgoing beam is also in this plane, and is characterized by the angles ϕ'_R, ϕ_R .

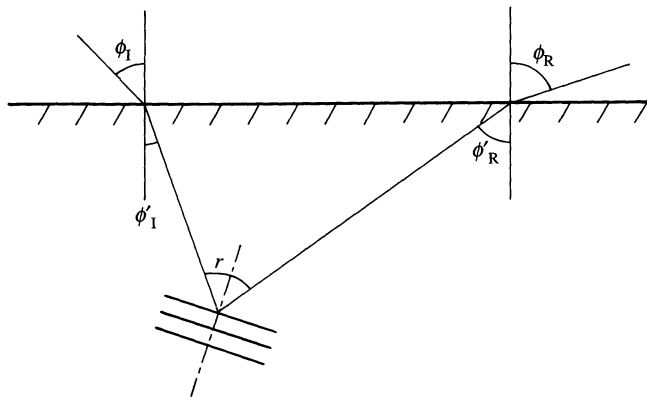


Fig. 6.9. Bragg reflection on a cholesteric polydomain sample. All rays are assumed to be in the plane of the sheet

Defining an angle r between the beam just before Bragg reflection, and \mathbf{q}_0 we can write in the first approximation of eqn (6.10)

$$P \cos r = m\lambda = m\lambda_v/\bar{n} \quad (6.37)$$

where λ_v is the wavelength in vacuum, \bar{n} the average refraction index, and we assume that $|n_e - n_0| \ll \bar{n}$. Figure 6.9 gives us the further relations

$$\begin{aligned} 2r &= \phi'_I + \phi'_R, \\ \sin \phi_I &= \bar{n} \sin \phi'_I, \\ \sin \phi_R &= \bar{n} \sin \phi'_R. \end{aligned} \quad (6.38)$$

Eliminating all internal angles between (6.37) and (6.38) we arrive at [11]

$$\lambda_v = \frac{P\bar{n}}{m} \cos \left\{ \frac{1}{2} \sin^{-1} \left(\frac{\sin \phi_I}{\bar{n}} \right) + \frac{1}{2} \sin^{-1} \left(\frac{\sin \phi_R}{\bar{n}} \right) \right\}. \quad (6.39)$$

This relation allows for a very simple measurement of P in polydomain samples. It is restricted to cases of small birefringence; with large birefringences, multiple reflections become important and the measurements are less accurate.

6.2 AGENTS INFLUENCING THE PITCH

From the discussions in Section 6.1, we see that the optical properties of a cholesteric material will often depend critically on the value of the pitch P .

In the present section we list some typical agents that can be used to change P and thus lead to various interesting applications.

6.2.1 Physicochemical factors

6.2.1.1 Temperature

In most cholesteric derivatives P is a *decreasing* function of temperature

$$\frac{dP(T)}{dT} < 0.$$

A typical curve for $P(T)$ was shown in Fig. 1.8. The order of magnitude of dP/dT is often surprisingly large; as can be seen again on Fig. 1.8, with cholesteryl nonanoate, in a certain temperature range around 74.6°C , one can reach values

$$\frac{1}{P} \left| \frac{dP}{dT} \right| \sim 100 \text{ deg}^{-1}.$$

These giant temperature variations have been observed in particular by Fergason and co-workers [11]. Their origin is not yet quite clear. The increase in P when T is decreased may be due to the onset of a short-range order of the smectic type; most of the compounds at hand have a smectic phase at lower temperatures, and the smectic stacking in equidistant planes is incompatible with twist [12].

In practice, the changes of P are reflected in colour changes provided that the Bragg reflections can occur in the visible spectrum; both the reflected wavelength and the temperature range of maximum sensitivity can be adjusted with suitable multicomponent mixtures [13]. This gives rise to a number of remarkable applications [14].

- Measurement of superficial temperatures.* The surface under study is painted with a thin film of cholesteric material; any temperature difference between two points on the surface will show up as a difference in coloration. This is used for medical purposes (detection of tumours, etc.) [15] and also for various industrial tests (microelectronic circuits, aircraft wings, etc.).
- Conversion of an infrared image into a visible image.* The infrared image is focused on a cholesteric film. In the irradiated areas of the film, some heat is liberated; the temperature rises and the pitch decreases. The local change of P is probed by a source of visible light, and observed either in reflection or in transmission.

This technique has been useful to visualize light patterns from infrared lasers [16]. It is also applicable to microwave patterns [17].

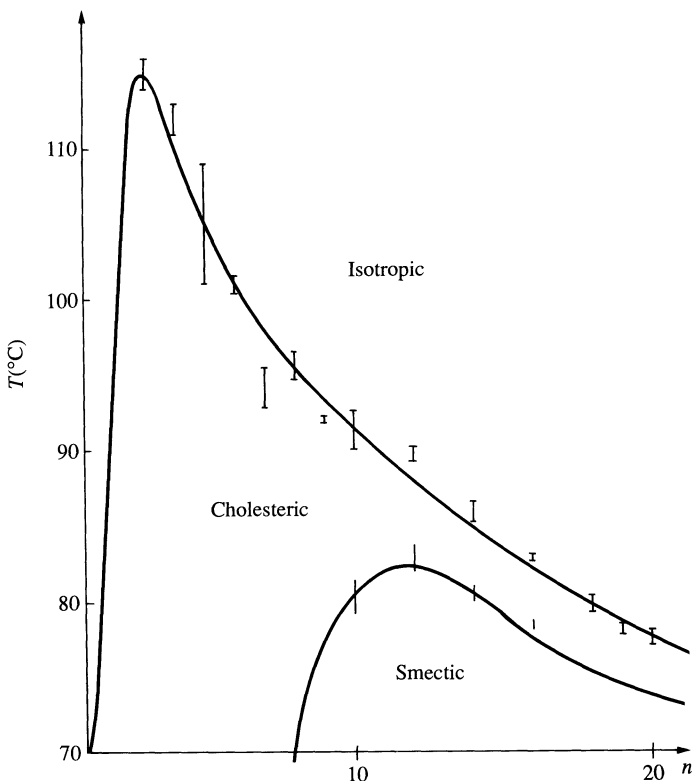


Fig. 6.10. Mesomorphism amongst aliphatic esters of cholesterol. n , number of carbon atoms in the fatty acid component. (Data from G. Gray and R. Ennulat, compiled in reference 18.)

6.2.1.2 Chemical composition

The overall temperature span of the cholesteric phase, the magnitude, and even the sign of the helical twist q_0 , vary greatly from one cholesteric compound to another. (The temperature intervals from aliphatic esters of cholesterol are shown in Fig. 6.10.) This immediately suggests that the properties of *mixtures* may be both flexible and interesting; a few examples will be discussed below.

Dilute solutions in a nematic mixture When a small concentration c of optically active material is dissolved in a nematic, the result is a cholesteric of large pitch P . In the dilute limit, P is inversely proportional to c [19]

$$Pc = \text{constant}. \quad (6.40)$$

A microscopic interpretation of this law, in terms of the long-range distortions

induced in the nematic by a single solute molecule, is given in the next problem. The result is conveniently written in the form

$$q_0 = \frac{2\pi}{P} = +4\pi\beta c \quad (6.41)$$

where c is the number of solute molecules/cm³, and β is a constant (with the dimension of a surface), dependent on the nature of both solvent and solute. We call β the 'microscopic twisting power' of the solute.

If we choose one particular nematic solvent N, we can measure the magnitude and sign of the microscopic twisting power for all chiral molecules that are soluble in N. In practice, such studies have been carried out for two groups of solvents N:

- (1) conventional nematics with two benzene rings such as PAA or MBBA.
- (2) special cholesteric mixtures with exact compensation; consider for instance a 1.75:1.00 mixture of cholesterol chloride–cholesterol myristate at 40°C. The pure chloride is right-handed ($q_0 > 0$) while the pure myristate is left-handed ($q_0 < 0$). This particular mixture has $q_0 = 0$, i.e. it is nematic. It has been used as a reference solvent by Baessler and Labes [20]. Typical results are given in Table 6.1 (in a slightly different notation).

The advantage of this mixture is that it provides a solvent involving the cholesterol skeleton that is clearly adequate for a study of twisting powers among cholesterol derivatives. The obvious drawback is that it can be used

Table 6.1. Macroscopic twisting power P_t of various solutes in a compensated (cholesterol chloride–cholesterol myristate) mixture at 40°C. P_t is defined by $c_w PP_t = 1$ where c_w is the weight concentration of solute and P is the resulting pitch (after reference 20).

Compound	No. of carbons on side chain	P_t
Cholesterol	0	+2.0
Cholesterol chloride	0	+2.96
Cholesterol formate	1	-0.67
Cholesterol acetate	2	-1.2
Cholesterol propionate	3	-3.22
Cholesterol butyrate	4	-3.45
Cholesterol valerate	5	-4.45
Cholesterol caproate	6	-4.70
Cholesterol myristate	14	-7.45

at one temperature only: if the temperature is changed, we do not have exact compensation any more.

Problem. Derive the pitch of a dilute solution of a cholesteric material in a nematic phase by a superposition of individual distortions.

Solutions. Our starting point is the discussion of distortions around one floating object in a nematic (problem p. 157, Chapter 3). In the one-constant approximation we found that the local rotation ω at a large distance r from the object had the form

$$\omega = \alpha \frac{1}{r} + \beta \cdot \nabla \left(\frac{1}{r} \right)$$

where α is a vector, and β a dyadic, both dependent on the orientation and shape of the object. As seen in Chapter 3, in the absence of specific torques acting on the object, the vector α vanishes. The dyadic β must be an even function of the unperturbed director n_0 , and has thus the general form†

$$\beta = -\beta + \beta_1 n_0 \cdot n_0.$$

However, the second term gives rise only to rotations around n_0 , which do not lead to any practical change. Thus we are left with

$$\omega = -\beta \nabla \left(\frac{1}{r} \right) = \beta \frac{\mathbf{r}}{r^3}.$$

Note that ω is an axial vector, while $\nabla(1/r)$ is a polar vector. Thus β is a pseudoscalar, and is non-vanishing only if the impurity differs from its mirror image. β has the dimensions of a surface. The general aspect of the distortion described by β is shown on Fig. 6.11.

† The choice of a $(-)$ sign in the scalar term will be convenient later: with this definition β will be positive when the solute is cholesterol chloride.

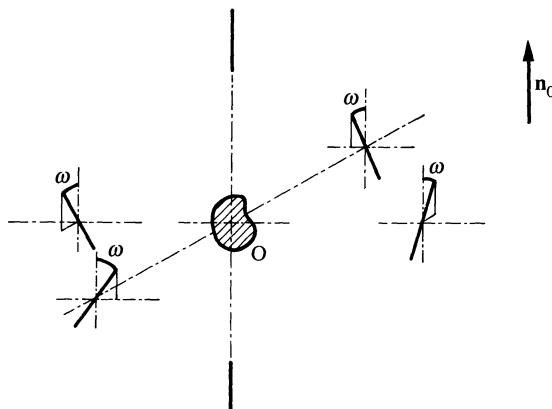


Fig. 6.11. Static distortions around a chiral object in a nematic matrix.

Let us now turn to a dilute solution with c impurities per cm³, each of them creating a distortion of this type. For small concentrations c , we may assume that the total rotation vector $\omega(\mathbf{r})$ at any point \mathbf{r} is obtained by superposition

$$\omega(\mathbf{r}) = \sum_p (-\beta) \nabla \frac{1}{r_p}$$

where the sum \sum_p is over all solute molecules. ω is identical to the electrostatic field that would result from charges β located at the various solute positions. Thus by Poisson's equation

$$\operatorname{div} \omega = +4\pi c\beta$$

and also

$$\operatorname{curl} \omega = 0.$$

The solution corresponds to a helical structure. Putting the helical axis along z , we have

$$\omega_z = q_0 z,$$

$$\omega_x = \omega_y = 0$$

with

$$q_0 = 4\pi c\beta.$$

Thus the helical wavevector q_0 is indeed proportional to the concentration.

Concentrated solutions For most mixtures between cholesterol derivatives, the twist \bar{q} of the mixture is nearly equal to the weight average of the component twists q_i [20]

$$\bar{q}(T) \simeq \sum_i c_i q_i(T) \quad (6.42)$$

where c_i is the (weight) concentration of component i . Note that in eqn (6.42) the various q_i s may be positive or negative: in particular, as already mentioned, if we have two components, one with $q_1 > 0$ and the other with $q_1 < 0$, a suitable mixture of the two will be nematic ($\bar{q} = 0$).†

There are, however, some exceptions to the additivity rule (6.42). Mixtures of cholesterol chloride–cholesterol laurate are one such exception; here the plot of \bar{q} versus concentration shows a well defined extremum [22], and is not at all linear on the laurate-rich side. Similar extrema are found with other esters of comparable length (Fig. 6.12). Their microscopic origin is unknown.‡

Effects of contaminants on the pitch Certain gases, when absorbed in a cholesteric film, cause a significant change of pitch, and thus of coloration

† Mixtures between two chiral antipodes are essentially ideal and obey eqn (6.42) exactly: see for instance D. Dolphin *et al.* [21].

‡ One possible interpretation would connect the low \bar{q} , observed for the laurate-rich mixtures, with smectic short-range order in the cholesteric phase. X-ray experiments will help to elucidate this point.

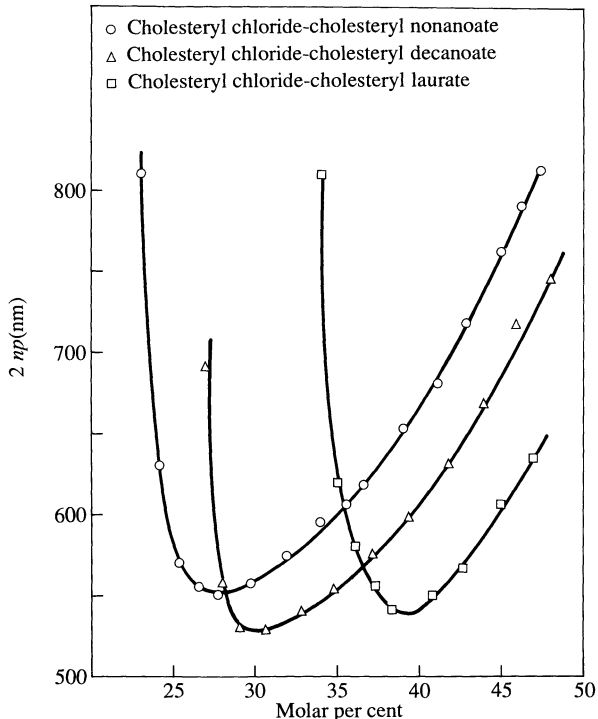


Fig. 6.12. Pitch versus composition for three binary mixtures of cholesterol esters (after reference 22).

[14]. A device transforming an ultraviolet image into a visible image, and based on a similar principle has been invented by the Xerox group [23]. The UV image is focused on a film containing a mixture of cholesteric esters and, in particular, some cholesterol iodide; this component is easily decomposed photochemically in the regions irradiated with UV light. Thus, in these regions, we have a change in chemical composition and a resulting change in pitch; the latter is then observed under visible light.

6.2.1.3 Pressure

The effects of a hydrostatic pressure on the helical pitch have not been measured up to now: they might be spectacular in the vicinity of the cholesteric-isotropic transition point, or also alternatively near a smectic-cholesteric transition.

6.2.2 External fields

It is possible to distort a cholesteric spiral by a magnetic or an electric field: this gives rise to rather remarkable magneto-optic or electro-optic effects,

which we shall now discuss. The starting point is to write a form for the free energy, as a function of the director $\mathbf{n}(\mathbf{r})$, for slow variations of \mathbf{n} in space.

6.2.2.1 Continuum theory for cholesterics

When we discussed the distortion energy F_d for a nematic fluid in Chapter 3, we discarded all terms linear in the gradients of \mathbf{n} : these terms are not compatible with an equilibrium conformation where $\mathbf{n} = \text{constant}$. For a cholesteric, however, this argument does not hold, since the equilibrium conformation is twisted. There are two terms that are linear in the spatial derivatives of \mathbf{n} , and rotationally invariant: $\text{div } \mathbf{n}$ and $\mathbf{n} \cdot \text{curl } \mathbf{n}$. Terms proportional to $\text{div } \mathbf{n}$ cannot occur in F_d because the states \mathbf{n} and $-\mathbf{n}$ are indistinguishable. On the other hand, the pseudoscalar quantity $\mathbf{n} \cdot \text{curl } \mathbf{n}$ may appear in F_d provided that the molecules are different from their mirror images. Adding to this the usual nematic terms (eqn (3.15)) we end up with a distortion energy of the form

$$F_d = \frac{1}{2}K_1(\text{div } \mathbf{n})^2 + \frac{1}{2}K_2(\mathbf{n} \cdot \text{curl } \mathbf{n} + q_0)^2 + \frac{1}{2}K_3(\mathbf{n} \times \text{curl } \mathbf{n})^2. \quad (6.43)$$

In eqn (6.43) we do find a term linear in the gradients, namely

$$K_2 q_0 \mathbf{n} \cdot \text{curl } \mathbf{n}$$

and a constant term $\frac{1}{2}K_2 q_0^2$. The meaning of eqn (6.43) becomes more transparent if we consider a situation of pure twist

$$n_x = \cos \theta(z), \quad n_y = \sin \theta(z), \quad n_z = 0.$$

Then eqn (6.43) reduces to

$$F_d = \frac{1}{2}K_2 \left(\frac{\partial \theta}{\partial z} - q_0 \right)^2. \quad (6.44)$$

We see from this that the equilibrium distortion corresponds to a helix of wavevector $\partial \theta / \partial z = q_0$.

Equation (6.43) is the correct form for the distortion free energy when both $\nabla \mathbf{n}$ and q_0 are small on the molecular scale. If q_0 were large ($q_0 a \sim 1$) the structure of F_d would become more complicated as discussed by Jenkins [24]. However, in all practical situations $q_0 a \sim 10^{-3}$ and the Jenkins corrections are not important.

We must add to the distortion F_d some extra terms that describe the coupling to \mathbf{H} or \mathbf{E} ; just as in the nematic case, they have the form

$$F_{\text{mag}} = -\frac{1}{2}\chi_a(\mathbf{H} \cdot \mathbf{n})^2, \quad (6.45)$$

$$F_{\text{el}} = -\frac{1}{8\pi}\epsilon_a(\mathbf{E} \cdot \mathbf{n})^2, \quad (6.46)$$

where $\chi_a = \chi_{||} - \chi_{\perp}$ and $\epsilon_a = \epsilon_{||} - \epsilon_{\perp}$. In eqns (6.45) and (6.46), only the \mathbf{n} -dependent terms have been retained. One quantitative point must be

mentioned at this stage. For cholesterol esters, where no benzene ring is present, the diamagnetic susceptibilities χ_{\parallel} and χ_{\perp} are considerably smaller than on conventional nematics: $|\chi_a|$ is of order 10^{-9} cgs units. Also χ_a is usually *negative* and in a magnetic field \mathbf{H} , the director tends to be aligned normal to \mathbf{H} . To obtain cholesterics with *positive* χ_a , the simplest procedure is to dissolve chiral molecules in a conventional nematic like MBBA.

The dielectric anisotropy $\epsilon_a = \epsilon_{\parallel} - \epsilon_{\perp}$ is positive for cholesterol halides, and negative for the aliphatic esters of cholesterol. It is also negative for dilute solutions of chiral molecules in MBBA.

Finally, it is also possible to use a.c. electric fields in these experiments (ϵ_a is then a function of the a.c. frequency): the a.c. regimes are sometimes useful to eliminate charge transport and electrohydrodynamic instabilities (we come back to this point in Section 6.3).

6.2.2.2 Negative anisotropy

A bulk cholesteric sample, with negative χ_a (or ϵ_a) minimizes its energy by putting the helical axis (\mathbf{q}_0) along the field; then the director \mathbf{n} is normal to the field at all points. No distortion energy is required and the helical pitch is independent of the field.

This very simple effect has been observed with a.c. electric fields (of frequency higher than ~ 1 kHz) in mixtures of MBBA and cholesterol esters [25]; as explained above, a finite frequency is required to eliminate the convective instabilities usually observed in MBBA (see Chapter 5). This experiment allows the transformation of a polydomain sample into a well ordered planar texture, and may be quite useful in practice.

6.2.2.3 Positive anisotropy

Let us start with a rather thick cholesteric sample, so that wall effects may be safely neglected. In low fields \mathbf{H} (or \mathbf{E}),[†] the helical structure is undistorted. The susceptibility measured along the helical axis is the perpendicular susceptibility χ_{\perp} ; when measured normal to the helical axis it is the average $\frac{1}{2}(\chi_{\perp} + \chi_{\parallel})$. If $\chi_{\parallel} > \chi_{\perp}$ this average is larger than χ_{\perp} . The system will tend to adjust in order to display the maximum susceptibility; the helical axis is thus *normal to the applied field*. This is well confirmed experimentally.

Let us now look for internal distortions of the helical structure. The initial situation for low fields is represented in Fig. 6.13(a), and that for intermediate fields in Fig. 6.13(b). In regions such as A, A', ... the molecules are favourably aligned along the field. In regions such as B, B', ... the molecules have an unfavourable orientation with respect to the field. Thus if the field becomes strong enough region A will expand. Region B, on the other hand, cannot

[†] We discuss here the case of a magnetic field; all formulae for electric fields are obtained by the substitution $\chi_a H^2 \rightarrow \epsilon_a E^2 / 4\pi$.

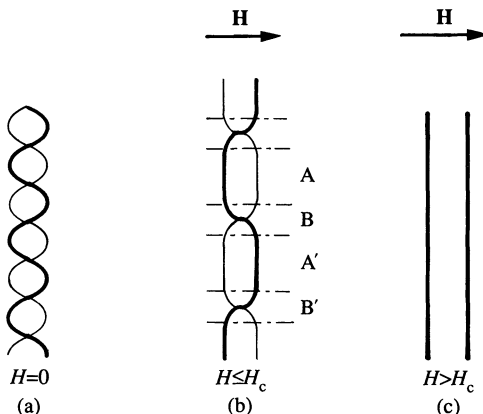


Fig. 6.13. Untwisting of a cholesteric spiral by a field \mathbf{H} . It is assumed that the molecules tend to lie *along* $\mathbf{H} (\chi_a > 0)$.

contract very much, since this would require too much twist energy. The overall result is an increase of the pitch P with field.

At somewhat higher fields, this leads to a succession of 180° walls separating large A regions. Each wall has a finite thickness, of order $2\xi_2(H)$, where ξ_2 is defined as usual

$$\xi_2 = \left(\frac{K_2}{\chi_a} \right)^{\frac{1}{2}} \frac{1}{H}. \quad (6.47)$$

The distance between walls $L = \frac{1}{2}P(H)$ is now much larger than ξ_2 . Finally, at a certain critical field H_c , the walls become infinitely separated ($P \rightarrow \infty$) and we obtain a nematic structure.

This cholesteric–nematic transition was observed first by Sackmann *et al.* [26] under magnetic fields, and by the Xerox group [27] under electric fields. More detailed studies [27–30] showed that the critical field is inversely proportional to the unperturbed pitch $P(0)$: in practice, to have reasonable critical field values, one always has to work in mixtures of large pitch.

The detailed variation of pitch with field has been measured in a few cases [28, 29] and is shown in Fig. 6.14. At low fields the pitch is essentially unperturbed: at higher fields P increases and finally diverges (weakly) at the critical field.

From a theoretical point of view, the transition can be studied rather simply from the continuum free energy (eqns (6.44) and (6.45)). In particular, the value of the critical field H_c (or E_c) may be derived as follows. For $H \rightarrow H_c$ we have well-separated walls, as shown in Fig. (6.13(b)); the interactions between walls become negligible, and it is enough to study the energy of one single wall in an infinite nematic medium. Assuming always a one-dimensional situation of pure twist ($n_x = \cos \theta(z)$, $n_y = \sin \theta(z)$) we find

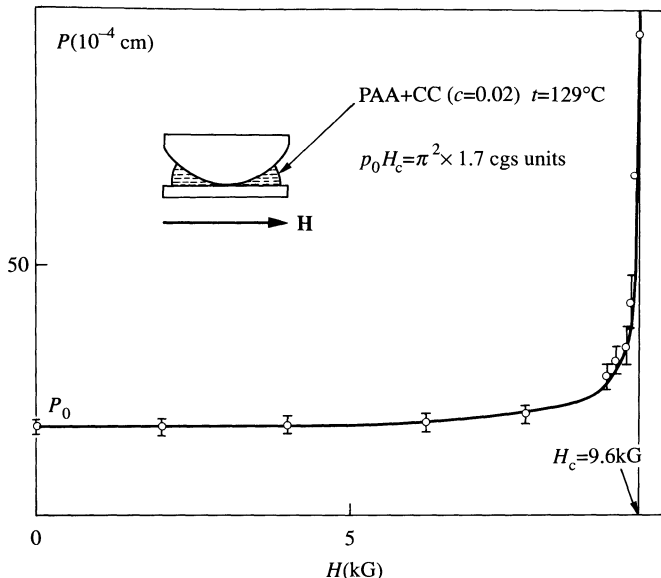


Fig. 6.14. Pitch $P(H)$ as a function of magnetic field for a mixture PAA–cholesterol ester. In this experiment the pitch was derived from the position of the discontinuities in a Cano wedge (see Fig. 6.20). (After reference 28.) The continuous curve is theoretical [31].

from eqns (6.44) and (6.45) the equilibrium equation

$$\xi_2^2 \frac{d^2\theta}{dz^2} = \sin \theta \cos \theta.$$

This, as in Chapter 3, has the first integral

$$\xi_2^2 \left(\frac{d\theta}{dz} \right)^2 = \sin^2 \theta, \quad (6.48)$$

ensuring that $d\theta/dz \rightarrow 0$ for $\theta \rightarrow \pi$. The free energy (per unit area) of one wall, compared to the energy of the nematic conformation, is then

$$\begin{aligned} F_w &= \int \left\{ \frac{1}{2} K_2 \left\{ \left(\frac{d\theta}{dz} - q_0 \right)^2 - q_0^2 \right\} + \frac{1}{2} \chi_a H^2 \sin^2 \theta \right\} dz, \\ \frac{F_w}{\chi_a H^2} &= \int \left\{ \frac{1}{2} \xi_2^2 \left(\frac{d\theta}{dz} \right)^2 - q_0 \xi_2 \frac{d\theta}{dz} + \frac{1}{2} \sin^2 \theta \right\}. \end{aligned} \quad (6.49)$$

From eqn (6.48) we see that the first and third terms in eqn (6.49) give equal

contributions

$$\begin{aligned} \frac{F_w}{\chi_a H^2} &= \int_0^\pi \xi^2 \left| \frac{d\theta}{dz} \right| d\theta - q_0 \xi_2 \int_0^\pi d\theta \\ &= \int_0^\pi \sin \theta d\theta - \pi q_0 \xi_2 \\ &= 2 - \pi q_0 \xi_2. \end{aligned} \quad (6.50)$$

Thus it becomes unfavourable to have walls when $\xi_2(H) < 2/\pi q_0$. Returning to eqn (6.47) we see that this corresponds to a critical field

$$H_c = \frac{\pi}{2} \left(\frac{K_2}{\chi_a} \right)^{\frac{1}{2}} q_0 = \pi^2 \left(\frac{K_2}{\chi_a} \right)^{\frac{1}{2}} \frac{1}{P_0} \quad (6.51)$$

where P_0 is the unperturbed pitch. Equation (6.51) was derived independently by Meyer [32] and by the present author [31]. It does show that (for fixed K_2 and χ_a) H_c is inversely proportional to P_0 .

Typically, for a dilute solution of chiral molecules in a conventional nematic, we might choose $K_2 \approx 10^{-6}$ dyne, $\chi_a = 10^{-7}$ cgs units, and $P_0/2 = 10 \mu\text{m}$, corresponding to $H_c = 15000 \text{ G}$.

At fields below critical, the energy of a single wall F_w (eqn (6.50)) becomes negative; thus walls tend to pile up in the sample, until the (repulsive) interactions between neighbouring walls lead to an equilibrium. These interactions decrease rapidly as a function of the interwall distance $L (= P/2)$: they are in fact proportional to $\exp(-L/\xi_2)$. For this reason, as soon as H is below H_c , we can have a rather large number of walls per unit length: the pitch $P(H)$ is only logarithmically divergent for $H = H_c$. As seen on Fig. 6.14, this feature is indeed quite apparent on the experimental data. We shall now list a few experiments giving some information on the distorted state.

1. *Electron spin resonance line-shape of a solute radical.* The resonance frequency, for a group of spins located in a region where the angle between director and field is θ , is of the form

$$\omega(\theta) = \omega_0 + \omega_1 \cos^2 \theta \quad (6.52)$$

where ω_1 is due to anisotropy in the g -factor, or in the hyperfine interactions of the spin label. From the frequency spread of the absorption line, one can thus derive the distribution law for $\cos^2 \theta$ in the distorted structure [33a].

2. *Optical studies* of the wavelength-dependent transmission for a beam parallel to the helical axis, in the distorted state [34].
3. *Macroscopic magnetic measurements* on the distorted state. In low fields the susceptibility χ is $\frac{1}{2}(\chi_{\parallel} + \chi_{\perp})$. At the critical field the susceptibility is χ_{\parallel} . The complete $\chi(H)$ curve has been measured by the Bordeaux group [33b].

The transition at $H = H_c$ has some interesting thermodynamic features. It is a second-order transition; the free energy (per cm³) $F(H)$ has a continuous slope at $H = H_c$. However, some hysteresis can be observed in the transition region! For instance, let us start from high fields ($H > H_c$) and assume that we have a good nematic single crystal between two polished glass walls (the easy axis of the wall being parallel to \mathbf{H}). Then let us decrease progressively; we find that nothing happens at $H = H_c$. For H slightly below H_c , we observe a metastable nematic phase [28]. At a somewhat lower field disclination loops nucleate and the equilibrium pitch is restored. In the metastable regime, as shown by eqn (6.50), it would be favourable to inject some 180° walls in the sample, but the boundary conditions create a barrier opposing wall nucleation.

Our discussion of external field effects with positive anisotropy has been restricted, up to now, to situations of pure twist, with the helical axis normal to the field. As explained at the beginning of this paragraph, this is indeed the usual situation for bulk samples. There are, however, some other possibilities, which we shall discuss now.

1. If the bend constant K_3 happens to be anomalously small ($K_3 < 4K_2/\pi^2$) there should occur, in increasing fields, a transition from the helical conformation (\mathbf{q} normal to \mathbf{H}) to a *conical conformation* [32] described by

$$\begin{aligned} n_y &= \cos(qx) \cos \psi, \\ n_z &= \sin(qx) \cos \psi, \\ n_x &= \sin \psi \end{aligned} \quad (6.53)$$

where ψ is a function of H only; the ‘conical axis’ x is parallel to the field. In practice, however, K_3 is larger than K_2 and this conical phase has not been observed.

2. If the sample is a thin slab, with tangential boundary conditions giving a planar texture, one can apply the field \mathbf{H} parallel to the unperturbed helical axis, in spite of the positive anisotropy [35]. In this case, above a certain threshold field a periodic distortion of the cholesteric planes takes place (Fig. 6.17). This possibility was invented by Helfrich, mainly in connection with electric field effects (including charge accumulation) [36]. A more detailed calculation, discussing both magnetic and electric field effects, is due to Hurault [37]. It has been tested by recent experiments of Rondelez *et al.* [35]. For the theory of magnetic distortions, the reader is referred to Section 7.1.6, where a similar problem is discussed for smectics. The electric case, which is more important in view of practical application, will be discussed later in the present chapter, after the introduction of some useful hydrodynamic concepts.

On the whole, the electro-optic effects, in cholesterics with positive

anisotropy, are remarkable. However, they are conveniently observed mainly on materials with large pitch ($P \sim 10 \mu\text{m}$) and it is not yet clear whether they will find interesting technical applications.

Problems. Construct a coarse-grained version of the continuum theory for cholesterics, applying when the distortions are very gradual in comparison with the pitch. (T. C. Lubensky and P. G. de Gennes, 1971).

Solution. In the unperturbed state the cholesteric planes are equidistant (interval P_0) and parallel (the unperturbed helical axis will be called the z -axis). In a slightly distorted state, each plane is displaced by an amount $u(\mathbf{r})$ along z ; u is a slowly varying function of \mathbf{r} . The coarse-grained free energy density F_{cg} must be a function of the gradients of u : the most general form (for small gradients $\nabla u \ll 1$) is

$$\begin{aligned} F_{\text{cg}} = & \frac{1}{2}B\left(\frac{\partial u}{\partial z}\right)^2 + \frac{1}{2}\tilde{K}\left(\frac{\partial^2 u}{\partial x^2} + \frac{\partial^2 u}{\partial y^2}\right)^2 \\ & + \frac{1}{2}K'\left(\frac{\partial^2 u}{\partial z^2}\right)^2 + K''\frac{\partial^2 u}{\partial z^2}\left(\frac{\partial^2 u}{\partial x^2} + \frac{\partial^2 u}{\partial y^2}\right). \end{aligned}$$

There is no term proportional to $(\partial u / \partial x)^2$; such a term would give a non-zero F_{cg} for a uniform rotation around the y -axis. There is also no term of the form

$$\frac{\partial u}{\partial z}\left(\frac{\partial^2 u}{\partial x^2} + \frac{\partial^2 u}{\partial y^2}\right).$$

This term is not compatible with the existence of a twofold axis of symmetry (parallel to the local direction \mathbf{n}) in the unperturbed structure. For a Fourier component of wavevector \mathbf{q} ($q \ll q_0$), the K' term is of the order of $\frac{1}{2}K'q_z^4u^2$ and is negligible in comparison with the B term $\frac{1}{2}Bq_z^2u^2$. The K term may also be dropped out for similar reasons. We are then left with two elastic constants, B and \tilde{K} . F_{cg} may be written in a slightly more general form by introducing a unit vector $\mathbf{d}(\mathbf{r})$ normal to the cholesteric planes

$$F_{\text{cg}} = \frac{1}{2}B\left(\frac{P}{P_0} - 1\right)^2 + \frac{1}{2}\tilde{K}(\text{div } \mathbf{d})^2$$

where P is the local value of the pitch in the distorted structure. The constant B is immediately derived from eqn (6.44) by considering a case where $\partial u / \partial z = \text{constant}$

$$B = K_2 q_0^2.$$

To obtain \tilde{K} we consider a ‘jelly-roll’ arrangement of cholesteric planes, in terms of cylindrical coordinates (r, ϕ, z) this corresponds to

$$n_r = 0,$$

$$n_\phi = \cos \theta(r),$$

$$n_z = \sin \theta(r).$$

We impose $\theta(r + P_0) \equiv \theta(r)$ (no change in pitch). The vector \mathbf{g} is parallel to the r -axis,

and $\operatorname{div} \mathbf{d} = 1/r$. Thus

$$F_{\text{cg}} = \frac{1}{2}\tilde{K}/r^2.$$

The local Frank free energy F is derived from eqn (6.43): after some calculation one obtains

$$F = \frac{1}{2}K_2 \left(\frac{d\theta}{dr} - q_0 - \frac{1}{r} \sin \theta \cos \theta \right)^2 + \frac{1}{2}K_3 \frac{1}{r^2} \cos^4 \theta.$$

We consider F in the limit $q_0 r \gg 1$ (weak distortions). The optimum form of $\theta(r)$ corresponds to

$$\frac{d\theta}{dr} = q_0 + \frac{1}{r} \sin \theta \cos \theta.$$

In the correction term on the right-hand side we may insert the unperturbed value $\theta = q_0 r + \text{const}$. The terms of order $1/q_0 r$ in θ may then be found by integration, and it may be checked that they are compatible with the periodicity condition $\theta(r + P_0) = \theta(P_0)$.

With this choice of $\theta(r)$ the twist contribution drops out. The bend contribution to the coarse-grained average may be obtained from the unperturbed form of θ ; the average over angles of $\cos^4 \theta$ is equal to $\frac{3}{8}$ and we obtain

$$\tilde{K} = \frac{3}{8}K_3.$$

6.3 DYNAMICAL PROPERTIES

Cholesterics are liquids, and very similar in their local structure to nematics; here too, we have some remarkable couplings between orientation and flow. The fundamental mechanical equations that describe these couplings have again been discussed by Leslie [38]. For the usual case of very weak twists on the molecular scale, negligible compressibility, and uniform temperature, the equations for cholesterics and nematics are *identical*. The entropy source is always given by eqn (5.21) of Chapter 5, in terms of the viscous stress $\sigma'_{\alpha\beta}$, the molecular field h_α , the shear rate tensor $A_{\alpha\beta}$, and the relative rotation velocity N_α of the director. The torque balance eqn (5.17) is also maintained, and the relations between fluxes ($A_{\alpha\beta}, N_\alpha$) and forces ($\sigma'_{\alpha\beta}, h_\alpha$) retain the form of eqns (5.31) and (5.32): they involve five independent coefficients with the dimension of a viscosity. The only difference is that the molecular field \mathbf{h} must now be derived from eqn (6.43) for the free energy.

However, in spite of these formal similarities, the physical flow effects and orientational effects are much more complex on a helical structure: in particular, as we shall see, the *apparent* bulk viscosity of a cholesteric sample may often be 10^5 times larger than the friction coefficients defined in the Leslie equations! Also, from an experimental point of view, it is often difficult to produce a situation where both the flow and the texture properties are adequately controlled; we shall restrict our attention here to a few situations of this class, where experiments have been done or at least look feasible.

6.3.1 Studies on small motions in a planar texture

6.3.1.1 Pulsed external fields

Consider for instance a cholesteric with positive χ_a , subjected to a time-dependent magnetic field $H(t)$ normal to the helical axis (z). The helix will distort with a certain time lag. For the example chosen, the only deformation involved is twist, and it may be shown that there is no backflow. Theoretical calculations for small-amplitude motions that are relevant to the present problem can be found in ref. [39]. Typical relaxation rates are of order $K_2 q_0^2/\gamma_1$, but the details of the relaxation depend on the average field. Experiments of this type provide a good measurement of γ_1 [40].

6.3.1.2 Ultrasonic attenuation of shear waves

The principle has been discussed in Chapter 5 in connection with nematics. A theoretical analysis for the planar texture of cholesterics has been given by F. Brochard [41a]; the regimes depend critically on the ratio between the acoustic penetration depth δ and the half-pitch $P/2$. To vary δ requires acoustic equipment working on a broad range of frequencies. It is simpler in practice to vary P , using for instance a mixture of MBBA and (dilute) cholesterol esters. The experiment gives two friction coefficients: they are in reasonable agreement with other data for MBBA [41b].

6.3.1.3 Inelastic scattering of light

No quantitative data on light scattering by cholesterics are available up to now, but the situation should soon improve. Both the intensity [42] and the frequency spectrum [39] of the scattered light have been analysed theoretically, at least for one case: namely for scattering wavevectors \mathbf{k} which are parallel to the helical axis.

For each \mathbf{k} , there are two orientational modes that are strongly coupled to the light. For \mathbf{k} parallel to \mathbf{q}_0 , these modes are very simple. One mode corresponds to *pure twist*: putting the helical axis along z , it may be described as follows

$$\begin{aligned} n_x &= \cos(q_0 z + u) \simeq n_x^0 - u \sin(q_0 z), \\ n_y &= \sin(q_0 z + u) \simeq n_y^0 + u \cos(q_0 z), \\ n_z &= 0 \end{aligned} \quad (6.54)$$

with $u = u_0 e^{iz}$. This type of twist deformation contributes only to one component of the dielectric tensor

$$\epsilon_{x,y} = \epsilon_a \{n_x^0 \delta n_y + n_y^0 \delta n_x\} = \epsilon_a \cos(2q_0 z) u_0 e^{iz}. \quad (6.55)$$

Thus it is associated with a scattering wavevector

$$k = l \pm 2q_0. \quad (6.56)$$

The thermal square amplitude of u is derived from eqn (6.44) and has the form

$$\langle |u_0|^2 \rangle = \frac{k_B T}{K_2 l^2}; \quad (6.57)$$

it diverges for $l \rightarrow 0$ or, equivalently, for $k \rightarrow \pm 2q_0$ (i.e. in the vicinity of the Bragg peaks). The corresponding relaxation rate is

$$\frac{1}{\tau_{lt}} = \frac{K_2 l^2}{\gamma_1}. \quad (6.58)$$

The second mode, detected with \mathbf{k} along q_0 , is what we might call the 'umbrella' mode, defined by

$$\begin{aligned} n_x &= \cos(q_0 z) \cos v \sim n_x^0, \\ n_y &= \sin(q_0 z) \cos v \sim n_y^0, \\ n_z &= \sin v \sim v, \end{aligned} \quad (6.59)$$

with $v = v_0 e^{ilz}$. This mode contributes to two components of the dielectric tensor

$$\begin{aligned} \epsilon_{x,z} &\simeq \epsilon_a n_x^0 \delta n_z = \epsilon_a \cos(q_0 z) v_0 e^{ilz}, \\ \epsilon_{y,z} &\simeq \epsilon_a n_y^0 \delta n_z = \epsilon_a \sin(q_0 z) v_0 e^{ilz}. \end{aligned}$$

We see that the scattering vector is now

$$k = l \pm q_0. \quad (6.60)$$

The thermal square amplitude of v is found to be

$$\langle |v_0|^2 \rangle = \frac{k_B T}{K_3 q_0^2 + K_1 l^2}. \quad (6.61)$$

It is maximum (but still finite) for $l = 0$ or $k = \pm q_0$, i.e. midway from the Bragg peaks. The relaxation rate for the umbrella mode is [39]

$$\frac{1}{\tau_{lu}} = \frac{(\alpha_2 + \alpha_4 + \alpha_5)(K_3 q_0^2 + K_1 l^2)}{\gamma_1(\alpha_4 + \alpha_5) - \gamma_2 \alpha_2}. \quad (6.62)$$

As is often found, the relaxation rate is minimal at the l value for which the intensity is maximal ($l = 0$). On the whole, we see that studies on the line width for \mathbf{k} parallel to \mathbf{q}_0 will give two relations on the Leslie coefficients (eqns (6.58) and (6.62)).

6.3.2 Macroscopic flow

6.3.2.1 Apparent viscosities and permeation

A typical viscosity measurement in ordinary fluids makes use of a capillary (of radius R); the pressure drop per unit length of the capillary p' is then

related to the mass flow Q and to the viscosity η by the Poiseuille law [43]

$$p' = \frac{8}{\pi} \frac{Q}{\rho R^4} \eta \quad (6.63)$$

(ρ = fluid density).

Measurements of this type (or with slightly more complicated geometries) have also been carried out on (unoriented) samples of cholesterics [44]. Unfortunately, the data have also always been taken with one same apparatus of fixed geometrical size (i.e. fixed R). Thus it has never been proven that the Poiseuille law holds for cholesterics—in fact, as we shall see, there are strong reasons to believe that it does *not*. However, it is customary to state the results of each measurement in terms of an *apparent viscosity* η_{app} : for instance, with a capillary, we would put

$$\eta_{\text{app}} = \frac{\pi \rho R^4 p'}{8Q}. \quad (6.64)$$

Typical data on η_{app} are shown in Fig. 6.15. Note the following features

1. η_{app} is considerably larger in the cholesteric phase than in the isotropic phase (the ratio may go up to 10^6 !)
2. η_{app} is very sensitive to the shear rate: the viscosity is ‘non-Newtonian’.

These properties have no counterpart in oriented nematic preparations; clearly they must be associated with specific properties of the helical phase. Their explanation has been given in a brilliant paper by W. Helfrich [45]. He considers a cholesteric planar texture which is assumed to be *blocked* (i.e. spatially immobile) because of certain anchoring effects at the walls, and assumes a uniform flow velocity \mathbf{v} , parallel to the helical axis \mathbf{q}_0 . The dissipation per unit volume in this situation is easily derived from the general eqn (5.21) for the entropy source

$$T\dot{S} = (\boldsymbol{\sigma} : \mathbf{A}) + \mathbf{h} \cdot \mathbf{N}. \quad (6.65)$$

For a uniform \mathbf{v} the shear rate tensor \mathbf{A} drops out. On the other hand, we must remember that

$$\mathbf{N} = \frac{d\mathbf{n}}{dt} - \boldsymbol{\omega} \times \mathbf{n}$$

involves the *total* derivative of the director \mathbf{n} , as experienced by a flowing molecule. In the present case, we have

$$\frac{d\mathbf{n}}{dt} = v \frac{\partial \mathbf{n}}{\partial z} = \boldsymbol{\Omega} \times \mathbf{n} \quad (6.66)$$

where z is an axis parallel to \mathbf{v} , and

$$\boldsymbol{\Omega} = v \mathbf{q}_0. \quad (6.67)$$

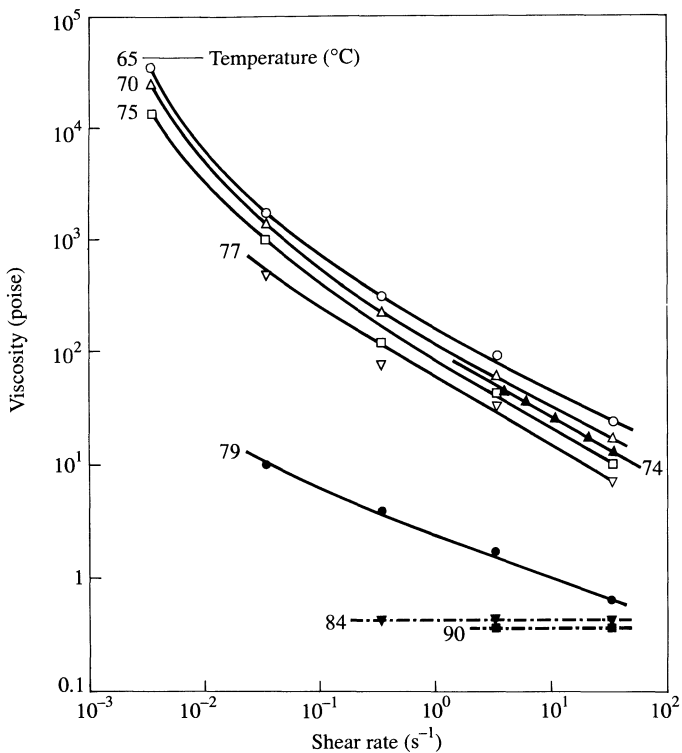


Fig. 6.15. Apparent viscosity of cholesterol myristate as a function of shear rate (after Sakamoto *et al.* [44]).

Also, since v is uniform, the local rotation velocity $\omega = \frac{1}{2} \operatorname{curl} v$ vanishes. Finally we may write the entropy source in the form

$$T\dot{S} = \Gamma \cdot \Omega \quad (6.68)$$

where the rotation velocity Ω is given by (6.67), and the torque $\Gamma = \mathbf{n} \times \mathbf{h}$ is given by eqn (5.32)

$$\begin{aligned} \Gamma &= \mathbf{n} \times (\gamma_1 \mathbf{N} + \gamma_2 \mathbf{A} \cdot \mathbf{n}) \\ &= \gamma_1 \Omega. \end{aligned} \quad (6.69)$$

Inserting this into eqn (6.68), and equating the result to the work done by the pressure gradient p' , we get

$$\begin{aligned} p'v &= \gamma_1 q_0^2 v^2, \\ p' &= \gamma_1 q_0^2 v. \end{aligned} \quad (6.70)$$

Equation (6.70) corresponds to an apparent viscosity

$$\eta_{\text{app}} = \frac{1}{8} \gamma_1 (q_0 R)^2. \quad (6.71)$$

Typical capillary radii R used in viscosity measurements are of the order of 300 μm while $q_0 = 2\pi/P$ is of order 10^5 cm^{-1} . Thus $\eta_{\text{app}}/\gamma_1$ may reach values of order 10^6 ; the dissipative process is not, as usual, a friction between neighbouring fluid regions flowing at slightly different velocities, but rather a friction between the individual molecules (in uniform flow) and a blocked cholesteric texture. The word ‘permeation’ has been introduced in this connection by Helfrich [45].

Of course, in practice, there is no reason for v to be exactly parallel to \mathbf{q}_0 in an unoriented sample; the details of the cholesteric texture achieved in the capillary will influence η_{app} . Conversely, the flow will react on the orientation of the domains, and this is probably the source of the non-Newtonian properties which are observed.

The Helfrich assumption ($v = \text{constant}$ in all the capillary section) may appear surprising at first sight, since, at the capillary walls, v must, in fact, vanish. However, we shall now show that the effects of this boundary condition are important only up to a small distance (of order P) from the walls; if, as is usual, the capillary is much larger than P in diameter, the Helfrich assumption is correct.

For simplicity, we shall discuss this not for a three-dimensional problem with a circular capillary, but rather for a two-dimensional problem of flow between two walls separated by a gap $2R$. Qualitatively, we may write the dissipation in the form

$$T\dot{S} = \gamma_1 q_0^2 v^2 + \bar{\eta} \left(\frac{\partial v}{\partial x} \right)^2 \quad (6.72)$$

where the x -axis is normal to the walls, while the velocity v is along the z -axis (in the plane of the walls). The viscosity $\bar{\eta}$ is a certain average of the Leslie coefficients. The force (per unit volume) along the z direction is then

$$-p' = \gamma_1 q_0^2 v - \bar{\eta} \frac{\partial^2 v}{\partial x^2} = 0. \quad (6.73)$$

This equation for v , plus the boundary condition $v(x = \pm R) = 0$, specifies the problem entirely. The solution is

$$v = \frac{p'}{\gamma_1 q_0^2} \left\{ 1 - \frac{\cosh \kappa x}{\cosh \kappa R} \right\} \quad (6.74)$$

where

$$\kappa^2 = \frac{\gamma_1}{\bar{\eta}} q_0^2. \quad (6.75)$$

Equation (6.74) does show that the Helfrich value $v = p'/\gamma_1 q_0^2$ is obtained

everywhere, except in a small region of thickness κ^{-1} near the walls. Since we expect $\bar{\eta}$ and γ_1 to be of comparable magnitude, we see from eqn (6.75) that κ^{-1} is roughly equal to $P/2\pi$: QED.

6.3.2.2 Future experiments

What are the experiments suggested by the Helfrich idea? First one should check that the ratio p'/v is independent of R (provided that $\kappa R \gg 1$). To pin strongly the cholesteric planes, one might substitute *optical gratings* for the walls (with a grating interval comparable to P).

Clearly, we need measurements on single-domain textures. This is hard to realize, but not entirely impossible, especially in cholesterics with negative local dielectric anisotropy ($\epsilon_{||} < \epsilon_{\perp}$). As explained in Section 6.2, it is possible in principle to induce a planar texture in such a case by suitable low-frequency a.c. electric fields [46]. It should then be possible to study viscous frictions in two very different situations.

1. When the flow velocity is parallel to \mathbf{q}_0 , where the Helfrich permeation dominates (if the texture is anchored).
2. When the flow is normal to \mathbf{q}_0 ; in this case the effective viscosity should be comparable in magnitude to the Leslie coefficients. This second case has been analysed theoretically by Leslie [38]. His calculation allows for local distortions of the helical pattern: these distortions turn out to be of order

$$\frac{\eta}{K q_0^2} A$$

where A is the shear rate. They could lead to some amusing mechano-optical effects.

Finally, the possible role of *dislocations* in the non-Newtonian viscosity should be studied (in analogy with the plastic properties of solid crystals).

6.3.3 Convective instabilities

A remarkable electro-optic effect has been observed in nematic–cholesteric mixtures by Heilmeier and his co-workers [47]. A thin slab, with the conventional planar texture, is driven by a static field \mathbf{E}_0 parallel to the helical axis. When E_0 exceeds a certain threshold E_c , the texture breaks up into small domains (of typical size $10 \mu\text{m}$) which have different orientations (different \mathbf{q}_0) and give rise to a strong scattering of light.

If the field \mathbf{E}_0 is turned off, the domains persist (the planar texture ‘heals’ very slowly): for this reason the process is referred to as the ‘*storage mode*’ of cholesterics. However, it is possible to erase the information (i.e., to accelerate the recovery of the planar texture) by an a.c. field (of frequency in the kilohertz range). This last effect is based simply on the

dielectric anisotropy and has been discussed in Section 6.2.2.2. It requires $\epsilon_{\perp} > \epsilon_{\parallel}$.

How do we explain the onset of the polydomain texture in increasing field E_0 ? The initial model proposed by Heilmeier assumed that the field produced an emulsion of cholesteric particles in a nematic matrix. Two observations apparently supported this idea.

1. No effect was observed on pure cholesterol derivatives.
2. The slow recovery of the planar texture is ruled by a kinetic law reminiscent of the Smoluchovski equation for the association of droplets.

However these facts were slightly misleading. We now tend to believe that the Carr–Helfrich process of charge accumulation governs the storage mode: nematic–cholesteric mixtures are helpful mainly because the nematic component is usually of low purity and high conductance (while pure cholesterol derivatives are better insulators). Also property 2 may occur with many textural transformations independently of a phase separation.

An elegant separation of the instability has been worked out by Helfrich [43]. The material is described by two conductances σ_{\parallel} (along the local director \mathbf{n}) and σ_{\perp} (normal to \mathbf{n}). The case of interest here is $\sigma_{\parallel} > \sigma_{\perp}$. Similarly there are two dielectric constants ϵ_{\parallel} and ϵ_{\perp} . We start with a planar texture and investigate the effects of a small distortion, as shown on Fig. 6.16. The spatial wavelengths involved are assumed to be much larger than the pitch. Then we can use a coarse-grained description, as in the problem at the end of Section 6.2. We take as our variable the displacement $u(\mathbf{r})$ of

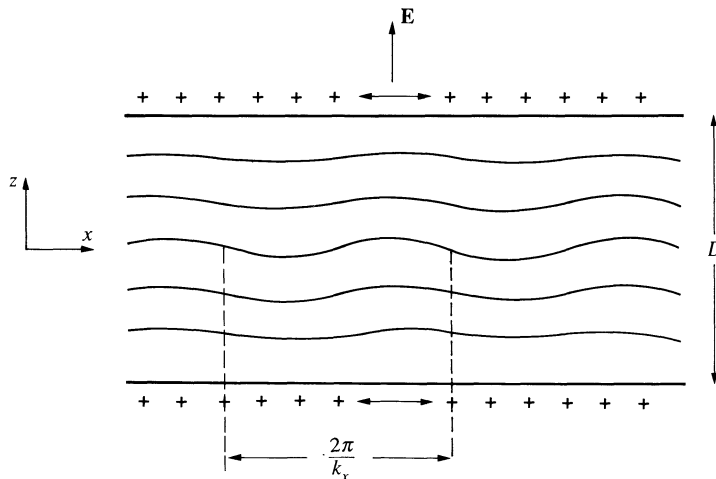


Fig. 6.16. The Helfrich distortion mode for a cholesteric planar texture under an electric field ($\epsilon_a > 0$). The square-lattice distortion of Fig. 6.17 is the superposition of two such distortions oriented at right angles (along x and y).

the cholesteric planes (the z -axis is put parallel to the unperturbed helical axis, and u is measured along z). The type of distortion discussed by Helfrich corresponds to

$$u = u_0 \exp(ik_x x) \sin(k_z z) \quad (6.76)$$

with $k_z = \pi/D$. This choice corresponds to $u = 0$ on both glass plates ($z = 0$ and $z = D$), D being the sample thickness. The wave vector k_x will be chosen later in order to maximize the instability. The local state of affairs may also be described by a unit vector \mathbf{d} normal to the layers. Here we have

$$\begin{aligned} d_z &\simeq 1, \\ d_x &\simeq -\frac{\partial u}{\partial x}. \end{aligned} \quad (6.77)$$

At this coarse-grained level, the cholesteric medium is uniaxial with conductances

$$\begin{aligned} \sigma_{\parallel \mathbf{d}} &= \sigma_{\perp} && \text{(along } \mathbf{d} \text{)} \\ \sigma_{\perp \mathbf{d}} &= \frac{1}{2}(\sigma_{\parallel} + \sigma_{\perp}) && \text{(normal to } \mathbf{d}). \end{aligned} \quad (6.78)$$

Note that $\sigma_{\perp \mathbf{d}} > \sigma_{\parallel \mathbf{d}}$ for the case of interest ($\sigma_{\parallel} > \sigma_{\perp}$). We may write, in dyadic notation:

$$\boldsymbol{\sigma} = \sigma_{\perp \mathbf{d}} + (\sigma_{\parallel \mathbf{d}} - \sigma_{\perp \mathbf{d}})\mathbf{d}:\mathbf{d} \quad (6.79)$$

Similar equations hold for the dielectric tensor.

Let us now write down the current \mathbf{J} present in the distorted structure. \mathbf{J} is due to the total field \mathbf{E} , the sum of the external field \mathbf{E}_0 plus the fields caused by the Carr–Helfrich charges

$$\mathbf{J} = \boldsymbol{\sigma} \cdot \mathbf{E} \quad (6.80)$$

Both vectors \mathbf{E} and \mathbf{d} have small components along x . Treating these components to first order we find that J_z is a constant, while

$$J_x = \sigma_{\perp \mathbf{d}} E_x + (\sigma_{\parallel \mathbf{d}} - \sigma_{\perp \mathbf{d}}) E_0 d_x. \quad (6.81)$$

The condition of charge conservation $\operatorname{div} \mathbf{J} = 0$ leads to $(\partial/\partial x) J_x = 0$ or finally to $J_x = 0$. This fixes the lateral field component

$$E_x = +E_0 d_x \frac{\sigma_{\perp \mathbf{d}} - \sigma_{\parallel \mathbf{d}}}{\sigma_{\perp \mathbf{d}}} = -E_0 \frac{\partial u}{\partial x} \frac{\sigma_{\perp \mathbf{d}} - \sigma_{\parallel \mathbf{d}}}{\sigma_{\perp \mathbf{d}}}. \quad (6.82)$$

Knowing the field distribution we can derive the corresponding charge densities.

1. The density of the mobile carriers ρ_c is given by

$$\rho_c = \frac{1}{4\pi} \operatorname{div}(\boldsymbol{\epsilon} \cdot \mathbf{E}) = \frac{\epsilon_{\perp \mathbf{d}} E_0}{4\pi} \frac{\partial^2 u}{\partial x^2} \left\{ \frac{\sigma_{\parallel \mathbf{d}}}{\sigma_{\perp \mathbf{d}}} - \frac{\epsilon_{\parallel \mathbf{d}}}{\epsilon_{\perp \mathbf{d}}} \right\}. \quad (6.83)$$

2. The total charge density (mobile carriers plus dielectric polarization) is

$$\rho = \frac{1}{4\pi} \operatorname{div} \mathbf{E} = -\frac{E_c}{4\pi} \frac{\partial^2 u}{\partial x^2} \frac{\sigma_{\perp d} - \sigma_{\parallel d}}{\sigma_{\perp d}}. \quad (6.84)$$

The vertical electric force due to the mobile carriers is

$$\phi_c = \rho_c E_0. \quad (6.85)$$

This is not the total electric force. There is another contribution ϕ_d , due to the following fact: the distortion of the cholesteric structure (described by u) imposes some changes on the dielectric tensor, and thus on the electrostatic energy. We can find ϕ_d from the dielectric torque Γ_d (directed along the y -axis) acting on the molecules

$$\Gamma_d = \frac{\epsilon_{\parallel d} - \epsilon_{\perp d}}{4\pi} E_0^2 \left(\frac{E_x}{E_0} - d_x \right). \quad (6.86)$$

In an infinitesimal transformation $u(x) \rightarrow u(x) + \delta u(x)$ the work done (per unit length along z) is

$$\begin{aligned} \int \Gamma_d \delta d_x dx &= - \int \Gamma_d \frac{\partial}{\partial x} \delta \mathbf{u}(x) dx \\ &= \int \frac{\partial \Gamma_d}{\partial x} \delta u(x) dx. \end{aligned}$$

This means that

$$\phi_d = \frac{\partial \Gamma_d}{\partial x} = \frac{\epsilon_{\parallel d} - \epsilon_{\perp d}}{4\pi} E_0^2 \frac{\sigma_{\parallel d}}{\sigma_{\perp d}} \frac{\partial^2 u}{\partial x^2} \quad (6.87)$$

(where we have made use of eqn (6.82)). The total electric force acting on the layers is

$$\phi_z = \phi_c + \phi_d = \frac{\epsilon_{\parallel}}{4\pi} \frac{\sigma_{\parallel} - \sigma_{\perp}}{\sigma_{\perp}} E_0^2 \frac{\partial^2 u}{\partial x^2}. \quad (6.88)$$

It is interesting (although not obvious) to note that ϕ_z is the product of the total charge density ρ and the displacement field $D_0 = \epsilon_{\parallel d} E_0$.

We must now balance ϕ_z against an elastic restoring force ϕ_{el} . We derive ϕ_{el} from the results of the problem on coarse-grained continuum theory (see end of Section 6.2). The elastic energy density is

$$F_{cg} = \frac{1}{2} K_2 q_0^2 k_z^2 u^2 + \frac{1}{2} \tilde{K} k_x^4 u^2 \quad (6.89)$$

where $\tilde{K} = \frac{3}{8} K_3$.

Thus

$$\phi_{el,z} = -(K_2 q_0^2 k_z^2 + \tilde{K} k_x^4) u. \quad (6.90)$$

The condition defining the threshold is

$$\phi_z = -\phi_{el,z}. \quad (6.91)$$

The ratio

$$-\frac{\phi_{el,z}}{\phi_z} = (K_2 q_0^2 k_z^2/k_x^2 + \tilde{K} k_x^2) \left(\frac{4\pi}{\epsilon_{||d} E_0^2} \right) \left(\frac{\sigma_{\perp d}}{\sigma_{\perp d} - \sigma_{||d}} \right) \quad (6.92)$$

is minimum when

$$k_x^2 = q_0 k_z (K_2/\tilde{K})^{\frac{1}{2}}. \quad (6.93)$$

This defines the wavelength of the perturbation which becomes unstable first in increasing fields. Since K_2 and \tilde{K} are comparable in magnitude, this wavelength is proportional to the geometric mean of the pitch $P = 2\pi/q_0$ and of the sample thickness $D = \pi/k_z$. Our analysis requires $k_z \ll q_0$; this condition is indeed satisfied if $D \gg P$. The Helfrich formula for the threshold field is then

$$E_c^2 = \frac{8\pi}{\epsilon_{||d}} \left(\frac{\sigma_{\perp d}}{\sigma_{\perp d} - \sigma_{||d}} \right) (K_2 \tilde{K})^{\frac{1}{2}} q_0 \frac{\pi}{D}. \quad (6.94)$$

Thus the threshold field is proportional to $(PD)^{-\frac{1}{2}}$. In the original Heilmeier experiments, the pitch P was small. The voltage DE_c was high, and, most important, the periodicity of the spatial pattern, $(PD)^{\frac{1}{2}}$, was too small for direct optical observations. More recent experiments have used nematic–cholesteric mixtures, where P is large and the instability can be studied more accurately (G. Gerritsma, private communication). As shown on Fig. 6.17, above the threshold, the undulations build up a square pattern (the superposition of two undulation waves at right angles). The dependence of E_c on both P and D , and also the dependence of the spatial wavelength on D (eqn (6.93)) have been verified in detail (G. Gerritsma, private communication): this gives a very strong confirmation of the Helfrich idea. The instability has also been studied under a.c. fields [48]. Depending on the frequency, one finds two regimes—roughly similar to the ‘conducting’ and ‘dielectric’ regimes of MBBA in a planar texture (see Section 5.3.4).

6.3.4 Torques induced by a heat flux

In any chiral liquid the symmetry of the physical laws is unusual, as stressed in particular by Pomeau [49]: for instance an electric field \mathbf{E} may induce a magnetic moment $\mathbf{M} = \alpha \mathbf{E}$! But these effects are usually very small. In a cholesteric, however, because of the long-range helical order, the orders of

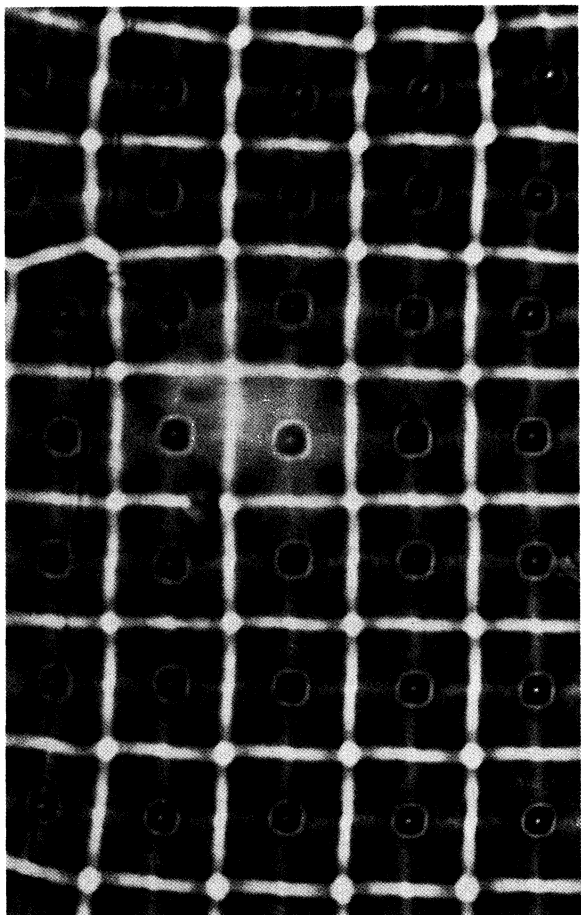


Fig. 6.17. Square-lattice distortion observed in a planar cholesteric textures by application of an electric field E . Note that this distortion is visible optically only with materials of large pitch P . The field E here is roughly 10 per cent higher than the threshold. At higher fields a very different pattern is observed. (Courtesy F. Rondelez.)

magnitude are much more favourable. An interesting class of such effects has been analysed by Leslie [50a] and will be briefly summarized here.

6.3.4.1 Transport equations

Let us consider a certain transport current J , which may describe an electric current, a heat current, or a diffusion current. With this current is associated a conjugate field E : for the three cases discussed above we would have

respectively

$$\begin{aligned}\mathbf{E} &= -\nabla V \quad (V = \text{electrical potential}), \\ \mathbf{E} &= -\frac{\nabla T}{T} \quad (6.95) \\ \mathbf{E} &= -\nabla \mu \quad (\mu = \text{chemical potential of the diffusing species}).\end{aligned}$$

The entropy source including flow, rotation of the director, and transport is of the form

$$T\dot{S} = \mathbf{A}:\boldsymbol{\sigma}' + \mathbf{h}\cdot\mathbf{N} + \mathbf{J}\cdot\mathbf{E}. \quad (6.96)$$

We shall define as fluxes the quantities \mathbf{A} , \mathbf{N} , and \mathbf{E} and as forces $\boldsymbol{\sigma}'$, \mathbf{h} , and \mathbf{J} . This choice is somewhat unsymmetrical because \mathbf{E} is even under time reversal, while \mathbf{A} and \mathbf{N} are odd. But it is convenient in practice.

The phenomenological equations between fluxes and forces may then be written in the form

$$\boldsymbol{\sigma}'_{\alpha\beta} = \sigma_{\alpha\beta}^H + \mu_1 n_\alpha (\mathbf{E} \times \mathbf{n})_\beta + \mu_2 n_\beta (\mathbf{E} \times \mathbf{n})_\alpha \quad (6.97)$$

$$\mathbf{h} = h^H + v\mathbf{n} \times \mathbf{E} \quad (6.98)$$

$$\mathbf{J} = \sigma_\perp \mathbf{E} + (\sigma_\parallel - \sigma_\perp)(\mathbf{n} \cdot \mathbf{E})\mathbf{n} + v\mathbf{n} \times \mathbf{N} - (\mu_1 + \mu_2)\mathbf{n} \times (\mathbf{A}:\mathbf{n}). \quad (6.99)$$

In these equations $\boldsymbol{\sigma}^H$ and \mathbf{h}^H are the standard contributions from nematodynamics† (they are linear functions of \mathbf{A} and \mathbf{N} given explicitly in eqns (5.31) and (5.32)) and σ_\perp and σ_\parallel are the usual conductivities. There are three new coefficients μ_1 , μ_2 , and v . Note the signs occurring in eqn (6.99); they express the fact that \mathbf{J} is odd in time reversal, while $\boldsymbol{\sigma}$ and \mathbf{h} are even. Finally the torque balance condition gives

$$\begin{aligned}\Gamma_z &= \sigma'_{yx} - \sigma'_{xy} = (\mathbf{n} \times \mathbf{h})_z, \\ \Gamma &= \mathbf{n} \times (\gamma_1 \mathbf{N} + \gamma_2 \mathbf{A} \cdot \mathbf{n}) - v\mathbf{E}_\perp\end{aligned} \quad (6.100)$$

where \mathbf{E}_\perp is the component of \mathbf{E} normal to \mathbf{n} , and v is related to μ_1 and μ_2 by the identity

$$v = \mu_1 - \mu_2. \quad (6.101)$$

Equation (6.100) shows that a field \mathbf{E} (which is a polar vector) may induce a torque (an axial vector) in a cholesteric: this is possible only because the cholesteric differs from its mirror image. Some consequences of the cross-

† The superscript H stands for 'hydrodynamics'.

terms have been discussed by Leslie [50a, b] and by Prost [51]. We shall here select one of them.

6.3.4.2 The Lehmann effect

A cholesteric droplet, when submitted to a thermal gradient parallel (or nearly parallel) to its helical axis, shows a uniform rotation of the local molecular axes. This effect was observed by Lehmann [52] and discussed later by Oseen [53]. It can be understood from the Leslie eqns (6.97)–(6.99). Consider for simplicity a flat slab with planar texture (helical axis parallel to the normal Oz to the slab) under a field $E = -\nabla T/T$ parallel to Oz. It is easily verified that in this situation there is no hydrodynamic flow ($\mathbf{A} \equiv 0$). The equation for the angle $\varphi(z)$ between the director and a fixed axis (x) in the plane of the slab is

$$\gamma_1 \frac{\partial \varphi}{\partial t} = K_2 \frac{\partial^2 \varphi}{\partial z^2} - vE. \quad (6.102)$$

The boundary conditions depend on the nature of the two limiting surfaces.

1. If we have a freely suspended film (a situation which is probably not too different from the Lehmann droplets) the condition is one of zero surface torque: this may be shown to give

$$\left. \frac{\partial \varphi}{\partial z} \right|_{z=0} = \left. \frac{\partial \varphi}{\partial z} \right|_{z=D} = q_0 \quad (6.103)$$

where the sample surfaces are located at $z = 0$ and $z = D$. Then the solution of (6.102) is

$$\varphi = q_0 z - \frac{vE}{\gamma_1} t + \text{constant}, \quad (6.104)$$

and the molecules rotate at a uniform speed vE/γ_1 .

2. If we have one anchored surface (at $z = 0$) and one free surface (at $z = D$) the boundary conditions may be taken as

$$\begin{aligned} \varphi(0) &= 0 \\ \left. \frac{\partial \varphi}{\partial z} \right|_D &= q_0 \end{aligned} \quad (6.105)$$

and the solution has the time-independent form

$$\varphi = qz + \frac{1}{2} \frac{vE}{K_2} z^2.$$

Here q is slightly different from the unperturbed value q_0 . To satisfy eqn

(6.105) we require

$$q = q_0 - \frac{vE}{K_2} D.$$

The quantity which would be most easily measured in such an experiment is the angle at the free surface

$$\varphi(D) = q_0 D - \frac{1}{2} \frac{vE}{K_2} D^2. \quad (6.106)$$

Let us guess the order of magnitude of v by a dimensional argument. When $E = -\nabla T/T$, v has the dimension of energy per unit area. Furthermore v must vanish when q_0 vanishes, and must be odd in q_0 . This suggests

$$v = x K_2 q_0 \quad (6.107)$$

where x is an unknown numerical coefficient. The estimate (6.107) gives

$$\frac{\varphi(D, E) - \varphi(D, 0)}{q_0 D} \sim x \frac{T(D) - T(0)}{T}.$$

Thus the distortion due to the head gradient may be quite sizeable. Of course the experiment should be done with a suitable mixture where the pitch is essentially independent of temperature ($dq_0/dT = 0$).

6.4 TEXTURES AND DEFECTS IN CHOLESTERICS

The ideal spiral arrangement which we have discussed up to now is easily distorted into more complicated textures: a lucid review of the main textures is given in the review article by G. Friedel [54]. Associated with the textures are various singular lines. The structure of these lines is often amazingly complex; in the present section, we shall present only the simplest types of textures and of lines.

6.4.1 Textures

6.4.1.1 Focal conics

If a common cholesteric liquid is cooled from the isotropic phase, between two glass plates, one does not usually obtain the simple planar texture (with helical axis normal to the plates); what is found is a different arrangement, where the planes of equal phase are distorted into curved surfaces (Fig. 6.18).

This texture is most easily obtained in rather thick samples, using cholesteric-nematic mixtures with pitches P in the $5 \mu\text{m}$ range. It is essentially identical to the ‘focal conic’ texture of smectics A, which will be

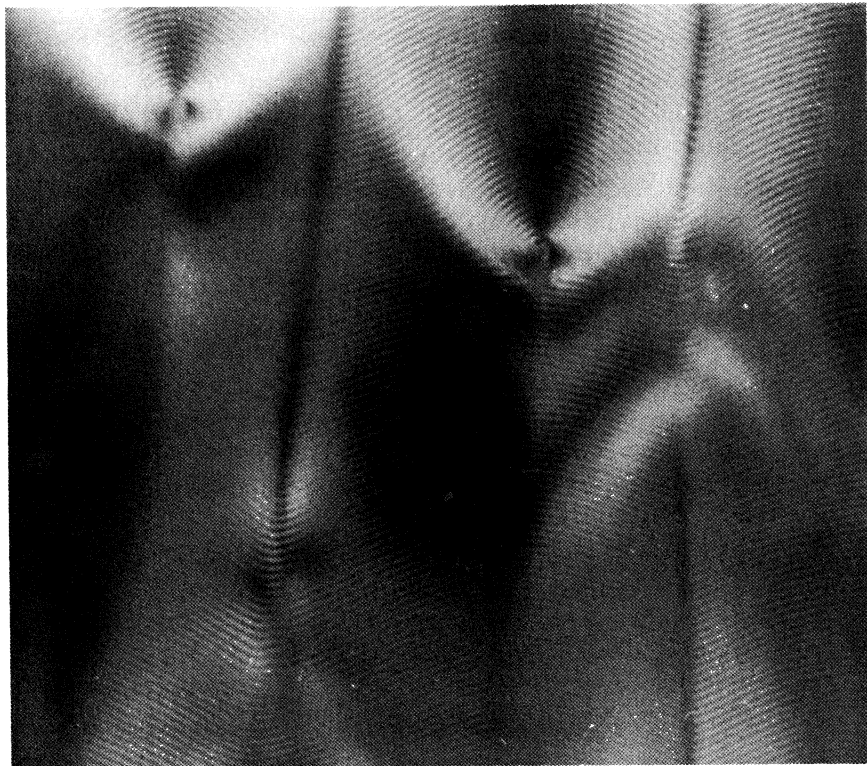


Fig. 6.18. Focal conics in a cholesteric (courtesy Y. Bouligand). Compare with Fig. 9.1 which is the analogue for smectics A. The geometry is explained in Fig. 9.5. The ideal arrangement shown here is rather rare. Usually one finds distorted focal conics [55].

described in more detail in Chapter 9. Both in cholesterics and in smectics we have lamellar structures, which can be deformed easily provided that the thickness of the layers is not altered. Of course this thickness is much larger in cholesterics ($\sim 1 \mu\text{m}$) than in smectics ($\sim 20 \text{\AA}$) but the geometrical consequences are similar. A detailed discussion of these textures, exhibiting clearly the similarities and differences with smectics A, has been given by Bouligand [55]. The similarity in textures between smectics A and cholesterics was a source of confusion in the early literature. One of the great achievements of G. Friedel was to show that the similarity is restricted to certain macroscopic features, and that cholesterics resemble nematics much more than smectics on the molecular scale.

To eliminate the focal conics, it is often sufficient to slightly displace one of the glass plates [54].

6.4.1.2 Cholesteric wedges

To probe the helical arrangement, it is interesting to insert a cholesteric, not between parallel plates, but rather in a small-angle wedge. Three cases must be distinguished.

1. Droplet with one free surface, and tangential boundary conditions (Fig. 6.19). On the bottom plate the molecules are anchored in one orientation, but at the free surface their orientation is arbitrary. The helix can then build up its natural pitch and is undistorted at all points. The orientation of the molecules to the free surface may be determined either by optical techniques or by 'surface labelling' with microprecipitates or bubbles, as explained in Chapter 4. One then sees a pattern of *arceaux*, as shown in Fig. 6.19.†

2. Cholesteric wedge between two oriented solid surfaces (Fig. 6.20). In the pioneering observations by Grandjean [58] this was obtained with a cleavage gap inside a sheet of mica. In more recent studies [6] the wedge is made with two polished glass surfaces. It is important to realize that in case 2 the number of turns allowed for the helix is quantized: the pitch of the spiral is modified, as is apparent in Fig. 6.20(a). One can probe the local pitch through the optical rotatory power, using the de Vries equations (e.g. eqn (6.36)). By this technique, Cano [6] has been able to show that the representation in Fig. 6.20 is correct: the local half-pitch $P/2$ is related to the local thickness d by

$$\frac{P}{2} = \frac{d}{n}$$

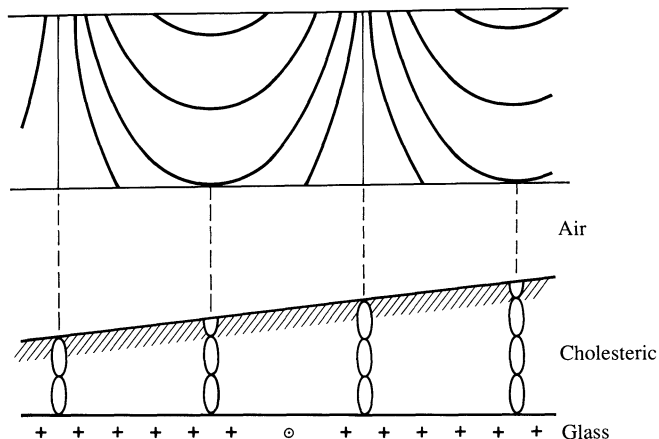
where n is an integer, chosen in such a way that P differs as little as possible from its unperturbed value P . A domain with n half-turns and a domain with $n + 1$ half-turns are separated by a sharp discontinuity: the nature of this discontinuity will be discussed later in this section.

Remark As first shown by J. Rault [59] by applying a horizontal field \mathbf{H} to a droplet with a free surface, it is possible to 'quench' the orientation at this surface,‡ and to go from case (1) to case (2): at a certain threshold field H_2 a set of discontinuities appears.

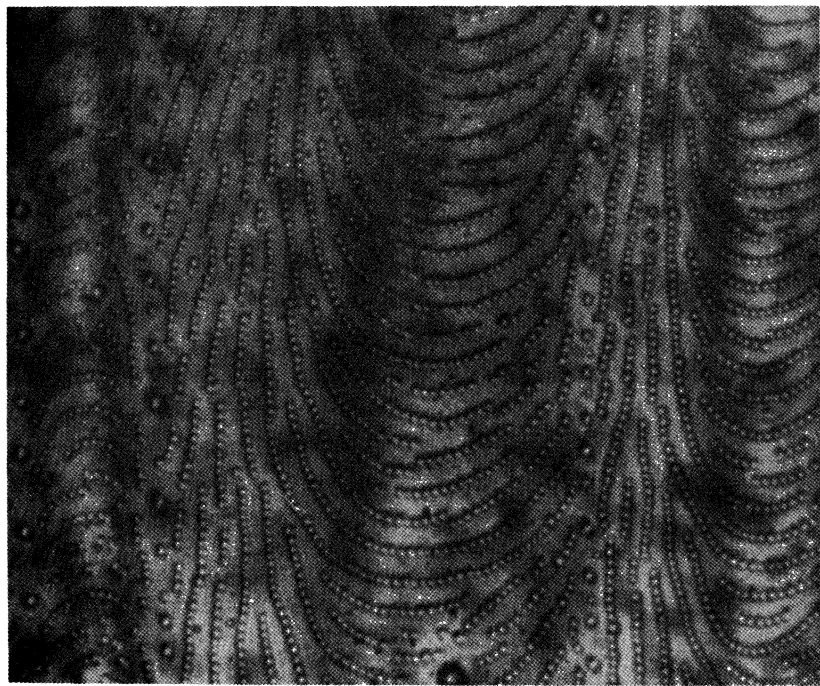
3. A situation very similar to (2) is obtained between two *parallel* polished plates (d fixed) if we use a cholesteric with a concentration gradient (say along X): the unperturbed pitch P_0 is then a function of X . The real pitch P is quantized, but tends to remain as close as possible to $P_0(X)$: again this leads to a succession of domains, separated by the same sharp discontinuities [60].

† The same pattern is found in electron micrographs of oblique cuts in the cuticle of certain crabs, where the building blocks are also arranged in a helix [57].

‡ The direction of alignment at the surface is not along \mathbf{H} , but at 45° from \mathbf{H} . This can be understood by an elementary calculation of the magnetic energy for a spiral of finite length [59].



(a)



(b)

Fig. 6.19. (a) Molecular arrangement in a cholesteric droplet with tangential boundary conditions. The lower part of the figure shows a small part of the droplet where the free surface makes a nearly constant angle with the horizontal plane. The upper part of the figure shows the arrangements of the molecules at the free surface as seen from above the droplet. The molecules at the free surface are disposed in *arceaux*. (b) Display of the *arceaux* by a decoration technique (after reference 56).

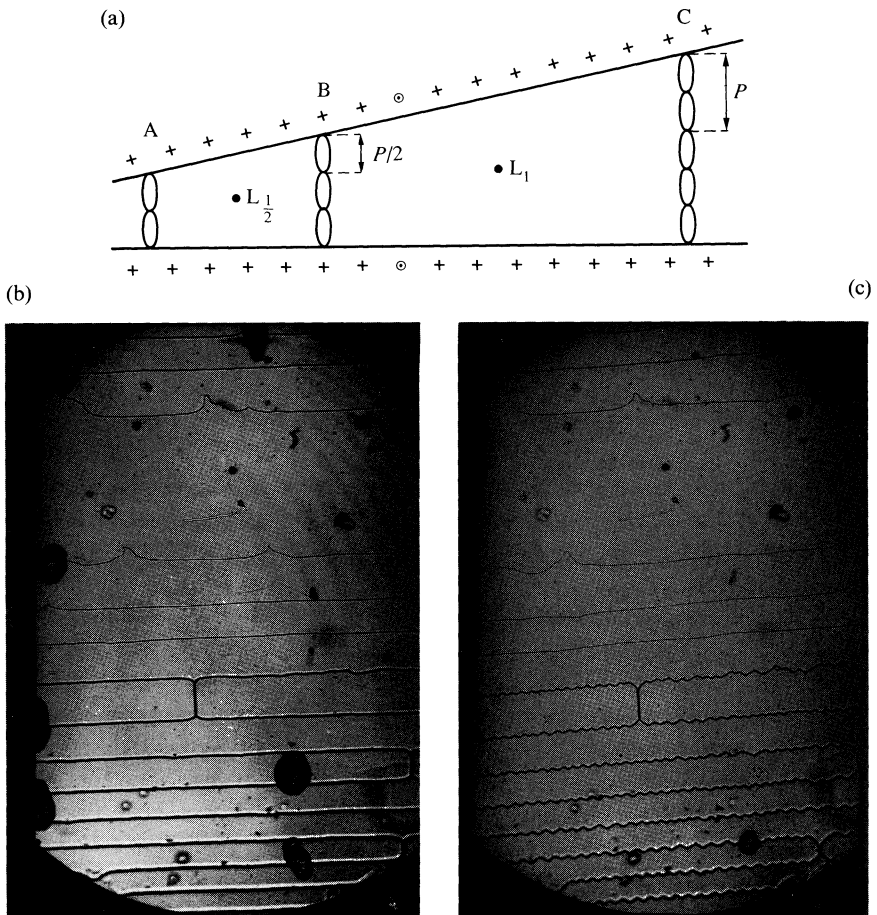


Fig. 6.20. (a) The Cano wedge. Region A with two half-turns is separated from region B (three half-turns) by a line $L_{1/2}$ (of strength $1/2$). Region B is separated from region C (five half-turns) by a line L_1 (strength 1). (b) Aspects of the lines in the wedge between a cylindrical lens and a flat plate. (Courtesy Orsay group.) The image refers to a field-free situation. The thin lines are of strength $1/2$. The thick ones are of strength 1. (c) On the lower image a field $H \sim 8000$ G has been applied normal to the lines. The lines $L_{1/2}$ are unaffected. The lines L_1 are deformed into zigzags.

6.4.1.3 ‘Fingerprint’ texture

With a cholesteric of large pitch observed just above the clearing point T_c , one often finds a texture where the helical axis is *in the plane of the plates*. This situation allows for a ‘side view’ of the helix, and for very simple measurements of the pitch. There are some minor complications.

1. Sometimes the helical axis deviates from the plane of the preparation.

- Near the glass slides that limit the sample at the bottom and at the top, the helix must distort to adjust to the boundary conditions (see reference 61).

But, on the whole, the fingerprint texture is extremely useful for the observation of certain defects (see Fig. 6.27).

6.4.2 Singular lines

Just as in nematics, we find in cholesterics certain singular lines where the director field is discontinuous. But, because the unperturbed structure is a helix, the lines are much more complex in a cholesteric: for this reason, we shall discuss their geometry first and come to the experiments at a later stage.

6.4.2.1 *The Volterra process*

A process generating singular lines inside an ordered medium was invented long ago by Volterra [62]. The application of this theoretical method to cholesterics is due to J. Friedel and M. Kleman [63]; we shall follow their presentation here.

Let us start from an ideal cholesteric helix, and carry out the following operations

- ‘Freeze’ the cholesteric into a solid body.
- Cut this solid along a certain surface S , limited by a line L .
- We displace one side (say S_1) of the cut with respect to the other side S_2 by a certain translation \mathbf{b} . We also rotate S_1 by an angle Ω around a certain axis \mathbf{v} .

We want to ensure, that after these operations, the displaced part S_1 is again ‘in register’ with S_2 along the entire cut: this imposes the condition that the translation \mathbf{b} and the rotation (Ω, \mathbf{v}) belong to the allowed symmetry operations of the unperturbed helix. (We shall list the possibilities below.)

- Fill any voids present with some extra cholesteric matter.[†] (Alternatively, if there is an overlap of the two parts, remove the excess.)
- ‘Defreeze’ the object; the director $\mathbf{n}(\mathbf{r})$ may adjust itself to minimize the Frank energy. At the same time, if the solid object has local dilations or compressions, they can be relaxed by displacing the molecules themselves.

Since the two sides S_1 and S_2 were ‘in register’, the director field $\mathbf{n}(\mathbf{r})$ is not discontinuous at S . But it will (usually) be discontinuous at L . Thus the process generates a *singular line* (which we call a disclination).

[†] The extra material must be positioned and oriented as the initial spiral: then it will be ‘in register’ with S_1 and S_2 .

For the specific case of cholesterics, what are the allowed operations (\mathbf{b} , Ω , \mathbf{v})? Here is a list of possibilities.

1. A translation \mathbf{b} normal to the helical axis has no effect on the director. It may create some local density changes in the frozen system but, when we defreeze, these compressions will relax to zero by viscous flow; no effect is obtained. Thus this type of translation may be omitted.
 2. A translation b along the helical axis: here, to satisfy the ‘in register’ condition we must have
- $$b = mP \quad (m = \text{integer or half integer}).$$
3. A rotation $\Omega = 2m\pi$ around an axis \mathbf{v} parallel to the helical axis. However, because of the screw symmetry of the helix, it is easily seen that this operation is no different from (2).
 4. A rotation $\Omega = 2m\pi$ with an axis \mathbf{v} normal to the helical axis. This will be an allowed symmetry operation if (and only if) \mathbf{v} is either parallel or perpendicular to the local director.

Of course, we can also use any combination of the possibilities 1–4.

It may be useful to compare this set of allowed operations with the allowed operations for a *nematic*: in the latter case all translations \mathbf{b} become allowed and trivial; the only useful operation is a rotation $\Omega = 2m\pi$ around an axis \mathbf{v} normal to the unperturbed director. The position of the rotation axis \mathbf{v} is irrelevant, since two rotations (Ω) around two parallel axes (\mathbf{v} and \mathbf{v}') differ only by a translation. This observation led to the simpler Volterra process described in Chapter 4 where each molecule is rotated around its own centre of gravity. For cholesterics, however, we must keep the full machinery.

6.4.2.2 Simple disclinations

Let us now go to some examples, and start with the Volterra process associated with operation 4 of the above list; it is enough to consider $\Omega = \pi$. Take first the case where the rotation axis \mathbf{v} is normal to the molecules in the unperturbed helix. The process is shown in Fig. 6.21. The result is a line called τ^- . The $(-)$ symbol recalls that, after the two lips S_1S_2 were separated, we have to fill in some voids. On Fig. 6.22 is shown a line λ^- (rotation Ω parallel to the local director).

If we move the two lips in the opposite sense, so that matter is subtracted rather than added we obtain two other lines, called λ^+ and τ^+ (Fig. 6.23). In practice there is an important difference between the λ s and the τ s. In a λ line the director is *continuous*: there is no core singularity.[†] On the other hand, a τ line has a core, and a higher line energy.

[†] The situation is reminiscent of the ‘escape in the third dimension’, which has been described for disclinations of integral strength in nematics (Chapter 4).

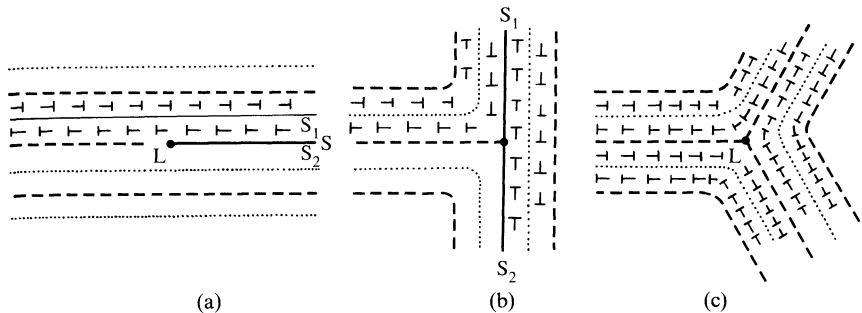


Fig. 6.21. The Volterra process. Example: generation of a τ^- line in a cholesteric. (a) The material is cut on a half-plane S. (b) The two lips S_1, S_2 of the cut are rotated around the axis L by a relative angle of π ($+\pi/2$ for S_1 and $-\pi/2$ for S_2). The empty space left on the right is then filled with cholesteric matter ‘in register’ with the director field on S_1 and S_2 . (c) The structure is relaxed: we are left with a singular line L. Dots, optical axis normal to the sheet; broken lines, axis parallel to the sheet; nail, tilted axis.

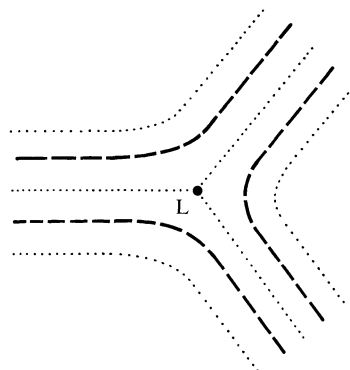


Fig. 6.22. Structure of a line λ^- . Notice that the director field $n(\mathbf{r})$ is continuous on the line itself. A λ line has no core.

It is important to realize that an isolated λ (or τ) line is not easily deformed. This can be understood from the Volterra process: near the line L the relative displacements of the two lips S_1, S_2 , must remain small, if we want to have a low line energy. To achieve this the rotation axis v must coincide with L: this implies that L is a straight line.

Let us turn now to the lines generated by operation 2 or by its equivalent 3: these are called χ lines. To each χ line is associated a value of the strength (m). A χ line can be viewed in two different ways: as a *dislocation* in a system of layers (via operation 2); or as a *disclination* in a twisted nematic (via operation 3).

One schematic example is shown in Fig. 6.24. Note that a χ line is more

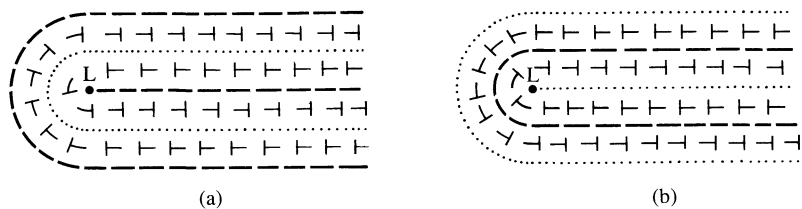


Fig. 6.23. (a) Line τ^+ . (b) Line λ^+ (no core).

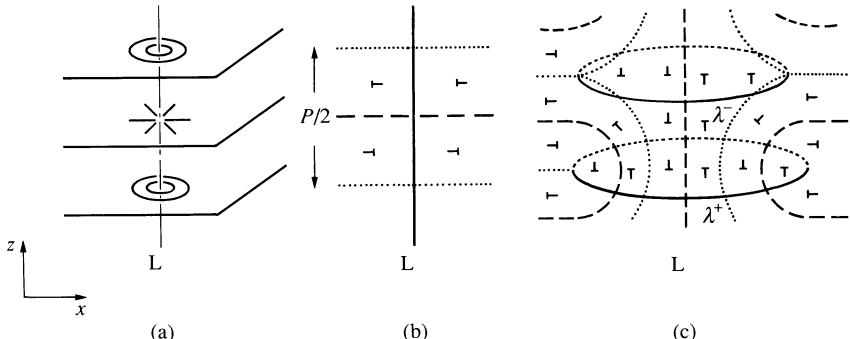


Fig. 6.24. Structure of a χ line of strength +1 normal to the cholesteric planes. (a) Naive model with a strong discontinuity at the core. (b) Same model: arrangement in one diametral plane (x, y). (c) Dissociated model: the line has no singularity at the core. It is surrounded by a periodic system of λ rings shown here in perspective. (After reference 64.)

flexible than a λ or a τ : if we generate the χ by a rotation \mathbf{v} parallel to the helical axis (*operation 3*) we impose relative displacements to S_1 and S_2 that are normal to this axis and that can be relaxed viscously: these displacements do not increase the line energy. Thus the χ line need not coincide with its rotation axis \mathbf{v} , and it may point in various directions.

6.4.2.3 Dissociation of a χ line

We have seen in Chapter 4 that, in nematic liquids, the disclinations of *integral* strength are generally unstable. A somewhat similar effect is found in cholesterics with the χ lines. Consider for instance a χ line of strength $m/2$, normal to the helical axis (Z) and parallel to the axis (Fig. 6.24). By analogy with eqn (4.1) we might, at first sight, expect an arrangement around the line of the form [65]

$$\begin{aligned} n_x &= \cos(q_0 z + m\psi + \alpha_0), \\ n_y &= \sin(q_0 z + m\psi + \alpha_0), \\ n_z &= 0 \end{aligned} \quad (6.108)$$

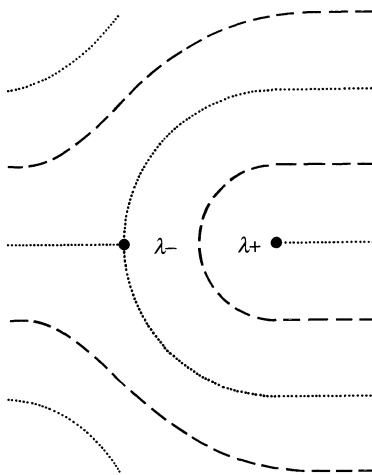


Fig. 6.25. Line of strength 1 (normal to the helical axis) dissociated into a $\lambda^- \lambda^+$ pair. This corresponds to the thick lines in Fig. 6.20(b).

where $\tan \psi = z/x$ and α_0 is a constant. This corresponds to a strong singularity in the director field $\mathbf{n}(\mathbf{r})$ at the line ($x \rightarrow 0, z \rightarrow 0$). This singularity may possibly be meaningful for $m = \pm \frac{1}{2}$.[†] But for $m = \pm 1$ the χ line will tend to dissociate into a pair

$$\chi(1) \rightarrow \lambda^+ + \lambda^-,$$

as shown in Fig. 6.25. This is favourable, because both λ lines have no core singularity. The pair ($\lambda^+ \lambda^-$) is called a P pair because the material on one side ($x \rightarrow +\infty$) has two extra cholesteric layers (or one full pitch P) when compared to the material on the other side ($x \rightarrow -\infty$).

This important dissociation process was invented by Friedel and Kleman [63]. Similar (although more complex) dissociations probably occur for χ lines that are oblique with respect to the cholesteric planes [64].

We may ask whether dissociation also takes place for χ lines of half-integral strength. It is indeed possible to consider the process

$$\chi(\frac{1}{2}) \rightarrow \lambda^+ + \tau^-,$$

which is displayed in Fig. 6.26, or the analogue $\chi(\frac{1}{2}) \rightarrow \lambda^- + \tau^+$. However, we now have a τ line in the final state, with a finite core energy: for lines of half-integral strength, it is not possible to eliminate the core singularity, as explained in Chapter 4. Thus it is not obvious that the dissociation into a $\lambda\tau$ pair will really lower the energy. (The $\lambda\tau$ pair is often a $P/2$ pair.)

[†] However, it must be pointed out that eqn (6.108), although correct for a twisted nematic is never rigorous for a cholesteric.

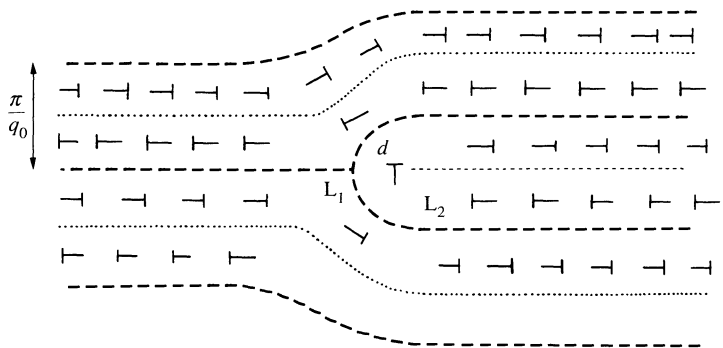


Fig. 6.26. Line of strength $1/2$ dissociated into a λ^+ - τ^- pair. This may be the structure of the thin lines of Fig. 6.20(b).

6.4.2.4 Observations on line defects

The most direct evidence for the λ lines and the λ^+ - λ^- pairs is obtained in the fingerprint texture (Fig. 6.27). But for quantitative studies, observations of defects in a planar texture are more accurate. To generate lines *normal to the helical axis*, two methods are particularly useful: one static and one dynamic.

1. *Cano wedge* (Fig. 6.20.) In *thin* wedges, the discontinuities studied by Cano [6] were always found to separate domains with n and $(n + 1)$ half turns. Cano first interpreted them in terms of sheet singularities, but it soon became clear that the discontinuities must be singular lines (of strength $\frac{1}{2}$). In *thicker* wedges, the Orsay group later observed that lines of strength 1 (separating n from $n + 2$) were systematically found [66]. At that time, the origin of this anomalous stability for ‘double’ lines was quite mysterious. Friedel and Kleman solved the paradox with the model of a $(\lambda^+\lambda^-)$ pair, devoid of any core singularity. If a magnetic field \mathbf{H} is applied normal to the lines and to the helical axis, the double lines take on a zigzag conformation (Fig. 6.20(c)) as soon as $H > H_z$ where H_z is a certain threshold field of order $H_c/2$ (H_c being the critical field for unwinding of the spiral). On the other hand, the simple lines are insensitive to the field. This difference in behaviour has been explained by Kleman and Friedel [63]: the experiments are made with nematic–cholesteric mixtures for which $\chi_a > 0$. Then, as seen earlier in this chapter, the helix prefers to have its axis normal to the field. The region between λ^+ and λ^- (Fig. 6.25) has a helical axis along x , and is thus in a high magnetic-energy conformation. The magnetic energy is lowered in the zigzag conformation. Kleman showed that qualitatively $H_z \sim H_c/m$ where $m/2$ is the strength of the line. Thus the lines of strength 1 have observable $H_z \sim H_c/2$.

(a)

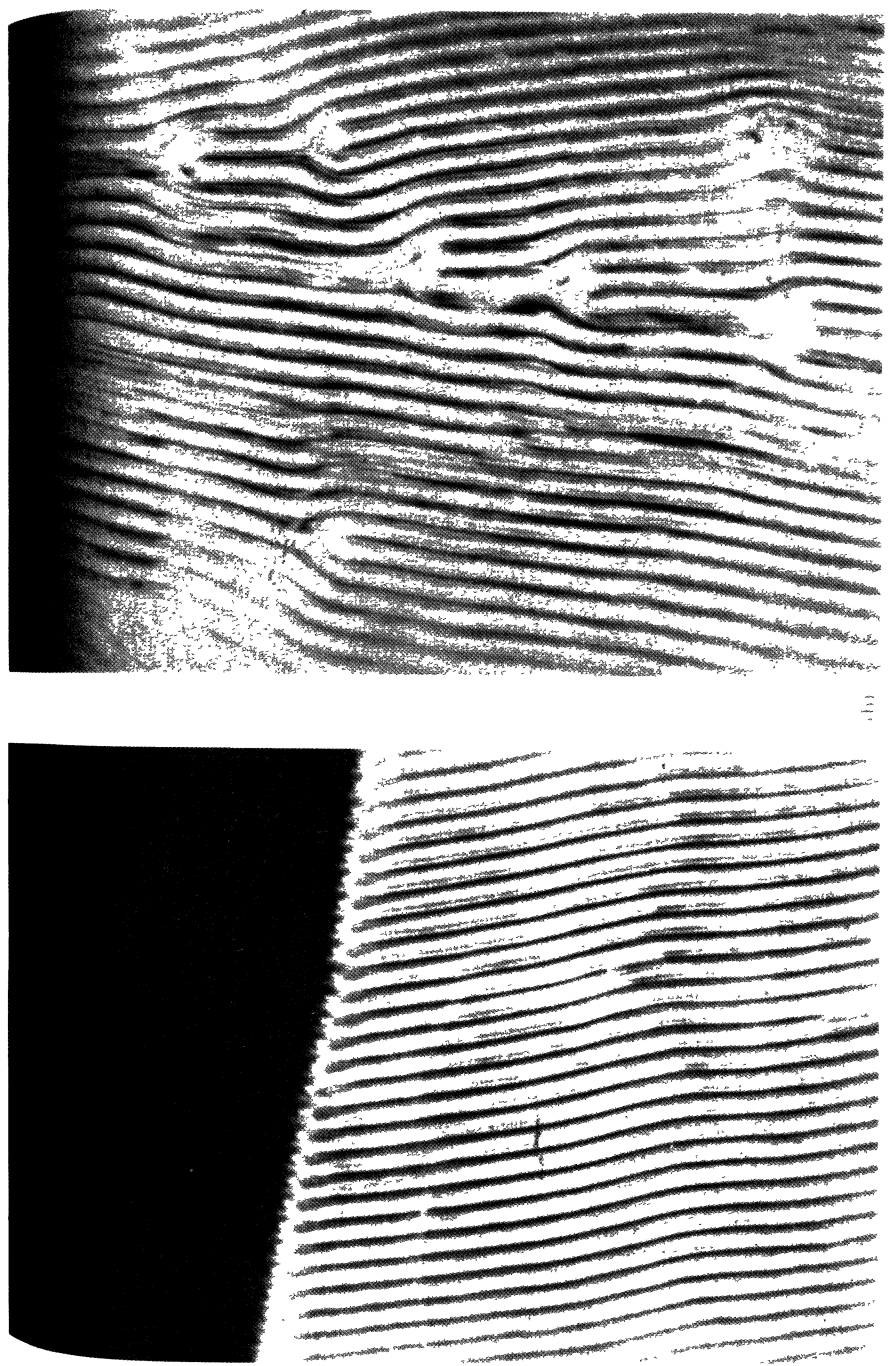


Fig. 6.27. (a) Fingerprint texture near a cholesteric-isotropic interface. (b) Defects in a fingerprint texture. Note that all the defects shown involve λ lines only (no core energy). (Courtesy P. Cladis and J. Rault.)

The observations do not allow conclusions on the structure of the lines of strength $\frac{1}{2}$: for instance the absence of field effects on these lines is explained as well in a pure χ model as in a $\lambda\tau$ model (where $H_Z \sim H_c$ and thus H_Z would not be detectable). Certain qualitative optical features [66] suggests that both types (dissociated and undissociated) of lines of strength $\frac{1}{2}$ may be present, depending on the sample thickness. To clarify this point is difficult, but one can think of the following technique: polymerize the cholesteric inside a Cano wedge (using for instance cholesterol acrylate as one constituent [67]) and study the resulting frozen texture by electron microscopy.

(2) *Mechanical twist.* This method of line generation is the analogue of the Meyer technique for nematics (Chapter 4). The cholesteric planar texture (with N_0 half-turn) is realized between two polished glass plates. An abrupt change in the twist is then imposed, either by a rotation of one plate, or by a change in spacing, or by a combination of both processes. In the equilibrium state for these new conditions, the optimum number of turns N_f will be usually different from N_0 . The transformation $N_0 \rightarrow N_f$ is realized by the migration of disclination loops. With suitable care one can generate lines of strength $\frac{1}{2}$ or of strength 1 [64] and measure their line tension or their mobility.

Up to now, we have discussed only the generation of lines normal to the helical axis. To observe χ lines parallel to this axis the following recipe is convenient [64]: one uses a cholesteric-mixture between a glass wall and a free surface (tangential boundary conditions). The transition from isotropic to cholesteric is obtained by slow evaporation of a passive solvent. One then obtains a planar texture with a few vertical χ lines present: the aspect is reminiscent of a *Schlieren* texture. Each χ line has the optical appearance of a *noyau*. Just as for nematics, by observations between crossed nicol prisms, one can determine the strength $m/2$ of the line.

The majority of the lines are found to have integral strength, and a rather thick core in optical observations. They are probably dissociated into pairs, but the geometry of these pairs is complex and not yet fully understood. Lines of half-integral strength are less frequent, and seem to have a thinner core. Detailed observations and plausible models for both are described in the doctoral work of Rault [64].

6.5 BLUE PHASES

6.5.1 Experimental observations

If, like Reinitzer in 1888, we observe under a polarizing microscope a mesogenic compound made of chiral molecules, we are very likely to see a ‘violet and blue colour phenomenon, which appears and then quickly disappears, leaving the substance cloudy but still liquid’ [68, 69]. The cloudy

substance was quite early shown to be the cholesteric phase, but the proper identification of the colour phenomenon as the manifestation of an equilibrium state of a matter is much more recent. Volumetric [70] and scanning calorimetry [71], together with accurate high-resolution enthalpic measurements [72], have established the existence of three phases (in the absence of external fields), called blue phases for historical reasons, separated from each other and from the isotropic and cholesteric phases by first-order transitions. The adjective blue does not prevent them from looking bright yellow or red in some instances. The colour can be traced back to the selective Bragg reflection of particular wavelengths, which indicates that the structure is periodic.

In reflection, one observes platelets that scatter a well defined colour under particular Bragg conditions. The scattered waves are circularly polarized. In transmission between crossed polarizers (or nearly so since the residual rotatory power is essentially negligible over a 100- μm thick slab), in the absence of Bragg reflection, the field of view is black; if one platelet Bragg-scatters a given wavelength with a given circular polarization, the opposite circular polarization is transmitted and gets through the linear analyser, giving rise to the same colour observation. The difference with reflection comes only from the fact that, across a typical slab, several platelets may satisfy different Bragg conditions and lead to colour superpositions.

The sequence of the Bragg reflections [73, 74], the optical isotropy, and the beautiful faceting of crystals [75, 76] when properly grown from the isotropic melt show that these phases are characterized by a cubic symmetry. The period of the structure, which is close to that of cholesterics, falls obviously in the optical wavelength range and thus there are about 10^7 – 10^8 molecules in a unit cell. Furthermore, X-ray studies show that local order is liquid-like! How can a local liquid be a macroscopic crystal? In fact, it is not too difficult to understand if one realizes that a cholesteric is itself a one-dimensional crystal (see, for example, the problem of Section 6.2.2). Thus blue phases appear as the three-dimensional counterpart of cholesterics. Their crystalline nature is further established by the fact that one can measure a shear elastic constant [76, 77]. Whether blue phases can be forced to flow or not depends on boundary conditions just as in ordinary crystals and not on their local fluid nature. Orders of magnitude are quite different from those for usual crystals, but dimensional analysis accounts for most of the observed facts. For instance, ordinary gravitational forces are large enough to exceed the yield stress and, under usual conditions, blue phases are observed to flow. In that respect they are very similar to the colloidal crystals made of polyballs. Their Bragg scattering characteristics differ from those of polyballs in that reflected wavelengths are circularly polarized in the same sense as in the cholesteric phase.

All these observations suggest that a pertinent description of blue phases should involve the same local description as for cholesterics (or even

nematics), i.e. that based on the order parameter $Q_{\alpha\beta}(\mathbf{r})$ introduced in Chapter 2. Since there is three-dimensional long-range order, $Q_{\alpha\beta}(\mathbf{r})$ can be expanded in a Fourier series

$$Q_{\alpha\beta}(\mathbf{r}) = \sum_{\mathbf{q}} Q_{\alpha\beta}(\mathbf{q}) \exp(i\mathbf{q}\cdot\mathbf{r} + \phi_{\mathbf{q}}) + \text{constant terms}, \quad (6.109)$$

in which the summation is over all possible wavevectors compatible with the three-dimensional space group symmetry of the structure.

The most obvious difference from ordinary crystals is that the mass (or electronic) density is replaced by the traceless nematic order parameter. This does not mean, however, that there is no density modulation in blue phases. Indeed, for finite wavevectors, density modulations can always couple to angular order parameter second variations. More precisely, one can always write

$$\tilde{\rho}(\mathbf{q}) = \lambda_{\tilde{\mathbf{q}}} q_{\alpha} q_{\beta} Q_{\alpha\beta}(\mathbf{q}). \quad (6.110)$$

Thus there is also a three-dimensional periodic density modulation in blue phases, but clearly this is only a side phenomenon. We can estimate from our knowledge of the isotropic–nematic transition that there is a few per cent relative modulation.

A typical diagram involving an isotropic, a cholesteric, and three blue phases in a (T, q_0) plane is given in Fig. 6.28 (q_0 is, for instance, the cholesteric wavevector far from any transition). For q_0 small, one observes a direct isotropic to cholesteric transition, but as q_0 increases, this opens stability domains usually a few tens of degrees wide (a few degrees in extreme cases)

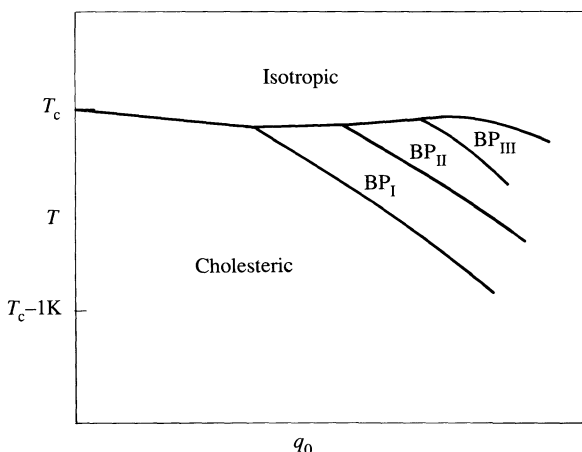


Fig. 6.28. Typical phase diagram in a temperature chirality plane. All lines correspond to first-order transitions.

for three distinct blue phases called blue phase I, II, and III (BP I, BP II, BP III). All the phase boundaries define first-order transitions [72]. A careful comparison with the experimental data of the Bragg selection rules for chiral structures constructed with $Q_{\alpha\beta}$ [78, 79] and observation of the faceting of monocrystals shows that!

- BP I is body-centred cubic.
- BP II is simple cubic.
- BP III is ‘amorphous’ but with short-range chiral order (of a few pitch lengths).

(For a detailed description and bibliography see references 74, 79, and 80.)

6.5.2 Double twist theories

The observations that we have quickly summed up in Section 6.5.1, strongly suggest that blue phases are the three-dimensional counterpart of cholesterics. Since they appear between the isotropic and the cholesteric phases a natural procedure to try to understand their occurrence is through the use of the chiral version of the Landau theory described in Chapter 2 [81, 82]. The main features of this approach will be sketched in the next section. However, we can have a simpler qualitative understanding of their stability, if we remark that, in general, cholesterics would like to develop their helicoidal precession in all directions perpendicular to the director simultaneously, rather than just choose one direction [83] (Fig. 6.29). The exact reason for this tendency is not as transparent as is often believed and, in particular, is not connected to chirality: a simple cholesteric helix can save as much twist energy as a double twist but costs additional saddle splay (if K_{24} is positive); hence the announced preference.

To understand the origin of the energy difference, we come back to the basic deformations (i.e. tensorial invariants) of a locally uniaxial medium

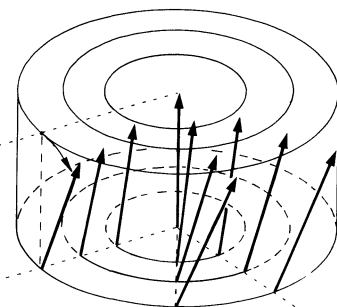


Fig. 6.29. Schematic representation of a double twist.

before any integration by parts. The two deformations that are pertinent in this problem are those of:

- tetrahedral symmetry, i.e. saddle splay, which is expressed via the traceless matrix (again for \mathbf{n} along z)

$$\begin{bmatrix} \frac{\partial n_x}{\partial x} - \frac{\partial n_y}{\partial y}, & \frac{\partial n_x}{\partial y} + \frac{\partial n_y}{\partial x} \\ \frac{\partial n_x}{\partial y} + \frac{\partial n_y}{\partial x}, & \frac{\partial n_y}{\partial y} - \frac{\partial n_x}{\partial x} \end{bmatrix}$$

with the corresponding energies

$$\frac{1}{2}K_2 \left(\frac{\partial n_x}{\partial y} - \frac{\partial n_y}{\partial x} - q_0 \right)^2 + \frac{1}{2}K_{24} \left\{ \left(\frac{\partial n_x}{\partial x} - \frac{\partial n_y}{\partial y} \right)^2 + \left(\frac{\partial n_x}{\partial y} + \frac{\partial n_y}{\partial x} \right)^2 \right\}. \quad (6.111)$$

Let us now compare, in the neighbourhood of the z -axis, the energies w_1 and w_2 for

$$\text{a simple twist } n_x = -qy, \quad n_y = 0, \quad n_z \simeq 1; \quad (6.112)$$

$$\text{a double twist } n_x = -q'y, \quad n_y = +q'x, \quad n_z \simeq 1, \quad (6.113)$$

$$w_1 = \frac{1}{2}K_2(q - q_0)^2 + \frac{1}{2}K_{24}q^2, \quad (6.114)$$

$$w_2 = \frac{1}{2}K_2(2q' - q_0)^2. \quad (6.115)$$

Note that, by a suitable choice of q and q' , the twist energy may be set to zero in both cases. However, simple twist involves a saddle splay, and the minimum of w_1 cannot be zero. w_1 can be in fact rewritten

$$w_1 = \frac{(K_2 + K_{24})}{2}(q - q'_0)^2 + \frac{1}{2}(K_2 K_{24}/(K_2 + K_{24}))q_0^2 \quad (6.116)$$

with

$$q'_0 = q_0 \frac{K_2}{K_2 + K_{24}}$$

and

$$w_{2\min} - w_{1\min} = -\frac{1}{2}(K_2 K_{24}/(K_2 + K_{24}))q_0^2. \quad (6.117)$$

For $K_{24} < 0$ simple twist is more stable than double twist. For $K_{24} > 0$ the reverse is true. Close to the isotropic phase, Landau theory shows that $K_{24} \simeq K_2 > 0$; hence the tendency for double twist. Note that in the preceding chapters and sections we called K_2 the sum $K_2 + K_{24}$ and that, for $K_2 = K_{24}$, the optimum wavevector is the same for simple and double twist, namely $q_0/2$.

Is it possible to extend this type of solution through all space?

The observation of Fig. 6.29 suggests that it is not. A more technical proof may be obtained in the following way [80]. Equation (6.113) may be

rewritten in tensor notation (the summation convention over repeated indices is used)

$$\frac{\partial n_j}{\partial x_i} = \frac{q_0}{2} \epsilon_{ijk} n_k \quad (6.118)$$

(in which ϵ_{ijk} is the complete antisymmetric tensor with $\epsilon_{xyz} = 1$, and the wave vector has been set directly to its optimum value). If (6.118) were to hold in a domain, one would be able to take its derivative with respect to x_l

$$\frac{\partial^2 n_j}{\partial x_l \partial x_i} = \frac{q_0}{2} \epsilon_{ijk} \frac{\partial}{\partial x_l} n_k$$

or, by using (6.118) for $\partial n_k / \partial x_l$, and with the identity $\epsilon_{ijk} \epsilon_{lkm} = \delta_{im} \delta_{jl} - \delta_{il} \delta_{jm}$,

$$\frac{\partial^2 n_j}{\partial x_l \partial x_i} = \frac{q_0^2}{4} (n_i \delta_{jl} - n_j \delta_{il}),$$

which is clearly inconsistent, since the left-hand side is symmetrical whereas the right-hand side is not. This proves that (6.118) cannot be satisfied in a continuous domain.[†] In fact, it can only be satisfied on a line.

Thus we are bound to consider arrays of such lines of double twist. Let us, for the sake of argument, consider the array of Fig. 6.30(a). The axes of the double twist cylinders are parallel to each other and their intersection with a plane normal to them defines a square lattice. The radius of the cylinders is such that there is no discontinuity in the director pattern at their contact points. The space between the cylinders defines an $s = -1$ disclination which we know requires no singularity, since the director field can escape in the direction parallel to the cylinders. This might at first sight look like an energy-saving solution since it involves a finite density of double twist lines. It turns out that it is not. To understand this point, one has to come back to the covariant expression of the saddle splay energy (remember Section 3.1.2)

$$\frac{K_{24}}{2} \{(\operatorname{div} \mathbf{n})^2 + 2 \operatorname{div}((\mathbf{n} \cdot \nabla) \mathbf{n} - \mathbf{n} \operatorname{div} \mathbf{n}) + (\mathbf{n} \cdot \operatorname{curl} \mathbf{n})^2\}. \quad (6.119)$$

The double twist (6.113) or (6.118) does not cost saddle-splay energy because:

- there is no splay;
- the second term exactly balances the third one.

However, this only holds locally on the axis of the double twist line. In a structure such as that of Fig. 6.30(a), the second term does not contribute, since it can be integrated out to an external surface, the influence of which

[†] Equation (6.118) can exactly be fulfilled in curved space, more precisely, on the three-dimensional surface of a four-dimensional sphere [84]. It allows, for example, a natural description of defects in blue phases [85].

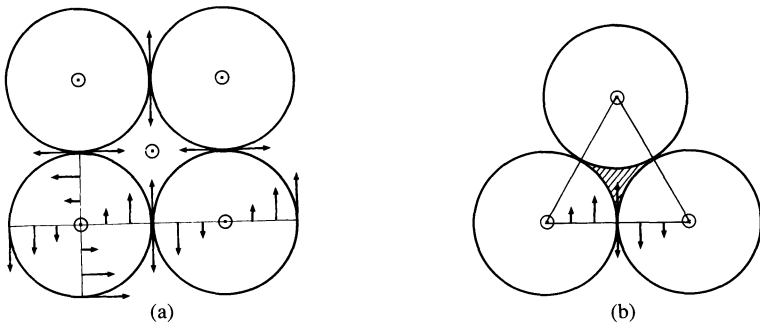


Fig. 6.30. (a) A square array of double twist cylinders. The cylinders are perpendicular to the figure and extend to infinity. Note the $s = -1$ disclination line and its escape in the third dimension. (b) A triangular array of double twist cylinders. The hatched region is supposed to be the isotropic phase.

vanishes for an infinite system. Thus even though double twist lines save energy locally (as compared to the cholesteric), the global structures does not because one loses exactly as much in other regions of space. Let us now consider the structure of Fig. 6.30(b) in which the hatched area is in the isotropic phase, with the generalization of the double twist configuration according to (in circular cylindrical coordinates) [83]

$$\mathbf{n} = \hat{\mathbf{z}} \cos \frac{q_0}{2} \rho + \hat{\mathbf{v}} \sin \frac{q_0}{2} \rho. \quad (6.120)$$

The total elastic energy involves twist, saddle splay, and bend. One can easily calculate its value per unit (triangular) cell in the one-constant approximation ($K_2 + K_{24} = 2K_{24} = K_3 = K$; the cholesteric energy is taken as the reference, the radius of the double twist cylinders as $R = \pi/q_0$), such that

$$W = \frac{\pi K}{2} \int_0^{\pi/q_0} \frac{d\rho}{\rho} \sin^2 \frac{q_0 p}{2} - \frac{\pi}{2} K \simeq -1.4\pi K. \quad (6.121)$$

The first term involves both bend and twist energies; the second involves only saddle splay. It can be either calculated directly or with the remark that the isotropic region is equivalent to a $-\frac{1}{2}$ disclination. In fact, since there is an isotropic domain, one should add its free energy difference with the cholesteric and the interfacial tension σ . Right at the would-be cholesteric-isotropic transition, we just have to take account of the interfacial tension, so that

$$W = -(1.4)\pi K + \pi R\sigma. \quad (6.122)$$

This structure is more stable than the cholesteric, provided that

$$\frac{\pi}{q_0} = R < 1.4K/\sigma.$$

In general, one does not know σ , but values measured at the isotropic–nematic interface provide a reasonable estimate [86]. With $\sigma \simeq 10^{-2}$ erg cm $^{-2}$, $K \simeq 3 \cdot 10^{-7}$ dyn, one finds $R < 0.4$ μm which compares rather well with experimental values. One sees from this simple example that blue phases exist only if the natural pitch is small enough.

Can one estimate the temperature range over which this phase would be stable? Equation (6.123) has to be completed by the introduction of the free energy difference between the isotropic and the cholesteric phase and the temperature dependence of K and σ such that

$$W = -1.4\pi K + \pi R\sigma + \left(\sqrt{3 - \frac{\pi}{2}} \right) f R^2. \quad (6.123)$$

Since the cholesteric–isotropic transition is first-order, we can assume (for $(T_c - T) \ll T_c$) that

$$f \simeq a(T_c - T), \quad K = K_c + K'(T_c - T), \quad \sigma = \sigma_c + \sigma'(T_c - T).$$

With the reasonable values, $a \simeq 8 \cdot 10^4$ erg K $^{-1}$ cm $^{-3}$ [83], $\sigma \simeq 2 \cdot 10^{-2}$ erg K $^{-1}$ cm $^{-2}$, and $K' \simeq 10^{-8}$ dyn K $^{-1}$, we find

$$W \simeq -6 \cdot 10^{-7} + (T_c - T) 3 \cdot 10^{-6} \text{ erg}.$$

This yields a 2 K temperature range for this ‘blue’ phase, which is small, but of the right order of magnitude. Note that if K' were much larger, one could increase considerably the stability domain and even get out of the validity range of the linear approximation. Although this structure has not been observed experimentally, this is the first that has been proved to be stable within the Landau description [81]. Note also that, if we had filled the intercylinder space with isotropic phase in the case of Fig. 6.30(a), we would also have found a stability domain.

We considered that an outer radius $R = \pi/q_0$ allowed us to build a two-dimensionally ordered blue phase. An outer radius $R = \pi/2q_0$, such that the director rotation is $\pi/4$ from the axis, allows us to build the cubic structures of Fig. 6.31 [83, 87] where the structure in Fig. 6.31(a) is simple cubic and that in (b) is body-centred. The $\pi/4$ direction rotation allows the absence of discontinuity at the cylinder’s contact point, but the structures require $-\frac{1}{2}$ disclination lines similar to that of Fig. 6.30(b). If in Fig. 6.31(b) one interchanges double twist axes and $-\frac{1}{2}$ disclination axes, one obtains another body-centred cubic structure (note that, in order to ensure a continuous director field, the rotation of the director has to be 54.7°). Detailed calculations (in which the director is allowed to relax to local

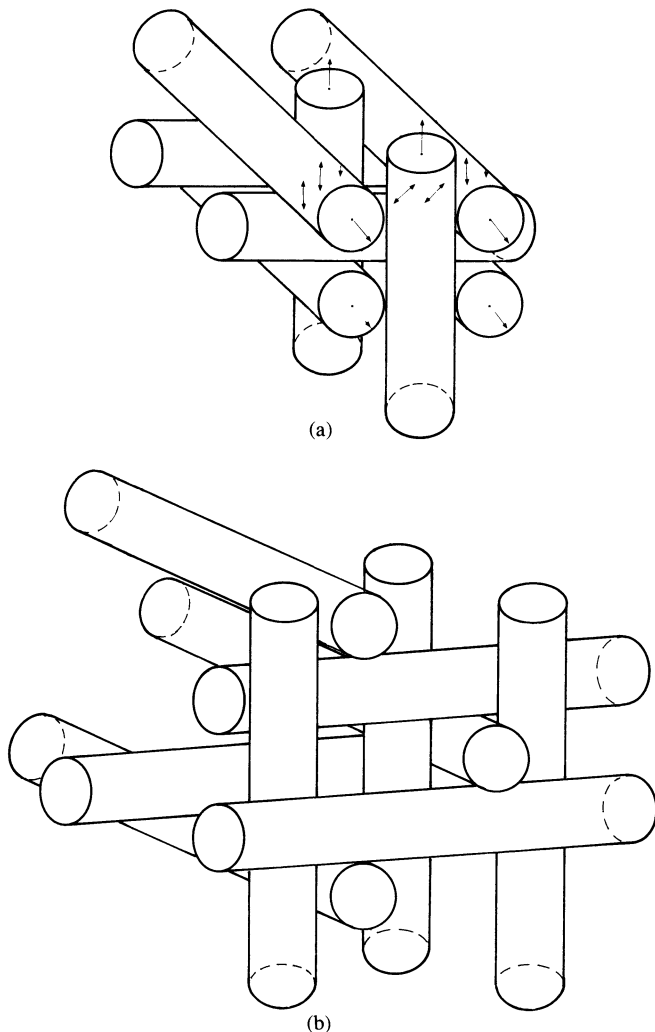


Fig. 6.31. (a) Simple cubic arrangement of double twist cylinders. Note that the $\pi/4$ tilt allows us to obtain a continuous director orientation at the cylinder's contact point. (b) Body-centred cubic arrangement of double twist cylinders.

equilibrium) show that these structures are stable in a narrow temperature range between the isotropic and cholesteric phases as seen experimentally. It thus seems correct that the 'double twist' tendency is an essential ingredient of the blue phase. We do not know, however, how close to real life these proposed structures are. We have seen that they require the simultaneous presence of isotropic and condensed domains. The description in terms of interfacial tension σ is correct only if the interface thickness is

small compared to the pitch. For that reason this approach has been called the low chirality limit [80]. Since correlation lengths close to the N–I transition are of the order of a few hundred Ångströms and the pitch is of the order of a few thousand, experimental systems should not be far from this limit. However, clearly, the interface with the isotropic phase could be described in more detail, and biaxiality should play a role (there is only a small biaxiality in the ordered region, but it is certainly much larger at the interface).

6.5.3 Landau theory

In Section 2.3.1 we introduced the Landau free energy, which can describe the isotropic–nematic transition. The expression relevant in the chiral case differs only because one can now accept pseudoscalars [88]. Hence, the homogeneous part is unchanged, but the gradient part has the addition term

$$\varepsilon_{\alpha\gamma\delta} Q_{\alpha\beta} \frac{\partial Q_{\delta\beta}}{\partial x_\gamma}.$$

(Other seemingly different expressions either vanish or are equivalent to this one.) This term, which is linear in the gradient, contains the natural twisting tendency.

Thus, in the chiral case, the isotropic–chiral nematic free energy can be written

$$F = F_0 + \int_v \left(\frac{1}{2} A(T) Q_{\alpha\beta} Q_{\beta\alpha} + \frac{1}{3} B Q_{\alpha\beta} Q_{\beta\gamma} Q_{\gamma\alpha} + \frac{1}{4} C (Q_{\alpha\beta} Q_{\beta\alpha})^2 + \frac{L_2}{2} \left(\varepsilon_{\alpha\gamma\delta} \frac{\partial Q_{\delta\beta}}{\partial x_\gamma} + 2q_0 Q_{\alpha\beta} \right)^2 + \frac{L_1}{2} \left(\frac{\partial Q_{\alpha\beta}}{\partial x_\beta} \right)^2 \right) d^3x. \quad (6.124)$$

As in Section 2.3.1, transitions are triggered by the sign change of $A(T)$. There is currently no exact solution minimizing F for finite q_0 and B . In the low-chirality limit, which seems to be relevant to the experimental situation, (6.124) could be used to calculate the interfacial and free energy difference between ordered and isotropic phases for given structures. This task is very complex, since one should allow for variations of the structure itself. Keeping the spirit of the previous section, it is possible to show that a double twist with amplitude going to zero at large distance is stable when immersed in isotropic surroundings for A slightly positive and q_0 sufficiently large [88].

This gives grounds for the description of the preceding section. However, the most efficient approach has been to use expansions such as (6.109) to calculate the corresponding energies. In principle, this type of treatment is not restricted to either a high- or low-chirality limit. However, it becomes extremely cumbersome in the low-chirality limit, since one has to retain a large number of Fourier components to provide a sensible description of

sharp interfaces. On the other hand, in the high-chirality limit (i.e. natural pitch shorter or comparable to the correlation lengths defined in Section 2.3.1), the fundamental of the modulations provides a satisfactory description of the phases. In view of the technicality of the calculations we only give a qualitative description of why blue phases can be stable. We follow the lines of reference 80; for more details, the reader is referred to references 79, 80, and 82.

We know from Chapter 2 that, for $B \neq 0$ and $q_0 = 0$,

- The stable low-symmetry phase is a uniaxial nematic.
- The transition is first order and occurs for positive A (such that $AC \sim B^2$).

What happens for $q_0 \neq 0$?

Using the notation and presentation of reference 80, with a suitable variable change, (6.124) becomes

$$\phi = \phi_0 + \int_v \left\{ \tau \chi_{\alpha\beta} \chi_{\alpha\beta} - \sqrt{6} \chi_{\alpha\beta} \chi_{\beta\gamma} \chi_{\gamma\alpha} + (\chi_{\alpha\beta} \chi_{\alpha\beta})^2 + K^2 \left[\left(\varepsilon_{\alpha\gamma\delta} \frac{\partial \chi_{\delta\beta}}{\partial x_\gamma} + \chi_{\alpha\beta} \right)^2 + \eta \left(\frac{\partial \chi_{\alpha\beta}}{\partial x_\beta} \right)^2 \right] \right\} d^3x \quad (6.125)$$

with lengths measured in units of $(1/2q_0)$, and

$$\begin{aligned} (\phi - \phi_0) &= (3^6 C^3 / 2^4 B^4)(F - F_0), \\ \tau &= 3CA/4B^2, \\ \chi_{\alpha\beta} &= -(3\sqrt{6C/4B})Q_{\alpha\beta}, \\ K &= (3^3 CL_2 q_0^2 / B^2)^{\frac{1}{2}} = q_0 \xi, \\ \eta &= L_1/L_2. \end{aligned}$$

$\xi = (3^3 CL_2 / B^2)^{\frac{1}{2}}$ is a correlation length over which the amplitude of the Q ordering may change. Equation (6.125) shows that, in the mean-field approximation, the topology of the phase diagrams involves three parameters only. Furthermore, the ratio of elastic moduli, $\eta = L_1/L_2$, is not expected to play an important role. So, in the proper units, the main parameters are the temperature τ and chirality $K = q_0 \xi$.

Let us consider the trial order parameter

$$\begin{aligned} \chi &= \sqrt{6} \lambda \cos \theta \begin{pmatrix} -\frac{1}{6} & 0 & 0 \\ 0 & -\frac{1}{6} & 0 \\ 0 & 0 & \frac{1}{3} \end{pmatrix} \\ &\quad + (\lambda/\sqrt{2}) \sin \theta \begin{pmatrix} \cos z & \sin z & 0 \\ \sin z & -\cos z & 0 \\ 0 & 0 & 0 \end{pmatrix}. \end{aligned} \quad (6.126)$$

χ depends on two parameters: λ describes the amount of angular ordering, θ that of biaxiality.

For example,

1. $\theta = 0 \rightarrow$ uniaxial nematic.
2. $\theta = \frac{2\pi}{3} \rightarrow$ uniaxial cholesteric

with $\chi_{ij} = \lambda \sqrt{\frac{3}{2}}(n_i n_j - \frac{1}{3}\delta_{ij})$
and $\mathbf{n} = (\cos z/2, \sin z/2, 0)$.

3. $\theta = \frac{\pi}{2} \rightarrow$ ‘strongly’ biaxial cholesteric

with $\chi_{ij} = \frac{\lambda}{\sqrt{2}}(n_i n_j - m_i m_j)$
and $\mathbf{n} = (\cos z/2, \sin z/2, 0)$, $\mathbf{m} = (\sin z/2, -\cos z/2, 0)$.

With the form (6.126), the energy (6.125) becomes

$$\bullet \quad (\phi/v) = (K^2/2 + \tau)\lambda^2 + \lambda^4 - \lambda^3 \cos 3\theta + \frac{1}{2}K^2\lambda^2 \cos 2\theta \quad (6.127)$$

in which v is the volume of integration (supposed large compared to the period).

Clearly, a large λ favours $\cos 3\theta = 1$, i.e. the uniaxial cholesteric phase. This is a sign that the standard cholesteric is favoured at low enough temperatures. On the other hand, large K^2 favours $\cos 2\theta = 1$, i.e. the strongly biaxial cholesteric. Note that with $\theta = \pi/2$ the third-order terms vanish and the transition may be second-order. Can this really be true?

Let us assume $\theta = \frac{\pi}{2} + \varepsilon$ with $\varepsilon \ll 1$. Minimization of (6.127) with respect to θ , leads to

$$\varepsilon \simeq \frac{3\lambda}{2K^2}$$

and

$$\bullet \quad (\phi/v) \simeq \tau\lambda^2 + \lambda^4 \left(1 - \frac{9}{4K^2}\right). \quad (6.128)$$

Thus, after minimization with respect to θ , one obtains the typical expression for second-order transitions. The phase transformation occurs with the sign change for τ . The procedure is self-consistent provided that the coefficient of the fourth-order term is positive, i.e. $K > 3/2$.[†] It does not mean, however,

[†] If $K = 3/2$, the transition is first-order with (the index c refers to values taken at the transition point)

$$\tau_c = \frac{1}{8}[1 - 4K^2 + (1 + \frac{4}{3}K^2)^{3/2}], \quad \cos 2\theta_c = -\frac{1}{2}(1 + \frac{4}{3}K^2)^{\frac{1}{2}}.$$

that this phase will be observed experimentally. Indeed, any order parameter obtained from the calculated one by a rotation or a transition gives the same free energy and, more important, any linear combination of these order parameters (properly normalized) gives the same second-order term. If, by any chance, a given combination leads to a non-vanishing cubic term, the corresponding phase is favoured over the ‘strongly’ biaxial cholesteric, since the condensation of the order will occur for positive τ . It turns out that it can always be achieved. Indeed, the general expression of the strong biaxial solution reads

$$\chi_{ij} = \text{Re}\{(n_i - im_i)(n_j - im_j) e^{i\mathbf{q} \cdot \mathbf{r}}\}$$

in which \mathbf{n} , \mathbf{m} , and \mathbf{q} are any triad of orthonormal vectors. If we now choose a linear combination of such expressions

$$\chi_{ij} = \sum_{\alpha=1}^N a^\alpha \{(n_i^\alpha - im_i^\alpha)(n_j^\alpha - im_j^\alpha) e^{i(\mathbf{q}_\alpha + \mathbf{q}_{\alpha'} + \mathbf{q}_{\alpha''}) \cdot \mathbf{r}}\} \quad (6.129)$$

in which a^α defines the amplitude and phase of a given biaxial helix. The cubic term then involves spatial averages of $e^{i(\mathbf{q}_\alpha + \mathbf{q}_{\alpha'} + \mathbf{q}_{\alpha''}) \cdot \mathbf{r}}$, which are non-zero if $\mathbf{q}_\alpha + \mathbf{q}_{\alpha'} + \mathbf{q}_{\alpha''} = 0$. Note that the simplest structure which allows this condition to be satisfied is the one in Fig. 6.30(b), but there are, in fact, many other possibilities (body-centred cubic, simple cubic, hexagonal, icosahedral). Such phases will have a stability domain, for τ positive ($\tau \sim 1$, like for nematics). Which structure is the most stable depends on detailed calculations. The results are in qualitative agreement with experiment, provided that higher harmonics are taken into account [89]. Because of the first-order nature of the transitions, the stability limit of blue phases is extended to $K \simeq 0.3$ on the low-chirality side. Furthermore, the very argument for the blue phase existence tells us that the stability range should be comparable to $(T_{NI} - T^*)$ (remember the notation of Chapter 2), i.e. of the order of one degree, which is essentially the correct order of magnitude.

Thus, this approach yields results that point in the same direction as the low-chirality limit. Everything is not yet understood.

- Some selection rules for Bragg reflection by a tensorial order parameter are not satisfied by BPII [90].
- Blue phase III fails to be described in this picture.

The first point is perhaps not too serious if one remarks that all scattering need not be coherent [91] and, furthermore, that there is also a density modulation that can scatter according to conventional selection rules.

Blue phase III is more puzzling. The suggestion that it might be a quasicrystal with icosahedral symmetry is appealing. Such a structure is indeed one of those that maximize the cubic term in the energy. It seems, however, that it has a slightly higher energy than the lowest energy b.c.c. structure [91]. Since quasicrystals carry more entropy than crystals, their

absence of stability is not really proved. One could also imagine other scenarios. For instance BPIII could be a three-dimensionally bond-ordered phase [92]. Indeed, since BPII is a crystal, its topological defects are dislocations. From dimensional analysis the dislocation line energy is an elastic modulus times the square of the Burger's vector of the dislocation. Furthermore, dislocation lines carry entropy (typically $k_B T q_0$ per unit length). Thus the dislocation free energy (per unit length) is

$$f \sim Bq_0^{-2} - k_B T q_0. \quad (6.130)$$

Since B goes to zero upon approaching the isotropic phase, f may change sign before the would-be BPII \rightleftharpoons isotropic transition and dislocation undergo an unbinding transition. Such a simple argument shows that this scenario is possible: experiment on monocrystals should tell whether this is the case or not. One cannot also rule out the possibility that BPIII is an isotropic liquid with a high degree of local order, separated from both BPII and the conventional isotropic liquid via first-order transitions.

REFERENCES

1. Mathieu, J. P. *Bull. Soc. fr. Minér. Cristallogr.* **62**, 172 (1939).
2. Berreman, D. W. and Scheffer, T. J. *Mol. Cryst. liquid Cryst.* **11**, 395 (1970).
3. Billard, J. *Mol. Cryst.* **3**, 227 (1968).
4. Taupin, D. *J. Phys. (Paris) Colloq.* **69** (Suppl. C4), 32 (1969).
5. Mauguin, C. *Bull. Soc. fr. Minér. Cristallogr.* **34**, 3 (1911).
6. Cano, R. *Bull. Soc. fr. Minér. Cristallogr.* **90**, 333 (1967); see also Kassubeck, G. and Meier, G. *Mol. Cryst. liquid Cryst.* **8**, 305 (1969).
7. de Vries, H. *Acta Crystallogr.* **4**, 219 (1951). Earlier calculations on the same lines are found in reference 5 and in Oseen, C. *Trans. Faraday Soc.* **29**, 833 (1933).
8. See, for example, Landau, L. D. and Lifshitz, E. M. *Quantum mechanics*, Section 104, p. 384. Pergamon, London (1959).
9. Levelut, A. and Billard, J. *Acta Crystallogr.* **A26**, 390 (1970).
10. Baessler, H *et al. Mol. Cryst.* **6**, 329 (1970).
11. Fergason, J. In *Liquid crystals, Proceedings of the Second Kent Conference* (ed. G. Brown, G. Dienes, and M. Labes), p. 89. Gordon and Breach, New York (1966); Fergason, J., Goldberg, N., and Nadalin, R. In *Liquid crystals, Proceedings of the Second Kent Conference* (ed. G. Brown, G. Dienes, and M. Labes), p. 105. Gordon and Breach, New York (1966); Adams, J. and Haas, W. *Mol. Cryst.* **11**, 229 (1970).
12. Alben, R. *Mol. Cryst. liquid Cryst.* **20**, 231 (1973).
13. See, for example, Magne, M. and Pinard, P. *J. Phys. (Paris) Colloq.* **30** (Suppl. C4), 117 (1960).
14. Fergason, J. *Sci. Amer.* **211**, 77 (1964); *Mol. Cryst.* **1**, 309 (1966); Ennulat, R. and Fergason, J. *Mol. Cryst. liquid Cryst.* **13**, 149 (1971).
15. Crissey, J. *et al. J. invest. Dermatol.* **43**, 89 (1965); Selawry, O. *et al. Mol. Cryst.* **1**, 495 (1966); Gautherie, M. *J. Phys. (Paris) Colloq.* **30** (Suppl. C4), 122 (1969).

16. Hansen, J., Fergason, J., and Okaya, A. *Appl. Opt.* **3**, 987 (1964); Keilmann, F. *Appl. Opt.* **9**, 1319 (1970).
17. Iizuka, K. *Electronics Lett.* **5**, 27 (1968).
18. Ennulat, R. *Mol. Cryst.* **8**, 247 (1969).
19. Cano, R. and Chatelain, P. *C.R. Acad. Sci., Paris* **B259**, 252 (1964); Adams, J., Haas, W., and Wysocki, J. *Liquid crystals and ordered fluids* (ed. R. S. Porter and J. F. Johnson), p. 463. Plenum Press, New York (1970).
20. Baessler, H. and Labes, M. *J. chem. Phys.* **52**, 631 (1970); Adams, J. and Haas, W. *Mol. Cryst. liquid Cryst.* **15**, 27 (1971).
21. Dolphin, D., Muljani, Z., Cheng, J., Meyer, R. B., *J. chem. Phys.* **58** (1), 413 (1973).
22. Adams, J., Haas, W., and Wysocki, J. *Phys. Rev. Lett.* **22**, 92 (1969).
23. Adams, J., Haas, W., and Wysocki, J. *Mol. Cryst. liquid Cryst.* **7**, 371 (1969).
24. Jenkins, J. T. Unpublished D.Phil. thesis, Johns Hopkins University (1969).
25. Haas, W., Adams, J., and Flannery, J. B. *Phys. Rev. Lett.* **24**, 577 (1970); see also Muller, J. H. *Mol. Cryst.* **2**, 167 (1966).
26. Sackmann, E., Meiboom, S., and Snyder, L. C. *J. Am. chem. Soc.* **89**, 5892 (1967).
27. Wysocki, J., Adams, J., and Haas, W. *Phys. Rev. Lett.* **20**, 1025 (1968); **21**, 1791 (1968); *Mol. Cryst.* **8**, 471 (1969).
28. Durand, G., Leger, L., Rondelez, F., and Veyssie, M. *Phys. Rev. Lett.* **22**, 227 (1969); Meyer, R. B. *Appl. Phys. Lett.* **14**, 208 (1969).
29. Kahn, F. *J. Phys. Rev. Lett.* **24**, 209 (1970).
30. Heilmeier, G. and Goldmacher, J. *J. chem. Phys.* **51**, 1258 (1969).
31. de Gennes, P. G. *Solid State Commun.* **6**, 163 (1968).
32. (a) Meyer, R. B. *Appl. Phys. Lett.* **14**, 208 (1969); (b) Meyer, R. B. Unpublished D.Phil. thesis, Harvard University (1969).
33. (a) Luckhurst, G. and Smith, H. *Mol. Cryst.* **20**, 319 (1973). (b) Regaya, B., Gasparoux, H., and Prost, J. *Rev. Phys. appl.* **7**, 83 (1972).
34. Chou Cheung, L. and Meyer, R. B. *Solid State Commun.* **2**, 977 (1972).
35. (a) Magnetic field effects: Rondelez, F. and Hulin, J. P. *Solid State Commun.* **10**, 1009 (1972). (b) Electric field effects: Gerritsma, G. and van Zanten, P. *Mol. Cryst. liquid Cryst.* **15**, 267 (1971); *Phys. Lett.* **37A**, 47 (1971); Rondelez, F. and Arnould, H. *C.R. Acad. Sci., Paris* **B273**, 549 (1971).
36. (a) Helfrich, W. *Appl. Phys. Lett.* **17**, 531 (1970); (b) Helfrich, W. *J. chem. Phys.* **55**, 839 (1971).
37. Hurault, J. P. *J. chem. Phys.* **59**, 2068 (1973).
38. Leslie, F. *Mol. Cryst. liquid Cryst.* **7**, 407 (1969).
39. Fan, C., Kramer, K., and Stephen, M. *Phys. Rev. A2*, 2482 (1970).
40. Gasparoux, H. and Prost, J. *Mol. Cryst. liq-Cryst.* **22**, 25 (1973).
41. (a) Brochard, F. *J. Phys. (Paris)* **32**, 685 (1971). (b) Martinoty, P. and Candau, S. *Phys. Rev. Lett.* **28**, 1361 (1972).
42. Pincus, P. *C.R. Acad. Sci., Paris* **B267**, 1290 (1968).
43. See, for example, Landau, L. D. and Lifshitz, E. M. *Fluid mechanics*, Chapter 2, p. 17. Pergamon, London (1952).
44. Sakamoto, K., Porter, R., and Johnson, J. *Mol. Cryst. liquid Cryst.* **8**, 443 (1969). See also Pochan, J. and March, D. *J. chem. Phys.* **57**, 1193 (1972).
45. Helfrich, W. *Phys. Rev. Lett.* **23**, 372 (1969).
46. Such experiments are very difficult to control experimentally. Wysocki, J. et al. *J. appl. Phys.* **40**, 3865 (1969).

47. Heilmeier, G. and Goldmacher, J. *Proc. IEEE* **57**, 34 (1969).
48. Arnould, H. and Rondelez, F. *Mol. Cryst.* **26**, 11 (1974).
49. Pomeau, Y. *Phys. Rev. Lett.* **A34**, 143 (1971).
50. (a) Leslie, F. *Proc. Soc. A* **307**, 359 (1968). (b) Leslie, F. In *Symposia of the Faraday Society*, no. 5. *Liquid crystals*, p. 63 (1971).
51. Prost, J. *Solid State Commun.* **11**, 183 (1972).
52. Lehmann, O. *Ann. Phys., Leipzig* **2**, 649 (1900).
53. Oseen, C. W. *Trans. Faraday Soc.* **29**, 883 (1933).
54. Friedel, G. *Ann. Phys., Paris* **18**, 273 (1922).
55. Bouligand, Y. *J. Phys. (Paris)* **33**, 715 (1972).
56. Cladis, P., Kleman, M., and Pieranski, P. *C.R. Acad. Sci., Paris* **273**, 275 (1971).
57. Bouligand, Y. *J. Phys. (Paris)* **30** (Suppl. C4), 90 (1969); **36** (Suppl. C1), 331 (1975).
58. Grandjean, F. *C.R. Acad. Sci., Paris* **172** 71 (1921).
59. Rault, J. *Mol. Cryst. liquid Cryst.* **16**, 143 (1972).
60. Kelker, H. *Mol. Cryst. liquid Cryst.* **15**, 347 (1972).
61. Kleman, M. and Cladis, P. *Mol. Cryst. liquid Cryst.* **16**, 1 (1972).
62. See, for example, Friedel, J. *Dislocations*. Pergamon, London (1964); for a more recent reference see Kleman, M. *Points, lignes, parois*, Vols I and II, les Editions de Physique (1977).
63. Kleman, M. and Friedel, J. *J. Phys. (Paris)* **30** (Suppl. C4), 43 (1969). See also Simmons, deWit, and Bullough (ed.) *Fundamental aspects of dislocation theory*, National Bureau of Standards Special Publication, no. 317, p. 1. National Bureau of Standards, Washington, DC (1970); Kleman, M. *Points, lignes, parois*, Vols I and II, les Editions de Physique (1977).
64. Rault, J. Unpublished D.Phil. thesis, Orsay (1971).
65. de Gennes, P. G. *C.R. Acad. Sci., Paris* **266**, 571 (1968).
66. Orsay Group on Liquid Crystals *Phys. Lett.* **A28**, 687 (1969); *J. Phys. (Paris)* **30** (Suppl. C4), 38 (1969).
67. Strzelecki, L. and Liebert, L. *Bull. Soc. chim., Paris*, no. 2, pp. 597, 603, 605 (1972). Bouligand, Y., Cladis, P., Liebert, L., and Strzelecki, L., *Mol. Cryst.* **25**, 233 (1974).
68. Kelker, H. *Mol. Cryst. liquid Cryst.* **21**, 000 (1973).
69. Pieranski, P. and Cladis, P. E. *Europhys. News* **17**, 113 (1986).
70. Armitage, D. and Price, F. P. *J. Phys. (Paris) Colloq.* **36** (Suppl. C1), 133 (1975).
71. Armitage, D. and Price, F. P. *J. chem. Phys.* **66**, 3414 (1977).
72. Thoen, J. *Phys. Rev. A* **37**, 1754 (1988).
73. Johnson, P. L., Flack, J. H., and Crooker, P. P. *Phys. Rev. Lett.* **45**, 641 (1980).
74. For general experimental references see Stegemeyer, H., Blümel, Th., Hiltrop, K., Onusseit, H., and Porsch, F. *Liquid Cryst.* **1**, 3 (1986).
75. Onusseit, H. and Stegemeyer, H. *Z. Naturforsch.* **36a**, 1083 (1981).
76. Marcus, M. *Phys. Rev. A* **30**, 1109 (1984); Cladis, P. E., Pieranski, P., and Joanicot, M. *Phys. Rev. Lett.* **52**, 542 (1984).
77. Clark, N. A., Vohra, S. T., and Handschy, M. A. *Phys. Rev. Lett.* **52**, 57 (1984).
78. Hornreich, R. M. and Shtrikman, S. *Phys. Lett.* **A84**, 20 (1981).
79. Belyakov, V. A. and Dmitrienko, V. E. *Usp. Fiz. Nauk.* **146**, 369 (1985) (*Sov. Phys. JETP* **28**, 636 (1985)).
80. Wright, D. C. and Mermin, N. D. *Rev. mod. Phys.* **61**, 385 (1989).
81. Brazovskii, S. A. *Zh. Eksp. Ter. Fiz.* **68**, 175 (1975) (*Sov. Phys. JETP* **41**, 85 (1975)).

82. Hornreich, R. M. and Shtrikman, S. *Mol. Cryst. liquid Cryst.* **65**, 183 (1988).
83. Meiboom, S., Sethna, J. P., Anderson, P. W., and Brinkman, W. F. *Phys. Rev. Lett.* **46**, 1216 (1981).
84. Sethna, J. P., Wright, D. C., and Mermin, N. D. *Phys. Rev. Lett.* **51**, 467 (1983).
85. Dubois Violette, E. and Pansu, B. *Mol. Cryst. liquid Cryst.* **165**, 151 (1988).
86. Langevin, D. and Bouchiat, M. A. *J. Phys. (Paris) Colloq.* **36** (Suppl. C1), 197 (1975).
87. Meiboom, S., Sammon, M., and Berreman, D. W. *Phys. Rev. A* **28**, 3553 (1983).
88. de Gennes, P. G., *Mol. Cryst. Liquid Cryst.* **12**, 193 (1971). Hornreich, R. M., Kugler, M., and Shtrikman, S. *Phys. Rev. Lett.* **48**, 1404 (1982).
89. Grebel, H. R., Hornreich, R. M., and Shtrikman, S. *Phys. Rev. A* **28**, 1114; **A28**, 3669 (1983); **A30**, 3264 (1984).
90. Tanimoto, K. and Crooker, P. P. *Phys. Rev. A* **29**, 1566 (1984).
91. Hornreich, R. M. and Shtrikman, S. *Z. Phys. B, Condensed Matter* **8**, 369 (1987) and references therein.
92. Nelson, D. R. and Toner, J. *Phys. Rev. B* **24**, 363 (1981).

MACROSCOPIC BEHAVIOUR OF SMECTICS AND COLUMNAR PHASES

7.1 CONTINUUM DESCRIPTION OF SMECTICS AND COLUMNAR PHASES: STATICS

In Chapter 1, after the description of smectic and columnar phases, we briefly discussed the influence of thermal fluctuations in these systems. To that end we introduced what we called a ‘poor man’s’ *elastic theory*. This allowed us to introduce the notions of *short-, long-, and quasilong-range order*. The main ingredient was the number of ‘liquid-like’ directions, but no attention was paid to the number of relevant variables. A closer contact with experiment requires a proper consideration of the symmetries involved. Because of their unique-characteristics, we consider chiral systems separately in Section 7.2.

7.1.1 Choice of variables

7.1.1.1 Smectics

We have already introduced in Chapter 1 the notion of layer displacement u in smectics. Clearly, small deformations of the structure from that of an ideal single-domain sample are well described by u . Is there any need for introducing other variables? Three cases have to be distinguished: smectics A, hexatic smectics B, and smectics C.

Smectics A In simple fluids, the density is commonly considered as the relevant variable. As a matter of fact, in the distorted material, the density ρ will usually differ from its equilibrium value ρ_0

$$\rho = \rho_0(1 - \theta(r)). \quad (7.1)$$

However, for the static distortions of interest here, $\theta(r)$ will adjust itself to minimize the free energy in a given $u(\mathbf{r})$ configuration: thus (in the absence of external pressure that would change ρ) it need not be treated as an independent variable.†

† This statement applies only for static phenomena: to study dynamic effects we must keep θ as an independent variable, because (7.1), which is an equilibrium relation, breaks down at acoustic frequencies.

In fact, the form of the relation between θ and u at equilibrium may be derived on pure symmetry grounds: we note first that a uniform displacement will not change ρ ; thus θ must depend only on derivatives of u , the leading ones being first-order derivatives. The only relation allowed by symmetry is

$$\theta = m \frac{\partial u}{\partial z} \quad (7.2)$$

in which m is a dimensionless constant, characteristic of the material, which may be positive or negative.

It is illustrative to discuss this example a little further. We have seen in Section 1.6.1 that a dilatation (compression) ($\partial u / \partial z$) of the layers causes a change in energy density: $\frac{1}{2}B(\partial u / \partial z)^2$. Similarly, a bulk dilatation induces an increase in the energy density, $\frac{1}{2}A\theta^2$. However, since θ and $(\partial u / \partial z)$ have similar symmetry properties, the simultaneous existence of $(\partial u / \partial z)$ and θ requires the inclusion of a third term $C\theta(\partial u / \partial z)$. The total energy is

$$F = \frac{1}{2}A\theta^2 + C\theta\left(\frac{\partial u}{\partial z}\right) + \frac{1}{2}B\left(\frac{\partial u}{\partial z}\right)^2. \quad (7.3)$$

The pressure follows the usual definition

$$p = -\frac{\partial F}{\partial \theta}. \quad (7.4)$$

In any experiment performed at constant pressure, $p = 0$ implies (7.2), with $m = -C/A$. Then (7.3) simplifies to

$$F = \frac{1}{2}\bar{B}\left(\frac{\partial u}{\partial z}\right)^2 \quad \text{with} \quad \bar{B} = B - C^2/A, \quad (7.5)$$

Suppose now that the experiment is performed in an air-tight undeformable vessel $\theta = 0$, and (7.3) simplifies to

$$F = \frac{1}{2}B\left(\frac{\partial u}{\partial z}\right)^2. \quad (7.6)$$

If, in the air-tight vessel, we include small air bubbles, then one must keep both $(\partial u / \partial z)$ and θ , and the effective elastic constant B^e will satisfy $\bar{B} \leq B^e \leq B$.

In practice, all experiments are conducted at constant pressure, and θ is not an independent variable.[†]

Similarly, the tilt of the molecules with respect to the layers is not an independent variable. We showed in Fig. 1.21 that the first-order derivatives $\partial u / \partial x$, $\partial u / \partial y$ correspond to a simple rotation of the smectic system. This, of

[†] Note that this type of analysis holds for any scalar variable and, in particular, for concentrations in mixtures.

course, cannot change the orientation of the molecules with respect to the layers. Thus, if we associate a unit director \mathbf{n} to the optical axis, it will have the components†

$$\left. \begin{aligned} n_x &= -\frac{\partial u}{\partial x} \ll 1, \\ n_y &= -\frac{\partial u}{\partial y} \ll 1. \end{aligned} \right\} \quad (7.7)$$

Equation (7.7) simply states that, at each point, \mathbf{n} is normal to the layers. It has the interesting consequence that

$$\mathbf{n} \cdot \operatorname{curl} \mathbf{n} = 0.$$

Thus we see that the twist deformation that was allowed in nematics becomes forbidden within smectics A.

Hexatic smectics ($S_{BH_{hex}}$) We have seen in Chapter 1 that $S_{BH_{hex}}$ are characterized by a sixfold modulation of the density-density correlation function in the layer directions (Fig. 1.15(b)). Is there any need for an extra variable? The answer is yes: one can rotate the sixfold modulation pattern (i.e. the bond order) of the X-ray figure independently of u around the normal to the layers. The knowledge of such a rotation Ω_z (Fig. 7.1(a)) is needed to specify the state of hexatic smectics. The layer is defined as in smectics A.

Smectics C The picture of a phase in which molecules are tiled with respect to the layers allows us to easily understand the need for an extra variable. One can indeed change the azimuthal direction of the molecules through a rotation Ω_z (Fig. 7.1(b)) independently of u , without changing the free energy. The situation is thus very similar to that of $S_{BH_{hex}}$.

Note. Since the symmetry of S_F , S_I , and S_K is the same as that of S_C , there is no need for any other macroscopic variable: the X-ray modulation follows exactly the molecular tilt.‡

7.1.1.2 Columnar phases

We introduced in Chapter 1 the ‘column displacement’ variable \mathbf{u}_\perp (Fig. 1.20). It is a two-dimensional vector since there is always a liquid-like order along the column direction (see the problem in Chapter 1). The remarks concerning the interdependence of ρ and \mathbf{u} in smectics have their counterparts:

† In more complicated situations an effective tilt with respect to the layers may occur on a ‘microscopic’ length scale $\lambda(T)$. For more details, see reference 1 and Chapter 10.

‡ If we call Ω_{z1} and Ω_{z2} the rotations of the tilt direction and of the bond order, respectively, a coupling proportional to $-\cos(6(\Omega_{z1} - \Omega_{z2}))$ can be introduced in the free energy. Equilibrium requires $\Omega_{z1} = \Omega_{z2} + k\pi/3$ ($k = \text{integer}$).

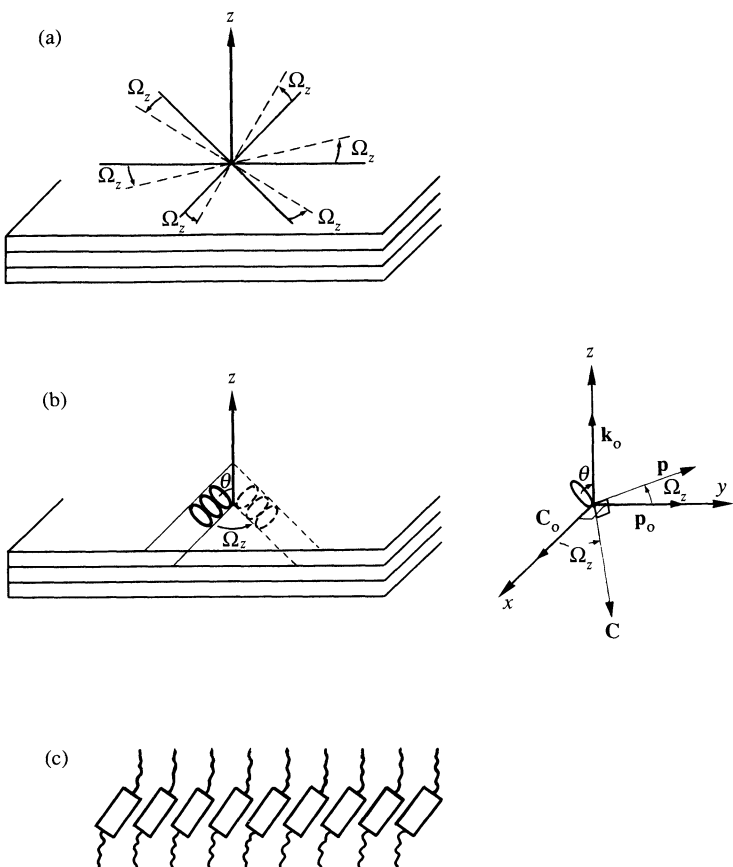


Fig. 7.1. (a) Rotation Ω_z of a $S_{B_{\text{hex}}}$ around the normal to the layers: the direction of the bond order changes (the solid lines are mapped on to the broken ones), but clearly the energy is unchanged. (b) Rotation Ω_z of a S_C around the normal to the layers: the tilt direction changes (again the solid line is mapped on to the broken one) and the energy is also unchanged. (c) Zigzag model of S_C according to Bartolino *et al.* [12].

with the same definition of θ , one can write on symmetry grounds

$$\theta = m \left(\frac{\partial u_x}{\partial x} + \frac{\partial u_y}{\partial y} \right). \quad (7.8)$$

(z is taken along the column direction.)

We have seen that there are many different ‘two-dimensionally’ ordered structures. Does one need to introduce extra variables as in smectics B_{hex} or C ? The answer is no. The reason is best demonstrated for the case of a molecular tilt.

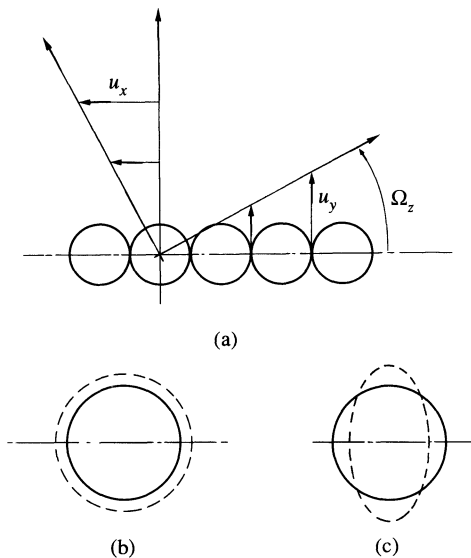


Fig. 7.2. (a) Rotation around the z -axis: note $\Omega_z = \frac{1}{2}[(\partial u_y / \partial x) - (\partial u_x / \partial y)]$. (b) Schematic representation of a uniform dilatation of the columns. (c) ‘Pure shear’ of the columns corresponding to a compression in one direction, and an equal dilatation in the perpendicular direction.

Assume a rectangular arrangement of the column axes: symmetry requires that x and y are extrema of the free energy for the tilt direction. Thus, in equilibrium, there will be a well defined relation between this direction and the x - and y -axes (note that there can be a finite number of minima, which play a role in domain formation, but we deal here with monodomain samples). As a result the tilt rotation is simply given by the lattice rotation (Fig. 7.2(a))

$$\Omega_z = \frac{1}{2} \left(\frac{\partial u_y}{\partial x} - \frac{\partial u_x}{\partial y} \right). \quad (7.9)$$

Similar arguments could be developed for more complicated structures: in that respect the situation in columnar phases is simpler than in smectics.

7.1.2 Distortion free energy of (non-chiral) smectics

7.1.2.1 Smectics

We have already quickly derived the free energy of a deformed smectic. It is worth giving a few more details. In this kind of ‘harmonic’ description, we shall constantly assume that $\text{grad } u$ is small. Physically, this means that we consider layers that are neither very much tilted from the x , y -plane nor strongly compressed (dilated). The assumption excludes certain interesting

cases, such as the focal conic textures, but it makes the algebra much more transparent.

Let us write the variations of u in the neighbourhood of a reference point \mathbf{r} as

$$\delta u = \nabla \mathbf{u} \cdot \delta \mathbf{r} + \frac{1}{2}(\delta \mathbf{r} \cdot \nabla \nabla u) \cdot \delta \mathbf{r} + O(\delta r^3), \quad (7.10)$$

$$\delta \mathbf{r} = \begin{cases} \delta x \\ \delta y, \\ \delta z \end{cases}, \quad \delta \mathbf{x}_\perp = \begin{cases} \delta x \\ \delta y \\ 0 \end{cases}.$$

This may be transformed with straightforward manipulations into

$$\begin{aligned} \delta u &= \left(\frac{\partial u}{\partial z} \right) \delta z - \mathbf{n}_\perp \cdot \delta \mathbf{x}_\perp + \frac{1}{4}(\delta x, \delta y) \begin{pmatrix} \frac{\partial u}{\partial x} + \frac{\partial u}{\partial y} & 0 \\ 0 & \frac{\partial u}{\partial x} + \frac{\partial u}{\partial y} \end{pmatrix} \begin{pmatrix} \delta x \\ \delta y \end{pmatrix} \\ &\quad + \frac{1}{2}(\delta x, \delta y) \begin{pmatrix} \frac{1}{2} \left(\frac{\partial u}{\partial x} - \frac{\partial u}{\partial y} \right) & \frac{\partial^2 u}{\partial x \partial y} \\ \frac{\partial^2 u}{\partial x \partial y} & \frac{1}{2} \left(\frac{\partial u}{\partial y} - \frac{\partial u}{\partial x} \right) \end{pmatrix} \begin{pmatrix} \delta x \\ \delta y \end{pmatrix} \\ &\quad + \delta z \delta \mathbf{x}_\perp \cdot \frac{\partial^2 u}{\partial z \partial \mathbf{x}_\perp} + \frac{1}{2} \delta z^2 \frac{\partial^2 u}{\partial z^2}. \end{aligned} \quad (7.11)$$

The physical meaning of the deformations is evident in (7.11).

- The first term is, of course, the compression (dilatation) of the layers.
- The second term is a mere tilt of the layers; it cannot enter the free energy because of rotational invariance.
- The third term has the symmetry of a vector in the z direction: it is the splay introduced in Section 3.1.2 (cf. $\mathbf{n}_\perp = -\nabla_\perp u$).
- The interpretation of the fourth term is simple if we choose axes that diagonalize the matrix

$$(\delta x_0, \delta y_0) \begin{pmatrix} a & 0 \\ 0 & -a \end{pmatrix} \begin{pmatrix} \delta x_0 \\ \delta y_0 \end{pmatrix}.$$

In the x_0 direction the layers have an upward curvature, whereas they have a downward one along y_0 (note: since the matrix is symmetrical, x_0 and y_0 are perpendicular): this is a saddle-splay deformation.

- The fifth term has the symmetry of a vector in the x, y -plane; it is nothing but the bend (also introduced in Section 3.1.2).

- The last term is clearly the rate of change of the compression along z . It exhibits the symmetry of a vector along z as the splay deformation.

The terms that may enter the free energy must be invariant in the operations that leave smectics A unperturbed (i.e. $z \rightarrow -z$ and rotations around the z -axis essentially). This requires us to take the scalar square of each term taken separately, plus the product of the third and sixth terms. In principle, a linear contribution $\partial u / \partial z$ may be included. Its presence gives a non-zero $\partial u / \partial z$ equilibrium value: this simply means that the choice of the equilibrium thickness of the later was inappropriate. In the following we omit such a linear dependence.

The saddle-splay contribution to the energy reads

$$\begin{aligned} & \frac{K}{2} \left[\left(\frac{\partial^2 u}{\partial x^2} - \frac{\partial^2 u}{\partial y^2} \right)^2 + 4 \left(\frac{\partial^2 u}{\partial x \partial y} \right)^2 \right] \\ &= \frac{K}{2} \left[\left(\frac{\partial^2 u}{\partial x^2} + \frac{\partial^2 u}{\partial y^2} \right)^2 + 4 \left(\left(\frac{\partial^2 u}{\partial x \partial y} \right)^2 - \frac{\partial^2 u}{\partial x^2} \frac{\partial^2 u}{\partial y^2} \right) \right]. \quad (7.12) \end{aligned}$$

One recognizes in the first term of the right-hand side of eqn (7.12), a contribution to the splay energy. The second can easily be shown to be a surface term.[†] Thus it will not appear in bulk equations. This does not mean that K should always be ignored: for a given system it has a well defined value, and its influence may be recognized in some cases.[‡] Similarly the bend energy differs from the product of the third and sixth terms of (7.11) only through a surface term.

With all these provisos we arrive at the form [3]

$$\begin{aligned} F = F_0 + \frac{\bar{B}}{2} \left(\frac{\partial u}{\partial z} \right)^2 + \frac{K_1}{2} \left(\frac{\partial^2 u}{\partial x^2} + \frac{\partial^2 u}{\partial y^2} \right)^2 + \frac{K'}{2} \left(\frac{\partial^2 u}{\partial z^2} \right)^2 \\ + \frac{K''}{2} \left(\frac{\partial^2 u}{\partial z^2} \right) \left(\frac{\partial^2 u}{\partial x^2} + \frac{\partial^2 u}{\partial y^2} \right). \quad (7.13) \end{aligned}$$

The last two terms in eqn (7.13) have been included for completeness but are in fact unobservable (with long-range distortions) because they contribute only if the displacement u varies along z . But, in this case, they are dominated by the terms $\frac{1}{2}\bar{B}(\partial u / \partial z)^2$, which is lower order in the space variations. Thus, in all that follows, we shall omit K' and K'' .

To summarize the static properties of a smectic A are described by two constants. \bar{B} (dimension: energy length⁻³) and K_1 (dimension: energy

[†] The Fourier transform of this expression is obviously identically zero. Thus any time a Fourier analysis is compatible with boundary conditions its contribution is rigorously zero. This is the case with samples of infinite extent in the x , y -directions.

[‡] In the DPPL lecithin-water system negative values of K have been deduced from the observation of focal conics [2].

length⁻¹). It is often convenient to introduce the associated length

$$\lambda = \left(\frac{K_1}{\bar{B}} \right)^{1/2}. \quad (7.14)$$

Far from phase transitions λ should be comparable to the layer thickness a_0 . Field effects may be included easily. The magnetic energy in a field parallel to the z direction can be written as

$$\frac{1}{2} \chi_a H^2 \left(\left(\frac{\partial u}{\partial x} \right)^2 + \left(\frac{\partial u}{\partial y} \right)^2 \right) = \text{const} - \frac{1}{2} \chi_a (\mathbf{n} \cdot \mathbf{H})^2. \quad (7.15)$$

The latter form is familiar from our discussion of nematics (Chapter 3). Usually the anisotropy χ_a will be comparable to what we found in that case (namely $\chi_a > 0$ and $\chi_a \sim 10^{-7}$ cgs units).

Electric fields with a perfectly insulating sample give a dielectric interaction similar to that of (7.15) (replace \mathbf{H} by \mathbf{E} and χ_a by $\epsilon_a/4\pi$). ϵ_a is also comparable to what we had in nematics: the increase in the angular order parameter S tends to give larger values of ϵ_a in the smectic phase, but antiferroelectric correlations tend, on the other hand, to decrease them. There are also flexoelectric terms (indeed we have recognized that three of the characteristic deformations have a vectorial symmetry)

$$e_1 E_z \left(\frac{\partial^2 u}{\partial x^2} + \frac{\partial^2 u}{\partial y^2} \right) + e_3 \left(E_x \frac{\partial^2 u}{\partial z \partial x} + E_y \frac{\partial^2 u}{\partial z \partial y} \right) + e_4 E_z \frac{\partial^2 u}{\partial z^2}. \quad (7.16)$$

Using $\text{curl } \mathbf{E} = 0$, we can transform (7.16) into

$$-(e_1 + e_3) \left(\frac{\partial E_x}{\partial z} \frac{\partial u}{\partial x} + \frac{\partial E_y}{\partial z} \frac{\partial u}{\partial y} \right) - e_4 \frac{\partial E_z}{\partial z} \left(\frac{\partial u}{\partial z} \right). \quad (7.17)$$

The existence of the flexoelectric coupling has been evidenced experimentally in both thermotropic and lyotropic smectics A [4, 5] but no values of the coefficients have been given.

7.1.2.2 Hexatic smectics ($S_{BH_{\text{Hex}}}$)

The distortion energy of $S_{BH_{\text{Hex}}}$ obviously comprises a contribution identical to (7.13). Indeed, sixfold symmetry behaves like infinite rotation symmetry, as far as elastic properties are concerned.

The Ω_z -dependent part can be written using a procedure exactly similar to the one we used for u (indeed, only gradients of Ω_z can enter the free energy. We obtain [6]

$$\frac{K_{\perp}}{2} \left[\left(\frac{\partial \Omega_z}{\partial x} \right)^2 + \left(\frac{\partial \Omega_z}{\partial y} \right)^2 \right] + \frac{K_{||}}{2} \left(\frac{\partial \Omega_z}{\partial z} \right)^2. \quad (7.18)$$

Can we write couplings between u and Ω_z ? The answer is no. Rotational

symmetry requires us to use the dot product of similar invariants for u and Ω_z (an expansion similar to (7.11) can be performed with Ω_z). However, u being the component of a ‘true’ vector and Ω_z that of a pseudovector, inversion symmetry forbids the existence of these terms.

What about field effects? Dielectric and diamagnetic couplings are obviously identical to these of smectics A. So are the flexoelectric ones. Since Ω_z is the component of a pseudovector, one might speculate on the existence of ‘flexomagneticity’ in $S_{B_{\text{Hex}}}$! In fact it is forbidden by time reversal symmetry ($t \rightarrow -t$: $\mathbf{H} \rightarrow -\mathbf{H}$ but $\Omega_z \rightarrow \Omega_z$).

7.1.2.3 Smectics (S_C)

As already emphasized in Section 7.1.1, a smectic C, like a smectic B_{Hex} , has two distinct types of degrees of freedom.

- The ‘vertical (along z) displacement of the layers, common to all smectic phases. Long-wavelength fluctuations of u are inexpensive and have large amplitude; all the related effects that we discussed for a smectic A have their counterpart here.
- The rotation Ω_z of the tilt direction. Equivalently one could use a unit vector \mathbf{c} parallel to the layers and pointing in the tilt direction (Fig. 7.1(b)). \mathbf{c} is somewhat similar to the director in a nematic, and smectics C have many features of nematics. A detailed correspondence between the two presentations may be found in reference 7. In the following we choose the x -axis along the unperturbed \mathbf{c} direction (\mathbf{c}_0).

We shall now sketch the static continuum for smectics C, in terms of the variable $\Omega_z(\mathbf{r})$ and $\mathbf{u}(\mathbf{r})$. Since a constant $\partial u / \partial y$ represents a rotation Ω_x along the x -axis, it is sometimes convenient to use simultaneously the three (small) rotation angles [8]

$$\Omega_x = \frac{\partial u}{\partial y}, \quad \Omega_y = -\frac{\partial u}{\partial x}, \quad \Omega_z. \quad (7.19a)$$

Note that eqn (7.19a) implies one relation

$$\frac{\partial \Omega_x}{\partial x} + \frac{\partial \Omega_y}{\partial y} = 0. \quad (7.19b)$$

Uniform rotations do not change the free energy F : thus the part F_d of F associated with elastic distortions must be a function of the gradients $\partial_x \Omega_\beta$ (or, more concisely $\nabla \Omega$). F_d will also depend on the changes in the interlayer distance, described by

$$\gamma = \frac{\partial u}{\partial z}.$$

To construct F explicitly, we note first that terms linear in $\nabla \Omega$ cannot occur

if the unperturbed structure has a centre of symmetry: in a reflection operation around this centre, a rotation vector (pseudovector) such as Ω is not changed, while the (∇) operator changes sign. Terms linear in γ will not occur either, if the unperturbed interlayer distance has its equilibrium value.

Finally, making use of the equivalence between terms which can be transformed into one another by partial integration and eliminating certain 'unobservable' terms (similar to K' and K'' in eqn (7.13)), we arrive at the structure

$$F_d = F_c + F_s + F_{cs} \quad (7.20)$$

where F_c is associated with distortions of the c director, for fixed layers, while F_s describes distortions of the layers. Finally, F_{cs} contains cross-terms coupling the two effects. Explicitly, one has

$$F_c = \frac{1}{2}B_1\left(\frac{\partial\Omega_z}{\partial x}\right)^2 + \frac{1}{2}B_2\left(\frac{\partial\Omega_z}{\partial y}\right)^2 + \frac{1}{2}B_3\left(\frac{\partial\Omega_z}{\partial z}\right)^2 + B_{13}\frac{\partial\Omega_z}{\partial x}\frac{\partial\Omega_z}{\partial z}, \quad (7.21)$$

$$F_s = \frac{1}{2}A\left(\frac{\partial\Omega_x}{\partial x}\right)^2 + \frac{1}{2}A_{12}\left(\frac{\partial\Omega_y}{\partial x}\right)^2 + \frac{1}{2}A_{21}\left(\frac{\partial\Omega_x}{\partial y}\right)^2 + \frac{1}{2}\bar{B}\gamma^2, \quad (7.22)$$

$$F_{cs} = C_1\frac{\partial\Omega_x}{\partial x}\frac{\partial\Omega_z}{\partial x} + C_2\frac{\partial\Omega_x}{\partial y}\frac{\partial\Omega_z}{\partial y}. \quad (7.23)$$

The first group (F_c) was introduced by Saupe [8]. The second and third groups were analysed in reference 9.† In eqn (7.23) we find two types of terms associated with pure distortions of the layer.

1. The terms A, A_{12}, A_{21} describe a curvature of the layers and are analogous (for a system of monoclinic symmetry) to the splay term occurring in a smectic A (eqn (7.13)). The reader will recall that this splay term has the form

$$\frac{1}{2}K_1\left(\frac{\partial^2 u}{\partial x^2} + \frac{\partial^2 u}{\partial y^2}\right)^2 = \frac{1}{2}K_1\left(\frac{\partial\Omega_x}{\partial y} - \frac{\partial\Omega_y}{\partial x}\right)^2.$$

2. The term B , associated with possible changes of the interlayer distance: just as in smectics A, one can show that these changes remain, in fact, small for most practical situations.

Finally, the F_{cs} terms of eqn (7.23) describe some rather subtle effects according to which a deformation imposed on the c director reacts on the curvature of the smectic planes.

As regards dimensions and orders of magnitude, we may note that the Saupe coefficients (B_1, B_2, B_3, B_{13}), the A coefficients (A, A_{12}, A_{21}) and the

† In this reference, the discussion was purposely restricted to cases of constant interlayer thickness ($\gamma = 0$). In the present discussion, we allow for finite values of γ : this adds one term $\frac{1}{2}\bar{B}\gamma^2$ to eqn (7.22).

C coefficients (C_1, C_2) have the dimensions of energy per unit length (dyn): they are probably comparable to the Frank elastic constants in a homologous nematic phase (i.e. of the order of 10^{-7} dyn). On the other hand, \bar{B} has the dimensions of energy per unit volume, as in smectics A.

Some of the elastic constants have been measured (e.g. \bar{B} is of the order of that found in S_A , or less [10], B_1 and B_2 are comparable to what can be estimated from a nematic comparison).†

Dielectric and diamagnetic tensors have three non-equivalent axes: the first nearly parallel to the direction of alignment (in the x, z -plane), the second one normal to the first in this same plane, and the third along y . In practice it appears that, for many compounds, the values measured along the second and third axis are nearly equal; the medium is almost uniaxial, but with an axis tilted by an angle θ , from the normal to the layer. The standard expression (3.47) (or its dielectric counterpart) may be used provided one expresses the ‘nematic director’ \mathbf{n} (i.e. the second eigen-axis) as a function of the normal to the layers, \mathbf{k} , and the tilt azimuthal direction \mathbf{c}

$$\mathbf{n} = \mathbf{k} \cos \theta + \mathbf{c} \sin \theta, \quad (7.24)$$

$$F_{\text{mag}} \simeq -\frac{1}{2}\chi_a(\mathbf{n} \cdot \mathbf{H})^2 = -\frac{1}{2}\chi_a(\mathbf{k} \cdot \mathbf{H} \cos \theta + \mathbf{c} \cdot \mathbf{H} \sin \theta)^2. \quad (7.25)$$

A magnetic field parallel to the layers specifies the \mathbf{c} -axis (in the absence of boundary conditions on \mathbf{c}) and exerts a torque on the layers. A magnetic field perpendicular to the layers also exerts a torque on them. In practical situations this is often negligible compared to the boundary effects (this remark does not hold for \mathbf{c} which is ‘nematic-like’; magnetic coherence lengths can be constructed with the B s just as with the K s in Chapter 3).

The limits of the ‘tilted uniaxial’ description of S_C s, is provided by a comparison of the tilt angle measurements as obtained by X-rays and optics [12]. The latter technique is sensitive to the orientation of the core of the molecule, whereas the first measures the projection of the molecular length along \mathbf{k} : for some molecules, a ‘zigzag’ model is more relevant than a simple tilt (Fig. 7.1(c)).

Flexoelectricity is also expected to exist with S_C s. The simplicity of nematics or S_A is, however, lost: one can count as many as 14 flexoelectric coefficients! In the tilted uniaxial picture, four of them survive. Not much is known about flexoelectricity in smectics C yet.

Problem. Find a covariant expression for the 14 independent vector fields that give rise to the 14 independent flexoelectric coefficients.

† The comparison is possible provided one takes into account the tilt angle dependence of the nematic constants [11]

$B_1 \simeq K_2 \sin^2 \theta \cos^2 \theta + K_3 \sin^4 \theta; \quad B_2 \simeq K_1 \sin^2 \theta; \quad B_3 \simeq K_2 \sin^4 \theta + K_3 \sin^2 \theta \cos^2 \theta$
where θ is the angle between the ‘long’ axis of the molecules and the normal to the layer: see Fig. 7.1(b).

Solution. It is convenient to use a representation with \mathbf{k} , \mathbf{c} , and $\mathbf{p} = \mathbf{k} \times \mathbf{c}$.

The symmetry elements of S_C (remember: the \mathbf{k} , \mathbf{c} -plane is a symmetry plane, \mathbf{p} is a c_2 -axis, and there is inversion symmetry) require that \mathbf{k} , \mathbf{c} enter the expression an even number of times (i.e. \mathbf{k} and \mathbf{c} considered without discrimination; \mathbf{kk} , \mathbf{kc} , and \mathbf{cc} are acceptable as well) and \mathbf{p} also, but separately from the first two (cf. it has a pseudovectorial character). Then we obtain:

(1) *Terms containing γ :*

$$(\mathbf{k} \cdot \nabla \gamma) \mathbf{k}$$

$$(\mathbf{k} \cdot \nabla \gamma) \mathbf{c}$$

$$(\mathbf{c} \cdot \nabla \gamma) \mathbf{k}$$

$$(\mathbf{c} \cdot \nabla \gamma) \mathbf{c}$$

$$(\mathbf{p} \cdot \nabla \gamma) \mathbf{p}$$

Note that the obvious expression $\bar{\nabla} \gamma$ is not independent of the retained ones.

(2) *Terms containing $\nabla \mathbf{k}$:*

$$(\mathbf{c} \cdot \nabla \mathbf{k} \cdot \mathbf{c}) \mathbf{k}$$

$$(\mathbf{c} \cdot \nabla \mathbf{k} \cdot \mathbf{c}) \mathbf{c}$$

$$(\mathbf{p} \cdot \nabla \mathbf{k} \cdot \mathbf{p}) \mathbf{k}$$

$$(\mathbf{p} \cdot \nabla \mathbf{k} \cdot \mathbf{p}) \mathbf{c}$$

$$(\mathbf{p} \cdot \nabla \mathbf{k} \cdot \mathbf{c}) \mathbf{p}$$

(or in index notation $c_i \nabla_i k_j c_j k_k$). Again other expressions that fulfil the symmetry requirements are not independent (i.e. $\nabla \cdot \mathbf{k}$ or $\mathbf{k} \cdot \nabla \mathbf{k} \cdot \mathbf{c} = \mathbf{c} \cdot \nabla \gamma$ to lowest order) or zero ($\mathbf{k} \cdot \nabla \mathbf{k} \cdot \mathbf{k}$, cf. $k^2 = 1$).

(3) *Terms containing $\nabla \mathbf{c}$:*

$$(\nabla \cdot \mathbf{c}) \mathbf{c}$$

$$(\nabla \cdot \mathbf{c}) \mathbf{k}$$

$$(\mathbf{c} \cdot \nabla \mathbf{c} \cdot \mathbf{p}) \mathbf{p}$$

$$(\mathbf{k} \cdot \nabla \mathbf{c} \cdot \mathbf{p}) \mathbf{p}$$

One can take $\nabla \cdot \mathbf{c}$ as the independent term since $\mathbf{c} \cdot \nabla \mathbf{c} \cdot \mathbf{c} = 0$ (cf. $\mathbf{c}^2 = 1$) and $\mathbf{k} \cdot \nabla \mathbf{c} \cdot \mathbf{k} = -\mathbf{k} \cdot \nabla \mathbf{k} \cdot \mathbf{c}$, $\mathbf{p} \cdot \nabla \mathbf{c} \cdot \mathbf{p} \simeq \mathbf{c} \cdot \nabla \gamma + \nabla \mathbf{c}$ to lowest order; similarly, $\mathbf{k} \cdot \nabla \mathbf{c} \cdot \mathbf{c} = 0$ and $\mathbf{c} \cdot \nabla \mathbf{c} \cdot \mathbf{k} = -\mathbf{c} \cdot \nabla \mathbf{k} \cdot \mathbf{c}$.

Hence the total number of 14 flexoterms.[†]

The easiest term to probe and perhaps the most interesting is certainly

$$(\nabla \cdot \mathbf{c})(\mathbf{k} \cdot \mathbf{E}) = E_z (\nabla \cdot \mathbf{c}).$$

[†] The number 12 obtained in reference 13 results from the failure to recognize $(\nabla \cdot \mathbf{c}) \mathbf{c}$, $(\nabla \cdot \mathbf{c}) \mathbf{k}$, $(\mathbf{c} \cdot \nabla \mathbf{c} \cdot \mathbf{p}) \mathbf{p}$, and $(\mathbf{k} \cdot \nabla \mathbf{c} \cdot \mathbf{p}) \mathbf{p}$ as independent contributions. All the expressions for $\gamma = 0$ were given in reference 7.

This tells that an electric field applied across the layers tends to induce a constant splay of the azimuthal tilt direction. This is not a space-filling structure: defects have to be introduced somewhere. In a way, a free surface (with layers parallel to the surface) acts like E_z : striped domains are often observed under these conditions. They have been interpreted in terms similar to those developed here [14].

The ‘tilted uniaxial’ description yields much simpler results: now one wants expressions involving \mathbf{n} only. They are, as in nematics, $\mathbf{n} \nabla \cdot \mathbf{n}$ and $(\mathbf{n} \cdot \nabla) \mathbf{n}$ with the additional terms involving the layer’s dilatation

$$(\mathbf{n} \cdot \nabla \gamma) \mathbf{n} \quad \text{and} \quad (\nabla \gamma - \mathbf{n} \mathbf{n} \cdot \nabla \gamma).$$

(Note that the coupling between E_z and the splay of the tilt direction still exists.)

7.1.2.4 Smectics F, I, and K

In Chapter 1 and Section 7.1.1 we pointed out that the symmetry of these phases was exactly that of S_C . As a result, everything in the preceding section holds. Differences can only be quantitative. Note, however, that the elastic properties of the phase in which the tilt direction is neither along the nearest neighbours nor along the next nearest neighbours as described in reference 32 of Chapter 1, will be different from that of S_C .

7.1.3 Distortion free energy of columnar phases

In Section 7.1.1 we showed that, for static phenomena, a description in terms of the two-dimensional vector field $\mathbf{u}(\mathbf{r})$ displacement of the columnar axes, is relevant. The derivation of the free energy expansion for small values of the derivatives of $\mathbf{u}(\mathbf{r})$ follows pretty much the lines used for smectics. In fact, it is even simpler: one has just to take the elastic energy of a crystal with the relevant point group symmetry, suppress all the terms containing u_z , or $\partial \mathbf{u} / \partial z$ (which is a rotation), and add the bend terms $\partial^2 \mathbf{u} / \partial z^2$ [15].

7.1.3.1 Uniaxial case

Although the procedure we just outlined is quite straightforward, we find it useful to give a few more details; as in (7.10), let us write the variations of $\mathbf{u}(\mathbf{r})$ in the vicinity of \mathbf{r}

$$\begin{pmatrix} \delta u_x \\ \delta u_y \end{pmatrix} = \begin{pmatrix} \frac{\partial u_x}{\partial x} & \frac{\partial u_x}{\partial y} \\ \frac{\partial u_y}{\partial x} & \frac{\partial u_y}{\partial y} \end{pmatrix} \begin{pmatrix} \delta x \\ \delta y \end{pmatrix} + \delta z \begin{pmatrix} \frac{\partial u_x}{\partial z} \\ \frac{\partial u_y}{\partial z} \end{pmatrix}. \quad (7.26)$$

The same manipulation as in (7.11) yields

$$\begin{aligned} \begin{pmatrix} \delta u_x \\ \delta u_y \end{pmatrix} &= \frac{1}{2} \begin{pmatrix} \frac{\partial u_x}{\partial x} + \frac{\partial u_y}{\partial y} & 0 \\ 0 & \frac{\partial u_x}{\partial x} + \frac{\partial u_y}{\partial y} \end{pmatrix} \begin{pmatrix} \delta x \\ \delta y \end{pmatrix} \\ &+ \frac{1}{2} \begin{pmatrix} \frac{\partial u_x}{\partial x} - \frac{\partial u_y}{\partial y} & \frac{\partial u_x}{\partial y} + \frac{\partial u_y}{\partial x} \\ \frac{\partial u_x}{\partial y} + \frac{\partial u_y}{\partial x} & \frac{\partial u_y}{\partial y} - \frac{\partial u_x}{\partial x} \end{pmatrix} \begin{pmatrix} \delta x \\ \delta y \end{pmatrix} \\ &+ \frac{1}{2} \begin{pmatrix} 0 & \frac{\partial u_x}{\partial y} - \frac{\partial u_y}{\partial x} \\ \frac{\partial u_y}{\partial x} - \frac{\partial u_x}{\partial y} & 0 \end{pmatrix} \begin{pmatrix} \delta x \\ \delta y \end{pmatrix} + \delta z \begin{pmatrix} \frac{\partial u_x}{\partial z} \\ \frac{\partial u_y}{\partial z} \end{pmatrix}. \quad (7.27) \end{aligned}$$

The last two terms correspond to rotations of the structure (Figs 1.21 and 7.2(a)) and cannot enter the free energy. The first one describes a radially homogeneous compression (dilatation) of the columns (i.e. diameter change; Fig. 7.2(b)). The second, which like the saddle-splay matrix of smectics can be diagonalized with two orthogonal eigendirections, represents an elliptical deformation of the columns ('pure shear'—at constant 'average' diameter; Fig. 7.2(c)).

To get a contribution to the free energy from the distortions in the z direction, as already remarked in Chapter 1, it is necessary to include second-order derivatives in z ; this is the bend of the tubes (note that it has the symmetry of a vector in the x, y -plane)

$$\frac{\partial^2 \mathbf{u}}{\partial z^2}.$$

Hence the energy is simply

$$\begin{aligned} F &= \frac{1}{2} \bar{B} \left(\frac{\partial u_x}{\partial x} + \frac{\partial u_y}{\partial y} \right)^2 + \frac{1}{2} C \left[\left(\frac{\partial u_x}{\partial x} - \frac{\partial u_y}{\partial y} \right)^2 + \left(\frac{\partial u_x}{\partial y} + \frac{\partial u_y}{\partial x} \right)^2 \right] \\ &\quad + \frac{1}{2} K_3 \left[\left(\frac{\partial^2 u_x}{\partial z^2} \right)^2 + \left(\frac{\partial^2 u_y}{\partial z^2} \right)^2 \right]. \quad (7.28) \end{aligned}$$

What happened to the splay and twist terms familiar in nematics? The tilt is given by

$$\delta n_x = + \frac{\partial u_x}{\partial z}, \quad \delta n_y = \frac{\partial u_y}{\partial z},$$

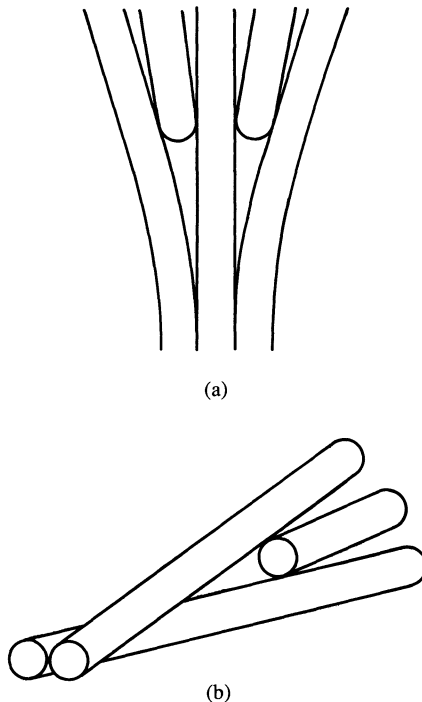


Fig. 7.3. Illustration of the necessity of introducing dislocations in (a) splayed and (b) twisted columnar structures.

the splay by

$$\operatorname{div} \mathbf{n} = \frac{\partial}{\partial z} \left(\frac{\partial u_x}{\partial x} + \frac{\partial u_y}{\partial y} \right),$$

and the twist by

$$\operatorname{curl} \mathbf{n}_z = \frac{\partial}{\partial z} \left(\frac{\partial u_y}{\partial x} - \frac{\partial u_x}{\partial y} \right).$$

Both types of deformation could be included in (7.28), but their observation would always be pre-empted by the first-order terms involving B and C . Note that a constant splay or twist requires the inclusion of dislocations (Fig. 7.3).

As in smectics, first-order elastic constants (B and C ; dimensions energy length $^{-3}$) coexist with second-order ones (K_3 ; dimension energy length $^{-1}$). One can define two associated lengths

$$\lambda_B = \left(\frac{K_3}{B} \right)^{1/2}, \quad \lambda_C = \left(\frac{K_3}{C} \right)^{1/2} \quad (7.29)$$

The absence of correlation between the columns suggests that these lengths should be of the order of a tube diameter.

Diagmagnetic and dielectric couplings are similar to those of smectic A or nematics, with $\delta n_x = \partial u_x / \partial z$ and $\delta n_y = \partial u_y / \partial z$. Flexoelectricity should exist and be described by four coefficients (corresponding to the vector fields: $\nabla_z^2 \mathbf{u}$, $\nabla_{\perp}^2 \mathbf{u}$, $\nabla_{\perp}(\nabla \cdot \mathbf{u})$, $\nabla_z(\nabla \cdot \mathbf{u})$).

Remark A few authors use a three-dimensional displacement variable [16, 17]; in the purely static limit we consider here, this procedure is not legitimate. However, if the time required for reaching the equilibrium density is large compared to the characteristic times involved in the experiment, an additional variable has indeed to be taken into account. A natural candidate is the bulk dilatation θ , which allows an easy extension to dynamical phenomena, but a variable u_z can also be used provided proper boundary conditions are imposed. In the following we will prefer θ since it sticks better to the physics of the problem. In this limit (7.28) is replaced by

$$F = \frac{1}{2}A\theta^2 + \frac{1}{2}B\left(\frac{\partial u_x}{\partial x} + \frac{\partial u_y}{\partial y}\right)^2 + \frac{1}{2}C\left[\left(\frac{\partial u_x}{\partial x} - \frac{\partial u_y}{\partial y}\right)^2 + \left(\frac{\partial u_x}{\partial y} + \frac{\partial u_y}{\partial x}\right)^2\right] \\ + D\theta\left(\frac{\partial u_x}{\partial x} + \frac{\partial u_y}{\partial y}\right) + \frac{1}{2}K_3\left[\left(\frac{\partial^2 u_x}{\partial z^2}\right)^2 + \left(\frac{\partial^2 u_y}{\partial z^2}\right)^2\right]. \quad (7.30)$$

(Note: $\bar{B} = B - D^2/A$.)

7.1.3.2 Biaxial columnar phases

This case is not much more complicated than the uniaxial one. The free energy reads [18]

$$F = \frac{1}{2}B\left(\frac{\partial u_x}{\partial x}\right)^2 + \frac{C}{2}\left(\frac{\partial u_y}{\partial y}\right)^2 + \frac{D}{2}\left(\frac{\partial u_y}{\partial x} + \frac{\partial u_x}{\partial y}\right)^2 + E\frac{\partial u_x}{\partial x}\frac{\partial u_y}{\partial y} \\ + K\left(\frac{\partial^2 u_x}{\partial z^2}\right)^2 + K'\left(\frac{\partial^2 u_y}{\partial z^2}\right)^2. \quad (7.31)$$

The only noticeable change results from the non-equivalence of the x and y directions. Note that (7.31) holds for D_{rob} as well as for D_r (remember from Chapter 1: D_r = ‘simple’ rectangular phases, i.e. the plane x, y is a plane of symmetry; D_{rob} = oblique rectangular, i.e. the point group symmetry is that of a smectic C). Indeed, in the oblique case, one could write expressions such as $\partial u_x / \partial x$, $\partial u_x / \partial z$ without violating the symmetry requirements, but since $\partial u_x / \partial z$ is a mere rotation, it does not change the energy.

The eigendirections of the dielectric permittivity or the diamagnetic susceptibility are x, y, z in D_r phases but not known *a priori* in the D_{rob} case. There should be nine (respectively 14) flexoelectric coefficients in the D_r (respectively D_{rob}) systems.

7.1.4 Boundary conditions

Having defined the relevant distortion and field energy, we are able, in principle, to derive equations for the equilibrium configuration $\mathbf{u}(\mathbf{r})$ that minimizes the overall free energy. However (just as in the case of nematics), not much insight is gained by writing down these equations in their full generality; we shall directly attack some specific examples where the algebra is comparatively simple. Most of these examples are connected with the competition between wall and field alignments. Thus we must begin by some statements concerning boundary conditions.

Detailed studies on wall alignment are rather rare. In many cases when put into contact with a glass surface or with a freshly cleaved crystal (e.g. mica) a smectic A will tend to put its layers parallel to the limiting surface. The molecules are then normal to the surface:[†] this type of alignment is called homeotropic (i.e. unless otherwise specified the epithet qualifies the optical axis). In the case of smectics C such a nomenclature becomes ill defined: one should independently specify the layers and the tilt orientation. The same remark holds for $S_{B\text{Hex}}$.

Other types of boundary conditions with the molecules tangential or oblique may be imposed by a suitable treatment, which we briefly described in Chapter 3: cooling carefully from the nematic phase usually preserves the molecular alignment. In the case of smectics A, a unique layer orientation follows. This is not the case with smectics C: obtaining a monocrystalline sample is not an easy task!

A particularly ‘clean’ case is an air–smectic interface: most of the time the layers run parallel to it. In the absence of any external constraint, the zz component of the stress must vanish. Hence $\partial u / \partial z = 0$ is the correct condition. In the presence of (small) curvatures, the stress of the layers must balance the pressure difference due to the Laplace force. Hence $B(\partial u / \partial z) = A_0 V_\perp^2 u$ (in which A_0 is the surface tension) is the correct condition (we assume that the hydrostatic pressure is uniform). Recent X-ray investigations of air–liquid crystal interfaces reveal that this is a ‘blind’ representation of what is going on close to the free surfaces [19, 20]. Quite often the first layer (or more!) is in an entirely different state (e.g. at an S_A –air interface it may well be S_C , at an $S_{B\text{Hex}}$ –air interface it is often crystalline!). Such subtleties are certainly present at solid–smectic interfaces, and very little is known about their influence on the expression of macroscopic boundary conditions. Furthermore, the notion of perfectly flat, or locally smooth surface is an *ad hoc* idealization. Even with ‘float’ glass, which is molecularly smooth, there are:

- long-wavelength undulations (to be described in the following problem);

[†] The mathematical expression of this condition is simply $\partial u / \partial x = \partial u / \partial y = 0$ at the surface.

- segregation of submicroscopic dust particles always contained in the smectic; this leads to surface dislocation densities (see Chapter 8).

The case of columnar phases is difficult as well. Coating the walls with molecules such as those of mellitic acid allows us to orient the columns perpendicular to the walls [21]. This type of orientation is often called homeotropic; this nomenclature does not define unequivocally the situation: it is better to explicitly specify the orientation of the columns and of the two-dimensional lattice; contrary to the nematic or the S_A case, a 'homeotropic texture' does not correspond to a monodomain sample. It usually involves grain boundaries, dislocations, etc. There is currently no really satisfactory way of producing a monodomain with the columns aligned parallel to the wall [22].

Problem. A smectic A is put in contact with an undulating glass surface (Fig. 7.4(a)). The smectic planes stay locally tangent to the surface. Study the distortions inside the smectic (G. Durand and N. Clark, 1972). Compare with a D_r phase (columns parallel to the surface: Fig. 7.4(b)).

Solution. Let z be the local amplitude of the undulation, and consider the case of a sine wave.

$$z(x, y) = \alpha \cos kx \quad (k\alpha \ll 1).$$

The smectic occupies the region above the surface ($z > 0$). The distortions in this region are of the form

$$u(x, y, z) = u_0(z) \cos kx$$

and the boundary condition requires that $u_0(0) = \alpha$.

The elastic energy, described in eqn (7.6) is (after averaging in the x, y -plane)

$$F = \frac{1}{2} \bar{B} \left(\frac{du_0}{dz} \right)^2 \langle \cos^2 kx \rangle + \frac{1}{2} K_1 k^4 u_0^2 \langle \cos^2 kx \rangle = \frac{1}{4} \bar{B} \left[\left(\frac{du_0}{dz} \right)^2 + \lambda^2 k^4 u_0^2 \right].$$

Minimizing the integral of F over the sample volume, we obtain an equation for u_0 ,

$$-\frac{d^2 u_0}{dz^2} + \lambda^2 k^4 u_0^2 = 0.$$

The appropriate solution is†

$$u_0 = \alpha \theta^{-z/l}$$

where l gives us the thickness of the distorted region and is given explicitly by

$$l = \frac{1}{k^2 \lambda}.$$

† The solution is correct only for very weak modulations $\alpha < a$. For $\alpha > a$ non-linear effects must be included, and they reduce the amplitude.

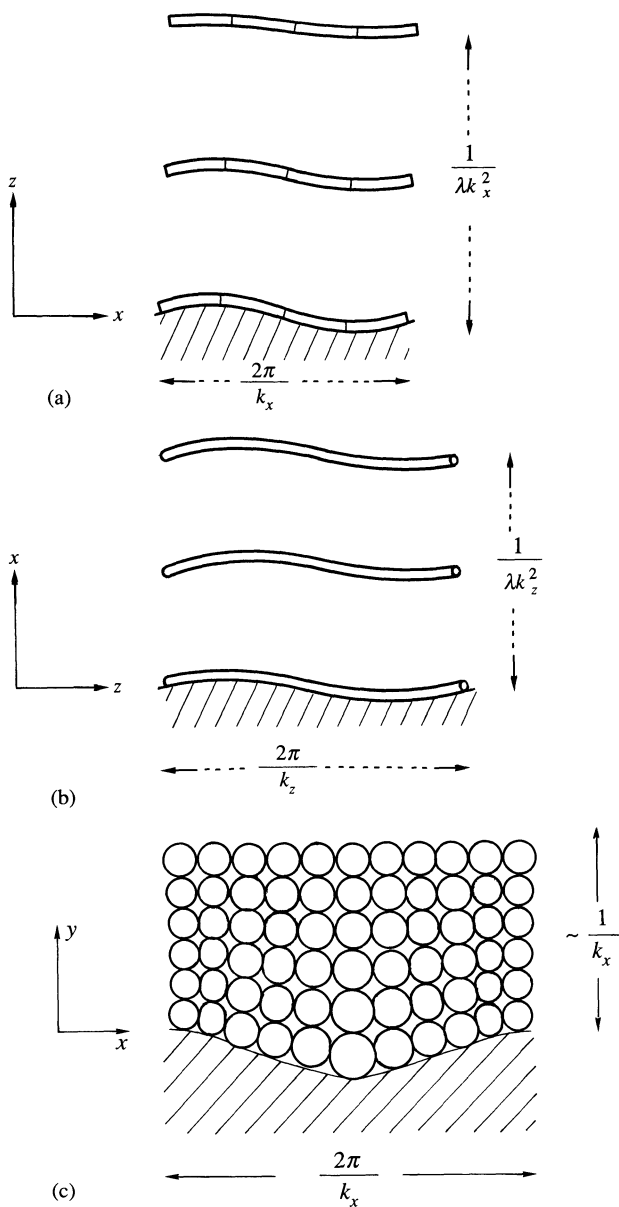


Fig. 7.4. (a) A small undulation at the surface of a smectic has far-reaching effects inside the sample. The penetration length is much larger than for nematics (compare with Fig. 3.9). (b) Undulation in a columnar phase: note the similarity of the two situations (i.e. if one is concerned only with the z , x -plane, there is no way of differentiating from (a). (c) When the columns are perpendicular to the undulation direction and parallel to the surface, the penetration length of the distortion is of the order of the wavelength $2\pi/k_x$, as in crystals.

Note that l is much larger than the wavelength ($2\pi/k$) of the undulation. For instance, if $2\pi/k = 10 \mu\text{m}$, and $\lambda = 20 \text{ \AA}$, $l \simeq 1.4 \text{ mm}$.

This remark is important from several different viewpoints, e.g. to prepare good single crystals of a smectic, it is clearly necessary to work with glass plates that are polished with great care. Also, the distortions react on the capillary properties of a smectic A. Consider an interface between the smectic A and an isotropic fluid where the layers are always assumed to be locally parallel to the interface. The surface tension energy associated with an undulation $\zeta(x)$ is (per cm along y)

$$A_0 \int \sqrt{(dx^2 + d\zeta^2)} \simeq \text{const.} + \frac{1}{2} A_0 \int \left(\frac{d\zeta}{dx} \right)^2 dx$$

where A_0 is the surface tension. For a sinusoidal distortion of amplitude α and wavevector \mathbf{k} this gives (per cm^2)

$$\frac{1}{2} A_0 k^2 \alpha^2 \langle \sin^2 kx \rangle = \frac{1}{4} A_0 k^2 \alpha^2.$$

But, in a smectic A, we must add to this the terms discussed above, namely

$$\int_0^\infty dz \frac{1}{4} \bar{B} \left[\left(\frac{du_0}{dz} \right)^2 + \frac{u_0^2}{l^2} \right] = \frac{1}{4} \frac{\bar{B} \alpha^2}{l} = \frac{1}{4} \bar{B} \lambda \alpha^2 k^2.$$

Thus the effective surface tension is increased by

$$\delta A = \bar{B} \lambda.$$

Even if we were able to make A_0 small by the use of suitable detergents, we would be left with a finite δA resulting from the bulk properties of the smectic.

What about columnar phases?

One can distinguish two cases:

1. The columns are parallel to the x direction. A quick look at Fig. 7.4(b) convinces us easily that all we said for smectics A is still valid provided we utilize the correspondence:

Smectic	D_h
u	$\rightarrow u_x$
x	$\rightarrow z$
z	$\rightarrow x$
\bar{B}	$\rightarrow (\bar{B} + C)$
K_1	$\rightarrow K_3$

2. The columns are perpendicular to the x direction (Fig. 7.4(c)). The situation is similar to that of a crystal. Let us assume $B \ll C$: this allows us to set $u_y = 0$ and simplify the algebra without changing the physics. As in the preceding case, one can write

$$u_x(x, y) = u_0(y) \cos kx$$

and the averaged energy

$$\begin{aligned} F &= \frac{1}{2}C \left[\left(\frac{du_0}{dy} \right)^2 \langle \cos^2 kx \rangle + k^2 u_0^2 \langle \cos^2 kx \rangle \right] \\ &= \frac{1}{4}C \left[\left(\frac{du_0}{dy} \right)^2 + k^2 u_0^2 \right]. \end{aligned}$$

The minimization condition reads

$$-\frac{d^2 u_0}{dy^2} + k^2 u_0 = 0;$$

hence

$$u_0 = \alpha e^{-ky}.$$

In contrast to the smectic case and the other orientation, the distortion dies off on a length scale comparable to the wavelength of the surface undulation. This result holds when one relaxes the condition $B \ll C$ (e.g. x and y may be scaled by kx and ky , respectively, to produce an energy (F/k^2) independent of k ; one would find in fact two length scales both linearly linked to k^{-1}).

The integrated energy (per cm²) takes the value

$$F = \frac{C}{4} \int \left[\left(\frac{du_0}{dy} \right)^2 + k^2 u_0^2 \right] dy = \frac{C}{4} k\alpha^2.$$

In contrast to the preceding case, it does not scale as a surface tension term, but is linear in wavevector (again this result survives if $B \neq 0$; C is simply replaced by a linear combination involving B and C).

The ratio of the energies of case one over case two is

$$\sim \lambda k.$$

Since one expects λ to be of the order of molecular dimensions, grooves of infinite extent should favour an alignment of the columns perpendicular to them (cf. $k\lambda \ll 1$ is easily realized).

7.1.5 Particular geometries

7.1.5.1 Three-dimensional systems

Simple geometries can be used to study the hydrodynamic and thermodynamic properties of both smectic and columnar phases. The simplest but perhaps most basic experiment consists in imposing a stress σ_{zz} on one of the boundaries of a S_A homeotropic sample and measuring how it is transmitted to the other boundary (reference axes as in Fig. 7.4(a): in principle, the zz component should be entirely transmitted. It is experimentally more interesting to impose a displacement δd [23]. The strain $\partial u / \partial z$ is simply given by $(\delta d/d)$, and the transmitted stress by $\bar{B}(\delta d/d)$. This experiment thus provides a direct measure of \bar{B} . This should be a static experiment, but defect motions relax the stress and only the short time

behaviour leads to \bar{B} . Typical values are a few 10^8 erg cm^{-3} , but can vary considerably from system to system.

What happens with columnar phases? There are two basic geometries.

1. Columns parallel to the walls. The behaviour is identical to that of smectics (one has, however, to be careful with lateral boundary conditions; i.e. axes defined as in Fig. 7.4(b)). With $\partial u_y / \partial y = 0$ one measures $(\bar{B} + C)$; with $\sigma_{yy} = 0$, one measures $4BC/(\bar{B} + C)$) [24].
2. Columns perpendicular to the walls: since we are exerting a stress in the liquid direction, there should be nothing but flow at vanishingly small frequencies. However, there is a time scale over which molecules cannot flow from one tube to the next: in a given column the number of molecules is a conserved quantity, and the pressure uniform.[†] Let us consider the case of a thin sample ($d \ll L$ = lateral size). Under such conditions the dilatation is entirely determined by boundary displacement (in the absence of buckling to be described in Section 7.1.7),

$$\theta = \frac{\delta d}{d}.$$

And the stress transmitted by the sample is simply a pressure term, $p = A(\delta d/d)$. The modulus A was found to be of the order of $5 \cdot 10^8 \text{ erg cm}^{-3}$ [25].

7.1.5.2 Reduced dimensionality

A technique that allows us to obtain a beautiful geometry ideally suited for the study of monocrystalline smectics was invented years ago by G. Friedel [26] and revived at Harvard [24, 27]. Spreading a smectic across a hole (typical diameter: a few millimetres) with a blade, produces a ‘free-standing film’, the thickness of which can be monitored by reflectivity measurements and varied from several thousand down to a few layers (Fig. 7.5(a)). This is a tool particularly adapted to the study of dimensionality effects (cross-over from three to two dimensions) and to high-resolution X-ray work [28, 29].

The reason for the film stability is the following. Breaking a film requires the creation of a hole, the energy of which comes essentially from two parts:

1. A positive line tension giving a contribution $2\pi N a_0 A_0 R$ (N , number of layers; a_0 , layer thickness; A_0 , air/liquid crystal interfacial tension; R , radius of the hole).
2. A negative interfacial term $-2(\pi A_0 R^2)$. (The factor 2 comes from the two sides of the film. The minus sign comes from the fact that, in the process

[†] The pressure is equilibrated on a time scale corresponding to the ratio of the column length over the sound speed: considering a $100 \mu\text{m}$ thick sample, one gets: $\tau \sim 10^{-2}/10^5 \sim 10^{-7} \text{ s}$.

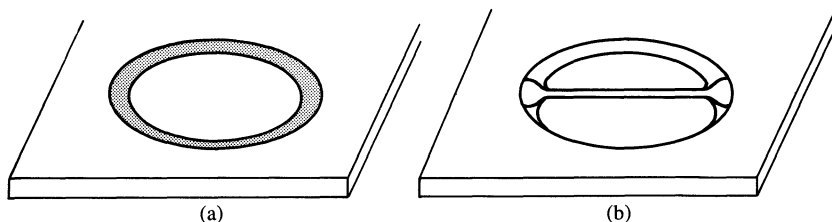


Fig. 7.5. (a) Typical appearance of a free-standing film: the holder may be a microscope coverslip; the middle of the sample is thin (a few layers to a few hundred or even thousand layers). The edges of the film are significantly thicker and act as ‘bulk reservoir’. (b) Freely suspended strand (developed in the spreading direction). The diameter ranges typically from a few micrometres to a few hundred micrometres. Again the ends of the strand, which are much thicker, act as ‘bulk reservoir’.

of creating the hole, molecules are removed from the interface to the bulk where they cost no interfacial energy.)

Thus the energy required to create a hole of radius R is

$$W_R = 2\pi A_0(Na_0R - R^2). \quad (7.32)$$

For small R , W_R is positive and nucleation of a hole costs energy. For large R , the system gains energy while opening up the hole more and more: the film pops.

There is a barrier (corresponding to the maximum of W_R at the critical radius $R_c = Na_0/2$),

$$W_c = \frac{\pi A_0}{2} (Na_0)^2 \quad (7.33)$$

for nucleating such holes. The nucleation frequency per unit area is

$$f \simeq f_0 \exp(-W_c/k_B T) \quad (7.34)$$

where f_0 is a natural frequency (per cm²) of the system. Taking the value of f_0 to be of the order of the speed of sound divided by a molecular diameter times a molecular area and taking a typical value of A_0 ($\simeq 30$ erg cm⁻²), we estimate

$$f \simeq 10^{26} \exp(-50N^2) \text{ s}^{-1} \text{ cm}^{-2}.$$

For $N = 1$, $f \simeq 2 \times 10^6 \text{ s}^{-1}$, while, for $N = 2$, $f \simeq 10^{-59} \text{ s}^{-1}$. The N^2 dependence of the energy barrier has a tremendous consequence. Whereas one-layer films will almost never be stable, two-layer or thicker films should last for months when kept in suitable conditions.

Why should the layers not pop one after the other? The answer is simple: there is no surface energy gain. Only a term linear in R remains and, unless elastic energy is gained (which requires a strained sample, and this will be

discussed in the next chapter), there is no instability and growth of R to be expected.

The corresponding geometry for columnar phases has been discovered by D. H. Van Winkle and N. A. Clark [30]: spreading columnar materials across holes similar to those utilized for making the smectic films, produces freely suspended strands (Fig. 7.5(b)). Their stability may be understood in the following way: in the cylindrical geometry (7.30) reads (with a radial distortion u_r , and assuming $u_\theta = 0$, plus no dependence on z and θ)

$$F = \bar{B}\pi \int \left(\frac{du_r}{dr} \right)^2 r dr. \quad (7.35)$$

Thus, expressing the extremum condition requires

$$\frac{1}{r} \frac{d}{dr} \left(r \frac{du_r}{dr} \right) = 0, \quad (7.36)$$

which gives

$$\frac{du_r}{dr} = \frac{r_0}{r} \quad (7.37)$$

or

$$u_r = r_0 \ln \left(\frac{r}{r_c} \right) \quad (7.38)$$

where r_0 is a constant to be determined and r_c a short-range cut-off of the order of a column diameter a_0 . Hence the total free energy, including interfacial tension A_0 , reads per unit length

$$F = 2\pi \left\{ \bar{B}r_0^2 \ln \left(\frac{R}{r_c} \right) + A_0 R \right\} \quad (7.39)$$

where R is the strand outer radius. If the number of columns is not conserved, the minimum energy is obtained for $R = 0$, i.e. the strand is not stable. This occurs if the maximum stress exceeds the critical value σ_c for breaking a column

$$\sigma_{\max} = \bar{B} \frac{r_0}{a_0} > \sigma_c.$$

If, on the contrary, $\sigma_{\max} < \sigma_c$, the strand is stable against the disappearance of the columns one after the other. The column conservation law reads

$$R - u_r(R) = Na_0$$

where N^2 is proportional to the number of columns in the strand (the proportionality factor depends on the exact columnar structure and is of the order of one).

After elimination of r_0 , the free energy reads

$$F = 2\pi \left\{ \bar{B} \frac{(R - Na_0)^2}{\ln\left(\frac{R}{r_c}\right)} + A_0 R \right\},$$

which always has a stable minimum for finite R . Thus, when the column number is conserved, the Rayleigh instability of liquid jets is pre-empted [31]. The ratio $A_0/\bar{B} = e$ has the dimension of a length which should be of the order of a_0 . Hence, for N reasonably large (macroscopic diameters larger than microns), R is close to Na_0 . Setting $R = Na_0 + u$ and minimizing F leads to

$$u \simeq -e \ln\left(\frac{Na_0}{r_c}\right).$$

Hence the column displacement is of the order of a few diameters but $\sigma_{\max} = -\bar{B}(e/a_0)$ is of the order of what can be reasonably expected for σ_c . Thus depending on the detailed properties of the system, strands can or cannot be stable.

High-resolution X-ray work [32] teaches us that in a strand a few tens of micrometres thick, several domains usually coexist although the column axis is remarkably well defined (mosaicity $< 0.3^\circ$). Sufficient annealing may produce monocrystals.

7.1.6 Transitions induced by external forces: Helfrich–Hurault effect

Let us consider first a smectic A in a homeotropic texture between two glass plates. The unperturbed layers are parallel to the plane (x, y) of the plates; the molecules are aligned along z . We add to this system a magnetic field \mathbf{H} in the x direction, and we assume that the diamagnetic anisotropy χ_a is positive. To minimize the magnetic energy, the system would like to rotate its optical axis. But the layers are strongly clamped at both walls. What will happen then?

If we were dealing with a nematic, we would expect to find, above a certain field threshold, a bend distortion of the Frederiks type, with the following structure for the director (see Chapter 3)

$$n_x(z) \neq 0 \quad (n_x \ll 1 \text{ just above threshold}),$$

$$n_y = 0,$$

$$n_z \simeq 1.$$

According to eqn (7.7) this would correspond to

$$u(x, y, z) = \text{const.} - xn_x(z),$$

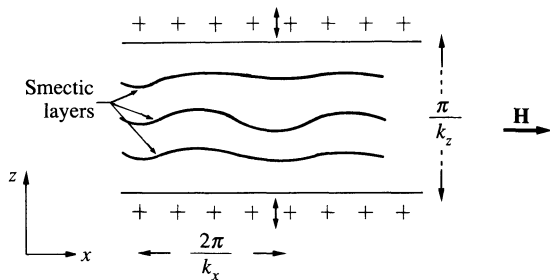


Fig. 7.6. The Helfrich–Hurault transition for smectics A. The transition can be induced in principle by a magnetic field \mathbf{H} . In practice, it is more convenient to apply a mechanical tension to the limiting plate.

i.e. to layers that cross from one plate to the other, piling up at very high densities near both plates, and giving infinite elastic energies through the \bar{B} term in eqn (7.13). Thus we must invent another solution, also leading to a non-zero n_x —i.e. to some partial alignment along \mathbf{H} .

A similar problem, for another layered system, has in fact been encountered in Chapter 6 in connection with cholesterics under electric fields (the Helfrich effect): the layers undergo a periodic distortion along x (Fig. 7.6). In terms of the displacements u , this corresponds to

$$u(x, z) = u_0(z) \cos kx \quad (7.40)$$

where k is a certain wavevector, the optimal value of which will be derived later. Equation (7.40) still contains a dependence in z , because the displacement must vanish on both plates. In fact, for small-amplitude distortions (just above threshold) we can take $u_0(z)$ as a sine wave, vanishing both for $z = 0$ and $z = d$, such that

$$\left. \begin{aligned} u_0(z) &= u_0 \sin(k_z z), \\ k_z &= \frac{\pi}{d}. \end{aligned} \right\} \quad (7.41)$$

This distortion of the layers corresponds to an optical axis locally defined by

$$\left. \begin{aligned} n_x &= -\frac{\partial u}{\partial x} = \epsilon \sin(k_z z) \sin kx, \\ n_y &= 0, \\ n_z &\simeq 1. \end{aligned} \right\} \quad (7.42)$$

Let us write down the elastic free energy $\langle F_{\text{el}} \rangle$ derived from the eqn (7.13)

(and averaged over the sample thickness)

$$\langle F_{\text{el}} \rangle = \frac{1}{2}\epsilon^2 \left[\bar{B} \left(\frac{k_z}{k} \right)^2 \langle \cos^2 k_z z \rangle \langle \cos^2 k_x + K_1 k^2 \rangle \langle \sin^2 k_z z \rangle \langle \sin^2 k_x \rangle \right]. \quad (7.43)$$

We must add to this the magnetic term: it differs from eqn (7.13) because, in the present example, the field is in the plane of the layers

$$\langle F_{\text{mag}} \rangle = -\frac{1}{2}\chi_a H^2 \langle n_x^2 \rangle = \frac{1}{2}\chi_a H^2 \epsilon^2 \langle \sin^2 k_z z \rangle \langle \sin^2 k_x \rangle. \quad (7.44)$$

All the averages of the form $\langle \sin^2 \theta \rangle$ or $\langle \cos^2 \theta \rangle$ are equal to $\frac{1}{2}$, and the total free energy becomes

$$\langle F_{\text{el}} + F_{\text{mag}} \rangle = \frac{\epsilon^2}{8} \bar{B} \left[\left(\frac{k_z}{k} \right)^2 + k^2 \lambda^2 \right] - \frac{\epsilon^2}{8} \chi_a H^2. \quad (7.45)$$

When the overall coefficient of ϵ^2 in eqn (7.45) is positive for all k values, the unperturbed arrangement is stable. Instability will occur first for that value of k at which the first bracket in (7.45) is minimum. This corresponds to

$$k^2 = k_z/\lambda = \pi/\lambda d. \quad (7.46)$$

Thus the optimal wavelength of the distortion ($2\pi/k$) is (apart from numerical coefficients) equal to the geometric mean of the sample thickness d and of the microscopic length λ . This result has been verified experimentally on cholesterics, where similar equations hold (λ being then related to the pitch [33]). But no experiments have been performed, up to now, on smectics: the problem is that one needs to have very large samples, or very large fields. To understand this, let us now write down the threshold field H_c obtained when the elastic and magnetic terms cancel exactly in eqn (7.45). We have

$$\chi_a H_c^2 = 2\bar{B} \left(\frac{k_z}{k} \right)^2 = 2\bar{B} k_z \lambda = 2\pi \frac{\bar{B} \lambda}{d}. \quad (7.47)$$

Equation (7.47) was derived by Hurault inspired by an earlier calculation of Helfrich [34]. It shows that H_c is proportional to $d^{-1/2}$. This behaviour is quite different from that which we have in a conventional Frederiks transition, where $H_c \sim d^{-1}$. Here the field decreases more slowly with sample thickness. Writing eqn (7.47) in the form

$$\chi_a H_c^2 = 2\pi \frac{K_1}{\lambda d} \quad (7.48)$$

and using the estimates $K_1 = 10^{-6}$ dyn, $\lambda = 20$ Å, $d = 1$ mm, and $\chi_a = 10^{-7}$, we arrive at $H_c \sim 60$ kG. To bring the value of H_c into a more convenient range (say 20 kG) we would need smectic monocrystals of thickness 1 cm. Samples of this size have been prepared. However, there is one serious

difficulty: above the threshold field H_c (say, for $H = 2H_c$) the distortion amplitude ϵ remains very small. The undulation of the layers is strongly limited by the requirement of (nearly) constant interlayer thickness: in such a situation we say that we have a ‘ghost transition’, which is formally present but hard to observe.[†]

Similar considerations may be developed for columnar phases. It is clear that the remarks concerning the observability of field effects in smectics hold in that case as well. Thus, unless one is able to produce large monocrystalline samples, field-driven instabilities will not be observed. For that reason we prefer to concentrate on mechanical instabilities to be described in the next subsection.

7.1.7 Transitions induced by external forces: undulation by mechanical tension

7.1.7.1 Smectics

When a homeotropic slab of a smectic A is put under mechanical tension, one observes a periodic undulation of the layers of the Helfrich–Hurault type, with a wavelength $2\pi/k$ proportional to the square root of the sample thickness d , as in eqn (7.46). This remarkable deformation appears only under tension (not under compression). It has been found and studied by Delaye, Ribotta, and Durand [36a], through the diffraction of light on the periodic undulations. The effect was also predicted independently by the Harvard group [36b].

This mechano-optic effect is easily understood if we assume that, during the time under study, the number of layers present in the sample thickness is constant. (Changes in this number must involve dislocation motion and will be discussed later.) Then, when the system is expanded, there are two different behaviours: either the layers expand uniformly (and this costs a rather high energy, proportional to the elastic modulus \bar{B}) or they keep a nearly constant thickness, but manage to fill the available space by undulations as shown in Fig. 7.6. At high strains the latter solution is preferable.

The threshold may be analysed in terms of a simple generalization of the elastic energy (7.13) allowing for finite strains. This generalization is useful in many practical problems and will be described here in some detail. It is still sufficient to write the energy associated to a dilatation γ of the layers in the form

$$F_{\text{dil}} = \frac{1}{2} \bar{B} \gamma^2, \quad (7.49)$$

[†] Light scattering experiments are sensitive enough to be able to evidence such distortions, but other phenomena have been preferred for the study of the peculiarities of smectic elasticity and the measurements of \bar{B} and K_1 . Another geometry leading to a similar ghost transition for a smectic A under a magnetic field is discussed in more detail in reference 35.

but the linear form $\gamma = \partial u / \partial z$ must be improved. Consider first a case where the layers are tilted uniformly. At lowest order

$$\begin{aligned}\frac{\partial u}{\partial z} &= 0, \\ \frac{\partial u}{\partial x} &= -n_x \quad (\ll 1).\end{aligned}$$

Remember now that, in our problem, the total number of layers is constant: this means that the distance between them, *measured along z* is still equal to the unperturbed interval a . But the true distance between them is $a \cos n_z \cong a(1 - \frac{1}{2}n_x^2) < a$.

Thus in this case, we have a small (second-order) dilatation

$$\gamma = -\frac{n_x^2}{2} = -\frac{1}{2} \left(\frac{\partial u}{\partial x} \right)^2.$$

Returning now to the general case (where u depends both on x and z , but the number of layers is still kept constant), we have

$$\gamma = \frac{\partial u}{\partial z} - \frac{n_x^2}{2}. \quad (7.50)$$

The elastic energy is still of the form

$$F = \frac{1}{2} \bar{B} \gamma^2 + \frac{1}{2} K_1 \left(\frac{\partial^2 u}{\partial x^2} \right)^2 \quad (7.51)$$

where γ is given by eqn (7.50). Let us now split the displacement u (or the resulting dilatations) into two terms

$$\begin{aligned}u &= u_0 + u_1(x, z), \\ \gamma &= \gamma_0 + \gamma_1\end{aligned} \quad (7.52)$$

where $u_0 = \gamma_0 z$ is the uniform displacement associated with the imposed strain γ_0 ($\gamma_0 > 0$), while u_1 will describe the undulation. We are interested in the threshold for the onset of the undulations: thus γ_0 and u_0 are finite, while u_1 is infinitesimally small. Let us then expand the free energy (7.51) up to order u_1^2 . We find

$$F = F_0 + \bar{B} \gamma_0 \frac{\partial u_1}{\partial z} - \bar{B} \gamma_0 \frac{n_x^2}{2} + \frac{1}{2} K_1 \left(\frac{\partial^2 u_1}{\partial x^2} \right)^2. \quad (7.53)$$

The term linear in $\partial u_1 / \partial z$ gives 0 by integration over the z variable (since u_1 is defined as vanishing on both plates). The new term of interest is the third term. It is identical in form to the effect of a destabilizing magnetic

field \mathbf{H} , the correspondence being given by

$$-\frac{1}{2}\chi_a H^2 n_x^2 = -\bar{B}\gamma_0 n_x^2. \quad (7.54)$$

Thus all our discussion of the Helfrich–Hurault threshold may be transposed to the present case: the spatial wavelength of the unstable mode is still given by eqn (7.46), and the threshold value of the strain γ_{oc} is obtained from eqns (7.47) and (7.54) as

$$\gamma_{oc} = 2\pi \frac{\lambda}{d}. \quad (7.55)$$

This corresponds to an increase in sample thickness $2\pi\lambda \sim 150 \text{ \AA}$, typically. It is thus quite easy to achieve strains γ_0 that are much larger than γ_{oc} . In this case, the distortions become quite visible: the mechanical coupling is much more convenient than the magnetic one.

Right at threshold the distortion has the same plane wave structure as in formulae (7.40) and (7.41). Subsequent dilatations induce a second instability that produces a square pattern and eventually results in a square array of parabolic focal conics [37].†

It must be emphasized that the distortions induced by tension are metastable: if we wait long enough, the number of layers present in the sample will tend to adjust itself through the motion of dislocations. In practice, the stability is found to depend strongly on the amplitude of the perturbation γ_0 : if γ_0 is not very large (although larger than γ_{oc}) the undulations persist only for a short time; while if γ_0 is large, the periodic distortions are not smooth any more (defects such as focal conics may be present). They are then much harder to heal; we have here the analogue of the storage mode of cholesterics, discussed in Chapter 6.

Note eventually that we have discussed the simplest modification of (7.13) which allows us to understand the undulation instability experiment; other non-linearities can be included (either of geometric or of physical origins) but under usual experimental conditions they do not play a fundamental role.

7.1.7.2 Columnar phases

Experiments show an undulation instability similar to that of smectics [22]. Looking at Fig. 7.6, it is hard to tell whether one is dealing with smectic layers seen from the side or with columns parallel to the plane of the figure (compare also Fig. 7.4(a) and (b)). This reveals that, for modes polarized in the x, z -plane, the two systems behave identically. Thus a straightforward extrapolation of the smectic results predicts the existence of an undulation instability beyond a displacement threshold [16]

$$\delta d = d\gamma_{oc} = 2\pi\tilde{\lambda}_3, \quad (7.56)$$

† A brief discussion of dislocations and focal conics in smectics is given in Chapter 9.

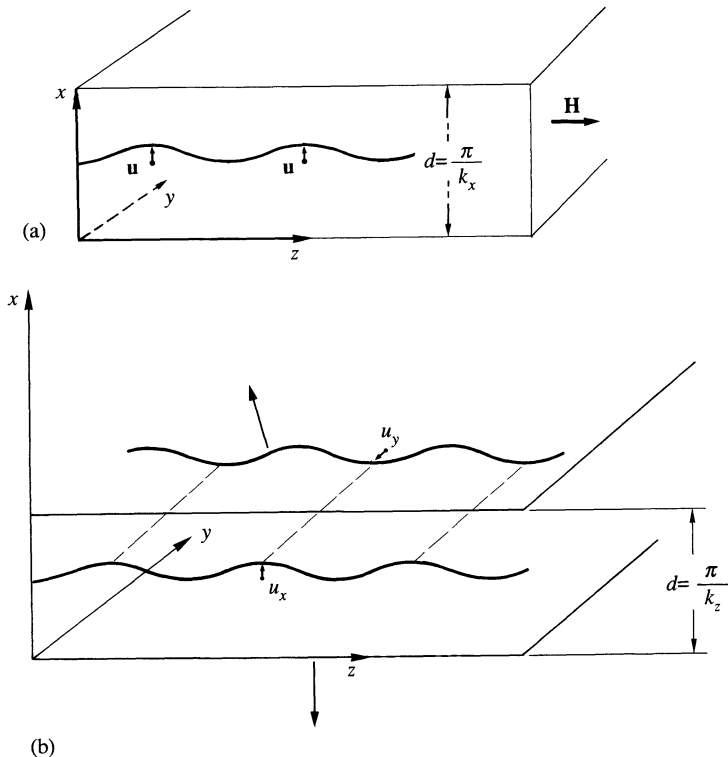


Fig. 7.7. (a) The Helfrich–Hurault transition in columnar phases. For $\frac{1}{2}B < C$, the case is identical to that for the smectics (distortion in the x, z -plane). (b) for $\frac{1}{2}B > C$, we get a two-dimensional pattern resulting from the imposed direction along x . (Note that both u_x and u_y differ from zero.)

in which

$$\tilde{\lambda}_3 = \sqrt{K_3/(B + C)} \quad (7.57)$$

with a wavevector along the columns

$$k^2 = \pi/\tilde{\lambda}_3 d. \quad (7.58)$$

In fact, the situation is more subtle: fluctuations to probe the y direction, and one must investigate the stability of the system versus displacements u_x and u_y of wavevectors $k_x = \pi/d$, k_y , k_z (Fig. 7.7(a, b)) [37].

For $2C > B$, the first instability is of the smectic type ($Uy \equiv 0$).

For $2C > B$, the columns deviate both in the x and y directions and the undulation pattern is bidimensional. The transition to this modulated state should be discontinuous. In terms of order of magnitude k_y scales as k_z (as $(\lambda d)^{-1/2}$) and the displacement at threshold as λ . This case has not been observed yet.

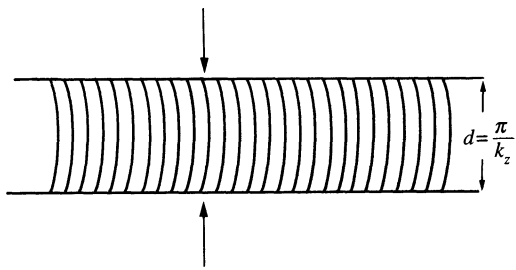


Fig. 7.8. Buckling instability in the ‘thin’ regime.

Another interesting instability is obtained when the columns, orthogonal to the surfaces, are submitted to a compressive stress (along z) (Fig. 7.8). Let us consider again the case of thin samples [16]. As already remarked in Section 7.1.3:

- At vanishingly small frequencies, nothing should happen except flow since we are squeezing the sample in the fluid direction.
- On time scales such that permeation cannot occur,† the number of molecules is a conserved quantity in a given column, and θ is directly given by this conservation equation (we assume $\nabla_y u_x = 0$ in the following).
- The relevant energy is given by (7.30).

The dilatation is then simply given by the total length change of a given column (divided by the equilibrium length d)

$$\theta = \frac{\delta d}{d} + \frac{1}{2d} \int_0^d (\nabla_z \mathbf{u})^2 dz. \quad (7.59)$$

Let us look for the simple buckling

$$u_x = \alpha \sin \frac{\pi z}{d}, \quad u_y = 0. \quad (7.60)$$

The generalization of (7.50) yields

$$\gamma_x = \frac{\partial u_x}{\partial x} - \frac{1}{2} \left(\frac{\partial u_x}{\partial z} \right)^2 = -\frac{\alpha^2 \pi^2}{2d^2} \cos^2 \frac{\pi z}{d}. \quad (7.61)$$

With (7.59)–(7.61) the α^2 part of the elastic energy (7.30) can be written (per cm^2) as

$$F = d \frac{\alpha^2}{4} \left((A - D) \frac{\delta d}{d} \frac{\pi^2}{d^2} + K_3 \frac{\pi^4}{d^4} \right). \quad (7.62)$$

† The characteristics of permeation will be described in Section 7.2.

This expression becomes unstable for a displacement (the minus sign corresponds to the fact that a compression is needed)

$$\delta d_c = -\frac{\pi^2 K_3}{d(A - D)}. \quad (7.63)$$

With $(A - D) \sim 10^9 - 10^8 \text{ erg cm}^{-3}$, $K_3 \sim 10^{-6} \text{ dyn}$, and $d \sim 10^{-3} \text{ cm}$, $\delta d_c \simeq 10^{-11} - 10^{-10} \text{ cm}$!! This extremely small number shows that, unless molecules can flow from column to column, these systems cannot be monocrystalline in practical cases.

Experiments do show the undulation and the buckling instability [20, 22, 38]. The thresholds turn out to be much larger than expected. If one considers that the results correspond to defect-free samples, this implies a K_3 value 10^6 times larger than the nematic one, if one assumes elastic constants 10^8 erg cm^{-3} . This observation may result from the existence of point defects linked by ‘strings’ [39].

7.1.8 Transitions induced by external forces: thermo-optic effect in smectics A

Another experimental set-up, generating the Helfrich–Hurault undulations in smectics A, has been discovered by Kahn [40]. A homeotropic sample is placed under a strong light beams, and is thus slightly heated because of the finite absorption of the material. The light intensity is then abruptly reduced: the sample cools down and the layers tend to contract. If the sample thickness d is fixed, this may be achieved by undulations; a distortion appears in the form of a very fine square lattice.

This Kahn effect suggests some interesting technical applications, since it allows us to store information on a very small scale in a smectic slab: the information can be written, read, and erased by light beams of suitable intensity [41].

Direct joule heating has basically the same effect [41]. In fact, in order to obtain a texture made of domains that are as small as possible, it is technically interesting to heat the sample to the isotropic phase. Fast cooling provides a strongly scattering texture, which can be used in display devices. This is the ‘write’ sequence. Erase is easily obtained by cooling under the action of an electric field. Note that this display has good multiplexing characteristics, since stray fields have no influence on the smectic site (cf. ghost transitions!), and good time response: the slowest one is provided by thermal diffusivity: $\tau \simeq 1/Kq^2$ where $q \simeq \pi/d$. With $d \simeq 10^{-3} \text{ cm}$, $K \sim 10^{-2} \text{ cm}^2 \text{ s}^{-1}$, one gets $\tau \sim 10^{-5} \text{ s}$. This is much faster than the typical nematic displays. One drawback, however: the power consumption is no longer negligible.

7.1.9 Fluctuations

7.1.9.1 Smectics A

Let us return to an unperturbed, single-domain smectic A and investigate the spontaneous fluctuations of the positions of the layers. These fluctuations control in particular the scattering of light and the scattering of X-rays (remember: Chapter 1 for X-rays).

To determine the amplitude of the fluctuations, we start from eqn (7.13) (putting $H = 0$ for simplicity) and go to the Fourier transform u_q of the displacement $u(r)$. In terms of the u_q s, the free energy F takes the form

$$F = \sum_q \frac{1}{2}(\bar{B}q_z^2 + K_\perp q_\perp^4)|u_q|^2 \quad (7.64)$$

where $q_\perp^2 = q_x^2 + q_y^2$. Applying the classical equipartition theorem to eqn (7.71), we arrive at the thermal averages

$$\langle|u_q|^2\rangle = \frac{k_B T}{\bar{B}q_z^2 + K_\perp q_\perp^4} = \frac{k_B T}{\bar{B}(q_z^2 + \lambda^2 q_\perp^4)}. \quad (7.65)$$

Let us now discuss how these fluctuations may be detected by light scattering [42]. In the unperturbed state, the dielectric tensor ϵ (at the light frequency of interest) has three non-vanishing components

$$\begin{aligned} \epsilon_{xx} &= \epsilon_{yy} = \epsilon_\perp, \\ \epsilon_{zz} &= \epsilon_{||} = \epsilon_\perp + \epsilon_a. \end{aligned} \quad (7.66)$$

In the fluctuating system, we will first have some modifications in the magnitude of $\epsilon_{||}$ and ϵ_\perp due to changes in the density and in the interlayer distance: they will be similar to what is found in conventional liquids and will not give rise to any spectacular effect (see reference 42) for more detailed discussion of this point). We also expect some deviations of the optical axis \mathbf{n} from the normal of the layers, contributing to the depolarized scattering—but, as already mentioned, these deviations are not important at small wavevectors \mathbf{q} ($q\lambda \ll 1$).

Finally, the most interesting contribution is related to possible *rotations* of the layer system, the molecules remaining normal to the local layers. The fluctuations $\delta\epsilon$ of the dielectric tensor associated with such rotations may be obtained by writing (as was done in Chapter 3 for nematics)

$$\epsilon = \epsilon_\perp + \epsilon_a \mathbf{n} \cdot \mathbf{n}$$

$$\delta\epsilon = \epsilon_a [\delta\mathbf{n} \cdot \mathbf{n} + \mathbf{n} \cdot \delta\mathbf{n}].$$

Using eqn (7.7), this gives two non-vanishing terms

$$\left. \begin{aligned} \delta\epsilon_{xz} &= -\epsilon_a \frac{\partial u}{\partial x}, \\ \delta\epsilon_{yz} &= -\epsilon_a \frac{\partial u}{\partial y}. \end{aligned} \right\} \quad (7.67)$$

Assuming that ϵ_a is not too large, the scattering intensity (for a given scattering wavevector \mathbf{q}) is given by the Born approximation formula

$$I(q) = \langle |\mathbf{i} \cdot \delta\epsilon(q) \cdot \mathbf{f}|^2 \rangle. \quad (7.68)$$

Thus, to have a strong scattering, it is favourable to have the ingoing polarization vector \mathbf{i} along z and the outgoing polarization vector \mathbf{f} in the x, y -plane (or the reverse). Let us assume that this condition is realized. Then, using eqns (7.65), (7.67), and (7.68), we arrive at

$$I = \frac{k_B T}{\bar{B}} \epsilon_a^2 \frac{q_\perp^2}{q_z^2 + \lambda^2 q_\perp^4}. \quad (7.69)$$

Equation (7.69) predicts the existence of two widely different regimes.

1. If \mathbf{q} is oblique ($q_z \sim q_\perp \neq 0$), we may write

$$I \sim \epsilon_a^2 \frac{k_B T}{\bar{B}} \frac{q_\perp^2}{q_z^2} \quad (7.70)$$

since $q\lambda \ll 1$ for visible light. The intensity I is then of the order of $k_B T/\bar{B}$, i.e. comparable to that found in a conventional liquid. Note that the ‘oblique’ situation corresponds to the majority of scattering events in transmission experiment; eqn (7.77) indicates that a smectic A (in a single-domain texture) should not be turbid like a nematic. This is indeed what is found.

2. If \mathbf{q} is in the plane of the layers ($q_z = 0$), the intensity becomes

$$I = \epsilon_a^2 \frac{k_B T}{\bar{B} \lambda^2 q^2} = \epsilon_a^2 \frac{k_B T}{K_1 q^2}. \quad (7.71)$$

Equation (7.71) has the form found in Chapter 3 for scattering by nematics, and predicts a very high intensity. Physically, the modes $q_z = 0$ are pure undulation modes (Fig. 7.9) for which the layers are deformed, but the interlayer distance is not altered; fluctuations of this type require very little energy, and have large amplitudes.

The condition $q_z = 0$ restricts the intense scattering to a cone (Fig. 7.10). The angle of this cone is very sharply defined: from eqn (7.69) we see that I

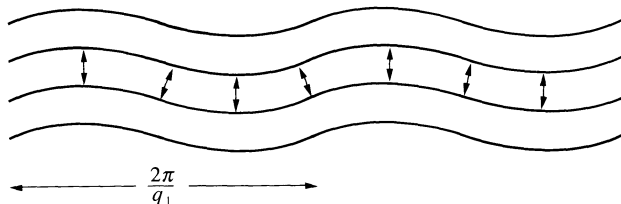


Fig. 7.9. The pure undulation of smectics. In this mode the interlayer distance is unaffected.

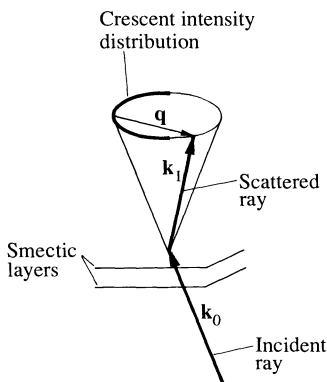


Fig. 7.10. Distribution of the light scattering intensity in an ideal smectic sample. For simplicity, the differences in refractive indices for the two polarizations **i** and **f** have been neglected: then \mathbf{k}_0 and \mathbf{k}_1 have the same length.

gets large when

$$\left. \begin{aligned} q_z^2 &< \lambda^2 q^4, \\ \frac{q_z}{q} &< \lambda q \sim 10^{-3}. \end{aligned} \right\} \quad (7.72)$$

This implies that scattering experiments must be performed only on excellent single-domain samples; also the thickness d of the sample must be large, to ensure that the undulation mode is not clamped by the limiting surfaces. The requirement on d is obtained by replacing $q_z \rightarrow \pi/d$ in eqn (7.72). Light scattering due to thermal undulation in this geometry has been observed [43] but the ‘planar’ geometry (i.e. layers perpendicular to the surfaces) is better adapted for this kind of study [44]. The full formula (7.65) may be tested and \bar{B} and K_1 obtained from the experiment. \bar{B} is again found in the 10^7 – 10^8 erg cm $^{-3}$ range and K_1 is often nearly identical to its nematic value.

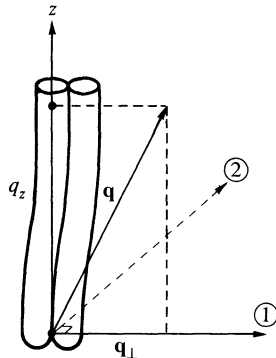


Fig. 7.11. Decomposition of the column displacement into independent components for a given wavevector.

7.1.9.2 Columnar D phase

As in nematics, the fluctuations of \mathbf{u} polarized in the $(\hat{\mathbf{z}}, \mathbf{q})$ plane (direction 1 of Fig. 7.11) and that polarized in a direction perpendicular to that plane decouple naturally in Fourier space. Thus

$$F = \sum_q \left\{ \frac{1}{2} [(\bar{B} + C)q_{\perp}^2 + K_z q_z^4] |u_1(q)|^2 + \frac{1}{2} [Cq_{\perp}^2 + K_z q_z^4] |u_2(q)|^2 \right\}. \quad (7.73)$$

The equipartition theorem gives (once more!)

$$\left. \begin{aligned} |u_1(q)|^2 &= \frac{k_B T}{(\bar{B} + C)q_{\perp}^2 + K_z q_z^4} \\ |u_2(q)|^2 &= \frac{k_B T}{Cq_{\perp}^2 + K_z q_z^4}. \end{aligned} \right\} \quad (7.74)$$

The similarity of (7.73) with (7.74) is striking, but note that \mathbf{q}_{\perp} and q_z have been interchanged: the contribution from first-order elastic constants vanishes in the plane $q_z = 0$ in smectics but only along the line $\mathbf{q}_{\perp} = 0$ in columnar phases.

With the same provisos used previously, the dominant dielectric tensor modulations read

$$\left. \begin{aligned} \delta\epsilon_{z1} &= \epsilon_a \frac{\delta u_1}{\delta z} \\ \delta\epsilon_{z2} &= \epsilon_a \frac{\delta u_2}{\delta z} \end{aligned} \right\} \quad (7.75)$$

and the scattered intensity is

$$I_{\text{HV}} \propto I_{\text{VH}} \propto \langle |\delta\epsilon_{z2}(a)|^2 \rangle = \epsilon_a^2 \frac{k_B T q_z^2}{C q_{\perp}^2 + K_z q_z^4}, \quad (7.76)$$

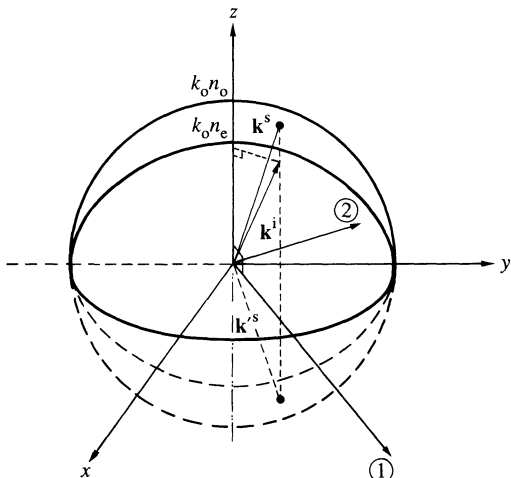


Fig. 7.12. I_{VH} geometry. The two spots of light scattered by the incident radiation of polarization in the $(1, z)$ plane. They correspond to light polarized in the 2 direction (note: the extremity of \mathbf{k}^i lies on the $k_0 n_e$ surface, those of \mathbf{k}^s and \mathbf{k}'^s on the $k_0 n_o$ one. $k_0 = \omega/c$.

$$I_{VV} \propto \langle |\delta\epsilon_{z1}(q)|^2 \rangle = \frac{k_B T q_z^2}{(\bar{B} + C)q_\perp^2 + K_3 q_z^4}. \quad (7.77)$$

(V refers to a polarization of the electric field in the $\{z, 1\}$ plane; H to a polarization in direction 2 of Fig. 7.11; as usual, the first (respectively second) subscripts refer to the polarization of incident (respectively scattered) light.)

Equations (7.76) and (7.77) hide geometrical factors: they turn out to be unimportant for (7.76) but important for (7.77). Indeed the source term responsible for the scattering may easily be shown to be proportional to

$$\delta\epsilon(q)(k_z^s D_z^1 - k_1^s D_1^1) \quad (\mathbf{k}^s = \mathbf{k}^i + \mathbf{q})$$

where \mathbf{D} is the displacement vector. When $\mathbf{q}_\perp = 0$, $k_1^s = k_1^i$, but $k_z^s = -k_z^i$ the source term ($\propto \mathbf{k}^i \cdot \mathbf{D}^i = 0$) vanishes. As a result, the scattering will be essentially concentrated on two spots (Fig. 7.12). (NB. Those corresponding to I_{VH} are geometrically different from those corresponding to I_{HV} .) This interesting peculiarity of columnar phases has not been observed yet, probably because of the difficulty of getting large high quality samples.

7.1.9.3 Smectic C films

The novel features of smectics C in comparison to smectics A have their basis in the existence of the extra hydrodynamic variable Ω_z . The free-standing film geometry is particularly well suited for singling out this

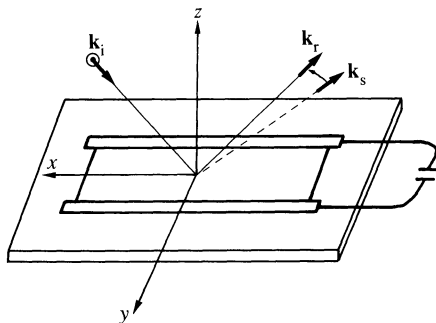


Fig. 7.13. Free smectic C film geometry, after Young *et al.* [24]. The inner parallelogram of the figure represents a rectangular hole in a glass microscope coverslip over which the smectic film is drawn. The electrodes on the ‘long sides’ of the hole make it possible to apply a field in the y direction which specifies the polarization direction \mathbf{P}_0 in the case of ferroelectric S_C^* . \mathbf{k}_i , \mathbf{k}_r , \mathbf{k}_s represent the incident, specularly reflected, and scattered wavevectors of the light beams interacting with the sample. In the example shown in the figure, $q_x \neq 0$, $q_y = 0$, the incident polarization is along y and the scattering one in the x , z -plane. The scattering is due to $\delta\epsilon_{xy}$ fluctuations directly proportional to Ω_z for small fluctuations.

variable, as shown by the Harvard group [24, 27]. For wavelengths large compared to the film thickness (which is basically always the case in light scattering experiments), free-standing smectics C behave essentially like two-dimensional nematics [45].

The free energy per unit surface may be written as

$$F = \int \frac{1}{2} \left[B_1^* \left(\frac{\partial \Omega_z}{\partial x} \right)^2 + B_2^* \left(\frac{\partial \Omega_z}{\partial y} \right)^2 \right] dx dy \quad (7.78)$$

where $B_1^* \simeq d\tilde{B}_1$ and $B_2^* \simeq d\tilde{B}_2$ (d is the film thickness). \tilde{B}_1 and \tilde{B}_2 are the bend and the splay elastic constants of the \mathbf{c} director.

Light scattering experiments allow the measurement of Fig. 7.13

$$\langle \Omega_z(\mathbf{q}) \Omega_z(-\mathbf{q}) \rangle = \frac{k_B T}{B_1^* q_x^2 + B_2^* q_y^2}. \quad (7.79)$$

Thin-film measurements show systematic deviations from the bulk value: this illustrates the structural differences between surface and bulk. They are best demonstrated by X-ray work, but cannot be described without reference to phase transitions.

In Chapter 1 we insisted on the notions of short-, long-, and quasilong-range order in liquid crystals and stated that nematics exhibit long-range order in three dimensions, but only quasilong-range order in two dimensions

[45]. Recently, a direct measure of $\langle \Omega_z^2(r, t)\Omega_z^2(r', t') \rangle$ has clearly demonstrated the logarithmic dependences linked with bidimensionality [46, 47].

7.2 CONTINUUM DESCRIPTION OF CHIRAL SMECTICS AND COLUMNAR PHASES

7.2.1 Chiral S_A^* and S_C^*

To what respect are S_A and S_A^* different? It is clear that the elastic and flexoelectric expressions are the same since we only used translational and rotational invariances in their construction. On the other hand one expects the existence of rotatory power in S_A^* (of the order of that expected in isotropic liquids) but not in S_A . Another interesting difference has been pointed out by R. B. Meyer [48]: the rotations $\Omega_x = -\delta n_y$, $\Omega_y = \delta n_x$, which are pseudovectors, can be dotted on to the electric field and contribute to the free energy. (NB. Pseudoscalar coefficients are now allowed.) Of course, a mere rotation cannot change the free energy: it can only be a rotation with respect to the layers. That is

$$F_e = e \left[\left(\Omega_x - \frac{\partial u}{\partial y} \right) E_x + \left(\Omega_y + \frac{\partial u}{\partial x} \right) E_y \right]. \quad (7.80)$$

The coupling describes the ‘electroclinic’ effect. Knowing that it requires an energy,

$$F' = \frac{1}{2} D \left[\left(\Omega_x - \frac{\partial u}{\partial y} \right)^2 + \left(\Omega_y + \frac{\partial u}{\partial x} \right)^2 \right], \quad (7.81)$$

in order to tilt the director away from the normal to the layers, one finds that an electric field induces such a tilt in a S_A^* . For instance, with fixed layers,

$$\Omega_x = -eE_x/D. \quad (7.82)$$

Since one is speaking of a rotation with respect to the layers, the characteristic time of the rotation does not depend on wavelength and is thus ‘microscopic’. (Typically, $\tau = \gamma/D$, the viscosity γ may be estimated to be of the order of the nematic twist viscosity ~ 1 poise, $D \simeq 10^7$ erg cm $^{-3}$ far from any transition [49], and thus $\tau \sim 10^{-7}$ s.) This linear electro-optic effect is intrinsically fast! Although small in early experiments [50], this effect may be sizeable in more recent systems and leads to interesting applications [49].

What about $S_{BH_{ex}}^*$? Obviously, the arguments developed for S_A^* still hold. Flexoelectric terms are those of $S_{BH_{ex}}$, but extra couplings between E and Ω_z on the one hand and ∇E and $\nabla \Omega_z$ on the other are allowed (Fig. 7.14(b)). However, the most important feature is the helicoidal precession of the bond ordering in the z direction (Fig. 7.14(a)). Indeed $\partial \Omega_z / \partial z$ is a pseudoscalar that can enter the free energy and, as a result, the ground state involves a non-zero $\partial \Omega_z / \partial z$.

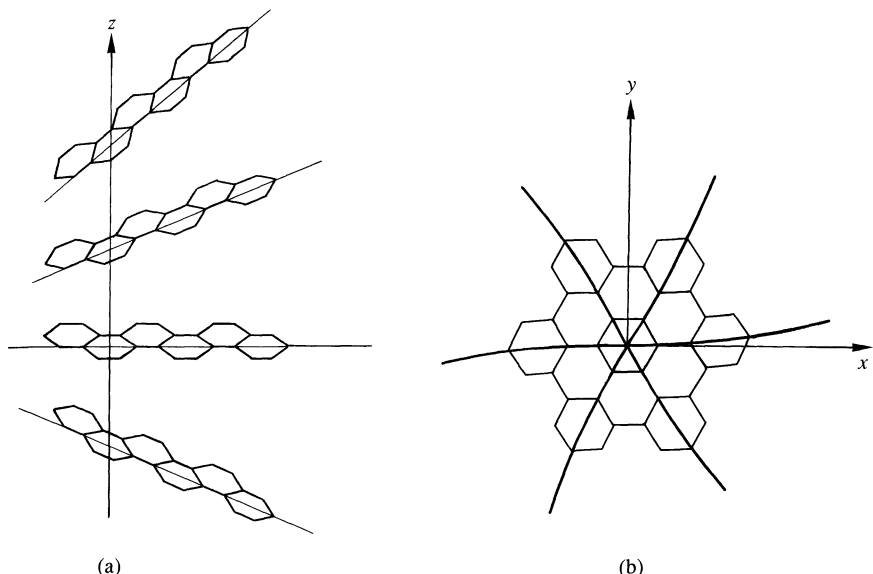


Fig. 7.14. (a) Twist of the bond order in S_B^* . (b) Distortion resulting from the action of a field E_z across the layers: $\nabla_{\perp}\Omega_z \propto E_z$. Note that one cannot fill space with such a distortion: beyond a given threshold a field should create an array of defects in a $S_{B\text{Hex}}^*$. Note that an E_x electric field would simply induce an x gradient of the twist $\partial\Omega_z/\partial z$. Note further than a splay $\nabla_{\perp}u$ and bend $\partial^2 u/\partial z \partial x$ have the same effects as E_z and E_x , respectively. In (a) and (b) the hexagons are a guide to the eye for visualizing bond order; they do not represent positional order.

7.2.2 Chiral S_C^* (S_I^* , S_F^* , and S_K^*)

As we have already noticed in Chapter 1, the symmetry element characterizing these systems is C_2 only. It is both perpendicular to the normal to the layers and to the tilt direction (c) defined in Section 7.1.2. We also made the point that, as a result, these phases should be ferroelectric, the electric polarization being along the C_2 axis.

Let us construct the elastic free energy for these systems in terms of the \mathbf{k} , \mathbf{c} , \mathbf{p} vectors defined in Section 7.1.2.3. In the non-chiral smectic C all terms linear in $\nabla\mathbf{k}(\mathbf{c}, \mathbf{p})$ were prohibited in the elastic free energy, because they were incompatible with the inversion symmetry. Now, some of these terms become allowed: they are the analogues of the $\mathbf{n} \cdot \text{curl } \mathbf{n}$ term in the Frank energy of cholesterics (Chapter 6).

In the problem of Section 7.1.2.3 we wrote all independent vectorial quantities characterizing a S_C . Those which point along the \mathbf{p} direction can enter the S_C^* free energy. (NB. The same argument as the one allowing for

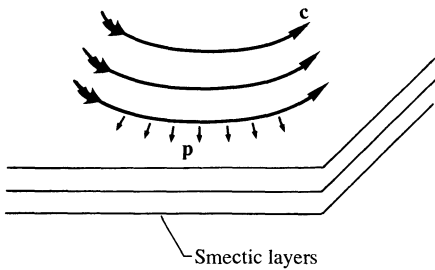


Fig. 7.15. One type of distortion mode in a chiral smectic C. The \mathbf{c} director tends to bend. However, this is not a space-filling structure.

a polarization holds.)

$$\left. \begin{aligned} & (\mathbf{p} \cdot \nabla \gamma) \mathbf{p}, \\ & (\mathbf{p} \cdot \nabla \mathbf{k} \cdot \mathbf{c}) \mathbf{p}, \\ & (\mathbf{c} \cdot \nabla \mathbf{c} \cdot \mathbf{p}) \mathbf{p}, \\ & (\mathbf{k} \cdot \nabla \mathbf{c} \cdot \mathbf{p}) \mathbf{p}. \end{aligned} \right\} \quad (7.83)$$

Thus the first-order part of the elastic energy reads†

$$F_1 = D_1(\mathbf{c} \cdot \nabla \mathbf{c} \cdot \mathbf{p}) - D_2(\mathbf{p} \cdot \nabla \mathbf{k} \cdot \mathbf{c}) + D_3(\mathbf{k} \cdot \nabla \mathbf{c} \cdot \mathbf{p}) + D_4(\mathbf{p} \cdot \nabla \gamma). \quad (7.84)$$

In the incompressible limit, the D_4 term may be omitted. In terms of the Ω vector field

$$F_1 = D_1 \frac{\partial \Omega_z}{\partial x} + D_2 \frac{\partial \Omega_x}{\partial x} + D_3 \frac{\partial \Omega_z}{\partial z} + D_4 \frac{\partial \Omega_x}{\partial z}. \quad (7.85)$$

Equations (7.84) and (7.85) suggest complementary interpretations.

Let us consider first the D_1 term: it tends to bend the \mathbf{c} director (i.e. splay the electric polarization) as shown in Fig. 7.15. But in fact, in many practical situations, D_1 has no observable effect. Indeed

$$(\mathbf{c} \cdot \nabla \mathbf{c} \cdot \mathbf{p}) = -(\mathbf{c} \times \text{curl } \mathbf{c}) \cdot \mathbf{p} = (\text{curl } \mathbf{c}) \cdot (\mathbf{c} \times \mathbf{p}) = (\text{curl } \mathbf{c})_z.$$

(Remember from Chapter 3 that, since $\mathbf{c}^2 = 1$, $\mathbf{c} \times \text{curl } \mathbf{c} = -(\mathbf{c} \cdot \nabla) \mathbf{c}$.)

If \mathbf{c} is continuous (no singular lines), the volume integral of $\text{curl } \mathbf{c}$ may be transformed into a surface integral: thus the D_1 term does not contribute to the volume energy. If the molecules are strongly anchored at the limiting surfaces (non-degenerate case), the surface term D_1 is unobservable. The only possible effect of D_1 in such a case would be to generate a finite density of defects [51]. To discuss their stability, one would have to consider the electric terms linked to their charge (e.g. $\text{div } \mathbf{p} \neq 0$) together with their core energy.

† The minus sign in front of D_2 is used to keep up with the convention of the previous edition.

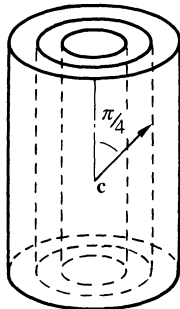


Fig. 7.16. Preferred angle of \mathbf{c} in a ‘jelly roll’ structure according to Dahl and Lagerwall [52]: S_C^* away from the centre.

The term D_2 tends to transform a flat layer into a twisted ribbon. This type of twist is entirely acceptable for a single layer. For a many-layer system, it is still locally acceptable, but it is not compatible with the rule of constant interlayer spacing for a macroscopic sample; thus in the absence of any defect it will also be unobservable (it could become significant in the presence of screw dislocation densities). An alternative interpretation has been put forward by Dahl and Lagerwall [52]. Consider a ‘jelly-roll’ of S_C^* (Fig. 7.16). Far from the centre distortions are small and linear terms are dominant. Depending on the sign of D_2 the \mathbf{c} will align at $\pm \pi/4$ of the cylinder axis.

The D_3 term leads to a strong and observable effect: it is indeed coupled to a simple twist of the \mathbf{c} director (Fig. 7.17)

$$q_0 = \frac{\partial \Omega_z}{\partial z} = -\frac{D_3}{B_3} \quad (7.86)$$

where B_3 is defined in (7.21). Thus the ground state of a S_C^* has a helielectric structure, which restores on a macroscopic scale the D_∞ symmetry of the S_A^* .

The D_4 term is again not compatible with the rule of a constant interlayer distance and requires the existence of a dislocation density. Needless to say, the quadratic part of the free energy is identical to that of the (non-chiral) S_C (eqns (7.21)–(7.23)).

7.2.3 Electric terms

Let us consider the perfectly insulating case. The electric energy contains two parts.

1. One due to the voltage imposed on the conductors surrounding the S_C^* ,

$$-\int \left(\mathbf{P}_0 \cdot \mathbf{E} + \sum_{\alpha=1}^{14} e_\alpha \mathbf{G}_\alpha \cdot \mathbf{E} + \frac{\mathbf{E} \cdot \boldsymbol{\epsilon} \cdot \mathbf{E}}{8\pi} \right) dv, \quad (7.87)$$

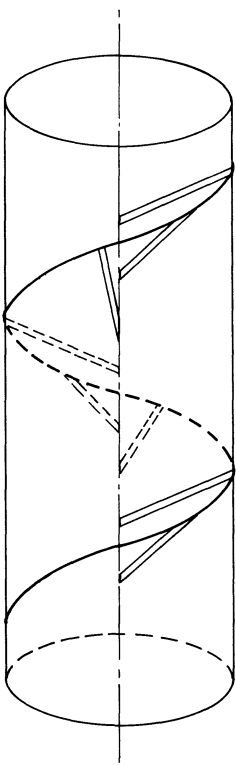


Fig. 7.17. Helical precession of the **c** director.

in which the integral extends over the whole system. \mathbf{P}_0 is the spontaneous polarization of the S_C^* ; as shown in Chapter 1 it is always directed along the normal to the tilt plane \mathbf{p} (as defined in Section 7.1.2)

$$\mathbf{P}_0 = P_0 \mathbf{p}.$$

\mathbf{G}_x are the 14 vector fields identified in the problem of Section 7.1.2.3, and e_x are the related flexocoefficients. Currently very little is known on the e_x ; one can expect values comparable to that of the nematic phase (i.e. a few 10^{-4} cgs units). P_0 has been extensively measured. On purely dimensional grounds

$$\begin{aligned} P_0 &= (\text{yield factor}) \times (\text{transverse molecular dipole}) \\ &\quad \times (\text{number of molecules per unit volume}). \end{aligned} \tag{7.88}$$

With a transverse dipole of the order of one debye per molecule,

$$\begin{aligned} P_0 &\simeq (\text{yield factor}) \cdot 10^{-18} \times 2 \times 10^{21} \\ &\simeq (\text{yield factor}) 2 \cdot 10^3 \text{ statcoulomb cm}^{-2}. \end{aligned}$$

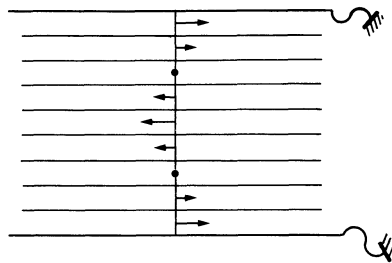


Fig. 7.18. S_C^* maintained between two grounded conducting plates, parallel to the layers. We assume ‘free boundary’ conditions in the example discussed in the text.

Experiments show that, depending on the compounds, the yield factor ranges from a few 10^{-3} to a few 10^{-1} . This is a direct measure of the molecular rotation around the long axis. Some of the S_C^* fit the picture of a phase that is almost locally uniaxial; some others are strongly biaxial. Obviously this latter case is favourable for getting a high spontaneous polarization.[†]

2. A second part corresponding to the Coulomb interaction between the polarization charges

$$\frac{1}{2} \int \int dv dv' \frac{\nabla \cdot (\mathbf{P}_0 + \sum_{\alpha=1}^{14} e_\alpha G_\alpha) \nabla \cdot (\mathbf{P}_0 + \sum_{\beta=1}^{14} e_\beta G_\beta)}{\epsilon |\mathbf{r} - \mathbf{r}'|}. \quad (7.89)$$

ϵ is an average of the permittivity coefficients in an ‘isotropic’ approximation. Due to charge screening, this contribution to the electric potential is often neglected. We will discuss in Section 7.2.5 an example in which its existence has been demonstrated [24].

Do the electric terms modify the pitch of the structure? In the absence of external charges, or with conductors maintained at zero potential, the answer is no. Let us illustrate this result using the simple geometry of Fig. 7.18. Suppose we maintain the two conducting plates grounded. The invariance of the fields along x and y , the conditions $\nabla \cdot \mathbf{D} = 0$ and $\text{curl } \mathbf{E} = 0$ together with the absence of charges on the conductors, yield

$$D_z = 0, \quad \mathbf{E} = 0; \quad \text{hence } \frac{\partial \Omega_z}{\partial z} = -D_3/B_3 \quad (7.90)$$

as in the absence of electric terms, which proves our statement. Furthermore $\mathbf{p} = 4\pi(\partial F/\partial E)$ in which F is the sum of eqns (7.21)–(7.23), (7.85), and (7.87)

[†] Values as high as $1000 \text{ statcoulomb cm}^{-2}$ have been reported [53]. (Note that data are usually given in $\text{nanocoulomb cm}^{-2} = 3 \text{ statcoulomb cm}^{-2}$.)

gives

$$\left. \begin{aligned} D_{\mathbf{p}} &= 4\pi \left(P_0 + e_{14} \frac{\partial \Omega_z}{\partial z} \right) = 4\pi P, \\ P &= (P_0 - e_{14} D_3 / B_3). \end{aligned} \right\} \quad (7.91)$$

$D_{\mathbf{p}}$ is the displacement field in the \mathbf{p} direction: it defines a total polarization \mathbf{P} , which precesses in a helicoidal fashion like \mathbf{P}_0 . Note that the total polarization involves the ‘spontaneous’ part \mathbf{P}_0 which exists in an unwound system, and a flexoelectric one due to the helicoidal precession in the ground state [48, 54]. Note also that in this geometry there is no charge–charge interaction: expression (7.89) is identically zero.

Remark One often finds in the literature formulae showing the influence of the flexoelectric coupling on the elastic modulus B_3 and on the spontaneous twist q_0 [55–57], although we do not find any here. There is no contradiction with the considerations developed above. Suppose we consider for the sake of simplicity polarizations and fields along the \mathbf{p} direction and constant precessions $\partial \Omega_z / \partial z$. Further suppose that we write the energy as a function of the deformations as in eqns (7.21)–(7.23), now not only taken at a constant temperature and pressure, but also at constant polarization (index the corresponding elastic constant with a subscript 0: D_{i0} , B_{i0}). The polarization-dependent part of the energy must then be explicitly added

$$F_{\mathbf{p}} = \int_v \left(\frac{P^2}{2\chi} - PE - \frac{e_{14}}{\chi} P \frac{\partial \Omega_z}{\partial z} - \frac{P_0 P}{\chi} \right) dv. \quad (7.92)$$

Expression (7.92) is allowed by symmetry and the notations are justified *a posteriori*. Indeed, the minimization with respect to P yields

$$P = \chi E + e_{14} \frac{\partial \Omega_z}{\partial z} + P_0, \quad (7.93)$$

which is identical to (7.91) in presence of a non-zero E field. Substitution in (7.92) gives

$$F_{\mathbf{p}} = -\frac{\chi E^2}{2} - \frac{e_{14}^2}{2\chi} \left(\frac{\partial \Omega_z}{\partial z} \right)^2 - \frac{P_0^2}{2\chi} - P_{14} E \frac{\partial \Omega_z}{\partial z} - P_0 E - \frac{P_0 e_{14}}{\chi} \frac{\partial \Omega_z}{\partial z}. \quad (7.94)$$

The fourth and fifth terms can be straightforwardly identified with their counterparts in (7.87): e_{14} is the fourteenth flexocoefficient and P_0 the spontaneous polarization. The first term is equivalent to $-(E^2 \epsilon_{pp} / 8\pi)$ provided the field vacuum energy is taken care of ($\chi = (\epsilon_{pp} - 1)/4\pi$ is the electric susceptibility). The second and last terms lead to a correction of B_3

and D_3

$$\left. \begin{aligned} B_3 &= B_{30} - \frac{e_{14}^2}{\chi}, \\ D_3 &= D_{30} - e_{11}P_0/\chi, \\ q_0 &= \frac{D_3}{B_3} = -\frac{D_{30} - e_{14}P_0/\chi}{B_{30} - e_{14}^2P_0/\chi}. \end{aligned} \right\} \quad (7.95)$$

Equations (7.95) relate the elastic moduli defined at constant temperature, pressure, and field to the same moduli defined at constant temperature, pressure, and polarization (all other thermodynamic variables being allowed to relax to their equilibrium value).

In this type of presentation one does find that flexoelectricity influences the spontaneous torsion of the structure and the corresponding elastic moduli but this is implicit in (7.90)

7.2.3.1 Uniaxial picture

It is interesting to illustrate in the ‘uniaxial approximation’ the origin of the flexoelectric term. In Chapter 3 we have mentioned that a pure twist is not coupled to flexoelectricity; if so, how can the pure twist of \mathbf{c} give rise to a flexoelectric polarization? The answer is that a pure twist of \mathbf{c} involves a bend of \mathbf{n} (Fig. 7.19). Indeed, according to (7.24),

$$\operatorname{div} \mathbf{n} = 0,$$

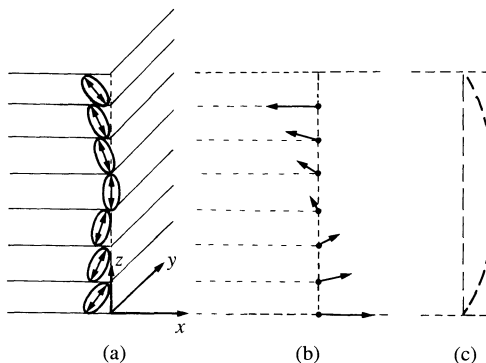


Fig. 7.19. Helicoidal precession of the S_c^* in the tilted uniaxial approximation. (a) The director \mathbf{n} ; (b) its projection in the x, y -plane: the characteristic twist of the structure is clear in this representation; (c) its projection in the x, z -plane: now the bend reveals itself clearly.

but

$$(\mathbf{n} \times \text{curl } \mathbf{n}) = \frac{1}{2} \left(\frac{\partial \Omega_z}{\partial z} \right) \sin(2\theta) \mathbf{p}. \quad (7.96)$$

The helical structure of the S_C^* involves a bend everywhere collinear with the spontaneous polarization. Hence, even in the ‘nematic’ picture, there is a contribution to the total polarization (using the notation of (3.68)),

$$\mathbf{P}_d = -\frac{1}{2} e_3 \frac{D_3}{B_3} \sin(2\theta) \mathbf{p} \quad (7.97)$$

with $e_3 \simeq 6 \cdot 10^{-4}$ cgs; $\partial \Omega_z / \partial z \simeq 4 \cdot 10^4 \text{ cm}^{-1}$; $\sin 2\theta \simeq \frac{1}{2}$ one gets $P_d \simeq 6 \text{ statcoulomb cm}^{-2}$.

P_0 measurements currently range from a few tens of statcoulomb cm^{-2} to 10^3 ! Thus in some cases the flexoelectric contribution may be entirely neglected; in others one should be more careful. Note that in the case of high polarization the ‘uniaxial picture’ is irrelevant and so is our estimate of P_d .

It is instructive to pursue this approximation further: (7.96) shows that a spontaneous bend is compatible with the symmetry of the structure. Thus the Oseen–Frank energy must be modified to include both a spontaneous twist and bend [48, 52],

$$F = \int \frac{1}{2} \{ K_1 (\nabla \cdot \mathbf{n})^2 + K_2 (\mathbf{n} \cdot \text{curl } \mathbf{n} + q_0)^2 + K_3 (\mathbf{n} \cdot \nabla \mathbf{n} + \mathbf{v}_0)^2 \} \, dv \quad (7.98)$$

in which q_0 has the same meaning as in (6.43), and $\mathbf{v}_0 = b_0 \mathbf{k} \times \mathbf{n}$ is the spontaneous bend. Making use of (7.24) and identifying (7.84) with (7.98) we get

$$D_3 = -(K_2 q_0 + K_3 b_0 \cos \theta) \sin^2 \theta. \quad (7.99)$$

Thus both the spontaneous twist and spontaneous bend of the nematic director \mathbf{n} , contribute to the helicity of the structure. For a suitable combination of spontaneous twist and bend, D_3 can be set to zero. The resulting structure may be totally unwound,† although truly ferroelectric ($P_0 \neq 0$). One such case has been observed, with a molecule in which two conflicting chiral centres interfere [58].

This illustrates clearly that P_0 and $\partial \Omega_z / \partial z = -(D_3/B_3)$ are two independent quantities, which can be manipulated at will in suitable mixtures. (For reasons that will become clear in Section 7.2.6 it is technologically important to reduce $\partial \Omega_z / \partial z$ as much as possible, while increasing P_0 .)

† This cancellation may occur accidentally at one point of a (P, T) diagram for a pure compound.

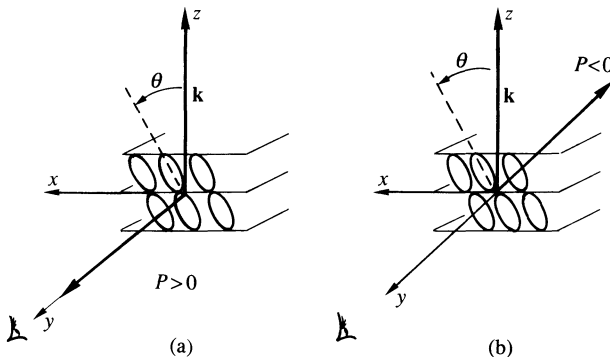


Fig. 7.20. Sign convention for \mathbf{p} : the observer looks in a direction parallel to the layers (y) such that a counterclockwise rotation of \mathbf{k} of amplitude θ around $\hat{\mathbf{y}}$ brings \mathbf{k} in the tilt direction. (a) $P > 0$, the polarization points towards the observer; (b) $P < 0$ the polarization points away from the observer. (Note that the definition is invariant in the change $\mathbf{k} \rightarrow -\mathbf{k}$ as it should be.)

7.2.3.2 Sign convention for P_0

A correct definition of a S_C^* system should give not only the handedness of the helicoidal precession, but also, independently, the sign of the spontaneous polarization [52]. \mathbf{P}_0 is said to be positive (respectively negative) if it points in the same (respectively opposite) direction as \mathbf{p} . One can determine the polarization sign operationally. Look at a S_C^* sample from a direction perpendicular to the normal to the layers, \mathbf{k} , such that the tilt direction[†] can be deduced from \mathbf{k} by a counterclockwise rotation around the observation axis (as seen by the observer). If \mathbf{P}_0 points towards the observer, it is said to be positive, if \mathbf{P}_0 points away from the observer, it is negative (Fig. 7.20).

7.2.4 Unwinding of the helix by an electric field

Consider the geometry of Fig. 7.21, i.e. a smectic C* sample sandwiched between conducting plates, the layer being anchored normally to the plates. Assume for the sake of simplicity that there is no easy axis for the polarization of the solid–liquid crystal interface,[‡] so that the helix can develop without defect in the sample. In the absence of any applied field the equilibrium

[†] As already pointed out, the ‘tilt direction’ of a S_C or S_C^* is ill defined. A better definition would involve the principal direction corresponding to the largest eigenvalue of the dielectric tensor (at a well defined optical frequency). Furthermore, the rotation must be restricted to angles smaller than $\pi/2$ for the specification to be complete.

[‡] In fact, such boundary conditions are never satisfied and ‘dechiralization lines’ are always observed close to the walls [59] (Fig. 7.25(a)). For thicknesses large compared to the helix pitch, the considerations developed above are relevant [60].

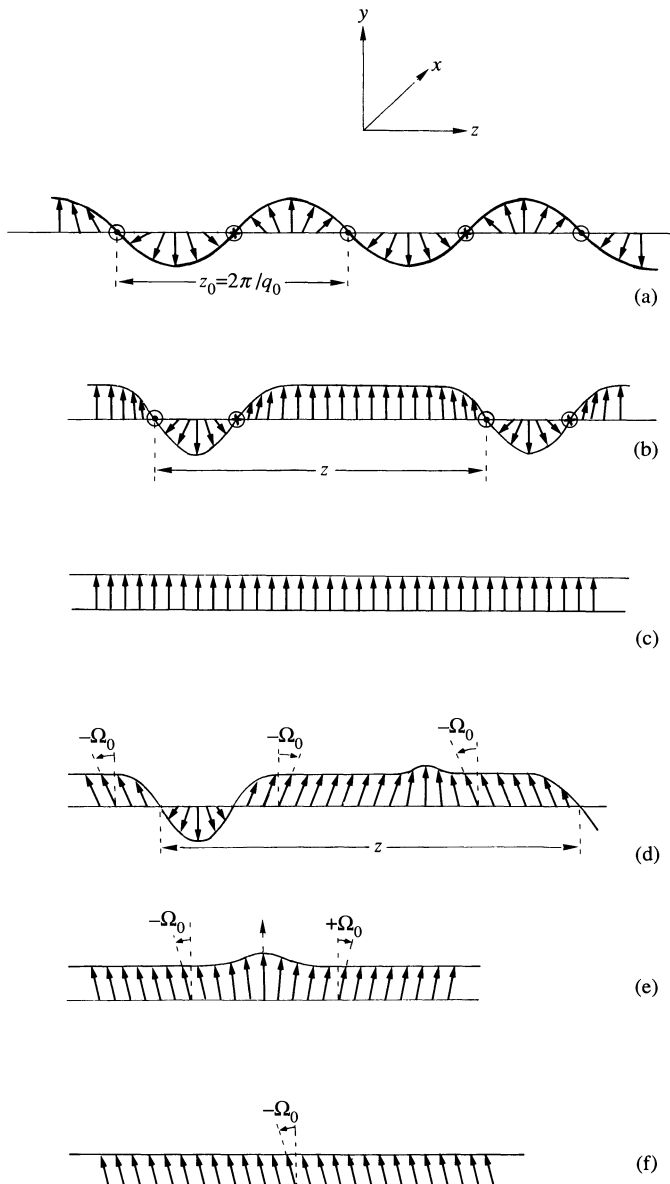


Fig. 7.21. Unwinding of a S^* by an ‘in-plane’ electric field (the arrows represent the permanent polarization. The field is applied in the positive y direction). (a) Structure in zero field: period z_0 . (b) Distorted structure: $E_y < E_c < E_0$. Note the existence of 2π walls. The structure is periodic. (c) Unwound structure $E_c < E_y < E_0$. (d) Distorted structure $E_0 < E_y < E_c$. Note the existence of two unequivalent types of walls (called W_1 and W_2 in the text). The structure is periodic. (e) ‘One-wall’ state $E_0 < E_c < E_y < E_1$. (f) Unwound state $E_1 < E_y$.

structure is obviously obtained for $\partial\Omega_z/\partial z = q_0$ (Fig. 7.21(a)). (\hat{z} is the normal to the layers, \hat{y} the normal to the conducting plates, \hat{x} parallel to the plates as shown in Fig. 7.21.) The behaviour of the S_c^* under an applied E field, is fairly similar to that of a cholesteric in a magnetic field (Section 6.2.2.3). Upon increasing the intensity of E , one observes the formation of walls, which move further and further apart (this increases the pitch just as described in Section 6.2.2.3) until they disappear at infinity when the critical field E_c is reached. If $\epsilon_{cc} - \epsilon_{pp} + \epsilon_{zc}^2/\epsilon_{zz} < 0$, the main difference from the case of cholesterics lies in the fact that the walls are not 180° walls but 360° ones:[†] this is a direct consequence of the S_c^* polarity (the up regions of Fig. 21(b), (d) increase in size until 360° walls are built). The case $\epsilon_{cc} - \epsilon_{pp} + \epsilon_{zc}^2/\epsilon_{zz} > 0$ is more complex; the existence of the two equally stable homogeneous states (corresponding to $\Omega_z \pm \Omega_0(E)$) beyond a field value E_0 , increases the number of possibilities.

- If $E_c < E_0$, the unwinding steps are basically identical to the one described above. However, when the field is further increased beyond E_0 , a deformed state in which Ω_z goes from $+\Omega_0$ to $-\Omega_0$ (or vice versa, respecting the natural chirality of the spontaneous helix, and keeping the total rotation smaller than 180°) is most stable. Eventually, if the field is further increased, a third critical value E_1 is reached beyond which the state is again homogeneous.
- If $E_c > E_0$, the unwinding is not complete and leaves a single wall ($\Omega_0 \rightarrow -\Omega_0$ as described above) until the field exceeds the value E_1 . The possibility of controlling a single wall is very attractive [61], but no experiment has confirmed it to date.

The different critical fields can be calculated in pretty much the same way as for cholesterics [48, 61, 62]. We will not go into details, but rather discuss the starting energy and the main features of the results.

The flexoelectric contribution being very small, the only important terms are the ‘ferroelectric’ and dielectric ones. Their angular-dependent part can be cast in the simple form

$$F(E_y) - F(E_y = 0)$$

$$= \int \left\{ \frac{B_3}{2} \left(\frac{d\Omega_z}{dz} - q_0 \right)^2 + \frac{\tilde{\epsilon}^a}{8\pi} \cos^2 \Omega_z E_y^2 - P_0 E_y \cos \Omega_z \right\} dz \quad (7.100)$$

in which $\tilde{\epsilon}^a = \epsilon_{cc} - \epsilon_{pp} + (\epsilon_{zc}^2/\epsilon_{zz})$ with the corresponding Euler–Lagrange equation

$$\frac{d^2\Omega_z}{dz^2} = -\frac{\tilde{\epsilon}^a E_y^2}{4\pi B_3} \cos \Omega_z \sin \Omega_z + \frac{P_0 E_y}{B_3} \sin \Omega_z. \quad (7.101)$$

[†] ϵ_{zc} refers to the off-diagonal component of the dielectric permittivity between directions z and c , ϵ_{cc} , ϵ_{pp} , ϵ_{zz} refer, respectively, to the diagonal components in the c , p , z directions.

Equations such as (7.101) are known as the ‘double’ Sine Gordon equation. If either $\tilde{\epsilon}^a = 0$ or $P_0 = 0$, one recovers the simple Sine Gordon case which describes the cholesteric–nematic transition.

The first integral is again easily found by multiplying (7.101) by $d\Omega_z/dz$ to give

$$\frac{1}{2} \left(\frac{d\Omega_z}{dz} \right)^2 = \frac{\tilde{\epsilon}^a E_y^2}{8\pi B_3} \cos^2 \Omega_z - \frac{P_0 E_y}{B_3} \cos \Omega_z + \text{const.} \quad (7.102)$$

The constant is determined by the minimum energy condition. Inversion of (7.102) gives the function $\Omega_z(z)$, which is periodic, the period diverging at a critical field E_c . Typical structures are illustrated in Fig. 7.21 in the cases $\tilde{\epsilon}^a > 0$ ($E > E_0$ in Fig. 7.21(d), (e)). The critical field can be analytically calculated using the same procedure as in Section 6.2.2.3. It is instructive to consider the unwound state first: if we call Ω_0 the azimuthal angle, we get

$$F(E_y) - F(E_y = 0) = \int \left(\frac{B_3}{2} q_0^2 + \frac{\epsilon_\perp^a}{8\pi} \cos^2 \Omega_0 E_y^2 - P_0 E_y \cos \Omega_0 \right) dz. \quad (7.103)$$

If $\tilde{\epsilon}^a < 0$ the minimum energy is obviously reached for $\Omega_0 = 0$.

If $\tilde{\epsilon}^a > 0$ and $E_c < E_y < 4\pi P_0/\epsilon_\perp^a = E_0$, again the minimum energy corresponds to $\Omega_0 = 0$.

If $\tilde{\epsilon}^a > 0$ and $E_0 = 4\pi P_0/\epsilon_\perp^a < E_c < E_y$, the minimum energy is obtained for

$$\cos \Omega_0 = 4\pi P_0/\epsilon_\perp^a E_y, \quad (7.104)$$

i.e. two equivalent angles $\pm \Omega_0$.

The difference $\delta F(E)$ between the energy of a one 2π -turn state and the totally unwound one is easily written in a form similar to (6.50), which allows us to write implicit expressions for E_c [61, 62].

Note that, if $E_c > E_0$, the 2π turn is composed of two walls: $W_1(-\Omega_0 \rightarrow +\Omega_0)$ followed by $W_2(+\Omega_0 \rightarrow 2\pi - \Omega_0)$ (Fig. 7.21(d)); the rotation sense has to be taken with the correct chirality). $\delta F(E_c) = 0$ can equivalently be written (with obvious notation)

$$\delta F(W_1) + \delta F(W_2) = 0. \quad (7.105)$$

Since the sum is zero, one of the two energies has to be negative. A detailed calculation shows $\delta F(W_1) < 0$. Hence, immediately above E_c , the ground state is not homogeneous but involves a single W_1 wall (Fig. 7.21(e)).† \mathbf{E}_1 is defined as the field at which $F(W_1) = 0$ [61]. In most practical situations the permanent polarization provides the leading term; the final state is

† Under such circumstances one can wonder if the calculation of E_c still has a meaning. The answer is yes: no matter how small the difference $E - E_c < 0$, the structure is periodic and, in an infinite sample, the twisted structure is favoured as compared to the single W_1 wall. The situation is, of course, more subtle in a finite size sample.

homogeneous with \mathbf{p} parallel to \mathbf{E} [48]. A good approximation for E_c is given by reference 62 as

$$E_c = \frac{\pi^2}{16} \frac{B_3 a_0^2}{P_0} \left(1 + \frac{\pi}{192} \frac{B_3 q_0^2 \tilde{\epsilon}^a}{P_0^2} \right). \quad (7.106)$$

With $P_0 \sim 1$ to 10^3 statcoulomb cm $^{-2}$, $q_0 \sim 10^4$ cm $^{-1}$, $B_3 \sim 10^{-7}$ dyn, and $\tilde{\epsilon}^a \simeq 1$ to 10 one gets $E_c \simeq 5 \cdot 10^{-3}$ to 5 statvolt cm $^{-1}$ (i.e. 1.5 to $1.5 \cdot 10^3$ V cm $^{-1}$), and the correction due to the dielectric coupling reaches at most a few per cent. Thus, under current practical situations, the simplest cholesteric analogy provides a satisfactory description.

Last but not least, S_C^* liquid crystals always contain conductive impurities: imposing a non-zero E_y requires that a current be maintained that cannot be homogeneous. Current gradients may react on the polarization orientation [63] and the whole problem is different from the one discussed here. The solution to this new problem requires the use of hydrodynamical equations.

7.2.5 Fluctuations

The characteristics of S_C^* fluctuations are best evidenced in the thin-film experiments similar to that described in Section 7.1.5 (25). The geometry is still that of Fig. 7.13, a weak electric field parallel to the film allows us to easily obtain a homogeneous orientation of \mathbf{p} (hence \mathbf{e}) throughout the sample.[†] The relevant free energy per cm 2 is obtained by adding to (7.78) electric terms characteristic of S_C^* (omitting contour integrals)

$$\begin{aligned} F = & \int dx dy \left[\frac{B_1^*}{2} \left(\frac{\partial \Omega_z}{\partial x} \right)^2 + \frac{B_2^*}{2} \left(\frac{\partial \Omega_z}{\partial y} \right)^2 - \mathbf{P}^* \cdot \mathbf{E} \right] \\ & + \int dx dy dx' dy' \frac{\nabla \cdot \mathbf{P}^*(\mathbf{r}) \nabla \cdot \mathbf{P}^*(\mathbf{r}')}{2|\mathbf{r} - \mathbf{r}'|}. \end{aligned} \quad (7.107)$$

($P^* \simeq P_0$; note that the charge–charge interaction occurs in three dimensions, which justifies the use of $1/|\mathbf{r} - \mathbf{r}'|$ rather than $\ln|\mathbf{r} - \mathbf{r}'|$ which would be relevant if the field created by the charges was confined to a plane.)

In the limit of small fluctuations (\mathbf{E} field along the y direction),

$$\left. \begin{aligned} -\mathbf{P}^* \cdot \mathbf{E} &\simeq \frac{1}{2} P_0^* E \Omega_z^2 - P_0^* E, \\ \nabla \cdot \mathbf{P}(\mathbf{r}) &\simeq P_0^* \nabla_x \Omega_z. \end{aligned} \right\} \quad (7.108)$$

[†] Note that the spontaneous helical precession of \mathbf{p} is entirely negligible in a film much thinner than the natural pitch.

Thus in Fourier space the energy reads

$$F = \sum_{q_x, q_y} \frac{1}{2}(B_1^* q_x^2 + B_2^* q_y^2 + P_0^* E + 2\pi P_0^{*2} q_x^2/q) |\Omega_z(q)|^2 \quad (7.109)$$

with $q = (q_x^2 + q_y^2)^{1/2}$. Equipartition yields

$$\langle \Omega_z(\mathbf{q}) \Omega_z(-\mathbf{q}) \rangle = \frac{k_B T}{B_1^* q_x^2 + B_2^* q_y^2 + P_0^* E + (2\pi P_0^{*2} q_x^2/q)}. \quad (7.110)$$

Depolarized Rayleigh scattering experiments for which the scattered intensity $I(\mathbf{q}) \propto \langle \Omega_z(\mathbf{q}) \Omega_z(-\mathbf{q}) \rangle$ confirm the existence of a term linear in $|q_x|$ for $q_y = 0$ [24] (Fig. 7.22). Equations (7.109) and (7.110) show clearly under what conditions charge-charge interactions are important.

- Splay deformations of \mathbf{p} (bend deformations of \mathbf{c}) are required (i.e. $q_x \neq 0$).
- Typical wavelengths must exceed a characteristic value: $\lambda_c^* = B_1^*/P_0^{*2} \simeq 10^{-2}$ cm. For a three-layer thick film as reported in reference 24, $B_1^* \simeq 2 \cdot 10^{-14}$ erg, $P_0^* \simeq 3 \cdot 10^{-6}$ statcoulomb).

Note that, in three dimensions, if one neglects layer spacing fluctuations and considers the case $q_0 = 0$, (7.109) is replaced by (F is now an energy per cm^3)

$$F = \sum_q \frac{1}{2} \left(B_1 q_x^2 + B_2 q_y^2 + B_3 q_z^2 + P_0 E + 4\pi\alpha P_0^2 \frac{q_x^2}{q^2} \right) |\Omega_z(q)|^2 \quad (7.111)$$

where the coefficient α is a function of the dielectric permittivities of order unity. The observation of charge-charge interactions requires the same geometric features, but the characteristic length is now

$$\lambda_c = (2\pi B_1)^{1/2}/P_0.$$

For $B_1 \simeq 10^{-7}$ dyn, $P_0 \simeq 3$ statcoulomb cm^{-2} and

$$\lambda_c \simeq 2 \cdot 10^{-4} \text{ cm}.$$

For $B_1 \simeq 10^{-7}$ dyn, $P_0 \simeq 1000$ statcoulomb cm^{-2} and

$$\lambda_c \simeq 10^{-6} \text{ cm!}$$

Thus, in most experiments involving a splay of the polarization, the charge terms dominate over standard elasticity: this is true only to the extent that ionic impurities do not screen these interactions out. Nowadays many compounds are pure and stable enough that screening cannot be complete.

7.2.6 Surface anchoring

Consider a smectic A at a vapour-liquid crystal (or glass-liquid crystal) interface. In the simplest approximation the anisotropic part of the interfacial

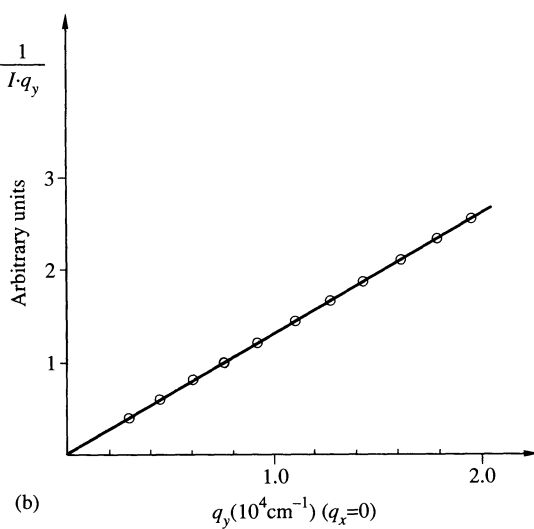
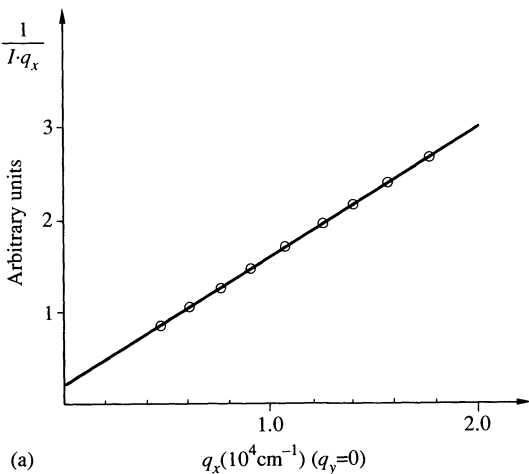


Fig. 7.22. Dependence of $(I \cdot q)^{-1}$ (I = intensity of the depolarized scattered light) for a three-layer thick film of octyloxybenzylidene-*B*-methyl-butyl aniline, according to the Harvard group [24]. (a) Mode involving charge-charge interactions (bend of **c**, i.e. $q_y = 0$, $q_x \neq 0$); note the non-zero intercept of the straight line $(Iq_x)^{-1} = f(q_x)$ with the ordinate axis: this is a measure of B_1^*/P_0^{*2} . (b) Pure nematic-like mode (splay of **c**, i.e. $q_y \neq 0$, $q_x = 0$): now the straight line $(Iq_y)^{-1} = f(q_y)$ goes through the origin, which proves the absence of electrostatic terms.

energy can be written

$$W_s = \frac{W}{2} (\mathbf{k} \cdot \mathbf{S})^2 \quad (7.112)$$

(\mathbf{k} and \mathbf{S} , layers and interface normals; remember that $+\mathbf{k}$ and $-\mathbf{k}$ are physically equivalent). Depending on the sign of W , the preferred orientation will be either with the layers parallel to the interface ($W < 0$) or perpendicular to it ($W > 0$). At this (oversimplified) level of approximation, there are only two possibilities.

Let us now write the equivalent of (7.112) for a ferroelectric liquid crystal. The orientational state of a S_C^* is specified by two fields; let us choose \mathbf{k} and \mathbf{p} . Since the polarization direction is a true vector (not a director), its scalar product with the surface vector can enter the expression of the surface energy. Thus, the simplest relevant expansion of W_s can be written

$$W_s = W_1 \mathbf{p} \cdot \mathbf{s} + \frac{W_2}{2} (\mathbf{p} \cdot \mathbf{s})^2 + \frac{W_3}{2} (\mathbf{k} \cdot \mathbf{s})^2. \quad (7.113)$$

W_2 and W_3 should have approximately the same order of magnitude as in the case of nematics (from a few erg cm^{-2} down to a few $10^{-2} \text{ erg cm}^{-2}$); as a rough rule of thumb one can consider that W_1 should be smaller by a factor similar to the yield factor introduced in (7.2.3) (i.e. a few 10^{-3}).

Minimization of (7.113) defines the optimum directions of \mathbf{k} and \mathbf{p} at the interfaces. No fewer than six different extremal states can be determined, some of them being simultaneously stable. This shows the complexity, but also the richness of interfaces involving S_C^* . There is no real point in going into details because, in fact, the problem is even more complex.

- The interface history seems to be important which suggests that thermodynamic equilibrium may not be locally reached.
- The interface structure is generally different from the bulk (e.g. crystalline layer) and necessitates a finite tilt for matching layer thickness [64] (Fig. 7.23).
- The analyticity of (7.113) is not guaranteed when \mathbf{k} is nearly parallel to \mathbf{S} .†

This last point is illustrated in Fig. 7.24. For a small tilt angle α of the layers with respect to the surface plane, a term linked to the dislocation density must replace (7.103)

$$\delta W_s = \frac{W_d}{b} |\alpha|. \quad (7.114)$$

W_d is the dislocation line energy, $b/|\alpha|$ the distance between dislocations. Such

† It is guaranteed for temperatures larger than the roughening transition of the interface.

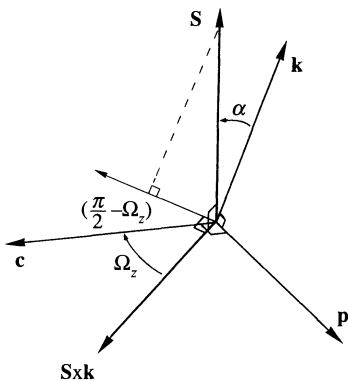


Fig. 7.23. Definition of the notation used in the text: \mathbf{S} , \mathbf{k} are respectively the surface and layer normal, \mathbf{c} and \mathbf{p} the tilt and polarization direction.

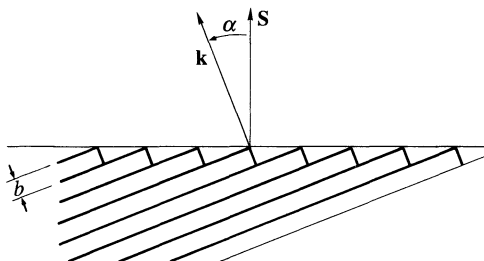


Fig. 7.24. Tilting the layers with respect to the surface requires the introduction of an array of edge dislocations (i.e. layer ending: see next chapter).

an expression is not included in (7.113). It stabilizes layers parallel to the interface.[†]

Note at last that (7.113) ignores gradient terms: those that are potentially the most important are those involving gradients parallel to the surface. Non-homogeneous states could be stable, as already quoted in the case of S_C with layers parallel to the surface (remember the interpretation of the striped domains of a S_C at a ‘free’ surface [14]).

7.2.7 Particular geometries

7.2.7.1 Slab with planes parallel to the boundaries: selective reflection of light
The simplest geometry *a priori* is that corresponding to an infinite slab bounded by two parallel interfaces (i.e. layers parallel to the interface). Under

[†] In systems which are S_C^* at temperatures above the roughening transition (7.113) is valid even for α small, and a stability analysis of (7.113), suggests that layers cannot run parallel to the interface.

favourable conditions the strips of reference 14 can be avoided and the single crystal of S_C^* grown (Fig. 7.18).† This geometry is interesting for many fundamental experiments such as the selective reflection of light of the 'cholesteric type' (as discussed in Section 6.1.4) [65, 66]. The easiest way of understanding the similarities and differences with the case of cholesterics is to come back to eqn (6.5) of Chapter 6 (or (3.81) of Chapter 3). Remember: if α represents the scattered amplitude and \mathbf{f} and \mathbf{i} the polarizations of the scattered wave of wavevector \mathbf{k}_1 and of the incident wave of wavevector \mathbf{k}_0 , respectively ($q = \mathbf{k}_0 - \mathbf{k}_1$),

$$\alpha = \mathbf{f} \cdot \boldsymbol{\epsilon}(q) \cdot \mathbf{i} \quad (7.115)$$

where $\boldsymbol{\epsilon}(q)$ is the Fourier transform of the dielectric tensor at the considered optical frequency.

Although slightly more complex, the expression of the dielectric tensor is very reminiscent of the cholesteric one

$$\boldsymbol{\epsilon}_{\alpha\beta}(\mathbf{r}) = \epsilon_{\alpha\beta}^0(\mathbf{r}) + \epsilon_{\alpha\beta}^1(\mathbf{r}). \quad (7.116)$$

$\epsilon_{\alpha\beta}^0$ has a structure similar to that of cholesterics (with α, β restricted to the **c**, **p**-plane)

$$\epsilon_{\alpha\beta}^0(\mathbf{r}) = \epsilon_{pp} \delta_{\alpha\beta} + (\epsilon_{cc} - \epsilon_{pp}) C_\alpha(\mathbf{r}) C_\beta(\mathbf{r}).$$

See the similarity with (6.6).

The second part of $\epsilon_{\alpha\beta}^1$ is connected to the tilt of the structure

$$\epsilon_{\alpha\beta}^1(\mathbf{r}) = \epsilon_{zz} \delta_{\alpha z} \delta_{\beta z} + \epsilon_{zc} (\delta_{\alpha z} c_\beta(\mathbf{r}) + \delta_{\beta z} c_\alpha(\mathbf{r})).$$

The \mathbf{r} -dependent part of $\boldsymbol{\epsilon}^0$ is bilinear in **c** and hence has a characteristic wavevector $\pm 2\mathbf{q}_0$ as in the cholesteric case. On the other hand, $\boldsymbol{\epsilon}^1(\mathbf{r})$ is linear in **c** and its characteristic wavevector is $\pm \mathbf{q}_0$.

For an incident wave propagating along the helix axis (or equivalently the normal to the layer, \mathbf{k}) it is clear that both the incident and reflected polarizations are in the **c**, **p**-plane: the behaviour is identical to that of cholesterics, since $\epsilon_{\alpha\beta}^0$ only is operative [67].

For oblique incident waves the genuine periodicity of S_C^* shows up through $\epsilon_{\alpha\beta}^1$ and Bragg reflection at the wavevectors $\pm \mathbf{q}_0$ is obtained (added to the 'more classic' one at $\pm 2\mathbf{q}_0$). More details may be found in reference 68.

7.2.7.2 Non-linear optics

All the optical properties discussed up to now were based on a linear relation between the displacement and the electric fields

$$D_\alpha = \epsilon_{\alpha\beta} E_\beta. \quad (7.117)$$

† In fact Ω_z is usually specified at the interface, for instance by gentle rubbing, but, if the thickness is large compared to the pitch, the complications due to these 'rigid' boundary conditions are negligible.

This linearity holds as long as the external electric field is small compared to the molecular one. However, if one uses pulsed lasers, one can get transient values which become non-negligible, and (7.117) must be expanded (we drop all indices for simplicity), such that

$$D = \varepsilon E + \chi_2 E^2 + \chi_3 E^3.$$

The cubic term corresponds to phenomena such as electrostriction and exists in all systems. When non-zero, the quadratic term leads to second harmonic generation. Indeed the term E^2 radiates power at the frequency 2ω , if the incident wave is at ω . In the presence of inversion symmetry, χ_2 is identically zero. On the other hand, the S_C^* have just the right symmetry for having $\chi_2 \neq 0$.

In fact, there is a second condition for getting appreciable second harmonic generation, called phase matching. Because of dispersion the harmonic wave does not travel at the same speed as the fundamental: as a result, in most situations, destructive interference decreases drastically the emitted harmonic. The condition for getting the same velocity is simply

$$k(2\omega) = 2k(\omega) \quad (7.118)$$

in which $k(\omega)$ (respectively $k(2\omega)$) are magnitudes of the wavevectors at the pulsation ω (respectively, 2ω). For waves with the same polarization this relation is never satisfied. The usual trick is to play with anisotropy and mode polarization to cancel the mismatch. With S_C^* the period of the helix allows another kind of phase matching. Equation (7.118) can be replaced by

$$k(2\omega) = 2k(\omega) - q_0 \cos \delta$$

in which $\cos \delta$ is the angle between $\mathbf{k}(\omega)$ and the helix axis. Experimentally observed, the second harmonic generation is small [69]. This situation may change with the recent discovery of high polarization materials.

Last but not least, the conoscopic observation in this geometry confirms our remark according to which the D_∞ symmetry is restored on a macroscopic scale: one obtains a beautiful Maltese cross similar to that obtained with a smectic A* (the only difference comes in the magnitude of the rotatory power observable at the centre of the cross) [70]. Application of an electric field in the layers plane tilts the conoscopic figure linearly in a direction perpendicular to the field: this was one of the early signatures of ferroelectricity [48, 70].

7.2.7.3 Slab with planes perpendicular to the boundaries; surface stabilized ferroelectric states

Suppose one starts from a smectic A* slab in the planar geometry, and more precisely in a ‘planar degenerate’ case. This means that the normal to the layers is everywhere parallel to the interface, but that no energy direction is specified. We can now impose a unique direction to the layers by either

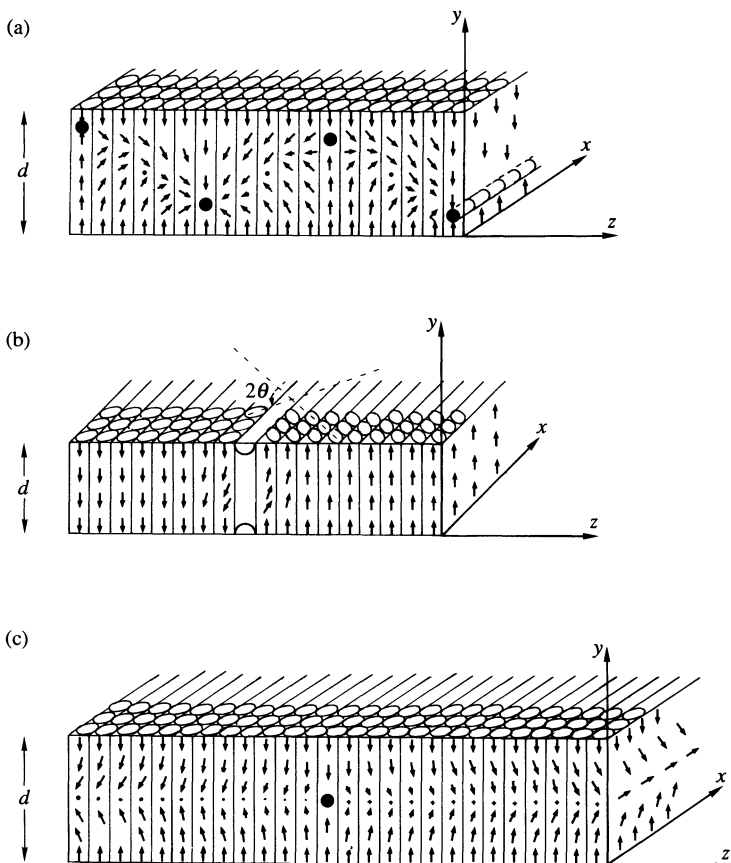


Fig. 7.25. Example of structures obtained between flat surfaces with ‘planar degenerate’ boundary conditions (the arrow represents the polarization, the ellipses the molecules). (a) Twisted state: the heavy dots represent 2π disclination lines (they run parallel to the x -axis). Note the ‘pure’ twist along z in the $y = d/2$ plane. The distance between two adjacent lines on the same side is close to $(q_0/2\pi)^{-1}$. (b) Two homogeneous domains separated by a π inversion wall [71]. In the hatched area the exact nature of the deformation is not known. Note the rotation 2θ of the molecular axis between the two domains, and the sign change of the polarization. (c) Splayed state: the existence of the splay is most obvious in the x , y -plane. Here again, there are two domains separated by a -2π disclination: they differ in the sign of the polarization in the $y = d/2$ plane ($-\hat{x}$ on the left of the figure; $+\hat{x}$ on the right).

gently shearing the sample (in the x , y -plane of Fig. 7.25; as a result \mathbf{k} is confined to the z direction), or by the action of an external magnetic field (provided $\chi_a > 0$). Slowly cooling the system into the S_C^* , one gets in the ideal case a state in which the orientation of the layers is preserved. At the

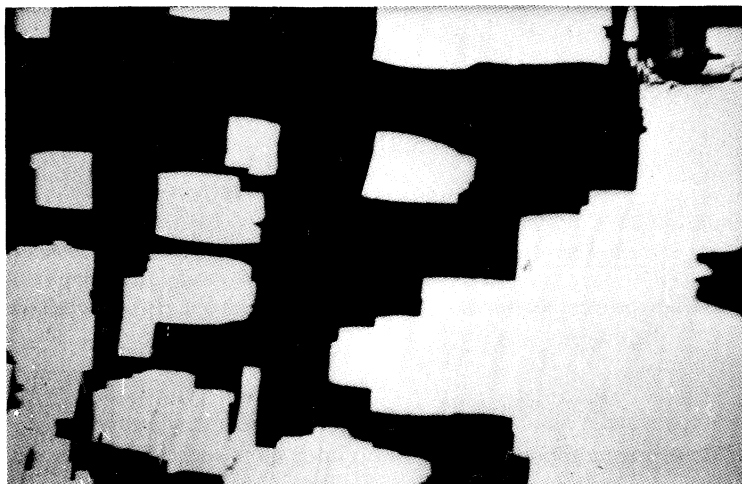


Fig. 7.26. First reported picture of the ferroelectric surface-stabilized state. (Courtesy S. Lagerwall.) The dark domains correspond to a molecular direction parallel to the polarizer. Note the good contrast between the two states. The spontaneously appearing domains corresponds to a polarization pointing towards and away from the observer, respectively, and give the surface-stabilized state properties that are characteristic of conventional, solid state ferroelectrics. In particular, the memorized state can be reversed by an applied external field.

interfaces the molecules can adopt only two directions respecting both the tilt requirement and the parallelism to the walls. On the other hand, the bulk of the sample has a tendency to adopt the helix structure of Fig. 7.21(a). This is a conflicting situation since the bulk helicoidal precession cannot match the boundary conditions. Experiment reveals that, for slabs thick enough, most of the system is in its twisted state, and that boundary conditions are met via an array in disclinations called dechiralization lines [59] (Fig. 7.25(a)).

Let us now reduce the thickness d : when $d \leq P_0$, the helix is suppressed. There are two possible scenarios.

1. A homogeneous state is formed (Fig. 7.25(b)). Everywhere the polarization is perpendicular to the interfaces: now a macroscopic polarization develops. This 'clever' geometry was discovered by Clark and Lagerwall and called bookshelf geometry [71, 52]; its practical importance was immediately recognized. Indeed, the polarization can point either up or down (Figs 7.25(b) and 7.26) which corresponds to a rotation of the 'molecular axis' (in loose language) of 2θ (Fig. 7.26). A field can easily switch the polarization and hence promote the 2θ rotation which is well 'coupled' to polarized light.

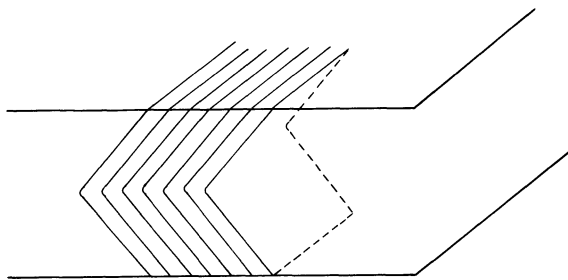


Fig. 7.27. Chevron texture obtained after cooling a smectic A in the bookshelf geometry.

2. A splayed state is reached first (Fig. 7.25(c)). The polarization points either outside or inside the liquid crystal on both interfaces. (In the case of thick samples, the polarization tends to point inside the liquid crystal which minimizes the surface electrostatic energy [60], but frequently both signs of splay are observed.)

By subsequent squeezing, one can obtain the uniform state. In fact quite often splayed and uniform states are simultaneously observed.

Remarks In a given sample, one can also find regions in which planes are tilted with respect to the interfaces [72]. These states seem to be simultaneously stable. This discussion is oversimplified in many ways. The most important shortcoming is that a pure bookshelf geometry is rarely achieved. Instead, the chevron texture of Fig. 7.27 is observed [72]. Experiment shows that the tilt of the layers results from a mismatch of the smectic periodicity in the bulk and at the surface. More precisely at the interface the periodicity a_s seems to be close to that of a smectic A, hence the layer tilt $\cos((\pi/2) - \alpha) \simeq a_s/a_0$ (a_0 periodicity of the bulk S_C). Often also the molecules are not exactly parallel to the interface.

Problem. Is there a simple way of understanding the helix unwinding?

Solution. Let us discuss in naïve terms the stability of the twisted state as compared to that of the homogeneous one. We assume that in both cases $\Omega_z = 0$ at the interfaces so that one does not have to worry about surface energies.

The increase of bulk energy (per unit surface of the slab) due to the helix unwinding is simply

$$F_h = \frac{B_3}{2} \int_0^d q_0^2 dy = \frac{B_3}{2} q_0^2 d. \quad (7.119)$$

On the other hand the energy (per unit surface) of the twisted state can be evaluated as the product of the line energy W of a disclination times the number n of

disclinations per unit length (in the z direction)

$$F_t = Wn.$$

The periodicity of the lines being close to that of the structure

$$n \simeq 2q_0/2\pi.$$

(NB. There are two arrays of lines.)

W is, in fact, very hard to calculate exactly: in principle it could depend on flexoelectric coefficients, charge density, Debye screening length, electric and elastic boundary conditions, elastic anisotropy, even thickness and layer dilatation might be involved. On purely dimensional grounds we can write

$$W = B_3 f \quad (7.120)$$

where f is a function of all other parameters. Keeping elastic terms only, we find [60] $f \simeq \frac{1}{4}\pi^2(B_1/B_3)^{1/2}$. Thus

$$F_t \simeq B_3 f q_0 / \pi.$$

The cross-over from the twisted to the untwisted state occurs for

$$q_0 d_c \simeq (2f/\pi). \quad (7.121)$$

This occurs, as observed experimentally, when the thickness is of the order of the pitch of the helix.

Remarks

- In the argument developed above, nothing differs from the cholesteric case (aside from the exact expression of f): indeed, in similar circumstances, cholesterics are unwound.
- The situation described here, which ignores the splayed state, can be achieved by using glass surfaces treated in such a way that an easy axis for the molecular direction is imposed.

If no easy axis is specified, the surface energy is minimized by symmetric directions for \mathbf{P} . For instance $\Omega_z = 0$ on the top surface; $\Omega_z = \pi$ on the bottom one. A possible representation of the twisted state with symmetric boundary conditions for \mathbf{P} is given in Fig. 7.25(a). Upon reducing the thickness, the natural candidate, as a stable state, is now the splayed one Fig. 7.25(c). This is, however, not always the case: symmetric configurations at the boundaries for \mathbf{P} minimize the surface energy† but not the bulk one, which diverges like B_1/d for small thicknesses. As a result the homogeneous state is always more stable for α sufficiently small; for weakly polar interfaces the splayed state may even never be stable. In a given sample and thickness range these states may be simultaneously observed. One can also induce splayed \rightarrow homogeneous transitions with the external fields [73].

† It also includes a bulk spontaneous bend contribution.

7.2.7.4 Importance of the bookshelf geometry

This geometry provides a very promising display device [71] which is characterized by good contrast, bistability, and speed.

Coupling to light The first point is easily understood by observing Fig. 7.26: viewed in transmission between crossed polarizers under suitable conditions, a S_C^* slab in the bookshelf geometry reveals black and white domains with a remarkable contrast. Indeed, if the incident polarization is parallel to the director† \mathbf{n} of one of the domains:

- the transmitted intensity through this domain is zero;
- the transmitted intensity through the second domain is given by

$$I = I_0 \sin^2(4\theta) \sin^2(\pi \Delta n d/\lambda)$$

where θ is the angle between \mathbf{k} and \mathbf{n} ; $\Delta n = n_n - n_0$ (n_n index in the \mathbf{n} direction; n_0 in the direction perpendicular to \mathbf{k} and \mathbf{n}).

Ideal transmission is obtained for $\theta = 22.5^\circ$.

$$\Delta n d/\lambda = \frac{1}{2}, \quad \text{that is, with } \lambda \simeq 0.5 \text{ }\mu\text{m and } \Delta n \simeq 0.2,$$

$$d \simeq 2.5 \text{ }\mu\text{m}.$$

For S_C^* characterized by pitches sufficiently larger than this value, one can take full advantage of this optical contrast provided θ has the right value. The skill of chemists is amazing since many compounds are known that exhibit θ values close to 22° . The rule of the game is then to prepare large pitch mixtures which preserve the polarization value: this is possible by mixing compounds characterized by q_0 of the same order but different sign.

Switching characteristics Bistability is illustrated in Fig. 7.25(b). The equivalence of the two states show that, once the system is either in the ‘up’ or the ‘down’ situation, it will stay there forever.‡

Switching is easy. The electric field E_y discriminates one state from the other: a non-zero electric field E_y , however small, will move the wall of Fig. 7.25(b).

If one starts from a pure ‘up’ state and turns on a ‘down’ electric field and if one can avoid disclination loop nucleation, one will observe the following sequence.

† Remember: the S_C^* is in fact biaxial and by director we mean the unit vector in the direction of the largest eigenvalue of the dielectric tensor at the optical wavelength.

‡ This is not true if the surfaces have an easy axis different from the ideal case.

1. At a very small applied field, a kind of Frederiks transition occurs. In this regime, the boundary conditions may be regarded as rigid, and the relevant energy reads (per unit surface of the slab)

$$F = \int_0^d \left[\frac{B_1}{2} \left(\frac{d\Omega_z}{dy} \right)^2 - P_0 E \cos \Omega_z \right] dy. \quad (7.122)$$

This situation is entirely analogous to that described in Section 3.2.3.2. The product $P_0 E$ is equivalent to $\chi_a H^2$ (note however that now the sign of E is important). A direct transcription of (3.64) gives the threshold field E_t at which the first deformation occurs

$$E_t = - \frac{B_1 \pi^2}{P_0 d^2} \quad (7.123)$$

or

$$V_t = - \frac{B_1 \pi^2}{P_0 d}. \quad (7.124)$$

Note. In contrast to the nematic case, the threshold voltage is thickness-dependent.

Plugging in numbers such as $B_1 \sim 10^{-7}$ dyn, $P_0 \simeq 100$ esu, and $d \simeq 3$ μm , one finds $V_t \simeq 10^{-2}$ V! This threshold is very small and, in fact, has not been studied. In this geometry, the important phenomenon is not the onset of the first distortion† but rather the full switching to the other state!

2. Let us raise the voltage to a few volts: the polarization now points along the field in most of the sample except at the surfaces within boundary layers reminiscent of the magnetic or electric coherence length introduced in Chapter 3. At a second critical field, the surface potential barrier of Fig. 7.28 disappears and the whole system is homogeneous again.

Dynamics Speed is the most interesting feature. The dynamics may be quite complicated. However, in the ‘high field’ regime, the behaviour is controlled by the electric response time τ , which can be easily obtained by equating the viscous torque $\eta \partial\Omega/\partial t$ to the electric torque $\mathbf{P} \cdot \mathbf{E} \sin \Omega$ (η is a viscosity similar to γ_1 in nematics), i.e.

$$\tau = \frac{\eta}{|\mathbf{P} \cdot \mathbf{E}|}. \quad (7.125)$$

With $\eta \simeq 0.1$ poise, $p \simeq 100$ esu, and $E = 10^5$ V/cm $^{-1}$ (i.e. 10 V over 1 μm). $\tau \sim 3 \cdot 10^{-6}$ s. This is considerably shorter than for nematics. Times shorter than a microsecond have been reported [71] and further improvements are to be expected. Speed and bistability open the way to highly multiplexed

† Although this might provide a measurement of B_1 !

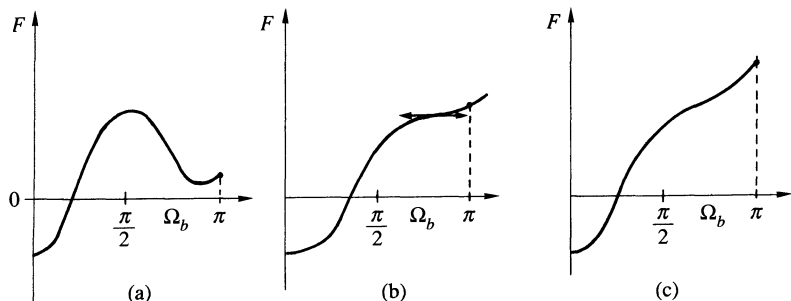


Fig. 7.28. Variation of the free energy of a S^*_C slab in the bookshelf geometry under an electric field. (a) $E < E_{t_2}$ (equivalently $\xi > 3\sqrt{(3b/2)}$) there is a potential barrier to overcome before reaching the more stable $\Omega_b = 0$ state. (b) $E = E_{t_2}$, the potential barrier is replaced by an inflection point. (c) $E > E_{t_2}$, F decreases monotonously with decreasing angle.

devices, such as display screens for computers, calculators, high-speed switches for fibre optics, for optical printers, etc.

Problem. Calculate the threshold E_{t_2} at which the surface anchoring barrier is overcome [75].

Solution. One can use (7.122) supplemented by surface terms (we neglect $\tilde{w}_2 \ll w_1$), and consider a semi-infinite medium in the y direction since in this limit d is no longer a relevant parameter (i.e. boundary layer \ll sample thickness). The free energy reads now (we choose $P_0 < 0$ so that the down states correspond to $\Omega_z = 0$; the system is initially defined by $\Omega_z = \pi$; $E < 0$)

$$F = \int_0^\infty \left(\frac{B_1}{2} \left(\frac{d\Omega_z}{dy} \right)^2 - P_0 E \cos \Omega_z \right) dy - \frac{w_1}{2} \cos^2 \Omega_b.$$

(Remember: $\Omega_b = \Omega_z(y=0)$.)

We are now familiar with the Euler–Lagrange equation:

$$\xi^2 \frac{d^2 \Omega_z}{dy^2} = \sin \Omega_z \quad (7.126)$$

where $\xi^2 = B_1/|P_0 E|$ defines the range of the boundary layer. The other length in the problem is the extrapolation length $b = B_1/w_1$, which enters boundary conditions. Clearly a regime change will occur when $\xi \sim b$.

The first integral of (7.126) can be calculated as in Chapters 3 and 6; one gets

$$\cos(\Omega_z/2) = \tanh((y + y_1)/\xi).$$

y_1 is defined by

$$\cos(\Omega_b/2) = \tanh(y_1/\xi).$$

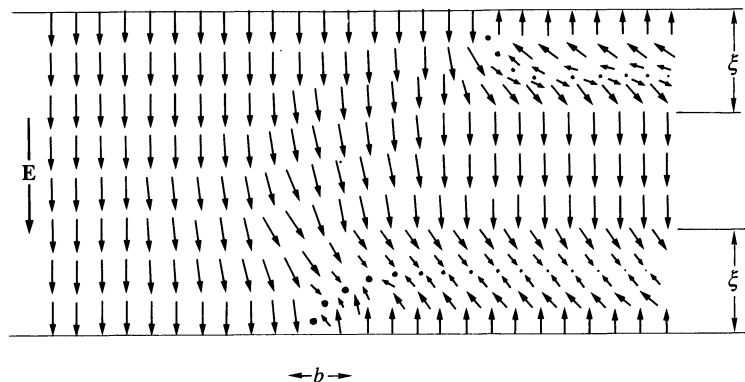


Fig. 7.29. S_C^* slab prepared in the up state, then submitted to a down electric field $E \leq E_{t_2}$. The distortions in the ξ boundary layers are relaxed by surface disclinations. (The core is probably of size b , and partially virtual.) The motion of the disclinations is from left to right.

F may be expressed as a function of Ω_b only. We have represented the three possible behaviours of $F(\Omega_b)$ with increasing field in Fig. 7.28.

- If $\xi > 3\sqrt{3}b/2$, the boundary layer is stable with respect to Ω_b fluctuations. The only way the system can relax to the down state is through nucleation and growth of surface disclinations of the type described in reference 74 (Fig. 7.29).
- If $\xi < 3\sqrt{3}b/2$ the surface angle Ω_b can relax homogeneously to the π value [75].
- $\xi = 3\sqrt{3}b/2$ defines the threshold $E_{t_2} = 4w_1^2/27P_0B_1$.

Implicit in this discussion is the fact that it is not possible to ignore the dynamics.

- For $E \ll E_{t_2}$ the down state is obtained through motions of walls like the one of Fig. 7.25(b).
- For $E \leq E_{t_2}$ and if the field has been switched on fast enough so that the former process has not taken place, the down state is reached through motion of surface disclinations.
- For $E > E_{t_2}$ and provided that the first two processes have not been operative, the surface orientation ‘flips’ as a solid body [75].

Remarks

1. The description we give here is highly idealized. As we have seen the boundary conditions may be very diverse. In the case of ‘molecules’ tilted with respect to the interface in the ground state, the process may be very different and, in particular, experimental observation suggests that the distortion may start from the surfaces [76].

2. The model we use is oversimplified in many ways: there are certainly space charges; the \mathbf{E} field is not uniform; flexoelectric and dielectric terms together with layer dilatation should also be considered.

7.2.7.5 *Polarization measurements*

The bookshelf geometry provides the most direct way of measuring the spontaneous polarization.

Suppose we start with a system prepared in the up direction, and sandwiched between two conductive plates (the planes: $y = 0$, $y = d$ of Fig. 7.25(b). Let us turn on a down field: as a result the polarization flips, and the polarization current $i_p = S(dP/dt)$ is generated in the electrical circuit (S is the surface of the conductive plates). The integral

$$\int_0^\infty i_p dt = SP. \quad (7.127)$$

provides a direct measure of the polarization. This method was first promoted by Martinot-Lagarde [77], using an external square wave voltage larger than the helix unwinding one and 'large' thicknesses (i.e. corresponding to Fig. 7.25(a) in the absence of the field). The polarization was differentiated from the one due to the capacitor charge simply by time resolution (i.e. capacitor charge was significantly faster than polarization reversal). The easiest way to obtain this discrimination is to use a triangular wave voltage [78]. The current, in the absence of polarization reversal is then a simple square wave; i_p appears as a 'bump' on a flat background and is thus easily integrated (Fig. 7.30). Bridge methods can also be used [79].

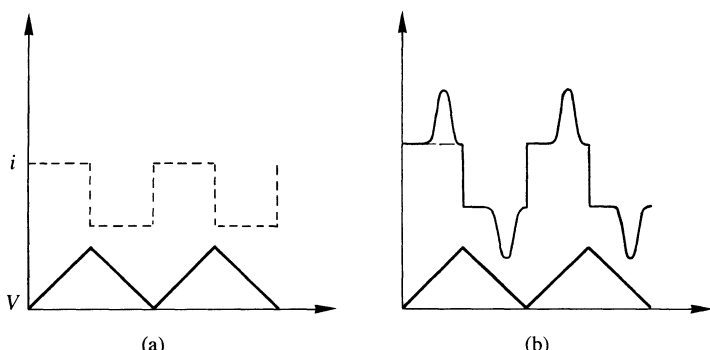


Fig. 7.30. Current i flowing through a planar capacitor containing a slab and corresponding voltage V . (a) Sample in the smectic A phase: the observed current corresponds to the charge of the capacitor plate and is simply the derivative of the voltage. (b) Sample in the ferroelectric S^* phase: the 'bump' corresponds to the polarization reversal current. The area under the peak gives the value of P_0 .

The pyroelectric effect may also be used in polarization measurements. In the same geometry with a monodomain sample when temperature is changed, a polarization current $i_p = (dP/dT)(dT/dt)$ (T = temperature; t = time) is induced in the electric circuit. One thus measures dP/dT and integration with respect to T yields P [80, 81]. This method has the advantage of being generalizable to polar phases in which \mathbf{P}_0 is locked to the structure (they are in general crystalline phases but could also be columnar).

REFERENCES

1. de Gennes, P. G. *Solid State Commun.* **10**, 753 (1972).
2. Boltenhagen, P., Lavrentovich, O., and Kleman, M. *J. Phys. (Paris) II* **1**, 1233 (1991).
3. de Gennes, P. G. *J. Phys. (Paris) Colloq.* **30** (Suppl. C4 to nos. 11, 12) (1969).
4. Prost, J. and Pershan, P. S. *J. appl. Phys.* **47**, 2298 (1976).
5. Marcerou, J. P., Rouillon, J. C., and Prost, J. *Mol. Cryst. liquid Cryst.* **102**, 211 (1984).
6. Mazenko, G. F., Ramaswamy, S., and Toner, J. *Phys. Rev. A* **28**, 1618 (1983).
7. Dahl, I. and Lagerwall, S. R. *Ferroelectrics* **58**, 215 (1984).
8. Saupe, A. *Mol. Cryst. liquid Cryst.* **7**, 59 (1969).
9. Orsay Group on Liquid Crystals. *Solid State Commun.* **9**, 653 (1971).
10. For recent measurements see Collin, D., Gallani, J. L., and Martinoty, P. *Phys. Rev. Lett.* **58**, 254 (1987).
11. Lagerwall, S. T. and Dahl, I. *Mol. Cryst. liquid Cryst.* **114**, 151 (1984).
12. Bartolino, R., Doucet, J., and Durand, G. *Ann. Phys., Paris* **3**, 389 (1978).
13. Brand, H. R. and Pleiner, H. *J. Phys. (Paris)* **45**, 563 (1984).
14. Meyer, R. B. and Pershan, P. S. *Solid State Commun.* **13**, 989 (1973).
15. Prost, J. and Clark, N. A. *Liquid Crystals, Proceedings of an International Conference held at the Raman Research Institute, Bangalore 1979* (ed. S. Chandrasekhar), p. 53. Heyden, Philadelphia (1980). See also Kats, E. *JETP* **48**, 916 (1978).
16. Kleman, M. and Oswald, P. *J. Phys. (Paris)* **43**, 655 (1982).
17. Palierne, J. F. and Durand, G. *J. Phys. (Paris) Lett.* **45**, L335 (1984).
18. Brand, H. and Pleiner, H. *Phys. Rev. A* **24**, 2777 (1981).
19. Pindak, R., Bishop, D. J., and Sprenger, W. O. *Phys. Rev. Lett.* **44**, 1461 (1980).
20. Moncton, D. E., Pindak, R., Davey, S. C., and Brown, G. S. *Phys. Rev. Lett.* **49**, 1865 (1982).
21. Vaucher, C., Zann, A., Le Barny, P., Dubois, J. C., and Billard, J. *Mol. Cryst. liquid Cryst.* **66**, 103 (1981).
22. Gharbia, M., Cagnon, M., and Durand, G. *J. Phys. (Paris) Lett.* **46**, L683 (1985).
23. Bartolino, R. and Durand, G. *Phys. Rev. Lett.* **39**, 1346 (1977).
24. Young, C., Pindak, R., Clark, N. A., and Meyer, R. B. *Phys. Rev. Lett.* **40**, 773 (1978).

25. Palierne, J. F. Thesis, Orsay (France) (1983).
26. Friedel, G. *Annales de Phys.* **18**, 273 (1922).
27. Pindak, R., Young, C., Meyer, R. B., and Clark, N. A. *Phys. Rev. Lett.* **45**, 1193 (1980).
28. Pindak, R., Moncton, D. E., Davey, S. C., and Goodby, J. W. *Phys. Rev. Lett.* **46**, 1135 (1980).
29. Sirota, E. B., Pershan, P. S., Sorensen, L. B., and Collett, J. *Phys. Rev. A* **36**, 2890 (1987).
30. Van Winkle, D. H., Clark, N. A. *Phys. Rev. Lett.* **48**, 1407 (1982).
31. Strutt, J. W. and Lord Rayleigh. *Proc. London math. Soc.* **10**, 4 (1879).
32. Safinya, C. R., Clark, N. A., Liang, K. S., Varady, W. A., and Chiang, L. Y. *Mol. Cryst. liquid Cryst.* **123**, 205 (1985).
33. Rondelez, F. and Hulin, J. P. *Solid State Commun.* **10**, 1009 (1972).
34. Helfrich, W. *Appl. Phys. Lett.* **17**, 531 (1970); Hurault, J. P. *J. chem. Phys.* **59**, 2086 (1973).
35. Rapini, A. *J. Phys.* **33**, 237 (1972).
36. (a) Delaye, M., Ribotta, R., and Durand, G. *Phys. Lett. A* **44**, 139 (1973).
(b) Clark, N. A. and Meyer, R. B. *Appl. Phys. Lett.* **30**, 3 (1973).
37. Rosenblatt, C. S., Pindak, R., Clark, N. A., and Meyer, R. B. *J. Phys. (Paris)* **38**, 1105 (1977).
38. Cagnon, M., Gharbia, M., and Durand, G. *Phys. Rev. Lett.* **53**, 938 (1984).
39. Prost, J. *Liquid Crystals* **8**, 123 (1990).
40. Kahn, F. *Appl. Phys. Lett.* **22**, 111 (1973).
41. Hareng, M. and Leberre, S. *I.E.D.M. Tech. Dig.*, p. 258 (1978) and references therein.
42. de Gennes, P. G. *J. Phys. (Paris) Colloq.* **30** (Suppl. C4), 65 (1969).
43. Ribotta, R., Durand, G., and Litster, J. D. *Solid State Commun.* **12**, 27 (1973).
44. Birecki, H., Schaetzing, R., Rondelez, F., and Litster, J. D. *Phys. Rev. Lett.* **36**, 1376 (1976).
45. de Gennes, P. G. *Symp. Faraday Soc.* **15**, 16 (1971).
46. Van Winkle, D. H. and Clark, N. A. *Phys. Rev. Lett.* **53**, 1157 (1984).
47. Van Winkle, D. H. and Clark, N. A. *Phys. Rev. A* **38**, 1573 (1988).
48. Meyer, R. B. *Mol. Cryst. liquid Cryst.* **40**, 33 (1977).
49. Anderson, G., Dahl, I., Kuczynski, W., Lagerwall, S. T., Skarp, K., and Stebler, B. *Ferroelectrics* **84**, 285 (1988).
50. Garov, S. and Meyer, R. B. *Phys. Rev. Lett.* **38**, 848 (1977).
51. Langer, S. A. and Sethna, J. P. *Phys. Rev. A* **34**, 5035 (1986); Hinshar, Jr, G. A., Petschek, R. G., and Pelcovits, R. A. *Phys. Rev. Lett.* **60**, 1864 (1988).
52. Dahl, I. and Lagerwall, S. T. *Ferroelectrics* **58**, 215 (1984); Lagerwall, S. and Dahl, I. *Mol. Cryst. liquid Cryst.* **114**, 151 (1984).
53. For instance, Bahr, C. and Heppke, G. *Mol. Cryst. liquid Cryst.* **150b**, 313 (1987).
54. Pikin, S. A. and Indenbom, V. L. *Sov. Phys. Usp.* **21**(6), 487 (1978).
55. Durand, G. and Martinot-Lagarde, Ph. *Ferroelectrics* **24**, 89 (1980).
56. Blinc, R. and Zecks, B. *Phys. Rev. A* **18**, 740 (1978).
57. Dumrograttana, S. and Huang, C. C. *Phys. Rev. Lett.* **56**, 464 (1986).
58. Martinot-Lagarde, Ph., Duke, R., and Durand, G. *Mol. Cryst. liquid Cryst.* **75**, 249 (1981).
59. Brunet, M. and Williams, C. *Ann. Phys., Paris* **3**, 237 (1978).

60. Glogarova, M., Lejček, L., Pavel, J., Janovec, V., and Fonsek, J. *Mol. Cryst. liquid Cryst.* **91**, 309 (1983).
61. Dmitrienko, V. E. and Belyakov, V. A. *Sov. Phys. JETP* **51**(4), 787 (1980).
62. Martinot-Lagarde, Ph. *Mol. Cryst. liquid Cryst.* **66**, 61 (1981).
63. Prost, J. *Ferroelectrics* **85**, 317 (1988).
64. Rieker, T. P., Clark, N. A., Smith, G. S., Parmar, D. S., Sirota, E. B., and Safinya, C. R. *Phys. Rev. Lett.* **59**, 2658 (1987); Ouchi, Y., Takezoe, H. and Fukuda, A. *Jap. J. appl. Phys.* **26**, 1 (1987).
65. Brunet, M. *J. Phys. (Paris) Colloq.* **36** (Suppl. C1), 321 (1975).
66. Belyakov, V. A., Dmitrienko, V. E., and Orlov, V. P. *Usp. Fiz. Nauk* **127**, 221 (1979).
67. Berreman, D. W. *Mol. Cryst. liquid Cryst.* **22**, 175 (1973); Parodi, O. *J. Phys. (Paris) Colloq.* **36** (Suppl. C1), 325 (1975).
68. Oldano, C. *Phys. Rev. Lett.* **53**, 2413 (1984).
69. Vtyupin, A. N., Ermakov, V. P., Ostrovski, B. I., and Shabanov, V. G. *Phys. Status Solidi* **B107**, 397 (1981).
70. Garov, S. and Meyer, R. B. *Phys. Rev. A* **19**, 338 (1979).
71. Clark, N. A., Lagerwall, S. T., and Dahl, I. *Phys. Lett.* **36**, 899 (1980).
72. See reference 64. Also see Clark, N. A., Rieker, T. P., and MacLennan, J. F. *Ferroelectrics* **85**, 79 (1988); Hiji, N., Chandani, A. D. L., Nishiyama, S. I., Ouchi, Y., Takezoe, H., and Fukuda, A. *Ferroelectrics* **85**, 99 (1988).
73. Handschy, M. A., Clark, N. A., and Lagerwall, S. T. *Phys. Rev. Lett.* **51**, 471 (1983); Yue, J., Clark, N. A., and Meadows, M. R. *Appl. Phys. Lett.* **53**, 2397 (1988).
74. Handschy, M. A. and Clark, N. A. *Appl. Phys. Lett.* **41**, 1 (1982).
75. Galvan, J. M. Unpublished D.Phil. thesis, no. 2179, Bordeaux (1987).
76. Ouchi, Y., Takezoe, H., and Fukuda, Z. *Eleventh International Liquid Crystal Conference*, Berkeley (1986).
77. Martinot-Lagarde, Ph. *J. Phys. (Paris)* **38**, L17 (1977).
78. Miyasato, K., Abe, S., Takezoe, H., Fukuda, A., and Kuze, E. *Jpn J. appl. Phys.* **22**, L661 (1983).
79. Ostrovski, B. I., Rabinovich, A. Z., Sonin, A. S., Strukov, B. A., and Chernova, N. I. *JETP* **25**, 80 (1977).
80. Yu, L. J., Lee, H., Bak, C. S., and Labes, M. M. *Phys. Rev. Lett.* **36**, 388 (1976).
81. Blinov, L. M. and Beresnev, L. A. *Sov. Phys. Usp.* **27**, 7 (1984).

DYNAMICAL PROPERTIES OF SMECTICS AND COLUMNAR PHASES

8.1 UNIFIED DESCRIPTION

8.1.1 Preliminary remarks

In Chapter 5 we saw that the long-wavelength, low-frequency behaviour of nematics could be described by a continuum theory. Here we consider the equivalent approach for smectics and columnar phases. We use the general framework constructed by Martin, Parodi, and Pershan [1] since it allows the use of the same presentation for all systems. The hydrodynamics of smectics was first discussed in reference 2 and of columnar phases in reference 3 (reference 4 for the biaxial case).

Common to all these theories are the hypotheses of local equilibrium and the existence of an analytic gradient expansion. We will see in the last part of this chapter how and when the second hypothesis breaks down. Local equilibrium requires that all variables that are not retained in the continuum description have time to adjust to the (slowly) fluctuating external conditions. Conversely, one needs a prescription for singling out the relevant hydrodynamic variables; they have to be slow compared to any ‘microscopic’ time of the system: Conserved quantities (mass, momentum, energy in a one-component system) satisfy this requirement since for an infinite wavelength perturbation they have an infinite lifetime: one will always be able to find a scale beyond which such variables will be slow compared to microscopic ones. These are already relevant in isotropic fluids. We have seen that the description of nematics required the introduction of a director \mathbf{n} : the relevance of \mathbf{n} is directly linked to rotational invariance. Indeed, a homogeneous rotation of \mathbf{n} does not lead to any restoring torque and thus the rotated state has an infinite lifetime. Similarly, in a smectic A system, a uniform layer displacement \mathbf{u} does not create any restoring force, since it corresponds to a simple translation: the translated state has an infinite lifetime. \mathbf{n} and \mathbf{u} are said to be ‘hydrodynamic’ variables linked to broken rotational and translational symmetries. Clearly, the hydrodynamic variables are those introduced in the elastic continuum description. They are listed in Table 8.1. In the following we restrict our considerations to small-amplitude distortions (i.e. linearized hydrodynamics).

It is interesting to understand why the director is not a ‘hydrodynamic’ variable in smectics A. Suppose that, at time $t = 0$, we move n_x out of its

Table 8.1. The hydrodynamic variables.

	Variables ^a linked to broken		No. of variables
	Translational symmetry	Rotational symmetry	
Isotropic fluids	None	None	5 ^b
Nematics	None	$\delta n_x, \delta n_y$	7
Smectics A	\mathbf{u}	None	6
Smectics B _{hex}	\mathbf{u}	Ω_z	7
Smectics C	\mathbf{u}	Ω_z	7
Columnar phases: hexagonal	u_x, u_y	None	7
Columnar phases: biaxial	u_x, u_y	None	7
Crystals	u_x, u_y, u_z	None	8

^a The displacement variables and the rotation Ω_z are defined in Chapter 7, the director variables in Chapter 5.

^b The five variables in the case of isotropic fluids correspond to mass, energy, and the three components of momentum.

equilibrium position (Fig. 8.1)

$$\left(n_x + \frac{\partial u}{\partial x} \right) = \theta \quad \text{at } t = 0.$$

θ relaxes to zero in a microscopic time independent of whether θ is homogeneous or not, because the smectic layers exert a torque depending directly on θ , not on its gradients. Thus in the hydrodynamic regime $n_x = -(\partial u / \partial x)$ is not an independent variable. As to order of magnitude, this time falls in the 10^{-7} s range [5]. For the same reason, angular variables are not independent in columnar phases and crystals. Smectics B_{hex} and C are very unusual in that their description requires the simultaneous use of \mathbf{u} and Ω_z .

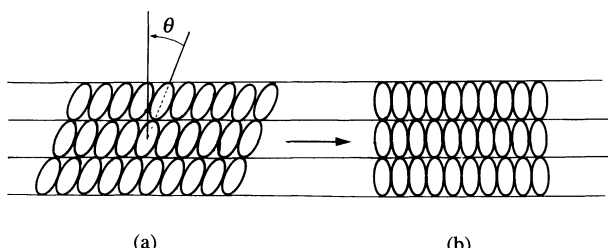


Fig. 8.1. In a smectic A, the time required for the distorted structure (sketched in (a)) to relax to its equilibrium state (sketched in (b)) depends on the local torque exerted by the layers on the molecules. It is finite even for homogeneous tilt θ .

The range over which hydrodynamics is valid is strongly system-dependent. Very often the largest non-hydrodynamic time is the one corresponding to longitudinal dipolar relaxation. It is usually in the 10^{-6} – 10^{-8} s range but can be as large as 10^{-3} s in some special cases [6]. The predictions of hydrodynamics are not altogether invalid on smaller time scales, but no rigorous statement can be made without paying closer attention to the system under consideration.

8.1.2 Basic equations

As we have seen in the nematic case, the rule of the game is to write down the equations for entropy production; this leads to the introduction of a set of fluxes and forces that are assumed to be linearly related in the lowest order approximation. The conservation equations are also central to the description of the dynamics; they read as usual

$$\frac{\partial \rho}{\partial t} + \partial_\alpha(\rho v_\alpha) = 0, \quad (8.1a)$$

$$\frac{\partial(\rho v_\alpha)}{\partial t} - \partial_\beta \sigma_{\alpha\beta} = 0, \quad (8.1b)$$

$$\frac{\partial \varepsilon}{\partial t} + \partial_\alpha J_\alpha = 0, \quad (8.1c)$$

Equations (8.1) are familiar: they express respectively mass, momentum, and energy conservation. Equations (8.1b) and (8.1c) can be considered as defining the stress tensor $\sigma_{\alpha\beta}$ and the energy flux J_α (ε is the energy density). Equation (8.1a) is particularly simple, because the mass flux is clearly equal to the momentum density ρv_α .

Local equilibrium implies (per unit volume)

$$d\varepsilon = \mu d\rho + T dS + v_\alpha d(\rho v_\alpha) + \sigma_{\alpha\beta}^u d(\partial_\beta u_\alpha) - h_\alpha d\Omega_\alpha. \quad (8.2)$$

The first three terms of the right-hand side of (8.2) are common to any system. $\mu = (\rho + \varepsilon^0 - \frac{1}{2}\rho v^2 - TS)/\rho$ is the chemical potential, S the entropy density. The last terms correspond to the existence of translational and rotational order: since we have seen that energy variations could result only from gradients in the displacement variable, the correct differential involves $d\partial_\beta u_\alpha$ instead of du_α . In principle, the same remark holds for the angular variable Ω : in the absence of any field the correct expression would be

$$h_{\alpha\beta} d\partial_\beta \Omega_\alpha. \quad (8.3)$$

The equivalence of (8.3) and (8.2) requires that $h_\alpha = \partial_\beta h_{\alpha\beta}$ (surface terms being once more omitted). If we allow for the presence of a magnetic field, (8.2) is better suited. At this point, $\sigma_{\alpha\beta}^u$ and h_α are the fields conjugate to $\partial_\beta u^\alpha$

and Ω^α ; their connection with $\sigma_{\alpha\beta}$ and J_α has to be determined.

$$\sigma_{\alpha\beta}^u = \left. \frac{\partial \varepsilon}{\partial \partial_\beta u_\alpha} \right|_{\rho, S, \rho v_\delta, \partial_\beta u_\gamma, \Omega_\gamma} \quad h_\alpha = \left. \frac{\partial \varepsilon}{\partial \Omega_\alpha} \right|_{\rho, S, \rho v_\delta, \partial_\beta u_\gamma, \Omega_\gamma} \quad (8.4)$$

($\alpha' \neq \alpha, \beta$). For instance, in the smectic A case

- The compression energy reads (the other variables ρ , S , etc. being maintained at their equilibrium value)

$$\delta \varepsilon = \frac{1}{2} B^0 (\nabla_z u)^2. \quad (8.5)$$

Thus $\sigma_{zz}^u = B^0 \nabla_z u$, in a static description this would be the zz components of the stress tensor (pressure omitted).

- The tilt energy is under similar conditions (in the presence of a magnetic field \mathbf{H} along z)

$$\delta \varepsilon' = \frac{\chi_a}{2} H^2 \left[\left(\frac{\partial u}{\partial x} \right)^2 + \left(\frac{\partial u}{\partial y} \right)^2 \right] + \frac{K_1}{2} \left(\frac{\partial^2 u}{\partial x^2} + \frac{\partial^2 u}{\partial y^2} \right)^2. \quad (8.6)$$

Thus,

$$\sigma_{zx}^u = \chi_a H^2 \frac{\partial u}{\partial x} - K_1 \frac{\partial}{\partial x} \left(\frac{\partial^2 u}{\partial x^2} + \frac{\partial^2 u}{\partial y^2} \right). \quad (8.7)$$

Note that, in the absence of magnetic field, σ_{zx}^u involves third-order derivatives only: this novel feature of smectics and columnar phases is responsible for the highly anisotropic behaviour of these systems.

Manipulations quite similar to those performed with simple fluids [1, 7] allow us to express the entropy production (i.e. making use of (8.1) and (8.2), taking into account the expression of the chemical potential, and neglecting higher order and surface terms) as

$$T \frac{\partial S}{\partial t} = - \frac{\partial_\alpha T}{T} \left(J_\alpha^e - (\varepsilon^0 + P) v_\alpha \right) + (\sigma_{\alpha\beta} + P \delta_{\alpha\beta}) \partial_\beta v_\alpha - \sigma_{\alpha\beta}^u \partial_\beta \dot{u}_\alpha + h_\alpha \dot{\Omega}_\alpha \quad (8.8)$$

where $\dot{u}_\alpha = \partial u_\alpha / \partial t$; $\dot{\Omega}_\alpha = \partial \Omega_\alpha / \partial t$. This expression of the entropy source still needs to be modified since \dot{u}_α and $\dot{\Omega}_\alpha$ each contain a reactive (i.e. reversible, non-dissipative) and a dissipative part (remember such a distinction has already been made at the end of Section 3.5.2). The dissipative part is the one that is expressed in the ‘flux–force’ linear relations. The reversible part has time-reversal properties opposite to those of the dissipative part and thus, to lowest order, one can write (with obvious notation)

$$\dot{u}_\alpha = \dot{u}_\alpha^r + \dot{u}_\alpha^d; \quad \dot{\Omega}_\alpha = \dot{\Omega}_\alpha^r + \dot{\Omega}_\alpha^d \quad (8.9)$$

where superscripts r and d refer, respectively, to the reversible and dissipative parts. Since u_α and Ω_α are even under time reversal, \dot{u}_α^r and $\dot{\Omega}_\alpha^r$ have to be

odd: the only variable of (8.2) that satisfies this requirement is v_α . Thus

$$\dot{u}_\alpha^r = A_{\alpha\beta} v_\beta + A_{\alpha\beta\gamma} \partial_\gamma v_\beta + \dots, \quad (8.10a)$$

$$\dot{\Omega}_\alpha^r = B_{\alpha\beta} v_\beta + B_{\alpha\beta\gamma} \partial_\gamma v_\beta + \dots. \quad (8.10b)$$

The A s and B s are coefficients that characterize the phase that we describe. Suppose we consider a system in its ground state at rest (in a given Galilean reference frame): $u_\alpha^r = \dot{\Omega}_\alpha^r = 0$. Let us now consider the same system, from another Galilean reference frame moving with a velocity v_α with respect to the former. From this new reference frame one sees $\dot{u}_\alpha = \dot{u}_\alpha^r = v_\alpha$; $\dot{\Omega}_\alpha = \dot{\Omega}_\alpha^r = 0$, but clearly no dissipation occurs.

Thus

$$A_{\alpha\beta} = \delta_{\alpha\beta}; \quad B_{\alpha\beta} = 0.$$

These relations express Galilean invariance.

In systems possessing inversion symmetry, $A_{\alpha\beta\gamma} = 0$; in chiral systems it may have non-vanishing terms. However, $A_{\alpha\beta\gamma}$ has the dimensions of a length: under current circumstances this length will be of molecular size and the contribution of the $A_{\alpha\beta\gamma} \partial_\gamma v_\beta$ term is down by a factor (a/λ) with respect to the Galilean term (if $a \approx 10^{-7}$, 10^{-6} cm and λ , the wavelength of the considered perturbation $\approx 10^{-4}$ Å cm, the second term contributes on the order of 10^{-2} – 10^{-3} in the reactive part). Thus in most practical situations (8.10a) may be written

$$\dot{u}_\alpha^r = v_\alpha. \quad (8.11)$$

Equation (8.10b) is more subtle: it contains terms linked to rotational invariance, but also terms of physical origin.[†] For instance, in nematics the reactive part of 5.37) can be rewritten[‡] ($i \in \{x, y\}$)

$$\dot{n}_i^r = \frac{1}{2}(\partial_z v_1 - \partial_i v_z) + \frac{\lambda}{2}(\partial_z v_i + \partial_i v_z). \quad (8.12)$$

(The unperturbed director is along z , and only linear terms are retained.)

As already explained in (5.22), the first part of the right-hand side corresponds to the rate of change of the director due to the rotation of the background fluid (rotational invariance implies, of course, the absence of any dissipation). The second part expresses the reversible torque exerted by the velocity gradients on the director.

[†] $B_{\alpha\beta\gamma}$ is non-zero in systems possessing inversion symmetry because it is a pseudo third-rank tensor. (NB. Ω_α is a pseudovector but $\partial_\beta v_\alpha$ a ‘true’ second-rank tensor.)

[‡] $\lambda = \gamma_2/\gamma_1$ is not to be confused with the smectic penetration length; everywhere else in the chapter $\lambda = \sqrt{(K_1/B)}$.

Using (8.11) and (8.10) in (8.8) allows us to rewrite the entropy production in terms of the dissipative fluxes

$$T \frac{dS}{dt} = -\frac{\partial_\alpha T}{T} J_\alpha^{\varepsilon^d} + \sigma_{\alpha\beta}^d \partial_\beta v_\alpha + \partial_\beta \sigma_{\alpha\beta}^u \dot{u}_\alpha^d + h_\alpha \dot{\Omega}_\alpha^d \quad (8.13)$$

with

$$J_\alpha^{\varepsilon^d} = J_\alpha^\varepsilon - (\varepsilon^0 + P)v_\alpha \quad \text{or} \quad J_\alpha^{\varepsilon^r} = (\varepsilon^0 + P)v_\alpha, \quad (8.14a)$$

$$\sigma_{\alpha\beta}^d = \sigma_{\alpha\beta} + P \delta_{\alpha\beta} - \sigma_{\alpha\beta}^u + B_{\gamma\alpha\beta} h_\gamma \quad (8.14b)$$

or

$$\sigma_{\alpha\beta}^r = -P \delta_{\alpha\beta} + \sigma_{\alpha\beta}^u - B_{\gamma\alpha\beta} h_\gamma,$$

$$\dot{u}_\alpha^d = \dot{u}_\alpha - v_\alpha, \quad (8.14c)$$

$$\dot{\Omega}_\alpha^d = \dot{\Omega}_\alpha - B_{\alpha\beta\gamma} \partial_\gamma v_\beta. \quad (8.14d)$$

The first term on the right-hand side of (8.13) represents the dissipation due to heat transport (a similar expression would be obtained if an electric field were added). The second term is familiar, and describes friction effects.

The third term corresponds to dissipation due to ‘permeation’ in the Helfrich sense [8]: it is non-zero when $\dot{u}_\alpha \neq v_\alpha$, i.e. when there is a mass transport through the structure. This is possible because the concept of structure (i.e. layers, columns, three-dimensional lattice) is macroscopic. Microscopically, there can be vacancies, interstitials, dislocation loops (to be defined in the next chapter) without preventing the existence of long-range or quasilong-range order: the motion of such defects allows mass transport at ‘constant structure’. The fourth term is identical in content to the last two terms of (5.35): it describes dissipation due to rotational motion of the angular variables (tilt direction, bond angle, nematic director).

Note that $\sigma_{\alpha\beta}^u$ indeed is found to contribute to the reactive part of the stress tensor; in a solid, a columnar phase, or a smectic A it is, in fact, equal to that stress as expected (aside from the pressure term). In smectics C and B_{hex} there are angular contributions as well. Note also that, in the absence of external fields ($\mathbf{H} = 0$), one can always choose a symmetric stress tensor via a suitable transformation (remember (5.44); see also reference 1). We choose

Fluxes	Forces	
$J_\alpha^{\varepsilon^d}$	$E_\alpha = -\frac{\partial_\alpha T}{T}$	
$\sigma_{\alpha\beta}^d$	$\partial_\beta v_\alpha$	
\dot{u}_α^d	$g_\alpha = \partial_\beta \sigma_{\alpha\beta}^u$	
$\dot{\Omega}_\alpha^d$	h_α .	

The flux-force relations read

$$\sigma_{\alpha\beta}^d = \eta_{\alpha\beta\gamma\delta} \partial_\delta v_\gamma, \quad (8.16a)$$

$$J_\alpha^{e^d} = K_{\alpha\beta} E_\beta + \mu_{\alpha\beta} g_\beta, \quad (8.16b)$$

$$\dot{u}_\alpha^d = \dot{u}_\alpha - v_\alpha = \mu_{\alpha\beta} E_\beta + \lambda_{\alpha\beta} g_\beta, \quad (8.16c)$$

$$\dot{\Omega}_\alpha^d = \dot{\Omega}_\alpha - B_{\alpha\beta\gamma} \partial_\gamma v_\beta = v_{\alpha\beta} h_\beta. \quad (8.16d)$$

$\eta_{\alpha\beta\gamma\delta}$ is the usual viscosity tensor; it has five independent components in all uniaxial systems, but 13 in S_C and 21 in a crystal of low symmetry! $K_{\alpha\beta}$ represents thermal conductivity (it has two components in uniaxial systems, four in S_C , six for a crystal of low symmetry). $\mu_{\alpha\beta}$ describes (8.16c) a kind of Soret effect. In a binary mixture a thermal gradient can induce a mass transport of one component with respect to the other. One has the equivalent here: a thermal gradient can induce a mass transport through the structure. Just as for the Soret effect, the existence of the corresponding current \dot{u}_α^d depends on boundary conditions (i.e. if u and v are fixed at the boundaries, g_α is built up until $\dot{u}_\alpha^d = 0$). $\lambda_{\alpha\beta}$ is the permeation tensor: it has one component in S_A , $S_{BH_{hex}}$, S_C , hexagonal columnar phases (D_h), two in biaxial columnar phases (D_r , D_0), and six in a low-symmetry crystal. $v_{\alpha\beta}^{-1}$ is the generalization of the twist viscosity of nematics. It has one component in S_C and $S_{BH_{hex}}$.

Because of time-reversal symmetry there are no dissipative cross-couplings between the stress and the g_α , E_α , h_α forces (note that there can be reactive ones, expressed in (8.14b)). Conversely, velocity gradients are not coupled to $J_\alpha^{e^d}$, $\sigma_{\alpha\beta}^d$, \dot{u}_α^d , $\dot{\Omega}_\alpha^d$ via dissipative terms.

Onsager reciprocal relations require that

$$K_{\alpha\beta} = K_{\beta\alpha}; \quad \mu_{\alpha\beta} = \mu_{\beta\alpha}; \quad \lambda_{\alpha\beta} = \lambda_{\beta\alpha}; \quad v_{\alpha\beta} = v_{\beta\alpha}; \quad \eta_{\alpha\beta\gamma\delta} = \eta_{\delta\gamma\alpha\beta}$$

(and one can always choose $\eta_{\alpha\beta\gamma\delta} = \eta_{\beta\alpha\gamma\delta}$ according to our remark concerning the symmetry of $\sigma_{\alpha\beta}$). They also justify the use of $\mu_{\alpha\beta}$ in both (8.16b) and (8.16c). We have not written down any cross-terms between angular variables and others. Indeed they would be expressed via pseudotensors of second rank which vanish for non-chiral nematics, S_C and $S_{BH_{hex}}$. (The case of chiral S_C^* and $S_{BH_{hex}}$ is different in that in the hydrodynamic limit it requires the use of two displacement variables in the same direction (say, z) corresponding to the periodicities of the layers and to the helicoidal precession of the structure [9].) The case of cholesterics is equivalent to that of S_A in the long-wavelength limit [10].

Equations (8.1), (8.14), and (8.16) specify the dynamical behaviour of the systems considered (in the small-amplitude, long-wavelength limit), provided that P , T , g_α , h_α are expressed as functions of the slow hydrodynamic variables. A convenient choice for ‘fast’ processes is ρ , S , v_α , u_α , Ω_α (entropy replaces energy with the use of (8.2)); for ‘slow’ processes the convenient choice is ρ , T , v_α , u_α , Ω_α . Fast or slow depends on the characteristic frequency

for heat diffusion:[†] above this frequency modes are adiabatic, below they are isothermal. The expressions for P , T , g_α , h_α are obtained through simple thermodynamic derivatives (which, as such, satisfy Maxwell relations) and define elastic constants such as B^0 (remember (8.5)), specific heat, etc. We find it more useful to give specific examples in what follows.

Before proceeding to this task, a last general remark has to be made: suppose we look for solutions of the type $\exp(i(\mathbf{k} \cdot \mathbf{r} - \omega t))$. We have $(5 + n + m)$ unknowns (n, m being the number of u_α and Ω_α variables) for $(5 + n + m)$ equations (all linear in ω). The determinantal equation (allowing for solutions different from zero) defines an algebraic equation of order $(5 + n + m)$ in ω . Thus the number of solutions $\omega(k)$ (called number of modes) is equal to the number of hydrodynamic variables. Furthermore, if $\omega(k)$ corresponds to a propagating mode, it must occur in pairs (e.g. if a wave propagates in a given direction, it also does so in the opposite one).

We can now proceed to give specific examples: let us start with a comparison between S_A and D_h phases.

8.1.3 Smectics A and columnar hexagonal phases

The general equations now simplify to

$$-\frac{\partial \theta}{\partial t} + \partial_\alpha v_\alpha = 0 \quad \left(\theta = -\frac{\delta \rho}{\rho} \right), \quad (8.17a)$$

$$\frac{\partial \varepsilon}{\partial t} + \frac{\partial \theta}{\partial t} (\varepsilon + P) = K_{\parallel} \partial_{zz}^2 T + K_{\perp} \Delta_{\perp} T - \mu \partial_\alpha g_\alpha, \quad (8.17b)$$

$$\frac{\partial u_\alpha}{\partial t} - v_\alpha = -\mu \frac{\partial_\alpha T}{T} + \lambda_p g_\alpha, \quad (8.17c)$$

$$\rho \frac{\partial v_\alpha}{\partial t} = -\partial_\alpha P + g_\alpha + \eta_{\alpha\beta\gamma\delta} \partial_\beta \partial_\delta v_\gamma, \quad (8.17d)$$

where subscripts \parallel and \perp mean, respectively, parallel and perpendicular to the optical axis, z , and λ_p is the permeation constant. For any uniaxial phase the viscous term involves five independent viscosities

$$\begin{aligned} \sigma'_{\alpha\beta} = \eta_{\alpha\beta\gamma\delta} \partial_\delta v_\gamma &= \alpha_0 \delta_{\alpha\beta} A_{\mu\mu} + \alpha_1 \delta_{\alpha z} \delta_{\beta z} A_{zz} + \alpha_4 A_{\alpha\beta} \\ &+ \alpha_5 (\delta_{\alpha z} A_{z\beta} + \delta_{\beta z} A_{z\alpha}) + \alpha_7 (\delta_{\alpha z} \delta_{\beta z} A_{\mu\mu} + \delta_{\alpha\beta} A_{zz}) \end{aligned} \quad (8.18)$$

where $A_{\alpha\beta}$ has the meaning given (5.18): $A_{\alpha\beta} = \frac{1}{2}(\partial_\alpha v_\beta + \partial_\beta v_\alpha)$. Stability

[†] Both cases must still be slow compared to any microscopic times of the system!

requirements lead to

$$\begin{aligned}
 (\alpha_0 + \alpha_1 + \alpha_4 + 2\alpha_{56} + 2\alpha_7) \left(\alpha_0 + \frac{\alpha_4}{2} \right) &\geq (\alpha_7 + \alpha_0)^2, \\
 \alpha_4 &\geq 0, \\
 \alpha_{56} + \alpha_4 &\geq 0, \\
 \alpha_0 + \alpha_4/2 &\geq 0, \\
 \alpha_0 + \alpha_1 + \alpha_4 + 2\alpha_{56} + 2\alpha_7 &\geq 0.
 \end{aligned}$$

Note. In the literature viscosities are often expressed in the Harvard notation [1]

$$\left. \begin{aligned}
 \eta_1 &= \alpha_0 + \alpha_1 + \alpha_4 + 2\alpha_{56} + 2\alpha_7, \\
 \eta_2 &= \alpha_4/2, \\
 \eta_3 &= \frac{\alpha_4 + \alpha_{56}}{2}, \\
 \eta_4 &= \alpha_0 + \alpha_4/2, \\
 \eta_5 &= \alpha_7 + \alpha_0.
 \end{aligned} \right\} \quad (8.19)$$

Stability conditions are particularly simple to express using this notation

$$\eta_1 \eta_4 \geq \eta_5^2, \quad \eta_2 \geq 0, \quad \eta_3 \geq 0, \quad \eta_4 \geq 0, \quad \eta_1 \geq 0.$$

For smectics A, a straightforward extension of eqn (7.13) gives

$$\begin{aligned}
 \varepsilon^0 &= \frac{1}{2} \left(B^0 (\partial_z u)^2 + K_1^0 (\Delta_\perp u)^2 + A^0 \theta^2 + \frac{T}{C_v} \delta s^2 \right) \\
 &\quad + C^0 \theta \partial_z u + F^0 \delta s \partial_z u + E^0 \delta s \theta + \frac{\chi_a}{2} H^2 [(\partial_x u)^2 + (\partial_y u)^2]. \quad (8.20)
 \end{aligned}$$

Similarly, for hexagonal columnar phases

$$\begin{aligned}
 \varepsilon^0 &= \frac{1}{2} \left\{ B^0 (\partial_x u_x + \partial_y u_y)^2 + D^0 ((\partial_x u_x - \partial_y u_y)^2 + (\partial_x u_y + \partial_y u_x)^2) \right. \\
 &\quad \left. + K_3 ((\partial_{zz}^2 u_x)^2 + (\partial_{zz}^2 u_y)^2) + A^0 \theta^2 + \frac{T}{C_v} \delta s^2 \right\} + C^0 \theta (\partial_x u_x + \partial_y u_y) \\
 &\quad + F^0 \delta s (\partial_x u_x + \partial_y u_y) + E^0 \delta s \theta + \frac{\chi_a}{2} H^2 [(\partial_z u_x)^2 + (\partial_z u_y)^2]. \quad (8.21)
 \end{aligned}$$

Remark. At frequencies larger than the heat diffusion frequency ($\omega \gg \omega_T = K_{||} q_z^2 + K_\perp q_\perp^2$), the processes are isentropic: one can set $\delta s = 0$ in (8.20) and (8.21). The bare elastic constants (B^0 , etc.) have to be considered.

For $\omega \ll \omega_T$, the processes are isothermal: $\delta T = \partial\varepsilon/\partial(\delta s) = 0$; the corresponding elastic constants are related to the bare elastic constants through

$$\left. \begin{aligned} B &= B^0 - F^{02}C_v/T, \\ C &= C^0 - C_vF^0E^0/T, \\ A &= A^0 - C_vE^{02}/T. \end{aligned} \right\} \quad (8.22)$$

The other rigidity moduli are not changed when crossing from the isentropic to the isothermal regimes.

Estimating F_0 and E_0 to be of the order of unity (i.e. a few kelvin which corresponds to dilatation coefficients of 10^{-3} typically), and with $C_v \simeq$ a few 10^7 erg cm $^{-3}$ K $^{-1}$, one finds corrections of the order of a few per cent to B^0 and C^0 (if B^0 and $C^0 \simeq 10^8$ erg cm $^{-3}$) and a few 10^{-4} to A^0 . Under most circumstances these effects are negligible. Except in particular directions, which will be described in (8.1.4) and (8.1.7), isentropic constants will be the relevant constants in the following discussion.

The forces are obtained from (8.3), (8.15), and (8.20) for S_A (in the isentropic regime)

$$\left. \begin{aligned} g_z &= \frac{\partial}{\partial z} \left(B^0 \frac{\partial u}{\partial z} + C^0 \theta \right) + \chi_a H^2 \left(\frac{\partial^2 u}{\partial x^2} + \frac{\partial^2 u}{\partial y^2} \right) - K_1 \left(\frac{\partial^2}{\partial x^2} + \frac{\partial^2}{\partial y^2} \right)^2 u, \\ g_x &= g_y = 0. \end{aligned} \right\} \quad (8.23)$$

From (8.3), (8.15), and (8.21) for hexagonal columnar phases,

$$g_z = 0,$$

$$\begin{aligned} g_x &= (B^0 + D^0) \frac{\partial^2 u_x}{\partial x^2} + D^0 \frac{\partial^2 u_x}{\partial y^2} + B^0 \frac{\partial^2 u_y}{\partial x \partial y} + C^0 \frac{\partial \theta}{\partial x} - K_3 \frac{\partial^4 u_x}{\partial z^4} + \chi_a H^2 \frac{\partial^2 u_x}{\partial z^2}, \\ g_y &= (B^0 + D^0) \frac{\partial^2 u_y}{\partial y^2} + D^0 \frac{\partial^2 u_y}{\partial x^2} + B^0 \frac{\partial^2 u_x}{\partial x \partial y} + C^0 \frac{\partial \theta}{\partial y} - K_3 \frac{\partial^4 u_y}{\partial z^4} + \chi_a H^2 \frac{\partial^2 u_y}{\partial z^2}. \end{aligned} \quad (8.24)$$

Let us consider modes polarized in the plane defined by the wavevector and the optical axis, and choose the wavevector in the x, z -plane ($\mathbf{q} = (q_x, 0, q_z)$). For S_A , $v_x, v_z \neq 0$; $v_y = 0$. For D_h , $v_z, v_x \neq 0$; $u_x \neq 0$; $v_y = u_y = 0$. With $\exp(i(\mathbf{q} \cdot \mathbf{r} - \omega t))$ dependences,

$$\begin{aligned} S_A: \quad g_z(q) &= -[B^0 q_z^2 + \chi_a H^2 q_x^2 + K_1 q_x^4] + iC^0 q_z \theta, \\ D_h: \quad g_x(q) &= -[(B^0 + D^0) q_x^2 + \chi_a H^2 q_z^2 + K_3 q_z^4] + iC^0 q_x \theta. \end{aligned} \quad (8.25)$$

The expressions are equivalent provided one switches the x - and z -axes, and replaces B^0 by $B^0 + D^0$ and K_1 by K_3 . It is easy to check that this equivalence also holds in (8.17). Thus all the modes polarized in the plane

defined by the wavevector and the optical axis are identical in S_A and D_h phases: they are described in Sections 8.1.4–8.1.6. (Note that this equivalence was already noticed in the problem of Section 7.1.4.)

8.1.4 The undulation mode

This type of mode is sketched in Fig. 7.4(a) and the light scattering intensities associated with it are discussed in Section 7.1.9. It corresponds to a wavevector \mathbf{q} in the plane of the layers in S_A (which we choose to be the x -axis) or along the column direction in D_h (z -axis). For this particular mode there is no change in layer spacing or column diameter. The only restoring forces \mathbf{g} are weak curvature forces, just as in a nematic. The mode is then very strongly damped and so slow that the conditions are usually isothermal rather than adiabatic.

For simplicity we shall also assume $\mathbf{H} = 0$. Then the equations of motion reduce to (we write explicitly the smectic case only since the columnar one can be deduced by the aforementioned transformation)

$$g_z = -K_1 q_x^4 u = \lambda_p^{-1}(\dot{u} - v_z), \quad (8.26)$$

$$\rho \dot{v}_z = -\eta_3 q_x^2 v_z + g_z. \quad (8.27)$$

The inertial term in eqn (8.27) is negligible: eliminating v_z between (8.26) and (8.27) we thus arrive at

$$\dot{u} + \frac{K_1}{\eta_3} q_x^2 (1 + \delta^2 q_x^2) u = 0. \quad (8.28)$$

$\delta = (\lambda_p \eta_3)^{1/2}$ has the dimensions of a length [11] and characterizes the flow properties of smectics (columnar phases). Under usual circumstances δ is expected to be of the order of magnitude of a layer thickness (or a column diameter). Hence, in the applicability range of hydrodynamics, the permeation contribution to the undulation mode is negligible $(-\dot{u} + v_z)/\dot{u} = \delta^2 q_x^2 \ll 1$; in fact, in the original derivation, permeation was omitted from the start [2].

Thus, the undulation relaxes with a rate

$$S_A: \quad \frac{1}{\tau_q} = K_1 q_x^2 / \eta_3, \quad (8.29)$$

$$D_h: \quad \frac{1}{\tau_q} = K_3 q_z^2 / \eta_3. \quad (8.30)$$

If there is a small compressional term ($q_z \ll q_x$ in S_A ; $q_x \ll q_z$ in D_h),

$$g_z = -(\tilde{B} q_z^2 + K_1 q_x^4) u. \quad (8.31)$$

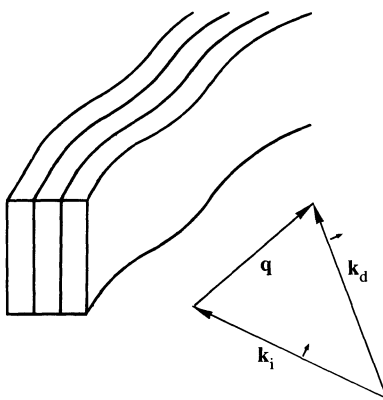


Fig. 8.2. Undulation mode in the planar geometry and scattering geometry for its observation.

Thus,

$$S_A: \frac{1}{\tau_q} = \left(\tilde{B} \frac{q_z^2}{q_x^2} + K_1 q_x^2 \right) / \eta_3, \quad (8.32)$$

$$D_h: \frac{1}{\tau_q} = \left((\widetilde{B+D}) \frac{q_x^2}{q_z^2} + K_3 q_z^2 \right) / \eta_3. \quad (8.33)$$

($\tilde{B} = B - c^2/A$; $B + D = B + D - c^2/A$ as already introduced in Chapter 7). These expressions are valid provided $\tilde{B} q_z^2 \sim K_1 q_x^4$ or

$$\widetilde{(B+D)} q_x^2 \sim K_3 q_z^4. \quad (8.34)$$

Equation (8.32) has been confirmed experimentally in two different geometries:

1. the homeotropic one, between glass slides [12] (Fig. 7.6). In this case the q_z component is quantized by boundary conditions ($q_z = n\pi/D$, if D is the sample thickness). In fact, only the fundamental, $n = 1$, has been observed by light beating spectroscopy, but the q_x dependence is nicely established.
2. The planar geometry (Fig. 8.2): tilting \mathbf{q} slightly with respect to the x direction allows us to check carefully the q_z -dependence of the relaxation time: the parabolic $\tau_q^{-1}(q_z)$ is well borne out by experiment [13].

No equivalent experiments have been performed yet on columnar phases.

Remarks

- With typical thermal diffusivities $K_{\perp}, K_{\parallel} \sim 10^{-4} \text{ cm}^2 \text{ s}^{-1}$, $K_1 \sim 10^{-6} \text{ dyn}$, $\eta_3 \sim 1 \text{ poise}$, $K_1/\eta_3 \ll K_{\parallel}$ and K_{\perp} , the undulation mode in smectics is indeed isothermal.

- In the homeotropic geometry, a one-mode analysis cannot meet all boundary conditions. They can only be satisfied via the introduction of a boundary layer of thickness $\zeta \simeq (\delta/q_x)^{1/2}$ [11]. Within this boundary layer, permeation takes place. In a typical experiment $q_x \simeq 10^2\text{--}10^4 \text{ cm}^{-1}$ and $\delta \simeq 10^{-7} \text{ cm}$ so that $\zeta \simeq 3 \times 10^{-6}$ or $3 \times 10^{-5} \text{ cm}$; this value is much smaller than usual sample thicknesses which explains the success of eqn (8.32).

8.1.5 Permeation mode

The second simple geometry is for $q_x = q_y = 0, q_z \neq 0$ in S_A , or $\mathbf{q}_\perp \neq 0, q_z = 0$ in D_h ; the spontaneous fluctuation modes of the layers or columns are dominated by the permeation process.

To understand this, let us restrict our attention to one simple limiting case. We assume that

1. The changes in density are negligible ($\theta = 0$ and thus $v_z = 0$ as can be seen from eqn (8.17a)).
2. The temperature fluctuations relax faster than the fluctuations of u (isothermal regime again).

With these assumptions (8.17c) reads

$$\dot{u} = \lambda_p g_z \quad (8.35)$$

with g_z given by (8.23) (but with isothermal elastic coefficients) as

$$g_z = \tilde{B} \frac{\partial^2 u}{\partial z^2}. \quad (8.36)$$

Comparing (8.35) and (8.36) we see that the displacement u obeys a simple diffusion equation [1]

$$\dot{u} = \lambda_p \tilde{B} \frac{\partial^2 u}{\partial z^2} \quad (8.37)$$

with a characteristic time

$$\frac{1}{\tau_q} = \lambda_p \tilde{B} q_z^2. \quad (8.38)$$

$\lambda_p \tilde{B}$ has the dimensions of a diffusivity. If we take $\delta = (\lambda_p \eta_3)^{1/2} \sim 10^{-7} \text{ cm}$,[†] $\eta_3 \simeq 1$ poise, and $\tilde{B} \simeq 10^8 \text{ erg cm}^{-3}$ we get $\lambda_p B \simeq 10^{-5} \text{ cm}^2 \text{ s}^{-1}$ that is of the same order of magnitude as a self-diffusion coefficient. If these figures are correct, the mode is indeed isothermal.

[†] Experiment does suggest that δ is of the order of one or several molecular sizes [14–16].

No direct experimental check of the validity of (8.38) (or its equivalent in columnar phases: $1/\tau_q = \lambda(B + D)q_x^2$) has been made to date.

8.1.6 Acoustic waves

When the wavevector \mathbf{q} is oblique with respect to the layers (respectively the tubes), e.g. in the x, z -plane, the situation is very different: the displacement u (respectively u_x) must be associated with some modulation of the interlayer spacing (Fig. 8.3) or tube diameter. Similarly the velocity v_x (respectively v_z) is linked to a bulk dilatation θ . For this reason we expect two types of acoustic waves, describing coupled oscillations of the density and of the interlayer spacing [2]. The following features must be noted.

1. Damping effects are weak: the frequencies are mainly real.
2. Permeation is again negligible.
3. The waves are adiabatic rather than isothermal.

These waves have been observed in S_A , both by acoustical methods [17, 18] and by Brillouin scattering of light [19] (Fig. 8.4). There is currently no comparable work on columnar phases. The dispersion relation can be easily obtained by neglecting all dissipative processes. Equation (8.17) now reads (with again $\exp(i(q_x x + q_z z - \omega t))$ dependences and adopting once again the S_A notation

$$\left. \begin{aligned} i\omega\theta + iq_x v_x + iq_z v_z &= 0 \\ -i\rho\omega v_z &= -iq_z P + g_z \\ -i\rho\omega v_x &= -iq_x P \end{aligned} \right\} \quad (8.39)$$

with $-i\omega u = v_z$, $g_z = -q_z^2 B^0 u + iC^0 q_z \theta$ and $-P = A^0 \theta + iC^0 q_z u$.

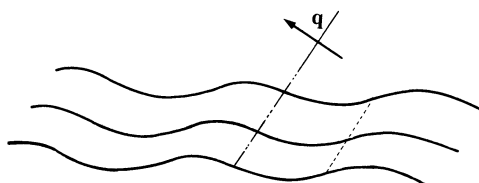


Fig. 8.3. Layer (tube) distortion, corresponding to an oblique wavevector: note that the layer spacing (tube diameter) is modulated (e.g. the thickness is not the same across the dotted and dash-dotted equiphase planes).

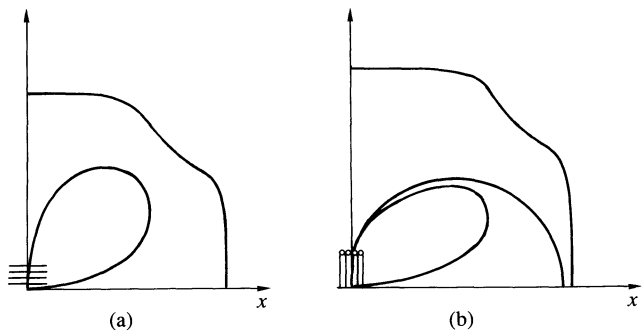


Fig. 8.4. (a) Polar plot of the sound speeds in the S_A phase. (b) Similar plot for columnar phases: note the additional curve, as compared to S_A , corresponding to third sound.

Equation (8.39) has non-zero solutions only if

$$\begin{vmatrix} \omega & q_x & -iq_z\omega \\ iq_z(A^0 + C^0) & 0 & \rho\omega^2 - (B^0 + C^0)q_z^2 \\ q_x A^0 & \rho\omega & iC^0 q_z q_z \end{vmatrix} = 0 \quad (8.40)$$

or

$$(\rho\omega^2)^2 - \rho\omega^2(A^0 q_x^2 + (A^0 + B^0 + 2C^0)q_z^2) + q_z^2 q_x^2 (A^0 B^0 - C^{0^2}) = 0. \quad (8.41)$$

The solution of (8.41) corresponds indeed to two pairs of propagating modes, $\rho\omega_1^2, \rho\omega_2^2$, satisfying

$$\left. \begin{aligned} (\rho\omega_1^2)(\rho\omega_2^2) &= q_z^2 q_x^2 (A^0 B^0 - C^{0^2}), \\ \rho\omega_1^2 + \rho\omega_2^2 &= A^0 q_x^2 + (A^0 + B^0 + 2C^0)q_z^2 \end{aligned} \right\} \quad (8.42)$$

or, introducing the speed of sound $C_i = \omega_i/q$ and the angle f between \mathbf{q} and the optical axis,

$$\left. \begin{aligned} C_1^2 C_2^2 &= \cos^2 f \sin^2 f (A^0 B^0 - C^{0^2})/\rho^2, \\ C_1^2 + C_2^2 &= (A^0 + (B^0 + 2C^0) \cos^2 f)/\rho. \end{aligned} \right\} \quad (8.43)$$

It is clear either from (8.39) or (8.43) that θ and u modulations are coupled in both propagating waves. A falls in general into the 10^{10} erg cm $^{-3}$ range; B and C can vary considerably from one system to the other [20]. Quite often $A \gg B, C$: then the two waves nearly decouple.

$$C_1 \simeq (A^0/\rho)^{1/2} \quad (8.44)$$

defines the speed of the ‘first sound’, which in this limit is essentially a density modulation.

$$C_2 \simeq (B^0/\rho)^{1/2} \sin f \cos f \quad (8.45)$$

defines the speed of the second propagating mode, which now essentially corresponds to a modulation of u . The name ‘second sound’ has been coined by analogy with superfluid helium where it is associated with fluctuations of the phase of a complex order parameter [2]. In smectics A, the displacement u is closely related to a phase (see for instance formula (1.11) and Chapter 10); hence the analogy.

The angular dependence of C_2 is remarkable. Equation (8.45) shows that $C_2 = 0$ when $f = \pi/2$. This mode corresponds to the undulation mode of Section 8.1.4. The continuous evolution from a propagating to an over-damped behaviour, together with the vanishing of the propagation velocity ($\sim \cos f$) have been experimentally confirmed in a forced Rayleigh experiment using the flexoelectric coupling [21]. C_2 vanishes also when $f = 0$, as is clear in Fig. 8.4. This feature was recognized, but left unexplained in reference 2. It has been fully clarified by Martin, Parodi, and Pershan [1]: for $f \rightarrow 0$, permeation effects become very important, and the mode described in Section 8.1.5 takes over.

Note that Brillouin experiments are performed at frequencies that are typically in the gigahertz domain. This does not correspond to our definition of the hydrodynamic regime, since several non-hydrodynamic modes (such as dipolar relaxation, the tilt with respect to the layers, the smectic order parameter mode, etc.) often fall below this frequency. Some of them have been discussed theoretically [22, 23]. The disappearance of the second sound for $f \geq \pi/4$ [19, 22] and the factor of 10 to 30 between the ‘high-frequency’ values of B [19, 24, 25] and the hydrodynamic regime [21] are striking: the smectic is considerably stiffer in the gigahertz range than in the kilohertz range. Measuring the compressional elastic constant is a tricky problem: above 10^6 – 10^7 Hz one gets out of the hydrodynamic regime; below 10^3 – 10^4 Hz defect motions interfere as we will see in the next section.

First and second sound should also exist in columnar phases with the correspondence defined in Section 8.1.3 but, as already pointed out, no experimental results are available to date.

8.1.7 Transverse modes

In smectics A, the transverse mode associated with the velocity v_y corresponds to vorticity diffusion: its characteristic frequency is $\eta_{\text{eff}} q^2 / \rho$, where η_{eff} is a certain average of the friction coefficients α and depends on the angle f ($\eta_{\text{eff}} = \frac{1}{2}(\alpha_4 + \alpha_{56} \cos^2 f)$). It cannot be observed with light scattering techniques but, as will be detailed in Section 8.2.1, can be directly observed in shear flow experiments (in the case $f = \pi/2$).

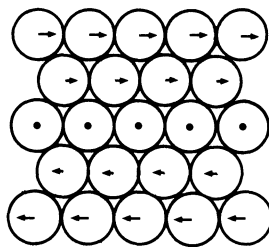


Fig. 8.5. Geometrical nature of third sound in columnar phases for $f = \pi/2$. The tube displacement is similar to that of a two-dimensional shear wave.

Now, since transverse modes sample the structure perpendicularly to the $\mathbf{q}, \hat{\mathbf{z}}$ -plane, the case of columnar phases is different. The relevant equations are easily derived. Setting $v_x, v_z, \theta = 0$ (note that this does not involve any density change), we get (with isentropic constants, in the absence of any temperature gradient and neglecting dissipation and bend)

$$\left. \begin{aligned} \frac{\partial u_y}{\partial t} - v_y &= 0, \\ \rho \frac{\partial v_y}{\partial t} &= g_y, \end{aligned} \right\} \quad (8.46)$$

and $g_y \simeq -D^0 q_x^2 u_y$ (with $\exp(i(q_x x + q_z z - \omega t))$ dependences again).

This leads to the dispersion relation

$$\rho \omega^2 = D^0 q_x^2, \quad (8.47)$$

i.e. a propagating wave of velocity

$$v_3 = (D^0 / \rho)^{1/2} \sin f. \quad (8.48)$$

Thus in columnar phases there is one more propagating mode than in smectics: it corresponds to a shear of the columns (Fig. 8.4(b)). In particular, for $f = \pi/2$, it has exactly the structure of a shear wave in two-dimensional crystals (Fig. 8.5). We can call it ‘third sound’, although it does not correspond to what is called third sound in liquid helium.[†]

For f small enough, it splits into a nematic-like undulation mode $\omega_r = K_3 q_z^2 / \eta_u$, and a vorticity diffusion one $\omega_v = \eta q_z^2 / \rho$.

8.1.8 $S_{B\text{hex}}$ and S_C hydrodynamics

There are two extra hydrodynamic variables as in the case of columnar phases but the difference is that one is of nematic (Ω_z) and the other of smectic type (\mathbf{u}).

[†] In bulk liquid helium there are only two propagating waves. What is called third sound exists in thin films only.

The general equations follow again directly from the considerations developed in Section 8.1.2 [1]

$$-\frac{\partial \theta}{\partial t} + \partial_\alpha v_\alpha = 0, \quad (8.49a)$$

$$\frac{\partial \varepsilon}{\partial t} + \frac{\partial \theta}{\partial t} (\varepsilon + P) = K_{\alpha\beta} \partial_{\alpha\beta}^2 T - \mu_{\alpha z} \partial_\alpha g_z, \quad (8.49b)$$

$$\frac{\partial u}{\partial t} - v_z = -\mu_{z\beta} \frac{\partial_\beta T}{T} + \lambda_p g_z, \quad (8.49c)$$

$$\frac{\partial \Omega_z}{\partial t} - B_{z\beta\gamma} \partial_\gamma v_\beta = -vh_z, \quad (8.49d)$$

$$\rho \frac{\partial v_\alpha}{\partial t} = -\partial_\alpha P + g_\alpha - B_{z\alpha\beta} \partial_\beta h_z + \eta_{\alpha\beta\gamma\delta} \partial_{\gamma\delta}^2 v_\beta. \quad (8.49e)$$

Clearly, from the definitions (8.3) and (8.15), $g_x = g_y = h_x = h_y = 0$. Equations (8.49) are quite similar to (8.17) if one excepts the Ω_z equation.

In $S_{BH_{hex}}$ the dissipative coefficients are identical to that of S_A , aside from the addition of the angular viscosity v^{-1} . (The minus sign in front of v is introduced for convenience.) The $B_{z\beta\gamma} \partial_\gamma v_\beta$ expression is particularly simple,

$$B_{z\beta\gamma} \partial_\gamma v_\beta = \frac{1}{2}(\partial_x v_y - \partial_y v_x). \quad (8.50)$$

Like the first term of the right-hand side of (8.12), it expresses the background rotation.

In S_C there are four thermal conductivity ($K_{zz}, K_{xx}, K_{yy}, K_{zx} = K_{xz}$), two Soret (μ_{zz}, μ_{xz}), and 13 viscosity coefficients! There are *a priori* four $B_{z\beta\gamma}$ allowed by symmetry: $B_{zxy}, B_{zyx}, B_{zyz}, B_{zzy}$. Expressing the fact that solid-body rotation cannot dissipate energy requires $B_{zxy} - B_{zyx} = 1/2$; $B_{zyz} = B_{zzy}$. Thus, (8.49d) can be written

$$\frac{\partial \Omega_z}{\partial t} - \frac{1}{2}(\partial_x v_y - \partial_y v_x) - \frac{b_1}{2}(\partial_x v_y + \partial_y v_x) - \frac{b_2}{2}(\partial_z v_y + \partial_y v_z) = -vh_z. \quad (8.51)$$

Just as in nematics, velocity gradients exert torques on the \mathbf{c} director. One can get further insight, using a version of (8.51) (assuming the layers unperturbed) in which the reference axes in the layers plane are arbitrary,

$$\frac{\partial \Omega_z}{\partial t} - \frac{1}{2}(\text{curl } v)_z - b_1 c_\alpha p_\beta A_{\alpha\beta} - b_2 p_\alpha A_{z\alpha} = -vh_z, \quad (8.52)$$

$$A_{\alpha\beta} = \frac{1}{2}(\partial_\alpha v_\beta + \partial_\beta v_\alpha).$$

$\mathbf{c}, \mathbf{k}, \mathbf{p}$ obey the definitions given in Chapter 7, i.e. they are, respectively, tilt direction, normal to the layers, and $\mathbf{p} = \mathbf{k} \times \mathbf{c}$.

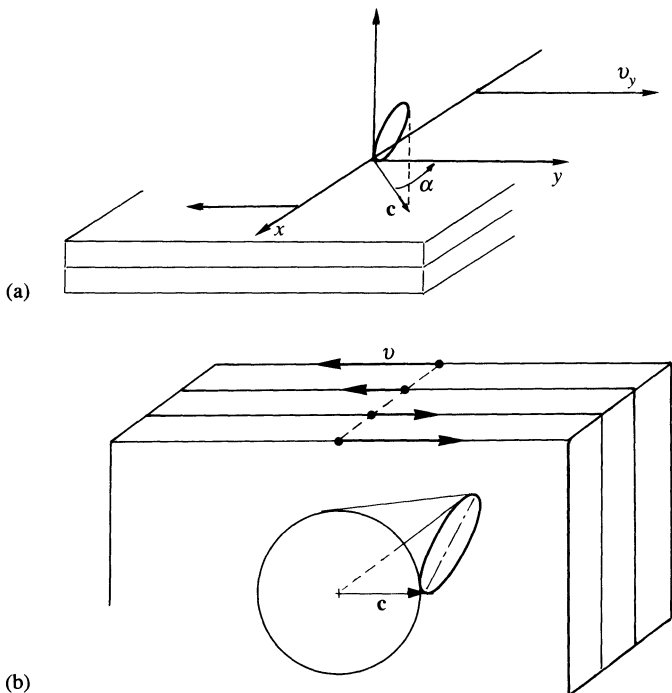


Fig. 8.6. Typical geometries coupling flow and c director in S_C^* . (a) Shear in the x, y -plane; (b) shear in the x, z -plane.

Let us first consider the action of a simple shear: $\partial_x v_y \neq 0$, $v_x = v_z = 0$, $\partial_y = \partial_z = 0$, $\mathbf{k} = \hat{\mathbf{z}}$ (Fig. 8.6(a)) where x is an arbitrary direction in the plane orthogonal to \mathbf{k} . A necessary condition for reaching a stationary state is

$$(b_1 + 1)p_y c_x \partial_x v_y + (b_1 - 1)p_x c_y \partial_x v_y = 0. \quad (8.53)$$

Or, introducing the angle α between the c director and the velocity field v_y , one finds that the simple shear $\partial_x v_y$ aligns the c director in a direction defined by

$$\cos 2\alpha = 1/b_1. \quad (8.54)$$

This relation is exactly the same as the one obtained in nematics (Section 5.2.3) if we identify b_1 with $\lambda = -\gamma_2/\gamma_1$ [26]. Note that the flow alignment in the direction defined by (8.54) will be stable only if $|b_1| > 1$. A well defined experimental geometry allowing us to probe (8.54) will be described in the next section [27].

Suppose now that $\partial_z v_x \neq 0$, $v_y = v_z = 0$ (Fig. 8.6(b)). The necessary condition for steady state reads simply $p_x = 0$: that is the tilt direction is aligned in the shear plane. (Note that a stable equilibrium will always be reached, which depends on the $b_2 \partial_z v_x$ sign; similar considerations would

hold with $\partial_x v_z \neq 0$, but the situation is harder to achieve since it requires permeation.)

The mode structure resulting from (8.49) may be guessed without much calculations [1]. We have seen in Section 8.1.6 that propagating modes resulted from the existence of first-order elastic constants in smectics A. Since these are identical in S_A and S_C one expects two pairs of propagating sounds in S_C just as in S_A . Only the dissipation and the behaviour in non-propagating directions should differ.

Note that, in general, Ω_z and \mathbf{u} are coupled (remember F_{cs} in Chapter 7) and, since Ω_z and the transverse velocity field are also coupled, in general, all polarizations are mixed in S_C . The situation is simpler for wavevectors in the x, z -plane: modes polarized in this plane mimic closely the S_A behaviour; those polarized in the y direction involve the velocity field v_y and Ω_z (equivalently the \mathbf{c} director): as in nematics it can be split into a fast vorticity diffusion mode and a slow one corresponding to the director reorientation.

To sum up: first and second sound, thermal and vorticity diffusion plus a nematic-like mode. The same holds for $S_{BH_{ex}}$, in which y -polarized modes are fully decoupled from x, z -polarized ones (for wavevectors in the x, z -plane [28]).

Problem. Derive hydrodynamic equations for the chiral smectics C* [29].

Solution. First question. What are the hydrodynamic variables? Obviously the conserved quantities are the same as in any other system and the layer displacement variable has also to be kept. What about the rotation Ω_z ? We have seen that in the ground state (eqn (7.25))

$$\Omega_z = q_0 z + \text{const} = q_0(z - z_0). \quad (8.55)$$

A homogeneous rotation $\delta\Omega_z$ of this structure changes neither the energy, nor the layer displacement: it is thus an independent hydrodynamic variable just like in ordinary S_C . However, it is clear from (8.55) that a homogeneous $\delta\Omega_z$ is equivalent to a translation $\delta z_0 = -q_0^{-1} \delta\Omega_z$ of the origin; in other words one could equivalently use a helix displacement variable $u_h = \delta\Omega_z q_0^{-1}$. This shows that, because of the helicoidal precession, $\delta\Omega_z$ has simultaneously the character of variables stemming from translational and rotational broken symmetry. Indeed, the helical pitch defines a period along the normal to the layers which is incommensurate† with the layer spacing, and one can consider that translational symmetry is ‘broken twice’ in this direction.

Second question. How does the existence of a macroscopic polarization affect the behaviour of S_C^* ? We have seen in the preceding chapter that the polarization vector is always perpendicular to the normal to the layers and the tilt direction; furthermore, its magnitude is a thermodynamic quantity determined by temperature and pressure. Thus it is not a new hydrodynamic variable. On the other hand, from (7.94) and

† This means that in general $(q_0 a)/2\pi = \text{irrational number } (a, \text{ smectic layer spacing})$.

(7.96) one sees that deformations are coupled with electric fields. Thus, to understand the dynamics of S_C^* , one needs to use not only the hydrodynamic equations but also the Maxwell equations.

Equations (8.14) and (8.16) can be used directly. Keeping in mind that $\delta\Omega_z$ has a mixed rotation translation character one gets

$$\left. \begin{aligned} -\frac{\partial\theta}{\partial t} + \partial_\alpha v_\alpha &= 0, \\ \frac{\partial\varepsilon}{\partial t} + \frac{\partial\theta}{\partial t}(\varepsilon + p) &= K_{\alpha\beta} \partial_{\alpha\beta}^2 T + K'_{\alpha\beta} \partial_\beta E_\alpha - \mu \partial_z g_z + \mu' \partial_z h_z, \\ \frac{\partial u}{\partial t} - v_z &= -\mu \frac{\partial_z T}{T} + \eta E_z + \lambda_p g_z - \lambda'_p h_z, \\ \frac{\partial\Omega_z}{\partial t} - q_0 v_z - \frac{1}{2}(\partial_x v_y - \partial_y v_x) &= v h_z - \lambda'_p g_z + \mu' \frac{\partial_z T}{T} + v' E_z, \\ \rho \frac{\partial v_\alpha}{\partial t} &= -\partial_\alpha p + (g_z - q_0 h_z) \delta_{\alpha z} + \frac{1}{2}\varepsilon_{\alpha\beta\gamma\delta} \partial_\beta h_z + \eta_{\alpha\beta\gamma\delta} \partial_{\gamma\delta}^2 v_\beta \\ J_\alpha &= \sigma_{\alpha\beta} E_\beta + K'_{\alpha\beta} \left(-\frac{\partial_\beta T}{T} \right) + (\eta g_z - v' h_z) \delta_{\alpha z} \end{aligned} \right\} (8.56)$$

where h_z and g_z are given by (8.3) and (8.15) as before. J_α is the electric current density; $K_{\alpha\beta}$, $K'_{\alpha\beta}$, $\sigma_{\alpha\beta}$ have a structure typical of uniaxial systems. These equations are fairly comparable to what we wrote for S_C . The main differences lie in the following.

- In the reactive term of $\partial\Omega_z/\partial t$, both velocity along and rotation around z have to be subtracted off.
- In the couplings. A strain gradient ($g_z \neq 0$) can induce a rotation and, conversely, a torque h_z can create a layer motion. Note, however, that for q_0 small compared to typical inverses of a molecular length these couplings should be small. The same remark holds for all primed coefficients, although they do not need to vanish with q_0 .[†] Note that the electric field can interact with the molecular orientation via two mechanisms: a reactive one linked to polarization (either spontaneous or induced) and a diffusive one which is reminiscent of the thermomechanical coupling in cholesterics.
- In the fact that electric fields cannot be omitted even in the absence of applied fields. Indeed, polarization charges develop and change the long-wavelength behaviour: we have seen in the preceding chapter that the dispersion relation involving the bend mode of the \mathbf{c} director involves a term linear in q (eqn (7.56)) (for two-dimensional deformations).

It should be kept in mind that these equations are valid in the long-wavelength limit, i.e. for wavelengths large compared to the helical pitch $2\pi/q_0$. At this scale the D_∞ symmetry is restored; this simplifies the tensorial nature of coupling coefficients

[†] They will if q_0 vanishes together with chirality (i.e. racemic mixture); on the other hand for an accidental vanishing of q_0 they have no reason to disappear.

but considerably restricts the utility of this approach. We will come back on this point in Section 8.2.3.2.

8.1.9 Remarks on the mode structure

As pointed out in Section 8.1.2, the number of modes in a given system equals the number of hydrodynamic variables. There are five in isotropic fluids, six in smectics A, seven in smectics $B_{B\text{Hex}}$, C and columnar phases, and eight in crystals (Table 8.1). In crystals the mode structure is particularly simple:

1. three propagating waves (i.e. six modes: remember propagating modes occur in pairs);
2. thermal conduction and permeation, which both are diffusive;
3. for a total of eight, this result holds irrespective of the wavevector orientation to the crystal axes.

In simple fluids one counts

4. one propagating wave (first sound);
5. thermal and vorticity (two polarizations) diffusion.

A total number of five. For binary mixtures one would have to add a sixth diffusive mode, corresponding to mass diffusion of one compound with respect to the other.

Depending on the wavevector orientation with respect to the layers normal \mathbf{n}_0 , smectics A behave either:

- like superfluid helium ($\mathbf{k} \cdot \mathbf{n}_0 \neq 0$, $\mathbf{k} \times \mathbf{n}_0 \neq 0$): two propagating (first and second sound) + two diffusive modes (vorticity and thermal diffusion);
- like a binary mixture: one propagating (first sound) + four diffusive modes. These are:
 1. $\mathbf{k} \cdot \mathbf{n}_0 = 0$: vorticity (two polarizations), thermal diffusion, and layer undulations.
 2. $\mathbf{k} \times \mathbf{n}_0 = 0$: vorticity (two polarizations), thermal diffusion, and permeation.

Smectics $B_{B\text{Hex}}$ and C behave pretty much like S_A with the addition of a nematic-like director mode. The most remarkable behaviour is provided by columnar phases (\mathbf{n}_0 = column axis).

- $\mathbf{k} \cdot \mathbf{n}_0 \neq 0$; $\mathbf{k} \times \mathbf{n}_0 \neq 0$: three propagating modes (first, second, third sounds) + one diffusive (thermal diffusion). This is reminiscent of crystals (if one subtracts off permeation), but the anisotropy is that of smectics for the modes polarized in the \mathbf{k} , \mathbf{n}_0 -plane.

- $\mathbf{k} \cdot \mathbf{n}_0 = 0; \mathbf{k} \times \mathbf{n}_0 \neq 0$: two propagating modes (first and third sounds) + three diffusive (thermal, vorticity diffusion + permeation). This structure is similar to $S_{BH_{ex}}$ or S_C for ordinary wavevectors.
- $\mathbf{k} \cdot \mathbf{n}_0 \neq 0; \mathbf{k} \times \mathbf{n}_0 = 0$: one propagating mode (first sound) + five diffusive (thermal, vorticity, two polarizations) + undulation modes (two polarizations). For a wavevector along the tube axis, columnar phases behave like a nematic!

Thus liquid crystals (and in particular columnar phases) give rise to the most anisotropic hydrodynamic behaviour known to date.

8.2 FLOW PROPERTIES

The existence of crystalline order in at least one direction of space manifests itself most dramatically in flow properties. In the following we choose to discuss a few illustrative examples rather than give a complete overview of the problem.

8.2.1 Typical geometries

They are summarized in Fig. 8.7 and Table 8.2; a pressure gradient of well defined direction forces a flow parallel to it. Any time the velocity field probes a liquid-like direction, a Poiseuille flow is expected as in isotropic fluids or nematics (parabolic shape of the velocity profile). Any time the velocity field probes a crystal-like direction, plug flow is expected just as in cholesterics with velocity along the helix axis (Chapter 6). The plug flow velocity profiles reads

$$v_1 = \lambda_p \frac{\partial P}{\partial x_1} \left(1 - \frac{\cosh(z/\delta)}{\cosh(d/2\delta)} \right). \quad (8.57)$$

Table 8.2. Characteristics of geometries (a)–(f) shown in Fig. 8.7.

Geometry	Type of flow	Viscosity	Boundary layer	Velocity component
a	Poiseuille	η_3		v_x
b	Poiseuille	$\alpha_4/2$		v_x
c	Plug	η_3	$\delta = (\lambda_p \eta_3)^{1/2}$	v_z
d	Poiseuille	η_3		v_z
e	Plug	η_3	$\delta = (\lambda_p \eta_3)^{1/2}$	v_x
f	Plug	$\alpha_4/2$	$\delta = (\lambda_p \alpha_4/2)^{1/2}$	v_x

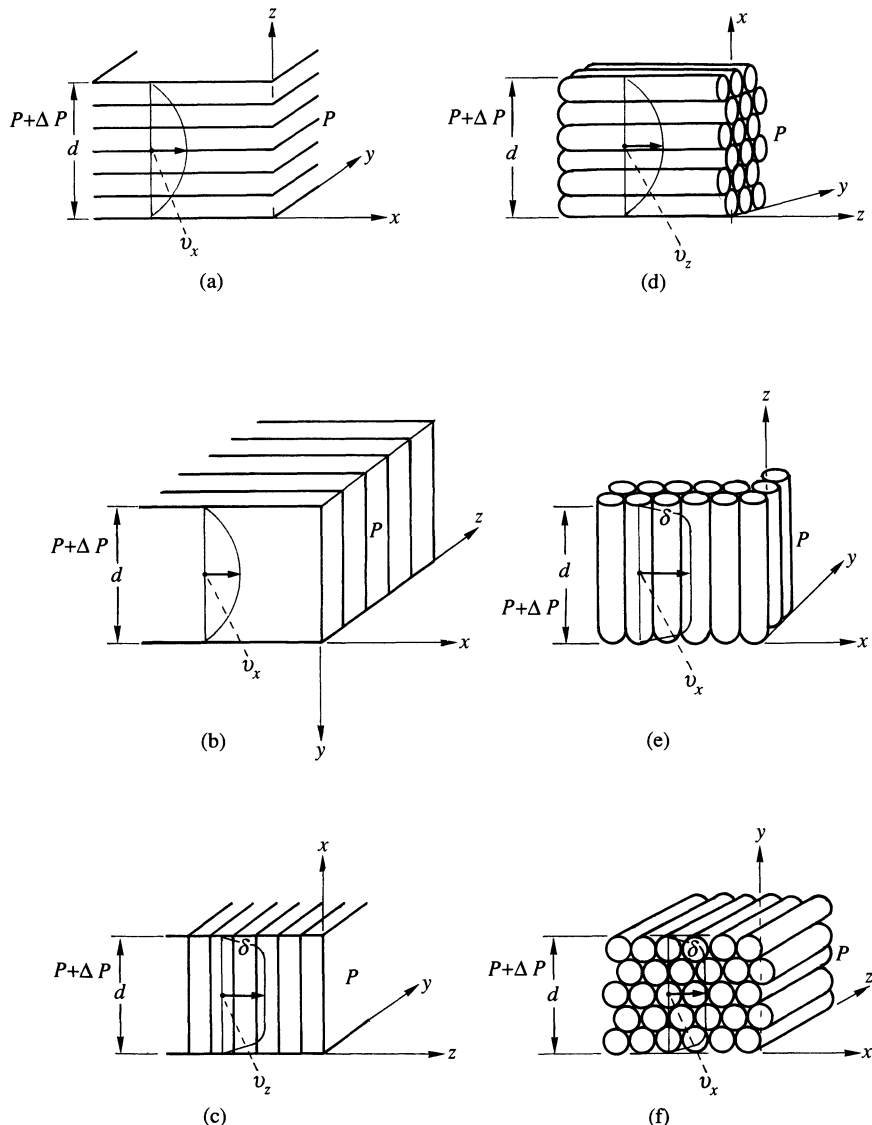


Fig. 8.7. Characteristic geometries for smectics A and columnar D_h phases. In all cases, a pressure head Δp is applied on the left part of the sample, to promote the flow. (a)–(c) Smectics: (a) velocity parallel, gradient perpendicular to the layers; (b) velocity and gradient parallel to the layers; (c) velocity perpendicular, gradient parallel to the layers. (d)–(e) Columnar phases: (d) velocity parallel, gradient perpendicular to the columns; (e) velocity perpendicular, gradient parallel to the columns; (f) velocity and gradient perpendicular to the columns. According to generalized hydrodynamic theories, Poiseuille flow should prevail in geometries (a), (b), and (d), and plug flow in geometries (c), (e), and (f).

As already quoted in Section 8.1.4, δ is of the order of a molecular length far from the nematic phase, and (8.57) is in most cases equivalent to Darcy's law. However, upon approaching the nematic phase, δ is expected to diverge; in principle, one could be able to achieve $d \ll \delta$ close enough to the transition temperature. The limit of (8.57) (in case (c) of Fig. 8.7) is then

$$v_z = \frac{\eta_3^{-1}}{2} \frac{\partial P}{\partial z} (z^2 - d^2/4) \quad (8.58)$$

which is just Poiseuille flow.

What is the experimental situation? Basically nothing is known for columnar phases. Geometries (a), (b), and (c) have been tested with smectics A [30, 31].

Geometry a Although the parabolic profile has not been checked experimentally, one can say that observations are roughly consistent with theoretical expectations. The observed flow is essentially Newtonian (the values of η_3 obtained are basically independent of shear rate, and comparable, although larger, to the nematic ones) [31]. There is, however, a sizeable difficulty in this geometry: the thickness d has to be kept constant over the whole sample with an accuracy better than $2\pi\lambda = 2\pi\sqrt{(K_1/B)} \simeq 100$ to 200 Å! This is not achievable currently in the usual viscometric set-up. Indeed, if thickness variations larger than $2\pi\lambda$ exist, during the flow the system will be alternatively dilated and compressed by the same amount: in the absence of dislocations when an integrated dilatation larger than $2\pi\lambda$ is reached, the buckling instability arises and eventually focal conic arrays appear [30].

Simple shear experiments [32] show the same behaviour. In fact, for low enough shear rates, dislocations can relax stresses due to thickness inhomogeneities. But they do contribute to dissipation and it is hard to know exactly what is their contribution to the apparent η_3 . The role of screw dislocations has also been discussed [33].

The experimental situation of Fig. 8.8 is more satisfactory in that, with a lateral displacement of the order of a few 10^2 Å, a plate parallelism of 10^{-4} rad, and thicknesses of 10^2 μm, residual strains ($\delta d/d$) as small as 10^{-8} can be achieved [34]. Even so, in the absence of dislocation motion, the residual normal stress† would be $\sigma_{zz} = B(\delta d/d) \simeq 1 \text{ erg cm}^{-3}$ (with $B \simeq 10^8 \text{ erg cm}^{-3}$), whereas the viscous stress $\sigma_{xz} = \eta_3(\partial v_x / \partial z) \simeq 10^{-4} \text{ erg cm}^{-3}$ (with $\eta_3 \simeq 1 \text{ poise}$, v_x corresponds to a lateral displacement of 10^2 Å at 1 Hz and with the same thickness). Thus, even if the detector had a sensitivity 10^4 larger for the x, z -component than for the z, z -component the two would contribute to the same degree to the measurement! Experimentally, a purely viscous behaviour is found: clearly, dislocation motion is

† In the following we use B for \tilde{B} to keep notation simple.

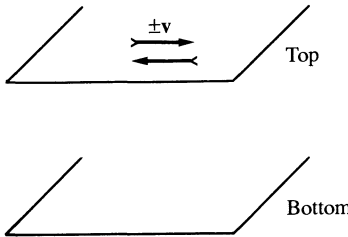


Fig. 8.8. An alternative way to probe flow properties of smectics or columnar phases is to force a controlled periodic motion of, say, the upper plate of a sample (at a given frequency) and synchronously detect the stress transmitted on the lower plate. The geometry can be any of the ones displayed in Fig. 8.7 [34].

again required to keep σ_{zz} low enough to prevent any interference with the σ_{xz} measurement. The factor of three to four difference in $\eta_u(\omega)$ between 1 Hz and 1 kHz may also be due precisely to the contribution of dislocation motion to the dissipation.

Geometry b As far as flow is concerned, this geometry is more puzzling. One does not find a purely viscous behaviour, but rather that of a Bingham plastic [31].

- Below a critical stress σ_0 no flow is observed.
- Above σ_0 the stress-shear relation is compatible with

$$\sigma_{xy} = \frac{\alpha_4}{2} \partial_x v_y + \sigma_0.$$

α_4 is found to be of the order of the nematic value (slightly higher), it is history-dependent. The smallest values are found after a vigorous flow, and measurements after annealing give larger values (typically a 15-min delay adds up to 20 per cent to the value). This is again an indication that defects play a role in the flow process, although at first glance this geometry seems the best suited for displaying the two-dimensional liquid character of the smectic layers. In fact, in this geometry, edge dislocations can cross the sample over the whole thickness and be pinned at the walls; this may be sufficient to transfer part of the normal stress in the x direction: dislocations cannot move freely to relax stress. Under those conditions, residual strains corresponding to a mismatch of one or a few layers may well subsist: $\sigma_{zz}^{\text{res}} \simeq B(na_0/L) \simeq n \cdot 30 \text{ erg cm}^{-3}$ (with a_0 = layer thickness = $3 \cdot 10^{-7}$; L -width of the capillary $\simeq 1 \text{ cm}$). The yield stress σ_0 experimentally found corresponds to a fraction of σ_{zz}^{res} ($\sigma_0 \sim 10 \text{ erg cm}^{-3}$) [31]. More subtle explanations of the existence of σ_0 have been put forward which are connected with the breakdown of hydrodynamics [35]: they are ruled out when all non-linearities are consistently taken into account [36].

Results obtained with the a.c. shearing technique of Fig. 8.8 have, on the other hand, confirmed the theoretical expectation of a viscous behaviour, and basically no frequency dependence is found for α_4 [37]. This shows the importance of working with small displacements in smectics and is a strong reminder of the validity range of linearized hydrodynamic theories discussed at the beginning of this chapter.

Geometry c Far from the nematic phase, the main observation is the absence of flow, unless the pressure head is large enough to break the layers [30, 31]. This is not in itself a proof of the existence of permeation. However, by a careful study of the nematic-smectic A phase change, Léger and Martinet have been able to give a good indication of the switch from the Poiseuille situation (8.58) at the transition, to the plug flow (8.57) with $\delta \ll d$, 0.3 K only away from it: the apparent viscosity is basically 150 times larger than η_3 measured in geometry a! One can estimate a permeation constant λ_p of the order of 10^{-8} – 10^{-9} g⁻¹ cm³ s, and a characteristic length $\delta \simeq 0.5$ µm. δ is large compared to molecular dimensions, but a linear extrapolation in $(T_{NA} - T)$ where T_{NA} is the N-S_A transition temperature gives $\delta_0 \sim 40$ Å, 30 K, away from T_{NA} , which is consistent with our previous estimate.[†]

In principle, the a.c. technique, with a displacement perpendicular to the plate, could, with suitable boundary conditions, be sensitive to the permeation process [39, 40] but here again defects play an important role that is hard to assess.

Geometry e We have said that basically nothing was known about the behaviour of columnar phases. This is true as far as the macroscopic flow properties are concerned, but not for the a.c. technique. Reasonably good e type macroscopic alignment has been achieved [41]. From generalized hydrodynamic theory one would expect a viscous behaviour controlled by η_3 . Nature is nasty since one observes an elastic behaviour! We have already pointed out in the preceding chapter that an optically homogeneous sample is not synonymous to a monocrystal in hexagonal columnar phases: there is a finite grain boundary density spanning the sample from top to bottom. Let us call l the average size of the grain boundaries going all the way through the sample (Fig. 8.9(a), (b)) and let us call w the grain boundary energy per unit surface. The excess energy F_e per unit surface of the sample is given by the excess energy of a grain (i.e. $w \cdot ld$), times the number of grains per unit surface (i.e. l^{-2}); $F_e \simeq w(d/l)$.

A displacement δ of the top interface with respect to the bottom increases the energy to: $F'_e \simeq w(d^2 + \delta^2)^{1/2}/l$. Thus $F'_e - F_e \simeq w(\delta^2/ld)$.

[†] In fact a better extrapolation would follow a $(T_{NA} - T)^{0.66}$ law [38] and yield $\delta_0 \sim 200$ Å which is still a microscopic number.

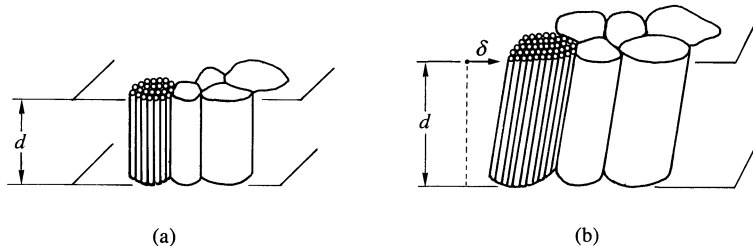


Fig. 8.9. Typical ‘microscopic’ aspect of an optically homogeneous uniaxial columnar sample. Each bundle is a microcrystal that shares only the z axis with its neighbours; two adjacent bundles are separated out by a grain boundary, characterized by a surface energy w . (a) Before shearing uniaxiality requires the grain boundaries to be on the average orthogonal to the sample surfaces; (b) after the shear δ of the upper plate, the grain surface has increased, which costs energy.

If the sample were characterized by a shear elastic constant c_{44} , the energy increase would read

$$\delta F_e = \frac{c_{44}}{2} \int \left(\frac{\partial u_x}{\partial z} \right)^2 dz = \frac{c_{44}}{2} d \left(\frac{\delta}{d} \right)^2.$$

Thus the grain boundary density gives rise to an apparent shear elastic constant

$$c_{44}^{\text{eff}} = \frac{2w}{l}.$$

The experimental value $c_{44}^{\text{eff}} \simeq 10^6 \text{ erg cm}^{-3}$ [41] with a reasonable w ($w \simeq B_x a_0 \simeq 10^2 \text{ erg cm}^{-2}$) gives an average size of the order of microns for the grains.

When the displacement is orthogonal to the plates, one expects at low frequency a purely dissipative behaviour since one probes the liquid-like direction of the columns. However, for this behaviour to be observed, molecules must have time to permeate through the columns. At higher frequencies one should get the elastic response discussed in the preceding chapter. This corresponds basically to the findings [41], but the cross-over frequency between elastic and dissipative behaviour is probably more linked to dislocation motion than to permeation.

8.2.2 Flow past obstacles

8.2.2.1 General considerations

Again this question has been addressed only in smectics A [11]. The difference with conventional fluids is striking, and comes from the existence of the characteristic length δ linked to permeation.

For:

1. steady-state flows;
2. static layer patterns, only slightly disturbed from their flat equilibrium state;
3. absence of emission of dislocations;
4. incompressible smectics;

the hydrodynamic equations (8.17) reduce to

$$0 = -\frac{\partial P}{\partial z} + \eta_3 \left(\frac{\partial^2}{\partial x^2} + \frac{\partial^2}{\partial y^2} + \beta_{\parallel} \frac{\partial^2}{\partial z^2} \right) v_z - v_z / \lambda_p, \quad (8.59a)$$

$$0 = -\frac{\partial P}{\partial x} + \eta_3 \left(\beta_{\perp} \left(\frac{\partial^2}{\partial x^2} + \frac{\partial^2}{\partial y^2} \right) + \frac{\partial^2}{\partial z^2} \right) v_x, \quad (8.59b)$$

$$0 = -\frac{\partial P}{\partial y} + \eta_3 \left(\beta_{\perp} \left(\frac{\partial^2}{\partial x^2} + \frac{\partial^2}{\partial y^2} \right) + \frac{\partial^2}{\partial z^2} \right) v_y. \quad (8.59c)$$

$\beta_{\parallel} = v_1 \eta_3$ and $\beta_{\perp} = (\alpha_4 / 2\eta_3)$ are assumed to be of order unity in the following. We include in the pressure P the term $(\alpha_7 + (\alpha_{56}/2)) \partial v_z / \partial z$ and note that

$$\tilde{v}_1 = \alpha_1 + \frac{\alpha_4}{2} + \alpha_{56}.$$

Condition 2 simply states that, since linearized hydrodynamics is used, the distortions considered have to be small. Note that one could well have a locally highly distorted state. Provided that the range of the non-linear distortion is finite (say, restricted to a linear dimension L) and that dislocation loops are not emitted far away from this region, the following discussion applies outside a domain of typical linear dimension $(L + 2\delta)$ (of course, a specific model for the dissipation inside the domain would have to be constructed).

The example of the permeative flow in a capillary (geometry c of Fig. 8.7) shows the existence of two regimes, when δ is small compared to the capillary thickness.

1. A region close to the boundary in which viscous friction is important and allows the fulfilment of the $v_z = 0$ boundary condition (i.e. velocity tangent to the wall and in the plane normal to the layers). It was called the proximal region in reference 11; eqn (8.57) shows that its extent is controlled by the characteristic length δ .
2. The rest of the capillary where $v_z = \lambda_p \partial P / \partial z$ holds with an excellent approximation. This domain has been called the distal region.

It is clear from (8.57) that this analysis in terms of two different scales, is valid provided $s = d/\delta \gg 1$. In the following we generalize the analysis of the distal field to obstacles of arbitrary shape (with the restrictions already mentioned) in the case $s = L/\delta \gg 1$ (L being a typical length scale in the problem: the linear size of the obstacle in simple cases, boundary layer thickness in others).

The starting point is the recognition that, in the distal region,

$$\frac{\partial P}{\partial z} = -v_z/\lambda_p. \quad (8.60)$$

One easy way to understand this is to look at the Fourier transform of (8.59a)

$$\frac{\partial P}{\partial z}(\mathbf{q}) = -\frac{v_z(\mathbf{q})}{\lambda_p} [1 + \delta^2(q_\perp^2 + \beta_{||} q_z^2)].$$

If we are interested in length scales larger than L , this means that q is bounded by an upper limit L^{-1} [i.e. $\delta^2 q^2 < d^2/L^2 \ll 1$] and thus

$$\frac{\partial P}{\partial z}(\mathbf{q}) = -\frac{v_z(\mathbf{q})}{\lambda_p}$$

neglecting terms of order $1/s^2$ [†] which is just the Fourier transform of (8.60).

Equation (8.60) along with (8.59b) and (8.59c) and together with the incompressibility condition provide the basic set of equations allowing us to discuss the distal region. Two cases have to be considered separately.

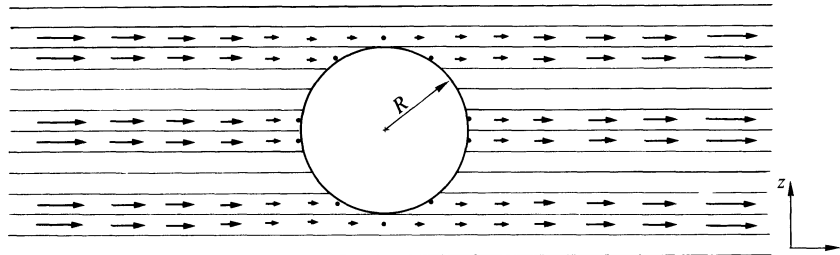
1. The obstacle does not perturb the flow at infinity. As an illustration we will consider a sphere moving along the x direction (Fig. 8.10).
2. The perturbation assumes the shape of a boundary layer going to infinity. We will illustrate this case with the problem of flow in the x direction past a semi-infinite rigid z , y -plane (Fig. 8.11) [16].

8.2.2.2 Flow past a sphere

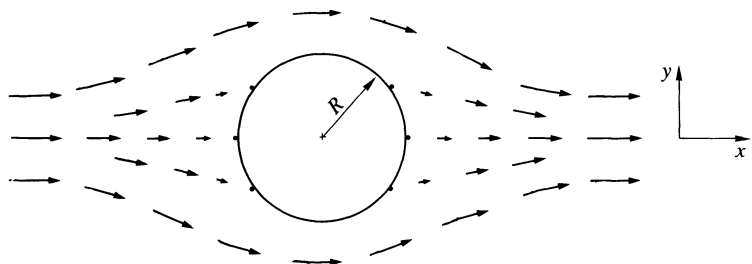
Eliminating pressure between (8.59a) and (8.59b), one gets (with x' (respectively, y' , $z' = x/R$ (respectively y/R , z/R) where R = sphere radius and $s = R/\delta$)

$$\begin{aligned} \frac{\partial v_z}{\partial x'} = \frac{1}{s^2} \left(\frac{\partial}{\partial x'} \left[\beta_{||} \frac{\partial}{\partial z'^2} + \left(\frac{\partial^2}{\partial x'^2} + \frac{\partial^2}{\partial y'^2} \right) \right] v_z \right. \\ \left. - \frac{\partial}{\partial z'} \left[\frac{\partial^2}{\partial z'^2} + \beta_\perp \left(\frac{\partial^2}{\partial z'^2} + \frac{\partial^2}{\partial y'^2} \right) \right] v_x \right), \end{aligned}$$

[†] Note: for $L \sim 10 \mu\text{m}$, $\delta \sim 100 \text{ \AA}$, $s \sim 10^3$ and thus $1/s^2 \sim 10^{-6}$, the approximation is quite good!



(a)



(b)

Fig. 8.10. Flow past a sphere in the distal region. (a) Note that $v_z = 0$ everywhere; (b) the in-plane flow is qualitatively similar to that of a usual liquid.

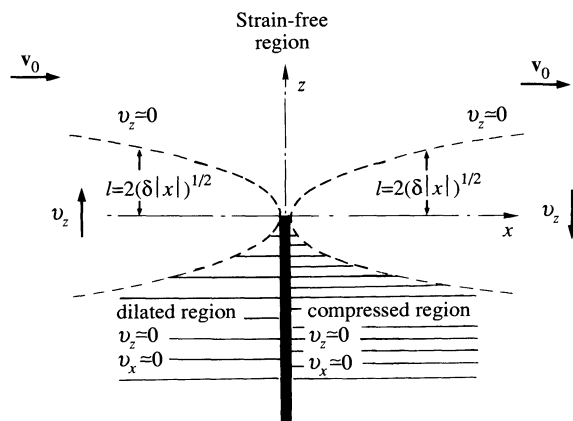


Fig. 8.11. Flow past a semi-infinite rigid z, y -plane extending in the $z < 0$ domain. Note that v_z is non-zero only in a parabolic boundary layer of width $2l$, indicated by the dotted lines.

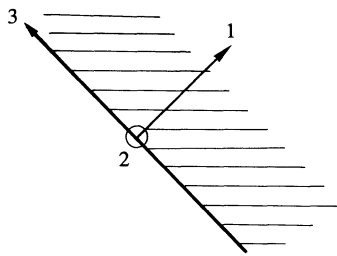


Fig. 8.12. Boundary conditions in the distal regime according to reference 11.

which, to order $1/s^2$, is simply

$$\frac{\partial v_z}{\partial x} = 0.$$

Similarly, $\partial v_z / \partial y = 0$. Thus in the distal region v_z is a function of z only. If the velocity field is homogeneous at infinity in all directions, one deduces

$$v_z = \text{const} \quad (8.61)$$

and the incompressibility condition now reads

$$\frac{\partial v_x}{\partial x} + \frac{\partial v_y}{\partial y} = 0, \quad (8.62)$$

which allows us to introduce the stream function such that

$$v_x = \frac{\partial \psi}{\partial y}, \quad v_y = -\frac{\partial \psi}{\partial x}. \quad (8.63)$$

Combining (8.59b) and (8.59c) after taking the proper derivatives yields the basic equation for the stream function,

$$0 = \left(\frac{\partial^2}{\partial z^2} + \beta_{\perp} \left(\frac{\partial^2}{\partial x^2} + \frac{\partial^2}{\partial y^2} \right) \right) \left(\frac{\partial^2}{\partial x^2} + \frac{\partial^2}{\partial y^2} \right) \psi. \quad (8.64)$$

Boundary conditions are set on \mathbf{v} . For a solid sphere it is clear that the component normal to the surface has to vanish: $v_1 = 0$ (Fig. 8.12).

Similarly, as in any liquid (made of small molecules) the no-slip boundary condition has to be fulfilled, i.e. in the fluid direction of smectics the velocity must vanish

$$v_2 = 0.$$

This leaves no choice for the third component v_3 , which, as in the example of the capillary flow, does not vanish in the distal approximation, and goes to zero in a boundary layer of thickness δ , described by the proximal regime.

The solution in the case of a sphere of radius R , at rest in a fluid moving at infinity with a velocity $\mathbf{v} = v_0 \hat{x}$, has been detailed in reference 11. The

centre of the sphere is at the origin (see Fig. 8.10) and β_{\perp} is taken equal to unity for the sake of simplicity). For $|z| < R$,

$$\psi = yv_0(r - R)^2/(x^2 + y^2). \quad (8.65a)$$

For $|z| > R$,

$$\psi = yv_0 \left(1 + \frac{2R(|z| - r)}{x^2 + y^2} \right) \quad (8.65b)$$

where $r = (x^2 + y^2 + z^2)^{1/2}$. One can check that ψ does respect the boundary conditions and leads to continuous velocity fields and field gradients in the physical domain. The corresponding flow field is displayed in Fig. 8.10.

What is the friction force due to the distortion of the flow lines? One way to perform the calculation is to integrate all stresses acting on the surface of the sphere. A more elegant method has been given in reference 11 and is based on the calculation of the ‘smectic Stokeslet’ (i.e. the velocity field induced by a point-like force perturbation). Equations (8.59b) and (8.59c) are transformed into (directly in Fourier space, and keeping $\beta_{\perp} = 1$)

$$\begin{cases} -\eta_3 q^2 v_x(\mathbf{q}) - iq_x P(\mathbf{q}) = F \\ -\eta_3 q^2 v_y(\mathbf{q}) - iq_y P(\mathbf{q}) = 0 \end{cases} \quad (8.66)$$

or, using a similar stream function (i.e. $v_x(\mathbf{q}) = iq_y \psi_s(\mathbf{q})$; $v_y(\mathbf{q}) = -iq_x \psi_s(\mathbf{q})$) and eliminating pressure,

$$(q_x^2 + q_y^2) \psi_s(\mathbf{q}) = \frac{iq_y}{q^2} (F/\eta_3) \quad (8.67)$$

or, in direct space,

$$\left(\frac{\partial^2}{\partial x^2} + \frac{\partial^2}{\partial y^2} \right) \psi_s = -\frac{F}{4\pi\eta_3} \frac{\partial}{\partial y} \left(\frac{1}{r} \right). \quad (8.68)$$

A direct inspection of (8.65) shows that ψ satisfies (8.68) exactly provided that

$$F = 8\pi\eta_3 R. \quad (8.69)$$

The long-range part of the flow field of a sphere is identical to that of the Stokeslet (in this particular geometry), and the only difference from an ordinary fluid is the change of 6 into 8. Differences are, in general, more dramatic as we will see in the next example.

Note. The case of a flow in the z direction is considerably more complicated [11].

- Boundary conditions are not compatible with the zero-order approximation.
- Dislocation loops are likely to be emitted from the sphere.

It would be interesting to perform experiments to test eqn (8.69); however, it is not easy to stabilize micron-size spheres in smectics.

8.2.2.3 Flow past a semi-infinite rigid plane

In the geometry of Fig. 8.11 it is clear that, in the absence of any symmetry-breaking instability, $v_y = \partial/\partial y = 0$. (This should be the case for the vanishing Reynolds numbers considered here.) The flow along the x direction (constant velocity $v_x = v_0$ for $z > 0$; $x = 0$) is totally blocked by the semi-infinite plane ($v_x = 0$ for $z < 0$; $x = 0$). This problem is not academic, since the boundary layer connected with this type of flow has been demonstrated in an elegant and simple experiment by N. A. Clark [16].

Let us come back to (8.59b) and (8.60); if we anticipate the existence of a boundary layer of width $2l = 4(x\delta)^{1/2}$ along z , it is clear that $\partial^2/\partial z^2 \sim 1/l^2 \gg \partial^2/\partial x^2 \sim 1/x^2$. Then the equations simplify to

$$\frac{\partial P}{\partial z} = -v_z/\lambda_p, \quad (8.70a)$$

$$\frac{\partial P}{\partial x} = \eta_3 \frac{\partial^2 v_x}{\partial z^2}, \quad (8.70b)$$

$$\frac{\partial v_x}{\partial x} + \frac{\partial v_z}{\partial z} = 0. \quad (8.70c)$$

From (8.70c) we see that we can again introduce a stream function such that

$$v_x = \frac{\partial \psi}{\partial z}, \quad v_z = -\frac{\partial \psi}{\partial x}.$$

Eliminating pressure between (8.70a) and (8.70b) yields

$$\delta^2 \frac{\partial^4 \psi}{\partial z^4} - \frac{\partial^2 \psi}{\partial x^2} = 0 \quad (8.71)$$

with boundary conditions $\partial\psi/\partial x(z, x = 0) = 0$; $\partial\psi/\partial z(z, x = 0) = v_0$, $z > 0$; $\partial\psi/\partial z(z, x = 0) = 0$, $z < 0$.

The mere observation of (8.71) confirms the existence of the boundary layer l . With $\partial/\partial z \sim 1/l$; $\partial/\partial x \sim 1/x$ one easily finds indeed that the two terms of (8.71) are comparable when $\delta^2/l^4 \sim 1/x^2$, i.e. $l^2 \sim |x|\delta$ as anticipated.

The solution to (8.71) with the proper boundary conditions reads

$$\psi = \int_{-\infty}^z dz_1 \int_{-\infty}^{z_1} h(z_2, x) dz_2 \quad (8.72)$$

in which h is a simple Gaussian

$$h(z, x) = \frac{v_0}{(4\pi\delta|x|)^{1/2}} \exp(-z^2/4|x|\delta). \quad (8.73)$$

Indeed, it is easy to check that

$$\delta \frac{\partial^2 h}{\partial z^2} - \frac{\partial h}{\partial x} = 0 \quad \delta \frac{\partial^2 \psi}{\partial z^2} + \frac{\partial \psi}{\partial x} = 2h\delta;$$

hence (8.71) is satisfied.

Furthermore, for $x \rightarrow 0$, $h(z, x) \rightarrow v_0 \delta_z$ in which δ_z is the Dirac distribution. Hence $v_x = \partial \psi / \partial z = \int_{-\infty}^z h(z_2, x) dz_2 \rightarrow v_0 \theta_z$ in which θ_z is the step function (0 for $z < 0$, 1 for $z > 0$). Thus the boundary conditions are satisfied. Note that, for $z \gg 2l = 4|x|\delta > 0$, $v_x \simeq v_0$ and $|z| \gg 2l$, but $z < 0$, $v_x \simeq 0$. The flow along x is homogeneous outside the boundary layer defined by $|z| \leq 2l$. The v_z expression is particularly simple:

$$v_z = \pm \frac{v_0}{(4\pi)^{1/2}} \left(\frac{\delta}{|x|} \right)^{1/2} \exp(-z^2/4|x|\delta). \quad (8.74)$$

The plus sign holds for $x < 0$; the minus one for $x > 0$. Note that the exact formula is $l = 2(|x|\delta)^{1/2}$.

The flow along z is different from zero only inside the boundary layer. For positive v_0 (Fig. 8.11), there is an upward permeative flow through the layers (i.e. toward positive z) before the obstacle (i.e. $x > 0$). The boundary layer extends not only in the wake, but is symmetrical for v_x and asymmetrical for v_z , with respect to x .

Note. For $x = 0$, $z \neq 0$, $v_z = 0$, the proper boundary condition is also satisfied on the obstacle, except at the origin ($z = 0$, $x = 0$). This means that the proximal behaviour is condensed in a small region of linear size δ around the origin.

The observation of flow past elongated bubbles confirms beautifully the existence of the boundary layer and thus permeation [16]. Two points are worth mentioning.

1. In order to get strong anchoring of the layers, one needs to use thin samples (in a planar geometry). Far enough from the bubble the boundary layer shape is no longer parabolic, but linear. Can one understand this feature?
2. The observation of the boundary layer makes use of the undulation instability, which proves the coupling of permeation with strain.

It is indeed easy to understand why the boundary layer gets straight: the flow in a thin sample is Poiseuille-like: $\partial/\partial y \sim 1/d \neq 0$ (d = sample thickness). Since $\partial/\partial z \sim 1/l$ decreases like $1/x^{1/2}$, one always reaches a regime in which (8.70) is replaced by

$$\frac{\partial P}{\partial x} = \frac{\alpha_4}{2} \frac{\partial^2 v_x}{\partial y^2}. \quad (8.75)$$

Getting rid of pressure and using the incompressibility condition, we obtain

(again with the simplifying assumption $\beta_{\perp} = \alpha_4/2\eta_3 = 1$)

$$\delta^2 \frac{\partial^4 v_x}{\partial z^2 \partial y^2} + \frac{\partial^2 v_x}{\partial x^2} = 0. \quad (8.76)$$

The functional dependence of the boundary layer thickness on x and d can readily be obtained by replacing $\partial/\partial z$ by $1/l$, $\partial/\partial y$ by $1/d$, $\partial/\partial x$ by $1/x$, and equating the two terms,

$$\frac{\delta^2}{l^2 d^2} \simeq \frac{1}{x^2} \quad \text{or} \quad l \simeq \frac{|x|\delta}{d}.$$

In fact, taking account of the Poiseuille character of the flow gives [16]

$$l = \frac{\sqrt{12}|x|\delta}{d}, \quad (8.77)$$

which is indeed a linear dependence.

What about the observation of the boundary layer? In view of the small values of the velocities involved ($10^{-4} \text{ cm s}^{-1}$) it is clear that the conventional velocimetric methods are totally unadapted to this problem. Fortunately, the coupling between layer distortions and flow provides a built-in way of visualizing the boundary layer. Indeed (8.17c) simplifies to

$$-\frac{v_z}{\lambda_p B} \simeq \frac{\partial^2 u}{\partial z^2} \quad (8.78)$$

which gives for the dilatation

$$\frac{\partial u}{\partial z}(z, x) = \frac{1}{\lambda_p B} \int_z^{\infty} v_z(z', x) dz'. \quad (8.79)$$

This solution is continuous everywhere, except on the obstacle, as required, and ensures a zero-averaged dilatation.

The corresponding strain pattern is given in Fig. 8.11. For $z > 0$, $|x| < z^2/4\delta$ (in the case of infinite extent in the y direction),

$$\nabla_z u \sim 0. \quad (8.80)$$

For $z < 0$, $x < 0$, $|x| < z^2/4\delta$,

$$\nabla_z u \simeq \frac{v_0 \delta}{2\lambda_p B}. \quad (8.81a)$$

For $z < 0$, $x > 0$, $|x| > z^2/4\delta$,

$$\nabla_z u \simeq \frac{-v_0 \delta}{2\lambda_p B}. \quad (8.81b)$$

Equations (8.81) show that the smectic is dilated in the upstream region, and compressed in the downstream one (for $z < 0$). This corresponds to the

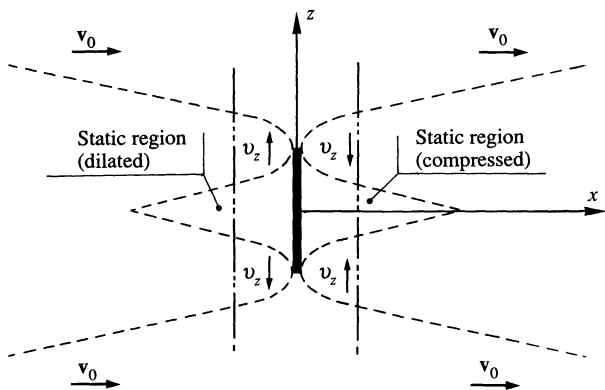


Fig. 8.13. Flow past a rigid obstacle. Layers are perpendicular to the z direction. The dashed lines again indicate the boundary layer. The dash-dotted lines indicate the cross-over between the parabolic and the linear regimes.

fact that, in order to force the flow through the boundary layer, there is necessarily a pressure head in the z direction pulling (pressing) the layers for negative (positive) x .

Equation (8.81a) reveals the profound originality of smectic hydrodynamics.

Since one finds a finite dilatation, no matter how small the velocity v_0 is, the flow we have been describing cannot be stable!

Indeed, we have shown in the preceding chapter that, for an integrated dilatation $2\pi\lambda = 2\pi\sqrt{(K_1/B)}$, a buckling instability would occur. For a sample of infinite extent in the z direction, no matter how small v_0 is, the integrated dilatation in the static region ($z < 0, x < 0, |x| < z^2/4\delta$) will always be larger than $2\pi\lambda$! Note that, since this region is static, the considerations of Chapter 7 are correct.

In the experimental geometry of reference 16 the obstacle has a finite size L in the z direction (Fig. 8.13). A good approximation to the flow field is the simple superposition of two boundary layers generated at each edge of the obstacle. Now the diluted region is finite and, for low enough v_0 , the linear solution holds. The buckling instability is reached in the large thickness regime, for a critical velocity v_{oc}

$$\left. \begin{aligned} L \frac{v_{oc}\delta}{2\lambda_p B} &\simeq 2\pi \sqrt{\left(\frac{K_1}{B}\right)}, \\ v_{oc} &\simeq 4\pi\sqrt{(K_1 B)} \left(\frac{\lambda_p}{\eta_3}\right)^{1/2} L^{-1}. \end{aligned} \right\} \quad (8.82)$$

Note that in this regime, since the dilatation is constant, the instability arises first close to the obstacle.

In the small thickness regime, the instability is expected at the largest x possible (i.e. where the two boundary layers generated by opposite edges meet). The critical velocity can be estimated using similar scaling arguments

$$v_{oc} \simeq \lambda_p B \frac{\lambda d}{\delta L^2} = \sqrt{(K_1 \bar{B})} \left(\frac{\lambda_p}{\eta_3} \right)^{1/2} \frac{d}{L^2}. \quad (8.83)$$

These predictions are strikingly well borne out by experiment [16].† One does observe the outset of the buckling instability in the static upstream region. When $d/L \ll 1$, the undulation instability occurs at the tip of the static region first; this was the experimental case. From $v_{oc} \sim 10^{-4} \text{ cm s}^{-1}$ one deduces $\delta \leq 100 \text{ \AA}$, which is in agreement with our previous considerations. Such small values of v_{oc} explain the difficulty of performing standard flow experiments.

This experiment is very rich for the following reasons.

1. The existence and shape of the boundary layer implies the existence of permeation.
2. The cross-over parabolic–linear implies the existence of Poiseuille flow in the geometry of Fig. 8.7(b), which was not obvious from standard hydrodynamic experiments.
3. The velocity threshold proves the coupling between permeation and strain, and allows an estimate of δ .

8.2.3 Flow alignment

We have seen in the last section that there is indeed a coupling between flow and strain in S_A . As a result, velocity gradients in general exert torques on the layers. However, when the effects become sizeable, they often amount to layer breaking and thus cannot be described by any simple theory of the kind developed here. On the other hand, as we have seen in Section 8.1.9, the c director of S_C behaves pretty much like that of nematics: this has been nicely illustrated in the experiments [27, 42] to be discussed now.

8.2.3.1 Flow alignment in freely suspended films of smectics C

A clever geometry has been studied by Cladis *et al.* [27]. Suppose you draw a smectics C free-standing film of the type described in Chapter 7 over a circular hole. Suppose now you punch the film right in the centre with a needle of radius r_0 without breaking it: you can exert a shear in the plane

† Note that this analysis is meaningful only to the extent that the undulation period is small compared to linear size in the x direction. It ceases to be valid when $l \sim 4\pi\delta^2\lambda/d^2$, i.e. quite close to the tip of the static region.

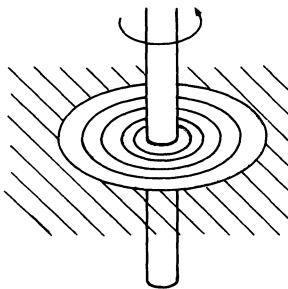


Fig. 8.14. Shear flow experiment with a free-standing film. The hatched area represents the holder, the circles the film.

of the layers by the mere rotation of the needle (Fig. 8.14). Angular speeds as high as 5000 r.p.m. can be achieved!

In such a cylindrical geometry, the equilibrium state corresponds to disclinations, the index s of which depends on boundary conditions. The analysis of the corresponding distortion is similar to the one developed for the nematics in Chapter 4, provided one considers integer values of s only. Two cases have been observed experimentally (Fig. 8.15(a)–(d)).

1. $s = 1$, radial distribution of the \mathbf{c} director;
2. $s = 0$, absence of disclination.

When a stationary state is reached, a good description of the flow field is given by the large-gap approximation to the Navier–Stokes equation of circular shear [27]

$$v_\phi = \omega_0 r_0^2 / \rho; \quad v_\rho = v_z = 0 \quad (8.84)$$

where the cylindrical coordinates ρ, ϕ, z are used and r_0 and R are the inner and outer radii, respectively (Fig. 8.16). Under such conditions (8.52) simplifies† (with $\Phi = \Omega_z - \varphi$)

$$\frac{\partial \Phi}{\partial t} + \frac{b_1 \omega_0 r_0^2}{\rho^2} \cos 2\Phi = v h_z. \quad (8.85)$$

Equation (8.85) exhibits the obvious solution: $\Phi = \pm \pi/4$ (2π), which corresponds to an $s = 1$ disclination. (Note that $h_z = 0$ in this case since $\Phi = \text{const}$ is an equilibrium configuration, at least in the one-constant approximation.)

The experiment confirms this prediction since one does observe $\Phi \simeq \pm 45^\circ$, when a $s = 1$ disclination is sheared.

For $s \neq 1$ (example $s = 0$ of Fig. 8.15(a), (b)) the topology entirely controls the dynamics. In contrast to the case $s = 1$ which is invariant in the rotation of the inner cylinder, if rigid and no-slip boundary conditions are assumed,

† The difference between this equation and equation (5) of reference 27 comes from the addition of a convective term in (8.5.2).

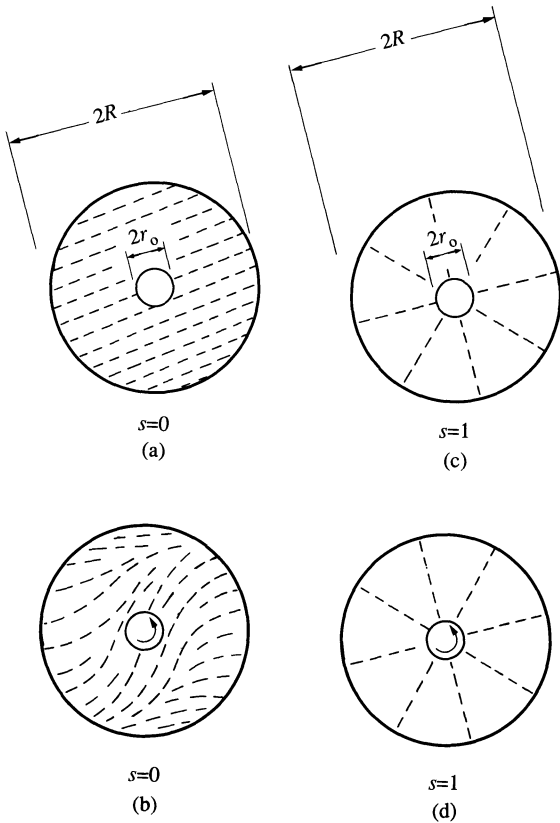


Fig. 8.15. Static distortions in a S_C film between two cylinders: (a) $s = 0$, absence of disclination homogeneous state; (b) $s = 0$, deformed state after a 90° rotation of the inner cylinder where rigid boundary conditions both for molecular orientation and position (no slip) are assumed; (c) $s = 1$, radial configuration; (d) $s = 1$, ‘undeformed’ state after a 90° rotation of the inner cylinder (with the same boundary conditions).

it is clear that the phase Φ has to wind up as the number of turns. The experiment supports the validity of such boundary conditions. When the inner cylinder is removed, the structure unwinds: the dynamics is compatible with

$$\Phi = \phi + \Phi_0 \frac{K_0(\rho/R)}{K_0(r_0/R)} \exp\left(-\frac{t}{\tau}\right), \quad (8.86)$$

$$\tau = R^2/Bv, \quad (8.87)$$

where K_0 is the modified Bessel function of second kind. Equation (8.86) is a solution of (8.85) if one neglects the coupling with the back flow and takes

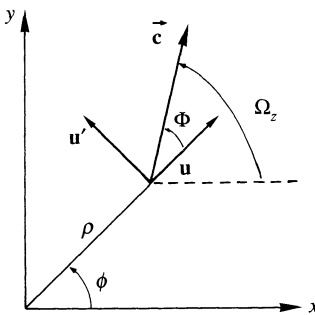


Fig. 8.16. Polar coordinates for the \mathbf{c} director in a S_C film.

the one-constant approximation for h_z

$$h_z = B \left(\frac{1}{\rho} \frac{\partial}{\partial \rho} \rho \frac{\partial \Phi}{\partial \rho} + \frac{1}{\rho^2} \frac{\partial^2 \Phi}{\partial \phi^2} \right) \quad (8.88)$$

where Φ_0 is the initial phase at $\rho = r_0$. The values of Bv obtained are compatible with those measured by light scattering on thin films [42] and approximately 100 times smaller than in nematics. (Note. The modulus B in (8.88) is a Frank constant defined in Chapter 7, not the compressional modulus.)

8.2.3.2 Flow alignment in chiral S_C^*

As we have seen in the preceding chapter, the helical precession of the polarization \mathbf{P} in S_C^* restores the D_∞ symmetry of S_A^* and, as a result, $\langle \mathbf{P} \rangle = 0$. On the other hand, if the structure is sheared, a uniform macroscopic polarization, proportional to the shear rate, sets in [43]

$$\langle P_\alpha \rangle = \lambda_{\alpha\beta\gamma} \partial_\gamma v_\beta. \quad (8.89)$$

Indeed, a shear is characterized by a D_{2h} symmetry, and the only common element with D_∞ is a C_2 along which a uniform polarization can develop (see Fig. 8.17). Equation (8.89) holds for S_A^* and cholesterics as well since its existence is derived from symmetry arguments only [44]. The induced polarization is however much larger in S_C^* . In the following, as an example, we calculate the coefficient λ_{xyz} , which corresponds to the clever geometry of Pieransky, Guyon, and Keller [43].

In the problem of Section 8.1.9, we noted that the hydrodynamic equations for S_C^* , in their linearized long-wavelength limit were not very useful. As we will see, the macroscopic polarization results from a modulation of the tilt direction in the shear flow at the period of the structure. So we need a description of the S_C^* valid at this scale. Since this period is large compared to molecular dimensions, one can still use a macroscopic hydrodynamic

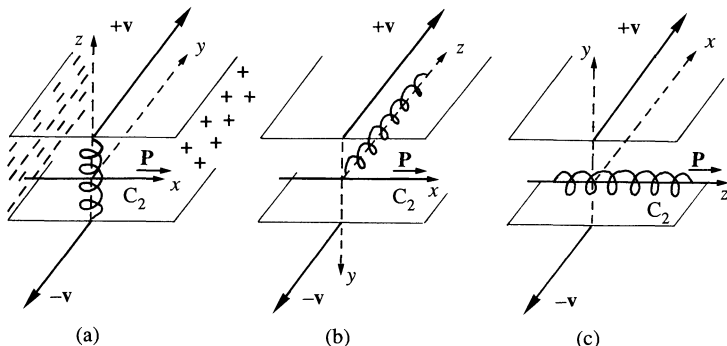


Fig. 8.17. Three typical geometries allowing the onset of a macroscopic uniform polarization in S_C^* under shear, but also in cholesterics and S_A^* . In all cases the polarization arises in the direction of the twofold axis C_2 , common element between the D_∞ group of the structure and the D_{2h} group of the shear. (a) $P_x = \lambda_{xyz} \partial_z v_y$ (an equivalent geometry would involve $\lambda_{xyz} = -\lambda_{xyz}$); the plus (minus) represents the surface charges resulting from bulk polarization. (b) $P_x = \lambda_{xyz} \partial_y v_z$ (an equivalent geometry would involve $\lambda_{yzx} = -\lambda_{xzy}$). (c) $P_z = \lambda_{zxy} \partial_y v_x$ (an equivalent geometry would involve $\lambda_{zyx} = -\lambda_{zxy}$).

theory, in which one considers the S_C^* as a twisted S_C (keeping in mind the lack of mirror symmetry). The approximation of small deviations from equilibrium for the c director has also to be removed because of the helicoidal precession. On the other hand, in many practical problems concerning S_C^* , the layers are either unperturbed or slightly displaced from their equilibrium position, so that one can keep the equations to lowest order in the u displacement variable and single out the normal to the layers, $\mathbf{k} = \hat{\mathbf{z}}$. Under such circumstances, (8.49) and (8.56) are replaced by [44]

$$-\frac{\partial \theta}{\partial t} + \partial_\alpha v_\alpha = 0, \quad (8.90a)$$

$$\frac{\partial \varepsilon}{\partial t} + \frac{\partial \theta}{\partial t}(\varepsilon + P) = \partial_\alpha [K_{\alpha\beta} \partial_\beta T - \mu_{az} g_z + \mu'_{az} h_z + \mu''_{\alpha\beta} E_\beta], \quad (8.90b)$$

$$\frac{\partial u}{\partial t} - v_z = -\mu_{za} \frac{\partial_\alpha T}{T} + \lambda_p g_z - \lambda'_p h_z + v_{z\beta} E_\beta, \quad (8.90c)$$

$$\frac{\partial \Omega_z}{\partial t} - v_z \partial_z \Omega_z - B_{z\alpha\beta} \partial_\beta v_\alpha = v h_z - \lambda'_p g_z + \mu'_{az} \frac{\partial_\alpha T}{T} + v'_{z\beta} E_\beta, \quad (8.90d)$$

$$\rho \frac{\partial v_\alpha}{\partial t} = -\partial_\alpha P + (g_z - q_0 h_z) \delta_{az} + \partial_\beta (-B_{z\alpha\beta} h_z + \eta_{\alpha\beta\gamma\delta} \delta_\beta v_\gamma), \quad (8.90e)$$

$$J_\alpha = K_{\alpha\beta} E_\beta + v_{az} g_z + v'_{az} h_z + \mu''_{\alpha\beta} \frac{\partial_\alpha T}{T}. \quad (8.90f)$$

In general (8.90) has to be completed by Maxwell equations.

$$\text{Furthermore: } B_{z\alpha\beta} \partial_\beta v_\alpha = \frac{1}{2}(\text{curl } v)_z + b_1 c_\alpha p_\beta A_{\alpha\beta} + b_2 p_\alpha A_{z\alpha}. \quad (8.91)$$

\mathbf{c} and \mathbf{p} obey the definitions used throughout this chapter, i.e. tilt direction and $\mathbf{k} \times \mathbf{c}$; $\mathbf{c} = (\cos \Omega_z, \sin \Omega_z, 0)$, $\mathbf{p} = (-\sin \Omega_z, \cos \Omega_z, 0)$. J_α is the electric current, $K_{\alpha\beta}^e$ the electric conductivity.

Equation (8.90) contains cross-terms absent in S_C because of the lack of mirror symmetry and in the long-wavelength description of S_C^* because of the low local symmetry (C_{2h}). We postpone their description for the end of this subsection, and consider an incompressible, isothermal smectic in the absence of external electric fields (in the frequency range considered here, incompressibility holds for the density and the layer spacing as well)

$$\frac{\partial \Omega_z}{\partial t} - \frac{b_2}{2} \cos \Omega_z \frac{\partial v_y}{\partial z} = v B_z \frac{\partial^2 \Omega_z}{\partial z^2}. \quad (8.92)$$

Let us consider for the sake of simplicity a shear sinusoidal in time (this corresponds precisely to the experimental situation), $\partial v_y^{\text{ext}} / \partial z = s e^{i\omega t}$. For s small enough, (8.92) may be linearized in terms of the distortion $\delta \Omega_z = \Omega_z - q_0 z$. The solution to (8.92) is then straightforward

$$\delta \Omega_z = \frac{b_2 \cos q_0 z \frac{\partial v_y^{\text{ext}}}{\partial z}}{2(i\omega t + q_0^2 v B_3)}, \quad (8.93)$$

i.e. the azimuthal tilt direction is modulated by the shear with the periodicity of the helix as announced.

One can now calculate the averaged polarization

$$\langle P_x \rangle = -P_0 \langle \sin \Omega_z \rangle = -P_0 \langle \sin(q_0 z + \delta \Omega_z) \rangle = \frac{-P_0 b_2 \frac{\partial v_y^{\text{ext}}}{\partial z}}{4(i\omega t + q_0^2 v B_3)}, \quad (8.94)$$

$$\langle P_y \rangle = P_0 \langle \cos \Omega_z \rangle = 0,$$

i.e.

$$\lambda_{xyz} = -P_0 b_2 / 4(i\omega t + q_0^2 v B_3). \quad (8.95)$$

The validity of (8.95) has been checked experimentally by the measure of the polarization charges appearing on the side surfaces as shown in Fig. 8.17(a). One does find a single Lorentzian that provides a measure of $B_3 v$. The amplitude of the induced charge is a measure of the product $P_0 b_2$. Since one knows P_0 from independent experiments, this is, in fact, a measure of b_2 , which seems to be significantly smaller than λ in nematics.

Up to now, we have taken the simplest approach. However, the assumption $v_x = 0$ is not valid, since the periodic angular modulation induces a

periodic backflow $v_x(z), v_y(z)$. (Note that the incompressibility condition imposes $v_z = 0$.) However, a more complete calculation shows that all results are preserved provided one replaces the viscosity ν by a ‘dressed’ viscosity $\tilde{\nu}$ [44]

$$\tilde{\nu} = \nu - \frac{b_2^2}{2(\eta_{czcz} + \eta_{pzpz})}$$

in which indices c and p refer to the **c** and **p** direction. Thus, as in nematics, the backflow leads to a lowering of the viscosity but does not alter the essential physics.

8.2.3.3 Electric field alignment in chiral S* revisited

In Chapter 7 we restricted our attention to the case of perfectly insulating smectics. Of course, this is not a physical situation. Let us again consider the geometry of Section 7.2.4 (Fig. 7.21), with a d.c. field E_y applied in the y direction. We assume that the layers are anchored at the walls, and consider only z -dependent, isothermal solutions. The condition for steady state reads

$$\left. \begin{aligned} 0 &= \lambda_p g_z - \lambda'_p h_z + v_{z\beta} E_\beta, \\ 0 &= -v h_z - \lambda'_p g_z + v'_{z\beta} E_\beta, \\ \partial_z J_z &= 0 \quad \text{or} \quad J_z = \text{const.} \end{aligned} \right\} \quad (8.96)$$

When dielectric coupling can be neglected, the absence of average electric field in the z direction may be shown to necessitate $J_z = 0$. Equation (8.96) then simplifies to

$$\tilde{\nu} h_z = \tilde{v}'_{z\beta} E_\beta \quad (8.97)$$

where $\tilde{\nu} = \nu + \lambda'^2/\lambda_p$ and $\tilde{v}'_{z\beta} = v'_{z\beta} + \lambda'_p v_{z\beta}/\lambda_p$ or, with

$$h_z = -B_3 \frac{\partial^2 \Omega_z}{\partial z^2} + P_0 E_y \sin \Omega_z \quad (8.98)$$

and

$$\tilde{v}'_{z\beta} E_\beta = \tilde{v}'_{zz} E_z + \tilde{v}'_{zc} \sin \Omega_z E_y, \quad (8.99)$$

(note: $\tilde{v}'_{zp} = 0$ because of the twofold symmetry) and, making use of the condition $J_z = 0$ to eliminate E_z , one eventually gets

$$-B_z \frac{\partial^2 \Omega_z}{\partial z^2} + \tilde{P} E_y \sin \Omega_z = 0, \quad (8.100)$$

$$\tilde{P} = P_0 - \frac{\tilde{v}_{zc}}{\tilde{\nu}} \quad \left\{ \begin{array}{l} \tilde{v}_{zc} = \tilde{v}'_{zc} - \tilde{v}'_{zz} K_{zc}/K_{zz} \\ \tilde{\nu} = \tilde{\nu} + \tilde{v}'_{zz}^2/K_{zz}. \end{array} \right. \quad (8.101)$$

Thus one finds an equation similar to (7.45) (in the absence of dielectric coupling), but with an ‘apparent’ dipole density that involves terms of dissipative origin: the electric current reacts on the **c** director with just the

same symmetry as the torque due to the polarization density. The importance of this term is not known today.

\tilde{v}_{zc} can be evaluated with the help of dimensional analysis.

$$\tilde{v}_{zc} = QM^{-1}L^{-1}T \quad \text{or} \quad \tilde{v}_{zc} = \left(\frac{Q}{L^3}\right)(M^{-1}LT)L$$

i.e. charge density \times characteristic length/viscosity. With a typical density $n \sim 10^{17} \text{ cm}^{-3}$ (clean case), a typical viscosity of 1 poise, and a characteristic length of molecular size we get

$$v_{zc} \sim \text{a few cgs units.}$$

If one includes a yield factor of typically 10^{-1} – 10^{-2} this term is negligible.

On the other hand, in the ‘dirty case’, $n \sim 10^{20}$ and, with the same yield factor, we get contributions ranging from a few 10 to 100 cgs units. This figure is now large. It would be interesting to study the influence of controlled ionic impurities in S_C^* systems.

8.3 BREAKDOWN OF ELASTICITY

Although the consequences of the gradient expansion failure are more spectacular in the dynamics, they were first predicted in the static case by Grinsteiner and Pelcovits [45]. In the following discussion we give the simplest derivation that allows us to understand the origin of the breakdown, and discuss additional information obtained in a more rigorous treatment.

8.3.1 Poor man’s derivation

We remark that the smectic free energy (7.13) is not rotationally invariant. We already introduced in Section 7.1.7 the lowest-order correction to the compressional energy due to rotational invariance (remember: it is responsible for the onset of the buckling instability)

$$\frac{B}{2} \int (\nabla_z u - \frac{1}{2}(\nabla_{\perp} \mathbf{u})^2)^2 dv. \quad (8.102)$$

Suppose that we take the validity of this expression for granted on a local scale: what is the effect of the strong layer fluctuations on the macroscopic measure of the elastic constant?

According to (8.102), the σ_{zz} stress is now a non-linear function of strains

$$\sigma_{zz} = B(\nabla_z u - \frac{1}{2}(\nabla_{\perp} \mathbf{u})^2). \quad (8.103)$$

Equation (8.103) is a local relation, and we want to calculate the macroscopic relation linking $\langle \sigma_{zz} \rangle$ and $\langle \nabla_z u \rangle$.

Suppose first that there is no external stress: $\langle \sigma_{zz} \rangle_0 = \sigma_{zz}^{\text{ext}} = 0$. Equation (8.103) shows that angular fluctuations renormalize the layer thickness of smectics (the subscript 0 emphasizes the fact that this average is taken at zero external stress)

$$\langle \nabla_z u \rangle_0 = \frac{1}{2} \langle (\nabla_{\perp} \mathbf{u})^2 \rangle_0. \quad (8.104)$$

The actual layer displacement $\bar{\mathbf{u}}$ has to be defined with respect to the average layer spacing,

$$\bar{u} = u - \frac{1}{2} \langle (\nabla_{\perp} \mathbf{u})^2 \rangle_0 z = u - \frac{1}{2} \langle (\nabla_{\perp} \bar{\mathbf{u}})^2 \rangle_0 z, \quad (8.105)$$

so that $\langle \nabla_z \bar{u} \rangle_0 = 0$.

Let us turn on an external stress (now the subscript σ_{zz}^{ext} in $\langle \cdot \rangle_{\sigma_{zz}^{\text{ext}}}$ indicates that this average is to be taken in presence of the external stress)

$$\langle \sigma_{zz} \rangle = \sigma_{zz}^{\text{ext}} = B(\langle \nabla_z u \rangle_{\sigma_{zz}^{\text{ext}}} - \frac{1}{2} \langle (\nabla_{\perp} \mathbf{u})^2 \rangle_{\sigma_{zz}^{\text{ext}}}), \quad (8.106)$$

$$\langle \sigma_{zz} \rangle = B(\langle \nabla_z \bar{u} \rangle_{\sigma_{zz}^{\text{ext}}} - \frac{1}{2}(\langle (\nabla_{\perp} \bar{\mathbf{u}})^2 \rangle_{\sigma_{zz}^{\text{ext}}} - \langle (\nabla_{\perp} \bar{\mathbf{u}})^2 \rangle_0)). \quad (8.107)$$

Angular fluctuations are modified by the external stress in just the same way as they are by an external magnetic field (remember remark (7.54)). As a result a compression reduces layer tilt fluctuations; a dilatation increases them. This is expressed by the susceptibility χ ,

$$\frac{1}{2}(\langle (\nabla_{\perp} \bar{\mathbf{u}})^2 \rangle_{\sigma_{zz}^{\text{ext}}(q)} - \langle (\nabla_{\perp} \bar{\mathbf{u}})^2 \rangle_0) = \chi(q) \sigma_{zz}^{\text{ext}}, \quad (8.108)$$

which immediately gives

$$\sigma_{zz}^{\text{ext}} = \frac{B}{1 + B\chi(q)} \langle \nabla_z \bar{u} \rangle \quad (8.109)$$

or

$$B^{\text{eff}} = \frac{B}{1 + B\chi(q)}. \quad (8.110)$$

$\chi(q)$ can be calculated using the fluctuation-dissipation theorem as

$$\chi(q) = \frac{1}{4k_B T} \langle (\nabla_{\perp} \mathbf{u})^2(q)(\nabla_{\perp} \mathbf{u})^2(-q) \rangle_0. \quad (8.111)$$

In the decoupling approximation,

$$\begin{aligned} & \langle (\nabla_{\perp} \mathbf{u})^2(q)(\nabla_{\perp} \mathbf{u})^2(-q) \rangle_0 \\ &= \frac{2k_B^2 T^2}{B^2} \int \frac{d^3 k}{8\pi^3} \frac{[\mathbf{k}_{\perp} \cdot (\mathbf{q}_{\perp} - \mathbf{k}_{\perp})]^2}{(k_z^2 + \lambda^2 \mathbf{k}_{\perp}^4)((q_z - k_z)^2 + \lambda^2 (\mathbf{q}_{\perp} - \mathbf{k}_{\perp})^4)}. \end{aligned} \quad (8.112)$$

Simple power counting shows that this integral diverges logarithmically. One finds (k_c is a cut-off corresponding to the molecular size at which the elastic

theory is no longer appropriate)

$$\chi(q) = \frac{k_B T}{64\pi B^2 \lambda^3} \ln \left[\frac{4k_c^4}{\max(\lambda^{-2}q_z^2, q_\perp^4)} \right] \quad (8.113)$$

and

$$B^{\text{eff}} = \frac{B}{1 + \frac{w}{32\pi} \ln \left(\frac{2k_c^2}{\max(\lambda^{-1}|q_z|, q_\perp^2)} \right)} \quad (8.114)$$

where $w = k_B T B^{1/2} / K^{3/2} = (k_B T / \lambda^3) / B$ is a dimensionless number, which determines the range of validity of conventional elasticity.

Note that for vanishing \mathbf{q} , B^{eff} goes to zero like $1/\ln(\text{const}/q)$, so that the usual notion of elastic constant breaks down. Local non-linear stress-strain relations such as (8.103) are present in any system (for example, crystals or columnar phases), and the same kind of treatment would also lead to a redefinition of the elastic constants. The difference lies in the fact that, for crystals and columnar phases, the integral (8.112) is a function of the upper cut-off wavevector only, i.e. of short-range order. The value of the elastic modulus is modified, but it is still a constant. On the contrary in smectics it goes to zero as \mathbf{q} goes to zero.

8.3.2 Splay modulus

The same type of argument can be developed in that case as well. Equation (8.7) (in the absence of a magnetic field) is replaced by

$$\sigma_{zx} = K_1 \frac{\partial}{\partial x} \Delta_\perp \mathbf{u} - B \left(\frac{\partial u}{\partial z} \right) \left(\frac{\partial u}{\partial x} \right) \quad (8.115)$$

where

$$\left\langle \frac{\partial u}{\partial z} \frac{\partial u}{\partial x} \right\rangle_{\sigma_{zx}} = \chi'(q) \sigma_{zx}^{\text{ext}}.$$

One finds

$$K_1^{\text{eff}} = K_1 / (1 + B\chi'(q)) \quad (8.116)$$

where

$$\chi'(q) = \frac{1}{k_B T} \frac{\partial}{\partial q_\perp^2} \left\langle \left(\frac{\partial u}{\partial z} \frac{\partial u}{\partial x} \right)(q) \left(\frac{\partial u}{\partial z} \frac{\partial u}{\partial x} \right)(-q) \right\rangle.$$

Again the integral is found to diverge logarithmically

$$K_1^{\text{eff}} = \frac{K_1}{1 - \frac{w}{64\pi} \ln \left(\frac{k_c^2}{\max(\lambda^{-1}|q_z|, q_\perp^2)} \right)}. \quad (8.117)$$

Note that K_1 is increased by the fluctuations; it is clear that the type of correction we have been discussing is valid only when it is small compared to one. Equation (8.117) predicts that K_1^{eff} goes to infinity for finite q , which is not reasonable. The proper long-wavelength limit can only be obtained in a renormalization group procedure (see Section 8.3.4) [47–49].

8.3.3 Macroscopic non-linear stress–strain relation

Up to now we have considered the finite wavevector response to external stress. What happens if a homogeneous stress σ_{zz} is applied to a smectic?

The procedure of Section 8.3.1 can be followed exactly from (8.102) to (8.111), in which one has to let \mathbf{q} go to zero to obtain the homogeneous behaviour. The divergence of the integral (8.112) shows that one misses something. Since a stress is applied, a non-zero $\langle \nabla_z \bar{u} \rangle$ results and the cubic term $\nabla_z \bar{u} \nabla_{\perp} u^2$ gives a quadratic $\langle \nabla_z \bar{u} \rangle \nabla_{\perp} \bar{u}^2$ contribution to the elastic energy. Hence the equipartition theorem gives

$$\langle \nabla_{\perp} \bar{u}(\mathbf{k}) \cdot \nabla_{\perp} \mathbf{u}(-\mathbf{k}) \rangle = \frac{k_{\perp}^2 k_B T}{B'(k_z^2 - \langle \nabla_z u \rangle k_x^2 + \lambda^2 k_x^4)}. \quad (8.118)$$

This provides a natural cut-off in the integral (8.112)

$$q_{\langle \nabla_z u \rangle} = \langle \nabla_z u \rangle / \lambda^2. \quad (8.119)$$

Note that the integral will be stabilized only if $\langle \nabla_z u \rangle < 0$, i.e. only with a compressional stress. In the opposite case we know that, no matter how small the external dilatative stress, the system will buckle in an infinite sample. One finds that the susceptibility χ is a function of the induced strain!

$$\chi(\mathbf{q} = 0) = \frac{k_B T}{32\pi B^2 \lambda^3} \ln \left[\frac{4\lambda^2 k_c^2}{|\langle \nabla_z u \rangle|} \right] \quad (8.120)$$

or

$$B_{(\sigma_{zz})}^{\text{eff}} \simeq \frac{B}{1 + \frac{w}{32\pi} \ln \left(\frac{2k_c^2}{(\sigma_{zz}/K_1)} \right)}. \quad (8.121)$$

For vanishing σ_{zz} the stress–strain relation is no longer linear, which is just the opposite of what happens in conventional systems (and on a local scale). More generally, the logarithm in B^{eff} is determined by the largest value of $\lambda^{-1}(q_z)$, q_{\perp}^2 , and σ_{zz}/K_1 .

8.3.4 Renormalization group results

The merit of the simple derivation we have given is to provide an understanding of the failure of Hooke's law. However, it is clearly insufficient, as one can see from the K_1 results and also from the fact that B appears in the

corrective term of eqn (8.114). The use of renormalization group provides a more satisfactory treatment which also answers other questions. We selected one particular non-linearity, namely, $\nabla_z u (\nabla_{\perp} u)^2$; why keep only this one when others such as $(\nabla_z u)^3$, $(\nabla_z u)^4$, $(\nabla_z u)^2 (\nabla_{\perp} \mathbf{u})^2$, $(\nabla_{\perp} u)^4$ are obviously allowed by symmetry?

The renormalization procedure allows us to calculate the long-wavelength expression of the elastic free energy, assuming that conventional elasticity is valid at short length scales. This procedure shows that the only important non-linearities at large scales are those stemming from the rotationally invariant form of the harmonic compression term (i.e. $-\nabla_z u (\nabla_{\perp} u)^2$, and $(\nabla_{\perp} u)^4$).

One finds expressions similar to (8.114) and (9.117) [48]

$$B^{\text{eff}}(q) = \tilde{B} \left(1 + \frac{5w}{128\pi} \ln \frac{2k_c^2}{\max(\lambda^{-1}|q_z|, q_{\perp}^2)} \right)^{-4/5}, \quad (8.122)$$

$$K_1^{\text{eff}}(q) = K_1 \left(1 + \frac{5w}{128\pi} \ln \frac{2k_c^2}{\max(\lambda^{-1}|q_z|, q_{\perp}^2)} \right)^{2/5}. \quad (8.123)$$

For the stress-controlled value of B one can again replace $\lambda^{-1}q_z$ by (σ_{zz}/K_1) in (8.122). Note that (8.114) and (8.117) are compatible with (8.122) and (8.123) in their range of validity.

Thus one finds that B goes to zero as $(\ln 1/q_z)^{-4/5}$ and K_1 to infinity as $(\ln 1/q_z)^{2/5}$. The usual gradient expansion fails at small wavevectors (or stress) where it should be, in principle, the most valid. This result is conceptually important, although hard to detect experimentally. Wavevectors, for which the logarithmic correction is of the order of one, correspond to enormous wavelengths, out of reach in the laboratory.

For small corrections (8.122) or (8.121) yield

$$\frac{B(q_2) - B(q_1)}{B(q_1)} \simeq \frac{w}{32\pi} \ln \left(\frac{q_{1z}}{q_{2z}} \right).$$

If $q_{2z} = q_{1z}/e$, one gets $(B(q_2) - B(q_1))/B(q_1) \simeq 10^{-2}$.

Problem. Derive a fully rotationally invariant form for the smectic elastic energy.

Solution. Let us use a procedure different from the original one [48]. Remark first that, in the absence of dislocation,

$$\oint \frac{1}{a} \mathbf{n} \cdot d\mathbf{l} = 0 \quad (8.124)$$

in which a and \mathbf{n} are the local layer thickness and normal. Thus one can always write

$$\frac{1}{a} \mathbf{n} = \nabla \phi \quad (8.125)$$

where ϕ is a phase that describes the position of the layers. Introducing the layer displacement variable amounts to choosing a reference system of period $a_0 = 2\pi/q_0$, in an arbitrary direction z , and expressing at each point the translation necessary to map ϕ on this reference. This gives simply

$$\phi(\mathbf{r}) = q_0(z - u(\mathbf{r})). \quad (8.126)$$

Note that z need not coincide with the average layer normal at all, nor a_0 with the actual layer spacing. Expressing the fact that \mathbf{n} is a unit vector yields

$$\frac{1}{a^2 q_0^2} = 1 - 2E(u)$$

with

$$E(u) = \nabla_z u - \frac{1}{2}(\nabla \mathbf{u})^2. \quad (8.127)$$

Since the elastic energy depends on layer thickness it depends on $E(u)$, which, according to (8.125), is rotationally invariant. Note that, since a_0 is not the equilibrium thickness *a priori*, any power of $E(u)$ starting from one enters the elastic energy. The correct form of (8.102) involves $E(u)$ with $(\nabla \mathbf{u})^2$ rather than $(\nabla_{\perp} \mathbf{u})^2$: there is no contradiction with the use of $(\nabla_{\perp} \mathbf{u})^2$ in Chapter 7, since, in the long-wavelength limit, only this term is relevant.

The splay term is easily expressed as

$$\operatorname{div}^2 \mathbf{n} = \operatorname{div}^2 \left(\frac{(\hat{\mathbf{z}} - \nabla \mathbf{u})}{(1 - 2E(u))^{1/2}} \right). \quad (8.128)$$

Note that one can write many other terms which will all be irrelevant in the long-wavelength limit.

8.4 BREAKDOWN OF HYDRODYNAMICS

8.4.1 Poor man's derivation

Again we take the simplest approach that will allow us to understand the essential results. To that end we consider an isothermal incompressible smectic and keep the $\frac{1}{2}\nabla_z u(\nabla_{\perp} \mathbf{u})^2$ static non-linearity only. Consider the force g_z conjugate to u . The local expression of the equations of motion may be written $[\exp(i(\mathbf{q} \cdot \mathbf{r} - \omega t))]$ omitted) as

$$g_z(\mathbf{q}, \omega) = L(\mathbf{q}, \omega)u(\mathbf{q}, \omega) + NL(u)(\mathbf{q}, \omega) \quad (8.129)$$

where $L(\mathbf{q}, \omega)$ is the linear part of the response. The nonlinear part, $NL(u)$, is obtained directly from the cubic term of the elastic energy

$$\begin{aligned} NL(u)(\mathbf{q}, \omega) &= \frac{B}{2} \int \frac{d^3 k}{8\pi^3} \frac{d\Omega}{2\pi} u(\mathbf{k}, \Omega) u(\mathbf{q} - \mathbf{k}, \omega - \Omega) \\ &\times \left[iq_z \mathbf{k}_{\perp} \cdot (\mathbf{q}_{\perp} - \mathbf{k}_{\perp}) + 2i\mathbf{q}_{\perp} \cdot (\mathbf{q}_{\perp} - \mathbf{k}_{\perp}) k_z \right]. \end{aligned} \quad (8.130)$$

As in Section 8.3.1 we look for the average relation between $\langle g_z \rangle$ and $\langle u \rangle$. It should obey linear response theory and, in particular, the fluctuation dissipation theorem

$$\langle g_z(\mathbf{q}, \omega) \rangle = \chi(\mathbf{q}, \omega) \langle u(\mathbf{q}, \omega) \rangle \quad (8.131)$$

with†

$$\chi''(q, \omega) = \frac{-\omega}{2k_B T} \langle g_z(\mathbf{q}, \omega) g_z(-\mathbf{q}, -\omega) \rangle \quad (8.132)$$

in which χ'' is the dissipative part of the response function. Making use of (8.129), and remarking that $\langle L(u) NL(u) \rangle = 0$, we find

$$\chi''(\mathbf{q}, \omega) = L''(\mathbf{q}, \omega) - \frac{\omega}{2k_B T} \langle NLu(\mathbf{q}, \omega) NLu(-\mathbf{q}, -\omega) \rangle \quad (8.133)$$

where $L''(q, \omega)$ is the dissipative part of the linear response function.‡ in the overdamped regime ($q_z \ll q_{\perp}$): $L''(\mathbf{q}, \omega) = -\omega(q_z^2 \eta_u^0 + q_{\perp}^2 \tilde{\eta}^0)$; $\tilde{\eta}^0 = v_1^0 + v_2^0 = \alpha_1 + \alpha_4 + \alpha_{56} = \eta_1 + \eta_2 - 2\eta_3 + \eta_4 - 2\eta_5$. The superscript 0 indicates bare values of the viscosities.

Evaluating the average in a decoupling (Gaussian) approximation,

$$\begin{aligned} \chi''(\mathbf{q}, \omega) &= L''(\mathbf{q}, \omega) - \frac{\omega B^2}{8k_B T} \int \frac{d^3 k}{8\pi^3} \frac{d\Omega}{2\pi} \langle u(\mathbf{k}, \Omega) u(-\mathbf{k}, -\Omega) \rangle, \\ &\quad \langle u(\mathbf{q} - \mathbf{k}, \omega - \Omega) u(\mathbf{k} - \mathbf{q}, \Omega - \omega) \rangle \Gamma(\mathbf{k}, \mathbf{q}). \end{aligned} \quad (8.134)$$

$\Gamma(\mathbf{k}, \mathbf{q})$ is obtained easily from the brackets in (8.130).

To quadratic order in the \mathbf{q} wavevector

$$\Gamma(\mathbf{k}, \mathbf{q}) = 2(q_z k_{\perp}^2 + 2k_z(\mathbf{q}_{\perp} \cdot \mathbf{k}_{\perp}))^2. \quad (8.135)$$

One still has to express $\langle u(k, \Omega) u(-k, -\Omega) \rangle$. To lowest order in perturbation, this is done easily, using the linear theory and the fluctuation dissipation theorem (in which g is considered as the force). A further remark has to be made: the modes that are important in (8.134) are those for which the amplitude of the fluctuations are large, i.e. those for which $k_z \sim \lambda k_{\perp}^2$. One knows that these modes are ‘nematic-like’, i.e. totally overdamped. It is then sufficient to use the overdamped response to calculate the u fluctuations. Thus one can take

$$\langle u(\mathbf{k}, \Omega) u(-\mathbf{k}, -\Omega) \rangle = \frac{2k_B T \eta_3 k_{\perp}^2}{(Bk_z^2 + K_1 k_{\perp}^4)^2 + (\omega \eta_3 k_{\perp}^2)^2}. \quad (8.136)$$

The $q_z^2(q_{\perp}^2)$ dependent part of the integral renormalizes $\tilde{\eta}(\eta_3)$. The most

† The minus sign corresponds to the fact that, since g_z is the field, the advanced response function has to be used.

‡ To obtain the correct sign for $L''(q, \omega)$ one has to pay attention to the fact that, when g_z is expressed as a function of \mathbf{u} , the retarded response has to be used.

dramatic dependence is obtained for $\tilde{\eta}$

$$\delta\tilde{\eta} = \tilde{\eta}^{\text{eff}} - \eta^0 = B^2 I(\mathbf{q}, \omega), \quad (8.137a)$$

$$I(\mathbf{q}, \omega) = \int \frac{\eta_3^2 k_B T k_{\perp}^8 (d^3 k / 8\pi^3) d\omega'}{[(B(k_z^2 + \lambda^2 k_{\perp}^4))^2 + (\omega' \eta_3 k_{\perp}^2)^2] \times [(B((k_z - q_z)^2 + \lambda^2(k_{\perp} - \mathbf{q}_{\perp})^4))^2 + ((\omega - \omega') \eta_3 k_{\perp}^2)^2]} . \quad (8.137b)$$

This integral is finite for ω and/or $\mathbf{q} \neq 0$, but diverges when both ω and \mathbf{q} go to zero. For $\omega(\eta_u/B) > (\lambda q_z, \lambda^2 q_{\perp}^2)$, the value of the integral is governed by the frequency cut-off

$$\delta\tilde{\eta} = \frac{Bw}{64\omega}. \quad (8.138)$$

The viscosity $\tilde{\eta}$ is found to diverge like ω^{-1} at low frequency! This is much more dramatic than in the static case. Ignoring $\tilde{\eta}^0$ for the sake of argument, suppose you measure a viscosity of 1 poise at one megahertz you will then measure 10 at 100 kilohertz, 100 at 10 kilohertz, etc.! Note that, at sufficiently small frequencies, the diverging part will always dominate the bare viscosity.

If ω is further reduced, the condition $\omega\eta_3/B > \max\{q_z\lambda, \lambda^2 q_{\perp}^2\}$ is no longer fulfilled. The viscosity is then governed by the wavevector and independent of frequency. The rule $\chi''(\omega = 0) = 0$ is thus satisfied, which would not be the case if (8.138) were holding all the way down to zero frequency.

$$\delta\tilde{\eta} = \begin{cases} \frac{1}{q_z} & q_z > \lambda q_{\perp}^2 \\ \frac{1}{\lambda q_{\perp}^2} & \lambda q_{\perp}^2 > q_z. \end{cases} \quad (8.139)$$

In finite-size samples, the largest possible viscosities are thus governed by the linear dimensions of the system.

Why these spectacular results? Damping describes how energy is transferred from one mode to all others existing in the system. Usually, it is governed by short-range interactions. The novelty here comes from the very large amplitude of the undulation mode: the lower the frequency the larger is the response and thus the contribution to the damping.

What about the shear viscosity η_3 ? The formula is almost the same

$$\begin{aligned} \delta\eta_3 &= \eta_3^{\text{eff}} - \eta_0 \\ &= \int \frac{4B^2 \eta_3^2 k_B T k_{\perp}^6 k_z^2 (d^3 k / 8\pi^3) d\omega'}{[(B(k_z^2 + \lambda^2 k_{\perp}^4))^2 + (\omega' \eta_3 k_{\perp}^2)^2] \times [(B((k_z - q_z)^2 + \lambda^2(k_{\perp} - \mathbf{q}_{\perp})^4))^2 + ((\omega - \omega') \eta_3 k_{\perp}^2)^2]} . \end{aligned} \quad (8.140)$$

The only sizeable difference is the replacement of k_\perp^8 by $k_\perp^6 k_z^2$. Since the integral is governed by wavevectors and frequencies such that $k_z \sim \lambda k_\perp^2 \sim \omega \eta_3 \lambda^{-1}/B$, taking $k_\perp = O(\varepsilon)$ and $k_z = \omega = O(\varepsilon^2)$, one finds by simple power counting that the integrand behaves at small (\mathbf{k}, ω') like ε^{-2} in (8.137) and like ε^0 in (8.140). Hence there is a ω^{-1} divergence for $\tilde{\eta}$, a logarithmic one of η_3 (for $\omega(\eta_3/B) > \max(\lambda q_z, \lambda^2 q_\perp^2)$) giving

$$\delta\eta_3 = \frac{w}{128\pi} \eta_3 \ln\left(\frac{k_c^2 K_1}{\rho_0 \eta_3 \omega}\right). \quad (8.141)$$

The difference comes only from the coupling to the undulation mode: since $k_z \sim \lambda k_\perp^2$, k_z is much less efficient than \mathbf{k}_\perp . As the shear viscosity η_3 appears on both sides of (8.141), we also see that the approximate procedure adopted here is not valid at very low frequencies.

One can also understand in the same manner the difference between the dynamics and the statics: the corrections to \tilde{B} depend on very similar integrals over correlation functions

$$\left. \begin{aligned} \delta\tilde{B} &\rightarrow \int d^3k k_\perp^4 \langle u(\mathbf{k})u(-\mathbf{k}) \rangle^2, \\ \delta\tilde{\eta} &\rightarrow \int d^3k k_\perp^4 d\omega' \langle u(\mathbf{k}, \omega')u(-\mathbf{k}, -\omega') \rangle^2. \end{aligned} \right\} \quad (8.142)$$

The difference stems from the u fluctuations: if $\langle u(\mathbf{k})u(-\mathbf{k}) \rangle = [O(\varepsilon^4)]^{-1}$ one deduces right away from the Kramers–Kronig relations that $\langle u(\mathbf{k}, \omega)u(-\mathbf{k}, -\omega) \rangle = [O(\varepsilon^6)]^{-1}$ which is a more dangerous divergence.

8.4.2 More general results

The simple derivation that we have adopted can be implemented in essentially two ways.

1. Lift the incompressibility assumption keeping the first-order approximation [46, 47].
2. Include other non-linearities, and go beyond the first-order approximation [46, 47, 36].

The first part of the programme can be performed in exactly the same way as was done in Section 8.4.1. It allows us to give detailed predictions concerning each of the five viscosities; the results are most easily expressed in the Harvard notation (remember (8.19))

$$\delta\eta_1 = (B - C)^2 I(\mathbf{q}, \omega) \quad (8.143a)$$

$$\delta\eta_2 = 0 \quad (8.143b)$$

$$\delta\eta_4 = C^2 I(\mathbf{q}, \omega) \quad (8.143c)$$

$$\delta\eta_5 = C(C - B)I(\mathbf{q}, \omega) \quad (8.143d)$$

$\delta\eta_3$ is still given by (8.141).

Relations (8.143a)–(8.143d) imply the important relation

$$\delta\eta_1 \delta\eta_4 = \delta\eta_5^2. \quad (8.144)$$

The absence of renormalization of η_2 seems at first sight natural since it corresponds to the ‘in-plane’ shear viscosity, characteristic of the two-dimensional fluid nature of smectic layers.

The inclusion of other non-linearities and of higher-order corrective terms does not change the ω^{-1} (or q_z^{-1}, q_\perp^{-2}) divergence of the viscosities. The coefficients appearing in (8.143) change, however; one does not know how different from the first-order expression they may be. An important result is that (8.143b) and (8.144) hold to all orders in perturbation theory [36].

η_3 is shown to obey a law similar to (8.123) in which the argument in the logarithm is that of (8.141) and the exponent of the order of 1/10 is not universal [47].

Remark. A straightforward use of Kramers–Kronig relations shows that the calculation of B from $\chi''(q, \omega)$ is compatible with (8.114) in the low-frequency regime. If $(\omega\eta_3/2B) > \max\{\lambda k_z, \lambda^{-2}k_\perp^2\}$, a formula similar to (8.114) holds, except for the replacement in the argument of the logarithm of λ^{-1} by $\lambda^{-2}\mu$. $\mu = \eta_3/(2pB)^{1/2}$ is the third length of smectic hydrodynamics usually much larger than molecular size.

8.4.3 Columnar phases

This case is fairly similar to that of smectics although the statics involves neither divergences of the elastic constants nor a Landau–Peierls instability [49]. The important non-linear coupling reads

$$(\nabla_z \mathbf{u}_\perp)^2 (\nabla_\perp \cdot \mathbf{u}_\perp), \quad (8.145)$$

which is reminiscent of the $\nabla_z u (\nabla_\perp \mathbf{u})^2$ in smectics but is not connected to the tube compressional elastic modulus. Indeed, a rotationally invariant expression of the elastic energy of a crystal involves the symmetrized strain tensor [50]

$$U_{ij} = \frac{1}{2}(\nabla_i u_j + \nabla_j u_i - \nabla_i u_k \nabla_j u_k). \quad (8.146)$$

Since there is no u_z variable in columnar phases, no symmetric $U_{z\perp}$ strain can be built. The column compression, and pure shear involve U_{xx}^2 and $(u_{\alpha\beta} u_{\alpha\beta} - \frac{1}{2}u_{xx}^2)$, respectively (in which $\alpha, \beta = x, y$), and are described as in (7.28) by the elastic constants \bar{B} and C . Note that they do not involve any $(\nabla_z \mathbf{u}_\perp)^2$. Expression (8.145) stems from the $U_{zz} U_{xx}$ invariant which is cubic

in the deformation (to lowest order) because $U_{zz} = -\frac{1}{2}\nabla_z U_\alpha \nabla_z U_\alpha$ ($\alpha = x, y$). It is characterized by an elastic modulus independent of B and C . Aside from this difference and the need for treating transverse fluctuations independently from longitudinal ones,[†] the procedure follows exactly the one adopted for smectics. A straightforward transposition of formula (8.137b) shows that the behaviour of the viscosities is controlled by integrals of the type

$$I(q, \omega) \propto \int \frac{k_z^8 d^3k d\omega'}{\left[(k_\perp^2 + \lambda^2 k_z^4)^2 + \left(\frac{\omega}{\Omega_0} k_z\right)^2 \right] \times \left[((\mathbf{k}_\perp - \mathbf{q}_\perp)^2 + \lambda^2(k_z - q_z)^4)^2 + \left(\frac{(\omega - \omega')}{\Omega'_0} k_\perp^2\right)^2 \right]} \quad (8.147)$$

in which Ω_0, Ω'_0 = (elastic constant/ η_3) are characteristic frequencies relevant to the longitudinal or transverse cases and λ^2 is a linear combination of λ_B^2 and λ_C^2 . Taking $k_z = O(\varepsilon)$ and $k_\perp = \omega = O(\varepsilon^2)$, one finds $I(q, \omega) \sim O(\varepsilon^{-1})$.

This shows that the integral diverges at low frequencies as $\omega^{-1/2}$ (or $q_\perp^{-1/2}, q_z^{-1}$ if the wavevector provides the cut-off). Thus viscosities are expected to diverge as $\omega^{-1/2}$ in columnar phases [49, 51]. The relation

$$\delta\eta_1 \delta\eta_4 = (\delta\eta_5)^2 \quad (8.148)$$

is predicted to hold again [49].

The correction to the shear viscosity η_3 is obtained by replacing k_z^8 in (8.147) by $k_z^6 k_\perp^2$. The integral now scales as $O(\varepsilon)$; hence it is well defined for $\mathbf{q} = \omega = 0$ and is dominated by the large wavevector cut-off (i.e. short-range order). η_3 is regular in columnar phases.

8.4.4 Experimental situation

Fundamental as they are, the Grinstein–Pelcovitz and Mazenko–Ramaswamy–Toner predictions attain their full importance only to the extent that they are experimentally observed.

We find (to first order)

$$\frac{\delta\eta}{B} \sim \frac{w}{64\omega}.$$

Far from any phase transition the dimensionless number w should be of order unity. Thus one expects

$$\frac{\delta\eta}{B} \sim \text{a few } 10^{-2}/\omega. \quad (8.149)$$

[†] Longitudinal fluctuations $\mathbf{u}_\perp = (1/q)(\mathbf{q} \cdot \mathbf{u}(\mathbf{q}))$; transverse fluctuations: $\mathbf{u}_\perp = \mathbf{u} - (1/q)(\mathbf{q} \cdot \mathbf{u}(\mathbf{q}))$.

Taking $B \sim 10^8 \text{ erg cm}^{-3}$, $\omega = 10^7 \text{ rad s}^{-1}$, gives the typical figure

$$\delta\eta \sim \text{a few } 10^{-1} \text{ g cm}^{-1} \text{ s}^{-1}$$

in the megahertz range. This correction is not easily observed. There are, however, two simple ways of getting a larger $\delta\eta$.

1. Consider a compound with a large B (more correctly, B or C , or their difference).
2. Measure η at a much lower frequency.

In both cases, resonance techniques have been used [52–54]. Early experiments using pulse techniques did reveal anomalous damping [55] but the measured effects were too large at least for one compound [56].

In the first-sound ($i = 1$) [52, 53] or in the second-sound ($i = 2$) [54] domains, the smectic response assumes a simple dependence of the type

$$(\text{slowly varying numerator})/(C_i^2(f)q^2 - \omega^2 - i\omega\eta_i(f)q^2\rho^{-1}) \quad (8.150)$$

in which $C_i(f)$ is the sound velocity given by (8.43), and $\eta_i(f)$ a direction-dependent viscosity (remember f is the angle between \mathbf{q} and the optical axis [1, 49]). For $C, B \ll A$:

$$\left. \begin{aligned} \eta^{(1)}(f) &= (\eta_2 + \eta_4) \sin^2 f + \eta_1 \cos^2 f (2\eta_3 - \tilde{\eta}) \cos^2 f \sin^2 f \\ \eta^{(2)}(f) &= \eta_3 + (\tilde{\eta} - 2\eta_3) \cos^2 f \sin^2 f. \end{aligned} \right\} \quad (8.151)$$

f is, as in (8.43), the angle between \mathbf{q} and the optical axis. The viscosities contain a $1/\omega$ diverging part. Expression (8.150) shows that, as usual, the analysis of the resonance provides a measure of the sound velocity (hence elastic constants) and of the viscosities. In well defined geometries, excitation of the harmonics provides a simple way of varying ω . One does find that the viscosities have an anomalous part, diverging like ω^{-1} . With ultrasonic techniques, for TBBA (terephthal-bis-*p*-*p*'-butyl aniline) the anomalous part of η_1 (the largest) has been found to be of the order of 2 poise at one megahertz (15 K away from the nematic phase). (This large value is linked to the ‘large’ value of $B - C \sim 5 \cdot 10^8 \text{ erg cm}^{-3}$ [53].) The angular dependence has also been successfully compared to theory, and the most striking result is certainly the fulfilment of the relation $\delta\eta_5^2 = \delta\eta_1 \delta\eta_4$ within 3 per cent uncertainty.† The K_1 value of TBBA being unknown, the validity of the first-order corrections could not be tested. The second-sound regime allows the measurement of $\delta\tilde{\eta}$ at frequencies ranging from the 10 to 200 kHz [54]; $\delta\tilde{\eta}$ reaches a value as large as 80 poise at 10 kHz for 8 CB (octyl cyanobiphenyl) (4 K away from the nematic phase)! Since K_1 and B are known for 8 CB, the first-order correction (8.138) could be compared to

† Recent measurements in the S_C phase of TBBA are compatible with the same angular dependence, but with $B < C$ (versus $B > C$ in the S_A case) [57].

experiment without adjustable parameter: it is satisfactory in terms of order of magnitude although small by a factor of about four.

Lower-frequency experiments would, in principle, allow us to demonstrate the finite size dependence of viscosities. This is, however, unpractical because dislocation motion perturbs the smectic behaviour at very low frequencies (typically below 10³ Hz).

REFERENCES

1. Martin, P. C., Parodi, O., and Pershan, P. S. *Phys. Rev. A* **6**, 2401 (1972).
2. de Gennes, P. G. *J. Phys. (Paris) Colloq.* **30** (Suppl. C4), 65 (1969).
3. Prost, J. and Clark, N. In *Liquid crystals, Proceedings of the International Conference, Bangalore 1979* (ed. S. Chandrasekhar), p. 53. Heyden, Philadelphia (1980).
4. Brand, H. and Pleiner, H. *Phys. Rev. A* **24**, 2777 (1981).
5. Delaye, M. and Keller, P. *Phys. Rev. Lett.* **37**, 1065 (1976). In the vicinity of the S_A–S_C transition this time diverges and can reach values as large as a few 10⁻⁴ s to 10⁻³ s a few millidegrees away from the transition.
6. De Jeu, W. H. In *Liquid crystals* (ed. L. Liebert), p. 109. Academic Press, New York (1978).
7. De Groot, S. and Mazur, P. *Non-equilibrium thermodynamics*. North-Holland, Amsterdam (1962).
8. Helfrich, W. *Phys. Rev. Lett.* **23**, 372 (1969).
9. Brand, H. and Pleiner, H. *J. Phys. (Paris)* **45**, 563 (1984).
10. Lubensky, T. C. *Phys. Rev. A* **6**, 452 (1972).
11. de Gennes, P. G. *Physics of Fluids* **17**, 1645 (1974).
12. Ribotta, R., Salin, D., and Durand, G. *Phys. Rev. Lett.* **32**, 6 (1974); Prost, J. and Pershan, P. S. *J. appl. Phys.* **47**, 2298 (1976).
13. Birecki, H., Schaetzing, R., Rondelez, F., and Litster, J. D. *Phys. Rev. Lett.* **36**, 1376 (1976).
14. Bartolino, R. and Durand, G. *J. Phys. (Paris)* **42**, 1445 (1981).
15. Oswald, P. and Kleman, M. *J. Phys. (Paris) Lett.* **43**, L411 (1982).
16. Clark, N. A. *Phys. Rev. Lett.* **40**, 1663 (1978).
17. The anisotropy of the 'first sound' has been widely studied. See, for example, for early work, Miyano, K. and Ketterson, J. B. *Phys. Rev. Lett.* **31**, 1047 (1973).
18. Second sound has been observed by acoustical methods and reported by Bacri, J. C. *J. Phys. (Paris) Colloq.* **37** (Suppl. C3), 119 (1976).
19. Liao, Y., Clark, N., and Pershan, P. S. *Phys. Rev. Lett.* **30**, 639 (1973).
20. In contrast to nematics, in which curvature elastic constants do not vary dramatically, smectics can exhibit compressional elastic constants ranging from a few 10⁹ erg cm⁻³ down to 10⁵ erg cm⁻³ and even smaller in lyotropic phases. See for example, Roux, D. and Safinya, C. R. *J. Phys. (Paris)* **49**, 673 (1987).
21. Ricard, L. and Prost, J. *J. Phys. (Paris) Colloq.* **40** (Suppl. C3), 83 (1979); *J. Phys. (Paris)* **42**, 861 (1981).
22. Brochard, F. *Phys. Lett.* **49A**, 315 (1974).
23. Liu, M. *Phys. Rev. A* **19**, 2090 (1979).

24. Kirby, F. and Martinoty, P. *J. Phys. (Paris)* **37** (Suppl. C3), 113 (1976); **39**, 1019 (1978).
25. Bradberry, G. W. and Vaughan, J. M. *Phys. Lett.* **62**, 225 (1977).
26. Brand, H. and Pleiner, H. *J. Phys. (Paris)* **43**, 853 (1982).
27. Cladis, P. E., Couder, Y., and Brand, H. R. *Phys. Rev. Lett.* **55**, 2945 (1985).
28. Pleiner, H. and Brand, H. *Phys. Rev.* **A29**, 911 (1984).
29. Brand, H. R. and Pleiner, H. *J. Phys. (Paris)* **45**, 563 (1984).
30. Léger, L. and Martinet, A. *J. Phys. (Paris)* **37** (Suppl. C3), 89 (1976).
31. Battacharya, S. and Letcher, S. V. *Phys. Rev. Lett.* **44**, 414 (1980).
32. Horn, R. G. and Kleman, M. *Ann. Phys. (Paris)* **3**, 229 (1978).
33. Oswald, P. and Kleman, M. *J. Phys. (Paris) Lett.* **45**, L319 (1984).
34. Cagnon, M. and Durand, G. *Phys. Rev. Lett.* **45**, 1418 (1980).
35. Ramaswamy, S. *Phys. Rev.* **A29**, 1506 (1984).
36. Milner, S. T. and Martin, P. C. *Phys. Rev. Lett.* **56**, 77 (1986).
37. Cagnon, M. and Durand, G. *J. Phys. (Paris) Lett.* **42**, L451 (1981).
38. Brochard, F. *J. Phys. (Paris)* **37** (Suppl. C3), 85 (1976).
39. Bartolino, R. and Durand, G. *J. Phys. (Paris) Lett.* **44**, L79 (1983).
40. Orsay Group on Liquid Crystals. *J. Phys. (Paris)* **36** (Suppl. C1), 305 (1975).
41. Cagnon, M., Gharbia, M., and Durand, G. *Phys. Rev. Lett.* **53**, 938 (1984).
42. Young, C. Y., Pindak, R., Clark, N. A., and Meyer, R. B. *Phys. Rev. Lett.* **40**, 773 (1978).
43. Pieranski, P., Guyon, E., and Keller, P. *J. Phys. (Paris)* **36**, 1005 (1975).
44. Prost, J. In *Symmetries and broken symmetries in condensed matter physics* (ed. N. Boccara), p. 123, IDSET, Paris (1981); *J. Phys.* **39**, 639 (1978); *Ferroelectrics* **84** (I), 261 (1988).
45. Grinstein, G. and Pelcovits, R. *Phys. Rev. Lett.* **47**, 856 (1981).
46. Mazenko, G. F., Ramaswamy, S., and Toner, J. *Phys. Rev. Lett.* **49**, 51 (1982).
47. Mazenko, G. F., Ramaswamy, S., and Toner, J. *Phys. Rev.* **A28**, 1618 (1983); see also Kats, E. I. and Lebedev, V. V. *Sov. Phys. JETP* **58**, 1172 (1983).
48. Kleman, M. and Parodi, O. *J. Phys. (Paris)* **36**, 671 (1975).
49. Ramaswamy, S. and Toner, J. *Phys. Rev.* **A28**, 3159 (1983).
50. Landau, L. D. and Lifshitz, E. M. *Theory of elasticity*. Pergamon, London (1959).
51. Kats, E. I. and Lebedev, V. V. *Sov. Phys. JETP* **59**, 325 (1984). The $\omega^{\sqrt{2}-2}$ regime proposed in this article holds if local dissipation is absent or negligible.
52. Gallani, J. L. and Martinoty, P. *Phys. Rev. Lett.* **54**, 333 (1985).
53. Collin, D., Gallani, J. L., and Martinoty, P. *Phys. Rev.* **A34**, 2255 (1986).
54. Baumann, C., Marcerou, J. P., Prost, J., and Rouillon, J. C. *Phys. Rev. Lett.* **54**, 1268 (1985).
55. Battacharya, S. and Ketterson, J. B. *Phys. Rev. Lett.* **49**, 997 (1982).
56. Gallani, J. L. and Martinoty, P. *Phys. Rev. Lett.* **53**, 1065 (1984).
57. Collin, D., Gallani, J. L., and Martinoty, P. *Phys. Rev. Lett.* **58**, 254 (1987).

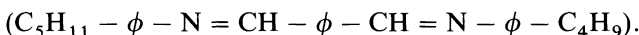
DEFECTS IN SMECTICS AND COLUMNAR PHASES

9.1 OBSERVATIONS

9.1.1 Large deformations in smectics

9.1.1.1 ‘Plages à éventail (‘fan texture’) in S_A

Observe under a microscope, between crossed polarizer and analyser, a few-micron-thick slab of terephthal-bis pentylaniline



At a temperature higher than 232°C, the compound is in its isotropic state and the field of view altogether black. Below 232°C, the ‘*texture à fils*’ (*Schlieren*) that we described in Chapter 4 appears. It corresponds, of course, to a nematic phase. Some of the regions may stay perfectly black (homeotropic regions) which shows that the system is uniaxial. If we keep on cooling down, below 213.5°C, a new texture appears (Fig. 9.1). The name ‘*texture à éventails*’ was given by Friedel [1] (‘fan-shaped texture’). On closer scrutiny one observes (Fig. 9.2(a)) two networks of polygons each located close to a liquid crystal–glass interface and containing ellipses that are tangent to each other and to the sides of the polygons. Their sides are curved: they are portions of hyperbolas. Only one of the foci of the ellipses is visible; from this focus a line emerges, which in some cases may be hinted to be a branch of hyperbola contained in a plane perpendicular to the ellipse. Often the slab exhibits bright colours characteristic of birefringence interferences.

There are remarkable geometrical peculiarities: if you consider two tangent ellipses (Fig. 9.2(b)), you can easily check that the line joining the visible focus F_1 of one ellipse to the invisible focus F_2 of the other goes exactly through the tangential point M! The same holds with the portion of hyperbola delineating the side of the polygons and the ellipses (Fig. 9.2(c)). Thus, if you draw the lines M_iF_i of ellipses tangent to the same side of a polygon, they all intersect in one point! These rules have been carefully checked on a fairly large number of examples [2]. They led to the conclusion that phases that gave these textures (i.e. smectics!) were made of layers even before X-rays gave more direct evidence of this [1, 3]. Nowadays, electron microscopy allows to visualize neatly the topology of these defects (Fig. 9.3) [4]. Note that the homeotropic regions are still perfectly black: the system

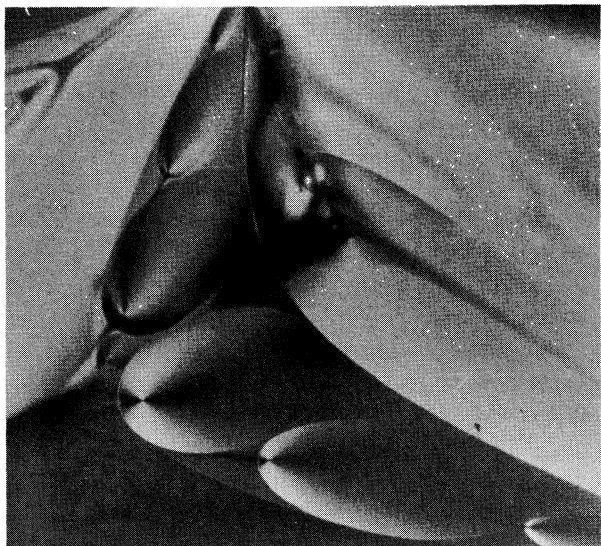


Fig. 9.1. ‘*Texture à éventails*’. Typical focal conics. The ellipses are just at the interface between the smectic sample and the cover glass. (The image is found on this plane.) The hyperolas are normal to the plane of the sheet. (Courtesy C. Williams.) The various ellipses are grouped in a polygonal superstructure as described in the text.

is in a smectic A phase that exhibits all the symmetry properties detailed in Chapter 7.

9.1.1.2 *Textures in other smectics*

If you keep on cooling, a new textural change occurs at 182.5°C . The polygonal network still exists but, in a given ellipse at locations where the appearance was homogeneous, one can sometimes observe two significantly different colours separated by a sharp line. Furthermore, the regions which used to be totally dark, exhibit a *Schlieren* texture fairly analogous to that of a nematic. These observations are characteristic of a S_C : in a given ellipse, the tilt direction may change and hence the colour. Decreasing the temperature below 153.5°C , one sees a faint front sweeping through the sample, which suggests another phase transition to a phase called S_F . The texture is essentially identical to that of S_C (at least within a few degrees from 153.5°C), the only difference lies in the much weaker intensity of the fluctuations. One might think that, in the absence of paramorphosis, this observation should be sufficient to infer that there is no symmetry difference between S_C and S_F . Although the conclusion is true, as careful X-ray analysis reveals (remember Section 1.4.3 of Chapter 1), the optical observation is not sufficient in itself. Indeed polygonal domains similar to that of S_A may be

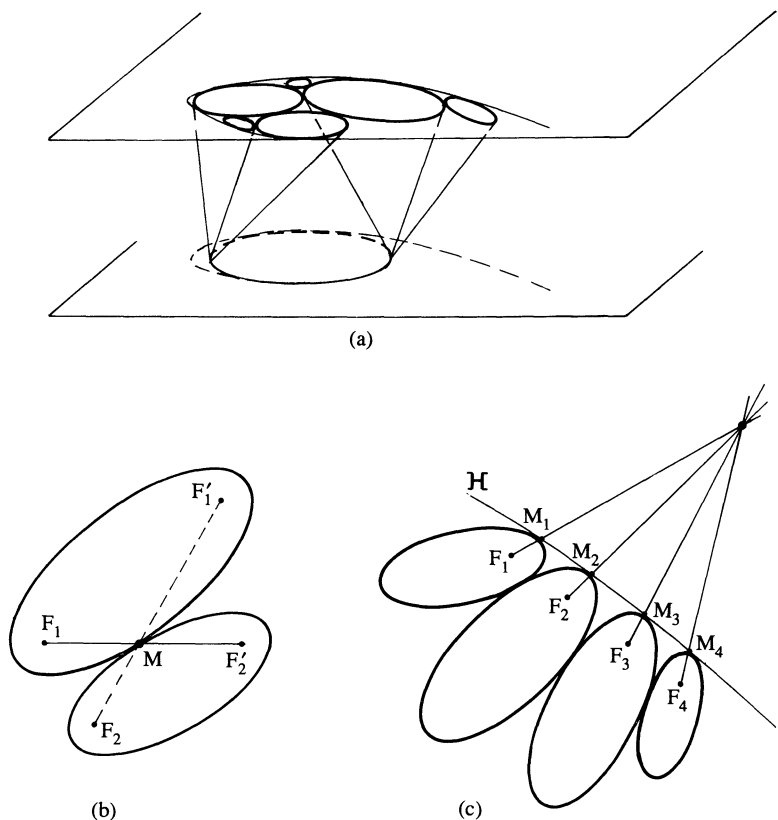


Fig. 9.2. (a) Arrangement of tangent focal conics building up polygonal domains. (b) The tangential point sits at the intersection of the segments joining the focal points. (c) All the lines F_iM_i joining the foci to the tangential points merge in a common point: the hyperbola focus.

seen in $S_{BH_{ex}}$, although it is a genuinely new phase (the new types of disclinations characteristic of $S_{BH_{ex}}$ are not directly coupled to light).

To sum up, in S_C and related phases one can see smectic A types of textures but also nematic-like *Schlieren* (we will see, however, that 1/2 disclinations do not exist in S_C).

9.1.1.3 Parabolic defect structure in S_A

Up to now we have described what happens when no special surface treatment is given to the coverslips containing the smectic. The observations are different when either homeotropic or parallel alignment is enforced. In the latter case, a uniform alignment is observed almost everywhere but, from place to place, one sees lines appearing in the form of ‘wishbones’, the tails



Fig. 9.3. Part of a focal domain as seen with electron microscopy. The tapped jelly roll character of the structure around the ellipse is clearly visible. The arrow 1, shows layers close to the hyperbola. Arrows 2 and 3 correspond to another domain. (Courtesy of M. Allain [18].)

of which are oriented normal to the undisturbed layers [5]. Measurements of the wishbone opening show that it can properly be represented by a parabola parallel to the coverslips and basically in the middle of the sample. The tail appears to be in focus above the plane of the parabola. Furthermore, tilting the sample reveals that the tail is itself a parabola located in a plane perpendicular to the slides (and to the unperturbed layers). Thus this type of defect is characterized by two intertwined parabolas with an antiparallel orientation and rotated 90° from each other about the unperturbed optic axis. The lines of the wishbone disappear sufficiently far from the centre of the defect leaving a perfectly oriented sample. We will see that, although the appearance of the wishbone texture is quite different from that of the fans, focal conics do provide the proper framework for the description of both observations.

The case of homeotropic alignment is somewhat different. Under perfectly controlled circumstances it is very hard to see any defect at all. However, when pulling the slides, one triggers as mentioned in Section 7.1.7 an undulation instability. Further pulling leads to a square lattice of defects that corresponds obviously to distortions larger than simple undulations (Fig. 9.4) [5]. As in the fan texture, there are two lattices in focus either near the top or the bottom slides: the vertex of one lattice sits in the centre of

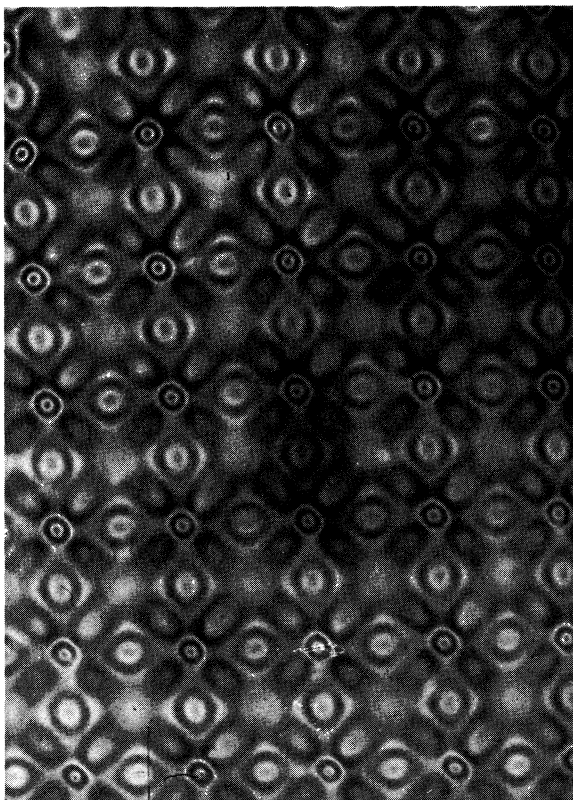


Fig. 9.4. Square pattern of undulation induced by mechanical tension in a cholesteric (courtesy F. Rondelez). Similar patterns are generated by mechanical tension in smectics: for large enough deformations one observes the square array of parabolic focal conics described in the text [5].

the other. Closer attention reveals that focal lines similar to the one described in the wishbone case emerge from the vertices (note that they run essentially perpendicular to the slides in this later case). This texture can again be understood in terms of focal conics. It can also be obtained by shear [6].

9.1.1.4 Focal conics

In the limit of incompressible layers, the geometrical objects that represent them are necessarily stacks of parallel surfaces. Families that involve only line singularities are Dupin cyclides. Their construction is depicted in Fig. 9.5. Starting from the jelly roll of Fig. 9.5(a), wrap it into a torus as depicted in Fig. 9.5(b). Fill the remaining space by piling layers on top of the torus. One now has two singular lines: the circle L_1 , located in the x, y -plane is the core of the $m = 1$ disclination originating from the initial

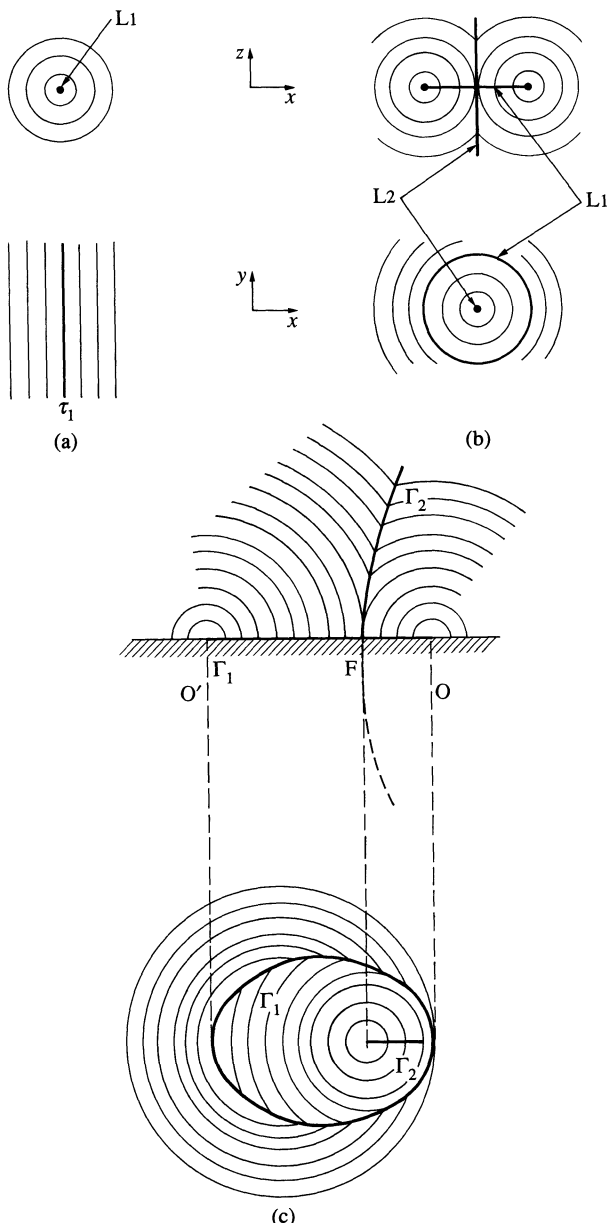


Fig. 9.5. Generation of a focal conic domain. (a) Simple 'jelly roll' or 'myelinic' arrangement generating a tube. (b) Tube closed into a torus: note the two singular curves (a circle and a straight line). The straight line L_2 is obtained by piling layers on the torus to fill space. (c) Generalization: the circle becomes an ellipse; the straight line becomes a hyperbola; with tangential boundary conditions for the molecules the ellipse is often stuck to the limiting surface.

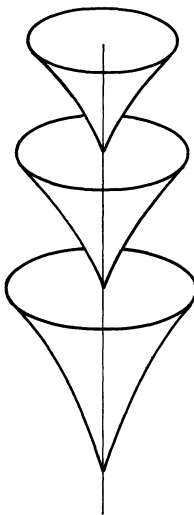


Fig. 9.6. Blow up of the L_2 line. Compare with Fig. 9.3, arrow 1.

'jelly roll' configuration. The straight line L_2 does not correspond to an *a priori* topologically stable defect of smectics: it corresponds to a stack of cone apexes (Fig. 9.6) [7]. From construction, the intersection of the x, y -plane with the smectic layers, are circles having the same centre—the origin. In the x, y -plane the L_1 line does not look singular. Let us now split this unique centre in two: one F for the layers contained inside L , the other F' for those contained outside (Fig. 9.5(c)). F which corresponds to the inner layers is visible experimentally; F' which corresponds to the outer ones has no physical existence. During the process L_1 is replaced by Γ_1 which now is also a stack of cone apexes like those of Fig. 9.6. For a point M moving on Γ_1 of Fig. 9.5(c), any time the distance MF is reduced by one layer thickness, the distance MF' is increased by exactly the same amount. Thus $MF + MF' = \text{const}$. Γ_1 is an ellipse with foci F and F' (only F is physically visible). During the same process, L_2 has been transformed into Γ_2 : similarly, the layer conservation rule tells us that, on Γ_2 , $MO' - MO = \text{const}$. Γ_2 is a hyperbola with foci O and O' . Γ_1 and Γ_2 are conjugate to each other (O is both the focus of Γ_2 and the apex of Γ_1 ; reciprocally, F is both the focus of Γ_1 and the apex of Γ_2). Layers delineate Dupin cyclides and their parallel stack forms a focal domain. One could imagine other arrangements, but they would, in general, involve surface singularities rather than lines and thus would cost more energy (J. Friedel; see reference 2).

Thus one understands the observations of Section 9.1.1.1: the ellipses and hyperbolas are the focal lines corresponding to Γ_1 and Γ_2 . The location of ellipses at the slides–liquid crystal interfaces is consistent with degenerate parallel boundary conditions (i.e. layers perpendicular to the interface but

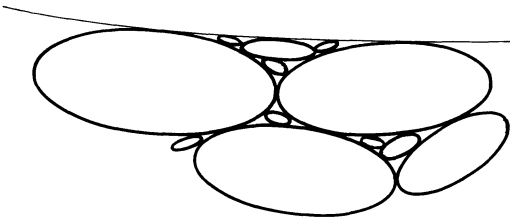


Fig. 9.7. Apollonius packing of ellipses.

no specified direction for the normal). Under such conditions neighbouring ellipses can only be tangent: indeed a given element cannot belong simultaneously to two different focal domains, except at the point of tangency. The alignment of $F_1MF'_2$ (F_1 the physical focus of ellipse 1, F'_2 the virtual focus of ellipse 2) follows. The same argument could be made for a contact point between a coplanar hyperbola and an ellipse. Thus all the rules mentioned in Section 9.1.1.1 are recovered.

However, to fill space with such rules, one needs an Apollonius packing of ellipses [2, 8] (Fig. 9.7). Careful observation, however, does not reveal self-similar textures over a large scale [9]. Focal conics are an idealization that cannot explain all of the smectics: this idealization neglects compressional energy and dislocations densities.

Note at last that, letting O' and F' go to infinity in Fig. 9.5(c), one obtains a figure involving two intertwined parabolas which correspond exactly to the description of Section 9.1.1.3.

9.1.2 Large deformations in columnar phases

9.1.2.1 ‘Flower texture’

When Chandrasekhar *et al.* [10] observed benzene-hexa-*n*-alkanoates (*n* ranging from 6 to 9) under a polarizing microscope, they observed, cooling from the isotropic phase, a new texture that they described as ‘flower-like’. Indeed, in many cases one can see nucleating from isolated points ‘petals’ that eventually fill the whole field of view. It is easy to check that the director is in the plane of the sample and wraps around the nucleation centre. (Sometimes, when the director is perpendicular to the plane of the sample, one sees facets during the growth process.) Often the visual observation resembles that of a broken fan texture as in a smectic C. There is, however, a sizeable difference: one cannot identify focal lines—neither ellipses nor hyperbolae. When the domains are complete, the nucleation centre appears as an $m = 1$ disclination. Close scrutiny shows that, in fact, it is often a pair of $m = 1/2$ disclinations. Different domains are separated by walls, which can be sharp or not depending on the director discontinuity across the wall [11]. Domains can also split into smaller ones leading to striations similar

to those seen in crystalline S_E [10, 11]. Any two-dimensionally ordered phase can lead to such observations. However, S_A usually look more like S_A simply because of paramorphosis and also because the two-dimensional order is ill coupled to light. On the other hand, S_C does give textures characteristic of biaxial columnar phases.

9.1.2.2 ‘Developable’ domains

Consider a developable surface S like that of Fig. 9.8, and the set of planes π which envelop S (they are tangent to S along the straight lines D). Around every point M of π one can draw a two-dimensional lattice corresponding to that of the columnar structure. Rotating π around S allows one to fill space with the columnar structure. In particular, the infinitesimal rotation from π to π' shows that the curvature centres of the tubes are on D , and that the tube deformation involves only bending (since the structure is obtained by local rotation of π only). Such geometrical objects are called developable domains [12]. If we call \mathbf{n} the local tube axis, the conditions

$$\left. \begin{aligned} \mathbf{n} \cdot \text{curl } \mathbf{n} &= 0 \\ \text{div } \mathbf{n} &= 0 \end{aligned} \right\} \quad (9.1)$$

are clearly satisfied. The first results from the orthogonality of \mathbf{n} everywhere to the planes π . The second expresses that in the generating process ($\pi \rightarrow \pi'$), the number of tubes is conserved. Conditions (9.1) can straightforwardly be obtained from the elastic energy in Section 7.2.8, when the first-order elastic constants \bar{B} and C , are allowed to go to infinity. Thus the developable domains correspond to a level of description comparable to that of focal conics for smectics.

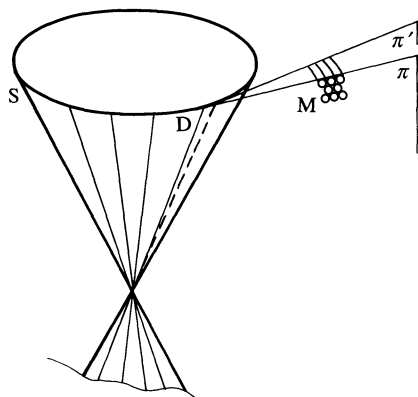


Fig. 9.8. General construction of a developable domain.

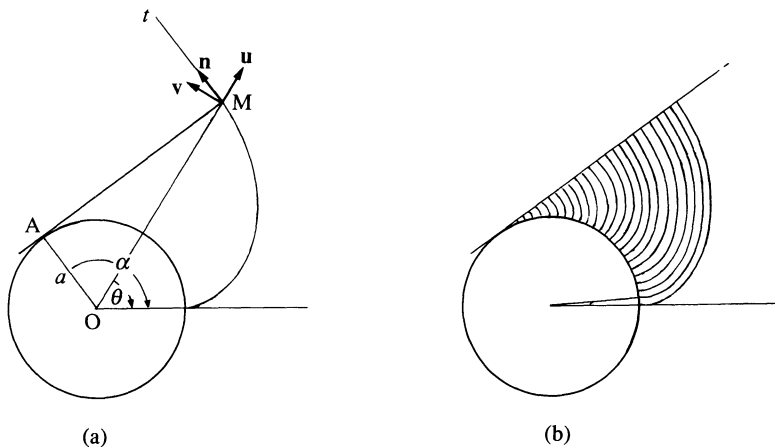


Fig. 9.9. Developable domain generated from a cylinder of revolution.

Problem. Describe mathematically a domain whose developable surface S is a cylinder of revolution, and calculate the corresponding elastic energy (Kleman reference 12).

Solution. Consider the construction of Fig. 9.9(a). In cylindrical coordinates, S is simply given by $\rho = a$. The D lines are parallel to the z -axis and the π planes are tangent to the cylinder. In M , the tube axis n is perpendicular to π , hence parallel to the vector OA . Expressing $n = d\mathbf{OM}/d\theta \propto OA$, one gets

$$\frac{1}{\rho} \frac{d\rho}{d\theta} = \frac{a}{\sqrt{(\rho^2 - a^2)}}.$$

As one could have guessed, the tube direction is perpendicular to the surface S at its starting point. The tube equation can be obtained by simple integration

$$a(\theta - \theta_0) = \int_a^\rho \frac{d\rho'}{\rho'} \sqrt{(\rho' - a^2)}.$$

It is easy to check that one can fill space with tubes of constant diameter (Fig. 9.9(b)): one just has to vary θ_0 by quantized amounts $\delta\theta_0 = \phi/a$ where ϕ is the tube diameter. The tube axis $n = d\mathbf{OM}/ds$ where s is the curvilinear abscissa along the tube is obtained by standard procedures

$$\mathbf{n} = \frac{a}{\rho} \mathbf{u} + \frac{\sqrt{(\rho^2 - a^2)}}{\rho} \mathbf{v}$$

where \mathbf{u} is the unit vector along OM ; and $\mathbf{v} = d\mathbf{u}/d\theta$. Furthermore,

$$\frac{d\mathbf{n}}{ds} = -\frac{\mathbf{u}}{\rho} + \frac{a}{\rho\sqrt{(\rho^2 - a^2)}} \mathbf{v} = \frac{\mathbf{n}_1}{R}$$

where \mathbf{n}_1 , the normal to the tube, points along MA and the curvature radius is given

by $R = \sqrt{(\rho^2 - a^2)}$, i.e. exactly MA. As announced in the general construction, the centre of curvature of the tube axis is located on a generatrix D of the developable surface S.

Now the curvature energy per tube is

$$w_t = \frac{\tilde{K}}{2} \int_{a+\varepsilon}^{\rho_0} \frac{ds}{R^2}$$

with $ds = \rho d\rho/a = R dR/a$ and ε a short-distance cut-off.

$$w_t = \frac{\tilde{K}}{2a} \int_{a+\varepsilon}^R \frac{dR}{R} = \frac{\tilde{K}}{2a} \ln\left(\frac{R_0}{\varepsilon}\right),$$

i.e. with $2\pi a/\phi$ tubes, an energy per unit length

$$w = \pi K_3 \ln\left(\frac{R_0}{\varepsilon}\right)$$

in which we have set $K_3 = \tilde{K}/\phi$. Note that the energy has to be cut off away from the developable surface S; indeed the curvature is infinite on the surface, which is not physical.

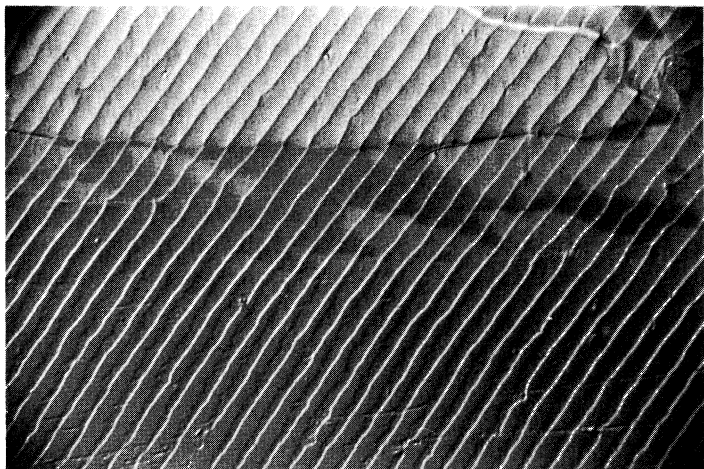
Two remarks have to be made.

1. The overall structure obtained is that of an $m = 1$ disclination line with a core of size a approximately. Yet the director pattern is fundamentally different from that of a nematic, and the energy does not depend on ' a ' explicitly but rather on the gap between S and the location where the developable domain structure starts to hold.
2. Experimentally, the core is large ($\sim 1 \mu\text{m}$) and, as already mentioned, developable domains corresponding to $m = 1/2$ rather than $m = 1$ lines are seen [11]. This will be discussed in Section 9.1.4.4.

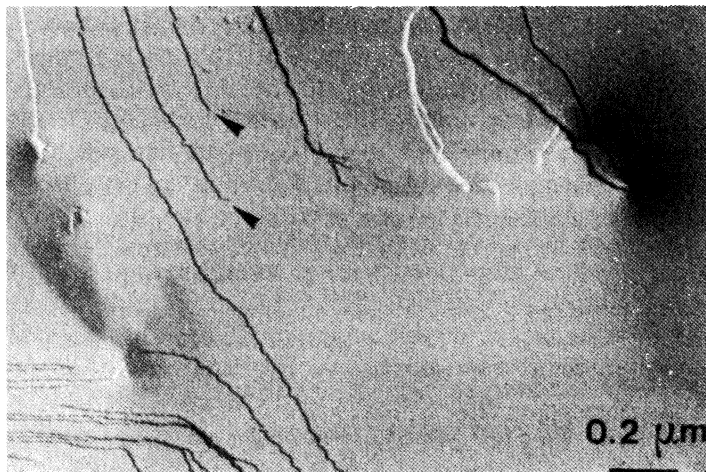
9.1.3 Dislocations

9.1.3.1 Direct evidence

In Section 6.4.2.4 we described the λ lines of cholesterics, which arise in the Cano geometry. The net effect of these lines is to add one pitch to adjust for the increase of the cell thickness in the wedge geometry. (In fact we have seen that, for thicker samples, lines of strength one are observed, which correspond to adding two pitches.) This property of cholesterics is due to their periodicity along the helical axis. Since smectics are also periodic along the normal to the layers, one expects them to exhibit similar lines in similar conditions. There is, however, one sizeable difference between the two systems: whereas in cholesterics the core of the lines falls naturally in the micron range and is thus well suited to microscopic observation, in smectics the core is of the order of a layer spacing (20–30 Å) and is, in general, unobservable with a polarizing microscope. Meyer, Stebler, and Lagerwall [13] have cleverly taken advantage of the S_A – S_C transition to increase



(a)



(b)

Fig. 9.10. (a) Array of edge dislocations in a wedge-shape sample (courtesy S. Lagerwall). For a schematic representation of edge dislocations see Figs 9.11 and 9.20. (b) Freeze-etching microscopy; the terrace ending shown by the arrow reveals the existence of a screw dislocation (courtesy M. Kleman): one can go continuously from one layer to the next by simply moving in a circle around the terrace extremity. For a schematic representation of screw dislocations see Fig. 9.18.

the contrast of the lines and have shown their existence experimentally (Fig. 9.10(a)). Such layer endings are called edge dislocations; in the experiment of reference 13 they were shown to correspond to a single added layer. More generally, the number of added layers is called the Burger's vector. (A better definition will be given in Section 9.2.) Four-component lyotropic systems

(dodecane, sodium dodecyl sulphate, pentanol, water) show a similar structure but with larger Burger's vectors (in the 10–20 range) the values of which are a function of the sample thickness [14]. In much thicker samples (100 µm), very large Burger's vectors had been previously observed by Williams and Kleman and the tendency to break up into focal conics explained [4, 15, 16].

Freeze-etching microscopy does show the existence of edge dislocations [17]. It also reveals another line defect: the screw dislocation. As is clear in Fig. 9.10(b), a screw dislocation introduces connectivity between adjacent layers.

Obviously, dislocations also exist in columnar phases, but their direct observation is not easy.

9.1.3.2 *Indirect evidences*

In many experiments dislocations play a role. For example, when we described the undulation instability in Section 7.1.7, we assumed that the total number of layers was constant. If the mechanical tension is set slowly enough, no undulation is observed. Similarly, if the plate displacement is maintained at a value not too different from threshold, the undulation disappears in a time of the order of a few tenths of second or less. This can be understood by assuming that edge dislocations move in to relax the imposed strain. The quantized nature of dislocations has even been revealed by the quantization of the relaxed part of the strain [19]. The failure of some of the focal conics packing rule is also blamed on dislocation densities [2, 20].

9.1.4 Disclinations

9.1.4.1 *Smeetics A*

We have introduced in Section 4.2 the notion of disclination lines. Since their description involves the director field \mathbf{n} only, everything that has been said for \mathbf{n} can be reproduced with the normal to the layers provided distortions involving bend and twist are excluded. In general, disclinations occur in pairs of opposite sign which restores the long-range order of the normal to the layers. It is clear in Fig. 9.11 that an $m = +\frac{1}{2}, -\frac{1}{2}$ pair is equivalent to a dislocation line of Burger's vector equal to twice the number of layers contained between the two disclination centres. The line energy of such a dislocation may easily be evaluated. In fact, this calculation was performed in the problem of Section 4.2.2.1, giving

$$\gamma = \frac{\pi}{2} K_1 \ln\left(\frac{ba_0}{2a}\right) \quad (9.2)$$

where a_0 is the layer thickness, a the molecular cut-off introduced in (4.6), and b the Burger's vector.

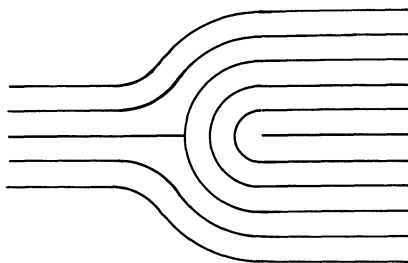


Fig. 9.11. Edge dislocation made of a $+ \frac{1}{2}, - \frac{1}{2}$ disclination pair.

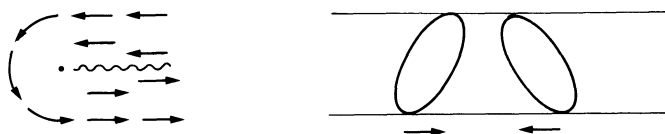


Fig. 9.12. Impossibility of having an $m = 1/2$ disclination in smectics C. In contrast to the nematic case, the arrow has a meaning: two opposite arrows correspond to tilts differing by an angle π in their azimuthal angle Ω_z . As a result the structure of the figure necessitates the presence of a wall (hatched area), and is not topologically stable.

9.1.4.2 Smectics C

In addition to disclinations related to the existence of the normal to the layers, \mathbf{k} , there can be disclinations in the tilt director field \mathbf{c} (we use the same conventions as in Chapter 7). They are best visualized in a geometry where the layers are perpendicular to the viewing axis: as we have mentioned in Section 9.1.1.1, one sees a *Schlieren* texture quite comparable to that of nematics. There are, however, important differences: one does not see brushes with two arms only. This reflects the fact that there are no $m = \frac{1}{2}(2n + 1)$ disclination lines in the \mathbf{c} director field [20] (Fig. 9.12). More generally, integer disclinations around any of the directions \mathbf{c} , \mathbf{k} , or $\mathbf{c} \times \mathbf{k}$ are possible together with half-integer disclinations around $\mathbf{c} \times \mathbf{k}$ [20] (\mathbf{c} , tilt director; \mathbf{k} layers' normal as in Chapter 7).

Similar disclinations can be observed in chiral smectics C*. They are particularly important in slabs with planar boundary conditions. In Section 7.2.7.3 we described how they can accommodate the natural twisting boundary condition. Up to now their description has been phrased in terms fairly similar to those used for nematics [21–24] but it would be useful to investigate the role of polarization charges.

9.1.4.3 Smectic B_{Hex}

An $m = k/6$ disclinations (with $k = \text{integer}$) in the bond-angle direction field should, in principle, exist in S_{B_{Hex}} (Fig. 9.13). However, the bond order

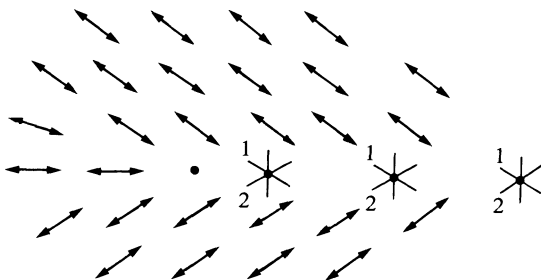


Fig. 9.13. $m = \frac{1}{6}$ disclination in an hexatic smectic. Note the $2\pi/6$ rotation of the bond order in a circuit embracing the disclination (i.e. bond 1, is transformed into bond 2 along the circuit).

parameter, which has sixfold local symmetry, is not coupled to light in any simple way. It is thus difficult to visualize them directly. The observation of the core splitting of 2π disclinations in S_I at low enough temperature does provide an elegant although indirect proof of their existence [25].

The observation goes as follows. Consider a two-layer thick film of the racemic 4-(2'-methyl butyl)phenyl)4-*n*-octylbiphenyl-4-carboxylate. By lowering the temperature one observes the sequence $S_A-S_C-S_I-S_J$. The last phase is a crystal. Although we have already insisted on the fact that there is no real symmetry difference between S_C and S_I , short-range order is very different: bond order is basically absent in S_C , whereas it extends over several hundred Å in S_I . In the S_C phase depolarized reflection microscopy shows *Schlieren* patterns characteristic of (2π) disclinations. Cooling into the S_I phase does not change the pattern, when one does not cool more than a few degrees below the transition. However about 4 degrees above the crystal S_I transition one sees a star of five straight radial arms growing from the centre of 2π disclinations. Across each arm the tilt direction undergoes a $\pi/3$ discontinuity (Fig. 9.14). The reversibility of the observation clearly demonstrates that it is an equilibrium structure. Upon approaching the S_J , the arm length seems to grow continuously to infinity.

How does this observation reveal the existence of bond order disclinations?

First, one has to assume that the tilt angle is locked to the bond direction everywhere except across the arms. This would necessarily be the case in three dimensions but it is not in a thin film [26–28]. However, the mere fact that the director fluctuations are essentially suppressed is a good indication that the assumption is meaningful.

Second, one has to recognize that, across an arm, the existence of a $\pi/3$ discontinuity of the tilt direction implies the very continuity of the bond order.[†]

Then, each arm ending is an $m = \frac{1}{6}$ disclination of the bond order: going

[†] In fact there is a slight discontinuity due to the coupling of tilt and bond orders [25].

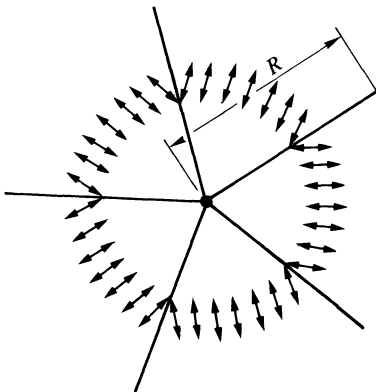


Fig. 9.14. Star defect in a smectic I. Note the five $2\pi/6$ disclinations at the arm extremities and the tilt discontinuity without bond discontinuity across the arms, leaving a $2\pi/6$ disclination in the center.

in a closed loop around such a point leads to a $2\pi/6$ change of the determination of the bond order (Fig. 9.13).

Thus, the existence of the five arms shows that the initially 2π ($m = 1$) disclination of the bond order (locked on to the tilt direction disclination) has split into five $m = \frac{1}{6}$ disclinations at the arm endings, plus one $m = \frac{1}{6}$ at the centre.

Problem. What determines the number of arms in the star? (Dierker *et al.*, reference 25)

Solution. The energy of a star defect made up of n arms of length R contains:

- the line energy of the n arms: $n\gamma R$;
- the energy of the n disclinations of strength $\frac{1}{6}$ at the tip of each arm: $B^*(\pi/6^2) \ln(R/a)$, where a is, as always, a short-scale cut-off;
- the far-field energy of the 2π disclination outside the arms: $B^*\pi \ln(L/R)$. L is on a large scale, comparable to the total size of the film, and, for this part of the defect, R plays the role of the short-scale cut-off;
- the energy of the central disclination of strength $(1 - (n/6))$:

$$B^*\pi \left(1 - \frac{n}{6}\right)^2 \ln\left(\frac{R}{a}\right).$$

(In principle the short distance cut-off should be different from a , but the physics is not deeply altered by this simplification.)

Thus the difference of the star defect energy from that of a regular strength one disclination reads

$$\Delta F = \frac{\pi B^*}{36} n(n-11) \ln\left(\frac{R}{a}\right) + n\gamma R$$

which is minimum for

$$R = \frac{\pi}{36} (11 - n) \frac{B^*}{\gamma}$$

and

$$\Delta F = \frac{\pi B^*}{36} n (11 - n) \left[1 - \ln \left(\frac{\pi}{36} (11 - n) \frac{B^*}{\gamma a} \right) \right].$$

The number of arms which minimizes ΔF depends on the ratio $B^*/\gamma a$. For $B^*/\gamma a \simeq 10^3$, it is compatible with $n = 5$ as observed in the experiment.

9.1.4.4 Columnar phases

In Section 9.1.2.1 we stressed that observations under the polarizing microscope revealed the presence of $m = 1/2$ disclination lines in columnar systems, and, in the problem of Section 9.1.2.2, we showed how the developable domain that issued from a cylinder of revolution was equivalent to an $m = 1$ disclination: the generalization to $m = 1/2$ can be made simply by using half a cylinder for the generating developable surface, and filling the remaining space with uniformly oriented columns as shown in Fig. 9.15. Similarly to the $m = 1$ case, the core is located inside a half-cylinder of diameter $(a + \varepsilon)$. Since the core size is macroscopic ($\sim 1 \mu\text{m}$), it is almost necessarily composed of columns parallel to its axis. One has to add a surface energy [11, 12] $\gamma = \gamma_0 + \gamma_2 \sin^2 \theta$ (θ is the angle between the tube axis and the tangent to the surface (see Fig. 9.15)) to the elastic energy of the problem in Section 9.1.2.2 (or half of it) in order to obtain the total energy. A straightforward minimization leads to the conclusion that an $m = 1/2$ line, is stable if $\gamma_2 < 0$ (homeotropic tendency) and $0.61 < -(\gamma_0/\gamma_2) < 0.83$.

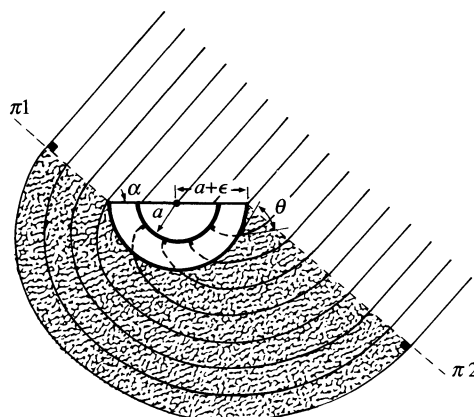


Fig. 9.15. $m = 1/2$ disclination in a columnar phase (after reference 11).

9.1.5 Walls

9.1.5.1 Small-angle discontinuity walls in smectics and D_h columnar phases

Up to now we have been interested mostly in defect structures involving line singularities (with the exception of developable domains). Can one have also surfaces like the twist walls of nematics in a magnetic field (remember Section 4.4)? As we will see, the answers are different for smectics and columnar systems, although walls are often made of planar arrays of the defects already described.

This observation can be explained using the following arguments. The calculations will be made using notation relevant to smectics, but they are also valid for columnar phases.

Consider a small-angle grain boundary like the one represented in Fig. 9.16: far from the z -axis (i.e. $|x|$ large compared to the width w of the wall) the smectic layers (respectively columns) are rotated by an angle $\pm\theta_\infty$ but have their equilibrium configuration.

We want to derive w as a function of the macroscopic elastic parameters, and calculate the energy of such a wall [11]. The starting point is the covariant smectic energy (8.106) (per unit surface in the z , y -plane)

$$F = \int \left[\frac{K_1}{2} \left(\frac{\partial^2 u}{\partial x^2} \right)^2 + \frac{B}{2} \left(\frac{\partial u}{\partial z} - \frac{1}{2} \left(\frac{\partial u}{\partial x} \right)^2 \right)^2 \right] dx. \quad (9.3)$$

(The more correct form involving $E(u) = \partial u / \partial z - \frac{1}{2}(\nabla u)^2$ is not needed here.)

We look for a wall that is translationally invariant along z . Thus $\partial u / \partial z$

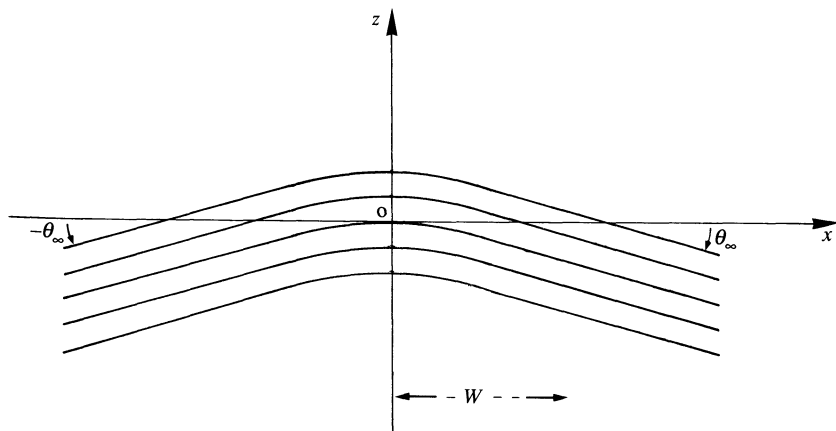


Fig. 9.16. Small-angle grain boundary in smectics and columnar phases. Note the necessary thickness difference between the middle of the wall and the wings [11].

can only be a function of x

$$\frac{\partial u}{\partial z} = f(x); \quad \text{this implies} \quad \frac{\partial u}{\partial x} = \int f'(x) dz + g(x).$$

Thus the only way to satisfy the z independence of $(\partial u / \partial x)$ is to choose $f'(x) = 0$, that is $\partial u / \partial z = \text{const}$. This constant can easily be evaluated with the requirement that, for large $|x|$, there is no compressional energy. With $-(\partial u / \partial x) = \theta$, one finds $\partial u / \partial z = \frac{1}{2}\theta_\infty^2$. Thus (9.3) can be written in terms of θ as

$$F = \int \left[\frac{K_1}{2} \left(\frac{d\theta}{dx} \right)^2 + \frac{B}{8} (\theta_\infty^2 - \theta^2)^2 \right] dx. \quad (9.4)$$

The corresponding Euler–Lagrange equation is

$$0 = -K_1 \frac{d^2\theta}{dx^2} + \frac{B}{4} [(\theta - \theta_\infty)(\theta + \theta_\infty)^2 + (\theta - \theta_\infty)^2(\theta + \theta_\infty)]. \quad (9.5)$$

Multiplying by $d\theta/dx$ and integrating, we get (where $\lambda = \sqrt{(K_1/B)}$ as usual)

$$\lambda^2 \left(\frac{d\theta}{dx} \right)^2 = \frac{1}{4}(\theta - \theta_\infty)^2(\theta + \theta_\infty)^2 + \text{const}. \quad (9.6)$$

The integration constant is clearly zero, and one obtains

$$\theta = \theta_\infty \tanh \left(\theta_\infty \frac{x}{\lambda} \right). \quad (9.7)$$

Thus the width of the wall is given by

$$w = \lambda/\theta_\infty. \quad (9.8)$$

For small θ_∞ , w is significantly larger than λ (although in general it cannot be resolved with a microscope). And the energy reads

$$F = \frac{2}{3}\sqrt{(K_1 B)}\theta_\infty^3. \quad (9.9)$$

The cubic dependence on θ_∞ suggests that the described structure will be stable only for small angles θ_∞ .

As a rough rule of thumb, the walls in smectics will acquire a modulation along y and eventually break up into focal conics when the integrated dilatation is of the order of λ (remember the ‘buckling’ instability)

$$\frac{1}{2}d\theta_\infty^2 \sim 2\pi\lambda \quad (9.10)$$

or

$$\theta_\infty \sim \left(\frac{4\pi\lambda}{d} \right)^{1/2}. \quad (9.11)$$

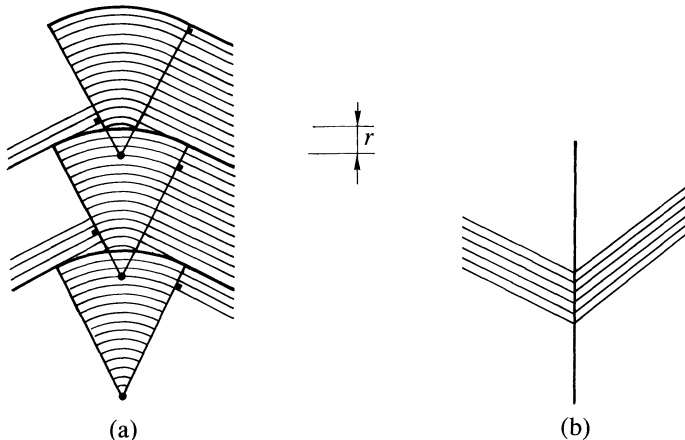


Fig. 9.17. Wall involving developable domains and grain boundaries in columnar phases [11].

(The wall is supposed infinite along y and of finite height d along z . Under such conditions the modulation period is $q_y \sim (\lambda d)^{-1/2}$.)†

Equation (9.11) shows that walls such as the one described in (9.7) are not stable in infinite-size smectics. For $d \sim 200 \mu\text{m}$, $\theta \sim 10^{-2} \text{ rad}$ is the largest possible angle; for $d \sim 2 \mu\text{m}$, $\theta \sim 10^{-1} \text{ rad}$. Reducing the lateral extent along y increases θ further; these figures probably explain why the chevron structure is observed in thin S_C^* samples [29].

The situation is qualitatively similar, but quantitatively different in columnar phases. Continuous walls such as described by (9.7) are stable up to $\theta_\infty \sim 10^{-1} \text{ rad}$ irrespective of the sample thickness. Beyond this value, the wall breaks up into developable domains and, eventually, for $\theta > 1 \text{ rad}$ evolves into a sharp grain boundary. The wall made of developable domains is represented in Fig. 9.17: according to Oswald and Kleman [11], it involves both developable domains and grain boundaries. Note that the grain boundary limit also exists in finite thickness smectics: this is the situation encountered in Cano wedges [30]. Twist walls composed of planar arrays of screw dislocations (Fig. 9.18) [30, 31] have also been predicted and observed.

9.1.5.2 Bloch walls in tilted columnar phases

We discussed in Chapter 7 the stability of strands in columnar systems. When the molecules are tilted with respect to the columnar axis, the

† A more careful analysis shows that the wall is destabilized not only via the mechanism responsible for the undulation instability but also because the q_y modulation relieves part of the splay. The dependences are, however, unaltered as far as scaling is concerned.

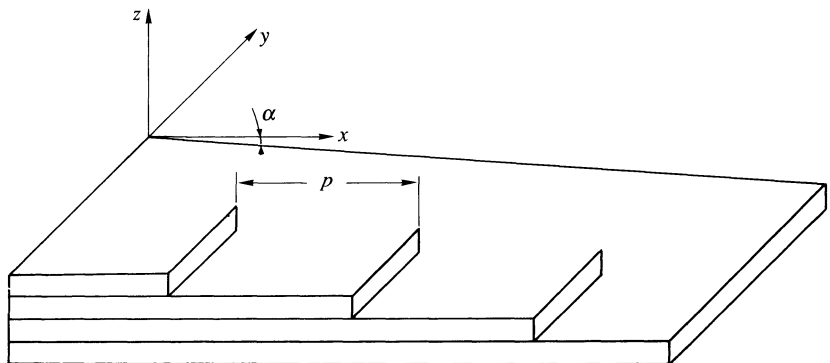


Fig. 9.18. Twist wall composed of a planar array of screw dislocations in a smectic A [30]. The steps at the upper part of the figure help visualize the structure but do not correspond to any discontinuity. The torsion α is simply given by $\alpha = a/p$ where a is the layer thickness and p the periodicity of the dislocation array.

observation of the optic axis direction reveals some interesting features [32].

1. An extrinsic smooth variation of the tilt direction, connected to a helicoidal distortion of the columnar structure resulting from the details of the strand history. (In fact one can get rid of this distortion.)
2. ‘Discrete’ jumps between energetically degenerate orientations where discrete simply means that the length over which the variation occurs is small compared to the resolution of the microscope. These jumps define Bloch walls in the tilt direction with respect to the two-dimensional columnar lattice. Their model is developed as follows.

Call ϕ the azimuthal angle of the tilt direction with respect to one of the lattice axes (say, x in Fig. 9.19) and assume that the structure we deal with is such that the tilt direction is preferentially along crystallographic directions. Then the energy of the system as a function of ϕ is minimum for $\phi = O + k(2\pi/6)$ (k is an integer);† the simplest function that represents this behaviour is

$$V(\phi) = -v \cos 6\phi \quad (v > 0). \quad (9.12)$$

For non-chiral compounds, one has to add a conventional elastic term

$$W_e = \frac{K_2}{2} \left(\frac{\partial \phi}{\partial z} \right)^2. \quad (9.13)$$

† The sixfold symmetry is, in fact, only approximate in general.

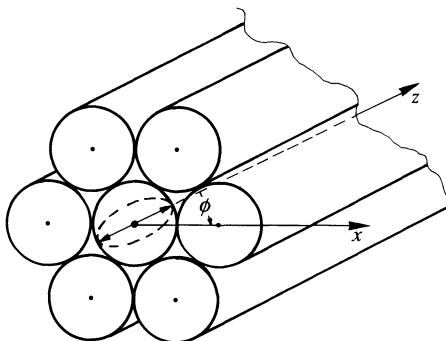


Fig. 9.19. The lattice of neighbouring columns act like a ‘magnetic field’ with sixfold symmetry for the tilt direction of molecules in the central column as described in the text.

(We consider only distortions along the z direction of Fig. 9.19: in principle, Néel walls could also exist and would require us to keep the x and y dependence, but the physics is essentially the same.) The situation is identical to that of describing walls in nematics submitted to a magnetic field (see Section 4.4) provided that we substitute 3ϕ for the angle θ between the nematic director and the magnetic field and the lock-in energy $12v$ (eqn (9.12)) for the magnetic energy $\chi_a H^2$ and divide the elastic constant by 3. The rest is identical to the treatment in Section 4.4 except that the lock-in energy is much larger than the magnetic one. On dimensional grounds one expects

$$v \simeq kT/l^3 \quad (9.14)$$

where l is a molecular length. That is $v \sim 10^8, 10^9 \text{ erg cm}^{-3}$. Thus the coherence length $\xi = (K/36v)^{1/2}$ is of molecular size. In fact, Landau theory shows that (9.14) has to be multiplied by the tilt angle to a power of six [33], which, for a tilt angle of the order of 20° , reduces v by a factor of roughly 10^3 and increases ξ 30 times.

9.2 DISLOCATION AND ASSOCIATED STRESS/STRAIN

9.2.1 Distortions in smectics

9.2.1.1 Dislocation ‘currents’

In Section 9.1.3 we saw that smectic layers could end (or start) on lines that we called dislocations. A mathematical description of such an object is certainly difficult since it involves short-scale as well as large-scale distortions. However, if one is interested only in the far-field patterns and if one agrees to treat the short-scale distortions through the introduction of

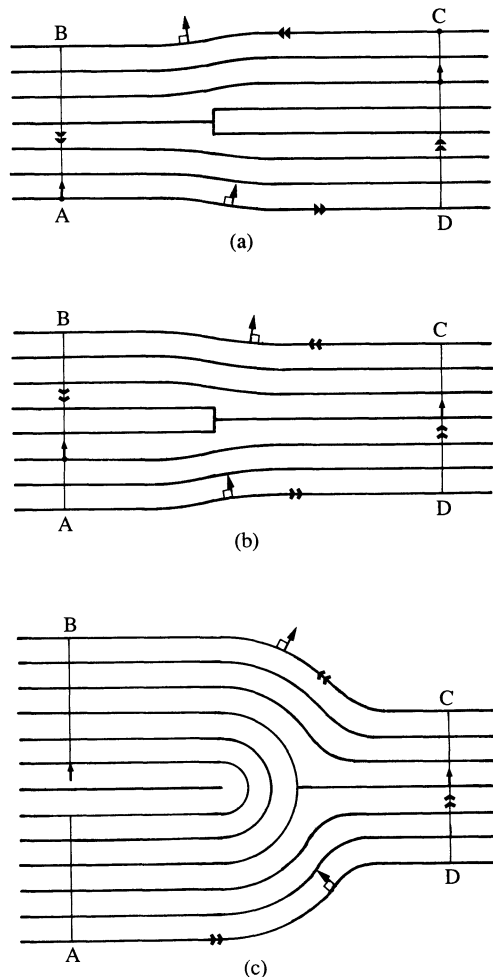


Fig. 9.20. Dislocations of different Burger's vectors: (a) $n = +1$ or $b = a_0$; (b) $n = -1$ or $b = -a_0$; (c) $n = -6$ or $b = -6a_0$.

large wavevector cut-offs in the energy calculations (this is, in general, legitimate because the short-scale effects appear with a characteristic length of molecular size far from phase transitions), the following procedure is valid.

Consider the same integral as in (8.124), but surrounding the dislocation of Fig. 9.20(a) (a , local layer thickness, \mathbf{n} local normal; counterclockwise rotation)

$$\oint \frac{\mathbf{n}}{a} \cdot d\mathbf{l} = +1.$$

Indeed, one counts: path AD $\rightarrow 0$; DC $\rightarrow +7$; CB $\rightarrow 0$; BA $\rightarrow -6$ (\mathbf{n} and $d\mathbf{l}$ opposite). This result is independent of the contour, as long as it embraces the dislocation core. Fig. 9.20(b) shows a negative dislocation of unit strength whereas Fig. 9.20(c) displays one of strength minus six. This strength n , once multiplied by the average thickness a_0 , is the Burger's vector b of the dislocation [34]

$$b = n a_0 \quad (n = \text{integer}). \quad (9.15)$$

The generalization is straightforward

$$\oint \frac{\mathbf{n}}{a} \cdot d\mathbf{l} = \sum_i n_i \quad (9.16)$$

where the summation extends over all sites embraced by the contour. The sign convention of Fig. 9.20 holds, that is negative when the layers appear upon moving toward the right of the figure and positive when the layers disappear upon moving toward the right of the figure. Introducing the dislocation current such that

$$\iint_S \mathbf{J} \cdot d\mathbf{s} = \sum_i n_i \quad (9.17)$$

yields a local relation between (\mathbf{n}/a) and \mathbf{J} , similar to that existing in magnetism between the induction \mathbf{H} and the electric current density \mathbf{J} , as remarked by Pershan [30]

$$\operatorname{curl} \left(\frac{\mathbf{n}}{a} \right) = \mathbf{J}. \quad (9.18)$$

Note that \mathbf{J} parallel (respectively perpendicular) to the layers represents edge (respectively screw) dislocations. Note also that, since a dislocation line is a layer ending or beginning, it is either closed on itself or ends at the boundaries of the system. In other words, \mathbf{J} is a conserved vector

$$\operatorname{div} \mathbf{J} = 0. \quad (9.19)$$

This further deepens the magnetic analogy.

Equation (9.18) holds irrespective of the local layer tilt value. If we restrict our attention to small deformations (i.e. exclude the core region of dislocations), (9.18) may be written (with the notation change $-a_0 \mathbf{J} \rightarrow \mathbf{J}$)

$$\operatorname{curl} \mathbf{m} = \mathbf{J} \quad (9.20)$$

in which we have used

$$\frac{\mathbf{n}}{a} \simeq \frac{\mathbf{n}_0}{a_0} + \frac{\delta \mathbf{n}_\perp}{a_0} - \frac{\mathbf{n}_0}{a_0} \left(\frac{\delta a}{a_0} \right) = \frac{\mathbf{n}_0}{a_0} - \frac{\mathbf{m}}{a_0} \quad (9.21)$$

with this definition of \mathbf{m} , away from the dislocation core,

$$\mathbf{m} = \nabla \mathbf{u}. \quad (9.22)$$

(Remember that $\delta \mathbf{n}_\perp = -\nabla_\perp \mathbf{u}$, $\nabla_z u = \delta a/a$.)

Note that, because of the presence of dislocations, the layer displacement is now a multivalued function. Aside from that, since energy densities are local and since \mathbf{m} is a well-defined single-valued deformation field, expression (7.13) is still valid and the corresponding Euler–Lagrange equation as well

$$-\frac{\partial m_z}{\partial z} + \lambda^2 \Delta_\perp (\nabla_\perp \cdot \mathbf{m}_\perp) = 0. \quad (9.23)$$

We can now illustrate these considerations using a few specific examples.

9.2.1.2 Isolated edge dislocations [35]

Let us consider first a straight edge dislocation at the origin in an infinite medium (line along the y direction) [35]

$$J_x = J_z = 0, \quad J_y = -a_0 n \delta_x \delta_z \quad (9.24)$$

where n represents the number of added (subtracted) layers. Clearly, $m_y = 0$ and $\partial/\partial y = 0$. Fourier transforming (9.20) and (9.23), and solving for m_x gives

$$m_x(\mathbf{q}) = \frac{ina_0 q_z}{q_z^2 + \lambda^2 q_x^4} \quad (9.25)$$

or

$$m_x(x, z) = na_0 \int \int \frac{iq_z}{q_z^2 + \lambda^2 q_x^4} e^{i(q_x x + q_z z)} \frac{dq_x}{2\pi} \frac{dq_z}{2\pi}, \quad (9.26)$$

i.e.

$$m_x(x, z) = \frac{\pm na_0}{4\pi} \int dq_x e^{iq_x x} e^{-\lambda q_x^2 |z|}, \quad (9.27)$$

$$m_x(x, z) = \frac{\pm na_0}{4\sqrt{(\pi\lambda|z|)}} \exp(-x^2/4\lambda|z|). \quad (9.28)$$

The + (respectively –) holds for positive (respectively negative) z .

From (9.27), one sees that, away from the $z = 0$ plane, we can define a layer displacement

$$u = \pm \frac{na_0}{4\pi} \int dq_x \frac{e^{iq_x x}}{iq_x} e^{-\lambda q_x^2 |z|} \quad (9.29)$$

(with the same sign convention), which gives the layer dilatation

$$m_z = \frac{\delta a}{a} = \pm \lambda \left(\frac{\partial m_x}{\partial x} \right), \quad (9.30)$$

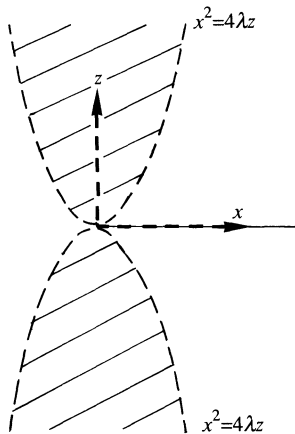


Fig. 9.21. The distortions induced by the dislocation decrease rapidly along x , but only slowly (as $|z|^{-1/2}$) along the optical axis. They are practically confined in two parabolic regions (hatched areas).

$$m_z = \frac{-xna_0}{8(\pi\lambda)^{1/2}|z|^{3/2}} \exp(-x^2/4\lambda|z|). \quad (9.31)$$

As expected, the tilt is odd in z and even in x , whereas the layer dilatation is even in z and odd in x . Equations (9.28) and (9.31) show that the distortion created by the dislocation is essentially contained inside the parabolas: $x^2 = 4\lambda|z|$ (Fig. 9.21). Along the $x = 0$ axis, the tilt and dilatation die off slowly as $1/z^{1/2}$ and $1/z^{3/2}$, respectively.

The line tension γ analogous to the one introduced in Section 4.2.3 can be calculated from (7.13). One finds

$$\gamma = \frac{(K_1 B)^{1/2} n^2 a_0^2}{2\xi} + e_c \quad (9.32)$$

where ξ is a cut-off length of molecular size ($\xi \sim na_0$) and e_c is the core energy of the dislocation. In general, core energies cannot be calculated from continuum theories. It is, however, possible when n is large. We have shown in Section 9.1.3.1 that a pair of $+1/2, -1/2$ disclinations is equivalent to a dislocation of Burger's vector equal to twice the number of layers contained between the two disclination centres. In that case e_c can be calculated from the nematic type of continuum theory, as pointed out by Williams and Kleman [15, 20]. In fact this calculation was performed in the problem of Section 4.2.2.1

$$e_c = \frac{\pi}{2} K_1 \ln\left(\frac{na_0}{2d}\right) \quad (9.33)$$

where d is the molecular cut-off introduced in (4.6).

Note that, since $\ln(n_1 + n_2) < \ln n_1 + \ln n_2$ for n_1 and $n_2 > 2$, one line with Burger's vector $a_0(n_1 + n_2)$ has less core energy than two lines with Burger's vectors a_0n_1 and a_0n_2 (as long as $\xi \sim na_0$). According to Williams and Kleman this remark explains the formation of very large Burger's vector dislocations in thick samples [4].

Note that, for n small, γ is of the order of K_1 (remember $\lambda = (K_1/B)^{1/2} \simeq a_0$ away from phase transitions); for n large γ is of the order of nK_1 .

Problem. In Section 4.2.2.1 we stressed that the two opposite disclinations attracted each other; what maintains them apart in smectics?

Solution. The answer is clearly the existence of the layers. More precisely the attractive force is balanced by the repulsive one due to the layer compression. If xa_0 is the distance between the disclination cores, the strain is

$$\left(x - \frac{n}{2}\right)a_0 / \left(\frac{n}{2}a_0\right) = \frac{2x - n}{n},$$

which extends over linear dimensions $(n/2)a_0$. Hence the compressional energy scales as

$$\frac{B}{2} \left(x - \frac{n}{2}\right)^2 a_0^2.$$

The total core energy then reads

$$e_c^t \simeq \frac{Ba_0^2}{2} \left[\left(x - \frac{n}{2}\right)^2 + \pi\alpha^2 \ln\left(\frac{xa_0}{d}\right) \right]$$

with $\alpha = \lambda/a_0$. Subtracting off (9.33),

$$e_c^t - e_c = \frac{Ba_0^2}{2} \left[\left(x - \frac{n}{2}\right)^2 + \pi\alpha^2 \ln\left(\frac{2x}{n}\right) \right].$$

This energy is minimum for

$$x = \frac{n + (n^2 - 8\pi\alpha^2)^{1/2}}{4}.$$

For large Burger's vectors, $x \simeq \frac{1}{2}n$ and formula (9.33) is recovered (with negative corrections of order α^4/n^2); more interesting is the existence of a critical n beyond which there is no possible stability: for $n_c \leq 2\sqrt{(2\pi)\alpha}$ the layers are irreversibly squeezed and dislocation cores made of two opposite disclination pairs are not possible. This sets up a lower limit for a core such as depicted in Figs 9.11 or 9.20(c), typically with $\alpha \simeq$ a few units (i.e. λ of the order of a layer spacing) and $n_c \sim$ a few times 5. The experiment of reference 14 seems to be compatible with $n_c \simeq 9$.

Note that, although compression is omitted in (9.33), e_c is always close to the actual value e_c^t . The largest value is obtained for $n \simeq n_c$

$$e_c^t - e_c = \frac{\pi}{2} K_1 [\frac{1}{2} - \ln 2],$$

i.e. $((e_c^t - e_c)/e_c) \simeq 10$ per cent. For large n the difference drops like $1/n^2$. Thus (9.33) practically always provides a good approximation.

9.2.1.3 Isolated screw dislocation [30]

Now the dislocation current reads

$$J_x = J_y = 0, \quad J_z = a_0 n \delta_x \delta_y \quad (9.34)$$

and $\mathbf{m}_z = \partial/\partial z = 0$. Equation (9.20) yields

$$\frac{\partial m_x}{\partial y} - \frac{\partial m_y}{\partial x} = n a_0 \delta_x \delta_y \quad (9.35)$$

and (9.23) becomes

$$\left(\frac{\partial^2}{\partial x^2} + \frac{\partial^2}{\partial y^2} \right) \left(\frac{\partial m_x}{\partial x} + \frac{\partial m_y}{\partial y} \right) = 0. \quad (9.36)$$

Fourier transforming as in the edge dislocation case provides us with

$$\left. \begin{aligned} m_x &= -n a_0 \frac{i q_y}{q^2}, \\ m_y &= n a_0 \frac{i q_x}{q^2}, \end{aligned} \right\} \quad (9.37)$$

or

$$\left. \begin{aligned} m_x &= \frac{-n a_0}{2\pi} \frac{y}{x^2 + y^2}, \\ m_y &= \frac{n a_0}{2\pi} \frac{x}{x^2 + y^2}. \end{aligned} \right\} \quad (9.38)$$

The corresponding (multivalued) layer displacement is similar to that found in crystals,

$$u = \frac{n a_0}{2\pi} \tan^{-1} \left(\frac{y}{x} \right). \quad (9.39)$$

The most important feature of screw dislocations is that, since $m_z = 0$ (no dilatation) and $\nabla \cdot \mathbf{m}_\perp = 0$ (no layer mean curvature), they do not have strain energy. They only have a core energy (note that for large Burger's vectors one can still have a core of the Williams-Kleman type). This result has its magnetic analogue: the energy of a solenoid is entirely confined to its interior.

Note, however, that the saddle-splay term is non-zero. Although we dropped it from (7.13) because it can be treated as a surface term (+ splay), it does give a contribution to the screw dislocation line energy.

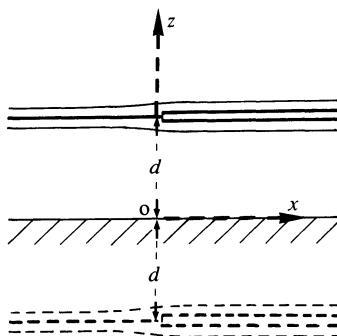


Fig. 9.22. The tilt induced by the dislocation in the $z = d$, $x = 0$ location is exactly cancelled by the one corresponding to the image in $z = -d$. Thus the layer at the hatched interface is flat ('rigid boundary'). (Solid lines represent actual layers, dotted ones the image.)

9.2.1.4 Boundary effect

Boundary effects have been discussed by Pershan in terms of image interaction [30]. If one places two edge dislocations of same strength n and direction 'on top of each other' (i.e. $J_y = n(\delta_x \delta_{z-d} + \delta_x \delta_{z+d})$), then, by symmetry, the resulting tilt m_x is identically zero in the $z = 0$ plane. In other words the corresponding layer is perfectly flat (see for example eqn (9.28)). If one wants now to calculate the distortion associated with the presence of one dislocation in a semi-infinite sample ($z > 0$) at $z = d$, $x = 0$, with a rigid boundary in $z = 0$ (Fig. 9.22), because of the linearity of the equations one can simply extend the problem to the whole space and add an image of the same sign in $z = -d$, $x = 0$. Since the sign is the same, a rigid boundary clearly repels the dislocation. (Note that, because of translational invariance, the force is necessarily along z .)

At a free surface, now, the relevant boundary condition is $\phi_z = Bm_z = 0$ (absence of normal stress). Suppose we consider a dislocation located in a semi-infinite sample ($z < 0$) at $z = d$, $x = 0$, the $z = 0$ plane being a smectic-air interface for instance (Fig. 9.23). From (9.31) it is now clear that one simply has to add an image of opposite sign at $z = d$, $x = 0$; since the sign is opposite, the free boundary attracts the dislocation (note that this boundary condition holds only if surface tension is negligible compared to $(K_1 B)^{1/2}$ [30]. Intermediate situations are more intricate and can only be treated in specific examples.

9.2.1.5 Magnetic analogy

Let us come back to the basic equations governing the strain in the presence of dislocations,

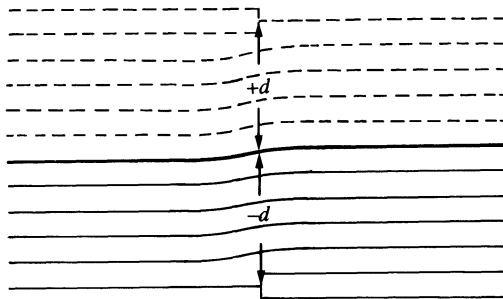


Fig. 9.23. Same conventions as in Fig. 9.22; the heavy line represents the free surface, which experiences a tilt but no normal stress.

$$\operatorname{curl} \mathbf{m} = \mathbf{J}, \quad (9.40)$$

$$\operatorname{div} \mathbf{J} = 0, \quad (9.41)$$

$$\operatorname{div} \phi = 0. \quad (9.42)$$

Equation (9.42) is just another way of writing (9.23) in which we have used

$$\phi_i = \sigma_{zi} = \frac{\delta F}{\delta m_i}, \quad (9.43)$$

that is, explicitly,

$$\left. \begin{aligned} \phi_z &= B m_z \\ \phi_{\perp} &= -K_1 \nabla_{\perp} (\operatorname{div} \mathbf{m}_{\perp}) \end{aligned} \right\} \quad (9.44)$$

As pointed out by Pershan [30] and Kleman [36], eqns (9.40)–(9.44) are entirely analogous to the equations governing magnetostatics. In fact, the analogy holds in solids, but is less transparent because of tensorial complications. One can make the following correspondence

$$\left. \begin{aligned} \text{dislocation current density } \mathbf{J} &\Leftrightarrow \text{electric current density } \mathbf{J} \\ \text{stress field} &\Leftrightarrow \phi \Leftrightarrow \text{magnetic flux } \mathbf{B} \\ \text{strain field} &\Leftrightarrow \mathbf{m} \Leftrightarrow \text{magnetic field } \mathbf{H} \end{aligned} \right\} \quad (9.45)$$

Since the elastic energy is a quadratic function of strains and the stress–strain relation is linear, the derivation of the force acting on a dislocation is exactly similar to that giving the Lorentz force in magnetism [30, 37], i.e.

$$\mathbf{F} = \phi \times \mathbf{J} \quad (9.46)$$

where \mathbf{F} is the force per unit length exerted by the ‘external’ stress on the dislocation. ‘External’ means everything which does not correspond to the self-stress of the dislocation in an infinite medium: in particular, images

contribute to the ‘external’ stress. Equation (9.46) is known in crystalline physics as the Peach–Koehler force [38].

Let us consider the case of Fig. 9.20(a), and apply an external stress $\nabla_z \mathbf{u}^{\text{ext}}$. Since the current is in the y direction and the stress in the z direction, the force is along x

$$\int F_x \, dx \, dz = -a_0 B \nabla_z u^{\text{ext}}. \quad (9.47)$$

A dilatation tends to move the added layer to the left of the figure, whereas a compression moves it to the right. Note the following.

- The motion is such that it tends to reduce the stress.
- In an infinite medium, there is no restoring force allowing the situation to reach equilibrium: no matter how small the stress ϕ_z , the dislocation moves and the structure flows. This absence of yield stress is characteristic of nematics, not of smectics! This important remark has been exploited by Nelson and Toner to describe the smectic A–nematic transition [39]. A smectic type of structure in which infinite-size dislocations can be thermally excited describes in fact a nematic.

This remark holds only in an infinite sample: we have already seen that one could find dislocation arrays of infinite length in wedge-shaped samples (remember Section 9.1.3.1).

Note eventually that an edge dislocation experiences no force in a splayed structure. A splay gradient along x is required for the motion of the dislocation of Fig. 9.20(a) to occur in the z direction.

9.2.1.6 Dislocation moments

In the following we consider an imperfect smectic, in which dislocation loops are present and pinned by dust particle impurities, etc. [40]. According to our remark of the preceding section, we describe a smectic behaviour only if

$$\int_S \mathbf{J} \cdot d\mathbf{s} = 0. \quad (9.48)$$

in which S is any cross-section of the considered sample. The situation is again similar to magnetostatics. Equation (9.48) implies that the average value of the dislocation current $\langle \mathbf{J} \rangle$ is given by the curl of its first moment [41]

$$\langle \mathbf{J} \rangle = \text{curl } \mathbf{P} \quad (9.49)$$

with

$$\int_u (\mathbf{r} \times \mathbf{J}) \, dv = \int_u \mathbf{P} \, dv \quad (9.50)$$

where \mathbf{P} is equivalent to the magnetic moment \mathbf{M} .

This in turn implies (taking the average of (9.40) and subtracting (9.49))

$$\operatorname{curl}(\langle \mathbf{m} \rangle - \mathbf{P}) = 0 \quad (9.51)$$

or

$$\langle \mathbf{m} \rangle = \nabla \mathbf{u} + \mathbf{P}. \quad (9.52)$$

What is the meaning of this relation? $\langle \mathbf{m} \rangle$ is the average of \mathbf{m} , the local layer dilatation and tilt. Equation (9.52) has a meaning only to the extent that \mathbf{P} varies slowly over the typical averaging volume. \mathbf{u} is a potential that appears as a macroscopic layer displacement: it differs from $\langle \mathbf{m} \rangle$ through the dislocation moment just as the average magnetic field \mathbf{B} differs from \mathbf{H} through the magnetic moment \mathbf{M} .

Note that the constant part of \mathbf{P} can be lumped in $\nabla \mathbf{u}$ and that one can worry about \mathbf{P} variations only. These variations can only come from the stress $\langle \phi \rangle$ in the linear domain (the minus sign is set for convenience)

$$\left. \begin{aligned} P_z &= -\chi_{zz} \phi_z, \\ \mathbf{P}_\perp &= -\chi_\perp \boldsymbol{\phi}_\perp. \end{aligned} \right\} \quad (9.53)$$

That is, using the average of (9.44) and (9.52)

$$\left. \begin{aligned} \phi_z &= B \nabla_z u / (1 + B \chi_{zz}), \\ \boldsymbol{\phi}_\perp &= -K_1 \nabla_\perp \Delta_\perp u, \end{aligned} \right\} \quad (9.54)$$

in which higher-order derivatives have been discarded. The splay elastic constant is not significantly perturbed by the presence of dislocation loops, but the compression modulus is

$$B^{\text{eff}} = B / (1 + B \chi_{zz}). \quad (9.55)$$

Equation (9.55) expresses a decrease of B , since $\chi_{zz} > 0$. The sign of χ_{zz} results from the fact that dislocations move to reduce the stress. How large is this effect?

Consider a dislocation pinned on two points separated from each other by a distance L (Fig. 9.24). Let us apply a stress $\phi_z = \phi_0 \sin(qy)$. (For the sake of simplicity we choose $q = (n\pi/L)n$ where n is an integer.)

The energy of the line is given by the increase in the line tension, plus the stress flux swept by the line during its deformation,

$$F = \gamma \int_0^L \frac{1}{2} \left(\frac{d\xi}{dy} \right)^2 dy - a_0 \int_0^L \phi_z \xi dy \quad (9.56)$$

where γ is the dislocation line tension, ξ the line displacement, and a_0 the Burger's vector of the dislocation ($n = 1$). The minimum of (9.56) is given by

$$\xi = \frac{a_0 \phi_0}{\gamma q^2} \sin qy. \quad (9.57)$$

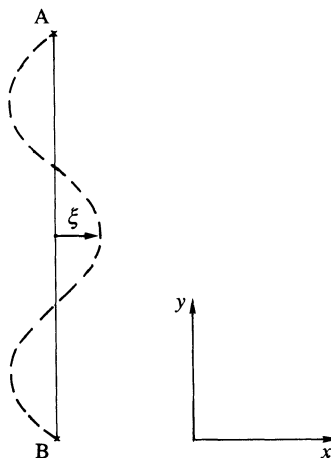


Fig. 9.24. Dislocation pinned at sites A and B. Solid line, ground state; dashed line, equilibrium shape resulting from the application of the sinusoidal stress discussed in the text.

The concept of dislocation moment is macroscopic: if d^{-2} pinned dislocations cut the unit (xz) surface (i.e. d average spacing between dislocations), (9.50) yields

$$P_z = -a_0 n \xi = -\frac{a_0^2 \phi_0}{\gamma q^2 d^2} \sin qy, \quad (9.58)$$

i.e.

$$\chi_{zz} = a_0^2 / \gamma q^2 d^2 \quad (9.59)$$

or

$$B^{\text{eff}}(q) = B / (1 + Ba_0^2 / \gamma q^2 d^2). \quad (9.60)$$

Equation (9.60) allows us to understand the large scatter of the early elastic constant measurements. Low-frequency experimental values depend on the dislocation loop sizes and densities and are weakly dependent on the bare elastic constant: the ‘dirty’ sample limit reads ($q^2 d^2 \ll 1$)

$$B^{\text{eff}}(q) = \frac{1}{2} \frac{\gamma}{a_0^2} q^2 d^2. \quad (9.61)$$

Equation (9.61) suggests two remarks.

1. The lower bound of B_{\min} can be orders of magnitude smaller than B provided $L^2 \gg d^2$.
2. If there exists a regime $q^2 d^2 \ll 1$ and $q^2 L^2 \gg 1$, in that regime the system

behaves as a nematic: indeed the energy $\frac{1}{2}B^{\text{eff}}(\nabla_z u)^2$ may be written

$$\frac{1}{2} \frac{\gamma}{a_0^2} d^2 q^2 q_z^2 |u^2(q)| = \frac{1}{2} \frac{\gamma}{a_0^2} d^2 q_z^2 |\delta n_q|^2 \quad (9.62)$$

(remember $\delta \mathbf{n} = -\nabla_{\perp} \mathbf{u}$). Expression (9.62) is a nematic type of energy with

$$K_3^{\text{eff}} = \frac{1}{2} \frac{d^2}{a_0^2} \gamma. \quad (9.63)$$

This is another way of understanding the dislocation unbinding picture, which describes the nematic-smectic A transition [39].

More generally, χ_{zz} may also stem from dust densities and impurities [40]. They can also give rise to sizeable osmotic stresses through (9.44) and (9.52): values as high as one atmosphere have been estimated.

9.2.1.7 Yield stress

Consider the energy of a dislocation loop of radius R in an infinite medium. It has a core energy $2\pi R\gamma$ with γ given by (9.32) provided R is larger than molecular sizes. When this loop is submitted to an external stress ϕ_z , it gains the ‘flux’ energy

$$-a_0 \int \phi_z \, ds = -\pi R^2 a_0 \phi_z. \quad (9.64)$$

Hence the total energy [40][†]

$$w = 2\pi R\gamma - \pi R^2 a_0 \phi_z. \quad (9.65)$$

Expression (9.64) holds for a loop corresponding to an extra layer. Equation (9.65) shows that a compressive stress ($\phi_z < 0$) will help in shrinking the loop to zero size. On the other hand, a dilatative stress gains energy: $w(R)$ exhibits no minimum but a maximum. Beyond $R_c = \gamma/a_0 \phi_z$, w is a decreasing function of R ; a new layer is nucleated.

Whether such a process is observable or not depends on nucleation rates. This problem is analogous to vortex nucleation in superfluid helium [42, 43]. The nucleation frequency (per unit volume) goes as

$$v \simeq v_0 \exp\left(-\frac{w_c}{k_B T}\right) \quad (9.66)$$

where w_c is the potential barrier obtained for $R = R_c$

$$w_c = (\pi\gamma^2/a_0\phi_z). \quad (9.67)$$

[†] In reference 40, due attention is paid to actual boundary conditions: ϕ_z is replaced by $(\phi_z - (Ba_0/2D))$ in which D is the sample thickness. This corresponds to the fact that one has to exceed a total displacement of half a layer thickness, in order to gain energy in nucleating a new layer. In the infinite D limit, however, this term is unimportant.

The nucleation is observable if $v \simeq v_1$ ($v_1 \simeq 1 \text{ s}^{-1} \text{ cm}^{-3}$) which defines a critical stress

$$\phi_z^c = \frac{\pi\gamma^2}{a_0 k_B T \ln(v_0/v_1)}. \quad (9.68)$$

with $\gamma \simeq \frac{1}{2}(K_1 B)^{1/2} a_0^2/\xi$, ones gets a critical strain

$$(\nabla_z u)^c \simeq \frac{\pi}{4} \left(\frac{B a_0^3}{k_B T} \right) \left(\frac{\lambda}{\xi} \right)^2 \frac{1}{\ln \left(\frac{v_0}{v_1} \right)}. \quad (9.69)$$

v_0 is a ‘short-scale’ fluctuation frequency per unit volume; it may be estimated to be comparable to a sound velocity divided by a molecular dimension, again divided by a molecular volume [40]

$$v_0 \simeq (10^5 \text{ cm s}^{-1}) / (2 \cdot 10^{-7} \text{ cm}) / (3 \cdot 10^{-22} \text{ cm}^3) \simeq 10^{33} \text{ s}^{-1} \text{ cm}^{-3}$$

with

$$B \sim \frac{k_B T}{a_0^3}, \quad \lambda \sim \xi,$$

one finds $\nabla_z^c u \sim$ a few 10^{-2} . Under the same conditions the critical radius would be of order of 100 times a molecular length which justifies the continuum approach. Such a strain is technically easy to realize but, just as in superfluids, a homogeneous nucleation is probably often pre-empted by heterogeneous nucleation due to pre-existing pinned dislocations. If we come back to the case of Fig. 9.24 in a homogeneous external stress the energy reads

$$w = \gamma R(2\theta - 2 \sin \theta) - a\phi_z R^2(\theta - \frac{1}{2} \sin 2\theta). \quad (9.70)$$

The line is unstable for $\phi_z > 2Ba_0/L$ or

$$(\nabla_z u)^c = \frac{2a_0}{L}. \quad (9.71)$$

If one accepts, as a rough rule of thumb, that L is of order of the largest dust particles ($\sim \mu\text{m}$ if no special case is taken), it is clear that the experimental yield stress will always be much smaller than the one corresponding to homogeneous nucleation.†

9.2.2 Strain fields in columnar phases

9.2.2.1 Formulation

The generalization of the considerations developed for smectics is straightforward. Since columnar phases are characterized by two-dimensional order,

† One can probably play with the characteristic times. Taking $v_1 \simeq 10^4$ would increase $(\nabla_z u)^c$ in a non-crucial way in (9.69), but could pre-empt the mechanism described in (9.71).

the Burger's vector is a two-component vector and (9.15) is replaced by

$$\mathbf{b} = n\mathbf{a}_1 + m\mathbf{a}_2 \quad (9.72)$$

where n and m are integers and \mathbf{a}_1 and \mathbf{a}_2 are basis vectors of the two-dimensional lattice. The generalization of (9.16) reads

$$\oint_c d\mathbf{u} = - \sum_J \mathbf{b}^J \quad (9.73)$$

where the sum over the J superscript runs over all dislocations of Burger's vector \mathbf{b}_J , embraced by the contour c . The dislocation current now specifies the direction of the line as in (9.17), but also that of the Burger's vector (i.e. second rank tensor)

$$\int_S d\mathbf{s} \cdot \mathbf{J}_\alpha = - \sum_J b_\alpha^J. \quad (9.74)$$

The integral is taken on any surface, bordered by the contour c . (The respective orientations of J and c follow the usual right-hand sense relations.) These equations are identical to those valid in crystals [44], with the only peculiarity being that (Greek) indices related to the Burger's vector run over the x, y components only.

Equations (9.73) and (9.74) can be combined (with $\mathbf{m}_\alpha = \nabla \mathbf{u}_\alpha$ away from the line) to give

$$\oint_c d\mathbf{l} \cdot \mathbf{m}_\alpha = \int_S d\mathbf{s} \cdot \mathbf{J}_\alpha$$

or

$$\text{curl } \mathbf{m}_\alpha = \mathbf{J}_\alpha. \quad (9.75)$$

To sum up, a dislocation in a columnar phase is determined by two directions (the line and the lattice shift) and an amplitude (that of the Burger's vector).

We have sketched three typical situations in Fig. 9.25(a)–(c). In (a)

$$\oint d\mathbf{u}_x = 0, \quad \oint d\mathbf{u}_y = -a, \\ \mathbf{J}_x = 0, \quad \mathbf{J}_y = -a \delta_x \delta_y \hat{\mathbf{z}}.$$

In (b)

$$\oint d\mathbf{u}_x = 0, \quad \oint d\mathbf{u}_y = a, \\ \mathbf{J}_x = 0, \quad \mathbf{J}_y = a \delta_y \delta_z \hat{\mathbf{x}}.$$

In (c)

$$\oint d\mathbf{u}_x = -a, \quad \oint d\mathbf{u}_y = 0, \\ \mathbf{J}_x = -a \delta_y \delta_z \hat{\mathbf{x}}, \quad \mathbf{J}_y = 0.$$

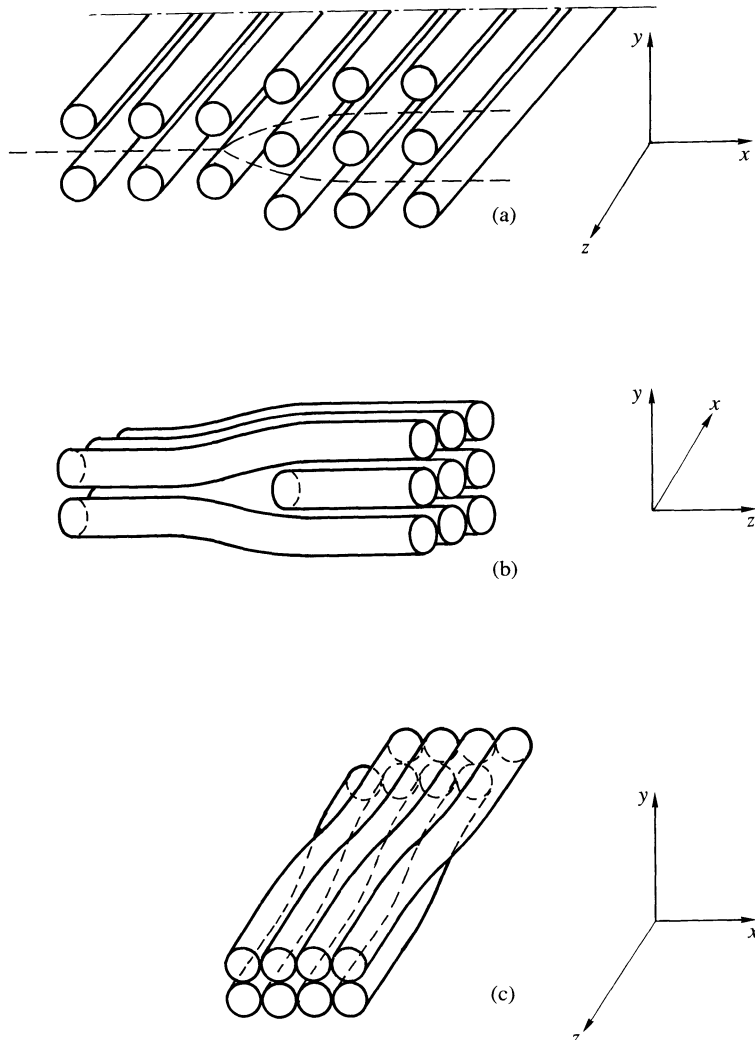


Fig. 9.25. Typical dislocations in columnar phases (the square lattice is chosen for the sake of simplicity): (a) longitudinal edge dislocation; (b) transverse edge dislocation; (c) screw dislocation (note that there is no column discontinuity).

Cases (a) and (b) correspond to longitudinal and transverse edge dislocations, case (c) to a screw dislocation. Note that screw dislocations do not involve discontinuities in the columns. Such dislocations have been discussed by Bouligand [45] and Kleman and Oswald [46].

Note that the magnetic analogy holds for each component α . In particular, a dislocation submitted to an external stress experiences a Peach-Koehler force

$$\mathbf{F} = \phi_x \times \mathbf{J}_x + \phi_y \times \mathbf{J}_y \quad (9.76)$$

in which ϕ_α is given by

$$\phi_{ia} = \sigma_{ia}^{\text{ext}} \quad (9.77)$$

where i runs over x , y , and z .

The effects of pinned dislocations, impurities, etc. could be discussed in pretty much the same way as in smectics.

9.2.2.2 Isolated edge dislocations

They can be calculated with the same procedure as the one used for smectics. One finds [46] the following using the notation of Chapter 7.

Case a of Fig. 9.25

$$\left. \begin{aligned} u_x &= \frac{a}{\pi} \left(\frac{\bar{B} + C}{4C} \ln(x^2 + y^2) + \frac{\bar{B} - C}{4C} \frac{y^2}{x^2 + y^2} \right), \\ u_y &= \frac{a}{2\pi} \left(\tan^{-1}(y/x) - \frac{\bar{B} - C}{2C} \frac{xy}{x^2 + y^2} \right), \end{aligned} \right\} \quad (9.78)$$

with a line tension

$$\gamma = \frac{C(\bar{B} - C)}{4\pi(\bar{B} + C)} a^2 \left(\ln\left(\frac{R}{r_c}\right) - 1 \right) + \gamma_c \quad (9.79)$$

where R corresponds to the size of the system in a direction perpendicular to the column axis, r_c to a small scale cut-off, and γ_c is the core energy. This result is identical to the one obtained with a two-dimensional crystal; in particular, the line energy diverges logarithmically with the size of the system. Such isolated dislocations should not be very frequent since they are energetically costly.

Case b of Fig. 9.25 It is clear that this situation is formally identical to that of smectics. One can directly transpose the results.

$$u_x = 0, \quad u_y \neq 0,$$

and, with $\mathbf{m} = \nabla \mathbf{u}_y$,

$$m_z = \frac{\pm a}{4(\pi\lambda_3|y|)^{1/2}} \exp(-z^2/4\lambda_3|y|). \quad (9.80)$$

The + (respectively -) sign holds for positive (respectively negative) y .

$$m_y = \frac{-za}{8(\pi\lambda_3)^{1/2}|y|^{3/2}} \exp(-z^2/4\lambda_3|y|) \quad (9.81)$$

with $\lambda_3^2 = K_3/(\bar{B} + C)$ and

$$\gamma = \frac{(K_3(\bar{B} + C)a_0^2)^{1/2}}{2\xi} + \gamma_c. \quad (9.82)$$

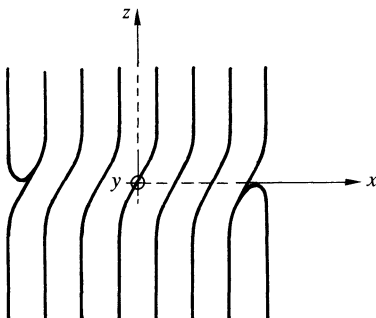


Fig. 9.26. ‘Lock-in fault’ segment joining two column extremities. All deformations are contained in the plane of the figure; the columnar sample is perfect immediately above and below this plane.

9.2.2.3 Isolated screw dislocation

The definition of \mathbf{J}_x in case (c) of Fig. 9.25 is identical to that of \mathbf{J}_y in case (b). This means that the $u_x(y, z)$ solution of the screw dislocation is formally identical to the transverse edge dislocation (with the replacement of $\bar{B} + C$ by C). Hence (9.80) now expresses the tilt of the columns in the z direction, and (9.81) the local rotation of the two-dimensional lattice. In contrast to the smectic case, screw dislocations exhibit a far-field distortion.

9.2.2.4 Point defect in columnar phases

We have seen that, in smectics, a layer may stop or start at some locations: since the border of a plane is a line, these locations were shown to be dislocation lines. The natural extension of this concept is a column extremity: since tubes are lines, these extremities are obviously points.

However, transverse edge dislocation lines are nothing but a linear array of such extremities (see for instance Fig. 9.25(b)). This tells us that column endings must always be part of a Burger’s circuit. A particular example is given on Fig. 9.26, in which the ‘lock-in fault’ line joining the two column extremities may be thought of as a screw dislocation ‘dipole’. Such defects may have a high density in some columnar phases and profoundly influence elastic properties such as the bending modulus [47] and even be responsible for an apparent shear modulus (G. Durand, personal communication).

REFERENCES

1. Friedel, G. *Ann. Phys., Paris* **2**, 273 (1922).
2. Bouligand, Y. *J. Phys. (Paris)* **33**, 525 (1972).
3. Grandjean, F. *Bull. Soc. Fr. Miner.* **39**, 164 (1916).
4. Williams, C. E. and Kleman, M. *J. Phys. (Paris) Colloq.* **36** (Suppl. C1), 315 (1975).

5. Rosenblatt, C., Pindak, R., Clark, N. A.. and Meyer, R. B. *J. Phys. (Paris)* **38**, 1105 (1977).
6. Oswald, P. and Kleman, M. *J. Phys. (Paris) Lett.* **43**, L411 (1982).
7. de Gennes, P. G. *C.R. Acad. Sci., Paris* **275B**, 549 (1972).
8. Bidaux, R., Boccara, N., Sarma, G., De Sèze, L., de Gennes, P. G., and Parodi, O. *J. Phys. (Paris)* **34**, 19 (1973).
9. Lavrentovich, O. D. *Zh. Eksp. Teor. Fiz.* **91**, 1666 (1986) [*Sov. Phys. JETP* **64**, 5 (1986)].
10. Chandrasekhar, S., Sadashiva, D. K., and Suresh, K. A. *Pramana (India)* **9**, 471 (1977).
11. Oswald, P. and Kleman, M. *J. Phys. (Paris)* **42**, 1461 (1981); Oswald, P. Thèse 3^{ème} Cycle, Orsay (1981).
12. Kleman, M. *J. Phys. (Paris)* **41**, 737 (1980).
13. Meyer, R. B., Stebler, B., and Lagerwall, S. R. *Phys. Rev. Lett.* **41**, 1393 (1978).
14. Nallet, F. and Prost, J. *Europhys. Lett.* **4**, 307 (1987).
15. Williams, C. E. and Kleman, M. *J. Phys. (Paris) Lett.* **35**, L49 (1974).
16. Williams, C. E. *Phil. Mag.* **32**, 313 (1975).
17. Kleman, M., Williams, C. E., Castello, M. J., and Gulik-Krzywicki, T. *Phil. Mag.* **35**, 33 (1977).
18. Allain, M. *J. Phys. (Paris)* **46**, 225 (1985).
19. Bartolino, R. and Durand, G. *Mol. Cryst. liquid Cryst.* **40**, 117 (1977).
20. Kleman, M. *Points, lignes, parois*, Vol. II. Editions de Physique, Orsay (1977).
21. Brunet, M. and Williams, C. *Ann. Phys., Paris* **3**, 237 (1978).
22. Yamashita, M. *Ferroelectrics* **58**, 149 (1984).
23. Lejček, L. *Czech. J. Phys.* **B35**, 655 (1985).
24. Lejček, L., Glogarova, M., and Pavel, J. *Phys. Stat. Solidi* **a82**, 47 (1984).
25. Dierker, S. B., Pindak, R., and Meyer, R. B. *Phys. Rev. Lett.* **56**, 1819 (1986); Selinger, J. V. and Nelson, D. R. *Phys. Rev. A* **39**, 3135 (1989).
26. Nelson, D. R. and Halperin, B. I. *Phys. Rev. B* **19**, 2456 (1979).
27. Nelson, D. R. and Halperin, B. I. *Phys. Rev. B* **21**, 5312 (1980).
28. Halperin, B. I. In *Symmetries and broken symmetries. Proceedings of the Colloque Pierre Curie, Paris, France* (ed. N. Boccara), p. 183–9, IDSET, Paris (1981).
29. Rieker, T. P., Clark, N. A., Smith, G. S., Parmar, D. S., Sirota, E. B., and Safinya, C. R. *Phys. Rev. Lett.* **59**, 2658 (1987).
30. Pershan, P. S. *J. appl. Phys.* **45**, 1590 (1974); see also Lejček, L. and Oswald, P. *J. Phys. II (France)* **1**, 931 (1991).
31. Allain, M. *Europhys. Lett.* **2**, 597 (1986).
32. Van Winkle, D. H. and Clark, N. A. *Phys. Rev. Lett.* **48**, 1407 (1982).
33. Prost, J. In *Symmetries and broken symmetries* (ed. N. Boccara), p. 159. IDSET, Paris (1981).
34. Friedel, J. and Kleman, M. *J. Phys. (Paris)* **30** (Suppl. C4), 43 (1969).
35. de Gennes, P. G. *C.R. Acad. Sci., Paris* **275B**, 939 (1972).
36. Kleman, M. *J. Phys. (Paris)* **35**, 595 (1974).
37. Dubois Violette, E., Guazelli, E., and Prost, J. *Phil. Mag. A* **48**, 727 (1983).
38. Peach, M. and Koehler, J. S. *Phys. Rev.* **80**, 436 (1950).
39. Nelson, D. R. and Toner, J. *Phys. Rev. B* **24**, 363 (1981).
40. Pershan, P. S. and Prost, J. *J. appl. Phys.* **46**, 2343 (1975).

41. Landau, L. D. and Lifshitz, E. M. *Electrodynamics of continuous media*. Pergamon, London (1960).
42. Langer, J. S. and Fisher, M. E. *Phys. Rev. Lett.* **19**, 560 (1967).
43. Vinen, W. F. In *Proceedings of the Enrico Fermi International School of Physics*, Course XXI (ed. G. Careri), p. 336. Academic, New York (1963).
44. Landau, L. D. and Lifshitz, E. M. *Theory of elasticity*. Pergamon, London (1959).
45. Bouligand, Y. *J. Phys. (Paris)* **41**, 1297 (1980).
46. Kleman, M. and Oswald, P. *J. Phys. (Paris)* **43**, 655 (1982).
47. Prost, J. *Liquid Cryst.* **8**, 123 (1990).

PHASE TRANSITIONS IN SMECTICS

Over the last 20 years there has been a considerable effort put into understanding the physics of phase transitions in liquid crystals. The main reason is probably that statistical mechanics has seemed ready to provide a comprehensive view of the successive phase changes that lead from liquids to crystals. This goal is almost reached, but not quite.

From the point of view of applications, it is important to understand the temperature behaviour of the macroscopic parameters that govern the characteristics of displays or sensors. Close to the nematic-smectic A transition ($N-S_A$), the onset of quasimectic features in the nematic phase may lead to a drastic change in certain important constants (elastic coefficients, transport properties, cholesteric pitch, etc.). For instance, it has been shown by Rondelez [1] that the ratio of the parallel to the perpendicular electric conductivity $\sigma_{\parallel}/\sigma_{\perp}$, which is usually larger than unity in nematics, may become significantly smaller than unity in the vicinity of a smectic transition (because the charge carriers do not cross the layers easily). The electrohydrodynamic effects on which some display devices are based, depend critically on $(\sigma_{\parallel}/\sigma_{\perp}) - 1$. Materials with positive dielectric anisotropy, which could not be used efficiently when $\sigma_{\parallel}/\sigma_{\perp} > 1$, become interesting.

The understanding of the transitions involving chiral smectics C^* is of direct importance for their use in the new generation of display devices.

Developing all aspects of transitions involving smectics or columnar phases would require a separate book. Obviously, this cannot be done here. Thus we avoid computational details and give more attention to the $N-S_A$ transition than to the others, in view of its generic importance. Furthermore, in view of the absence of detailed experimental studies on phase transitions in columnar phases, we omit any description of them.

10.1 THE $A \rightleftharpoons N$ TRANSITION

10.1.1 Mean-field description

In spite of early controversies, it is now well documented that the $N-S_A$ transition is continuous in the absence of special circumstances[†] [2, 3], as first suggested by McMillan for a specific model [4].

[†] Of course, one can never exclude discontinuities so small that they cannot be detected experimentally (see Section 1.1.7).

The smectic A phase is characterized by a density modulation, in a direction $\hat{\mathbf{z}}$ orthogonal to the layers

$$\rho(\mathbf{r}) = \rho(z) = \rho_0 + \rho_1 \cos(q_s z - \Phi) + \dots \quad (10.1)$$

where ρ_1 is the first harmonic of the density modulation and Φ an arbitrary phase. In a nematic $\rho_1 = 0$. A natural choice for the S_A order parameter is thus ρ_1 . We discuss later on, in this section and in Section 10.4, the role of higher harmonics.

In the vicinity of the N– S_A transition, the free energy (per unit volume) may be expanded in powers of ρ_1

$$f_s = \frac{1}{2} r \rho_1^2 + \frac{1}{4} u_0 \rho_1^4 + \dots \quad (10.2)$$

Only even powers of ρ_1 may come in, since $\pm \rho_1$ differ only in the origin of the reference axis choice (through Φ). At a certain temperature T_0 , the coefficient $r \simeq \alpha(T - T_0)$ vanishes. Above this temperature it is positive. The coefficient u_0 is always positive. With these ingredients alone, one could have a second-order transition $T_{AN} = T_0$. There are, however, a number of complications.

The simplest comes from the coupling between ρ_1 and S , the nematic order parameter defined in Chapter 2. If the alignment measured by S increases, the average attractions between molecules in a smectic layer in general increase. Because of this coupling the optimal value of S does not coincide with $S_0(T)$ obtained in the absence of smectic order (e.g. as given by the Maier–Saupe theory). We shall put

$$\delta S = S - S_0(T). \quad (10.3)$$

The coupling term, to lowest order, must have the form

$$f_1 = -C \rho_1^2 \delta S \quad (10.4)$$

(note again: no odd power of ρ_1). C is a constant, positive in general. Finally we must include in f the nematic free energy f_N which is minimum for $\delta S = 0$,

$$f_N = f_N(S_0) + \frac{1}{2\chi} \delta S^2. \quad (10.5)$$

Here $\chi(T)$ is a response function, which is large (although finite) near the nematic–isotropic transition point T_{NI} , but which is small for $T < T_{NI}$ (since S_0 is then nearly saturated and cannot fluctuate very much). The overall free energy f obtained by adding f_s, f_1, f_N must then be minimized with respect to δS , giving

$$\delta S = \chi C \rho_1^2, \quad (10.6)$$

$$f = f(S_0) + \frac{\Gamma_0}{2} \rho_1^2 + \frac{u}{4} \rho_1^4, \quad (10.7)$$

$$u = u_0 - 2C^2\chi. \quad (10.8)$$

The order of the transition depends critically on the sign of u .

1. If $T_0 \sim T_{\text{NI}}$, $\chi(T_0)$ is large and u is negative. Then terms in ρ_1^6 must be added to (10.2) to ensure stability, and the resulting plots of $f(\rho_1)$ show that, for $T = T_0$, the minimum of f is already at non-zero ρ_1 . The transition takes place at a higher temperature $T_{\text{AN}} > T_0$, and it is first order.
2. If T_0 is significantly smaller than T_{NI} , the response function $\chi(T_0)$ is small and $u \sim u_0 > 0$. Then, looking at the plots of $f(\rho_1)$, one easily sees that the transition is of second order and the transition point is T_0 (in this mean-field description).
3. The point at which $u = 0$ is a tricritical point to be discussed later. The change from second to first order is thus induced by a coupling between the order parameter ρ_1 and an external variable (S). This is the exact counterpart of the so-called ‘Rodbell–Bean’ effect in magnetism [5]. In the magnetic case, the order parameter is the magnetization M , and the external variable is the density (or lattice parameter a). The coupling is due to the dependence of exchange interactions on a . If the magnetic crystal is strongly compressible (large χ), the transition becomes first order. There are, in fact, many such couplings. Indeed, all scalar degrees of freedom[†] will give rise to the same kind of effect.

We shall now see that there are many other sources of complications.

10.1.2 The analogy with superconductors

We have already seen in Chapters 1 and 8 that layer fluctuations play an important role in smectics. The layer displacement $u(\mathbf{r})$ come naturally through[‡]

$$\Phi(\mathbf{r}) = -q_s u(\mathbf{r}). \quad (10.9)$$

Clearly, close to the transition, one also has to allow for fluctuations in the modulation intensity ρ_1 (which becomes $\rho_1(\mathbf{r})$). An elegant way of including both features is to introduce the complex order parameter [7, 8]

$$\psi(\mathbf{r}) = \rho_1(\mathbf{r}) e^{i\Phi(\mathbf{r})}. \quad (10.10)$$

Since we allow for the order parameter to vary from place to place, we have to add gradient terms that express the tendency for the smectic to be homogeneous. The free energy now reads

$$F_s = \frac{1}{2} \int_v d^3x \left\{ r|\psi|^2 + \frac{u}{2} |\psi|^4 + C_{\parallel} \left| \frac{\partial \psi}{\partial z} \right|^2 + C_{\perp} \left(\left| \frac{\partial \psi}{\partial x} \right|^2 + \left| \frac{\partial \psi}{\partial y} \right|^2 \right) \right\} \quad (10.11)$$

[†] The second harmonic of the layer modulation ρ_2 plays the same role as will be shown in Section 10.4 [6].

[‡] The layer displacement $u(\mathbf{r})$ is not to be confused with the coefficient of the fourth-order term u .

where $C_{\parallel} \neq C_{\perp}$ because of the nematic anisotropy. If one could stop here, the N-S_A problem would be analogous to that of the condensation of superfluid helium on the ground that ψ is a complex order parameter (the anisotropy can be removed with simple scale changes).†

Upon writing (10.11), we made the implicit assumption that the director is fixed in the z direction. In reality \mathbf{n} fluctuates. The gradient terms have to be taken in directions that are, respectively, parallel and perpendicular to \mathbf{n} . At the required order of expansion, only the C_{\perp} term is modified. It becomes (with the notation $\nabla_{\perp} = (\partial/\partial x, \partial/\partial y)$)

$$C_{\perp}|(\nabla_{\perp} - iq_s \delta\mathbf{n}_{\perp})\psi|^2 \quad (10.12)$$

in which $\delta\mathbf{n}_{\perp} = \mathbf{n} - \hat{\mathbf{z}}$. (Note that, since $n^2 = 1$, at the lowest order, $\delta\mathbf{n}$ is the x, y -plane.)

This can be easily understood in the following way. A rotation δn_x of the layers implies a displacement, $u = -\delta n_x x$ and thus a smectic order parameter

$$\psi = \psi_i e^{+iq_s \delta n_x x} \quad (10.13)$$

where ψ_i is the ‘intrinsic’ order parameter (i.e. defined in its local reference frame). Hence (10.12) is nothing but

$$C_{\perp}|\nabla_{\perp}\psi_i|^2 \quad (10.14)$$

and expresses, as wished, the intrinsic smectic fluctuations perpendicularly to the director.

The total free energy, of course, includes the Frank–Oseen elastic contribution. Finally, the N-S_A transition is described by the functional

$$F_{NA} = \frac{1}{2} \int d^3x \left\{ r|\psi|^2 + \frac{u}{2}|\psi|^4 + C_{\parallel} \left| \frac{\partial \psi}{\partial z} \right|^2 + C_{\perp} |(\nabla_{\perp} - iq_s \delta\mathbf{n}_{\perp})\psi|^2 + K_1 \operatorname{div}^2 \delta\mathbf{n}_{\perp} + K_2 (\hat{\mathbf{z}} \cdot \operatorname{curl} \delta\mathbf{n}_{\perp})^2 + K_3 \left(\frac{\partial}{\partial z} \delta\mathbf{n}_{\perp} \right)^2 \right\}. \quad (10.15)$$

Or, after a simple anisotropic scale change,

$$F_{NA} = \frac{1}{2} \int d^3x \left\{ r|\psi|^2 + \frac{u}{2}|\psi|^4 + C |(\nabla - iq_s \delta\mathbf{n}_{\perp})\psi|^2 + \tilde{K}_1 \operatorname{div}^2 \delta\mathbf{n}_{\perp} + \tilde{K}_2 (\hat{\mathbf{z}} \cdot \operatorname{curl} \delta\mathbf{n}_{\perp})^2 + \tilde{K}_3 \left(\frac{\partial}{\partial z} \delta\mathbf{n}_{\perp} \right)^2 \right\}. \quad (10.16)$$

† In helium, what we have is a Bose condensation [9]. A macroscopic number of helium atoms are occupying one quantum state, described by a wave function $\psi(r)$. This is the order parameter and it is complex. The independence of F on ϕ is called gauge invariance.

This expression bears a striking resemblance to the Landau–Ginzburg functional describing the normal–superconductor transition [7, 8, 10, 11]

$$F_{\text{SC}} = \frac{1}{2} \int d^3x \left\{ r|\psi|^2 + \frac{u}{2} |\psi|^4 + \frac{1}{m} \left| \left(\hbar \nabla - i \frac{q}{c} \mathbf{A} \right) \psi \right|^2 + \frac{1}{8\pi\mu} (\text{curl } \mathbf{A})^2 \right\} \quad (10.17)$$

where ψ is the superconductor ‘gap’ order parameter [10], \mathbf{A} the magnetic vector potential, m, q the particles’ mass and charge, c the speed of light, \hbar Planck’s constant, and μ the magnetic permittivity.

In clear correspondence:

Smectics	Superconductors
ψ smectics	$\rightarrow \psi$ superconductors
$\delta \mathbf{n}_\perp$	$\rightarrow \mathbf{A}$ magnetic vector potential
‘elastic constant’ C	$\rightarrow m^{-1}$ where m = mass of the superconducting pairs
q_s	$\rightarrow q/c$ charge of the superconducting pairs (divided by the speed of light)
K_1 Frank constants	$\rightarrow 1/\mu$ inverse magnetic permittivity
gradient energy	\rightarrow kinetic energy
Frank–Oseen elastic energy	\rightarrow magnetic energy

What do we learn from this analogy [8]?

Just as superconductors expel magnetic fields from their bulk (Meissner effect [12]), smectics expel bend and twist. As a result the bend and twist moduli should diverge upon approaching the smectic from the nematic phase. This will be discussed in the next section.

In superconductors, there are two important lengths:

1. the order parameter coherence length, $\xi = (|r|m)^{-1/2}$;
2. the London penetration length, $\lambda = (4\pi\mu|r|/um)^{-1/2}$.

ξ describes the scale over which ψ can vary, whereas λ sets the penetration depth of a magnetic field.

In smectics, there are two classes of such length:

1. two order parameter coherence lengths (Fig. 10.1), $\xi_{\parallel, \perp} = (C_{\parallel, \perp}/|r|)^{1/2}$;
2. four penetration lengths (Fig. 10.2), $\lambda_{\parallel, \perp}^{2;3} = (K_{2,3}u/C_{\parallel, \perp}|r|)^{1/2}$.

One has to further add $\lambda_1 = (K_1 u/C_\parallel |r|)^{1/2} = (K_1/B)^{1/2}$, the importance of which has been widely discussed in Chapters 8 and 9 (i.e. it weights the bending energy versus the compressional one).

There are too many possible cases to permit a detailed classification of them. The analogy helps us in that it suggests two basically distinct behaviours.

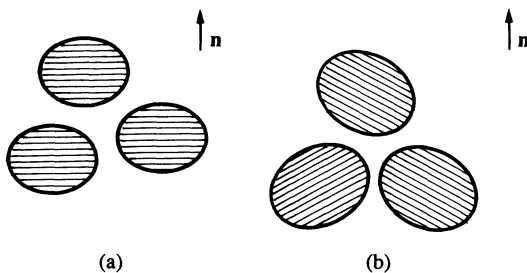


Fig. 10.1. Cybotactic groups above a smectic–nematic transition: (a) smectic A–nematic; (b) smectic C–nematic.

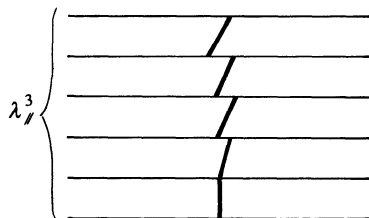


Fig. 10.2. Finite penetration length of a molecular tilt in the smectic layers (here $(\lambda_{||}^3)$).

- Type one ($\lambda_{||}/2 < \xi$). Below a critical field H_c , one observes a perfect Meissner effect. For $H > H_c$, the system becomes normal. H_c is such that the magnetic energy balances the pair condensation energy.
- Type two ($\lambda_{||}/2 > \xi$). At a field $H_{c1} < H_c$, vortices bearing a quantized flux $\Phi_0 = \hbar/q$ penetrate the system. The flux quantization results from the fact that the phase of the superconductors order parameter increases by exactly 2π if we follow a closed circuit embracing the vortex line. At a field $H_{c2} > H_c$, the system becomes normal. ($H_{c1}H_{c2} \sim H_c^2$ in which H_c is still defined as the field for which the magnetic energy balances the condensation energy.)

One can thus expect two basically different responses from a smectic submitted to a bending or twisting stress. Either it could resist, until a critical stress induces a transition toward the nematic state (type one), or at a lower threshold dislocations may come in and allow for the distortions to take place (type two). Indeed, the direct analogy of a vortex is a dislocation (cf. 2π increase of the phase $-q_s u$ in a circuit embracing the dislocation line). Observation of dislocation arrays suggests that smectics are in general type two [13], but type one behaviours have also been reported [14].

Another interesting feature of the analogy is that smectics provide a system with a short coherence length at zero temperature $\xi_0 = (m\alpha T_0)^{-1/2}$ (if

$r = \alpha(T - T_0)$), so that we expect to see critical fluctuations at the N-S_A transition, whereas it is not possible to do so with conventional superconductors. In this last case, ξ_0 is large (e.g. 5000 Å in simple metals) and the transition is perfectly described by mean field. The recent discovery of high T_c superconductors [15], which are characterized by ξ_0 comparable to that of smectics ($10 \sim 20$ Å), gives a new dimension to the analogy since we should be able to compare the critical behaviours. There are, however, important differences, which concern:

- gauge invariance;
- the absence of smectic long-range order (remember Chapters 1 and 8).

Equation (10.17) is invariant in the transformation

$$\left. \begin{aligned} \mathbf{A}' &= \mathbf{A} - \nabla L, \\ \psi' &= \psi \exp\left(-\frac{iq}{\hbar c} L\right). \end{aligned} \right\} \quad (10.18)$$

As a result any gauge choice is physically acceptable. One often used is the Coulomb gauge, $\text{div } \mathbf{A} = 0$.

In the smectic problem, one can consider the same type of transformation, namely (we use the notation \mathbf{A} to stress that the transformed vector has in general three components),

$$\left. \begin{aligned} \mathbf{A}' &= \mathbf{A} - \nabla L, \\ \psi' &= \psi \exp(-iq_s L). \end{aligned} \right\} \quad (10.19)$$

The situation is, however, more complex:

1. Only one gauge has a physical meaning, namely $A_z = 0$, i.e. $\mathbf{A} = \delta \mathbf{n}_\perp$.
2. In contrast to the magnetic energy, the Frank–Oseen energy is not invariant, because of the splay term.

How severe these differences are is not fully understood yet.

Problem. Show that in the Coulomb gauge the transformed smectic order parameter exhibits true long-range order [16, 17].

Solution. According to (10.13)

$$\begin{aligned} \int \frac{d^3x}{2m} |(\nabla - i\delta \mathbf{n}_\perp q_s)\psi|^2 &= \int \frac{d^3x}{2m} |(\nabla - i\mathbf{A}q_s)\psi'|^2 \\ &= \frac{1}{2m} \int \{ |\nabla \psi'|^2 - iq_s \mathbf{A} \cdot (\psi' \nabla \psi'^* - \psi'^* \nabla \psi') + q_s^2 \mathbf{A}^2 |\psi'|^2 \} d^3x \end{aligned}$$

or, with $\psi' = |\psi'| e^{i\phi'}$,

$$= \frac{1}{2m} \int \{|\nabla\psi'|^2 - 2q_s|\psi'|^2 \mathbf{A} \cdot \nabla\phi' + q_s^2 \mathbf{A}^2 |\psi'|^2\} d^3x.$$

The absence of long-range order in smectics comes from phase fluctuations, so that one can consider a constant modulus in what follows. Integrating the cross-term by parts yields

$$\frac{1}{2m} \int |\psi'|^2 \{(\nabla\phi')^2 + 2q_s \phi' \operatorname{div} \mathbf{A} + q_s^2 \mathbf{A}^2\} d^3x.$$

In the Coulomb gauge $\operatorname{div} \mathbf{A} = 0$ and the fluctuations of ϕ' and \mathbf{A} are decoupled; the $(\nabla\phi')^2$ term which involves first derivatives ensures that ϕ' exhibits true long-range order (remember the case of crystals in Chapter 1).

Note. In this gauge, the splay term reads

$$\frac{K_1}{2} \int (\Delta L)^2 d^3x$$

where the condition $\delta n_z \simeq 0$ imposes (in Fourier space)

$$A_z(q) - iq_z L(q) = 0.$$

Thus, one can write the splay energy

$$\frac{1}{2} K_1 \int \frac{q^4}{q_z^2} |A_z(q)|^2 \frac{d^3q}{(2\pi)^3}.$$

In the Coulomb gauge the splay term is a non-analytic function of the vector potential. This has two important consequences.

1. K_1 cannot be renormalized by ψ fluctuations to any order in perturbation theory.[†]
2. In a renormalization group procedure, K_1 will simply evolve according to power counting and is an eigendirection of renormalization equations. This implies that the physical K_1 does not diverge at T_{NA} .

10.1.3 Critical phenomena

In the smectic phase, just above the transition point T_{AN} , we expect to see small domains with a local smectic organization (Fig. 10.1). This has been recognized by de Vries [18] who called these domains cybotactic clusters. From the point of view of X-ray scattering, one has two peaks of intensity

[†] This does not forbid the existence of a direct $|\psi|^2$ dependence of K_1 , leading to irrelevant terms in the renormalization group jargon, but non-trivial temperature dependence of $(dK_1/dT) \sim |T - T_{NA}|^{-\alpha}$.

in reciprocal space, concentrated near the points $\mathbf{q} = \pm q_s \mathbf{n}$. The width of these peaks gives some information on the size ξ of the clusters.

According to (10.15) the X-ray structure factor should be given by (in the harmonic approximation)

$$\langle \psi(\mathbf{q})\psi^*(\mathbf{q}) \rangle = \frac{k_B T}{r + C_{||} q_z^2 + C_{\perp} q_{\perp}^2} = \frac{\chi}{1 + q_z^2 \xi_{||}^2 + q_{\perp}^2 \xi_{\perp}^2}. \quad (10.20)$$

Equation (10.20) helps us to understand the definition of $\xi_{||, \perp}$ as the coherence length of the smectic order parameter in directions, respectively, parallel and perpendicular to the nematic director. In other words, the clusters are anisotropic: experimentally one finds $\xi_{||} \sim 5\xi_{\perp}$ [18–21]. χ is the smectic susceptibility

$$\chi = (k_B T/r) \propto t^{-\gamma} \quad (10.21)$$

with $\gamma = 1$ and

$$t = \frac{T - T_{NA}}{T_{NA}}.$$

The mean-field relations predict a divergence of ξ upon approaching the transition

$$\xi_{||} \sim \xi_{\perp} \propto t^{-1/2}. \quad (10.22)$$

If the helium analogy were to hold, one would expect $\xi_{||} \propto \xi_{\perp} \propto t^{-v}$ with $v \simeq 0.67$ and $\chi \propto t^{-\gamma}$ with $\gamma \simeq 1.32$. We will see in the following that the experimental situation is more complex.

We learned at the end of the preceding chapter that one expects a divergence of K_2 and K_3 upon approaching the smectic phase from the nematic side. An effect of this sort in K_3 was first found by the Freiburg group [22]. However, the systems at hand were smectics C rather than smectics A, which complicates the situation. On the theoretical side, a calculation of the anomaly has been described in references 8 and 16. It predicts an increase $(\delta K_2, \delta K_3)$ proportional to the size ξ of the cluster. The calculation may be presented qualitatively as follows.

Consider for instance a *bend* deformation imposed on a cybotactic cluster (Fig. 10.3). The strains imposed to the layers are of order $\delta\theta$ where $\delta\theta$ is the angle between optical axes on both sides of the cluster

$$\delta\theta \sim \frac{\partial\theta}{\partial z} \xi.$$

The elastic energy due to layer distortion (per cm³) is

$$\frac{1}{2} \tilde{B} (\delta\theta)^2$$

where \tilde{B} has been defined in eqn (7.5) below T_c , but is now used for a cluster

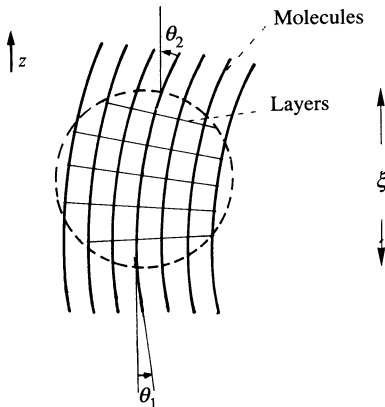


Fig. 10.3. Effect of a bending deformation on a cybotactic group, just above an $A \Leftrightarrow N$ transition: the layers cannot remain equidistant.

above T_c . The correction to the bend energy is thus

$$\frac{1}{2}\tilde{B}\xi^2\left(\frac{\partial\theta}{\partial z}\right)^2 = \frac{1}{2}\delta K_3\left(\frac{\partial\theta}{\partial z}\right)^2. \quad (10.23)$$

We must now estimate \tilde{B} for a cluster, i.e. in a temperature region where the order parameter ψ defined in eqn (10.15) is small. \tilde{B} vanishes with ψ and must be even in ψ : it is natural to assume that $\tilde{B} \sim |\psi|^2$. The complete calculation shows that, in fact, for the present problem, we must put

$$\tilde{B} = \text{const} \langle \psi^*(0)\psi(R) \rangle_{R \sim \xi}. \quad (10.24)$$

To a good approximation, the correlation function $\langle \psi\psi \rangle$ has the Ornstein–Zernike form

$$\langle \psi^*(0)\psi(R) \rangle = \frac{\text{const}}{R} \exp(-R/\xi).$$

Then

$$\tilde{B} \sim \langle \psi^*(0)\psi(\xi) \rangle \sim 1/\xi$$

and

$$\delta K_3 \simeq \tilde{B}\xi^2 \simeq \xi. \quad (10.25)$$

A similar argument holds for the twist constant

$$K_2 = K_{20} + \delta K_2.$$

Keeping track of the anisotropy, gives

$$\delta K_3 \propto \xi_{\parallel}, \quad \delta K_2 \propto \xi_{\perp}^2/\xi_{\parallel}. \quad (10.26)$$

Note that, as already pointed out, we expect no divergence of the splay elastic constant.

10.1.4 Anisotropic scaling

In fact, experiment suggests the existence of anisotropic scaling laws (i.e. $\xi_{\parallel} \propto t^{-v_{\parallel}}$; $\xi_{\perp} \propto t^{-v_{\perp}}$ with $v_{\parallel} \neq v_{\perp}$).

Let us consider the consequences resulting from the following scaling laws [23, 24],

$$f(t, K_1) \simeq k_B T \xi_{\parallel} \xi_{\perp}^2, \quad (10.27a)$$

$$\begin{aligned} \langle \psi(\mathbf{q}) \rangle &= G(q_{\parallel}, q_{\perp}, t, K_1) \\ &= t^{-(2-\eta_{\perp})v_{\perp}} G(t^{-v_{\parallel}} q_{\parallel}, t^{-v_{\perp}} q_{\perp}, t^{\tau v_{\perp}} K_1), \end{aligned} \quad (10.27b)$$

$$\begin{aligned} \langle \delta n_{\alpha}(\mathbf{q}) \delta n_{\beta}(-\mathbf{q}) \rangle &= G_{\alpha\beta}(q_{\parallel}, q_{\perp}, t, K_1) \\ &= t^{-(2-\eta_n)v_{\perp}} G_{\alpha\beta}(t^{-v_{\parallel}} q_{\parallel}, t^{-v_{\perp}} q_{\perp}, t^{\tau v_{\perp}} K_1) \end{aligned} \quad (10.27c)$$

where f is the free energy density, G the order parameter two-point correlation function, and $G_{\alpha\beta}$ the director correlation function. The presence of the exponents η_{\perp} and η_n reflects the need of scaling the amplitudes of ψ and δn respectively, upon rescaling wavevectors. K_1 is kept explicitly since it is an eigendirection of renormalization group equations.

We get immediately from (10.27b) and keeping the definition (10.21)

$$\left. \begin{aligned} \gamma &= (2 - \eta_{\perp})v_{\perp}, \\ \xi_{\parallel} &= t^{-v_{\parallel}}; \quad \xi_{\parallel} = t^{-v_{\perp}}. \end{aligned} \right\} \quad (10.28)$$

Equation (10.27a) implies for the critical part of the specific heat†

$$\delta C_p \propto t^{-\alpha} \quad \text{with} \quad 2 - \alpha = 2v_{\perp} + v_{\parallel}. \quad (10.29)$$

Keeping the notation of Chapter 3, on the nematic side

$$\langle \delta n_1(q) \delta n_1(-q) \rangle = \frac{k_B T}{K_1 q_{\perp}^2 + K_3 q_z^2}, \quad (10.30a)$$

$$\langle \delta n_2(q) \delta n_2(-q) \rangle = \frac{k_B T}{K_2 q_{\perp}^2 + K_3 q_z^2}. \quad (10.30b)$$

Imposing the structure (10.27c) on (10.30) requires

$$K_2 \propto t^{-\eta_n v_{\perp}} \quad K_3 \propto t^{-2(v_{\parallel} - v_{\perp}) - \eta_n v_{\perp}} \quad (10.31)$$

and remembering that K_1 is unchanged imposes the equality

$$\tau = \eta_n. \quad (10.32)$$

† Note that for $\alpha < 0$, a more correct expression is: $\delta C_p \propto \text{const} + A^{\pm} t^{-\alpha}$, since the critical part of the specific heat is finite at the critical point.

Similarly, on the smectic side

$$\langle |u(q)|^2 \rangle = \frac{k_B T}{Bq_z^2 + K_1 q_\perp^4} \quad (10.33)$$

(with $u(q)$ = Fourier transform of the layer displacement $u(\mathbf{r})$) and

$$\langle \delta n_1(q) \delta n_1(-q) \rangle = \frac{k_B T q_\perp^2}{Bq_z^2 + K_1 q_\perp^4}. \quad (10.34)$$

Insisting that (10.27c) should be valid below T_{NA} as well requires

$$B \propto t^{(4 - \eta_n)v_\perp - 2v_\parallel} \quad \text{and again} \quad \tau = \eta_n. \quad (10.35)$$

Finally, with

$$\langle \delta n_2(q) \delta n_2(-q) \rangle = \frac{k_B T}{D + K_2 q_\perp^2 + K_3 q_z^2} \quad (10.36)$$

where D describes the energy required to tilt the director away from the layer normal, one obtains that K_2 and K_3 diverge symmetrically upon approaching T_{NA} from above and below and that

$$D \propto t^{v_\perp(2 - \eta_n)}. \quad (10.37)$$

The simultaneous scaling of q_z , q_\perp , and δn imposes the following transformation of the smectic wavevector

$$q_s^2 \rightarrow t^{(v_\parallel - 2v_\perp + v_\perp \eta_n)} q_s^2. \quad (10.38)$$

Expressing the fact that q_s has a finite value at the transition necessitates

$$\eta_n = \frac{2v_\perp - v_\parallel}{v_\perp} \quad \text{or} \quad 2 - \eta_n = v_\parallel/v_\perp. \quad (10.39)$$

Hence the final scaling laws

$$\xi_\parallel = \xi_0 t^{-v_\parallel}, \quad \xi_\perp = \xi_0 t^{-v_\perp}, \quad (10.40a)$$

$$\delta K_2 \propto \xi_\perp^2 / \xi_\parallel, \quad \delta K_3 \propto \xi_\parallel \quad (10.40b)$$

(both above and below T_{NA}),

$$B \propto \xi_\parallel / \xi_\perp^2, \quad D \propto \xi_\parallel^{-1}, \quad (10.40c)$$

$$2 - \alpha = v_\parallel + 2v_\perp, \quad \gamma = (2 - \eta_\perp)v_\perp \quad (10.40d)$$

(again above and below T_{NA}).

10.1.5 Experimental situation

All the predicted behaviours can be checked experimentally.

1. ξ_\parallel , ξ_\perp , and γ can be obtained by X-ray scattering using eqn (10.20) directly. Early experiments showed the need for a more complex form [19].

More recent data [25] prove the validity of a slightly amended version of (10.20), namely,

$$\langle \psi(q)\psi^*(q) \rangle = \frac{\chi}{1 + \xi_{\parallel}^2 q_z^2 + \xi_{\perp}^2 q_{\perp}^2 (1 + C \xi_{\perp}^2 q_{\perp}^2)}. \quad (10.41)$$

There is no fundamental difficulty in accepting the existence of the $C \xi_{\perp}^4 q_{\perp}^4$ term, but it is unexpectedly large.[†] The most remarkable result is that, for basically all compounds studied to date, one does find scaling behaviours such as predicted by (10.40a), with $v_{\parallel} > v_{\perp}$ but the values of the exponents seem to depend continuously on the nematic range. Since the power law is followed in general over three decades, it seems hard (although possible) to blame the apparent dependence on a cross-over regime. (Note, however, that one does see the evolution toward tricritical exponents[‡] in well chosen chemical series [26], but the anisotropy is always present).[§]

Typical values are $v_{\parallel} \simeq 0.57\text{--}0.75$ and $v_{\perp} \simeq 0.45\text{--}0.60$, and $\gamma \simeq 1.3\text{--}1.5$.

2. The divergence of elastic constants has been studied with great accuracy, especially in the latest experiments [27–33] both with light scattering and Fredericks transitions. The results are fully consistent with X-ray data and relations (10.40b). Some of the studies are carried out over one of the largest reduced temperature ranges ever achieved ($10^{-5} \leq t \leq 10^{-1}$).

Note. What happens to the cholesteric pitch upon approaching the smectic phase? If q is the twist, the free energy for a cholesteric may be written as

$$F_{\text{chol}} = \frac{1}{2} K_2 q^2 - k_2 q + F_{\text{nem}}. \quad (10.42)$$

We find thus for the equilibrium twist

$$q_0 = \frac{k_2}{K_2}.$$

k_2 stems from molecular chirality and is only weakly influenced by the smectic order [34]. Thus the cholesteric twist vanishes according to $t_0 \propto \xi_{\perp}^2 / \xi_{\parallel}$. The corresponding divergence of the pitch has been carefully studied in reference 35.

3. The vanishing of the compressional elastic constant has been measured via the undulation instability [36, 37], Rayleigh scattering [30], and second-sound resonances [38–42]. B is indeed found to vanish continuously

[†] A more satisfactory form would be $C(\xi_{\perp} q_{\perp})^{4-2\eta}$.

[‡] At the critical point, $\nu = 0$, one expects $\gamma = 1$, $\alpha = 0.5$, and $v_{\parallel} = v_{\perp} = 0.5$. For a more complete analysis see Section 10.1.7.

[§] Recent experiments on a monolayer smectic show a clear-cut cross-over from helium to tricritical (Nounesis, G., Garland, C. W., and Shashidhar, R., personal communication).

according to a power law

$$B \propto t^x.$$

However, x is often found to be quite small ($x \simeq 0.3$). The data are only marginally consistent with (10.40c). Most recent results point toward $x \simeq 0.40$ irrespective of the system under consideration [42] and a non-vanishing modulus at the transition.

4. Much attention has also been paid to the specific heat critical behaviour [43–50]. One does find a critical contribution

$$\delta C_p \propto t^{-\alpha}.$$

The scaling relation (10.40d) is borne out by experiment within experimental uncertainties. The cross-over from critical to tricritical is well documented, together with the onset of the first-order transition [49]. It occurs for nematic ranges much smaller than expected from molecular theories, but follows the idea developed in Section 10.1.1 that one needs a large nematic response function χ , in order to obtain the u sign change. We will discuss the peculiarities of the tricritical point in Section 10.1.7.

To sum up,

- The constancy of K_1 and the divergences of K_2 , K_3 , C_p are well borne out by experiment.
- The scaling relations (10.40) seem to hold reasonably well.
- For large nematic ranges the critical exponents are quite close to an XY , helium-like behaviour (i.e. $\gamma = 1.32$; $v_{\parallel} = v_{\perp} = 0.67$; $\alpha = -0.007$), but a small anisotropy remains [51, 52].
- The values of the critical exponent seem to depend continuously on the width of the nematic range.

Before discussing further the theoretical questions raised by these results, it is worth mentioning two pitfalls, which may not always be avoided.

1. In the case of mixtures, the exponents may suffer the so-called Fisher renormalization [53]: if the slope of the phase boundary $T_{AN}(x)$ is large enough (x concentration of compound 2 in a (1–2) mixture) and α positive, the observed exponents are divided by $(1 - \alpha)$ (with the exception of α^{eff} which obeys $\alpha^{eff} = -\alpha/(1 - \alpha)$). This seems to be the case in mixtures involving dissimilar molecules (for instance: polar–non-polar) [54].
2. In mixtures again the prefactors may become a function of temperature. This should, however, not be too serious close enough to the transition.

With these words of caution, it is reasonable to think that there is indeed a theoretical challenge.

10.1.6 The search for an anisotropic fixed point

The relations (10.40) hold if, in a renormalization procedure, an ‘anisotropic’ fixed point (i.e. with $v_{\parallel} \neq v_{\perp}$) is found [23]. Several attempts toward finding such a fixed point have been conducted. They use:

- the ϵ -expansion [23, 55];
- the $1/n$ expansion [56];
- dislocation-mediated theories [57–62].

The first two are based on a generalization of (10.16) to an order parameter with $n/2$ complex components in a d -dimensional space ($\epsilon = 4 - d$) [63, 64]. We give a heuristic picture of the last in Section 10.1.8. Although technically different, they should all share in common the following important feature [23, 65].

As a note in the problem on gauge transformation we pointed out that K_1 renormalizes according to its power counting. In other words† (for $d = 3$):

$$\frac{dK_1}{dl} = -\eta_n K_1(l) = -\left(\frac{2v_{\perp} - v_{\parallel}}{v_{\perp}}\right) K_1(l) \quad (10.43)$$

where $K_1(l)$ is the renormalized K_1 after rescaling the wavevectors by a e^l factor in the q_{\perp} direction and $e^{(v_{\parallel}/v_{\perp})l}$ in the q_z direction.

It is clear from (10.43) that there are only three possibilities for the fixed point K_1^* .

1. $K_1^* = 0$: for $2v_{\perp} > v_{\parallel}$, this is a stable fixed point. The problem reduces exactly to the superconductor–normal conductor transition [23]. This implies immediately $v_{\parallel} = v_{\perp}$. Note, however, that there is no stable fixed point in dimensions $d = (4 - \epsilon)$ in this last case for $n < 365.9$ [17] (remember for smectics $n = 2$) [8]. The $1/n$ expansion also gives an isotropic fixed point at $K_1^* = 0$ [23, 17], but it seems likely that it disappears at some critical value $n_c > 2$ [17].
2. $K_1^* = \infty$. It is stable if $v_{\parallel} > 2v_{\perp}$. There is no such fixed point for $n < 238.2$. For $n > 238.2$, one does find an anisotropic fixed point, but with $v_{\parallel} < 2v_{\perp}$: it is unstable. On the other hand, the $1/n$ expansion does find an anisotropic fixed point with $K_1^* = \infty$ [23]. Again, it seems hard to extrapolate down to $n = 2$.
3. K_1^* finite. This requires (in three dimensions) $v_{\parallel} = 2v_{\perp}$. This anisotropy is very large, and does not fit the experimental behaviour.

† The generalization of (10.43) is straightforward in d dimensions, $\eta_n = 5 - d - v_{\parallel}/v_{\perp}$.

Note that one does not find physically acceptable fixed points of that sort in a $(4 - \epsilon)$ expansion, although they exist for non-physical values of K_2^* and K_3^* .

What can we conclude from all these quite elaborate studies?

First, they have been taken as a sign of the first-order nature of the N-S_A transition. We illustrate in the next section the reason why. The strong experimental suggestion that the transition is continuous has prompted a new generation of theoretical approaches: the dislocation-mediated theory.

10.1.7 Nature of the N-S_A transition

For ‘type one’ smectics, one can neglect the ψ fluctuations (this approximation is correct for type one superconductors). In this limit, the $\delta\mathbf{n}_\perp$ fluctuations are Gaussian, and can be simply integrated out to define a simple Landau energy for ψ . Following Halperin, Lubensky, and Ma [17], we write

$$e^{-F(\psi)/k_B T} = \int D\{\delta\mathbf{n}_\perp\} e^{-F_{NA}(\psi, \delta\mathbf{n}_\perp)/k_B T}. \quad (10.44)$$

The functional integral is taken over all possible δn_\perp configurations and F_{NA} is given by (10.15) where ψ is considered constant.

Differentiating with respect to ψ , one gets

$$\frac{1}{V} \frac{dF(\psi)}{d\psi} = r\psi + u\psi^3 + C_\perp q_s^2 \psi \langle \delta\mathbf{n}_\perp^2 \rangle. \quad (10.45)$$

$\langle \delta\mathbf{n}_\perp^2 \rangle$ is simply calculated using the equipartition theorem,

$$\langle \delta\mathbf{n}_\perp^2 \rangle = \int \frac{k_B T}{C_\perp q_s^2 \psi^2 + Kq^2} \frac{d^3 q}{(2\pi)^3}. \quad (10.46)$$

(For the sake of simplicity, we have ignored the nematic anisotropy, but this does not change the nature of the discussion.) Close enough to T_{NA} , (10.46) can be expressed as

$$\langle \delta\mathbf{n}_\perp^2 \rangle = \frac{k_B T_{NA}}{K} \left(\frac{q_c}{2\pi^2} - \frac{C_\perp^{1/2} q_s |\psi|}{4\pi K^{1/2}} \right) \quad (10.47)$$

where q_c is the large wavevector cut-off (at which the elastic theory breaks down). Hence (10.45) corresponds to a Landau expansion

$$F(\psi) = \frac{\tilde{\Gamma}}{2} |\psi|^2 - \frac{w}{3} |\psi|^3 + \frac{u}{4} |\psi|^4, \quad (10.48)$$

where

$$\tilde{\Gamma} = r_0 + C_\perp q_s^2 k_B T_{NA} / 2\pi^2 K, \quad (10.49a)$$

$$w = C_\perp^{3/2} q_s^3 k_B T_{NA} / 4\pi K^{3/2}. \quad (10.49b)$$

Equation (10.49a) describes a decrease in the transition temperature which we can write as

$$\frac{T_0 - \tilde{T}_{\text{NA}}}{T_0} = \frac{\xi_0^2 q_s^2 q_c k_B T_{\text{NA}}}{2\pi^2 K}. \quad (10.50)$$

If one plugs smectic values into (10.50), one finds a sizeable depression of the transition temperature, which proves that the director fluctuations are somehow important. Equation (10.49b) is conceptually more original: the presence of a cubic term forces the transition to be first order. Note that the non-analyticity comes from long-wavelength fluctuations; a local Landau expansion could never contain a similar term.

A measure of the strength of the discontinuity is given by

$$\frac{T_{\text{NA}} - \tilde{T}_{\text{NA}}}{T_{\text{NA}}} = \frac{2w^2}{9\alpha u T_{\text{NA}}} \quad (10.51)$$

where $\alpha = \tilde{r}/(T - \tilde{T}_{\text{NA}})$. Plugging numbers into this expression is not really meaningful, since experiment shows clearly that ψ fluctuations are important in smectics.

In one instance the figures are much more favourable—in the vicinity of the tricritical point discussed in Section 10.1.1 [66, 52]. According to the Ginzburg criterion, the critical domain in which ψ fluctuations cannot be neglected vanishes like u^2 whereas the discontinuity predicted by (10.51) increases like u^{-1} : at some temperature there must be a cross-over, for which (10.51) will appear in the mean-field regime. Exactly at $u = 0$, (10.51) is replaced by

$$\frac{T_{\text{NA}} - \tilde{T}_{\text{NA}}}{T_{\text{NA}}} = \frac{w}{4\alpha k_B T_{\text{NA}}} \left(\frac{w}{2v}\right)^{1/3}. \quad (10.52)$$

In which $(v/6)$ is the coefficient of $|\psi|^6$ needed for stability in the free energy. If one assumes

$$\alpha \simeq k_B q_{||c} q_{\perp c}^2; \quad K \simeq C_{\perp} \simeq k_B T q_{\perp c}; \quad v \simeq k_B T q_{||c} q_{\perp c}^2$$

where $q_{||c}$, $q_{\perp c}$ are cut-off wavevectors corresponding to molecular dimensions, one finds

$$\frac{T_{\text{NA}} - \tilde{T}_{\text{NA}}}{T_{\text{NA}}} \simeq \frac{1}{2} \left(\frac{1}{4\pi}\right)^{4/3} \left(\frac{q_s}{q_{\perp c}}\right)^{2/3} \simeq 10^{-2}$$

where we have assumed that $q_{||c} \simeq q_s$. This is quite measurable, and observations of the corresponding discontinuities have been reported [66, 67]. In that picture, nothing particular occurs for $u = 0$; the sharp appearance of a second-order regime for u switching from $u < 0$ to $u > 0$ is replaced by a continuous cross-over from a mean-field first-order transition to a fluctuation-driven first-order transition.

There are two possibilities upon entering more deeply into the $u > 0$ region:

1. The transition is still first order but the discontinuities are too small to be detected. This would be in agreement with ϵ expansions [55].
2. At some original multicritical point the transition becomes truly second order.

The second scenario requires the existence of a fixed point in a renormalization group procedure. The absence of such fixed points in the ϵ expansion has prompted the description in terms of dislocation unbinding transitions which we discuss in the next section.

10.1.8 ‘Poor man’s’ dislocation unbinding transition

The usual approach of phase transitions consists in considering excitations from the high-symmetry ground state and finding that some of them are unstable at a given critical temperature (or other relevant external parameters). Nothing prevents us, however, from starting from the low-symmetry side. In smectics, the natural topological excitations are dislocations.

We have seen in Chapter 9 that dislocations are characterized by a line tension γ ,[†] and we calculated the part linked to long-range elastic distortion. The total line tension, which is a free energy (per unit length), must include the entropy contribution [58]

$$\gamma = \gamma_0 - k_B T x^{-1} \quad (10.53)$$

where γ_0 contains the elastic and core energies and $k_B T x^{-1}$ measures the entropic part (x has the dimensions of a length). Upon raising temperature γ_0 decreases, the entropic part increases, and, at some temperature, γ becomes negative: dislocations spontaneously nucleate and the nematic phase is reached.

The essence of the picture can be understood with formulae (9.61) and (9.63), assuming that all lengths close to the critical point scale like the correlation length ξ . (In the following we ignore the anisotropy; only a more elaborate approach could keep track of anisotropic scaling.)

For small wavevectors, q is bounded by ξ^{-1} , thus $qd \simeq 1$. Furthermore, (9.66) must be generalized to Burger’s vectors of order ξ . This yields

$$B^{\text{eff}} \simeq \frac{\gamma_\xi}{2\xi^2}. \quad (10.54)$$

If one takes

$$\gamma_\xi \simeq \xi \frac{k_B T}{a_0^2}. \quad (10.55)$$

[†] In this section, the line tension γ is not to be confused with the susceptibility critical exponent.

(This is compatible with formula (9.35) taken for a Burger's vector ξ and bare elastic constants.) Then one obtains, in agreement with (10.40c)

$$B^{\text{eff}} \simeq \frac{k_B T}{a_0^2 \xi}. \quad (10.56)$$

Similarly, (9.68) yields an expression compatible with (10.40a) (omitting factors of two),

$$K_3^{\text{eff}} \simeq \frac{\xi k_B T}{a_0^2}. \quad (10.57)$$

In this picture ξ is the average distance between dislocations, the average length, and the average Burger's vectors. Note that dislocations must be seen as composite objects made up of other dislocations. It is clear that, if any of these lengths were scaling differently from the others, anisotropic scaling would result. More elaborate techniques, which go beyond the scope of this book, are needed for a more careful description. Their most important merit is to show the existence of a fixed point and thus the possibility for the N-S_A transition to be continuous [60, 61]. Hence the inability of the ϵ expansion to find a fixed point does not necessarily imply the first-order character of the transition. This fixed point is isotropic and belongs to the superfluid helium universality class.

The other important result of the dislocation unbinding picture is the inversion of the high- and low-temperature sides: this seems natural since we discuss excitations in the low-symmetry phase which diverge in the high-symmetry one. (It also comes out of elaborate calculations [60, 61].) For instance, the specific heat is expected to diverge according to

$$\delta C_p = \text{const}^+ A^\pm t^{-\alpha}. \quad (10.58)$$

The universal ratio (A^+/A^-) should be just the inverse of that found in the superfluid helium case.

10.1.9 Twisted grain boundary phase

Question. What happens to the smectic A*-cholesteric transition in this picture? (Renn, S. R. and Lubensky, T. C. [68].)

From the analogy with superconductors we can expect the existence of a type two phase [8, 10], in which a periodic array of screw dislocation walls such as those described in Chapter 9 allow an overall twist of the structure (Fig. 10.4). In the following we give qualitative arguments suggesting under what conditions this phase is stable: we estimate the cost of a twist wall and compare it to the gain in twist energy.

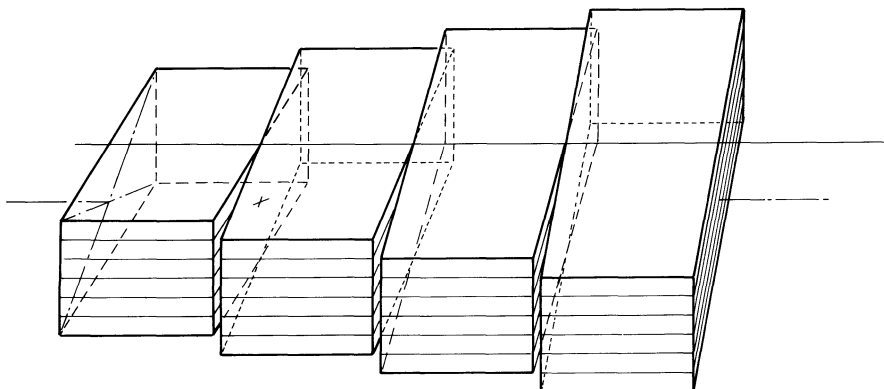


Fig. 10.4. Twist grain-boundary phase. Note the discontinuous rotations in opposition to the continuous twist of cholesterics.

In Chapter 9 we have shown that a screw dislocation involves only core energy (γ_s in the following). In the type two cases, we expect the twist elastic modulus K_2 to enter the expression of γ_s . Since it has the dimensions of a line energy, it must be multiplied by a dimensionless quantity. Since we further expect γ_s to depend on the square of the Burger's vector, we are naturally led to write

$$\gamma_s \simeq K_2 b^2 / \lambda^2 \quad (10.59)$$

in which λ is essentially λ_2 as defined in Section 10.1.2. Thus a wall made of parallel screw dislocations a distance d apart from each other spends an energy per unit surface

$$W = K_2 b^2 / \lambda^2 d. \quad (10.60)$$

The same wall gains a spontaneous twist energy

$$W' = k_2 \delta n_x$$

where $\delta n_x = b/d$ and $k_2 \simeq K_2/P_0$ (P_0 is the pitch in the cholesteric phase far from the C_h-S_A transition).

Thus these walls (and hence the twisted phase) will be stable if

$$\lambda > (P_0 b)^{1/2}. \quad (10.61)$$

Equation (10.61) shows the following.

- Deep in the S_A^* phase, $\lambda \simeq a_0$ and, since $b > a_0$ and $P_0 \gg a_0$, twist grain boundaries do not spontaneously nucleate.
- Close to the S_A^* -cholesteric transition when $\lambda \simeq (P_0 a_0)^{1/2}$ a twist grain boundary phase is more stable than both the S_A and the cholesteric phase (with $b = a_0$). Assuming a mean-field temperature dependence for λ and $a_0/P_0 \simeq 10^{-3}$, one can estimate a stability domain of a few tenths of

degrees for the twist grain boundary phase. If for particular reasons λ is large (this is, in particular, the case in the vicinity of the N-S_A-S_C point), the stability domain may be greatly enhanced [68].

This beautiful phase has been identified by a number of complementary techniques including optics and X-ray [69], independent of and simultaneous to the theoretic development.

10.1.10 Current situation

We have already pointed out that the latest experiments involving very large nematic domains provide results very close to the helium analogy [51, 52]. One could be tempted to conclude that all other results are perturbed by the ‘small’ range of the nematic phase. This is not very likely since most of the experiments are performed over a wide range of reduced temperature. Furthermore, pure XY behaviour is expected with inverted temperatures only, but experiment is consistent with non-inverted temperatures [54]. The gauge transformation would allow us to understand $v_{\parallel} \neq v_{\perp}$ as measured by X-ray but not as measured from critical behaviour of the elastic constants [65]; however, the correlation length critical exponents are found to be identical (within experimental accuracy) whether they are determined by X-ray or by the divergence of the elastic constants. It seems that we almost understand, but not quite.

10.2 SNECTIC A-SMECTIC C TRANSITION

10.2.1 Superfluid analogy

The early finding [70] that the A \rightleftharpoons C transition is continuous has been accurately confirmed by direct calorimetric measurements [71–74], by optical techniques [75–79] or X-ray scattering [81–83]. ESR [89], NMR [85], and neutrons [86] have also been used but they are less accurate.

For a given set of layers, to describe the ordered C state, one must specify the magnitude ω of the tilt angle, and also the azimuthal direction of tilt, specified by an angle ϕ (Fig. 10.5). Thus we can characterize the onset of order by two real parameters ω and ϕ or, equivalently, by the complex number (as in (10.10))

$$\psi = \omega e^{i\phi}. \quad (10.62)$$

This brings a remarkable analogy with superfluid helium, and the free energy is formally identical to (10.11) [87]. (Indeed, an overall change of the phase ϕ does not modify the free energy F .) This leads to the following expectations.

1. The transition C \rightleftharpoons A may be continuous. When it is, the specific heat

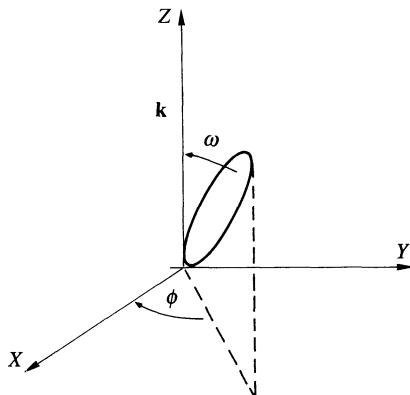


Fig. 10.5. Smectic C tilt angle: \mathbf{k} is the layer normal, ω the tilt amplitude, ϕ the azimuthal angle, relative to an arbitrary in-plane direction X .

should show a singularity

$$\delta C_p \simeq \text{const} + A^\pm |t|^{-\alpha} \quad (10.63)$$

where $\alpha \simeq -0.007$ and $t = (T - T_{CA})/T_{CA}$.

2. Below T_{CA} , the tilt angle should vary according to the law

$$\omega = \text{const} |t|^\beta \quad (10.64)$$

where $\beta \simeq 0.35$.

3. Above T_{CA} if we apply a magnetic field \mathbf{H} that is oblique with respect to the optical axis (O_z) of the smectic phase (e.g. in the x, z -plane), we induce a tilt angle

$$\omega = C \frac{\chi_a H_x H_z}{k_B T_{CA}} t^{-\gamma} \quad (10.65)$$

where C is a numerical constant of order unity, χ_a is the diamagnetic anisotropy per molecule, and $\gamma \simeq 1.33$ is the susceptibility critical exponent.

The tilt predicted by (10.65) is small (about 10^{-2} rad for $t \simeq 10^{-4}$ near room temperature) because the diamagnetic energy $\chi_a H^2$ is very weak when compared to $k_B T_{CA}$. However, optical experiments are sensitive enough to allow for reliable measurements [75, 77, 78].

Similar experiments can be conceived with electric fields \mathbf{E} . But, as explained in Chapter 2, the electric effects are usually much more complex than their magnetic counterparts.

4. Again starting from the smectic A phase and decreasing T toward T_{CA} , we expect to see the onset of a strong (depolarized) light scattering due

to fluctuations in the tilt angle. In the (usual) situation, where the wavelength of light is larger than the size ξ of the fluctuating domains, the scattered intensity I is of the form

$$I = I_0 + I_1 t^{-\gamma}. \quad (10.66)$$

I_0 , the normal scattering in the smectic A phase, is small (except for very special circumstances as explained in Chapter 7). Equation (10.66) has been used to measure γ [76]. In fact even ξ has been extracted from

$$(I(0) - I(q))/I(0) \simeq q^2 \xi^2. \quad (10.67)$$

Indeed for back scattering, $q \simeq 8\pi \cdot 10^4 \text{ cm}^{-1}$, and if relative intensity of a few per cent can be measured, correlation lengths as small as a hundred Å can be estimated [76]. ξ should vary according to

$$\xi_{\parallel} \simeq \xi_0 t^{-\nu} \quad \text{with } \nu \simeq 0.66. \quad (10.68)$$

The helium analogy is valid asymptotically close to the transition point. Whether the corresponding critical regime is attainable or not is discussed in the following section.

10.2.2 Ginzburg criterion

The superfluid analogy is expected to hold asymptotically close to the A \rightleftharpoons C transition, and the natural question is how close. The next question is what kind of mean field holds outside this regime? This leads us to distinguish three types of cross-over temperatures:

- temperatures such that the fluctuation contribution to a given property is comparable to the mean field discontinuities;
- temperature at which fluctuations become non-Gaussian† and helium-like behaviour starts to be observable;
- in the mean-field regime the temperature at which the influence of the sixth-order term shows up.

The first two sets of temperatures are often assumed to be equivalent. The original Ginzburg criterion was defined by comparing the mean-field specific heat discontinuity ΔC_p to its fluctuation-induced contribution δC_p estimated in a Gaussian approximation [88]. With

$$\Delta C_p = C_p(T_{\text{CA}}^-) - C_p(T_{\text{CA}}^+) = \frac{r'^2 T_c}{2U} \quad (10.69)$$

† Gaussian means that the quartic term u is neglected in the probability weight of the fluctuations and hence that the equipartition theorem is valid.

where $r \simeq r'(T - T_{\text{CA}})$ and

$$\delta C_p(T) \simeq -\frac{r'^2}{2} T \frac{\partial}{\partial r} \langle |\psi|^2 \rangle \quad (10.70)$$

in which only the leading term is kept, one gets from $\delta C_p(T_G) \simeq \Delta C_p$

$$T_G - T_{\text{CA}} \simeq r'^{-1} (k_B T u / 4\pi C_\perp C_{||}^{1/2})^2. \quad (10.71)$$

With the reasonable choices,

$$r' \simeq k_B q_{||C}, \quad C_{||} \simeq k_B T q_{||C}, \quad C_\perp = k_B T q_{\perp C}, \quad u = k_B T q_{||C} q_{\perp C}^2 \quad (10.72)$$

(as in Section 10.1.7, $q_{||C}$ and $q_{\perp C}$ are wavevectors of (inverse) molecular dimensions), we get

$$T_G - T_{\text{CA}} \simeq T_{\text{CA}} / 16\pi^2. \quad (10.73)$$

According to these figures the helium-like behaviour extends over a few degrees, but this range depends strongly on the chosen values. The sensitivity to the wavevector cut-offs is well known, and explains the mean-field behaviour of conventional superconductors [88]. An anomalously small u value has been invoked in the A \leftrightarrow C case [89]. Indeed, if our estimate is reasonable for u_0 taken at constant layer thickness, it is not correct for u which is defined at zero normal stress. Experiment suggests that

$$u \simeq u_0 / 10. \quad (10.74)$$

Indeed the coupling between tilt and layer thickness reads†

$$f_{\text{CA}} = \lambda \omega^2 \left(\frac{\delta a}{a_0} \right) \quad (10.75)$$

where $(\delta a/a_0)$ is the layer dilatation and λ a coupling constant. A simple minimization with respect to $(\delta a/a_0)$ leads to a result similar to (10.8)

$$u = u_0 - 2\lambda^2/B \quad (10.76)$$

where B is the compressional elastic modulus at constant pressure, u , u_0 , λ , and B can be measured by combined calorimetric and acoustic experiments, hence the estimate (10.74), and the reduction of the critical regime as compared to (10.73) by a factor of 100. This means that the A-C transition is naturally close to tricriticality, a remark which had been made independently from this argument [71]. Under such circumstances, a sixth-order term $(V/6)|\psi|^6$ has been added in the free energy to properly represent the experimental results [71, 90].

Had we been comparing the jump in the mean-field compressional elastic modulus ΔB , to its fluctuation-induced correction δB , the result would have been totally different [89].

† There are similar couplings with the mass density, which can also be measured experimentally [89] and also can decrease u .

In the smectic C phase (10.75) generates a bilinear coupling between the tilt fluctuations $\delta\omega$ and the dilatation of the layers

$$f_{CA}' = 2\lambda\omega_0 \delta\omega \left(\frac{\delta a}{a_0} \right) \quad (10.77)$$

where $\omega_0 = (-r/u)^{1/2}$. Minimization with respect to $\delta\omega$ yields for the elastic modulus in the C phase

$$B(T < T_{CA}) = B - \frac{2\lambda^2}{u_0} \quad (10.78)$$

or

$$\Delta B = -\frac{2\lambda^2}{u_0}. \quad (10.79)$$

δB may be written

$$\delta B(T) = \lambda \frac{\partial \langle |\psi^2| \rangle}{\partial \left(\frac{\delta a}{a_0} \right)} = 2\lambda^2 \frac{\partial}{\partial r} \langle |\psi^2| \rangle. \quad (10.80)$$

Comparison of (10.79) and (10.80) leads to the same criterion as (10.71) provided u is replaced by u_0 ! Whether or not fluctuations can be seen, depends on the accuracy of the considered experiment. Typically, experiments are designed in such a way that a few per cent of the mean-field discontinuities can be detected. Under such circumstances, elastic modulus measurements can be 100 times more sensitive to fluctuations than specific heat ones.

This does not tell us whether fluctuations are Gaussian or helium-like. One possible measure of the cross-over location may be obtained by equating the bare inverse susceptibility r to its fluctuation-induced correction. Again one finds an expression similar to (10.71), but with the replacement of $u/4$ by u . This corresponds to a 16-fold increase in the helium-like domain compared with (10.71) and leaves the possibility for observation of helium-like behaviour fairly open.

Remark one In the presence of an applied σ_{zz} stress, (10.77) may be written

$$f_{CA} = \frac{1}{2}(r + \sigma_{zz})\omega^2 + \frac{u}{4}\omega^4 + \frac{v}{6}\omega^6.$$

Close enough to the transition, a uniaxial compressive stress can induce the A-C transition. This stress-induced transition has been experimentally observed [92].

Remark two When the sixth-order term is included, there is another important temperature

$$t_0 = 3u^2/4r'v. \quad (10.81)$$

The mean-field low-temperature tilt and specific heat read

$$\left. \begin{aligned} \omega &= \left(\frac{u}{2v} \right)^{1/2} \left[1 - 3 \left(\frac{T_{\text{CA}} - T}{t_0} \right)^{1/2} - 1 \right]^{1/2}, \\ C_p(T < T_{\text{CA}}) - C_p(T = T_{\text{CA}}) &= \frac{r'^2}{2uT_{\text{CA}}} \left(1 - \frac{3(T_{\text{CA}} - T)}{t_0} \right)^{-1/2}. \end{aligned} \right\} \quad (10.82)$$

For $|T_{\text{CA}} - T| > t_0$, (10.82) corresponds to dependences that one expects at a tricritical point.

10.2.3 Experimental findings

The basic picture sketched in the last two sections is fairly well borne out by experiment.

Specific heat measurements show an essentially mean-field behaviour with a sizeable sixth-order term $t_0 \sim 1 \text{ K}$ [71–74, 90]. The strength of u is found to depend on the proximity of the N–S_A transition [90]. In some instances [91], the fluctuation corrections to C_p can be measured, but the range of observation is too small to allow for an estimate of the specific heat exponent α [74].

The ω temperature dependence is consistent with both (10.64) and (10.82) [81, 83, 93]. The asymptotic behaviour very close to T_{CA} ($T_{\text{CA}} - T < 10 \text{ mK}$) seems to favour (10.64) in one compound [93]. Consistency with specific heat measurements require a helium–mean-field cross-over in the 10–100 mK range which seems reasonable, according to (10.64), with the correct u . (Note that the cross-over is probably from the full expression (10.81) directly to (10.64), without sensitivity to a simple $(T_{\text{CA}} - T)^{-1/2}$ law, and is thus hard to spot directly.)

Susceptibility measurements are consistent with the above figures: values close to one may be found [75, 83] but a critical behaviour with $\gamma = 1.33$ is also possible with some systems if data outside the 0.1 K range are excluded [93].

Eventually, elastic constant measurements and sound attenuation show undoubtedly [94] (although not always [95]) the existence of helium-like fluctuations.

10.2.4 First-order S_A ⇄ S_C

Other couplings have a structure similar to (10.75). The most natural candidate is biaxiality: a tilt always induces a biaxiality (i.e. a difference

$\epsilon_{xx} - \epsilon_{yy} = \eta$, the tilt direction being, for instance, \hat{y}), but the reverse is not true (remember the possibility of a smectic with D_{2h} point group symmetry, mentioned in Chapter 1).

Thus the energy increment reads

$$f_\eta = \lambda\omega^2\eta + \frac{1}{2\chi}\eta^2 \quad (10.83)$$

where λ describes the coupling between tilt and biaxiality and χ is a response function quite similar to the one introduced in (10.5). If the system is close enough to an isotropic phase, χ is large. The equivalent of (10.8) reads

$$u^{\text{eff}} = u - 2\lambda^2\chi. \quad (10.84)$$

One can again have a first-order transition if u^{eff} is negative. Equation (10.76) could also lead, in principle, to a negative u , but it seems more likely that the known cases of $S_A \rightleftharpoons S_C$ first-order transition result from the coupling with biaxiality [96, 97].

This first-order transition leads to the existence of an interesting new critical point, in the case of chiral S_C^* [98, 99]. We have seen in Chapter 7 that, if a field E_x is applied on a chiral S_A^* , a tilt ω results in the y direction [75]. Thus E_x is the field conjugate to the order parameter. The total free energy now reads

$$f_{C^*A^*} = -h\omega + \frac{\Gamma}{2}\omega^2 + \frac{w}{3}\omega^3 + \frac{u}{4}\omega^4 + \frac{w'}{5}\omega^5 + \frac{v}{6}\omega^6 + \dots \quad (10.85)$$

Symmetry requires (at the lowest order)

$$h \sim w \sim w' \sim E_x.$$

The $\omega(T)$ curves at constant E_x show a discontinuity in ω , which decreases with increasing E_x (Fig. 10.6) [98]. The set of curves is very similar to the isobars $v(P)$ near a conventional liquid-vapour critical point. The location of the critical point, in the T, E_y -plane and the critical tilt are defined by the conditions

$$\frac{\partial f}{\partial \omega}(\omega_c, T_c, E_{yc}) = \frac{\partial^2 f}{\partial \omega^2}(\omega_c, T_c, E_{yc}) = \frac{\partial^3 f}{\partial \omega^3}(\omega_c, T_c, E_y) = 0.$$

Can the universality class be the same as that of the liquid-vapour case (i.e. Ising)?

At first, one might be tempted by a positive answer since (10.95) is exactly isomorphous to the free energy used in the liquid-vapour transition. The following argument shows that the problem is more complicated.

- Close to the critical point the variations of tilt angle and layer thickness, and polarization are proportional $P - P_c \propto \omega - \omega_c \propto (\nabla_z u)$ (if the reference layer thickness is taken at the critical point).

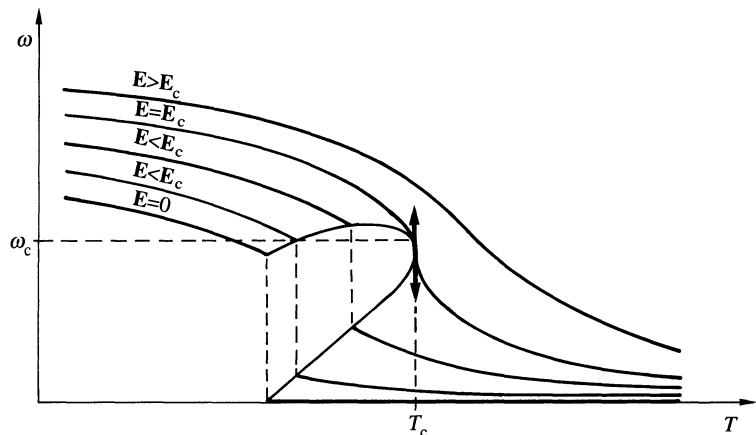


Fig. 10.6. Plot of the tilt angle versus temperature for different applied fields in the case of a first-order $S_A^*-S_C^*$ transition (after reference 98). Note the decrease of the ω discontinuity upon the field increasing and its disappearance at the critical field E_c . Note the similarity with the $V(T)$ isobars in the liquid-vapour case.

A proper energy must contain all terms allowed by symmetry, but since the three above-mentioned variables are linearly coupled, one can choose any of them as the basic order parameter of the transition. The layer displacement allows one to express more easily rotational invariance around the y direction. With this choice of order parameter, there are three non-equivalent cubic terms in the free energy (not just one as suggested by the mean-field expression (10.85)): $(\nabla_z u)^3$, $\nabla_z u(\nabla_z u)^2$, $\nabla_z u(\nabla_y u)^2$. Two of them are relevant in the renormalization group sense [101], which shows that the transition cannot just be Ising-like. Not only can liquid crystals provide useful analogies, but they can give rise to original problems that have the potential for defining new universality classes.

10.2.5 N-A-C point

The existence of an N-A-C multicritical point was shown by the Bordeaux and the Kent groups independently [101, 102]. It represents the intersection of the N- S_A , S_A-S_C , and N- S_C phase boundaries. We have already discussed the first two. The originality of the third one was recognized early on [103]: whereas at the N- S_A transition, only two components of the mass density wave show large fluctuations near T_C , in the N- S_C case ‘skewed’ cybotactic groups (i.e. S_C -type fluctuations) are concentrated on two rings in reciprocal space (Fig. 10.7), such that

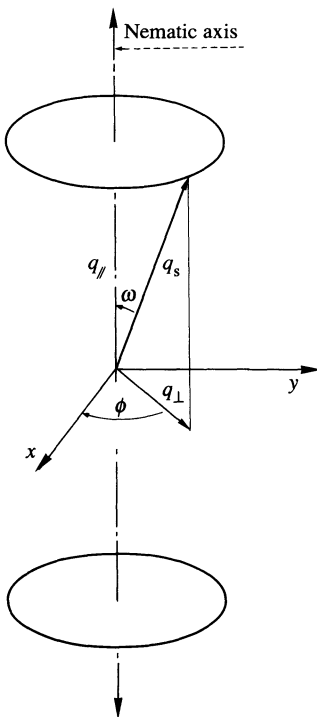


Fig. 10.7. Scattering ring in a nematic close to a transition in a smectic C.

$N-S_A \Leftrightarrow \rho(q_s)$ and $\rho(-q_s)$ exhibit critical fluctuations;

$N-S_C \Leftrightarrow$ all Fourier components $\rho(q)$ satisfying

$$\left. \begin{aligned} q_{\parallel} &= q_s \cos \omega \\ q_p &= q_s \sin \omega \end{aligned} \right\} \text{ are simultaneously critical.} \quad (10.86)$$

Thus the natural order parameter has an infinite number of components. A description of the N-A-C point must allow one to go from one type of fluctuations to the other. This is most naturally done in the Chen-Lubensky model [104].

- Consider as previously fluctuations of the mass density

$$\tilde{\rho}(\mathbf{r}) = \rho(\mathbf{r}) - \bar{\rho}$$

where $\bar{\rho}$ is the average density.

- Fix the nematic director on the z axis. The tendency for building up a mass density wave at a wavevector q_{\parallel}, q_{\perp} is simply expressed by a free

energy density, directly written in Fourier space as

$$\int F d^3r = \sum_q \frac{1}{2}(r + D_{||}(q_z^2 - q_{||}^2)^2 + C_{\perp}q_{\perp}^2 + D_{\perp}q_{\perp}^4)\tilde{\rho}(q)\tilde{\rho}(-q) \\ + \sum_{q,q',q''} \frac{u}{4}\tilde{\rho}(q)\tilde{\rho}(q')\tilde{\rho}(q'')\tilde{\rho}(-q-q'-q''). \quad (10.87)$$

The sign change of r favours the appearance of a non-zero $\tilde{\rho}$ and ($u > 0$) provides stability to the model; the second term favours condensation of the mass density wave $q_z = \pm q_{||}$. The second and third terms allow one to describe the change from smectic A to smectic C character.

1. For $C_{\perp} > 0$, the fluctuations are clearly S_A-like, i.e. centred around $q_{\perp} = (q_x^2 + q_y^2)^{1/2} = 0$, $q_z = \pm q_{||}$.
2. For $C_{\perp} < 0$, they are centred on two rings $q_p = (-C_{\perp}/2D_{\perp})^{1/2}$, $q_z = \pm q_{||}$. The ‘crystallographic’ tilt ω is defined by: $\tan \omega = q_{||}^{-1}(-C_{\perp}/2D_{\perp})^{1/2}$.

Thus, the nature of the condensed phase is controlled by the variation of C_{\perp} . In a one-component system the C_{\perp} sign change occurs in general at lower temperature than r and one observes the phase sequence with decreasing temperature: N–A–C. In less frequent cases, C_{\perp} changes sign at temperatures higher than r : they yield a direct N–S_C transition. In order to obtain the N–S_A–S_C point, one needs to control two external parameters such as temperature (T) and pressure (P), or temperature and concentration, in a binary mixture (note that chemical potential would be more appropriate). Thus the usual Landau hypothesis now reads

$$\left. \begin{aligned} r &= r_1(T - T_0) + r_2(P - P_0) \\ C_{\perp} &= C_1(T - T_0) + C_2(P - P_0) \end{aligned} \right\} \quad (10.88)$$

where T_0 , P_0 define the location of the N–A–C point in the mean-field approximation. The phase diagram is displayed in Fig. 10.8

$$\left. \begin{aligned} \text{N–S}_A \text{ line: } & r = 0, \\ \text{N–S}_C \text{ line: } & r = \frac{C_{\perp}^2}{2D_{||}}, \\ \text{S}_A\text{–S}_C \text{ line: } & C_{\perp} = 0. \end{aligned} \right\} \quad (10.89)$$

The simultaneous vanishing of C_{\perp} and r defines the N–A–C point as a Lifshitz point. General renormalization group studies of similar cases can be found in references 105 and 106, but the rotational invariance in smectics and the lack of long-range order render the problem very difficult. We have seen in the previous sections the difficulties connected with the N–S_A and S_A–S_C transitions. One has to add those of the N–S_C transition. Perturbation

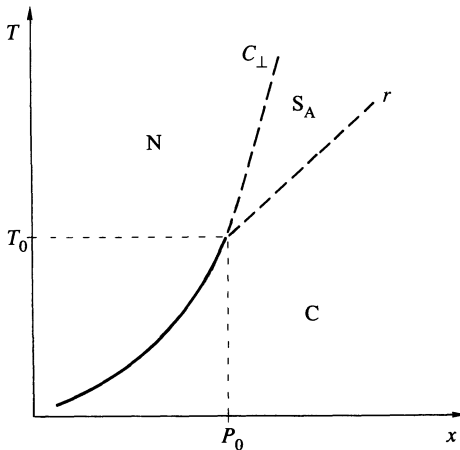


Fig. 10.8. Typical mean-field N-S_A-S_C diagram as predicted by the Chen-Lubensky model. The r and C_{\perp} axes have been chosen arbitrarily in order to reproduce the gross features of the experimental diagram of Fig. 10.10. Dotted lines represent second-order transitions.

expansions [107, 108] reveal some of the peculiarities of the problem. To illustrate the role of fluctuations, let us write ($\tilde{r} = r - C_{\perp}^2/2D_{\parallel}$)

$$r^{\text{eff}} = \tilde{r} + u\langle\tilde{\rho}^2\rangle. \quad (10.90)$$

With

$$\langle\tilde{\rho}^2\rangle = \int d^3q \langle\rho(q)\rho(-q)\rangle \quad (10.91)$$

and

$$\langle\rho(q)\rho(-q)\rangle = \frac{k_B T}{\tilde{r} + D_{\parallel}(q_z^2 - q_{\parallel}^2)^2 + D_{\perp}(q_{\perp}^2 - q_p^2)^2}, \quad (10.92)$$

one obtains for the leading terms

$$r^{\text{eff}} = \tilde{r} + uq_p a \ln\left(\frac{b}{r^{\text{eff}}}\right) \quad (10.93)$$

where a, b are unimportant constants. The logarithm comes from the integration in the vicinity of the two rings defined by (10.86).

Equation (10.93) always has a positive solution of r^{eff} as a function of \tilde{r} no matter how large and negative \tilde{r} can be. This means that, if there is any N-S_C transition at all, it must be of first order [107, 108]. One also sees that the strength of this effect is proportional to q_p ; the discontinuity must vanish with q_p .

The vanishing of the N-S_C latent heat along the N-S_C line upon approaching the N-A-C point was first seen with conventional techniques

[101, 102], high-resolution a.c. calorimetry [109, 110], and, more recently, with high-resolution adiabatic calorimetry [74, 111]. Although it seems very likely that the vanishing occurs right at the N–A–C point, it is not possible to assess this fact experimentally with total confidence. At last, the A–C transition goes to a Landau tricritical point at, or very near the N–A–C point.

Arguments similar to those we developed in Section 10.1.3 can be used to predict the behaviour of the Frank–Oseen elastic constants. The toroidal shape of the integration volume yields a ξ^2 divergence rather than ξ in the N–S_A problem [104]. Note that, in contrast to the N–S_A case, all three elastic moduli K_1 , K_2 , K_3 diverge [103]. Light scattering experiments far from the multicritical point agree with this ξ^2 divergence, but show the importance of both tilt and layer fluctuations close to it [112].

Note. In order to calculate the K_1 renormalization, one needs a covariant expression of (10.87). This is done naturally in real space by replacing ∇_z by $(\mathbf{n} \cdot \nabla)$ and ∇_{\perp} by $[\nabla - \mathbf{n}(\mathbf{n} \cdot \nabla)]$. The same expression holds for $C_{\perp} > 0$, and one can check that it reduces to (10.15) when the proper limits are taken and the bare Frank–Oseen energy included.

The X-ray diffuse scattering cross-section in the nematic phase, is obtained from (10.87) as

$$\sigma(q) \propto \langle \rho(-q) \rho(-q) \rangle = \frac{k_B T}{r + D_{\parallel}(q_z^2 - q_{\parallel}^2)^2 + C_{\perp} q_{\perp}^2 + D_{\perp} q_{\perp}^4}. \quad (10.94)$$

- If $C_{\perp} > 0$, it is S_A-like.
- If $C_{\perp} < 0$, it is maximum on the two rings defined by (10.85).

These predictions are reasonably well borne out by experiment [113] except in the immediate vicinity of the N–A–C point. In particular, the existence of a line $C_{\perp} = 0$ is well established in the nematic phase, and is found essentially parallel to the N–I line in the 8S5.7S5 mixture (octyl and heptyl oxy-p'-pentylphenylthiolbenzoate), but not in the 7S5 + 80CB (80CB = octyl oxycyanobiphenyl).

Other theoretical approaches, in which the mass density wave and tilt are considered as independent coupled variables, can be found [114–117]. The differences with the Chen–Lubensky model come from a specific physical assumption: if all couplings allowed by symmetry were included, they should be identical to (10.87) at the same level of expansion. In reference 116 sixth-order terms are included since we know that they are important close to the S_A–S_C line. Reference 117 includes the description of the isotropic phase and predicts that the $C_{\perp} = 0$ line should be parallel to the N–I boundary.

In all these theoretical approaches, the role of fluctuations in the immediate vicinity of the N–A–C point has not been assessed. A dislocation

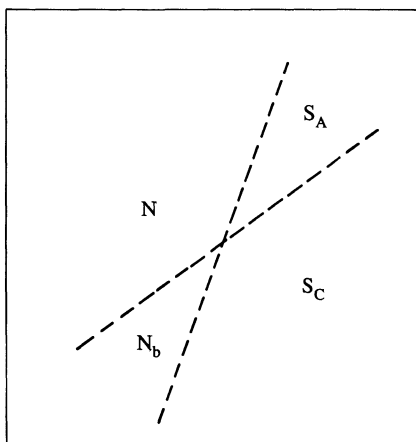


Fig. 10.9. $N-N_b-S_A-S_C$ multicritical point according to the dislocation disclination melting model [118]. In the N_b phase, the fluctuations depicted in Fig. 10.1(b) do not possess azimuthal degeneracy.

and disclination unbinding picture of the type described in Section 10.1.8, predicts an interesting behaviour [118, 119].

S_A-N and S_C-S_A meltings should be (inverted) helium-like second-order transitions. This implies that, whenever the $N-S_A$ and S_A-S_C second-order lines meet, they define a tetracritical point (if all lines are second order) (Fig. 10.9). The most important consequence is the existence of a new biaxial nematic phase, in which the azimuthal degeneracy of the layers normal fluctuations is broken (Fig. 10.9).

High-resolution phase diagrams both in the temperature-concentration [120, 113] and temperature-pressure planes [121] reveal a remarkable universality (Fig. 10.10). The phase boundaries obey simple power laws

$$\left. \begin{aligned} T_{NA} - T_{NAC} &= A_{NA}|X - X_{NAC}|^{\phi_1} + B(X - X_{NAC}), \\ T_{NC} - T_{NAC} &= A_{NC}|X - X_{NAC}|^{\phi_2} + B(X - X_{NAC}), \\ T_{AC} - T_{NAC} &= A_{NC}|X - X_{NAC}|^{\phi_3} + B(X - X_{NAC}), \end{aligned} \right\} \quad (10.95)$$

Note that T_{NAC} is certainly different from T_0 because of fluctuations, and X is either the pressure or the concentration.

All experiments are consistent with $\phi_1 = \phi_2 \simeq 0.57 \pm 0.03$ and $\phi_3 \simeq 1.4-1.7$. According to (10.95) the $N-A$ and $N-C$ lines have the same slope parallel to the temperature axis at the $N-A-C$ point, whereas that of the $A-C$ line is orthogonal. An alternative fit has been proposed in which $\phi_1 = \phi_3 \simeq 0.67 \pm 0.03$ and $\phi_2 \simeq 0.87 \pm 0.04$. With this fit, all phase boundaries are tangent and parallel to the temperature axis at the $N-A-C$ point [122]. This can only be fortuitous and approximate. Indeed, what the

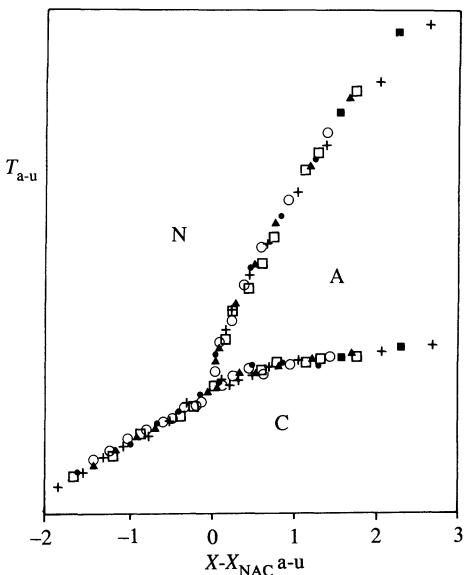


Fig. 10.10. Universality topology of the $N-S_A-S_C$ phase diagram. Coordinates have been rescaled and translated in order to obtain the superposition [120–22].

data suggest is that there are scaling fields that follow power laws at the phase boundaries but, as is clear from (10.88), these scaling fields have no reason (in particular no symmetry reason) to be just $(T - T_{NAC})$ and $(X - X_{NAC})$. A more appropriate form would be

$$t = p^\phi \quad \text{with both } t \text{ and } p \text{ linearly related to } T - T_{NA}, X - X_{NA}.$$

The main message is:

- the absence of the biaxial nematic phase;
- the experimental universality of the diagram;
- the framework of the Chen–Lubensky model seems to be valid, but there is a clear need for a comprehensive analysis of fluctuations at the $N-S_A-C$ point. Hartree corrections go in the right direction [123].

Remark. The absence of the biaxial nematic phase does not necessarily invalidate the dislocation–disclination unbinding model. Whenever first-order lines show up, the biaxial phase may be squeezed out; even if taken separately the $N-S_A$ and S_A-S_C were to be continuous [124].

10.2.6 The S_A-S_C transition in two dimensions

As we have seen, the S_A-S_C transition belongs to the helium universality class; since the normal–superfluid helium transition is expected to have very

special features in two dimensions, it is of interest to investigate the characteristics of the S_A-S_C transition in thin films. This has been done by the Harvard group in a beautiful series of experiments [125–127]. The S_C thin film behaviour bears some resemblance to two-dimensional nematics first discussed in reference 128. We have already described the long-wavelength fluctuations of the smectic c director in Chapter 7. We concentrate here on topological excitations (disclinations), which may drive the transition according to the Kosterlitz-Thouless mechanism [129–131; see also 128]. As usual we stick to the simplest possible description.[†]

First, in the one-constant approximation, the Frank-Oseen elastic free energy reads (Fig. 10.5; ϕ is the angle between the tilt director and an arbitrary axis)

$$F = \frac{1}{2}K \int (\nabla\phi)^2 d^2r. \quad (10.96)$$

Disclinations can be discussed in exactly the same way as in Chapter 5. In particular, the energy of an isolated disclination reads

$$E_0 = \pi Km^2 \ln\left(\frac{R}{a_0}\right) + E_C \quad (10.97)$$

where m is the strength of the disclination, a_0 is a molecular cut-off as already discussed, and R the overall size of the film. In an infinite sample, E_0 is infinite. The leading part of the free energy of a system with one free disclination reads (ignoring all interactions with existing pairs of $\pm m$ disclinations)

$$F = E_0 - k_B T \ln\left(\frac{R}{a_0}\right)^2 = (\pi m^2 K - 2k_B T) \ln\left(\frac{R}{a_0}\right), \quad (10.98)$$

in which the second term originates from translational entropy.

For T large enough the free energy is negative: the system spontaneously nucleates disclinations. This occurs first for

$$m = \pm 1; \quad k_B T_C = \frac{\pi}{2} K_C. \quad (10.99)$$

Equation (10.99) implies that, if this mechanism works, the ratio K_C/T_C should be universal, independent of the system under consideration. In the following we consider $m = \pm 1$ only.

Two questions:

1. Is this state with free disclinations really a S_A?
2. What is the role of disclination pairs in the process?

[†] When long-wavelength fluctuations are also included, one can still derive a condition such as (10.107), but one has to be more careful (see reference 132, for example).

They can be answered by the use of an electric analogy, similar in spirit to the magnetic one we used in Section 10.1.8. The existence of a disclination at the origin requires that, on any contour encircling it,

$$\oint \mathbf{m} \cdot d\mathbf{l} = \pm 2\pi \quad (10.100)$$

in which \mathbf{m} is identical to $\nabla\phi$ away from the disclination core.

Equation (10.100) becomes, with the introduction of the field \mathbf{E} perpendicular to \mathbf{m} in each point,

$$\mathbf{E} = (\hat{\mathbf{z}} \times \mathbf{m})(-2\pi K) \quad (\hat{\mathbf{z}} \text{ normal to the film}), \quad (10.101)$$

$$\int_{\Gamma} \mathbf{E} \cdot d\mathbf{s} = \pm 4\pi^2 K \quad (10.102)$$

where now $d\mathbf{s}$ is the normal to the curve Γ . This shows that \mathbf{E} obeys a Gauss theorem

$$\operatorname{div} \mathbf{E} = \pm \frac{4\pi}{\epsilon} \delta \quad (10.103)$$

$$\epsilon = 1/\pi K \quad (10.104)$$

and δ is the two-dimensional Dirac distribution. If one now has a local density of disclinations,

$$\operatorname{div} \mathbf{E} = \frac{4\pi}{\epsilon} \rho(r) \quad (10.105)$$

in which $\rho(r) = n_+ - n_-$ is the difference between the number of positive and negative disclinations per unit area. Since disclinations obey conservation rules, in the absence of externality imposed deformations, there is the same number of positive and negative disclinations

$$\int \rho(r) d^2r = 0 \quad (10.106)$$

The minimization of (10.96) requires that

$$\operatorname{div} \mathbf{m} = 0$$

i.e.

$$\operatorname{curl} \mathbf{E} = 0, \quad (10.107)$$

which completes the electrostatic analogy.

In the S_C phase, free disclinations cannot exist but pairs of opposite signs have a finite energy, namely (remember the problem in Section 4.2.2.1),

$$F_i = 2\pi K \ln\left(\frac{|r - r'|}{a_0}\right) + \text{const.} \quad (10.108)$$

This means that, at any temperature different from zero, there is a finite number of such pairs, which act like dipole densities in dielectrics.

One expects thus that, at large scales, macroscopic equations such as (10.97), (10.103), and (10.104) are still valid, but with constants that are renormalized by the screening of the field by the disclination pairs. More precisely

$$\epsilon_R = \epsilon + 4\pi\chi \quad (10.109)$$

where χ is the macroscopic polarizability of the system. In terms of the Frank modulus, (10.109) reads

$$K_R = \frac{K}{1 + 4\pi^2\chi K} \quad (10.110)$$

which is exactly similar to (9.60).

The nice feature of this two-dimensional problem is that it allows a calculation of ϵ_R by an iteration procedure. The surprise is that the transition is obtained not for infinite χ (i.e. zero K_R as at the N-S_A transition) but for finite χ in agreement with (10.99).

The argument goes as follows. First, we pair up all the disclinations (which is possible since $\int \rho(r) d^2r = 0$), starting from short length scales. This allows us to define the number of pairs with separation $|r - r'|$ as $P(|r - r'|) d^2r d^2r'$. Since we are dealing with thermal equilibrium, we should have

$$P(|r - r'|) \propto \exp(-E_i/k_B T). \quad (10.111)$$

Equation (10.111) neglects interaction between pairs, and is only valid for a 'dilute gas' of pairs.

We accept now the idea that one can define a dielectric permittivity $\epsilon(|r - r'|)$ for which the screening by pairs separated by distances smaller than $|r - r'|$ have already been taken into account. In particular, E_i is given by (10.108) with the replacement of K (or ϵ) by $K(|r - r'|)$ (respectively $\epsilon(|r - r'|)$).

Equation (10.109) tells us now that

$$\epsilon(r + dr) = \epsilon(r) + 4\pi d(\chi) \quad (10.112)$$

where $d(\chi)$ corresponds to the susceptibility of all the pairs separated by a distance r . This is simply the polarizability of one pair $|r - r'|^2/k_B T$ times the number of pairs per unit area

$$d\chi = \frac{|r - r'|^2}{2k_B T} \cdot 2\pi|r - r'| P(|r - r'|) dr'. \quad (10.113)$$

Or, setting r at the origin,

$$\frac{d\epsilon(r')}{dr'} = \frac{4\pi^2 r'^3}{k_B T} P(r'). \quad (10.114)$$

We still need an equation for $P(r')$. According to (10.111) and (10.108), it simply reads

$$P(r' + dr') = P(r') \exp(-2 dr'/r' k_B T \epsilon(r')), \quad (10.115)$$

i.e.

$$\frac{dP(r')}{dr'} = \frac{2P(r')}{r' \epsilon(r') k_B T}. \quad (10.116)$$

We are interested in the macroscopic behaviour, i.e. $r \rightarrow \infty$; we thus have to integrate equations (10.114) and (10.116) with the short-length scale condition

$$P(r \simeq a_0) \simeq a_0^{-4} e^{-(E_c/k_B T)}. \quad (10.117)$$

The prefactor corresponds to the availability of sites, and the Boltzmann factor to the core energy

$$\epsilon(r \simeq a_0) = 1/\pi K = \epsilon_0. \quad (10.118)$$

Equation (10.118) is identical to (10.104) since, at these short-length scales, one does not expect screening to occur.

The solution of (10.114) and (10.116) does not involve any major difficulty. Setting $r' = a_0 e^l$, $\tilde{\epsilon} = k_B T \epsilon$, $y^2 = r'^4 P(r')$, leads to

$$\frac{d\tilde{\epsilon}}{dl} = 4\pi^2 y^2, \quad (10.119a)$$

$$\frac{dy}{dl} = (2 - \tilde{\epsilon}^{-1}) y, \quad (10.119b)$$

or, taking the derivative of (10.119a) and using (10.119b),

$$\frac{d^2\tilde{\epsilon}}{dl^2} = 2(2 - \tilde{\epsilon}^{-1}) \frac{d\tilde{\epsilon}}{dl}$$

and, after integration

$$\frac{d\tilde{\epsilon}}{dl} = 4(\tilde{\epsilon} - \tilde{\epsilon}_0) - 2 \ln\left(\frac{\tilde{\epsilon}}{\tilde{\epsilon}_0}\right) + 4\pi^2 e^{-(E_c/k_B T)} \quad (10.120)$$

in which (10.117) and (10.118) are satisfied.

The phase behaves like a smectic C, if at large r (large l equivalently), $\tilde{\epsilon}$ (resp. $K(r)$) reaches a well defined limit. This requires the existence of $\tilde{\epsilon}$ values such that $d\tilde{\epsilon}/dl$ vanishes. A graphic solution of the equation,

$$\tilde{\epsilon} - \tilde{\epsilon}_0 + \pi^2 e^{-(E_c/k_B T)} = \frac{1}{2} \ln \frac{\tilde{\epsilon}}{\tilde{\epsilon}_0}, \quad (10.121)$$

is sketched in Fig. 10.11. For ϵ_0 small enough, there are two solutions to eqn (10.121), but, since recursion relations start from ϵ_0 and ϵ increases

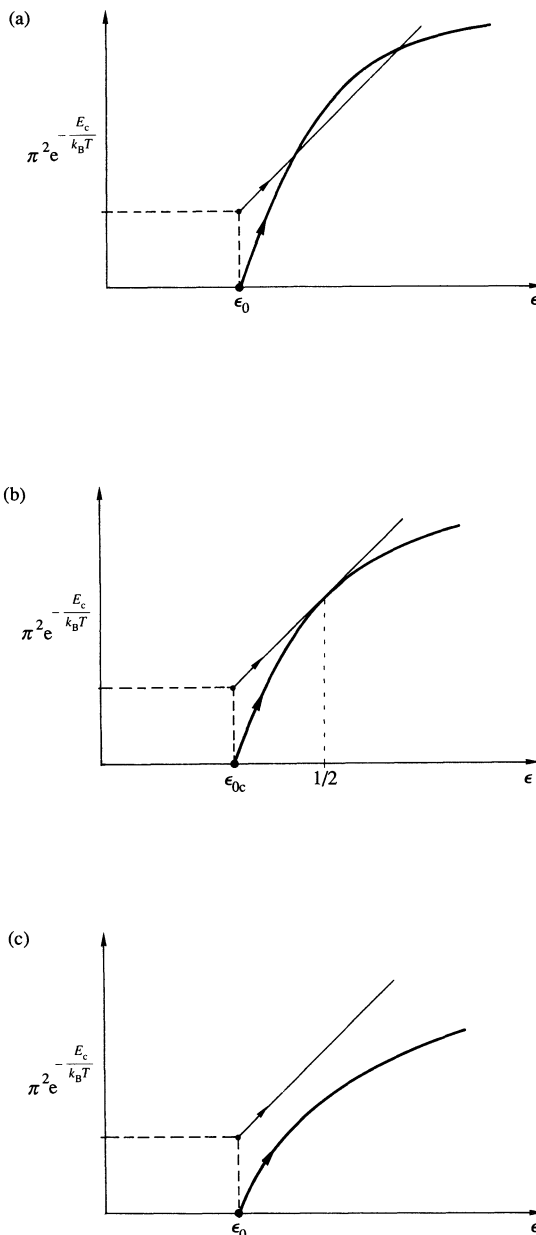


Fig. 10.11. Graphic solution of eqn (10.121): the straight line represents the left-hand side of (10.121), and the curved one the right-hand side. (a) $\epsilon_0 < \epsilon_c$: the two curves intersect; since $\epsilon(l)$ increases starting from ϵ_0 , the first intersection is the physically relevant one. (b) $\epsilon_0 = \epsilon_{0c}$: the dielectric permittivity is driven toward 1/2 at large scales. (c) $\epsilon_0 > \epsilon_c$: there is no intersection; the dielectric permittivity goes to infinity.

monotonically, the smallest solution corresponds to the experimental ϵ at large distances. Upon increasing ϵ_0 , the logarithmic contribution decreases: for $\epsilon = \epsilon_c$ the two solutions coincide. This is obtained when (10.121) and its derivative hold, which implies that

$$\tilde{\epsilon}_c = 1/2. \quad (10.122)$$

This condition is identical to (10.99), in which ϵ and K are taken at the large r or macroscopic limit. On the other hand, (10.121) relates the transition temperature to the local values of K and the core energy E_c . If one increases ϵ_0 further, there is no longer any solution for (10.121) and ϵ goes to infinity with r .

One can now answer the two questions.

1. For $\epsilon_0 < \epsilon_{oc}$ or $T < T_c$, ϵ goes to a well defined value at large scale. The system is in its smectic C phase since a Frank modulus $K = 1/\pi\epsilon$ can be defined.
2. For $\epsilon_0 > \epsilon_{oc}$ or $T > T_c$, ϵ goes to infinity as larger and larger scales are investigated. The corresponding Frank modulus goes to zero, which is characteristic of the smectic A phase.

For $T < T_c$, at large scale, $r^4P(r)$ vanishes: disclinations play a role, at short scale only.

For $T > T_c$, at large scale, $r^4P(r)$ diverges, which simply means that disclinations play a crucial role in the vanishing of K .

$T > T_c$ one can define a correlation length beyond which C types of fluctuations are no longer correlated (typically, that length for which $r^4P(r) \simeq 1$)

$$\xi \simeq a_0 \exp\left(\frac{\text{const}}{\sqrt{T - T_c}}\right). \quad (10.123)$$

If the critical part of the free energy is given by scaling,

$$F_s \propto k_B T / \xi^2. \quad (10.124)$$

This implies that there is no thermodynamic singularity at the transition, even in the specific heat.

Relaxing the one-constant approximation does not change the picture [133, 134]; one mainly has to set

$$K = \frac{1}{2}(K_s + K_b) \quad (10.125)$$

where K_s and K_b are the splay and bent moduli. Electric interactions in the case of ferroelectric S_C^* have also been shown to be negligible [134].

The merit of the Kosterlitz–Thouless picture is to show the possibility of a continuous transition with no thermodynamical singularities and a universal relation between the transition temperature and the rigidity

modulus. It has given impetus to an impressive effort toward the understanding of phase transitions in two dimensions. The very existence of continuous transitions has been challenged by computer simulations [135]; the existence of cusps in the specific heat have also been suggested [136, 137].

What does experiment say? Smectic C films are rather unique in that they are totally substrate-free. Relations such as (10.99) and (10.122) could not be tested directly: the Frank moduli are so small near the transition that they are very hard to measure directly. On the other hand, the tilt angle can be measured, and from it the K values inferred. Whereas the fulfilment of (10.122) requires a tilt θ at the transition of 4.5° , the experiment reveals a sharp drop of θ between 4 and 5° [127]. This tells that the Kosterlitz-Thouless picture has captured some of the physics of the two-dimensional transition. Heat capacity measurements are not available yet but, as we will see in the next section, beautiful measurements have been performed on thin hexatic films. It is still too early to make definite statements concerning relations such as (10.123) or (10.124), but they confirm the existence of continuous two-dimensional transitions [138].

10.3 TRANSITIONS INVOLVING HEXATIC PHASES

10.3.1 $S_A \rightleftharpoons S_{B\text{Hex}}$ transition

We have seen in Chapter 1 that the $S_{B\text{Hex}}$ phase differs from the S_A phase, by the existence of a sixfold modulation of the X-ray diffuse scattering ring corresponding to in-plane molecular correlations. For an incident X-ray beam orthogonal to the smectic planes the angular dependence of the maximum of the X-ray scattering intensity (Fig. 10.12) may be written as

$$I(\chi) = I_0 + I_6 \cos 6(\chi - \phi) + \text{higher harmonics} \quad (10.126)$$

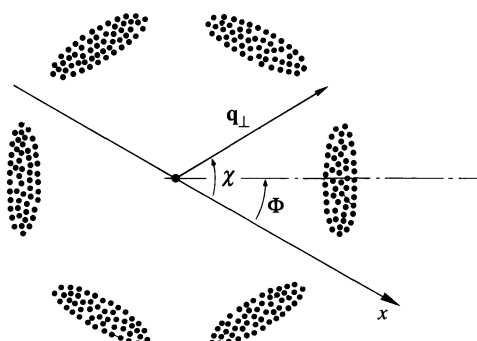


Fig. 10.12. Typical X-ray diffuse scattering pattern corresponding to in-plane order (wavevector transfer parallel to the smectic plane) in a $S_{B\text{Hex}}$.

where χ is the angle between the in-plane component of the wavevector transfer \mathbf{q} and an arbitrary reference axis x .

- In the smectic S_A phase: $I_6 = 0$.
- In the $S_{B\text{Hex}}$ phase: $I_6 \neq 0$.

The structure of (10.126) is similar to (10.1). Thus, using the same procedure as in (10.1.1), we can choose a complex order parameter

$$\psi_6 = I_6 e^{6i\phi}. \quad (10.127)$$

Since it is again a complex order parameter, a Landau free energy exactly similar to (10.11) may be written, and one expects the $S_A \leftrightarrow S_{B\text{Hex}}$ transition to belong to the superfluid helium universality class [139].

In particular, the exponent of the specific heat should be negative

$$\alpha = -0.007. \quad (10.128)$$

High-resolution a.c. calorimetry but also refractive index measurements give values of the order of 0.6, which are inconsistent with any available theory but not too far from the tricritical value 0.5 [140, 141]. The short-range chevron order, which one often sees in these systems, can be responsible for the existence of a tricritical point in a way similar to the one we describe in (10.1.1) and (10.2.4) [142]. It is, however, unlikely as an explanation for the 0.6 values that are observed for many compounds and also in mixtures for wide composition ranges. The strong coupling of the hexatic order parameter to the mass density, together with the importance of fluctuations, is revealed by the sizeable sound attenuation at the approach of the $S_A \leftrightarrow S_{B\text{Hex}}$ transition [143].

There are many other transitions related to the hexatic order, such as

$$S_{B\text{Hex}} \leftrightarrow S_{B\text{Xtal}}, \quad S_C \leftrightarrow S_F, \quad S_F \leftrightarrow S_G, \quad \text{etc.}$$

(Remember: $S_{B\text{Xtal}}$ and S_G are, in fact, crystals.)

In three dimensions, the transitions toward a crystalline phase are of first order because of the existence of the cubic invariant

$$\rho(\mathbf{q}_1)\rho(\mathbf{q}_2)\rho(-\mathbf{q}_1, -\mathbf{q}_2).$$

In two dimensions, the $S_{B\text{Hex}} \leftrightarrow S_{B\text{Xtal}}$ can be second order in a dislocation unbinding picture [144, 145]. The arguments are quite similar to those developed in Section 10.2.6. The important remark of the Halperin–Nelson–Young theory is that dislocations destroy positional long-range order without destroying bond ordering, as hinted early by Landau and Lifshitz [146]. The very existence of hexatic order in smectics is a beautiful success of the Halperin–Nelson–Young concept of bond ordering.

Experiments on thin films that are only a few layers thick will allow us to test the theories on two-dimensional melting in a similar way to that

which we discussed in Section 10.2.6. A very clever a.c. calorimetric technique has been set up for that purpose, which shows clearly the difference between two- and three-dimensional behaviour [147, 148]. As already stated in Section 10.2.6, these experiments confirm the existence of a continuous $S_A - S_{B\text{Hex}}$ transition. Eight-, four-, three-, and two-layer thick films have been investigated [138, 148]. The outer layers of the film have transition temperatures separate from that of the interior. In fact, in more than four-layer thick films, three transitions can be seen: that of the outermost layers, that of the layers next to them, and that of the remaining. The first one corresponds to a two-dimensional hexatic– S_A phase change. It corresponds qualitatively to expectations. The others cannot really be compared to them since they are in some sense lock-in transitions.

The $S_I \leftrightarrow S_F$ transition may be described by introducing the I_{12} harmonic, that is by constructing a Hamiltonian containing ψ_6 and $\psi_{12} = I_{12} e^{i12\phi}$. Formally, this problem is similar to the monolayer–bilayer ordering in S_A to be discussed in Section 10.4.3. The interesting point is the prediction of a new phase, similar to S_I and S_F but in which the molecular tilt is intermediate between the nearest-neighbour directions and the bisectors of these directions [149]. This phase is formally equivalent to the incommensurate smectic also to be discussed in Section 10.4.3. This can explain the observation of such an intermediate phase in the lecithin–water system [150].

The most satisfactory results with the hexatic order concern the study of higher harmonics in (10.126), as we shall see in the next subsection.

10.3.2 Harmonics of hexatic ordering and scaling properties

In (10.126) we have only made explicit the fundamental of the sixfold modulation. Away from the critical point, there should always be harmonics; experiments performed by the MIT group on monocrystalline samples allow to measure up to the seventh harmonic [151]. They can be fitted by the expression

$$I(\chi) = I_0 + \left\{ \frac{1}{2} \sum_{n=1}^{\infty} C_{6n} \cos(6n\chi) \right\} + I_{BG} \quad (10.129)$$

where I_{BG} is a background intensity. Equation (10.129) is written in such a way that $C_{6n} = 1$ for perfect bond order (the origin has been set up at $\phi = 0$ for convenience). In other words,

$$C_{6n} = \text{Re}\langle\psi_{6n}\rangle = \text{Re}\langle\psi_6^n\rangle. \quad (10.130)$$

On one hand, mean-field analysis leads to

$$C_{6n} = C_6^n \quad (10.131)$$

On the other hand, experiments show a remarkable scaling with

$$C_{6n} = C_6^{\sigma_n}, \quad (10.132)$$

$$\sigma_n = n + \lambda n(n - 1), \quad (10.133)$$

and $\lambda \simeq 0.295$.

The result can be easily understood in the neighbourhood of the $S_A-S_{B\text{Hex}}$ transition [152]. Indeed, the calculation of $\langle \psi_6^n \rangle$ can be performed with the addition of the term

$$H_n = g_n \int d^d r \operatorname{Re} \psi^n. \quad (10.134)$$

to the free energy (10.11) in which ψ is given by (10.62). C_{6n} can be expressed by

$$C_{6n} = \left. \frac{\partial F}{\partial g_n} \right|_{g_n=0} \quad (10.135)$$

in which F is the free energy associated to (10.11) plus (10.134), considered as a Hamiltonian.

Close to the $S_A-S_{B\text{Hex}}$ transition, F exhibits scaling properties

$$F(t, g_n) = |t|^{2-\alpha} F\left(\frac{g_n}{t^{\phi_n}}\right) \quad (10.136)$$

where $t = (T - T_c)/T_c$ and ϕ_n is the cross-over exponent corresponding to the field g_n . T_c is the $S_A-S_{B\text{Hex}}$ transition temperature.

Equations (10.135) and (10.136) lead to

$$C_{6n} \propto t^{2-\alpha-\phi_n} \propto C_6^{\sigma_n} \quad (10.137)$$

with

$$\sigma_n = (2 - \alpha - \phi_n)/(2 - \alpha - \phi_1). \quad (10.138)$$

ϕ_n can be calculated with ϵ expansion techniques ($\epsilon = 4 - d$) where d is the dimension of space) [152]. One finds

$$\sigma_n = n + x_n n(n - 1)/(d - 2 + \eta) \quad (10.139)$$

where η is the exponent associated to the ‘anomalous dimension’.

Unlike the experimental finding, x_n depends on n , but weakly so,

$$x_n \simeq 0.3 - 0.008n \quad (10.140)$$

which is remarkably good compared to experiment. In fact, (10.132) and (10.133) seem to hold even outside the validity domain of (10.139). A cross-over toward tricritical behaviour may be included which broadens the validity domain of relations such as (10.133), but λ becomes a function of temperature. The beauty of this analysis is that, in a single experiment, cross-over exponents which required separate work on different systems, or could not even be attained previously, can be measured simultaneously. For

instance ϕ_2 could be obtained by the action of uniform magnetic fields on uniaxial ferromagnets, ϕ_3 by that of a uniaxial stress on a [111] direction of a cubic ferromagnet, ϕ_4 appeared most visibly in structural phase transitions [152].

In fact, although recent experiments, using electron scattering rather than X-rays, have been truly performed on a $S_{BH_{ex}}$ phase [154], most of the data have been collected on tilted phases. This is interesting in several ways.

- The use of a magnetic field parallel to the layers allows us to obtain a monodomain sample in the smectic C phase and slowly cooling into the tilted hexatic phase preserves the orientation.
- One can directly check that there is no symmetry change between tilted hexatic (S_I or S_F) and S_C .

One can indeed measure sixfold order even in the smectic C phase, and follow continuously its increase through what was called the S_C-S_I transition [151]. Thus, as already stated, there is either no transition, or a first-order one [153]. One can easily understand the existence of sixfold order in S_C , the sixth power ψ^6 of the tilt order parameter acting as a field on the ψ_6 bond order parameter.

Since first-order S_C-S_I transitions have already been reported, there must be in appropriate phase diagrams (concentration–temperature for instance) isolated critical points of the liquid–vapour type or of the $S_{C^*}-S_{C^*}$ one as detailed in (10.2.4). In fact, this point must bear more resemblance to the S_A-S_A critical point to be described in Section 10.4.4. It could control part of the region of the rapid increase of C_6 , where $\lambda(T)$ turns out to be markedly temperature-dependent in contrast with (10.139).

10.4 FRUSTRATED SMECTICS

10.4.1 Experimental facts

Up to now, we have considered that S_A were characterized by their $D_{\infty h}$ point group symmetry, and a periodic molecular distribution along the C_∞ axis. In principle, this is enough but one can wonder if this symmetry-based classification is able to characterize all the diversity of observations related to the smectic A ordering. The existence of S_A-S_A transitions first revealed by Sigaud *et al.* [155, 156] in the DB5–TBBA binary phase diagram, suggests that the problem may be more complicated (DB5 = 4-pentyl-phenyl 4-cyanobenzoyloxy benzoate: $C_5H_{11}-\phi-OOC-\phi-OOC-\phi-CN$; TBBA = terephthal-bis-4n-butylaniline: $C_4H_9-\phi-N=CH-\phi-CH-N-\phi-C_4H_9$) (Fig. 10.13). How can two smectic A phases differ?

Let us replace DB5 with DB7 (i.e. C_5H_{11} by C_7H_{15}): a third smectic A phase appears (Fig. 10.14) [157]!

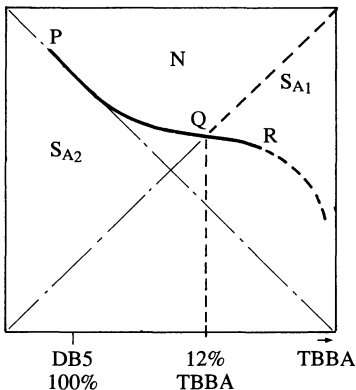


Fig. 10.13. Binary phase diagram obtained by mixing DB5 and TBBA [155, 156]. Note the existence of a monolayer–bilayer S_{A_1} – S_{A_2} transition line of the Ising type.

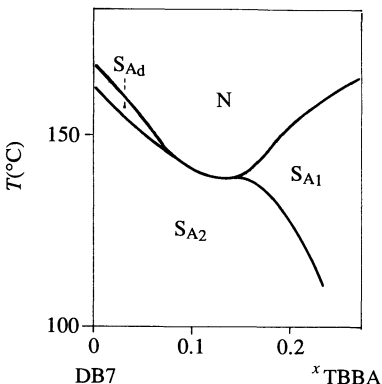


Fig. 10.14. DB7–TBBA phase diagram [157]. Note the existence of a new smectic A phase separated from the bilayer S_{A_2} by a first-order transition line. There are three different S_A phases and three N – S_A lines in this diagram.

Replace TBBA with a more polar compound named C₅ stilbene ($C_5H_{11}-\phi-CH=CH-\phi-OOC-\phi-CN$) (note that it still has three aromatic rings). Another phase labelled $S_{\tilde{A}}$ appears in a diagram already containing two S_A s [158]. Replace TBBA with T8 ($C_8H_{17}-O-\phi-OOC-\phi-CH=N-\phi-CN$) and the three S_A phases appear in addition to the $S_{\tilde{A}}$ one [159] (Fig. 10.15). The T8-rich domain is also interesting since it involves a re-entrant nematic domain (N_{Re}): re-entrant means that the nematic may be found both at higher and lower temperatures than the S_A [160]. Let us change the sens of a benzoate link in the DB_n series and join the DB7–DB9 diagrams side by side: we obtain a topology typical of a bicritical point [157, 161], which appears to be connected with re-entrant behaviour

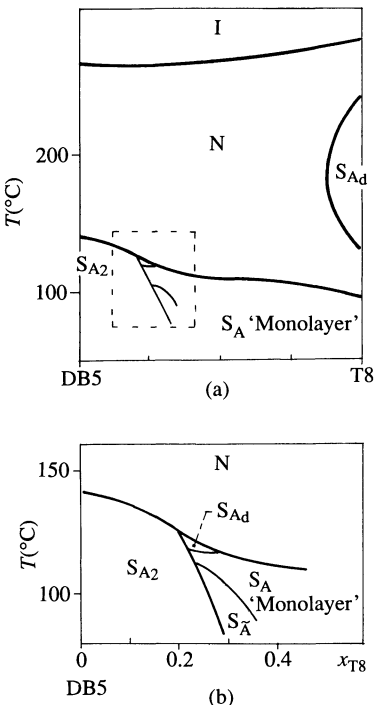


Fig. 10.15. DB5–T8 phase diagram [159]. (a) Remark the wide re-entrant nematic (N_{re}) domain. (b) Blow-up corresponding to the interior of the rectangle of (a). Note the appearance of the $S_{\bar{A}}$ phase.

(Fig. 10.16). If we now replace the cyano group with a nitro NO_2 of comparable polarity but larger steric hindrance, the binary diagram again includes three S_A phases, a re-entrant domain looking like a bicritical point, and one more phase labelled $S_{\bar{C}}$ [160] (Fig. 10.17). In all the aforementioned cases, the molecular changes are not dramatic, whereas the diagrams are significantly different.

X-rays reveal the existence of the following.

- S_{A_1} , a monolayer smectic A characterized by a quasi-Bragg peak at a reciprocal wavevector $q_2 \simeq 2\pi/l$; l = molecular length. There may be diffuse scattering of different origins but the only important point is the existence of the quasi-Bragg peak.
- S_{A_2} , a bilayer smectic, characterized by a quasi-Bragg peak at a reciprocal wavevector $q'_1 = \pi/l$, i.e. the period is twice that of the molecule. There is automatically another Bragg peak at $2q'_1 = q_2$ and, of course, diffuse scattering.

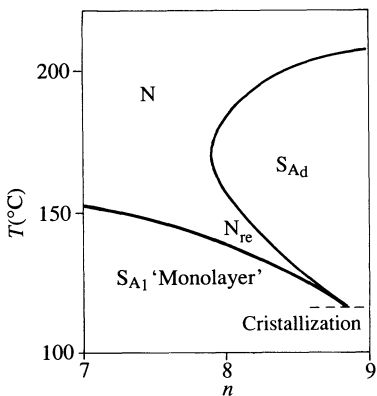


Fig. 10.16. DB 7–8 and 8–9 diagrams placed side by side [157]. Note the wide re-entrant domain and the topology of the N–S_{Ad}, N–S_{A1} suggesting the existence of a bicritical point.

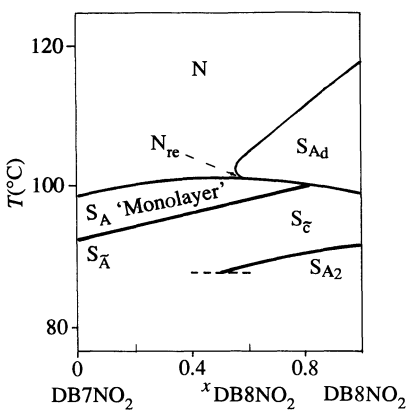


Fig. 10.17. DB7NO₂–DB8NO₂ phase diagram [160]. Note two S_A phases (S_{A1} and S_{Ad}) separated by a first-order phase boundary. The N–S_{A1}–S_{Ad} point suggests again the existence of a bicritical point, connected to re-entrance but of much smaller range than in Figs 10.15 and 10.16. For large DB8NO₂ concentrations, note the appearance of another phase: the S_C tilted antiphase.

- S_{Ad}, a partial smectic, characterized by a quasi-Bragg peak at a reciprocal wavevector $q_1 = 2\pi/l'$; l' corresponds to the length of molecular pairs. Experimentally l' is found to vary between 1 and $2l$.
- The S_Ā and S_{Ā̄}, called antiphases and tilted antiphases, have already been described in Chapter 1. They are two dimensionally ordered like columnar phases, but the local molecular arrangement is similar to that of smectics. A closer scrutiny of diagrams such as those of Figs 10.15 or 10.17 shows

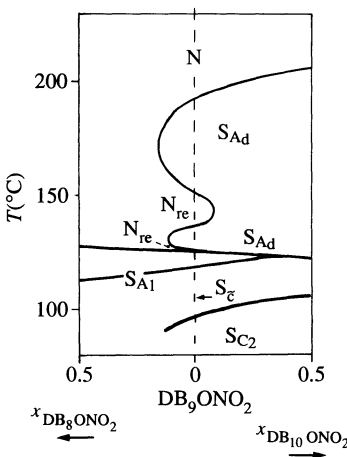
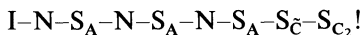


Fig. 10.18. Multiple re-entrance in the DB_8ONO_2 - DB_9ONO_2 - $\text{DB}_{10}\text{ONO}_2$ diagram [164].

that S_{A_2} and $S_{\tilde{A}}$ or $S_{\tilde{C}}$ phases are separated out by a small stability domain of a $S_{\tilde{A}}$ antiphase. $S_{\tilde{A}}$ differs from $S_{\tilde{A}}$ in that the two dimensional lattice is non-centred in $S_{\tilde{A}}$ but centred in $S_{\tilde{A}}$ (remember Chapter 1) [163].

The story does not stop here! Among other diagrams that are qualitatively distinct, we can quote DB_8ONO_2 - DB_9ONO_2 and DB_9ONO_2 - $\text{DB}_{10}\text{ONO}_2$ [164] (Fig. 10.18). Note that, for pure DB_9ONO_2 , there is the following sequence upon lowering temperature



What can be said about this multiple ‘re-entrance’?

Let us now consider the XC_n series ($\text{C}_n\text{H}_{2n+1}\text{O}-\phi-\text{COO}-\phi-\text{OCH}_2-\phi-\text{CN}$) (Fig. 10.19): the first-order line separating S_{A_d} and S_{A_2} disappears somewhere in the middle of the diagram [165]! In the case of the 90BCB (nonyloxybiphenyl cyanobenzoate: $\text{C}_9\text{H}_{15}\text{O}-\phi-\phi-\text{COO}-\phi-\text{CN}$) 4M6Cl (1-4 di (4-methylhexyloxybenzoate)2-chlorophenyl) an $S_{A_d}-\text{S}_{A_1}$ line ends in a closed nematic domain surrounded by the smectic [166] (Fig. 10.20). The name ‘nematic bubble’ was coined by Cladis and Brand (with chiral compounds, there is a cholesteric bubble). Eventually, Ratna *et al.* have suggested, in the mixture of 8OCB (octyloxycyanobiphenyl: $\text{C}_8\text{H}_{17}\text{O}-\phi-\phi-\text{CN}$) with DB_7OCN , the existence of a smectic A incommensurate phase (S_{A_i}) characterized by two incommensurate quasi-Bragg peaks [167–169] (Fig. 10.21).† Can one make sense of these apparently disconnected observations?

† A recent experiment [170] contradicts this statement, showing that in this system the incommensurate Bragg peaks correspond to a two-phase coexistence.

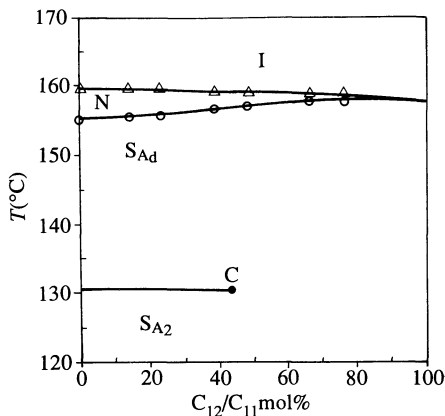


Fig. 10.19. $\text{XC}_{12}-\text{XC}_{11}$ phase diagram. Note the disappearance of the $\text{S}_{\text{Ad}}-\text{S}_{\text{A}2}$ first-order line, at the isolated critical point C [165].

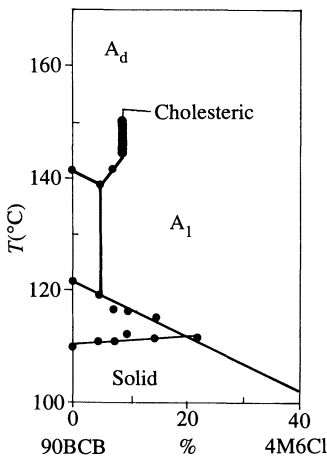


Fig. 10.20. 90BCB-4M6Cl phase diagram. Note the disappearance of the $\text{S}_{\text{Ad}}-\text{S}_{\text{A}1}$ first-order line, in a closed cholesteric stability domain called a 'cholesteric bubble' [166].

In the following sections we will show that the unifying feature of all these systems is the simultaneous presence of two incommensurate lengths:

1. that of the molecule;
2. that of a pair of molecules.

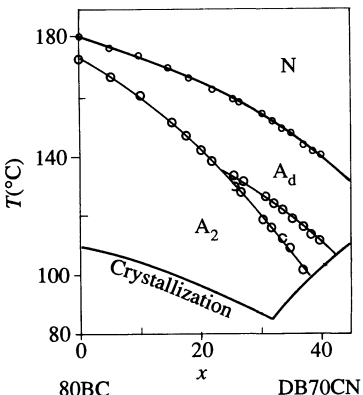


Fig. 10.21. 80BC–DB70CN phase diagram. Note the existence of a large two-phase region (see the footnote on p. 555). The line drawn between the S_{A_d} and S_{A_2} domains does not correspond to a phase transition, but rather to a locus of maximum specific heat [168, 162].

10.4.2 Frustrated smectics model

Most of the molecules involved in the observations of the preceding section are very asymmetrical. If we want more information than just the existence of a density modulation, we cannot stick to the description of Section 10.1.1. One parameter representing unambiguously the vectorial symmetry of molecules is, for example,

$$\mathbf{P}(\mathbf{r}) = \frac{1}{v} \sum_i P_i \delta(\mathbf{r} - \mathbf{r}_i) \quad (10.141)$$

where the summation is performed inside the volume v and P_i is the dipole of molecule i . This parameter describes the antiferroelectric order which tends to condense at the wavelength of molecular pairs [171]. In most of the following, we can make the simplifying choice of potential where, in the absence of charges, \mathbf{P} is derived as order parameter, $\mathbf{P}(\mathbf{r}) = 1/4\pi \nabla\phi$.

The mass density, of course, is still a relevant order parameter. We assume that it tends to condense at a wavelength corresponding to the molecular length.

The rule of the game is to build the Landau expansion with ρ and ϕ . Let us note that the introduction of an order parameter linked to dipolar ordering does not imply any assumption on the nature of interactions. In fact, the type of Landau expansion we will use requires only that the interactions be short-range. Polymeric systems, in which interactions are different, sometimes show behaviours similar to the ones described in the preceding section [172]. An equally good choice of order parameters

would be

$$\phi = \frac{\rho_A - \rho_B}{2}; \quad \rho = \frac{\rho_A + \rho_B}{2}, \quad (10.142)$$

in which we distinguish part A from part B in the molecule (say, head and tails) and ρ_A, ρ_B , respectively, is the density of part A, B. Again ρ can be assumed to condense at the molecular length; ϕ describes the segregation between heads and tails and thus can be assumed to condense at the pair length. ϕ will be called the antiferroelectric order parameter in what follows.

The expansion of the free energy results simply from the scalar nature of ρ and ϕ ; any power of ρ and ϕ is, in principle, allowed. The expansion up to fourth order reads

$$\begin{aligned} F = \int dv \left\{ & \frac{1}{2} A_1 \phi^2 + \frac{1}{3} B_1 \phi^3 + \frac{1}{6} C_1 \phi^4 + \frac{1}{2} A_2 \rho^2 + \frac{1}{3} B_2 \rho^3 + \frac{1}{6} C_2 \rho^4 \right. \\ & + A_{12} \phi \rho - \frac{1}{\sqrt{2}} B_{12} \phi^2 \rho - \frac{1}{\sqrt{2}} B_{21} \rho^2 \phi + \frac{1}{3} C_{12} \rho^2 \phi^2 \\ & \left. + \frac{1}{3} C'_{21} \rho \phi^3 + \frac{1}{3} C'_{12} \rho^3 \phi \right\}. \end{aligned} \quad (10.143)$$

The natural tendency for the system to form layers with either the pair length or the monomolecular length is expressed in A_1 and A_2

$$\left. \begin{aligned} A_1 \phi^2 &= a_1 \phi^2 + A''_1 ((\Delta + q_1^2) \phi)^2 + A_1^\perp ((\nabla - \mathbf{n}(\mathbf{n} \cdot \nabla)) \phi)^2, \\ A_2 \rho^2 &= a_2 \rho^2 + A''_2 ((\Delta + q_2^2) \rho)^2 + A_2^\perp ((\nabla - \mathbf{n}(\mathbf{n} \cdot \nabla)) \rho)^2 \end{aligned} \right\} \quad (10.144)$$

where \mathbf{n} is the nematic director and a_1, a_2 depend on two externally imposed intensive parameters such as temperature and pressure, or temperature and chemical potential. Their sign change drives the transitions toward phases with nonzero ρ and ϕ .

Let us set

$$\phi = \frac{1}{\sqrt{2}} (\psi_1 e^{i\mathbf{q} \cdot \mathbf{r}} + \text{complex conjugate}), \quad (10.145)$$

in which for the sake of argument we consider ψ_1 constant.

$$\begin{aligned} (\Delta + q_1^2) \phi &= \frac{\psi_1}{\sqrt{2}} (q_1^2 - q^2) e^{i(\mathbf{q} \cdot \mathbf{r})} + \text{complex conjugate}, \\ \int_V ((\Delta + q_1^2) \phi)^2 dv &= dv \psi_1 \psi_1^* (q^2 - q_1^2). \end{aligned} \quad (10.146)$$

This expression is minimum for $|q| = q_1$, which gives the tendency for the antiferroelectric order parameter to condense at a period l' . Similarly, the

$((\Delta + q_2^2)\rho)^2$ term favours condensation of a density modulation at a q_2 wavevector (i.e. the molecular length).

The $((\nabla - \mathbf{n}(\mathbf{n} \cdot \nabla))\phi)^2$ contribution to F (or the same with ρ) expresses the tendency for the smectic layers to be perpendicular to the nematic director. This can easily be shown if one neglects \mathbf{n} fluctuations. Then $\nabla = \hat{\mathbf{z}}$, and

$$\nabla - \mathbf{n}(\mathbf{n} \cdot \nabla) = \nabla_{\perp}, \quad (10.147)$$

$$\int_V (\nabla_{\perp}\phi)^2 dv = vq_{\perp}^2 \psi_1 \psi_1^* \quad (10.148)$$

which is minimum for $\mathbf{q}_{\perp} = 0$. Clearly, cubic terms such as ρ^3 and ϕ^3 do not contribute to F when order parameters such as (10.145) are relevant.

Two cases should be distinguished.

1. $l' \simeq l$. The product $\rho\phi$ is very important. To realize this, we look for order parameters given by (10.145) and

$$\rho = \frac{1}{\sqrt{2}} (\psi_2 e^{i\mathbf{q} \cdot \mathbf{r}} + \text{complex conjugate}). \quad (10.149)$$

Then integrating over the volume V :

$$\int_V \frac{A_{12}}{2} \rho\phi dv = \frac{VA_{12}}{2} (\psi_1 \psi_2^* + \psi_1^* \psi_2) = VA_{12} |\psi_1 \psi_2| \cos(\phi_1 - \phi_2) \quad (10.150)$$

with $\psi_1 = |\psi_1| e^{i\phi_1}$; $\psi_2 = |\psi_2| e^{i\phi_2}$. Whatever the A_{12} sign, this coupling favors a phase locking of the two waves (with $\phi_1 = \phi_2$ if $A_{12} < 0$, and $\phi_1 - \phi_2 = \pi$ if $A_{12} > 0$). This means that one cannot satisfy simultaneously the condensation of ρ at q_2 , ϕ at q_1 , and the lock-in condition (10.150).

2. $l' \simeq 2l$. The product $\phi^2\rho$ is now very important. Setting

$$\rho = \frac{1}{\sqrt{2}} (\psi_2 e^{i2qz} + \text{complex conjugate}) \quad (10.151)$$

and keeping $\phi = (1/\sqrt{2})(\psi_1 e^{iqz} + \text{complex conjugate})$, yields

$$-\int \frac{B_{12}}{\sqrt{2}} \phi^2 \rho dv = -V \frac{B_{12}}{4} (\psi_1^2 \psi_1^* + \psi_1^* \psi_2^2) = -\frac{VB_{12}}{4} |\psi_1^2 \psi_2| \cos(2\phi_1 - \phi_2). \quad (10.152)$$

Equation (10.152) again favours phase locking of ρ and ϕ but with a wavelength ratio of one to two. ψ_2 appears in that case as the harmonic of ψ_1 . Note that the $A_{12}\rho\phi$ contribution is negligibly small.

Satisfying simultaneously the tendency for ρ and ϕ to condense at incommensurate wavevectors and the lock-in terms (10.150) or (10.152) is not possible; hence the name frustrated smectics [173]. It is a somewhat

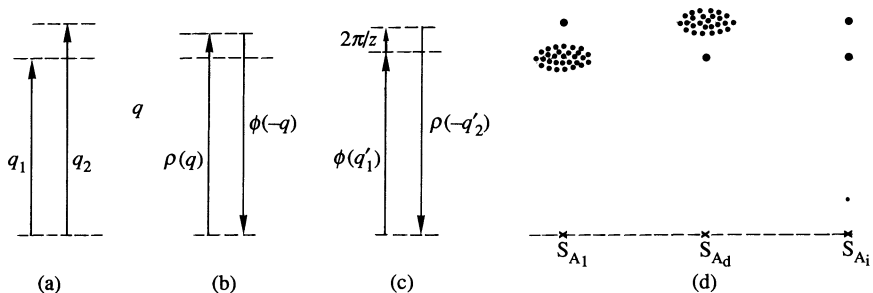


Fig. 10.22. Case $l' \simeq l$. (a) Natural wavevectors: q_2 for the mass density modulation ρ , q_1 for the antiferroelectric order parameter. Note $q_2 \simeq q_1$. (b) Smectic A compromise: the actual wavevector q is intermediate between q_1 and q_2 . (c) Incommensurate smectic $S_{A_{ii}}$; elastic energy is released by the introduction of a periodic array of discommensurations of period z . (d) S_{A_d} , S_{A_i} , $S_{A_{ii}}$ typical X-ray patterns (wavevector transfer perpendicular to the layers): the cross corresponds to the incident beam, the dots to quasi-Bragg spots, the ‘clouds’ to diffuse scattering. The light dots in $S_{A_{ii}}$ may be very hard to observe experimentally.

improper appellation since it does not correspond to the general notion of frustration connected to contour integrals.

10.4.3 Bilayer, partial bilayer smectics, incommensurate phases, and antiphases

Although one cannot simultaneously satisfy incommensurability and lock-in, some structures can provide a good compromise and correspond to stable states. There is no real point in going through detailed calculations of the stability domains of the different phases, but it is interesting to understand how they arise. Again, one has to distinguish the cases $l' \simeq l$ and $l' \simeq 2l$.

$l' \simeq l$ The existence of (10.150) shows that the condensation of ρ will always drive that of ϕ and vice versa. There is no pure density modulation without some antiferroelectric ordering, and no pure antiferroelectric ordering without density modulation. The simplest solution corresponds to the compromise of Fig. 10.22(b).

- The density and antiferroelectric modulations adopt the same wavevector q ; this costs elastic energy (measured by the coefficients A_1^{\parallel} and A_2^{\parallel}) but gains lock-in energy through (10.150). The structure is that of an ordinary smectic A, with essentially sinusoidal density and antiferroelectric modulations. Depending on numbers, the actual layer spacing $a_0 = 2\pi/q$ can vary from l to l' . When $a_0 \simeq l$, one usually speaks of monolayer smectics

S_{A_1} and, when $a_0 \simeq l'$, of partial bilayer smectics S_{A_4} , but there is no qualitative difference between the two. As a result, one can go either continuously from one case to the other, or through a first-order transition. We will come back to that point in Section 10.4.5.

- If we allow the phases ϕ_1 and ϕ_2 to depend on z , the coordinate along the normal to the layers, one can transform (10.143) into an expression involving the difference $(\phi_1 - \phi_2)$ only, which is isomorphous to that describing the cholesteric–nematic transition induced by an external magnetic field [173, 174].

The cholesteric pitch corresponds to the incommensurability $(q_2 - q_1)$, the twist elastic constant to a suitable average of A_1^{\parallel} and A_2^{\parallel} , and the magnetic field to the lock-in coefficient A_{12} . The discussion of Section 6.2.2.3 helps us to understand the different possibilities. For sufficiently large magnetic field, the cholesteric helix is unwound, i.e. the angle of the director is locked on the field direction. In our case this means that $(\phi_1 - \phi_2)$ is fixed and ρ and ϕ are locked: this is the description of the S_A of the preceding paragraph. Upon reducing the field, one reaches a critical value at which a regular array of Bloch walls starts to come in and macroscopic twist to appear. In our case, the phases ϕ_1 and ϕ_2 undergo a 2π phase shift with respect to each other, in regions corresponding to the Bloch walls (called discommensurations and sometimes solitons although they are static entities; Fig. 10.23): the periodicity Z of the walls is such that the wavevector conservation rule of Fig. 10.22(c) and the lock-in condition (10.150) are satisfied. This phase, in which incommensurate wavevectors coexist, is an incommensurate smectic, labelled $S_{A_{ii}}$. In the limit of vanishingly small magnetic field the pure cholesteric structure is obtained: the phase difference $\phi_1 - \phi_2$ is linear in z , which allows the wavevectors of ρ and ϕ to have their preferred values q_1

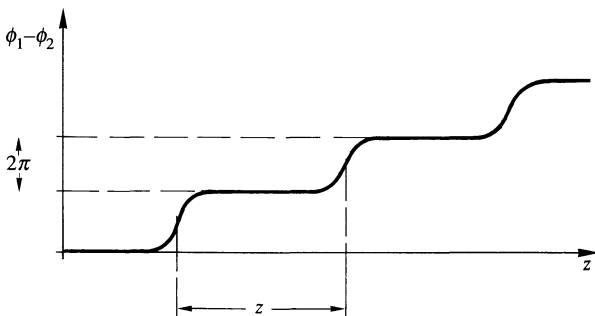


Fig. 10.23. Incommensurate $S_{A_{ii}}$ phase. Plot of the phase difference between the density and antiferroelectric modulations. The flat regions correspond to an ordinary smectic structure. In the 2π jumps, which are analogous to Bloch walls, the two modulations evolve independently from each other.

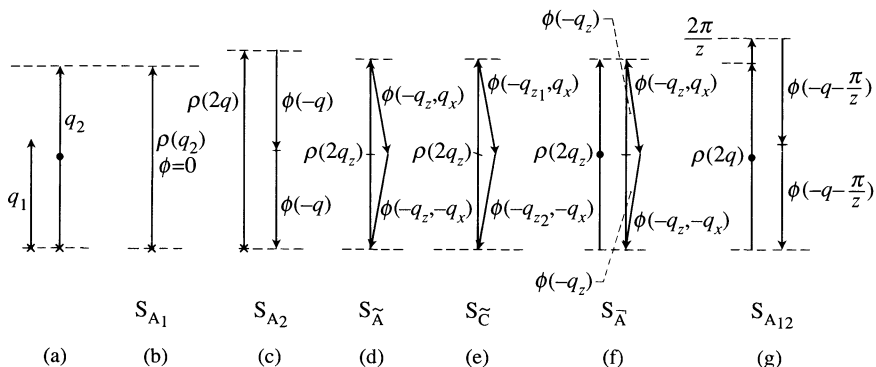


Fig. 10.24. Case $l' \simeq 2l$: (a) Natural wavevectors: q_2 for the mass density modulation ρ ; q_1 for the antiferroelectric order parameter. Note that $q_2 \simeq 2q_1$. (b) Monolayer smectic S_{A1} . Note the absence of antiferroelectric order and the optimum value of the wavevector at the inverse molecular length spacing. (c) Bilayer smectic S_{A2} . Both density modulation and antiferroelectric order are condensed. Note the exact ratio 1/2 in the wavevectors. (d) Smectic A antiphase $S_{\tilde{A}}$. Tilting the antiferroelectric wavevectors with respect to the mass density wavevector allows one to release compressional strain energy while keeping the wavevector matching. (e) Smectic C antiphase $S_{\tilde{C}}$. The symmetry of (d) is broken, but wavevector matching is still satisfied. (f) Crenellated smectic A antiphase $S_{\tilde{A}}$. The diagram appears as a superposition of (c) and (d). (g) Incommensurate bilayer smectic. Wavevector matching is now satisfied via the introduction of a periodic array of discommensurations different from those of Fig. 10.23 in that they involve ϕ^2 and ρ rather than ϕ and ρ .

and q_2 . In this limit, the incommensurate phase corresponds to two independent modulations. This is possible in three dimensions since the two incommensurate lattices can percolate through each other.

An incommensurate smectic E, although strictly speaking crystalline, may be relevant to the same physics [175].

$l' \simeq 2l$ This case is much richer than the preceding. Six different phases can be found with the interplay of the $\phi^2\rho$ coupling and incommensurability. Any time the wavevector phase-matching rule is satisfied, energy is gained from (10.152) and the rule of the game is to lose as little as possible in the gradient terms.

In Fig. 10.24 these are the different order parameter combinations and the wavevector matching which correspond to local minima of the free energy F , together with their physical identification, and Fig. 10.25 shows the typical X-ray patterns.

The simplest case is one in which $\phi(q = q_2/2) = 0$. This occurs when a_1 is sufficiently large and positive and a_2 negative. $\rho(q = q_2) \neq 0$: such a phase is called S_{A1} , since the period corresponds to a molecular length.

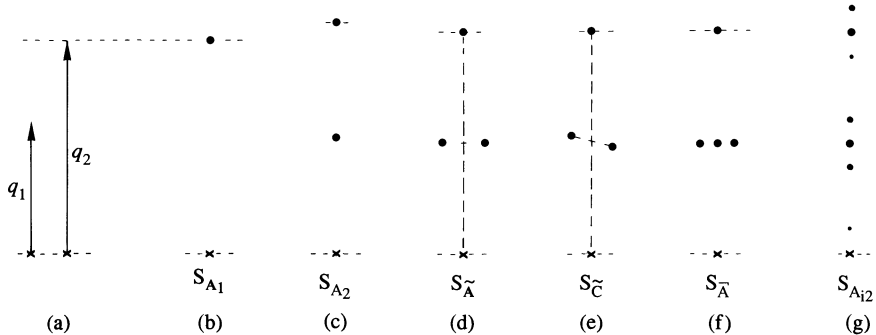


Fig. 10.25. Typical X-ray patterns for incident beam parallel to the layers: (a) natural wavevectors; (b) monolayer smectic S_{A_1} ; (c) bilayer smectic S_{A_2} ; (d) antiphase $S_{\tilde{A}}$; (e) tilted antiphase $S_{\tilde{C}}$; (f) 'crenelled antiphase' $S_{\bar{A}}$; (g) incommensurate bilayer $S_{A_{12}}$.

When a_1 decreases sufficiently, the system gains energy, with the condensation of a non-zero ϕ .

If the wavevectors stay collinear and matched, one obtains a bilayer smectic S_{A_2} : the fundamental period is $(2\pi/q \simeq 4\pi/q_2)$ which is close to two molecular lengths. The X-ray pattern is characterized by a strong harmonic modulation. The $S_{A_1}-S_{A_2}$ transition corresponds to the condensation of the fundamental $\phi(q)$ in the harmonic matrix $\rho(2q)$ which is already condensed. This transition can be second order and belongs to the Ising universality class [171]. The easiest way to understand this is to come back to the lock-in term (10.152). Matching the phases requires

$$2\phi_1 - \phi_2 = 0 \quad (\text{mod } 2\pi) \quad (\text{for } B_{12} > 0)$$

or

$$\left. \begin{aligned} \phi_1 &= \phi_2/2, \\ \phi_1 &= (\phi_2/2) + \pi. \end{aligned} \right\} \quad (10.153)$$

The transition corresponds to the segregation of heads and tails: one choice amounts to putting the heads in one pre-existing layer; the other choice to putting them in the next (Fig. 10.26). This binary choice corresponds exactly to spin up or down; hence the Ising universality class. More elaborate treatments confirm this result with minor corrections due to layer fluctuations [176]. Experiments fit remarkably well this picture provided Fisher renormalization is taken into account [177–179].

Matching is also obtained if one chooses [180, 181]

$$\left. \begin{aligned} \phi &= \sqrt{2} \cos(q_x x) (\psi_1 e^{iq_z z} + \text{complex conjugate}), \\ \rho &= \frac{1}{\sqrt{2}} (\psi_2 e^{i2qz} + \text{complex conjugate}). \end{aligned} \right\} \quad (10.154)$$

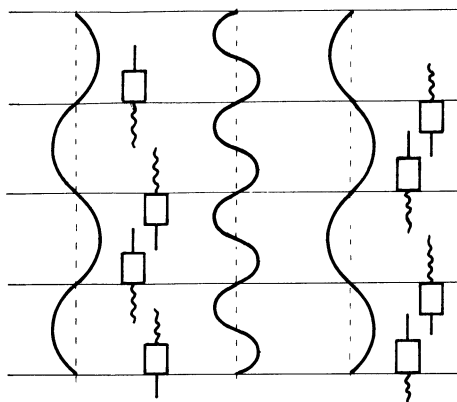


Fig. 10.26. The two possible choices of the bilayer order for a given monolayer order (density modulation) (the maximum of ϕ being taken as the maximum density of dipoles). (Left) The dipolar heads are located in the first order (and the rest follows). (Right) The dipolar heads are located in the second layer.

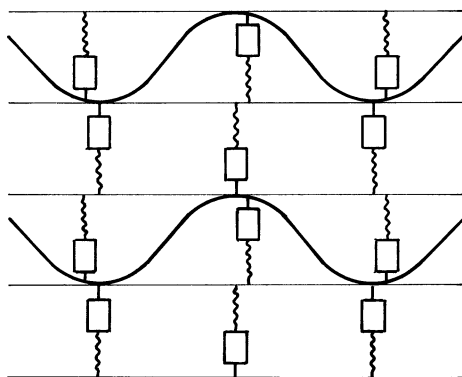


Fig. 10.27. Real space representation of the $S_{\tilde{A}}$ structure.

Indeed, with this choice (10.152) is unchanged together with the $\int a_1 \phi^2$ term. The actual wavevector of the structure comes now from a compromise between the natural tendency to satisfy $2q = q_2$, and $q_1 = \sqrt{(q^2 + q_x^2)}$ but also to choose q_x as small as possible (cf. (10.148)). The physical picture that emerges from (10.154) is very simple: moving along the x direction at constant z , the sign of ϕ changes periodically. This means that we meet successively regions rich in heads, and regions rich in tails. In between the amplitude of ϕ vanishes: there is an equal number of heads and tails. We give in Fig. 10.27 the real space picture of the $S_{\tilde{A}}$. The pure cosine description ($\cos q_x x$) fits the diagram in Fig. 10.24(d). It is possible to include higher harmonics [182], in which case a picture with walls is better suited [158].

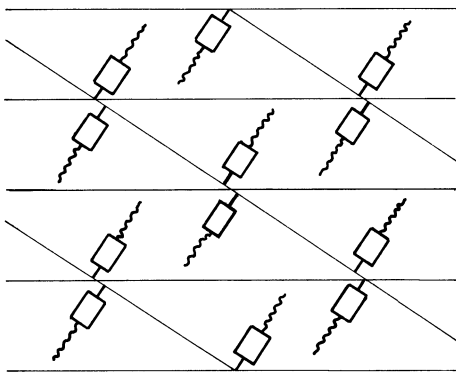


Fig. 10.28. Real space representation of the S_C structure.

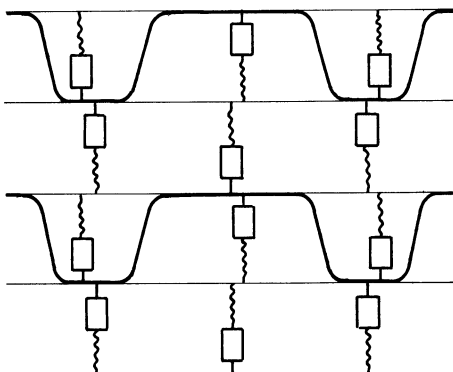


Fig. 10.29. Real space representation of the $S_{\bar{A}}$ structure.

Experiment [163] and theory [182] show that one goes continuously from one to the other. The importance of $S_{\bar{A}}$ -like fluctuations and the progressive lock-in of ϕ^2 on ρ have been nicely evidenced by X-ray scattering [183].

We could also give analytic expressions of $\phi_1 \rho$ for S_C and $S_{\bar{A}}$ [181, 182]. It is, however, more illustrative to come back to the real space picture of the phases (Figs 10.28 and 10.29), keeping in mind that the location of heads and tails is determined by ϕ .

The last possible matching of Fig. 10.24(g) describes a ‘bilayer incommensurate’ phase $S_{A_{12}}$ [173, 184, 182]. Its real space structure is depicted in Fig. 10.30. Like a S_{A_1} , it corresponds to a periodic array of discommensurations, but the important phase difference is now $2\phi_1 - \phi_2$, and the locked regions have a bilayer character. Again the limiting case is that of two independent modulations percolating through each other. The discommensuration regime was reported in reference 169. High-resolution

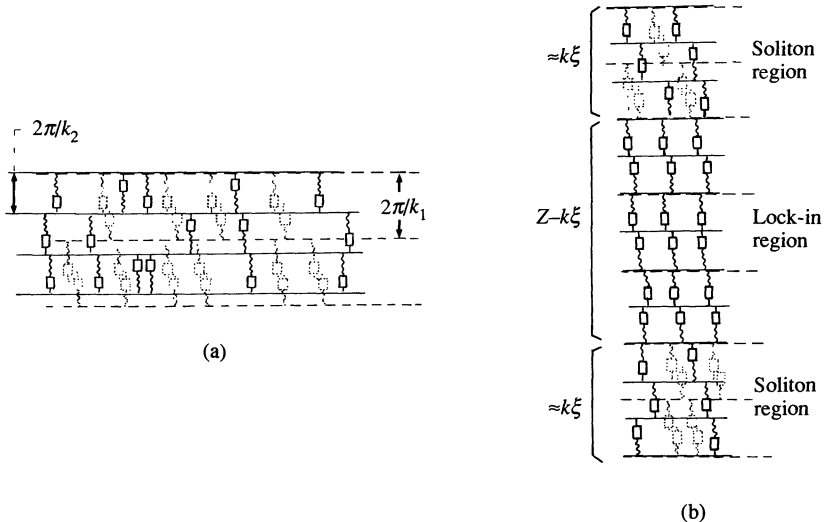


Fig. 10.30. Real space structure of the S_{A_2} incommensurate phase. (a) Weak-coupling limit (equivalent to a vanishing magnetic field in the cholesteric–nematic transition). (b) Discommensuration regime (equivalent to the Bloch wall regime in the cholesteric–nematic transition). (b) Discommensuration regime (equivalent to the Bloch wall regime in the cholesteric–nematic transition).

X-ray analysis needs to be performed on these systems, since, in one other instance, it revealed incommensurate modulations on a large scale (several hundred Å) but not condensed [185].†

We give in Fig. 10.31(a)–(d) five examples of diagrams that one can get from (10.143) by direct minimization of the free energy.

- (a) corresponds to the case of weak incommensurability [171]. Note the similarity with Fig. 10.13; the topology corresponds exactly to experiment, even the S_{A_1} – S_{A_2} tricritical point has been found.
- (b) is obtained upon increasing incommensurability, when the bilayer elastic constant is large compared to the partial bilayer [186, 187]. Note that the first-order S_{A_2} – S_{Ad} phase boundary ends on an isolated critical point. The topology is similar to that of Fig. 10.14 with, however, the absence of the isolated critical point in the physically accessible domain. Such a point can be seen in Figs. 10.19 and 10.21.
- (c) is obtained with moderate incommensurability when tilting the ϕ lattice with respect to ρ does not cost ‘too much’ energy [182, 186]. The relative position of N , S_{A_1} , S_{A_2} , S_{Ad} , and $S_{\tilde{A}}$ is correct when compared to

† Recent measurements show again that one deals, in fact, with two- and three-phase domains (Prem Patel, Li Chen, and Satyendra Kumar; preprint).

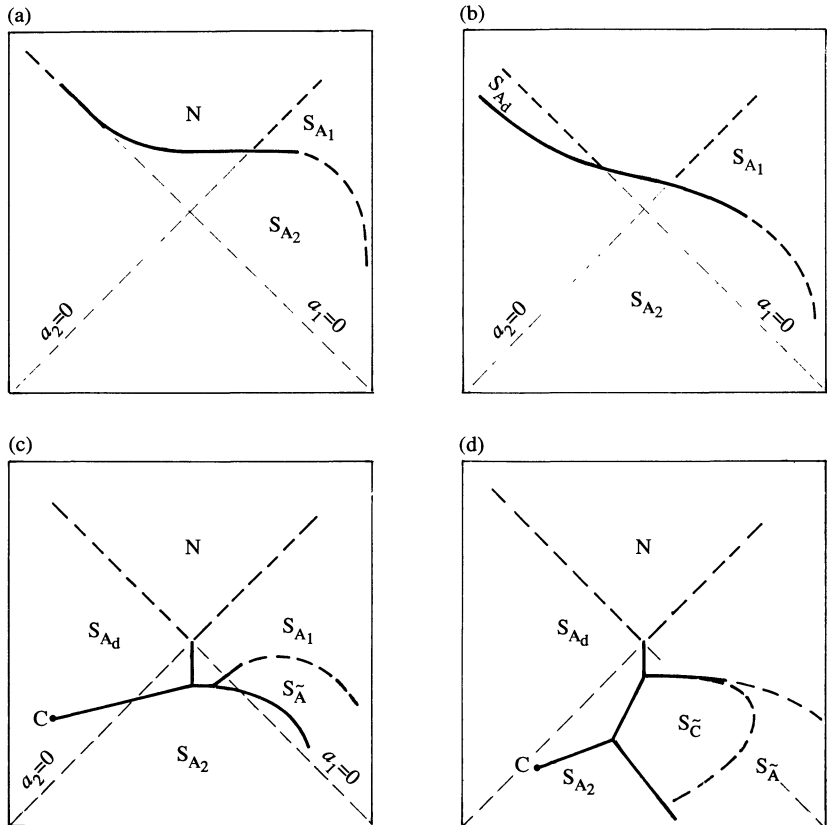


Fig. 10.31. Examples of diagrams obtained in the (dotted) a_1, a_2 -plane; full lines indicate second (first)-order boundaries. (a) Weak incommensurability: note the similarity with Fig. 10.13. (b) Intermediate incommensurability: note the similarity with Fig. 10.14. (c) Intermediate incommensurability, A_1^\perp 'small': note the similarity with Fig. 10.15. (d) Stronger incommensurability: note the similarity with Fig. 10.17.

Fig. 10.15, but the S_{Ad} domain is not closed as the experiment suggests. A high-resolution experimental diagram should check this point. More accurate experiments show that S_{A_2} and $S_{\tilde{A}}$ are separated out by a small $S_{\bar{A}}$ stability domain [163]. Computer calculations including higher-order Fourier components show that $S_{\bar{A}}$ and $S_{\tilde{A}}$ have very close energies in the vicinity of S_{A_2} [182].

(d) is obtained with larger incommensurability [182, 186], the relative positions of N , S_{A_1} , S_{Ad} , $S_{\tilde{C}}$, and S_{A_2} again compares favourably with experiment.

There are many other possible topologies and other 'axes' can be chosen

[184]: mean-field calculations provide surprisingly good results. There are, however, three instances in which fluctuations cannot be neglected:

1. the $S_{A_1}-S_{\bar{A}}$ transition;
2. the re-entrant phenomenon of Figs. 10.15, 10.16, and 10.17;
3. the S_A-S_A isolated critical point and the connected ‘nematic bubble’.

The last two cases are discussed in the following sections. The first one is similar to the $N-S_C$ transition: although the mean-field calculations predict that this transition might be continuous, because fluctuations are located on a cone in \mathbf{q} space they drive the transition to become first-order [107]. This feature is well borne out by experiment [163, 183, 188].

10.4.4 Re-entrant behaviour

First demonstrated by Cladis [189], the re-entrant behaviour has been observed in many different systems.

Is ‘re-entrance’ specific to the $N-S_A$ problem? Is there a universal explanation for this phenomenon?

The answer to both questions is no. Re-entrant behaviour exists in several other systems and sometimes can be understood using a microscopic description of the interactions. Even in the $N-S_A$ problem, there may well be re-entrances of different physical origins.

Single re-entrance may be understood using purely mean-field arguments. In the following we discuss the $S_{A_1}-S_{A_2}$ phase boundary because of its simplicity (i.e. its second-order domain and negligible incommensurability [171]). The $N-S_A$ problem is similar since the coupling of the nematic order parameter S to the smectic order parameter is identical, but the first-order nature of the $N-I$ transition complicates the algebra a little [117, 190, 191]. The relevant part of the free energy (10.143) reads

$$\int d\mathbf{v} \frac{1}{2}(A_2 - \sqrt{2B_{21}\psi_2 + C_{12}\psi_2^2})\psi_1^2 + \dots \quad (10.155)$$

with $\psi_2^2 = -2A_1/C_1$. The sign change of the ψ_1^2 coefficient defines the onset of the ψ_1 bilayer order in the ψ_2 monolayer matrix. Figure 10.31(a) shows the strong curvature of the phase boundary, which comes from the interplay of ψ_2 and ψ_2^2 with opposite signs. With suitable dependences of A_1 and A_2 on temperature and concentration or temperature and pressure, this may lead to re-entrant behaviour. This is a single re-entrance.

What about double re-entrance as in Figs 10.15–10.17? We already stated that the topology was very reminiscent of that of a bicritical point. Mean-field analysis of (10.143) predicts the existence of an $N-S_{A_1}-S_{A_d}$ bi- or tetracritical point. In the vicinity of this multicritical point, the relevant part of (10.143)

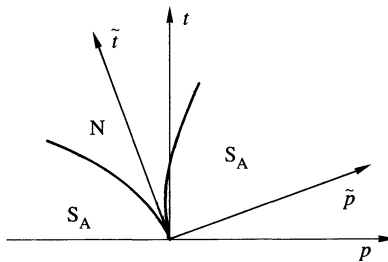


Fig. 10.32. Topology near a multicritical point: the two boundaries separating the high-symmetry phase from the low-symmetry ones are tangent to the \tilde{t} scaling axis. However, the physical t -axis is rotated from it by a non-universal amount. Thus varying temperature will always lead to re-entrant behaviour for well chosen parameters.

reads

$$F = \int dv \left(\frac{r_1}{2} \psi_1^2 + \frac{1}{2} (\nabla \psi_1)^2 + \frac{r_d}{2} \psi_d^2 + \frac{1}{2} (\nabla \psi_d)^2 + \frac{u_1}{4} \psi_1^4 + \frac{u_d}{4} \psi_d^4 + \frac{u_{1d}}{2} \psi_1^2 \psi_d^2 \right) \quad (10.156)$$

where ψ_1 and ψ_d describe the mono and partial bilayer order parameters (shifted in k space) and proper transformations have been made for the coefficients of the gradient terms to be set to 1/2. If one takes into account fluctuations, the existence of a multicritical point imposes that the smectic correlation functions G_1 and G_d obey scaling relations such as (Lubensky, T. C., unpublished and reference 192)

$$G(t, p) = \tilde{t}^{-\gamma} f(\tilde{p}/\tilde{t}^\psi) \quad (10.157)$$

where $t = (T - T_m)/T_m$, $p = (P - P_m)/P_m$ are the reduced temperature and pressure (T_m , P_m temperature and pressure at the multicritical point) and \tilde{p} and \tilde{t} are linear combinations of t and p . Equation (10.157) requires that the phase boundaries obey the relation

$$\tilde{g} = w^\pm \tilde{t}^\psi. \quad (10.158)$$

As is clear on Fig. 10.32, suitable rotation and translation of p , t with respect to \tilde{p} , \tilde{t} implies the doubly re-entrant behaviour. Note the similarity with Fig. 10.16. This interpretation is very general and does not depend on the particular system under study; any competing order parameters coupled to fourth order as in (10.156) should give the same behaviour.

In fact, as shown experimentally [193, 194] and theoretically,† the exact topology can be more subtle, but in any case can be described by (10.156)

† In particular, first-order transitions that involve differences in the smectic fluctuations may appear in the nematic phase (see reference 124, for example).

with fluctuations, or in other words by the competitions among the S_{A_1} and S_{A_d} fluctuating orders.

10.4.5 S_A - S_A isolated critical point and nematic bubble

Figure 10.31(c) and (d) exhibit first-order S_{A_2} - S_{A_d} lines that terminate on an isolated critical point. A similar point may exist in the S_{A_1} - S_{A_d} case, which is easier to illustrate analytically [195, 196]. For $l' \simeq l$, with the order parameters choices given in (10.145) and (10.149), the free energy (10.143) becomes (per unit volume)

$$\begin{aligned} f = & \frac{1}{2}(A_1 + (q^2 - q_1^2)^2)\phi_1^2 + \frac{1}{2}(A_2 + (q^2 - q_2^2)^2)\phi_2^2 - A_{12}\phi_1\phi_2 \\ & + \frac{C}{4}(\phi_1^4 + \phi_2^4) + \frac{C_{12}}{2}\phi_1^2\phi_2^2 \end{aligned} \quad (10.159)$$

in which we have set $a_1 \rightarrow A_1$, $a_2 \rightarrow A_2$, $A_1^{\parallel} = A_2^{\parallel} = 1$, $C_1 = C_2 = C$, $C'_{21} = C'_{12} = 0$, and the phases $\phi_1 = \phi_2 = 0$ ($A_{12} > 0$) for convenience. With the variable change $\phi_1 = \tilde{\rho} \cos \theta$, $\phi_2 = \tilde{\rho} \sin \theta$, and after minimization with respect to q , one obtains

$$2q^2 = (q_1^2 + q_2^2) + \cos 2\theta(q_1^2 - q_2^2) \quad (10.160)$$

$$f = \frac{r(\theta)}{2}\tilde{\rho}^2 + \frac{u(\theta)}{4}\tilde{\rho}^4 \quad (10.161)$$

with

$$r(\theta) = \frac{1}{2}(A_1 + A_2 + (A_1 - A_2)\cos 2\theta) - A_{12}(\sin 2\theta - 1) - \frac{(q_2^2 - q_1^2)^2}{4}\cos^2 2\theta.$$

$$u(\theta) = 2[(C + C_{12}) + (C - C_{12})\cos^2 2\theta].$$

The N- S_A transition is obtained when the smallest (θ) value vanishes or

$$r(\theta) = \frac{\partial r}{\partial \theta}(\theta) = 0. \quad (10.162)$$

Equation (10.162) gives a parametric representation of the phase boundary

$$A_1 = f(\theta), \quad A_2 = g(\theta). \quad (10.163)$$

In the smectic phase, the energy reads simply

$$f = -\frac{r^2(\theta)}{4U(\theta)}. \quad (10.164)$$

Note that one still has to minimize f with respect to θ .

Depending on the parameter values, one can calculate the topologically different diagrams, some of which exhibit an S_{A_1} - S_{A_d} critical point. Because of the (1, 2) symmetry this point must occur on the diagonal $A_1 = A_2$, and

for $\theta = \pi/4$ (when it is unique). One can thus expand (10.164) for small $\epsilon = \cos 2\theta$

$$(4f - f_0) = a_1\epsilon + a_2\epsilon^2 + a_3\epsilon^3 + a_4\epsilon^4 + \dots \quad (10.165)$$

It is straightforward to show that, on the diagonal $A_1 = A_2$, $a_1 = a_3 = a_{2n+1} = 0$. A critical point is reached when $a_2 = 0$, $a_4 > 0$. (For more details see references 195 and 196.) That is,

$$A_{1c} = A_{2c} = \left(2CA_{12} - \frac{(q_2^2 - q_1^2)^2}{4} (3C + C_{12}) \right) / (C - C_{12}). \quad (10.166)$$

For $a_2 < 0$, the line $A_1 - A_2$ is the coexistence line, for $a_2 > 0$ this is the isochoore (equal layer thickness lines).

This type of analysis corresponds exactly to that relevant at the liquid–vapour critical point.

According to (10.160) the layer spacing a is linearly related to the order parameter ϵ , such that

$$\frac{a - a_c}{a_c} \simeq \frac{\epsilon}{2} \frac{q_2^2 - q_1^2}{q_1^2 + q_2^2} \quad (10.167)$$

with

$$a_c = \frac{2\pi}{q_c} = (2/(q_1^2 + q_2^2))^{1/2}$$

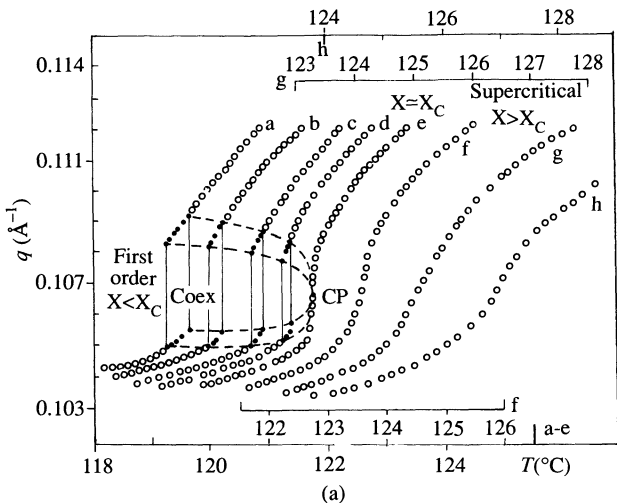
Equation (10.167) tells us that the $S_A - S_A$ transition corresponds to an amplitude change of the monolayer versus partial bilayer orders, together with a layer spacing change. It also tells us that we can choose $\partial u/\partial z = \delta a/a_c = -(\delta q/q_c)$ as well as ϵ for the order parameter. The analogy with $V(T)$ isobars in the liquid–vapour problem is striking. To the vanishing of a_2 corresponds that of the elastic constant B . Thus, the isolated $S_{A_1} - S_{A_d}$ critical point is characterized by the vanishing of the compressional elastic constant. (The same would hold at an $S_{A_2} - S_{A_d}$ critical point.) Figure 10.33 provides a nice illustration of these considerations [197].

To what extent can the liquid–vapour analogy hold? We have seen in Chapter 7 that the correct rotationally invariant expression for the compression–dilatation variable is not $\partial u/\partial z$ but $E(u) = \partial u/\partial z - \frac{1}{2}(\nabla \mathbf{u})^2$. This implies that the expansion (10.165) involves two third-order terms in the gradients of u , namely

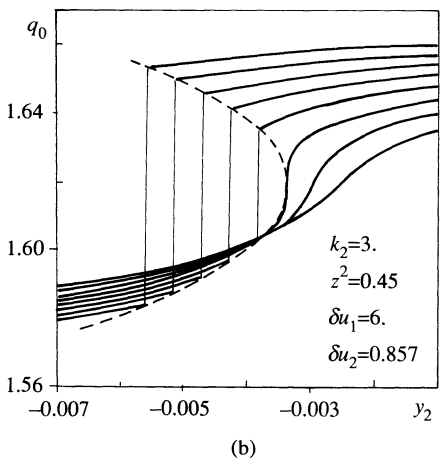
$$\frac{w_1}{3!} \left(\frac{\partial u}{\partial z} \right)^3$$

which comes from $a_3\epsilon^3$ and $a_2\epsilon^2$, and

$$\frac{w_2}{2} \frac{\partial u}{\partial z} \left(\left(\frac{\partial u}{\partial x} \right)^2 + \left(\frac{\partial u}{\partial y} \right)^2 \right)$$



(a)



(b)

Fig. 10.33. (a) Wavevector temperature dependence for different concentrations of the mixture 90BCB + 11OPCBOB [197]. 90BCB: $C_9H_{19}-O-\phi-\phi-OOC-\phi-CN$; 11OPCBOB: $C_{11}H_{23}-O-\phi-OOC-\phi-O-CH_2-\phi-CN$). Concentrations a, b, c, d give rise to a first-order transition; concentrations f, g, h lead to supercritical behaviour (i.e. no singularity); concentration e corresponds to the critical concentration, and goes through the criticalpoint CP. (b) Corresponding theoretical diagram in the $S_{A_2}-S_{A_d}$ case [186].

which comes from $a_2\epsilon^2$ (with the further requirement that $w_2 = -B$, on the line $A_1 = A_2$ or, more generally, on the isochore $a = a_c$).

This situation is quite different from that of the liquid-vapour problem in which the cubic term can always be suppressed by a simple variable

change. As a result the S_A - S_A critical point defines a new universality class [198]: the upper critical dimension is six, and anisotropic scaling with $v_{\parallel} \neq v_{\perp}$ holds. Experiments confirm the vanishing of B [199] and point toward the existence of a new universality class [199, 200].

Right at the critical point, since the compressional elastic constant vanishes, the system is very close to a nematic. It is then legitimate to wonder if, in some cases, this point could not be replaced by a nematic ‘bubble’. The analysis of the S_A - S_A critical point in terms of layer displacement cannot allow us to describe the nematic phase, unless we use dislocation distributions as in Section 10.1.8. The net result is that, depending on bare parameters, a nematic bubble or the S_A - S_A critical point may be observed [196]. This can be understood with the following simple argument. We have already stated in Section 10.1.8 that the free energy of an infinite dislocation per unit length reads

$$f_d = W - TS \quad (10.168)$$

where W is the energy and S the entropy of the dislocation. When $f_d < 0$ the nematic phase sets in. In general, W and S are monotonic slowly variable functions of temperature: as a result one observes a high-temperature nematic phase for $T > W/S$. However, W contains two types of contribution:

1. a local contribution that has no reason to exhibit strong temperature dependences;
2. one that arises from the elastic strain field and is essentially governed by B .

Since B vanishes at the critical point, W exhibits a sharp dip at this point. If the system is close to a nematic phase, this may be enough to give rise to a nematic bubble. We illustrate this possibility in Fig. 10.34(a)–(c). Note that the size of a nematic bubble depends on the ‘proximity’ of the high-temperature phase. When the bubble merges with the main nematic domain, conditions are met for multiple re-entrance (Fig. 10.34(d) [196, 201]).

It is important to close this subsection with a few remarks. Although we have distinguished S_{A_1} , S_{A_d} , and S_{A_2} phases, there is only one smectic A *sensu stricto* [198]. We have shown that one can go without any phase transition from S_{A_1} to S_{A_d} ($l' \simeq 1.2l$) and S_{A_d} ($l' \simeq 1.4l$). But it is also clear that one can go without phase transition from S_{A_d} ($l' \simeq 1.4l$) to S_{A_d} ($l' \simeq 1.6l$) and S_{A_d} ($l' \simeq 1.8l$). We also have diagrams in which one goes without phase transition from S_{A_d} ($l' \simeq 1.8l$) to S_{A_2} . Thus one can go from S_{A_1} to S_{A_2} in principle without any transition: this agrees with the statement that all smectic A phases have the same symmetry, but yet this does not contradict the fact that one can also observe a direct second- (or first-) order S_{A_1} - S_{A_2} transition (we illustrate this feature in Fig. 10.35).

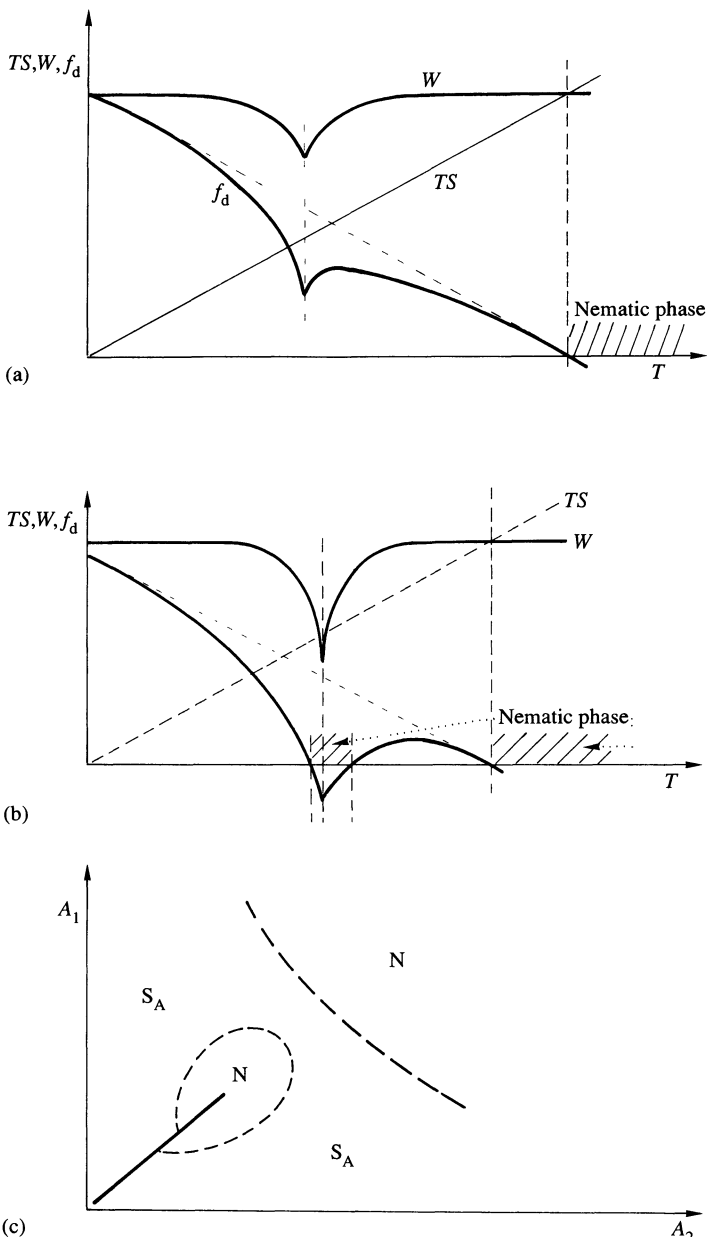


Fig. 10.34. Isolated S_A-S_A critical point versus nematic bubble. The dip in the dislocation energy $W(T)$ (light solid line), generates a dip in the dislocation free energy $f_d(T)$ (heavy solid line). (a) f_d is positive in the dip region: the S_A-S_A critical point is observed. (b) The proximity of the high-temperature nematic allows f_d to be negative in the dip region: a nematic 'bubble' is observed. (Continued opposite.)

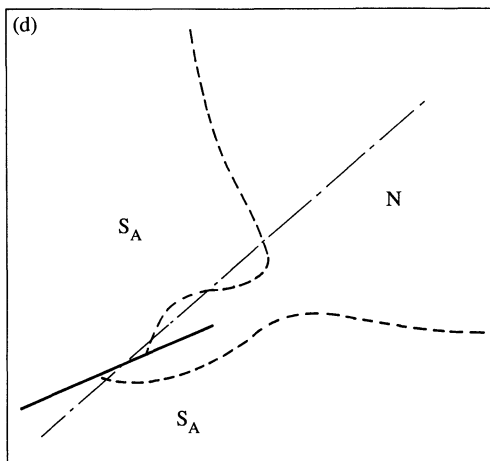


Fig. 10.34 (continued). (c) Phase diagram resulting from case (b) [196]: note the existence of a nematic–nematic critical point. Across the first-order nematic–nematic line, the phases differ in their smectic fluctuations. (d) Merging of the ‘bubble’ with the main nematic domain. Note the multiple re-entrance along the dash-dotted axis.

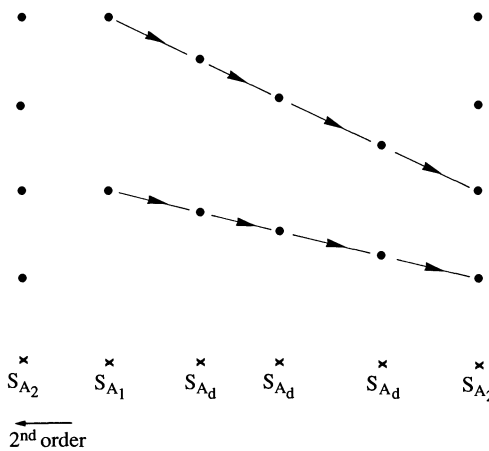


Fig. 10.35. X-ray scattering spectrum of S_A phases. Note the two possibilities: (1) following the arrows: a gradual change from S_{A_1} to S_{A_2} (with or without first-order transitions); (2) on the left of the figure: appearance of a quasi-Bragg peak at $(2\pi/2l)$, defining a second-order transition.

10.4.6 Molecular aspects

If the phenomenological approach provides a unifying framework for the description of the ‘frustrated’ smectics, it does not give much detail on what is happening at a molecular scale. At that level, there are many theories that

retain some of the physics involved in smectic-ordering, but it is hard to tell which corresponds best to real life! Most of them have been devoted to the understanding of the re-entrant or doubly re-entrant phenomenon.

One can distinguish two classes of approach. In the first the main role is played by the alkyl chain; in the second, dipolar interactions are considered to be dominant.

In its simplest version, the first explanation goes as follows [202]. When the chains have enough *cis* conformation, their entropy of mixing provides an amphiphilic interaction that is responsible for the smectic ordering. The ordering occurs in a well defined temperature range. At higher temperatures, one observes a conventional melting toward a nematic phase when the amphiphilic interaction is outweighed by the translational entropy. At lower temperature, the chains adopt less and less the *cis* conformations and the amphiphilic interaction decreases drastically; translational entropy again wins and one obtains the re-entrant nematic. This type of theory is successful in finding the chain length required for giving re-entrance and in finding the S_{A_d} phase. It does not locate properly the S_{A_1} phase and cannot describe the S_{A_2} . The early explanation proposed by Cladis [189, 190] had the further ingredient that the cores are more bulky than the chains, which leads to the idea of an optimum density for forming the smectic phase [203].

Dipolar interactions have been considered in the mean-field approximation [204–206] and in a ‘frustrated spin gas model’ [207–209]. In the first case, re-entrance results from treating the systems as a mixture of monomers and dimers: at lower temperature the dimer concentration increases and, above a certain concentration of associated molecules, a smectic phase sets in. Re-entrance is caused by the unfavourable packing of the dimers according to the Cladis argument. A one-particle description of S_{A_2} , S_{A_1} and of a hypothetical longitudinal ferroelectric phase is also proposed [205]. (The distinction of two monolayer smectic phases is not relevant.) The most successful microscopic theory is probably the spin gas model. Triplets of molecules on a two-dimensional triangular lattice are considered. The interaction between molecules is of dipolar type

$$V_{12} = \frac{AS_1 \cdot S_2}{r_{12}^3} - \frac{3B(S_1 \cdot \mathbf{r}_{12})(S_2 \cdot \mathbf{r}_{12})}{r_{12}^5}. \quad (10.169)$$

For purely dipolar interaction $A = B$. S_1 and S_2 are unit vectors along the z direction perpendicular to the two-dimensional lattice and $\mathbf{r}_{12} = \mathbf{r}_1 - \mathbf{r}_2$ where \mathbf{r}_i is the position of the dipolar head of molecule i . $A > B$ means that steric hindrance wins, and $A < B$ that Van der Waals or amphiphilic attraction wins. The presence of the tails is mimicked by imposing quantized positions for the heads (Fig. 10.36): n positions separated by a distance $1/n$. Vibrational motion around these positions is also quantized (displacement $\delta \ll 1/n$, labelled by an index m).

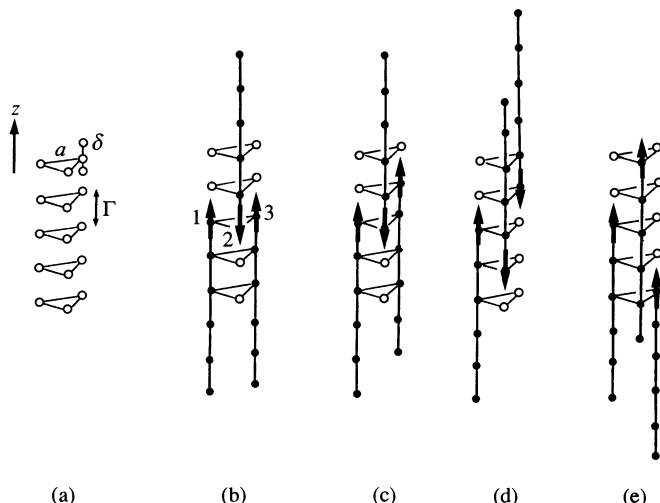


Fig. 10.36. Example of triplet configurations according to references 207–209. (a) The quantized positions introduced to mimic the chain hindrance are represented by the triangles (distance $\Gamma = 1/n$); δ is the short-scale librational jump allowed in the model. (b)–(e) Different allowed positions.

N– S_A phase boundaries are approximated in the following way. In a first step, partial summation of the partition function is taken over the z positions. This allows us to define ‘dress’ interactions, according to

$$\exp(K_s S_1 S_2 + K_l S_2 S_3 + K_w S_3 S_1 + G) = \sum_{\{r_i\}}^{n^2 m^3} \exp\{-(V_{12} + V_{23} + V_{13})/k_B T\} \quad (10.170)$$

where K_s , K_l , K_w correspond to the strongest, intermediate, and weakest couplings, specific to each positional configuration.

The transition to the smectic phase is estimated with Houtappel’s condition [210]

$$\sinh 2K_s \sinh 2K_s + \sinh 2K_l \sinh 2K_w + \sinh 2K_w \sinh 2K_s > 1. \quad (10.171)$$

This is a condition corresponding to a two-dimensional distorted triangular Ising model. If K_s and K_l are both positive, in-plane ferromagnetic order sets in. This corresponds to $\langle s_1 s_2 \rangle \simeq 1$ and $a \simeq 1$. The authors identify this phase with S_{A_1} although, since the piling of such planes is not considered, it could be S_{A_2} or longitudinal ferroelectric as well. If $K_s \cdot K_l < 0$, $\langle (s_1 - s_2) \rangle < 0$, local antiferroelectric order sets in, which describes the S_{A_d} phase. Since Houtappel’s condition corresponds to a two-dimensional system, the transitions are, of course, strongly displaced toward low temperatures as compared to what they should be in a three-dimensional system. However,

short-range statistics seem to capture an interesting part of the physics involved in the smectic ordering. Double re-entrance like that of Fig. 10.16, but also multiple re-entrance like that of Fig. 10.18 are satisfactorily reproduced. The number of quantized positions n that give rise to multiple re-entrance agrees with the number of carbon atoms (i.e. nine) in the alkyl chain of the molecule leading to this observation. In this picture, the outset of the S_{A_1} phase corresponds to the breaking of the antiparallel pairs, whereas at the $N-S_{A_d}$ transitions their number is nearly constant. As a result, the specific heat anomaly at the $N-S_{A_1}$ transition is much larger than at the $N-S_{A_d}$, which is true experimentally [211]. The near constancy of the number of antiparallel pairs in the S_{A_d} and re-entrant nematic phase is also in agreement with dielectric measurements [212]. The predicted sextuple, octuple, etc. re-entrances seem very unlikely experimentally. In its present form, the spin gas model cannot describe the S_A-S_A transition and the more ordered phases, but the fact that it is able to predict smectics with different thicknesses gives ground for the phenomenological theory (the same remark holds for reference 205). To end, an interesting remark has been made by the Bangalore group. Whereas permanent dipole-permanent dipole interactions favour antiparallel short-range order, permanent dipole-induced dipole interactions favour parallel short-range order. The interplay between these two tendencies may also explain the existence of two natural lengths and re-entrances [213].

REFERENCES

1. Rondelez, F. *Solid State Commun.* **12**, 1675 (1972).
2. Marynissen, H., Thoen, J., and Van Dael, W. *Mol. liquid Cryst.* **97**, 149 (1983).
3. Anisimov, M. A., Voronov, V. P., Kulkov, A. O., and Kholmurodov, F. J. *Phys. (Paris)* **46**, 2137 (1985).
4. McMillan, W. L. *Phys. Rev.* **A4**, 1238 (1971).
5. Bean, C. P. and Rodbell, D. *Phys. Rev.* **126**, 104 (1962); for a more recent and complete analysis see Bergman, D. J. and Halperin, B. I. *Phys. Rev.* **B13**, 2145 (1976).
6. Meyer, R. B. and Lubensky, T. C. *Phys. Rev.* **A14**, 2307 (1976).
7. McMillan, W. L. *Phys. Rev.* **A6**, 936 (1972); McMillan, W. L. *Phys. Rev.* **A7**, 1673 (1973).
8. de Gennes, P. G. *Solid State Commun.* **10**, 753 (1972).
9. London, F. *Superfluids*, Part I; Penrose, O. and Onsager, L. *Phys. Rev.* **104**, 576 (1956).
10. de Gennes, P. G. *Superconductivity of metals and alloys*. W. A. Benjamin Inc., New York (1966).
11. Ginzburg, V. L. and Landau, L. D. *J. exp. theor. Phys. (USSR)* **20**, 1064 (1950).
12. Meissner, W. and Ochsenfeld, R. *Naturwissenschaft* **21**, 787 (1933).
13. Lagerwall, S. T., Meyer, R. B., and Stebler, B. *Ann. Phys., Paris* **3**, 249 (1978); Meyer, R. B., Stebler, B., and Lagerwall, S. T. *Phys. Rev. Lett.* **41**, 1393 (1978).

14. Cladis, P. E., and Torza, S. *J. appl. Phys.* **46**, 584 (1975); Cladis, P. E. *Phil. Mag.* **29**, 641 (1974).
15. Bednortz, J. G. and Müller, K. A. *Z. Phys.* **B64**, 189 (1986).
16. Jähnig, F. and Brochard, F. *J. Phys. (Paris)* **35**, 301 (1974).
17. Halperin, B., Lubensky, T. C., and Ma, K. S. *Phys. Rev. Lett.* **32**, 292 (1974).
18. de Vries, A. *Mol. Cryst. liquid Cryst.* **10**, 31 (1970); **10**, 219 (1970); **11**, 361 (1970).
19. McMillan, W. L. *Phys. Rev. A7*, 1419 (1973).
20. Litster, J. D., Als-Nielsen, J., Birgeneau, R. J., Dana, S. S., Davidov, D., Garcia-Golding, F., Kaplan, M., Safinya, C. R., and Schaetzing, R. J. *J. Phys. (Paris)* **40** (Suppl. C3), 339 (1979).
21. Litster, J. D., Birgeneau, R. J., Kaplan, M., Safinya, C. R., and Als-Nielsen, J. In *Ordering in strongly fluctuating condensed matter systems* (ed. T. Riste), p. 357. Plenum, New York (1980).
22. Gruler, H. *Z. Naturforsch.* **28**, 474 (1972).
23. Lubensky, T. C. and Chen, J.-H. *Phys. Rev. A17*, 366 (1978).
24. The isotropic version of the scaling discussion has been given by Brochard, F. *J. Phys. (Paris)* **35**, 301 (1973).
25. Als-Nielsen, J., Birgeneau, R. J., Kaplan, M., Litster, J. D., and Safinya, C. R. *Phys. Rev. Lett.* **39**, 352 (1977).
26. Ocko, B. M., Birgeneau, R. J., Litster, J. D., and Neubert, M. E. *Phys. Rev. Lett.* **52**, 208 (1984). See also reference 50.
27. Cheung, L., Meyer, R. B., and Gruler, H. *Phys. Rev. Lett.* **31**, 349 (1973).
28. Léger, L. and Martinet, A. *J. Phys. (Paris)* **37** (Suppl. C3), 89 (1976).
29. Birecki, H. and Litster, J. D. *Mol. Cryst. liquid Cryst.* **42**, 33 (1977).
30. Von Känel, H. and Litster, J. D. *Phys. Rev. B23*, 363 (1981).
31. Delaye, M., Ribotta, R., and Durand, G. *Phys. Rev. Lett.* **31**, 443 (1973).
32. Garland, C. W., Meichle, M., Ocko, B. M., Kortan, A. R., Safinya, C., Yu, L. J., Litster, J. D., and Birgeneau, R. J. *Phys. Rev. A27*, 3234 (1983).
33. Mohmood, R., Brisbin, D., Khan, I., Gooden, C., Baldwin, A., and Johnson, D. L. *Phys. Rev. Lett.* **54**, 1031 (1985).
34. Alben, R. *Mol. Cryst.* **20**, 231 (1973).
35. Pindak, R., Huang, C.-C., and Ho, J. T. *Phys. Rev. Lett.* **44**, 1461 (1974).
36. Clark, N. A. *Phys. Rev. A14*, 1551 (1976).
37. Ribotta, R. C. R. *Acad. Sci., Paris B279*, 295 (1974).
38. Ricard, L. and Prost, J. *J. Phys. (Paris)* **40** (Suppl. C3), 83 (1979).
39. Ricard, L. and Prost, J. *J. Phys. (Paris)* **42**, 861 (1981).
40. Fisch, M., Sorensen, L. B., and Pershan, P. S. *Phys. Rev. Lett.* **47**, 43 (1981).
41. Fisch, M. R., Pershan, P. S., and Sorensen, L. B. *Phys. Rev. A29*, 2741 (1984).
42. Benzekri, M., Marcerou, J. P., Nguyen, H. T., and Rouillon, J. C. *Phys. Rev. B41*, 9032 (1990); Benzekri, M., Claverie, J., Marcerou, J. P., and Rouillon, J. C. *Phys. Rev. Lett.* **68**, 2480 (1992).
43. Johnson, D. L., Hayes, C. F., de Hoff, R. J., and Schantz, C. A. *Phys. Rev. B18*, 4902 (1978).
44. Brisbin, D., de Hoff, R., Lockhart, T. E., and Johnson, D. L. *Phys. Rev. Lett.* **43**, 1171 (1979).
45. Garland, C. W., Kasting, G. B., and Lushington, K. J. *Phys. Rev. Lett.* **43**, 1420 (1979).

46. Kasting, G. B., Garland, C. W., and Lushington, K. J. *Phys. (Paris)* **41**, 879 (1980).
47. Thoen, J., Marynissen, H., and Van Dael, W. *Phys. Rev.* **A26**, 2886 (1982).
48. Birgeneau, R. J., Garland, C. W., Kasting, G. B., and Ocko, B. M. *Phys. Rev.* **A24**, 2624 (1981); Birgeneau, R. J. and Ocko, B. M. *Z. Phys.* **B62**, 487 (1986).
49. Thoen, J., Marynissen, H., and Van Dael, W. *Phys. Rev. Lett.* **52**, 204 (1984); *Mol. Cryst. liquid Cryst.* **124**, 195 (1985); Stines, K. J. and Garland, C. W. *Phys. Rev.* **A39**, 3148 (1989).
50. Anisimov, M. A., Voronov, V. P., Kulakov, A. O., Petukhov, V. N., and Kholmurodov, F. *Mol. Cryst. liquid Cryst.* **150b**, 399 (1987).
51. Evans-Lutterodt, K. W., Chung, J. W., Ocko, B. M., Birgenau, R. J., Chiang, C., Garland, C. W., Chin, E., Goodby, J., and Tinh, N. H. *Phys. Rev.* **A36**, 1387 (1987).
52. Garland, C. W., Nounesis, G., and Stines, K. J. *Phys. Rev.* **A39**, 4919 (1989); Garland, C. W., Nounesis, G., Stines, K. J., and Heppke, G. *J. Phys. (Paris)* **50**, 2291 (1989).
53. Anisimov, M. A. *Mol. Cryst. liquid Cryst.* **162A**, 1 (1988); Fisher, M. E. *Phys. Rev.* **176**, 257 (1968).
54. Huster, M. E., Stines, K. J., and Garland, C. W. *Phys. Rev.* **A36**, 2364 (1987); Hill, J. P., Keimer, B., Evans-Lutterodt, K. W., Birgenau, R. J., and Garland, C. W. *Phys. Rev.* **A40**, 4625 (1989); Stine, K. J. and Garland, C. W. *Phys. Rev.* **A39**, 4919 (1989).
55. Chen, J.-H., Lubensky, T. C., and Nelson, D. R. *Phys. Rev.* **B17**, 4274 (1978).
56. Dunn, S. G. and Lubensky, T. C. *J. Phys. (Paris)* **42**, 1201 (1981).
57. Hubermann, B. A., Lubkin, D. M., and Doniach, S. *Solid State Commun.* **17**, 485 (1975).
58. Helfrich, W. *J. Phys. (Paris)* **39**, 1199 (1978).
59. Nelson, D. R. and Toner, J. *Phys. Rev.* **B24**, 363 (1981).
60. Dasgupta, C. and Halperin, B. I. *Phys. Rev. Lett.* **47**, 1556 (1981); Dasgupta, C. *J. Phys. (Paris)* **48**, 957 (1987).
61. Toner, J. *Phys. Rev.* **B26**, 462 (1982).
62. Day, A. R., Lubensky, T. C., and McKane, A. J. *Phys. Rev.* **A27**, 1461 (1983).
63. Wilson, K. G. and Kogut, J. *Phys. Rep.* **12**, 77 (1974).
64. Ma, K. S. *Modern theory of critical phenomena*. Benjamin, Reading, Massachusetts (1976).
65. Lubensky, T. C. *J. Chim. Phys.* **80**, 31 (1983).
66. Anisimov, M. A., Voronov, V. P., Gorodetskii, E. E., Podnek, V. E., and Kholmudorov, F. *JETP Lett.* **45**, 425 (1987).
67. Cladis, P. E., Van Saarloos, W. D., Huse, A., Patel, J. S., Goodby, J. W., and Finn, P. L. *Phys. Rev. Lett.* **62**, 1764 (1989).
68. Renn, S. R. and Lubensky, T. C., *Phys. Rev.* **A38**, 2132 (1988).
69. Goodby, J. W., Waugh, M. A., Stein, S. M., Chin, E., Pindak, R., and Patel, J. S. *Nature* **337**, 449 (1989); Srajer, G., Pindak, R., Waugh, M. A., and Goodby, J. W. *Phys. Rev. Lett.* **64**, 1545 (1990).
70. Taylor, T. R., Fergason, J. L., and Arora, S. L. *Phys. Rev. Lett.* **24**, 359 (1970); **25**, 722 (1970).
71. Huang, C. C. and Viner, J. M. *Phys. Rev.* **A25**, 3385 (1982).
72. Thoen, J. and Seynhaeve, G. *Mol. Cryst. liquid Cryst.* **127**, 229 (1985).

73. Meichle, M. and Garland, C. W. *Phys. Rev. A* **27**, 2624 (1983).
74. Anisinov, M. A., Voronov, V. P., Kulkov, A. O., and Kholmurodov, F. *J. Phys. (Paris)* **46**, 2137 (1985).
75. Garov, S. and Meyer, R. B. *Phys. Rev. Lett.* **38**, 848 (1977).
76. Delaye, M. *J. Phys. (Paris) Colloq.* **40** (Suppl. C4), 350 (1979).
77. Galerne, Y. *Phys. Rev. A* **24**, 2284 (1981).
78. Rosenblatt, C. and Litster, J. D. *Phys. Rev. A* **26**, 1809 (1982).
79. Galerne, Y. *J. Phys. (Paris) Lett.* **44**, L461 (1983).
80. Doucet, J., Levelut, A. M., and Lambert, M. *Mol. Cryst. liquid Cryst.* **24**, 317 (1973).
81. Safinya, C. R., Kaplan, M., Als-Nielsen, J., Birgeneau, R., Davidov, D., Litster, J. D., Johnson, D. L., and Neubert, M. *Phys. Rev. B* **21**, 4149 (1980).
82. Cladis, P. E., Guillon, D., Stamatoff, J., Aadsen, D., Neubert, M. E., and Griffith, R. F. *Mol. Cryst. liquid Cryst. Lett.* **49**, 279 (1979).
83. Birgeneau, R. J., Garland, C. W., Kortan, A. R., Litster, J. D., Meichle, M., Ocko, B. M., Rosenblatt, C., Yu, L. J., and Goodby, J. *Phys. Rev. A* **27**, 1251 (1983).
84. Gelerinter, E. and Fryburg, G. C. *Appl. Phys. Lett.* **18**, 84 (1971).
85. Wise, R. A., Smith, D. H., and Doane, J. W. *Phys. Rev. A* **7**, 1366 (1973).
86. Hervet, H., Lagomarsino, S., Rustichelli, F., and Volino, F. *Solid State Commun.* **17**, 1533 (1973).
87. de Gennes, P. G. *C.R. Acad. Sci., Paris* **B274**, 758 (1972).
88. Ginzburg, V. L. *Sov. Phys. Solid State* **2**, 1824 (1960).
89. Benguigui, L. and Martinoty, P. *Phys. Rev. Lett.* **63**, 774 (1989).
90. Dumrograttana, S., Nounesis, G., and Huang, C. C. *Phys. Rev. A* **33**, 2181 (1986); Dumrograttana, S., Huang, C. C., Nounesis, G., Lien, S. C., and Viner, J. M. *Phys. Rev. A* **34**, 5010 (1986).
91. Andereck, B. S. and Swift, J. *Phys. Rev. A* **25**, 1084 (1982).
92. Ribotta, R., Meyer, R. B., and Durand, G. *J. Phys. (Paris) Lett.* **35**, L49 (1974).
93. Galerne, Y. *J. Phys. (Paris)* **46**, 733 (1985).
94. Collin, D., Gallani, J. L., and Martinoty, P. *Phys. Rev. Lett.* **61**, 102 (1988); note that C_p measurements on the same compound as the one studied in this reference show no sign of fluctuations in agreement with arguments developed in reference 89 and Section 10.2.2: Das, P., Ema, K., and Garland, C. W. *Liquid Cryst.* **4**, 205 (1989).
95. Battacharia, S., Cheng, B. Y., Sarma, B. K., and Ketterson, J. B. *Phys. Rev. Lett.* **49**, 1015 (1982).
96. Lien, S. C. and Huang, C. C. *Phys. Rev. A* **30**, 624 (1984).
97. Shashidhar, R., Ratna, B. R., Geetha, G. Nair, and Krishna Prasad, S. *Phys. Rev. Lett.* **61**, 547 (1988). For chiral compounds the physical origin of the discontinuity may, however, be different: Liu, H. Y., Huang, C. C., Bahr, Ch., and Heppke, G. *Phys. Rev. Lett.* **61**, 345 (1988).
98. Bahr, C. and Heppke, G. *Mol. Cryst. liquid Cryst.* **150b**, 313 (1987).
99. Dupont, L., Galvan, J. M., Marcerou, J. P., and Prost, J. *Ferroelectrics* **84**, 317 (1988).
100. Défontaines, A.-D. and Prost, J. *Phys. Rev. E* (in press).
101. Sigaud, G., Hardouin, F., and Achard, M. F. *Solid State Commun.* **23**, 35 (1977).

102. Johnson, D., Allender, D., Dehoff, D., Maze, C., Oppenheim, E., and Reynolds, R. *Phys. Rev.* **B16**, 470 (1977).
103. de Gennes, P. G. *Mol. Cryst. liquid Cryst.* **21**, 49 (1973).
104. Chen, J.-H. and Lubensky, T. C. *Phys. Rev. A* **14**, 1202 (1976).
105. Mukamel, D. and Hornreich, R. M. *J. Phys. C* **13**, 161 (1980).
106. Hornreich, R. M., Luban, M., and Shtrikman, S. *Phys. Rev. Lett.* **35**, 1678 (1975).
107. Brazovskii, S. A. *Zh. esp. teor. Fiz.* **68**, 175 *Sov. Phys. JETP* **41**, 85 (1975).
108. Swift, J. *Phys. Rev. A* **14**, 2274 (1976).
109. de Hoff, R., Bigger, R., Brisbin, D., and Johnson, D. L. *Phys. Rev. A* **25**, 472 (1982).
110. Huang, C. C. and Lien, S. C. *Phys. Rev. Lett.* **56**, 2268 (1981).
111. Thoen, J. and Parret, R. *Liquid Cryst.* **5**, 479 (1989).
112. Witanachi, S., Huang, J., and Ho, J. T. *Phys. Rev. Lett.* **50**, 594 (1983).
113. Safinya, C. R., Martinez-Miranda, L. J., Kaplan, M., Litster, J. D., and Birgeneau, R. J. *Phys. Rev. Lett.* **50**, 56 (1983); Martinez-Miranda, L. J., Kortan, A. R., and Birgeneau, R. J. *Phys. Rev. Lett.* **56**, 2264 (1986); Martinez-Miranda, L. J., Kortan, A. R., and Birgenau, R. J. *Phys. Rev. A* **36**, 2372 (1987).
114. Chu, K. C. and McMillan, W. L. *Phys. Rev. A* **15**, 1181 (1977).
115. Benguigui, L. *J. Phys. (Paris) Colloq.* **40** (Suppl. C3), 419 (1979).
116. Huang, C. C. and Viner, J. M. *Phys. Rev. A* **25**, 3385 (1982).
117. Gorodetskii, E. E. and Podnek, V. E. *Sov. Phys. Crystallogr.* **29**, 618 (1984).
118. Grinstein, G. and Toner, J. *Phys. Rev. Lett.* **51**, 2386 (1984).
119. Grinstein, G., Lubensky, T. C., and Toner, J. *Phys. Rev. B* **33**, 3306 (1986).
120. Brisbin, D., Johnson, D. L., Fellner, H., and Neubert, M. E. *Phys. Rev. Lett.* **50**, 178 (1983).
121. Shashidhar, R., Ratna, B. R., and Krishna Prasad, S. *Phys. Rev. Lett.* **53**, 2141 (1984).
122. Anisimov, M. A. *Mol. Cryst. liquid Cryst.* **162A**, 1 (1988).
123. Gorodetskii, E. E. and Podnek, V. E. *Phys. Lett. A* **136**, 233 (1989).
124. Prost, J. and Pommier, J. *J. Phys. I* **1**, 383 (1991).
125. Young, C. Y., Pindak, R., Clark, N. A., and Meyer, R. B. *Phys. Rev. Lett.* **40**, 773 (1978).
126. Rosenblatt, C., Pindak, R., Clark, N. A., and Meyer, R. B. *Phys. Rev. Lett.* **42**, 1220 (1979).
127. Rosenblatt, C., Meyer, R. B., Pindak, R., and Clark, N. A. *Phys. Rev. A* **21**, 140 (1980).
128. de Gennes, P. G. In *Symposia of the Faraday Society*, no. 5, *Liquid Crystals*, p. 16 (1971).
129. Kosterlitz, J. M. and Thouless, D. J. *J. Phys. C* **6**, 1181 (1973).
130. Kosterlitz, J. M. *J. Phys. C* **7**, 1046 (1974); Kosterlitz, J. M. and Thouless, D. J. *J. Phys. C* **6**, 1181 (1973).
131. Kosterlitz, J. M. and Thouless, D. J. In *Progress in low temperature physics*, Vol. VIIB (ed. D. F. Brewer). North-Holland, Amsterdam (1978).
132. For more details see, for instance, Halperin, B. I. *Proceedings of the Kyoto Summer Institute on Low Dimensional Systems*, Kyoto (1979). *Physics of low dimensional systems* (ed. Nagaoka and S. Hikami), p. 53. Publications Office, Progress of Theoretical Physics, Kyoto, 1979.

133. Nelson, D. and Kosterlitz, J. M. *Phys. Rev. Lett.* **39**, 1201 (1977).
134. Pelcovits, R. A. and Halperin, B. I. *Phys. Rev.* **B19**, 4614 (1979).
135. Abraham, F. F. *Phys. Rep.* **80**, 339 (1981).
136. Tobochnik, J. and Chester, G. W. *Phys. Rev.* **B20**, 3761 (1979).
137. Van Himbergen, J. and Chakravarty, S. *Phys. Rev.* **B23**, 359 (1981).
138. Geer, R., Huang, C. C., Pindak, R., and Goodby, J. W. *Phys. Rev. Lett.* **63**, 540 (1989); Geer, R., Stoebe, T., Huang, C. C., Pindak, R., Goodby, J. W., Cheng, M., Ho, J. T., and Hui, S. W. Letters to *Nature* **355**, 152 (1992).
139. Pindak, R., Moncton, D. E., Davey, S. C., and Goodby, J. W. *Phys. Rev. Lett.* **46**, 1135 (1981).
140. Huang, C. C., Viner, J. M., Pindak, R., and Goodby, J. W. *Phys. Rev. Lett.* **46**, 1289 (1981).
141. Pitchford, T., Nounesis, G., Dumrograttana, S., Viner, J. M., Huang, C. C., and Goodby, J. W. *Phys. Rev.* **A32**, 1938 (1985) and references therein.
142. Aepli, G. and Bruinsma, R. *Phys. Rev. Lett.* **53**, 2133 (1984).
143. Gallani, J. L., Martinoty, P., Guillon, D., and Poeti, G. *Phys. Rev.* **A37**, 3638 (1988).
144. Halperin, B. I. and Nelson, D. R. *Phys. Rev. Lett.* **41**, 121 (1978); Nelson, D. R. and Halperin, B. I. *Phys. Rev.* **B19**, 2457 (1979).
145. Young, A. P. *Phys. Rev.* **B19**, 1855 (1979).
146. Landau, L. D. and Lifshitz, E. M. *Statistical physics*, p. 466. Addison-Wesley, Reading, Massachusetts (1969).
147. Pitchford, T., Huang, C. C., Pindak, R., and Goodby, J. W. *Phys. Rev. Lett.* **57**, 1239 (1986).
148. Geer, R., Huang, C. C., Pindak, R., and Goodby, J. W. *Phys. Rev. Lett.* **63**, 540 (1989).
149. Seliger, J. V. and Nelson, D. *Phys. Rev. Lett.* **61**, 416 (1988).
150. Smith, G. S., Sirota, E. B., Safinya, C. R., and Clark, N. A. *Phys. Rev. Lett.* **60**, 813 (1988).
151. Brock, J. D., Aharony, A., Birgeneau, R. J., Evans-Lutterodt, K. W., and Litster, J. D. *Phys. Rev. Lett.* **57**, 98 (1986).
152. Aharony, A., Birgeneau, R. J., Brock, J. D., and Litster, J. D. *Phys. Rev. Lett.* **57**, 1012 (1986); Brock, J. D., Birgeneau, R. J., Litster, J. D., and Aharony, A. *Contemp. Phys.* **30**, 321 (1989).
153. Garland, C. W., Litster, J. D., and Stines, K. J. *Mol. Cryst. liquid Cryst.* **170**, 71 (1989).
154. Cheng, Ming, Ho John, T., Hui, S. W., and Pindak, R. *Phys. Rev. Lett.* **61**, 550 (1989).
155. Sigaud, G., Hardouin, F., and Achard, M. F. *Phys. Lett.* **72A**, 24 (1979).
156. Sigaud, G., Hardouin, F., Achard, M. F., and Gasparoux, H. *J. Phys. (Paris) Colloq.* **40** (Suppl. C3), 356 (1979).
157. Hardouin, F., Levelut, A. M., Achard, M. F., and Sigaud, G. *J. Chim. Phys.* **80**, 53 (1983).
158. Sigaud, G., Hardouin, F., Achard, M. F., and Levelut, M. *J. Phys. (Paris)* **42**, 107 (1981).
159. Levelut, A. M., Tarento, R. J., Hardouin, F., Achard, M. F., and Sigaud, G. *Phys. Rev.* **A24**, 2180 (1981).

160. Hardouin, F., Nguyen, H. T., Achard, M. F., and Levelut, A. M. *J. Phys. (Paris) Lett.* **43**, L327 (1982).
161. Kosterlitz, J. M., Nelson, D. R., and Fisher, M. E. *Phys. Rev. B* **13**, 412 (1976).
162. Garland, C. In *Geometry and thermodynamics* (ed. J. C. Toledano), p. 251. Plenum, New York (1990).
163. Levelut, A. M. *J. Phys. (Paris) Lett.* **45**, L603 (1984).
164. Nguyen, H. T., Hardouin, F., and Destrade, C. *J. Phys. (Paris)* **43**, 1127 (1982).
165. Hardouin, F., Achard, M. F., Nguyen, H. T. and Sigaud, G. *J. Phys. (Paris) Lett.* **46**, L123 (1984).
166. Cladis, P. E. and Brand, H. *Phys. Rev. Lett.* **52**, 2210 (1984).
167. Ratna, B. R., Shashidhar, R., and Raja, V. N. *Phys. Rev. Lett.* **55**, 1476 (1985).
168. Das, P., Ema, K., Garland, C. W., and Shashidhar, R. *Liquid Cryst.* **4**, 581 (1989).
169. Shashidhar, R. and Ratna, B. R. *Liquid Cryst.* **5**, 421 (1989).
170. Kumar, S., Chen, Li, and Surendranath, V. *Phys. Rev. Lett.* **67**, 322 (1991).
171. Prost, J. *J. Phys. (Paris)* **40**, 581 (1979).
172. Mauzac, M., Hardouin, F., Richard, H., Achard, M. F., Sigaud, G., and Gasparoux, H. *Eur. Polymer J.* **22**, 137 (1986).
173. Prost, J. In *Proceedings of the Conference on Liquid Crystals of One and Two Dimensional Order*, Garmisch Partenkirchen, p. 125. Springer Verlag, Berlin (1980).
174. de Gennes, P. G. *Solid State Commun.* **6**, 163 (1968); see also Meyer, R. B. *Appl. Phys. Lett.* **14**, 208 (1968).
175. Brownsey, G. J. and Leadbetter, A. J. *Phys. Rev. Lett.* **44**, 1608 (1980).
176. Wang, J. and Lubensky, T. C. *Phys. Rev. A* **29**, 2210 (1984).
177. Chan, K. K., Pershan, P., Sorensen, L. B., and Hardouin, F. *Phys. Rev. Lett.* **54**, 1694 (1985); *Phys. Rev. A* **34**, 1420 (1986).
178. Chiang, C. and Garland, C. W. *Mol. Cryst. liquid Cryst.* **122**, 25 (1985); Garland, C. W., Chiang, C., and Hardouin, F. *Liquid Cryst.* **1**, 81 (1986).
179. Huse, D. A. *Phys. Rev. Lett.* **55**, 2228 (1985); Anisimov, M. A., Voronel, A. V., and Gorodetskii, E. E. *Sov. Phys. JETP* **33**, 605 (1971).
180. Barois, P., Coulon, C., and Prost, J. *J. Phys. (Paris) Lett.* **42**, L107 (1981).
181. Prost, J. and Barois, P. *J. Chim. Phys.* **80**, 65 (1983).
182. Barois, P., Pommier, J., and Prost, J. In *Solitons in liquid crystals* (ed. L. Lam and J. Prost), Chapter 6. Springer Verlag, Berlin (1991).
183. Safinya, S. R., Varady, W. A., Chiang, L. Y., and Dimon, P. *Phys. Rev. Lett.* **57**, 432 (1986).
184. Barois, P. *Phys. Rev. A* **33**, 5008 (1987).
185. Fontes, E., Heiney, P. A., Barois, P., and Levelut, A. M. *Phys. Rev. Lett.* **60**, 1138 (1988). See also Fontes, E., Lee, W. K., Heiney, P. A., Nounesis, G., Garland, C. W., Riera, A., McCauley, J. P., and Smith III Jr., A. B. *J. chem. Phys. (In press)*.
186. Barois, P. Unpublished D.Phil. thesis, no. 875, Bordeaux (1986).
187. Barois, P., Prost, J., and Lubensky, T. C. *J. Phys. (Paris)* **46**, 391 (1985).
188. Ema, K., Garland, C. W., Sigaud, G., and Nguyen, H. T. *Phys. Rev. A* **39**, 1369 (1989).
189. Cladis, P. E. *Phys. Rev. Lett.* **35**, 48 (1981).
190. Cladis, P. E. *Cryst. liquid Cryst.* **67**, 833 (1981).
191. Gorodetskii, E. E. and Podnek, V. E. *JETP Lett.* **39**, 624 (1984).

192. Prost, J. *Adv. Phys.* **33**, 1 (1984).
193. Raja, V. N., Shashidhar, R., Ratna, B. R., Heppke, G., and Bahr, Ch. *Phys. Rev. A* **37**, 303 (1988).
194. Ema, K., Nounesis, G., Garland, C. W., and Shashidhar, R. *Phys. Rev. A* **39**, 2599 (1989).
195. Prost, J. In *From crystalline to amorphous* (ed. C. Godrèche), p. 273. Les Editions de Physique, Paris (1988).
196. Prost, J. and Toner, J. *Phys. Rev. A* **36**, 5008 (1987).
197. Shashidhar, R., Ratna, B. R., Krishna Prasad, S., Somesekhara, S., and Heppke, G. *Phys. Rev. Lett.* **59**, 1209 (1987).
198. Park, Y., Lubensky, T. C., Barois, P., and Prost, J. *Phys. Rev. A* **37**, 2197 (1988).
199. Prost, J., Pommier, J., Rouillon, J. C., Marcerou, J. P., Barois, P., Benzekri, M., Babeau, A., and Nguyen, H. T. *Phys. Rev. B* **42**, 2521 (1990).
200. Jeong, Y., Nounesis, G., Garland, C. W., and Shashidhar, R. *Phys. Rev. A* **40**, 4022 (1989).
201. Hardouin, F., Achard, M. F., Nguyen, H. T., and Sigaud, G. *Mol. Cryst. liquid Cryst. Lett.* **3**, 7 (1986).
202. Dowell, F. *Phys. Rev. A* **28**, 3526 (1983); **31**, 2464 (1985); **31**, 3214 (1985).
203. Pershan, P. S. and Prost, J. *J. Phys. (Paris) Lett.* **40**, L27 (1979).
204. Longa, L. and de Jeu, W. H. *Phys. Rev. A* **26**, 1632 (1982).
205. Longa, L. and de Jeu, W. H. *Phys. Rev. A* **28**, 2380 (1983).
206. Mirantsev, L. V. *Mol. Cryst. liquid Cryst.* **133**, 151 (1986).
207. Berker, A. N. and Walker, J. S. *Phys. Rev. Lett.* **47**, 1469 (1981).
208. Indekeu, J. O. and Berker, A. N. *Phys. Rev. A* **33**, 1158 (1986).
209. Indekeu, J. O. and Berker, A. N. *J. Phys. (Paris)* **49**, 353 (1988).
210. Houtappel, R. F. M. *Physica* **16**, 425 (1950).
211. Indekeu, J. O., Berker, A. N., Chiang, C., and Garland, C. W. *Phys. Rev. A* **35**, 1371 (1987).
212. Ratna, B. R., Shashidhar, R., and Rao, K. V. In *Proceedings of the International Liquid Crystal Conference, Bangalore* (ed. S. Chandrasekhar), p. 135. Heyden, London (1980); Benguigui, L. and Hardouin, F. *J. Phys. (Paris) Lett.* **42**, LIII (1981); Legrand, C., Parneix, J. P., Chapoton, A., Nguyen, T., and Destrade, C. *Mol. Cryst.* **124**, 277 (1985).
213. Madhusudana, N. V. and Jyotsna Rajan. *Liquid Cryst.* **7**, 31 (1990).

AUTHOR INDEX

- Aadsen, D. 581
Abbot, A. 197
Abe, S. 407
Abragam, A. 94, 250, 261
Abraham, F. F. 583
Achard, M. F. 40, 581, 583, 584, 585
Adams, J. 161, 333, 334
Aeppli, G. 583
Aharony, A. 583
Alben, R. 70, 83, 95, 96, 333, 579
Alcantara, J. 148
Alexander, E. 40
Alexander, S. 39, 89, 97
Allain, M. 469, 505
Allender, D. 582
Als-Nielsen, J. 40, 579, 581
Andereck, B. S. 581
Anderson, G. 406
Anderson, P. W. 336
Anisimov, M. A. 96, 578, 580, 581, 582, 584
Armitage, D. 335
Arnould, H. 334, 335
Arora, S. L. 580
Atkin, R. J. 260
Atten, P. 96
- Babeau, A. 585
Bacri, J. C. 464
Baessler, H. 283, 333, 334
Bahadur, B. 40
Bahr, Ch. 581, 585
Bak, C. S. 407
Baldwin, A. 579
Barois, P. 584, 585
Bartolino, R. 340, 405, 464, 465, 505
Barton, J. 40
Barton, L. 260, 262
Battacharia, S. 465, 581
Baumann, C. 465
Baur, G. 197
Bean, C. P. 578
Beauvais, de, F. 262
Bednortz, J. G. 579
Belyakov, V. A. 335, 407
- Benattar, J. J. 40
Benedek, G. 260
Benguigui, L. 581, 582, 585
Benoit, H. 39
Benzekri, M. 579, 585
Beresnev, L. A. 407
Bergman, D. J. 578
Berker, A. N. 585
Berreman, D. W. 161, 279, 333, 336, 407
Bevers 95
Bidaux, R. 505
Bigger, R. 582
Billard, J. 39, 40, 97, 276, 333, 405
Birecki, H. 406, 464, 579
Birgeneau, R. J. 40, 579, 580, 581, 582, 583
Bishop, D. J. 405
Blech, I. 39
Blinc, R. 261, 262, 406
Bilnov, L. M. 407
Blümel, Th. 335
Boccaro, N. 39, 505
Boix, M. 161
Boltenhagen, P. 405
Borel, J. 105
Bouchiat, M. 147, 161, 162, 336
Bouligand, Y. 183, 190, 197, 309, 335, 502,
 504, 506
Boxtel, van, A. 262
Bradberry, G. W. 465
Brand, H. R. 405, 464, 465, 555, 584
Brand, P. 40
Brazowskii, S. A. 335, 582
Brière, G. 262
Brinkman, W. F. 336
Brisbin, D. 579, 582
Brochard, F. 97, 105, 130, 161, 189, 197, 224,
 225, 260, 295, 334, 464, 465, 579
Brock, J. D. 583
Brown, G. H. 38, 39
Brown, G. S. 405
Brownsey, G. J. 584
Bruinsma, R. 583
Brun, L. 102
Brunet, M. 406, 407, 505
Bucher, H. 261

- Cabane, B. 95, 261
 Cagnon, M. 405, 465
 Caillé, A. 40
 Candeau, S. 187, 197, 213, 216, 217, 260, 262, 334
 Cano, R. 271, 278, 310, 318, 333, 334
 Carr, E. F. 135, 161, 237, 261
 Casagrande, C. 97
 Castello, M. J. 505
 Chakravarty, S. 583
 Chan, J. W. 39
 Chan, K. K. 584
 Chandani, A. D. L. 407
 Chandrasekhar, S. 39, 95, 261, 473, 505,
 Chapoton, A. 585
 Charvolin, J. 95
 Chatelain, P. 109, 114, 139, 140, 148, 161, 334
 Chen, Jing-Huei 535, 579, 580, 582
 Chen, Li 566, 584
 Cheng, B. Y. 581
 Cheng, J. 334
 Cheng, Ming 583
 Chernova, N. I. 407
 Chester, G. W. 583
 Cheung, L. 579
 Chiang, C. 580, 584, 585
 Chiang, L. Y. 406, 584
 Chin, E. 580
 Chistiakov, I. G. 39
 Chou Cheung, L. 334
 Chu, B. 96
 Chu, K. C. 582
 Chuen-Shyr 95
 Chung, J. W. 580
 Ciferri, A. 39
 Cladis, P. E. 105, 161, 182, 196, 197, 260, 319, 335, 445, 465, 555, 568, 576, 579, 580, 581, 584
 Clark, N. A. 40, 95, 96, 335, 354, 360, 397, 405, 406, 407, 441, 464, 465, 505, 579, 582, 583
 Clarke, W. G. 95, 261
 Claverie, J. 579
 Clerc, J. F. 40
 Coles, H. J. 96
 Collet, A. 39
 Collett, J. 406
 Collin, D. 405, 465, 581
 Constant, E. 96
 Constant, M. 96
 Cotter, M. 65, 95
 Couder, Y. 465
 Coulon, C. 584
 Creagh, L. T. 161
 Crissey, J. 333
 Crooker, P. P. 335, 336
 Currie, P. K. 260
 Dafermos, C. 196
 Dahl, I. 379, 405, 406, 407
 Dana, S. S. 579
 Das, p. 584
 Dasgupta, C. 580
 Davey, S. C. 40, 405, 406, 583
 Davidov, D. 579, 581
 Day, A. R. 580
 Debeauvais, F. 197
 Decoster, D. 96
 Défontaines, A. D. 581
 Dehoff, D. 582
 Delaye, M. 364, 406, 464, 579, 581
 Deloche, B. 50, 51, 95
 Demus, D. 38, 40
 Destrade, C. 39, 95, 96, 584, 585
 Deuling, H. 161
 Diehl, P. 48, 95
 Diele, S. 40
 Dierker, S. B. 481, 505
 Dijon, J. 40
 Dimic, V. 262
 Dimon, P. 584
 Dmitrienko, V. E. 335, 407
 Doane, J. W. 39, 247, 261, 262, 581
 Dolphin, D. 285, 334
 Domon, M. 97
 Donald, A. M. 95
 Doniach, S. 580
 Doucet, J. 405, 581
 Dowell, F. 585
 Dreyer, J. F. 95, 164
 Dubois, J. C. 405
 Dubois Violette, E. 197, 244, 245, 253, 261, 336, 505
 Duke, R. 406
 Dumrograttana, S. 406, 581, 583
 Dunmur, D. A. 96
 Dunn, S. G. 580
 Dupont, L. 581
 Durand, G. 104, 105, 162, 234, 240, 241, 260, 262, 334, 354, 364, 405, 406, 464, 465, 504, 505, 579, 581
 Eden, D. 262
 Ema, K. 584, 585
 Emsley, J. W. 48, 95
 Englert, G. 94, 95
 Ennulat, R. 333, 334
 Eppenga, R. 75, 96
 Erickson, J. L. 99, 103, 107, 150, 160, 162, 196, 199, 219, 220, 259, 260
 Ermakov, V. P. 407
 Etherington, G. 40
 Evans-Lutterodt, K. W. 580, 583
 Evereva, G. 261

- Fan, C. P. 96, 334
 Farinha Martins, A. 259, 261, 262
 Fauré, M. 40
 Felici, N. 261
 Fellner, H. 582
 Fergason, J. L. 39, 130, 279, 281, 333, 334, 580
 Filev, V. M. 96
 Filippini, J. C. 96
 Finkelman, H. 95, 97
 Finn, P. L. 580
 Fisch, M. R. 579
 Fischer, F. 105
 Fishel, D. 261
 Fisher, J. 218, 219, 260
 Fisher, M. E. 506, 580, 584
 Flack, J. H. 335
 Flannery, J. B. 161, 334
 Flory, P. J. 63, 95
 Fonsek, J. 407
 Fontes, E. 584
 Ford, G. W. 261
 Forster, D. 162, 259
 Frank, F. C. 99, 103, 160, 163, 166, 170, 196
 Franklin, W. 251, 262
 Frederiks, V. K. 34, 40, 124, 135, 160
 Frederikson, A. G. 260, 262
 Freiser, M. J. 71, 96
 Frenkel, D. 75, 96
 Freund, L. 39
 Friedel, E. 18, 39
 Friedel, G. 10, 15, 18, 39, 163, 165, 168, 171,
 183, 196, 227, 260, 309, 335, 358, 406, 466,
 504
 Friedel, J. 169, 180, 196, 197, 313, 317, 318,
 335, 472, 505
 Fryburg, G. C. 581
 Fukuda, A. 407
- Gahwiller, J. 213, 260
 Galerne, Y. 20, 39, 96, 105, 199, 262, 581
 Gallani, J. L. 405, 465, 581, 583
 Galvan, J. M. 407, 581
 Garcia-Golding, F. 579
 Garland, C. W. 262, 519, 579, 580, 581, 583,
 584, 585
 Garov, S. 20, 39, 406, 407, 581
 Gaspard, F. 261, 262
 Gasparoux, H. 39, 95, 96, 105, 161, 260, 334,
 583, 584
 Gautherie, M. 333
 Geer, R. 583
 Geetha, G. Nair 581
 Gelbart, W. M. 96
 Gelerinter, E. 581
 Gennes, de, P. G. 95, 96, 161, 196, 197, 260,
 261, 262, 291, 293, 334, 335, 405, 406, 464,
 505, 578, 581, 582, 584
 Genova, D. 261
 George, K. L. 96
 Gerritsma, G. 129, 161, 304, 334
 Gharbia, M. 405, 465
 Giannessi, C. 39
 Ginzburg, V. L. 578, 581
 Gladstone, G. 261
 Glogarova, M. 407, 505
 Gohin, A. 96
 Goldberg, N. 39, 333
 Goldmacher, J. 334, 335
 Golombok, R. 95
 Goodby, J. W. 38, 40, 406, 580, 581, 583
 Gooden, C. 579
 Gorodetskii, E. E. 580, 582, 584
 Gosh, S. 261
 Gramsbergen, E. F. 87, 96
 Grandjean, F. 109, 160, 163, 227, 310, 335, 504
 Gratias, D. 39
 Gray, G. W. 38, 40, 92
 Grebel, H. R. 336
 Griffith, R. F. 581
 Grinstein, G. 40, 452, 465, 582
 Groot, de, S. 200, 204, 207, 260, 464
 Grubel, W. 161
 Gruler, H. 105, 135, 160, 161, 186, 261, 579
 Guazzelli, E. 505
 Guillou, D. 581, 583
 Gulari, E. 96
 Gulik-Krzywicki, T. 40, 505
 Gutowsky, H. S. 94
 Guyon, E. 40, 105, 161, 212, 225, 245, 260, 261,
 448, 465
- Haas, W. 161, 333, 334
 Haller, I. 105, 161, 260, 261
 Halperin, B. I. 40, 505, 522, 548, 578, 579, 580,
 582, 583
 Handschy, M. A. 335, 407
 Hansen, J. 334
 Hardouin, F. 40, 581, 583, 584, 585
 Hareng, M. 406
 Hayes, C. F. 579
 Heilmeier, G. 230, 239, 260, 261, 262, 300, 301,
 304, 334, 335
 Heilmeier, G. H. 40
 Heiney, P. A. 584
 Helfrich, W. 39, 80, 96, 130, 136, 161, 188, 197,
 230, 237, 238, 239, 261, 292, 297, 299, 301,
 302, 304, 334, 363, 406, 464, 580
 Heppke, G. 406, 580, 581, 585
 Herino, R. 261, 262
 Herrmann, K. 40
 Hervet, H. 581
 Hessel, F. 95
 Hewitt, R. C. 260
 Hiji, N. 407

- Hill, J. P. 580
 Hiltrop, K. 335
 Hinshar, Jr., G. A. 406
 Ho, J. T. 579, 582, 583
 Hoff, de, R. J. 579, 582
 Hogenboom, D. 261
 Horn, R. G. 465
 Hornreich, R. M. 39, 335, 336, 582
 Houtappel, R. F. M. 577, 585
 Huang, C. C. 406, 579, 580, 581, 582, 583
 Huang, J. 582
 Hubermann, B. A. 580
 Huggins, H. A. 161
 Hui, S. W. 583
 Hulin, J. P. 334, 406
 Humphries, R. L. 52, 95
 Hurault, J. P. 292, 334
 Huse, D. A. 580, 584
 Huster, M. E. 580
- Iizuka, K. 334
 Imura, H. 262
 Indekeu, J. O. 585
 Indenbom, V. L. 406
 Indovina, E. 261
 Ishihara, A. 95
 Itachi, C. 40
- Jähnig, F. 250, 259, 262, 578
 James, P. G. 52, 95
 Janik, J. A. 262
 Janik, J. M. 262
 Janovec, V. 407
 Jen, S. 53, 95
 Jenkins, J. T. 287, 334
 Jeong, Y. 585
 Jérôme, D. 95
 Jeu, de, W. H. 96, 129, 161, 464, 585
 Joanicot, M. 335
 Johnson, D. L. 221, 261, 579, 581, 582
 Johnson, J. F. 260, 334
 Johnson, P. L. 335
 Jouffroy, J. 97
 Jyostsna Rajan, 585
- Kahn, F. J. 334, 369, 406
 Kaneko, E. 40
 Kaplan, M. 40, 579, 581, 582
 Kapustin, A. 261, 262
 Kashnow, R. 240
 Kassubeck, G. 333
 Kast, W. 38
 Kastelejn, P. W. 95
 Kasting, G. B. 579, 580
 Kats, E. I. 405, 465
- Keilmann, F. 334
 Keimer, B. 580
 Kelker, H. 92, 335
 Keller, P. 39, 448, 464, 465
 Kemp, K. 262
 Ketterson, J. B. 464, 465, 581
 Keyes, P. H. 96
 Khalatnikov, I. 249, 262
 Khan, I. 579
 Khetrapel, C. L. 48, 95
 Kholmurodov, F. J. 578, 580, 581, 582
 Kiry, F. 465
 Klapperstruck, M. 40
 Kleman, M. 169, 182, 194, 196, 197, 313, 317,
 318, 335, 405, 464, 465, 475, 477, 478, 491,
 492, 495, 502, 504, 505, 506
 Klingbeil, R. 261
 Kmetz, A. R. 161
 Knobler, C. 97
 Koehler, J. S. 505
 Koelmans, H. 262
 Kogut, J. 97, 580
 Kohil, M. 95
 Kortan, A. R. 579, 581, 582
 Korzhenevskii, A. L. 97
 Kosterlitz, J. M. 541, 582, 583, 584
 Kramer, K. 334
 Krigbaum, W. R. 39
 Krishna Prasad, S. 581, 582, 585
 Kruger, A. 161
 Kuczynski, W. 406
 Kugler, M. 336
 Kulkov, A.O. 578, 580, 581, 582
 Kumar, S. 566, 584
 Kuze, E. 407
- Labes, M. M 262, 283, 334, 407
 Labrunie, G. 105
 Largerwall, S. R. 40, 379, 397, 405, 406, 407,
 476, 477, 505, 578
 Lagomarsino, S. 581
 Lalanne, J. R. 96, 262
 Lambert, M. 40, 581
 Landau, L. D. 40, 77, 95, 96, 160, 161, 249,
 260, 262, 333, 334, 465, 505, 506, 548, 578,
 583
 Langer, J. S. 506
 Langer, S. A. 406
 Langevin, D. 39, 147, 161, 162, 260, 336
 Lanning, J. L. 161
 Larkin, A. I. 96
 Lavrentovich, O. D. 405, 505
 Leadbetter, A. J. 40, 584
 Le Barny, P. 405
 Lebedev, V. V. 465
 Leberre, S. 406
 Lee, H. 407
 Lee, J. 262

- Lee, W. K. 584
 Léger, L. 104, 105, 190, 191, 197, 224, 260, 261,
 334, 434, 465, 579
 Legrand, C. 585
 Lehmann, O. 161, 307, 335
 Lejček, L. 407, 505
 Leonard, M. 95
 LeRoy, P. 197
 Leslie, F. M. 161, 199, 259, 260, 294, 300, 305,
 307, 334, 335
 Letcher, S. V. 262, 465
 Levelut, A. M. 26, 27, 40, 95, 333, 581, 583, 584
 Levinson, P. 97
 Levy, M. 39
 Liang, K. S. 406
 Liao, Y. 464
 Lieb, E. H. J. 95
 Lieberman, E. 262
 Liebert, L. 20, 39, 95, 335
 Lien, S. C. 581, 582
 Lifshitz, E. M. 95, 160, 161, 260, 262, 333, 334,
 465, 505, 506, 548, 583
 Lin, L. 39, 97
 Lindon, J. C. 48, 95
 Link, V. 40
 Litster, J. D. 40, 96, 260, 262, 406, 464, 579,
 581, 582, 583
 Liu, H. Y. 581
 Liu, M. 464
 Lockhart, T. E. 579
 London, F. 578
 Longa, L. 96, 585
 Lord, A. E. 262
 Luban, M. 582
 Lubensky, T. C. 97, 162, 247, 259, 261, 293,
 464, 522, 525, 535, 569, 578, 579, 580, 582,
 584, 585
 Lubkin, D. M. 580
 Luckhurst, G. R. 52, 95, 224, 260, 334
 Lushington, K. J. 579, 580
 Lüthi, B. 262
 Luzzati, V. 39, 40
- Ma, K. S. 522, 579, 580
 McCauley, J. P. 584
 McColl, J. 95, 96
 McKane, A. J. 580
 MacLennan, J. F. 407
 McMillan, W. L. 507, 578, 579, 582
 McMullen, W. E. 96
 Madhusudana, N. V. 96, 585
 Magne, M. 333
 Maier, W. 96, 161, 245, 261
 Malthête, J. 39, 95
 Mamnitskii, V. M. 96
 Marcerou, J. P. 96, 405, 465, 579, 581, 585
 March, D. 334
- Marcus, M. 335
 Martianova, L. 262
 Martin, A. J. 261
 Martin, P. C. 161, 162, 216, 259, 408, 423, 464,
 465
 Martinand, J. L. 105, 162, 260
 Martinet, A. 197, 434, 465, 579
 Martinez-Miranda, L. J. 582
 Martinot-Lagarde, Ph. 404, 406, 407
 Martinoty, P. 213, 216, 217, 260, 262, 334,
 405, 465, 581, 583
 Martire, D. E. 95
 Marynissen, H. 96, 578, 580
 Mathieu, J. P. 278, 333
 Mattis, D. C. 39
 Mauguin, C. 99, 108, 126, 127, 160, 161, 179,
 227, 268, 279, 333
 Mauzac, M. 584
 Maze, C. 582
 Mazenko, G. F. 405, 465
 Mazur, P. 200, 204, 207, 260, 464
 Meadows, M. R. 407
 Meiboom, S. 260, 334, 336
 Meichle, M. 579, 581
 Meier, G. 135, 160, 161, 197, 245, 261, 333
 Meisner, W. 578
 Mermin, N. D. 335, 336
 Meunier, J. 39
 Meyer, R. B. 20, 22, 39, 127, 133, 134, 158, 161,
 178, 182, 183, 184, 186, 190, 194, 196, 197,
 224, 253, 260, 291, 334, 376, 405, 406, 465,
 476, 505, 578, 579, 581, 582, 584
 Miesowicz, M. 210, 211, 260
 Migliori, A. 261
 Milkovich, R. 39
 Milner, S. T. 465
 Mirantsev, L. V. 585
 Mitchell, G. R. 95
 Miyano, K. 95, 464
 Miyasato, K. 407
 Mohmood, R. 579
 Moll 147, 162
 Moncton, D. E. 40, 405, 406, 583
 Mondon, F. 261, 262
 Moon, F. 262
 Moussa, F. 40
 Mukamel, D. 582
 Muljani, Z. 334
 Mullen, M. 262
 Muller, J. H. 334
 Müller, K. A 579
 Murphy, J. A. 262
- Nabarro, F. R. N. 184, 197
 Nadalin, R. 39, 333
 Nallet, F. 505
 Neff, V. D. 39

- Nehring, J. 95
 Nelson, D. R. 39, 40, 97, 336, 496, 505, 548,
 580, 583, 584
 Neubert, M. E. 579, 581, 582
 Nguyen, H. T. 39, 95, 579, 584, 585
 Nickerson, M. 261
 Nishiyama, S. I. 407
 Nolle, A. W. 261
 Nolm, C. H. 94
 Nounesis, G. 519, 580, 581, 583, 584, 585
- Ochsenfeld, R. 578
 Ocko, B. M. 579, 580, 581
 Oh, C. S. 39
 Okano, K. 262
 Okaya, A. 334
 Oldano, C. 407
 Onsager, L. 59, 61, 95, 578
 Onusseit, H. 335
 Oppenheim, E. 582
 O'Reilly, D. 261
 Orlov, V. 407
 Ornstein 147, 162
 Oseen, C. W. 99, 103, 160, 279, 307, 333, 335
 Ostrovski, B. I. 407
 Oswald, P. 405, 465, 485, 502, 505, 506
 Otnes, K. 95, 262
 Ouchi, Y. 407
- Palierne, J. F. 405, 406
 Pansu, B. 336
 Papoular, M. 161
 Park, Y. 585
 Parmar, D. S. 407, 505
 Parneix, J. P. 585
 Parodi, O. 158, 197, 199, 206, 244, 253, 259,
 261, 407, 408, 423, 464, 465, 505
 Parret, R. 582
 Patel, J. S. 580
 Patel, P. 566
 Pavel, J. 407, 505
 Peach, M. 505
 Peierls, R. E. 40
 Pelcovits, R. A. 40, 406, 452, 465, 583
 Penrose, O. 578
 Penz, P. A. 261
 Pershan, P. S. 39, 95, 162, 259, 405, 406, 408,
 423, 464, 489, 494, 495, 505, 579, 584, 585
 Peterson, E. 261
 Petschek, R. G. 406
 Petukhov, V. N. 580
 Pieranski, P. 40, 105, 161, 167, 196, 212, 225,
 245, 260, 261, 335, 448, 465
 Pikin, S. A. 406
 Pinard, P. 333
 Pincus, P. 95, 247, 261, 334
- Pindak, R. 40, 405, 406, 465, 505, 579, 580,
 582, 583
 Pirš, J. 262
 Pitchford, T. 583
 Pleiner, H. 405, 464, 465
 Pochan, J. 334
 Podneks, V. E. 580, 582, 584
 Poeti, G. 583
 Poggi, Y. 96
 Pomeau, Y. 304, 335
 Pommier, J. 582, 584, 585
 Pontikis, V. 105
 Porsch, F. 335
 Porter, R. S. 218, 260, 334
 Pouligny, B. 96
 Press, M. 197
 Price, F. P. 335
 Priest, R. G. 97
 Priestley, E. B. 95
 Prost, J. 96, 105, 161, 260, 262, 307, 334, 335,
 405, 406, 407, 464, 465, 505, 506, 579, 581,
 582, 584, 585
 Proust, J. E. 161
 Pynn, R. 95
- Rabinovich, A. Z. 407
 Raioni, A. 197
 Raja, V. N. 95, 584, 585
 Ramaswamy, S. 405, 465
 Rameska, S. 95
 Ranoni, L. 262
 Rao, K. V. 585
 Rapini, A. 161, 197, 216, 242, 406
 Ratna, B. R. 95, 555, 581, 582, 584, 585
 Rault, J. 166, 182, 190, 196, 197, 310, 319, 320,
 335
 Rayleigh, Lord 406
 Regaya, B. 105, 161, 334
 Renn, S. R. 525, 580
 Reynolds, R. 582
 Ribotta, R. C. R. 364, 406, 464, 579, 581
 Ricard, L. 464, 579
 Richard, H. 584
 Rieker, T. P. 407, 505
 Riera, A. 584
 Riste, T. 95, 262
 Robert, J. 105
 Robin, Y. 96
 Robinson, C. 39, 95
 Rodbell, D. 578
 Rondelez, F. 104, 105, 261, 292, 305, 334, 406,
 464, 507, 578
 Rose, P. I. 161
 Rosenblatt, C. S. 97, 406, 505, 581, 582
 Rouillon, J. C. 405, 465, 579, 585
 Roux, D. 464
 Rowell, J. C. 95

- Ryschenkov, G. 194, 197
 Rustichelli, F. 581
- Sackmann, E. 289, 334
 Sackmann, S. 40
 Sadashiva, D. K. 39, 95, 505
 Safinya, C. R. 40, 406, 407, 464, 505, 579, 581, 582, 583, 584
 Sakamoto, K. 298, 334
 Salin, D. 464
 Saludjan, P. 39
 Sammon, M. 336
 Sarma, B. K. 581
 Sarma, G. 505
 Saupe, A. 39, 50, 58, 67, 94, 95, 96, 104, 160, 197, 245, 261, 346, 405
 Savithramma, K. L. 96
 Schadt, M. 96, 136, 161
 Schaetzing, R. J. 406, 464, 579
 Schechter, E. 40
 Scheffler, T. J. 160, 186, 279, 333
 Schmidt, D. 136, 161
 Schmidt, M. 259
 Schroder, I. 92, 97
 Selawry, O. 333
 Selinger, J. V. 583
 Sethna, J. P. 336, 406
 Seynhaeve, G. 580
 Sèze, de, L. 505
 Shabanov, V. G. 407
 Shalaev, B. N. 97
 Shashidhar, R. 519, 581, 582, 584, 585
 Shaw, G. H. 38
 Shechtman, D. 39
 Shen, Y. R. 96, 97, 262
 Shih, C. S. 95, 96
 Shtrikman, S. 39, 129, 161, 335, 336, 582
 Shulka, P. 96
 Sigaud, G. 40, 90, 551, 581, 583, 584, 585
 Sirota, E. B. 40, 406, 407, 505, 583
 Skarp, K. 406
 Skoulios, A. E. 39
 Sluckin, T. J. 96
 Smith III Jr., A. B. 584
 Smith, D. H. 581
 Smith, G. S. 40, 407, 505, 583
 Smith, H. J. 260, 334
 Snyder, L. C. 95, 334
 Somesekhara, S. 585
 Sonin, A. S. 407
 Sorensen, L. B. 406, 579, 584
 Sorkin, E. L. 96
 Sosnovskii, A. 40, 104, 260
 Spach, G. 39
 Spegt, P. A. 39
 Spence, R. D. 94
 Sprenger, W. O. 405
 Srager, G. 580
 Srikanta, B. C. 95
 Stamatoff, J. 581
 Stanley, H. E. 197
 Stebler, B. 406, 476, 505, 578
 Stegemeyer, H. 335
 Stein, S. M. 580
 Stephen, M. J. 96, 259, 262
 Stieb, A. 197
 Stine, K. J. 580, 583
 Stinson, T. W. 96, 262
 Stoebe, T. 583
 Strukov, B. A. 407
 Strutt, J. W. 406
 Strzelecki, L. 39, 95, 335
 Surendranath, V. 584
 Suresh, K. A. 39, 505
 Svedberg, T. 233, 251, 261, 262
 Swift, J. 162, 259, 581, 582,
 Szwarc, M. 39
 Tajbakhsh, A. 40
 Takezoe, H. 407
 Tanimoto, K. 336
 Tardieu, A. 40
 Tarr, C. 261
 Tarento, R. J. 583
 Taupin, D. 333
 Taylor, T. R. 580
 Teaney, D. 261
 Ter-Minassian, L. 161
 Tettamanti, E. 261
 Thoen, J. 96, 578, 580, 582
 Thouless, D. J. 541, 582
 Tinh, N. H. 580
 Tobochnik, J. 583
 Toner, J. 39, 97, 336, 405, 465, 496, 505, 580, 582
 Tsvetkov, V. N. 34, 40, 223, 224, 237, 260
 Urbach, W. 39, 161
 Van Dael, W. 96, 578, 580
 Van Doorn, D. 129, 161
 Van Himbergen, J. 583
 Van Laar, J. J. 92, 97
 Van Raulte, J. 40
 Van Saarloos, W. D. 580
 Van Winkle, D. H. 360, 406, 505
 Varady, W. A. 406, 584
 Vaucher, C. 405
 Vaughan, J. M. 465
 Veysse, M. 97, 104, 105, 262, 334
 Vieillard-Baron, J. 66, 96
 Vigman, P. B. 96
 Vilfan, M. 247, 261, 262

- Vincy, C. 95
Vinen, W. F. 506
Viner, J. M. 580, 581, 582, 583
Visintainer, J. 261
Vitek, B. 197
Vohra, S. T. 335
Volino, F. 581
Von Känel, H. 579
Voronel, A. V. 584
Voronov, V. P. 578, 580, 581, 582
Vries, de, A. 514, 579
Vries, de, H. 272, 279, 333
Vtyupin, A. N. 407
- Wadati, M. 95
Whal, J. 105, 218, 219, 260
Walker, J. S. 585
Wang, J. 584
Wang, X. J. 40
Ward 95
Waugh, M. A. 580
Williams, C. E. 105, 194, 197, 406, 467, 478,
 491, 492, 504, 505
Williams, R. 40, 176, 181, 183, 196, 197, 233,
 261
Williamson, R. 262
Wilson, K. G. 90, 97, 580
Windle, A. H. 95
Wise, R. A. 581
- Witanachi, S. 582
Wolff, U. 161
Wong, G. 96, 97
Wong, W. 262
Wright, D. C. 335, 336
Wysocki, J. 334
- Yamashita, M. 505
Yeates, R. N. 95
Yin, G. 262
Young, A. P. 548, 583
Young, C. Y. 375, 405, 406, 465, 582
Young, W. 261
Yu, L. J. 39, 50, 95, 407, 579, 581
Yue, J. 407
Yun, C. K. 230, 260
- Zann, A. 405
Zanoni, J. 40, 260
Zanten, van, P. 129, 161, 334
Zaprudskii, V. M. 96
Zaschke, H. 38, 40
Zecks, B. 406
Zimmerman, H. 39
Zocher, H. 99, 120, 125, 160
Zolina, V. 40, 160
Zupančič, I. 262
Zvetkov, V. 104, 135, 160, 262

SUBJECT INDEX

acoustic waves 213–18, 248–50, 258, 295, 421–3
amphiphiles 9, 576
anchoring
 strong 114
 weak 114
anisotropy, dielectric 133–5, 148
antiphases 27–8, 554, 562, 563
arceaux 310, 311

bend deformations 515, 516
birefringence, flow 256
Bloch–Floquet 272
blue phases 320–33
bond ordering 548
bookshelf geometry 397–404
Bragg reflection 264–8, 321
Brillouin scattering 421, 423
buckling instability 368–9
Burger's vectors 477, 478, 501

Cano wedges 312, 318, 485
capillary waves 217
Carr–Helfrich effect 80, 237, 240, 301
Chen–Lubensky model 535, 537, 538, 540
chevrons 239–40, 241
cholesteric–nematic transition 289
cholesterics 13–17, 263–333
 storage mode of 300
 cholesteric wedges 310–12
 fingerprint texture 310–13
chromatography 92
clusters, cybotactic 512, 514–16
coherence lengths 76
 magnetic 120–3, 143
 order parameter 511
columnar phases, *see* phases, columnar
conductance, static 232
conductivities 232
conics, focal 308–9, 470–3
conoscopy 126–7
consolute points 93, 94
continuum theory
 for cholesterics 287–8, 293–4

for columnar phases and smectics 337–52, 408–30
for nematics 98–117
convective instabilities 230–45
copolymers, block 9
Cotton–Mouton effect 79, 85
Coulomb gauge 513
crystals
 colloidal 3
 definition of 1

diamagnetism, molecular 117–20
dielectric constants 58, 230
dielectric relaxation 245
diffusion 250–4
diffusivity
 orientational 225
 thermal 225
disclinations 163, 166–8, 478–82, 492, 541–6
 disclination lines 168–80, 478, 482
 instability theorem for 180–3
 strength of 169
 disclination loops 129, 168, 223
 pairs of 541, 543
 point 168, 180–5
 see also point defects
 discommensurations 561, 566
dislocations 315, 333, 351, 392–3, 476–8, 487–504
 boundary effect 494
 dislocation currents 489–90, 493, 495, 501
 dislocation loops 496
 dislocation unbinding transitions 524–5
 edge 393, 477, 502
 isolated 490–2, 503
 screw 478, 502, 525–6
 isolated 493–4, 504
display systems 34–5
Dupin cyclides 470

elastic constants 102–5
 compressional 519–20, 530, 531
electric birefringence 80
electroclinic effect 376

- electrode effects 232
 energy
 anchoring 194, 196
 distortion, *see* distortion energy
 Frank-Oseen elastic 510, 511, 538
 isotropic-chiral nematic 329
 tilt 411
 entropy
 production of 410, 413
 sources of 200
 final formula for 203
 translational 576
 EPR (electron paramagnetic resonance) 51,
 54
 Ericksen law 219–20
 Ericksen stress 153, 201
- ferronematics 130
 films, smectic 358–9, 374–6
 Fisher renormalization 520
 flexoelectric coefficients 136, 347–9, 352, 380
 flexoelectric effect 135–9
 Flory model 63–4
 Frank elasticity 138
 Frederiks transition 123–33, 189–90, 194,
 225
 friction
 coefficients 204–5
 temperature variation of 254
 see also Leslie coefficients
- Ginzburg criteria 87, 523, 529–32
 grain boundaries 483, 485, 525
- Helfrich–Hurault effect 361–4
 helium, superfluid 510, 525, 527, 540–1
 homeotropic texture 353, 354
 hydrodynamics
 basic equations for smectics and columnar
 phases 410–15
 breakdown of 457–64
 of columnar phases 417–18, 419, 421,
 461–2
 mode structure 429–30
 of smectics A 408–9, 415–24
 variables in 408–9, 429
- incommensurability 560, 566–7
- Kerr effect 80, 85, 258
 Kosterlitz–Thouless mechanism 541, 546–7
- Landau–Peierls instability 31, 461
 Leslie coefficients 206, 254, 259, 296
- light scattering 80–2, 85, 139–41, 144–50,
 528–9
 inelastic 217, 227–30, 256–8, 295–6
 line tension 178–80, 491, 524
 liquids, isotropic, definition of 1–2
 lyotropic systems 6
- magnetic birefringence 79
 magnetic fields, external 220–7
 oscillating 220–3
 pulsed 225–7, 295
 rotating 223–5
 magnetic susceptibilities 58
 Maier–Saupe (MS) theory 55, 56, 69
 Mauguin limit 268–9, 276
 MBBA 54
 carrier mobilities in 252, 253
 conductivity of 232
 elastic constants of 105, 147
 viscosities of 231
 Meissner effect 511, 512
 miscibility 25, 91
 molecular field 107, 150
 molecules
 alkyl chains in 50–1, 576
 chiral 13
 flexible 48
 rigid 45–8
 small discoid organic 6
 small elongated organic 3–6
 vectorial symmetry of 557
 Monte Carlo studies 74, 85, 90
- nematic–isotropic transition,
 phenomenological description
 of 76–90
- nematics
 alignment fluctuations in 139–50
 biaxial 12, 57, 70–3, 539, 540
 definition of 2, 34
 deformations in 98
 re-entrant 552, 568
 sensitivity to weak external
 perturbations 34
 turbidity of 147
 uniaxial order in 51, 67
 nematogens 4, 92
 neutron scattering 55
 NMR spectra 12, 43
 NMR quadrupole splitting 47, 48
 noyaux 163–6, 168, 183
- Onsager model 59–62, 74
 ordering matrix 45, 50